

AD701235

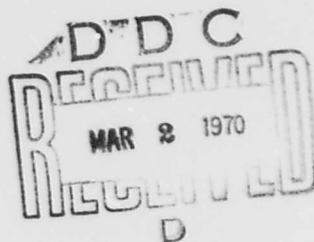
FOREIGN TECHNOLOGY DIVISION



PRINCIPLES OF SOLID-FUEL ROCKET DESIGN

By

Ya. M. Shapiro, G. Yu. Mazing  
N. Ye. Prudnikov



This document has been approved  
for public release and sale; its  
distribution is unlimited.

Distribution of this document is  
unlimited. It may be released to  
the Clearinghouse, Department of  
Commerce, for sale to the general  
public.

Reproduced by the  
**CLEARINGHOUSE**  
for Federal Scientific & Technical  
Information Springfield Va. 22151

400

FTD-HT-23-268-69

(JPRS)

## EDITED TRANSLATION

PRINCIPLES OF SOLID -FUEL ROCKET DESIGN

By: Ya. M. Shapiro, G. Yu. Mazing, N. Ye. Prudnikov

English Pages: 389

Source: Osnovy Proyektirovaniya Raket na Tverdom  
Toplive, 1968, pp. 1-352

THIS TRANSLATION IS A RENDITION OF THE ORIGINAL FOREIGN TEXT WITHOUT ANY ANALYTICAL OR EDITORIAL COMMENT. STATEMENTS OR THEORIES ADVOCATED OR IMPLIED ARE THOSE OF THE SOURCE AND DO NOT NECESSARILY REFLECT THE POSITION OR OPINION OF THE FOREIGN TECHNOLOGY DIVISION.

PREPARED BY:

TRANSLATION DIVISION  
FOREIGN TECHNOLOGY DIVISION  
WP-AFB, OHIO.

FTD-HT- 23-268-69 (JPRS)

Date 19 Nov 19 69

**BLANK PAGE**

## TABLE OF CONTENTS

	<u>Page</u>
Foreword	1
Chapter I. Basic Types of Solid-Fuel Rocket Designs	1
1.1. Basic Solid-Fuel Rocket Concepts and Classifications	1
1.2. Peculiarities of Design and Arrangement Layouts of Solid-Fuel Rocket Engines and Elements of Designs	17
1.3. Characteristic Peculiarities of Design Layouts of Unguided Reactive Missiles	34
Bibliography	43
Chapter II. Basic Relations of the Internal Ballistics of Guided Rockets	46
2.1. The Rocket as a Variable Mass Body	46
2.2. The Gravitational Field of the Earth	53
2.3. The Terrestrial Atmosphere	58
2.4. Aerodynamic Forces and Moments	62
2.5. The Trajectory of Movement of a Guided Ballistic Rocket. The Parts of the Trajectory	74
2.6. The Equation for Motion of the Rocket in the Active Part of the Trajectory	77
2.7. Approximate Calculation of Elements of Active Section of Trajectory by the Method of Successive Integration	82
2.8. Calculation of the Initial Passive Section of the Trajectory by Arcs	90
2.9. Movement of the Rocket on the Passive Airless Section of the Trajectory in the Central Field of the Earth's Attraction	96

Table of Contents (continued)

	<u>Page</u>
2.10. Range of Flight of a Rocket. The Angle of Greatest Range. Height of Trajectory	102 106
2.11. Time of Flight	108
2.12. Calculation of the Final Section of the Trajectory	
2.13. Over-All Computation of the Elements of the Trajectory. The Method of Fictitious Initial Conditions	115
2.14. Trajectory of Flight of an Earth Satellite	117
2.15. The Trajectory of Movement of a Satellite Relative to a Rotating Earth	122
Bibliography	126
 Chapter III. Ballistic Designing of Guided Rockets	 128
3.1. Statement of the Problem	128
3.2. Weight Equation of Single-Stage Ballistic Rocket	131
3.3. The Weight Coefficient of a Solid-Fuel Rocket Engine	134
3.4. Relationship Between Admissible Changes in Unit Impulse and Weight of Engine Structure for Given Velocity of Rocket at End of Active Section	141 145
3.5. Determination of Basic Dimensions of Charge	150
3.6. Dependence of Start Weight of Rocket Upon Initial Thrust-Weight Ratio	153
3.7. Selection of Initial Transverse Loading	
3.8. Connection Between the $x$ Parameter and the Pressure in the Forward Part of the Engine (Taking Erosive Combustion into Account)	157
3.9. Selection of Optimum Values of Working Pressure and of the Loading Parameter	168
3.10. Selection of Optimum Degree of Expansion of Cone	170
3.11. Determination of Basic Characteristics of Rocket	172
Bibliography	173
 Chapter IV. Solid-Fuel Rocket Engine Strength Computation	 175
4.1. Working Loads, Computed Cases, and Peculiarities of Computation for Strength of Engines	175
4.2. Calculating the Casing of the Engine for Strength	181
4.3. Evaluation of the Reliability of the Structure of Large Solid-Fuel Rocket Engines	191
 Chapter V. Strength of Charges of Solid Fuel	 203
5.1. Working Characteristics and Character of Deformation of Solid-Fuel Rocket Charges	203
5.2. Mechanical Properties of Solid Rocket Fuels	206

Table of Contents (continued)

	<u>Page</u>
5.3. The Strength Criterion	215
5.4. Calculation of a Solid Fuel Charge for Strength During Working of Rocket Engine	218
5.5. Analysis of Concentrations of Stresses in Solid Fuel Charge Having Compound Perforations of the Internal Channel of the Burner	221
5.6. Strength Calculation of Rocket Charge Allowing for Elastic-Plastic Deformation and Rheological Properties of Solid Fuel	223
5.7. Taking Temperature Stresses Into Account in Calculating a Solid Fuel Charge for Strength	231
5.8. Calculating Elastic-Plastic Deformations in a Solid Fuel Charge Under the Effect of Weight	232
Bibliography	233
 Chapter VI. Executant Organs for Guidance of a Rocket Having Solid Fuel Engine	 234
6.1. Regulation of Thrust in Amount	234
6.2. Interception of Thrust	238
6.3. Regulating the Vector of Thrust as Regards Direction	244
6.4. Controlling the Vector of Thrust by Injecting Gas or by Injecting Liquid Into the Post-Critical Part of the Cone	255
Bibliography	261
 Chapter VII. Motion of the Center of Mass of an Unguided Rocket	 263
7.1. Equations for the Motion of an Unguided Rocket Over the Active Part of Its Trajectory	263
7.2. Integration of Equations for Motion of Rocket in Active Section of Trajectory, in First Approximation	265
7.3. Allowing for Air Resistance	270
7.4. Determining the Full Range of Flight of the Rocket	278
Bibliography	280
 Chapter VIII. Plane Oscillations and Dispersion of Fimmed Unguided Rockets	 281
8.1. Factors Determining Dispersion of Unguided Rockets	281
8.2. Motion of the Rocket Along the Guide	282
8.3. Differential Equations of Plane Oscillation of the Rocket in the Active Part of the Trajectory	289
8.4. Oscillation of a Rocket in the Presence of Eccentricity of Reactive Force	291

Table of Contents (continued)

	<u>Page</u>
8.5. The Critical Section of the Trajectory	297
8.6. Oscillation of a Rocket in the Presence of Initial Disturbances $\varphi$ and $\psi$	299 303
8.7. Axial Rotation of Finned Rockets	306
8.8. Influence of Wind on the Flight of Finned Rockets	310
Bibliography	
<b>Chapter IX. Rotary Motion of Turbojet Missiles</b>	<b>311</b>
9.1. Drawing up Differential Equations for Motion of a Rocket	311
9.2. Integrating the Equations for Rotary Motion of a Rocket	316
9.3. The Condition of the Gyroscopic Stability of Turbojet Missiles	321 324
9.4. Over-All Dispersion of Unguided Rockets	325
Bibliography	
<b>Chapter X. Ballistic Planning of Unguided Rocket Missiles</b>	<b>326</b>
10.1. Posing the Problem	326
10.2. The Weight Equation for an Unguided Rocket Missile	329
10.3. Change of Ballistic and Structural Characteristics of Guided Rocket Missile With Length of Charge. Condition of Maximum Range	331
10.4. Connection Between Dimensions of Charge and Coefficient of Charging $\alpha$ for Charges of Various Shapes	334
10.5. Determination of Basic Design Parameters of Optimum Ballistic Model for Charge Consisting of Cylindrical Single-Channel Burners	343
10.6. Determination of Basic Design Parameters of Optimum Ballistic Model for Charge of Any Given Shape (Generalized Graph-Analytical Method of Solution)	347
10.7. Selection of Optimum Design Variant of Unguided Rocket Missile	355 361
10.8. Peculiarities of Planning Turbojet Missiles	
10.9. Determination of Basic Design Parameters of Model Having Set Charge Combustion Time	366
10.10. Initial Data and Project Parameters Determining Basic Design Characteristics of an Unguided Rocket Missile. Weight and Over-All Dimensions of Warhead	374
Bibliography	380

Table of Contents (continued)

	<u>Page</u>
Annex I. Changes in Meteorological Elements With Altitude	381
Annex II. $U_1 - U_2; U_2 = \frac{1}{2} (U_1)^2$	383
Annex III. Graphs for Function $\Phi_2 (\eta, u, \mu)$ for Chapter II	385

6T5.2  
Sh23

UDC 621.455.001

PRINCIPLES OF SOLID-FUEL ROCKET DESIGN

352 pages, 5,500 copies  
1 ruble 25 kopecks

Ya. M. Shapiro, G. Yu. Mazing,  
and N. Ye. Prudnikov

On the basis of materials published in the domestic and foreign press this book offers a survey of the designs of guided and unguided rockets for various purposes and having solid-fuel engines. The design elements of individual assemblies and units, the composition layouts of rockets, and questions relating to the regulation of thrust as regards quantity and direction are examined. Engineering methods for calculating the elements of trajectories of guided and unguided rockets are given, as they apply to the problems of ballistic designing. The factors affecting the scatter of unguided rockets are examined. Optimum parameters for rockets and design units are evaluated via synthesis and analysis of weight equations for rockets, approximate external ballistic relations being utilized. The fundamentals of calculations of solid-fuel rocket engines and of charges for them as regards sturdiness are set forth.

The book can be used as a manual for engineers working in the field of rocket technology, and also for students at institutes of higher education.

## FOREWORD

Recent decades have been characterized by a surging development of rocket technology. At present rockets are being worked out both for military purposes and for the investigation of outer space. After the sending up of the world's first artificial earth satellite which opened the era of space flights Soviet science and technology have registered significant successes in the investigation and conquest of outer space.

In the practice of designing rockets of various classes rocket engines using solid fuel (RDTT) find widespread application. For this reason questions relating to the theory, design, and use of these engines are of great interest to specialists in rocket technology and to designers.

This book sets forth the basic data and relationships necessary for designing solid-fuel rockets. It sets forth the basic design systems and characteristics of modern solid-fuel rockets.

It examines questions related to the external ballistics and the ballistic designing of solid-fuel rockets as these are introduced into engineering calculations, and it also examines calculations for the strength of the rocket chamber and for the charge of solid fuel.

It offers a generalization of experimental and theoretical investigations regarding current questions of RDTT designing: regarding the reliability, regulation, and strength calculation for solid-fuel charges, taking into account elastic-plastic deformations, rheological properties, and temperature stresses.

The book is based upon the basic assumptions of RDTT theory, and constitutes a logical continuation of the book The Theory of the Solid-Fuel Rocket Engine by the same authors.

Since it is not possible to cover in a single book of no great scope all of the questions associated with the designing of rockets of various classes, the authors have found it necessary, in setting forth

their material, to limit themselves to the field of guided, single-stage rockets and of unguided rocket projectiles of the "surface-to-surface" class. Many of the methods and relationships examined are nevertheless of universal application and may be used in designing rockets of other classes. Among these are included a number of external ballistics relationships, strength calculations for the basic design units, gravimetric equations, formulas linking dimensions of charge with loading parameters, limit solutions for ballistic design problems, etc.

The exposition of basic methods of calculation is illustrated by numerical solutions. Where the characteristics of engines, fuels, and materials taken from foreign literature are used in the examples, references are made to the literature sources. In other examples having a purely methodical purpose arbitrarily selected quantities not associated with actual objects are used.

Chapters II, VII, VIII, and IX have been written by Professor Ya. M. Shapiro (Meritorious Scientific and Technical Worker of the RSFSR, Doctor of Technical Sciences); chapters III and X by G. Yu. Mazing (Candidate in Technical Sciences, Lecturer); and chapters I, IV, V, and VI by N. Ye. Prudnikov (Candidate in Technical Sciences, Lecturer).

M. N. Stepanov (Candidate in Technical Sciences) took part in the writing of heading 10.7.

## CHAPTER I. BASIC TYPES OF SOLID-FUEL ROCKET DESIGNS

### 1.1. Basic Solid-Fuel Rocket Concepts and Classification

A rocket consists of a carrier rocket and the object transported (a warhead, instruments for scientific investigation, radio transmitting apparatus, and other loads). If the carrier rocket and the object transported are inseparable, the term "rocket" relates to the flying apparatus as a whole, for example, short-range military rockets or guided zenith rockets. If the carrier rocket and the object transported separate during the trajectory of the flight, the term "rocket" relates to the carrier.

The creation of the theory of reactive movement by the distinguished Russian scholar K. E. Tsiolkovskiy played an enormous part in the working out of rocket flight apparatus for various purposes. In 1924 Soviet engineers created military rockets using smokeless powder (1). At the beginning of the Great Fatherland War only solid fuel rockets were among our armaments. Gunpowder of ballistic type was used as solid fuel in these rockets.

After the Second World War, in the light of the imperfection of solid fuel the field of its application was exclusively that of small-caliber unguided missiles. It was in this period that a sharp distinction among rockets, depending on the range of their action, became defined. In long-range rockets liquid fuels were used, and solid-fuel rockets became a basic combat instrumentality for land-based short-range rocket artillery.

The genesis of mixed solid fuel and the bringing to perfection of the technology of its production considerably expanded the field of application of the solid-fuel rocket. At present solid-fuel rocket engines (RDIT) are used in all forms of weapons (see Table 1.1).

The considerable part played by the solid-fuel rocket in present-day rocket technology is occasioned by advantages which solid-fuel rockets have as compared with liquid fuel ones:

- high reliability of functioning and constant readiness for re-lease;
- simplicity and compactness of apparatus;
- simplicity of use, and the simplicity of ground equipment and servicing associated with this;
- possibility of prolonged storage in final missile form;
- uncomplicated nature of production technology and lower cost of manufacture as compared with other rocket engines;
- possibility of ensuring high thrust-weight ratio (use as start engine).

Among the deficiencies of the solid-fuel rocket engine are the following: existence of considerable dependence of characteristics of engine upon initial temperature of charge of solid fuel, more complicated solution of problems associated with ensuring guidance and multistage start-up of engine.

Guided rockets are the most widespread form of flight apparatus. Guided rockets are divided into two groups according to their aerodynamic shape and arrangement:

- winged rockets;
- ballistic, or wingless, rockets.

In winged rockets aerodynamic lift coefficient in the system of forces determining flight on the trajectory plays a substantial part.

As an example of such a design one may take the winged "Lacrosse" solid-fuel rocket (Figure 1.1).

In the system of forces determining the flight of a ballistic rocket upon a trajectory lift coefficient does not play a substantial part. The trajectory of a ballistic rocket, with the exception of the initial portion, constitutes the trajectory of flight of a body fired at an angle to the horizon. As an example of such a design we may cite the two-stage "Pershing" solid-fuel ballistic rocket (Figure 1.2).

In their design layouts and tactical and technical characteristics existing solid-fuel rockets are decidedly variegated. Depending on the place of start and the final target rockets are divided into classes: "surface to surface," "surface to air," etc. (Figure 1.3).

Ballistic rockets of the "surface-to-surface" class are shown in Figures 1.4 and 1.5.

Table 1.1. Basic Tactical and Technical Characteristics of Solid-Fuel Rockets (1)

<u>No in Order</u>	<u>Designation or Index of Rocket</u>	<u>Number of Stages and Weight at Start, Tons</u>	<u>Maximum Range, Kilometers</u>
"Surface-to-Surface" Class Rockets			
1	"Lacrosse" (USA)	1/1.0	32
2	"Mace" (USA)	2/8.2 (7.0)* start. RDTT + TRDj -- 33	> 1,600 (2,220)*
3	"Minuteman A" (USA)	3/30.9	9,200
4	"Minuteman B" (USA)	3/31.5	10,200
5	"Minuteman C" (USA)	3/33.0	12,000 (13,366)*
6	"Athena" (USA)	4/7.2	--
7	"Pershing A" (USA)	2/4.54	750 (185-740)*
8	"Pershing B" (USA)	2/5.0	1,500
9	"Sergeant" (USA)	1/4.54	46-140 (320)*
10	"Honest John" (USA)	1/2.0	Up to 32 (19)*
11	"Little John" (USA)	1/0.360	16
12	"Slim John" (USA)	1/2.2	32
13	"SS-10" (France)	1/0.015	1,500

Table 1.1 (continued from page 7)

<u>No in Order</u>	<u>Length of Rocket, Meters</u>	<u>Diameter of First Stage, Meters</u>	<u>Take-Off Apparatus</u>	<u>Remarks</u>
1	5.86	0.52	Automotive release apparatus.	Winged rocket.
2	13.4	1.37		Idem.
3	16.2	1.65	From stationary start positions. Release from shaft.	Intercontinental ballistic rocket.
4	17.03	1.65		
5	18.00	1.68		
6	16.2	--	Take-off from rail chute 9 meters in length.	Head of rocket reached altitude of 180 kilometers for investigation of re-entry of ballistic rockets into atmosphere.
7	10.6 (10.7)*	1.0	Mobile, on ground.	Ballistic rocket.
8	10.0	1.0	Idem.	Idem.
9	10.0 (10.5)*	0.8	Idem.	Idem.
10	7.6	0.76	Release from automobile trailer.	Unguided rocket missile.
11	4.4	0.3	Release from automobiles.	--
12	7.3 (7.6)*	0.76	Mobile -- release from automobile.	--
13	0.86	0.152	Antitank arm.	Wire-guided missile.

Table 1.1 (continued from page 7)

<u>No in Order</u>	<u>Designation or Index of Rocket</u>	<u>Number of Stages and Weight at Start, Tons</u>	<u>Maximum Range, Kilometers</u>
14	"SS-11" (France)	1/0.029	3.5
15	TOW	2/0.073 (0.018)*	0.075-3.500
16	"Vigilant" (Great Britain)	1/0.0147	1.65
"Surface-to-Air" Class Rockets			
17	"Diamant" (France)	3/--; II and III stages -- RDTT	Height of perigee 530 kilometers; height of apogee 2,680 kilometers
18	Antisatellite device on basis of carrier rocket "IAT-Edjen" and "TAT-Delta" (USA)	2/58.0 ZhRD + three RDTT	--
19	"Nike-Zeus" (USA)	3/10.3 (13.6)*	240-370
20	"Sprint" (USA)	2/4.54	Height of interception of target 30-50 kilometers
21	"Hibex" (USA)	2/--	Interception of rockets at low altitudes

Table 1.1 (continued from pages 9 and 8)

<u>No in Order</u>	<u>Length of Rocket, Meters</u>	<u>Diameter of First Stage, Meters</u>	<u>Take-Off Apparatus</u>	<u>Remarks</u>
14	1.17	0.152	--	--
15	1.35	0.14	Release tube.	Charge of first stage consumed in release tube and thrusts missile out. Charge of second stage ignited after exit of missile from release tube.
16	0.91	0.13	--	--
17	--	1.4	Release apparatus for releasing artificial earth satellite /ISZ/.	Rocket carries "A-1" apparatus into space in orbit of artificial earth satellite.
18	18.2	2.4	Stationary release apparatus.	Missile intended to intercept satellites in orbits of about 640 kilometers altitude.
19	14.7	1.17	Stationary release apparatus.	--
20	8.2	1.4	Fired from underground release apparatus.	Antirocket device.
21	--	--	Starting engine ignited in shaft.	Antirocket device.

Table 1.1 (continued from page 9)

<u>No in Order</u>	<u>Designation or Index of Rocket</u>	<u>Number of Stages and Weight at Start, Tons</u>	<u>Maximum Range, Kilometers</u>
22	"Bomark" (USA)	2/7.3 RDTT + 2PVRD	800 (700)*
23	"Nike-Hercules" (USA)	2/4.5	> 130
24	"Bloodhound" (Great Britain)	2/-- 4RDTT + 2PVRD	--
25	"Thunderbird" (Great Britain)	2/1.8	50-60
26	"Roland" (France and German Federal Republic)	1/0.06; RDTT with two thrust stages	0.5-7.0
27	"Ready" (USA)	1/0.009; RDTT with two thrust stages	3-5
28	"Hawk" (USA)	1/0.58; RDTT with two thrust stages	35-40
29	"Mauler" (USA)	1/0.055; RDTT with two thrust stages	0.450-15.0
30	"Short Matra and Disso Aramis" (Great Britain and France)	--	--
"Air-to-Surface" Class Rockets			
31	"Skybolt" (USA)	2/4.0-5.0	1,850
32	"Nord Aviation" (France)	2/0.5 -- 2RDTT in single hull	11.0
33	"SAAB-305" (Sweden)	RDTT	--

Table 1.1 (continued from pages 11 and 10)

<u>No in Order</u>	<u>Length of Rocket, Meters</u>	<u>Diameter of First Stage, Meters</u>	<u>Take-Off Apparatus</u>	<u>Remarks</u>
22	14.3	0.89	--	--
23	12.1	0.8	--	--
24	2.03	0.55	--	--
25	6.4	0.53	Transporters, trailers; transportable by air	--
26	2.5	0.5	Release apparatus designed for eight missiles and discharges them in pairs.	--
27	1.2	0.076	Fired from shoulder from release tube.	--
28	5	0.36	Release apparatus on transporters and trailers.	--
29	1.8	0.14	Caterpillar amphibious transporter.	--
30	2.5	Span of wing 0.3	Transporter.	
31	11.7	1.0	Release from aircraft.	Ballistic rocket released from airplane.
32	3.8	0.35	Aircraft release apparatus.	For armament of tactical aviation.
33	3.53	0.305	Idem.	--

Table 1.1 (continued from page 11)

<u>No in Order</u>	<u>Designation or Index of Rocket</u>	<u>Number of Stages and Weight at Start, Tons</u>	<u>Maximum Range, Kilometers</u>
34	"Shrike" (USA)	RDIT 0.227	20.0
"Air-to-Air" Class Rockets			
35	"Falcon" (USA)	1/0.068	8.0
36	"Falcon (GAR-9)" (USA)	RDIT/0.36	160 (> 40)* Altitude about 21 kilometers
37	"Phoenix" (USA)	1/0.227; RDIT with two thrust stages	65-75
38	"Sparrow-3" (USA)	1/0.17 RDIT	8-15
39	"Red Top" (Great Britain)	1/0.132	13 (17)*
40	"Sidewinder" (USA)	1/0.07	7-16
41	"Matra" (France)	1/0.195; RDIT with two thrust stages	14 (18.5)*
"Ship-to-Air" Class Rockets			
42	"Terrier" (USA)	2/1.6	≈ 37
43	"Tartar" (USA)	1/0.68; RDIT with two thrust stages	17-20
44	"Sislag" (Great Britain)	2/1.8	32

Table 1.1 (continued from pages 13 and 12)

<u>No in Order</u>	<u>Length of Rocket, Meters</u>	<u>Diameter of First Stage, Meters</u>	<u>Take-Off Apparatus</u>	<u>Remarks</u>
34	≈ 3.0	0.2	--	Rocket intended to strike radio-locator set-ups of antiaircraft defenses (PVO).
35	2.17	0.164	Aircraft release apparatus.	For armament of fighter aircraft.
36	3.8	0.34	Idem.	For armament of fighter-interceptor planes.
37	--	0.15	Idem.	For armament of naval fighters.
38	3.6-3.66	0.21	Idem.	Idem.
39	3.5	0.22	Idem.	For aircraft armament.
40	2.87	0.127	Idem.	For armament of fighter planes.
41	3.3	0.26	Idem.	For armament of all-weather fighters.
42	9.0	0.33	Shipboard release apparatus.	For antiaircraft defense of surface vessels.
43	≈ 4.5	0.33	Idem.	For defense of /esmintsey/ against aircraft.
44	6.0	0.41	Idem.	For antiaircraft defense of surface vessels.

Table 1.1 (continued from page 13)

<u>No in Order</u>	<u>Designation or Index of Rocket</u>	<u>Number of Stages and Weight at Start, Tons</u>	<u>Maximum Range, Kilometers</u>
45	"Siket" (Great Britain)	1/-- RDIT with two thrust stages	8
46	"Mazurka" (France)	2/1.450-1.850	30-40
47	"Regulus" (USA)	2/6.7 -- 2RDIT + route TRD	800-900
"Submarine-to-Surface" Class Rockets			
48	"Polaris A-1" (USA)	2/12.8	2,200
49	"Polaris A-2" (USA)	2/14.5	2,800
50	"Polaris A-3" (USA)	2/15.9	4,600
51	"Poseidon C-2" (USA)	2/--	4,600
"Ship-to-Submarine" Class Rockets			
52	"Terne III" (Norway)	1/0.12	5.6
53	"Asroc" (USA)	1/0.450 -- RDIT + torpedo electric motor	1.6-15

Table 1.1 (continued from pages 15 and 14)

<u>No in Order</u>	<u>Length of Rocket, Meters</u>	<u>Diameter of First Stage, Meters</u>	<u>Take-Off Apparatus</u>	<u>Remarks</u>
45	6.0	0.41	Shipboard release apparatus.	For defense of surface vessels and strikes against surface and shore targets.
46	8.5-8.6	0.4	Idem.	For anti-aircraft defense of vessels.
47	10-10.4	1.37	Idem.	Missile aircraft released from shipboard release apparatus.
48	8.7	1.37	Release apparatus of submarine.	Release of rocket takes place from beneath water against terrestrial armaments.
49	9.6	1.37	Release apparatus of water-surface stationary base and release apparatus of submarine.	--
50	9.8	1.37	Release apparatus of water-surface stationary base and release apparatus of submarine.	--
51	--	1.47	--	--
52	1.98	0.3	Shipboard release apparatus	--
53	4.6 → (overall length of device) 2.54 → (length of missile)	0.3	--	For combat against atomic submarines /nuclear submarines/.

Table 1.1 (continued from page 15)

<u>No in Order</u>	<u>Designation or Index of Rocket</u>	<u>Number of Stages and Weight at Start, Tons</u>	<u>Maximum Range, Kilometers</u>
54	"Malafon-2" (France)	1/1.4 -- 2 start RDTT + torpedo motor	≈ 18
55	"Sabroc" (USA)	RDTT/1.80	40-50 (65-80)*

\* The characteristics appearing in parentheses have been taken from other data.

The acronyms have the following meanings:

PU -- release apparatus  
 TRD -- turbojet engine  
 PVRD -- ram-jet engine  
 PVO -- antiaircraft defense  
 ISZ -- artificial earth satellite

Table 1.1 (continued from pages 17 and 16)

<u>No in Order</u>	<u>Length of Rocket, Meters</u>	<u>Diameter First Stage, Meters</u>	<u>Take-Off Apparatus</u>	<u>Remarks</u>
54	6.0	0.53-0.63	Shipboard release apparatus.	For armament of escort vessels.
55	6.4	0.553	Torpedo apparatus.	Ballistic rocket with release from submarine.

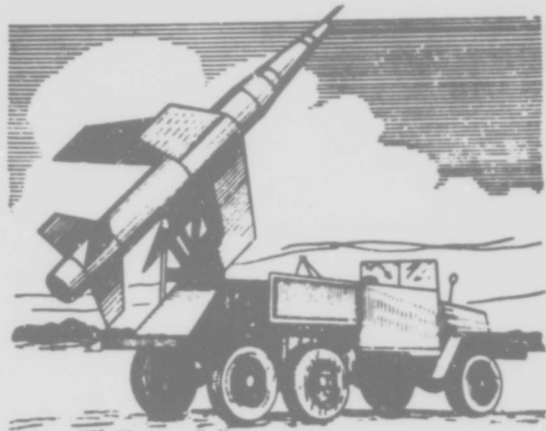


Figure 1.1. Winged "Lacrosse" solid-fuel rocket.



Figure 1.2. Two-stage "Pershing" ballistic rocket with solid-fuel engines.

For striking aerial targets zenith guided rockets (ZUR) belonging to the "surface-to-air" class are used. In this class of rockets the solid-fuel engine is as a rule used as a starting stage. Interceptor rockets also fall among the means of anti-aircraft defense. In Figure 1.6 we show an interceptor rocket of the "surface-to-air" class with solid-fuel rocket engines set up on the start and the route stages.

Antimissile rockets, intended to intercept the warheads of intercontinental ballistic rockets and medium-range ballistic missiles at relatively low altitudes, occupy a special place among rockets of the "surface-to-air" class. The "Sprint" antimissile rocket (Figure 1.7), of cone

shape, represents a two-stage design with solid-fuel engines. It is fired from an underground release shaft in order to accelerate the velocity of ascent of the antimissile rocket (1).

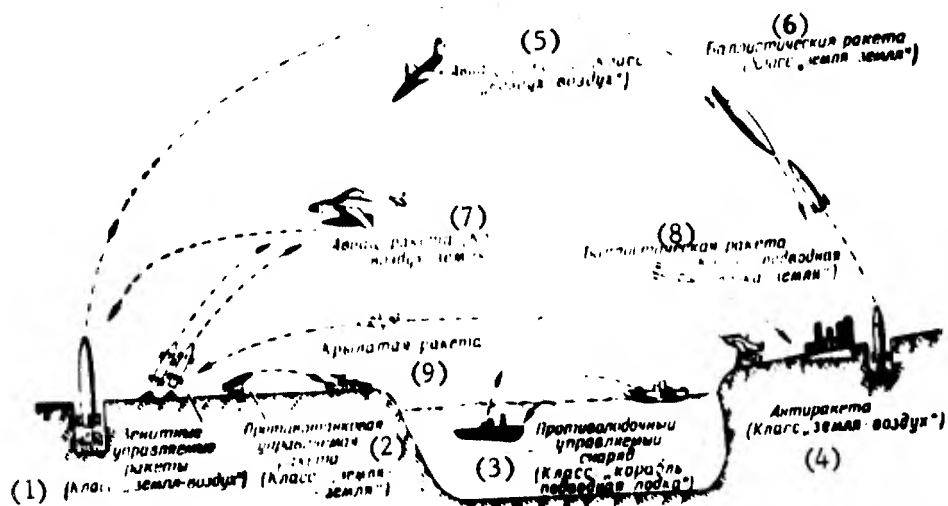


Figure 1.3. Solid-fuel rockets of various classes, and trajectories of their flights.

1 -- Zenith guided rockets ("surface-to-air" class); 2 -- Antitank guided rocket ("surface-to-surface" class); 3 -- Antisubmarine guided missile ("ship to submarine" class); 4 -- Antimissile rocket ("surface-to-air" class); 5 -- Aviation rocket ("air-to-air" class); 6 -- Ballistic rocket ("surface-to-surface" class); 7 -- Aviation rocket ("air-to-surface" class); 8 -- Ballistic rocket ("submarine-to-surface" class); 9 -- Winged rocket.

With the help of "surface-to-air" rockets one can study the structure of the atmosphere and physical phenomena in space and can carry out biological experiments and photograph the surface of the earth.

The release devices of apparatus of "air-to-air," "air-to-ship," and "air-to-surface" classes are set up on carrier aircraft. In these cases the velocity of the aircraft itself is added to the velocity of the rocket.

An example of a rocket of the "submarine-to-surface" class, starting from an underwater position, is the "Polaris" solid-fuel ballistic missile (Figure 1.8). There are 16 such rockets in the armament of an atomic submarine.

Rockets of the "ship-to-air" class are used for the antiaircraft defense of surface vessels (Table 1.1).

The classification set forth here makes it possible to introduce a certain order into the description of rockets of the various classes. At the same time, rockets are pretty diversified and are distinguished

from one another by their design layouts, their working characteristics, and other features. On this account, in studying the technological, design, and use peculiarities of rockets and establishing logical fields for their use it is possible to classify them also according to other features (purpose, sort of solid fuel used, etc.).

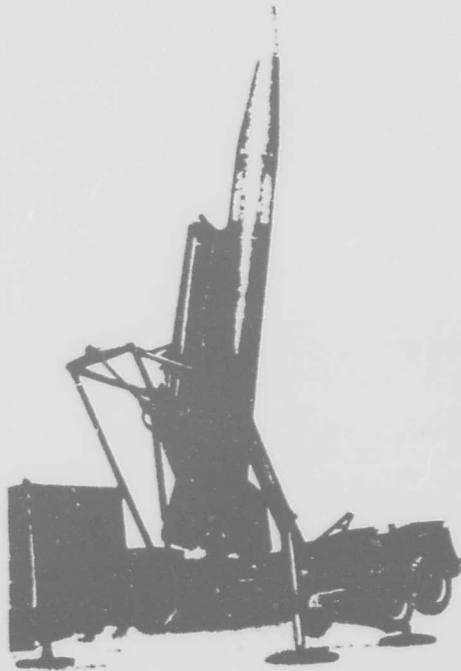


Figure 1.4. "Sergeant" guided rocket using solid fuel.

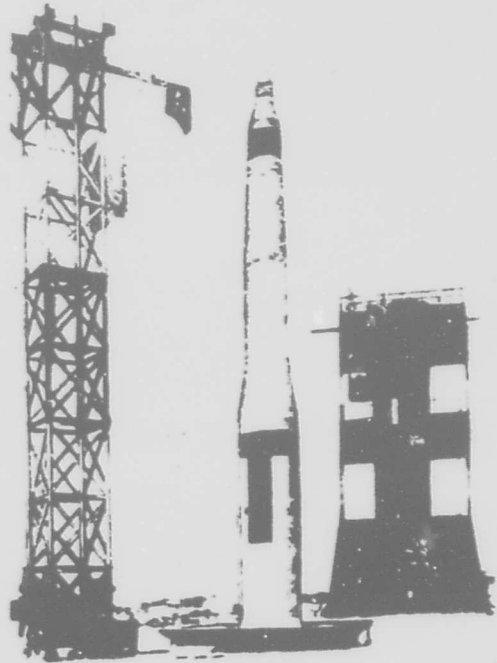


Figure 1.5. "Minuteman" intercontinental ballistic rocket using solid fuel.

## 1.2. Peculiarities of Design and Arrangement Layouts of Solid-Fuel Rocket Engines and Elements of Designs

### RDTT Design Layouts

The solid-fuel rocket engine is the basic structure of a rocket. Joined to it are the instrument block, the executive organs of guidance, and also the stabilizers, rudders, wings, and other elements. In Figure 1.9 we present a present-day design layout for a RDTT with a mixed charge attached to the walls of the chamber. The basic properties of this fuel are ability to burn steadily at a working pressure of 30-40 kilograms per square centimeter and possibility of charging the engine by pouring into a combustion chamber of any dimensions. Combustion of the fuel takes

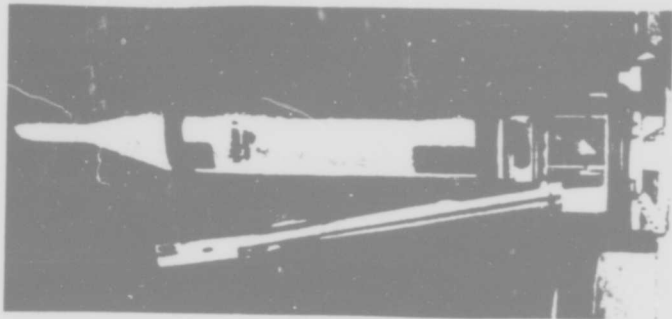


Figure 8. "Polaris" solid-fuel ballistic missile.



Figure 7. "Sprint" rocket for interception of warheads of ballistic rockets.

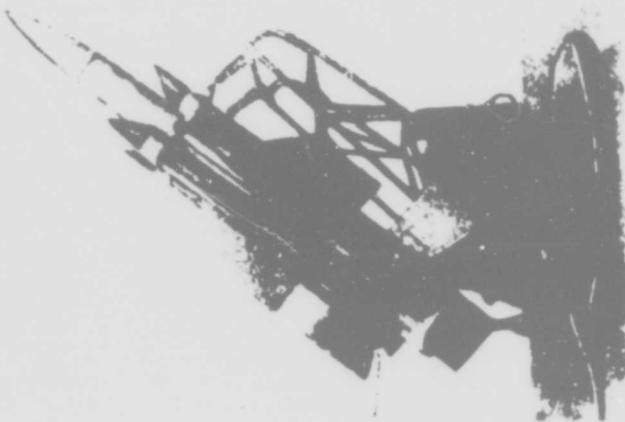


Figure 6. Two-stage "Thunderbird" interceptor rocket.

place from the inner surface of the central channel. In this process the walls of the combustion chamber are protected from the thermic action of gases by the whole thickness of the charge. In order to make the rocket chamber structural materials having high unit strength  $\frac{\sigma}{\gamma}$ , such as alloy

steel, titanium, aluminum alloys, beryllium alloys, glass plastics, and the like, are used. As a result of this it has been possible to reduce the weight of the casing of the engine, and to increase the working time of the engine to some tenths of a second (3). The value of the structural quality factor  $\sigma$ , representing the ratio of the structure to the weight of the fuel, comes to about 0.08-0.1 for a RDIT of the layout under consideration.

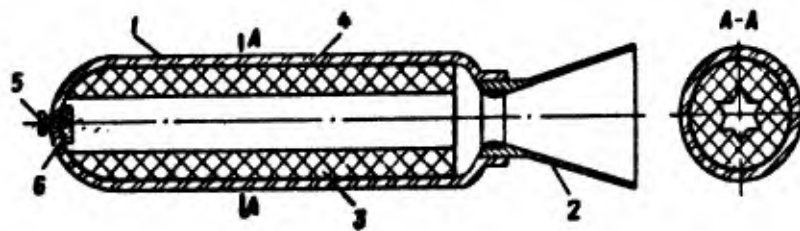


Figure 1.9. Diagram of Solid Fuel Rocket Engine with Charge Attached to Chamber Walls

1 -- Rocket chamber; 2 -- Nozzle unit; 3 -- Solid fuel charge; 4 -- Charge jacket; 5 -- Charge igniter; 6 -- Ignition unit.

According to communications in the foreign press some American firms (4) are working out RDIT's of 3-, 4-, and 6.6-meter calibers, intended for intercontinental ballistic missiles and the carrier rockets of space ships. The basic characteristics of the engines are set forth in Table 1.2 (5).

Table 1.2

Engine	Characteristics					
	Length L, meters	Weight Q <sub>engine</sub> , tons	Weight of Fuel $\omega_{fuel}$ , tons	Thrust P, tons	Working Time $\tau$ , seconds	Pressure in Chamber p, kilograms per square centimeter
RDIT of 3-meter caliber	11.3	--	90	273	--	--
RDIT of 4-meter caliber	23.75	352	316	635	130	50

Table 1.2 (continued)

Engine	Characteristics					Pressure in Chamber p, kilograms per square centimeter
	Length L, meters	Weight Q <sub>engine</sub> , tons	Weight of Fuel $\omega_{fuel}$ , tons	Thrust P, tons	Working Time $\tau$ , seconds	
The same, with fixed cone /nozzle/ for jet/	$\approx 30$	--	362.8	1,360	--	--
RDIT of 6.6-meter caliber	42.7	--	3,175	1,588	120	53
	24.4	680	1,475	$\approx 800$	< 120	--

The RDIT of 4-meter caliber (Figure 1.10) consists of a section with the upper end wall, a central section, and a section with the lower end wall and a rotatory cone. The charge is made of mixed fuel on a basis of polybutadiene with acrylic acid and aluminum additives. Combustion of the section of the fuel charge takes place from the side of a cylindrical channel 1.65 meters in diameter and from the end faces. In stand tests of a RDIT with fuel of the composition indicated a single-impulse value of 245 kilogram · second per kilogram was secured.

New design layouts for RDIT's having high thrusts\* cannot be analyzed separately from the form and weight of the fuel charges.

As may be seen from Table 1.2, the weight of the fuel for engines of large diameters reaches many hundreds of tons. For this reason in working out charges for the most powerful solid-fuel rocket engines new problems arise, the solution of which is associated not only with dimensions and weight, but also with their transport to the start platforms (4). At present technological processes for pouring fuel into the casing of a RDIT actually upon the start platform itself are being worked out (6). In Figure 1.11 we show the setting up of the mandrel into the casing of a RDIT before the pouring of solid fuel into the engine. In addition, in order to facilitate transport of large-dimension RDIT's and to increase the firmness of the solid-fuel charge sectional engines are being worked out. The charge of fuel can consist of a number of sections, separated by inert partitions (Figure 1.12). The sections are assembled at the place of the start.

\* In the foreign press high-power engines are called boosters.

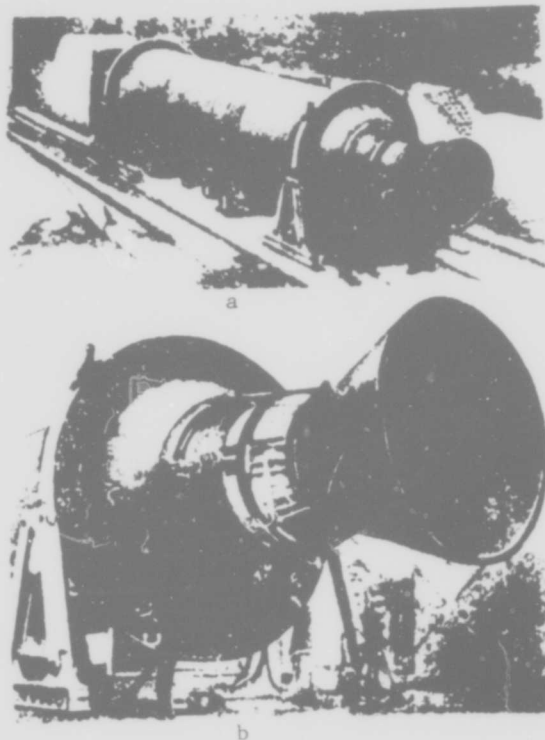


Figure 1.10. Solid-fuel rocket engine of high power: a -- general view of engine of 4-meter caliber; b -- part of engine bearing rotatory cone.



Figure 1.11. Rocket chamber and spine-core section before pouring of solid fuel at start platform.

For the most powerful engines modular burners are used (Figure 1.13), made up of a number of cast and individually polymerized fuel element modules (6). The individual modules are more transportable, are accessible to quality checking, and are easily replaced in case of need. In Figure 1.14 we show the assembling of a modular burner at the moment when the forward part of the engine is being let down to unite with the fifth section of the fuel charge.

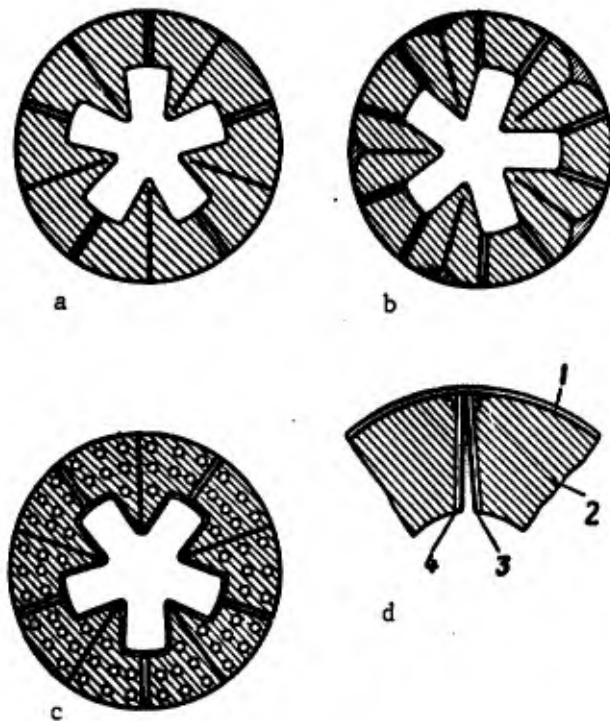


Figure 1.12. Shapes of sectional burners: a -- burner divided by five vertical partitions; b -- burner divided by 10 vertical partitions; c -- burner having horizontal support shelves; d -- divergent coupling: 1 -- wall of casing; 2 -- fuel; 3 -- heat-insulating covering; 4 -- vertical supporting plate of reinforced plastic.

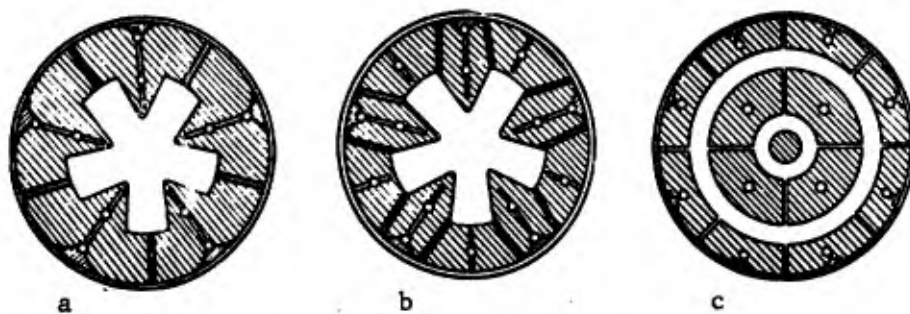


Figure 1.13. Shapes of modular burners: a -- five modules; b -- 10 modules; c -- 30 modules.

#### Composition Layouts for Engines

In their composition layouts existing RDIT's are exceedingly variegated. This is to be explained by the fact that solid-fuel rocket

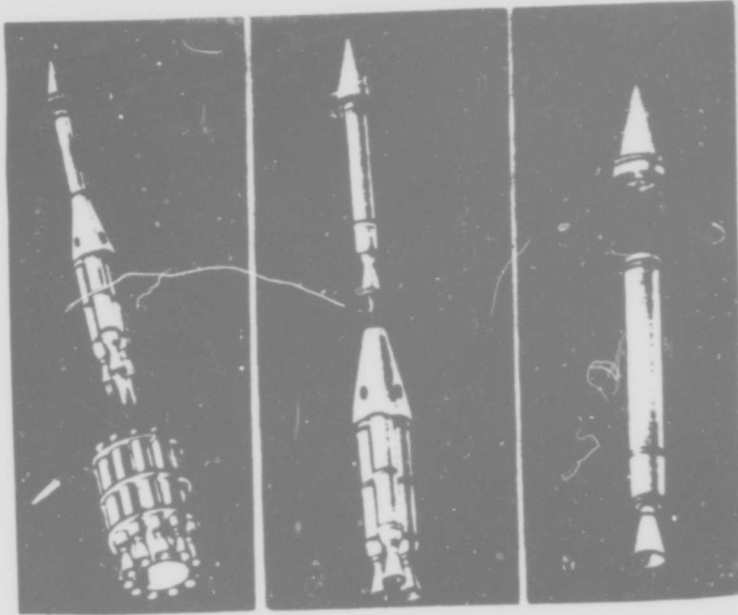


Figure 1.15. Line diagram of separation of stages in multiple-stage solid-fuel rocket.

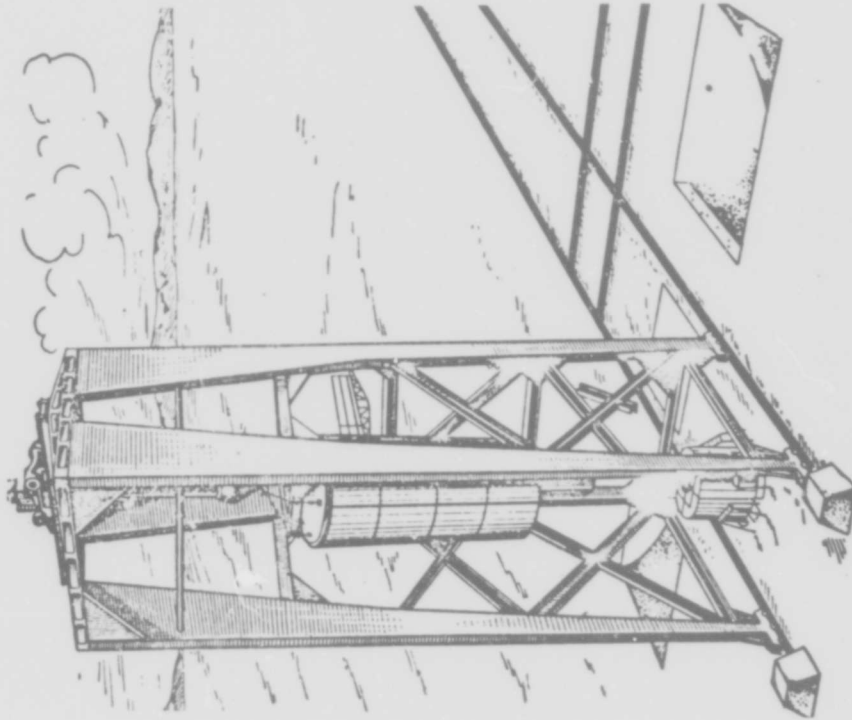


Figure 1.14. Assembling of modular burner on start platform.

engines, by reason of simplicity of design and convenience in use, have become widespread in rockets of most diversified types.

On the basis of the general composition and in harmony with tactical and technological requirements types of carrier designs and fastening points for engines, and also methods of transmitting basic loads and of joining the warhead and the cone block to the rocket chamber, are selected.

Depending on range of flight, character of combat effect at target, and other factors, rockets may be single-stage or multiple-stage.

In Figure 1.9 we show one of the widespread RDIT layouts for a single-stage guided missile. The casing of the engine is made in the form of an axially symmetrical structure. The cone block is attached directly to it, and the casing is connected to the instrument compartment and the warhead via the traversible end wall.

One of the type composition layouts for a multiple-stage rocket RDIT is shown in Figure 1.15.

In this rocket the first and second stages are grouped in a package layout, while the third (last) stage consists of a single rocket engine. During the flight of the multiple-stage rocket the engines which have burned out and are not necessary for further flight are dropped off, and the engine which is functioning is able to communicate supplementary velocity to the lightened rocket.

The composition layout of a RDIT depends essentially on the purpose of the rocket, and also on the character and working regime of the engine. For zenith, antitank, and some other designs of rockets ordinarily the first-stage engine plays the part of an accelerator and is intended for rapid build-up of the velocity necessary to ensure steady flight. Such engines are called start engines. The engine ensuring the further flight of the rocket upon its trajectory is called a route engine. The working regimes of start and route engines (thrust and time) are substantially differentiated from each other. The charge of a start engine is made of fuel having a high burning speed; it has a low thickness of burning arc and a large burning surface. For the charge of a route engine it is wise to use fuel having a lower combustion speed.

In setting start engines around the route engine the cones can be adjusted parallel to the rocket axis, or at an angle. If the cones are set at a certain angle to the axis of the rocket, the line of action of the thrust vector of each of the rocket chambers ordinarily runs through the over-all center of gravity of the rocket. When this is the case, the possibility of the stream of gases that issue from the cones striking the casing of the rocket is eliminated.

In order to reduce as much as possible differences in the thrusts of individual engines, and also in order to achieve simultaneous cut-off

("shut-down") of the working engines, identical combustion regimes must be maintained in each engine. In designing all these problems are resolved by making use of gasodynamic links between engines. In Figure 1.16 we show RDTT layouts in which the chambers are connected to each other by a pipe or a single cone; this brings about evening-off of pressures within the separate rocket chambers and ensures simultaneous release and cut-off of all engines in the set (16).

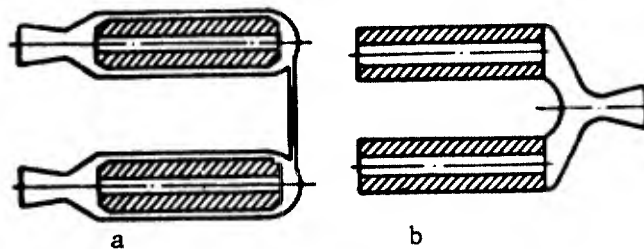


Figure 1.16. Composition layout of RDTT: a -- layout of engines joined via pipe conduit in order to ensure fire linkage; b -- layout of engines connected to single common cone.

In some composition layouts (Figure 1.17) for single-stage rockets engines are used which operate on two regimes (start and route). In Figure 1.17, a and b, engine layouts are shown in the rocket chambers of which there are in each case two solid fuel charges having different combustion times. In Figure 1.17, c and d, we show engine layouts having a number of chambers positioned in a single casing.

#### The Rocket Chamber

The rocket chamber, which operates under circumstances of high pressure and temperature, is a basic part of the engine. For this reason structural and heat-resistant steels, and also alloys of light metals, titanium alloys (6 percent Al, 4 percent Va), and plastics, are used as materials for the manufacture of RDTT rocket chambers.

Thus, for example, the steel casing of the engine of the first stage of the "Minuteman" rocket (Figure 1.18) consists of a cylindrical shell, and two caps (upper, 2, and lower, 3). The spherical or ellipsoidal caps (end walls) are made of isotropic materials (steel, titanium, etc.). The upper cap is welded to the cylindrical portion, and the lower is threaded on. The inward surface of the upper cap is covered with a shaped rubber insulation 10 millimeters thick. The insulation of the lower cap consists of fiberglass 50 millimeters thick and a two-layer rubber coating which ensures compensation of the expansion of the fuel upon change in temperature. The interior surface of the casing of the engine is covered with a double layer of rubber insulation 4, 5 millimeters in thickness. A protective coating 5 is applied to the exterior surface of the casing; it protects the engine against the action of gases upon release from the shaft, and also against aerodynamic heating-up during flight through the atmosphere (7).

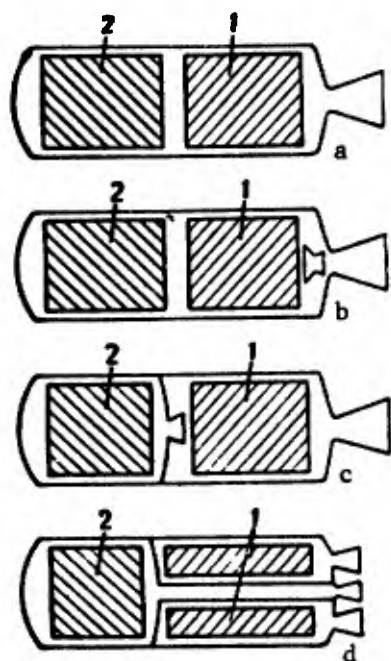


Figure 1.17. Layouts for theoretically possible designs of RDTT's having two thrust stages: a, b -- single-chamber; c, d -- two-chamber: 1 -- charge of start regime; 2 -- charge of route regime.

Heat-treated steel in the manufacture of rocket chambers is gradually being supplanted by plastic materials reinforced with glass fiber distinguished by very marked anisotropic properties. Standard brands of glass plastics are manufactured on the basis of epoxy resins (optimum resin content about 15-20 percent). When ordinary epoxy resin is used the strength of glass plastics declines to 25 percent at a temperature as low as 149° C. Work is continuing on the creation of resins which retain great strength up to a temperature of 260° C (3). Fibers can be made not only of glass and nylon, but also of steel and other materials (8). Fibers made of oxides of beryllium and boron show promise. In Table 1.3 we set forth comparative data on the mechanical properties of compound beryllium-steel systems (9).

In manufacture of the cylindrical casings for combustion chambers by the coil method a combined coil of thread (at various angles), making it possible to take up not only gas pressure but also the deflecting forces arisen from the operation of inertial forces, is used.

The casings of the RDTT's of both stages of the "Polaris A-3" rocket, and also the engine of the third stage of the "Minuteman" rocket, are manufactured by a similar method.

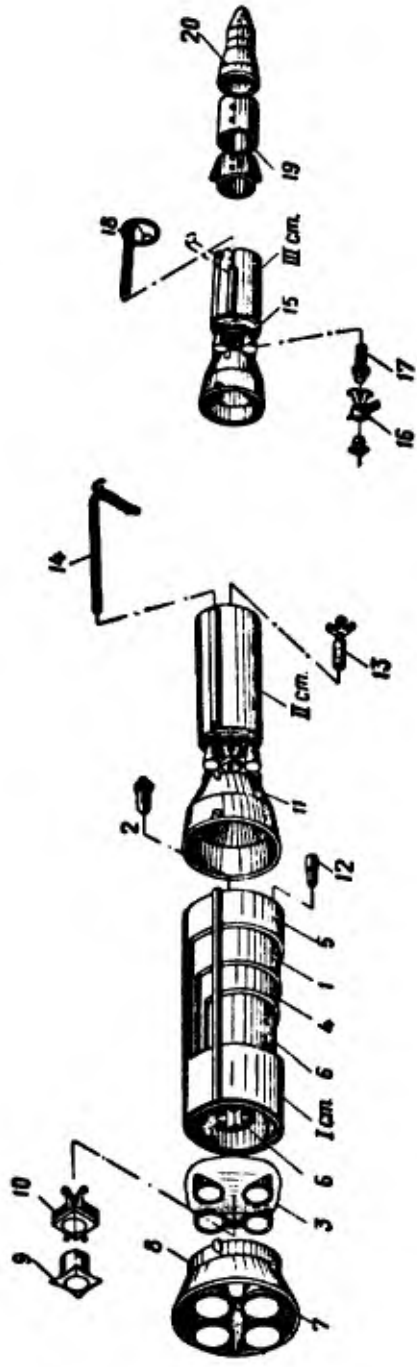


Figure 1.18. Composition layout of "Minuteman" solid-fuel rocket: 1 -- casing; 2 -- upper cap of casing; 3 -- lower cap of casing; 4 -- internal insulation; 5 -- external insulation; 6 -- Fuel; 7 -- cone block; 8 -- "skirt"; 9 -- heat reflector; 10 -- block for positioning cones; 11 -- intermediate section connecting first and second stages; 12 -- autodestruct device; 13 -- igniter for second stage engine; 14 -- autodestruct device in form of cumulative charge; 15 -- cone block of third stage; 16 -- block for positioning cones; 17 -- igniter; 18 -- autodestruct device; 19 -- compartment containing equipment for guidance and adjustment system; 20 -- separable warhead of rocket.

Table 1.3

<u>Material</u>	<u>Resistance Over Time</u>		<u>Module of Elasticity</u>	
	<u>Mean (kilo-gram per square centimeter)</u>	<u>Specific (centimeter)</u>	<u>Mean (kilo-gram per square centimeter)</u>	<u>Specific (centimeter)</u>
Boron				
Short-fiber	35,000	$1.35 \cdot 10^7$	$4.2 \cdot 10^6$	$1.62 \cdot 10^9$
Continuous fiber	28,100	$1.02 \cdot 10^7$	$4.2 \cdot 10^6$	$1.52 \cdot 10^9$
E glass fiber	35,000	$1.37 \cdot 10^7$	$0.73 \cdot 10^6$	$0.28 \cdot 10^9$
Beryllium	6,300	$0.33 \cdot 10^7$	$3.1 \cdot 10^7$	$1.68 \cdot 10^9$
Steel	1,970-42,100	$(0.025-0.53) \cdot 10^7$	$2.1 \cdot 10^6$	$0.28 \cdot 10^9$

Comparative weight data for steel and plastic (glass plastic) casings of the engines of three modifications of the "Polaris" rocket are set forth in Table 1.4 (9).

Table 1.4

<u>Modification of Rocket</u>	<u>Casing Material</u>	<u>Strength (grams per square centimeter)</u>	<u>Thickness of Wall (milli-meters)</u>	<u>Length of Cylindrical Part (meters)</u>	<u>Weight of Casing Without Heat Protection (kilograms)</u>
First stage					
A-1	Steel	7.8	5.6	2.6	862
A-2	Steel	7.8	4.8	3.4	773
A-3	Glass plastic (S-994 glass fibers)	2.0	8.1	3.5	433
Second stage					
A-1	Steel	7.8	2.3	0.9	238
A-2	Glass plastic (E glass fiber)	2.1	4.6	0.9	173
A-3	Glass plastic (S-994 glass fiber)	2.0	3.7	1.1	95

In Table 1.5 the characteristics of a number of structural materials are set forth, making it possible to perform a comparative analysis of the desirability of using them (8).

Table 1.5

<u>Name of Material</u>	<u>Time Resistance to Rupture (kilograms per square centimeter)</u>	<u>Specific Weight (grams per square centimeter)</u>	<u>Specific Strength (centimeters · 10<sup>6</sup>)</u>	<u>Specific Resistance to Annular Stress (centimeters · 10<sup>6</sup>)</u>	<u>Heat Conductivity Coefficient (kilocalories per meter · hours · °C)</u>
RS 140 steel	15,700	7.8	2.010	--	12-19
L71 aluminum alloy	4,400	2.8	1.580	--	100-170
Titanium	9,400	4.5	2.090	--	12-16
Phenol-asbestos plastic					
Type A	2,040	1.75	1.160	--	--
Type B	3,640	1.8	2.030	--	--
Type C	420	1.8	0.236	--	--
Glass plastic (S-994 glass fiber; longitudinal coiling)	8,400*	2.0	--	4.2	--
Glass plastic (E brand glass fiber; spiral coiling)	7,000*	2.1	--	3.3	--
Glass plastic (S-994 glass fiber; spiral coiling)	10,500*	2.0	--	5.3	--

\* Values for strength limits for glass plastics are given for annular stress.

## The Rocket Cone Block

The design of the supersonic cone of the RDTT and the reciprocal positioning of the cone and the rocket chamber affect the amount of thrust and the reliability of the engine's functioning. The configuration of the entry (precritical) and exit (postcritical) parts of the cone are selected to meet conditions of assuring minimal losses of energy upon the issuance of gases from the cone. Depending on the purpose of the RDTT, an optimum degree of widening of the cone is selected. The exit portion of the cone can have the shape of a cone of 16-40° aperture, or in the form of a curve of a profile determined so as to assure a straight and even flow upon the section of the cone (profiled cone).

The critical part of the cone is made of graphite or heat-resistant metal, and the expansion part of thermoreactive resin with a filler in the form of metal powders or graphite, asbestos, or ceramic fibers (10). A plastic cone may have self-regulating sublimation cooling (11). Experiments with cones having sublimation cooling have shown satisfying results: after 56 seconds of engine operation the thickness of the covering was reduced only by 0.1-0.2 millimeter (12).

To make cone inserts pyrographite, secured by pyrolysis of hydrocarbons in a vacuum furnace at high temperature, is used. Pyrographite is a strong, impenetrable material, resistant to erosion. It stands up well to oxidation up to a temperature of 1,000° C, has anisotropic properties, and starts to disintegrate at a temperature of 3,500° C.

For engines in which the charge is firmly fastened to the walls of the rocket chamber, a plastic cone block can be fastened to the fuel charge as well (Figure 1.19). Such fastening considerably reduces the weight of the cone block and the thermic load on the structural elements adjacent to the cone.

In Figure 1.20 we show the design of a rotatory cone for a RDTT of 4-meter caliber. An articulated ring, 3, of 2-meter diameter is fastened on two pivots, 2, to the stationary precritical part of the cone, 1. The movable part of the cone, 4, which can be inclined to an angle of 5° in two planes, is fastened to the articulated ring at an angle of 90° to the first two pivots (13). In the gap between the stationary and the movable parts a filler ring made of a special kind of rubber is inserted. In order to prevent burning the ring is covered with a silicon lubricant. The steel casings of the units of the movable cone are covered with graphite and carbon fabrics, and also with glass plastic saturated with phenolic resin.

Translator's note: The cone "rotates" to a limited extent relative to its longitudinal axis; "swinging" would perhaps be a better term than "rotatory."

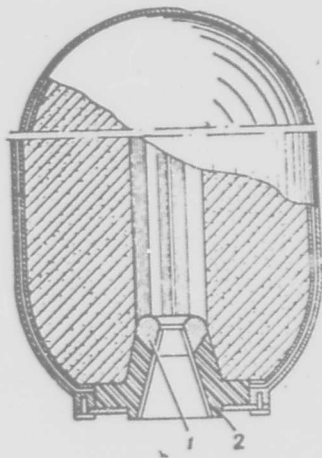


Figure 1.19. Layout of RDTT with cone attached directly to solid fuel charge: 1 -- critical part of cone; 2 -- expanding part of cone.

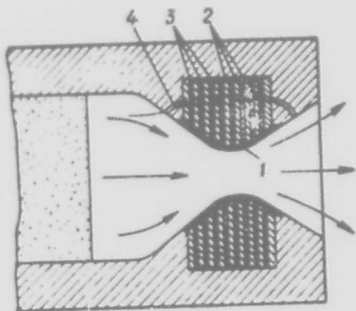


Figure 1.21. Design of cone having special form of heat insulation: 1 -- porous insert; 2 -- plates of metallic hydride; 3 -- steel plates; 4 -- channel for passage of gases.

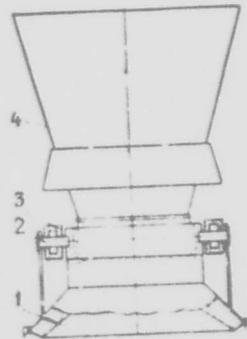
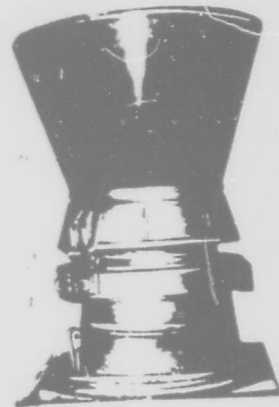


Figure 1.20. Swinging cone for RDTT of 4-meter caliber: 1 -- stationary part of cone; 2 -- pivot; 3 -- power ring of rocker assembly; 4 -- movable part of cone.

As heat flows in the wall of the cone reach their maximum value in the critical section of the cone (about  $10^7$  kilocalories per square meter

times hours), great importance is laid upon its heat insulation. Thus, for example, in the critical section of the cone of the first stage of the "Minuteman" rocket a tungsten insert having six graphite rings is inserted (7). In the design of the cone illustrated in Figure 1.21 cooling of the critical section of the cone takes place by virtue of the decomposition of the metallic hydrides  $\text{LiH}$ ;  $\text{LiBH}_4$ ;  $\text{NaBH}_4$ ; and  $\text{KBH}_4$ . Above the porous insert, 1, there is a set of plates of metallic hydrides, 2, alternating with steel plates, 3. As hot gases flow through the cone the metallic hydride plates heat up. (For intensification of heating the hot gases may be supplied to the plates through a piercing, 4.) Under the action of the high temperature, the metallic hydride decomposes with release of hydrogen which, passing through the porous insert, forms a gas film on the surface of the cone, which reduces the heat flow from the hot gases to the cone (11).

Curvilinear cones have found application in designs of RDTT's for guided rockets. Various forms of curvilinear cones with forced declination of flow are shown in Figure 1.22. Three possible types apply to these: annular cones, cones with a central body, and saucer-like cones (or the cone with a "skirt"). All the types set forth are characterized by high thrust characteristics, have a relatively small length (weight), and create an even and straight-line flow upon issuance from the cone.

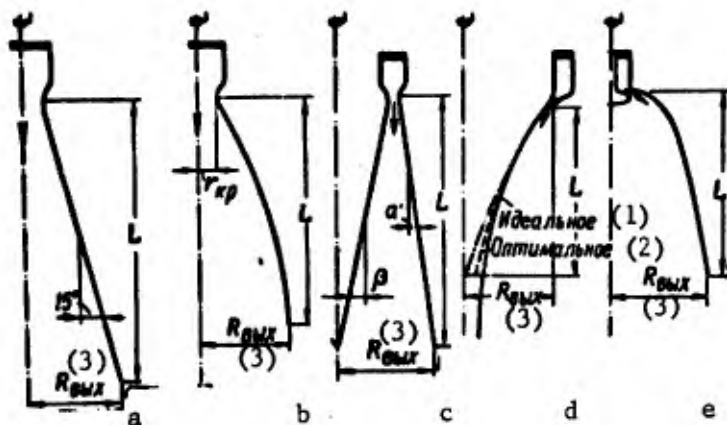


Figure 1.22. Various forms of curvilinear cones with forced declination of stream: a -- cone of conical form; b -- cone with optimum contour; c -- annular cone; d -- cone with central body; e -- saucer-like cone.  
1 -- ideal; 2 -- optimum; 3 -- radius at exit.

At present cones having a central body are being widely used (Figure 1.23). The inner boundary of the stream along such a cone is a free surface. While the altitude of flight is changing the free surface of the gas stream bathing the central body is constantly undergoing adaptation to surrounding conditions, and the magnitude of the area of section of the stream at the end of the central body is automatically set in

harmony with the degree of expansion. Inasmuch as a cone having a central body operates as a cone having a ratio of sections which can be regulated, the characteristics of the cone at regimes lower than the calculated one are higher than the characteristics of usual Laval cones (Figure 1.24). The physical significance of the advantage referred to lies in the nature of the self-regulation of the flow. The work of a cone having a central body is identical with the process of bathing a convex obtuse angle with a supersonic flow (Prandtl-Meyer stream).

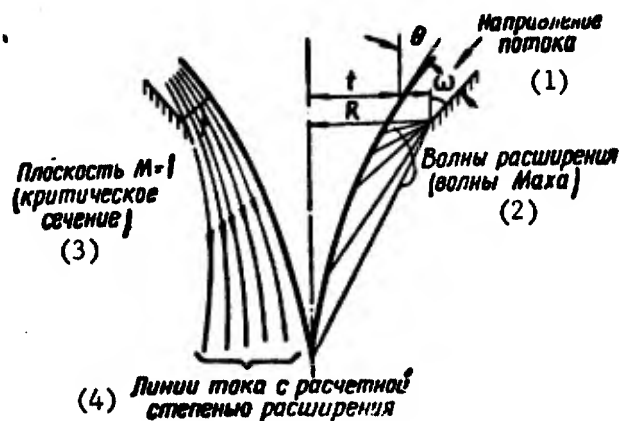


Figure 1.23. On the question of the physical picture of the process occurring in cone having central body.  
 1 -- direction of flow; 2 -- expansion waves (Mach waves);  
 3 -- plane  $M = 1$  (critical section); 4 -- lines of flow with calculated degree of expansion.

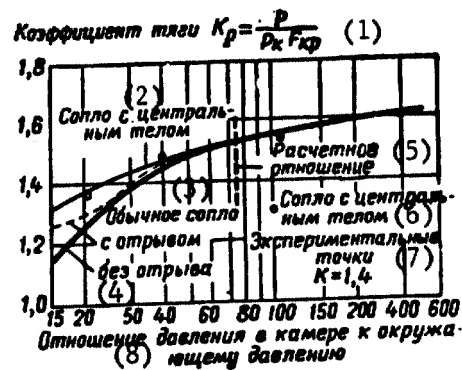


Figure 1.24. Thrust characteristics of cones of various types.  
 1 -- coefficient of thrust  $K_p = P/P_k F_{kp}$ ; 2 -- cone having central body; 3 -- usual cone, with break; 4 -- without break; 5 -- calculated ratio; 6 -- cone having central body; 7 -- experimental points  $K = 1.4$ ; 8 -- ratio of pressure in chamber to surrounding pressure.

Increase of pressure on the parts of the central body increases thrust of the cone from the central body as compared with thrust of a Lavalle cone. At degrees of expansion which exceed the calculated degree, the thrust characteristics of the cones compared coincide (Figure 1.24). This is to be explained by the fact that any expansion of a stream of gases in the atmosphere when there is a ratio of pressures greater than the calculated one does not affect the flow moving along the wall of a cone of any type (15).

The use of a central body opens up new possibilities in controlling the vector of thrust according to direction.

### 1.3. Characteristic Peculiarities of Design Layouts of Unguided Reactive Missiles

It is indicated in the foreign press that although guided rockets are at present fundamental in military rocket technology, unguided reactive missiles (NRS) still occupy an important position in the system of army armaments (17).

NRS's are simple in layout, and their release apparatus are dependable, light, and small in dimensions.

In Figures 1.25-1.27 we show various patterns of Soviet NRS's dating from the period of the Second World War (2, 18).

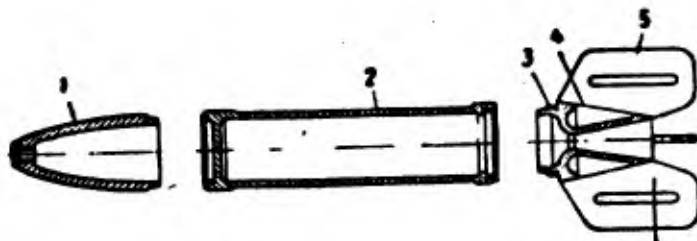


Figure 1.25. M-8 rocket missile (USSR), 82-millimeter caliber, start weight 8 kilograms, maximum velocity 315 meters per second: 1 -- warhead; 2 -- rocket chamber (with solid front wall); 3 -- cone; 4 -- deflector; 5 -- stabilizer.

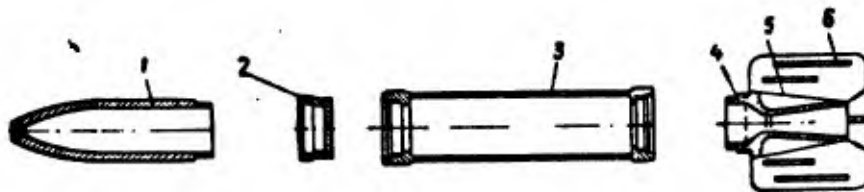


Figure 1.26. M-13 rocket missile (USSR), caliber 132 millimeters, start weight 42.5 kilograms, maximum velocity 355 meters per second: 1 -- warhead; 2 -- intermediate unit; 3 -- rocket chamber; 4 -- cone; 5 -- deflector; 6 -- stabilizer.

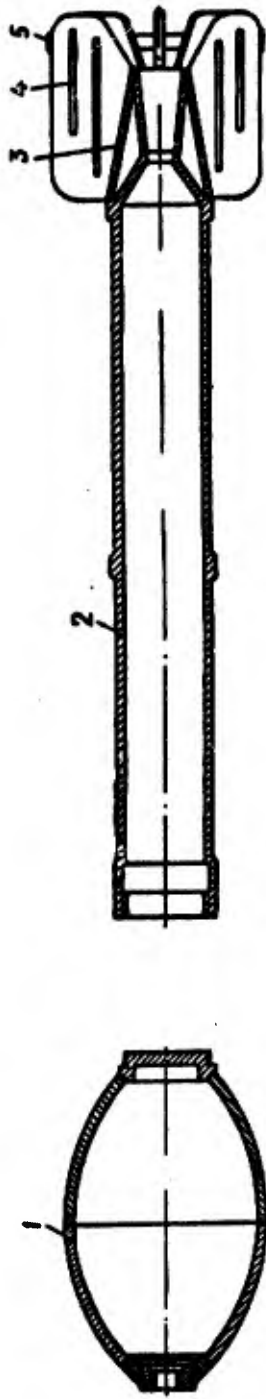


Figure 1.27. M-31 rocket missile (USSR), 300-millimeter caliber, start weight 94.6 kilograms, maximum velocity 255 meters per second: 1 -- warhead (assembly); 2 -- rocket chamber (made in single piece with cone); 3 -- deflector; 4 -- stabilizer; 5 -- directional ring of stabilizer.

Unguided rocket missiles are distinguished by the variety of their composition and design layouts. In selecting an optimum composition layout the purpose of the missile, the weight and composition of the useful load, the character and effectiveness of operation of the missile at the target, and the type of explosive device are taken into account.

There are a number of layouts for mutual positioning of the warhead and the rocket parts in the over-all composition of a rocket missile having a solid fuel engine (Figure 1.28). One should regard as the basic design the so-called normal RS design -- warhead in front, rocket part behind (Figure 1.29). Some RS's for field artillery having shrapnel effect are made on the reverse system -- rocket part forward, warhead behind (Figure 1.30), which heightens the effectiveness of operation at the target on the part of the missile in question (18).

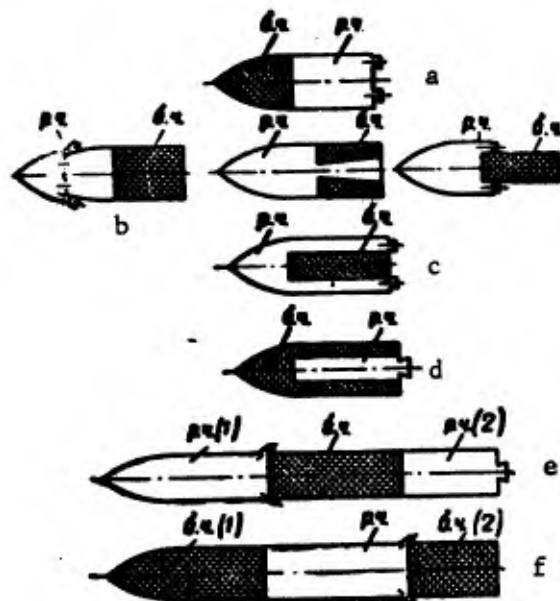


Figure 1.28. Possible layouts for structural composition of rocket missiles having solid-fuel engines: a -- warhead forward, rocket chamber behind; b -- rocket chamber forward, warhead behind; c -- warhead inside rocket chamber; d -- rocket part within warhead; e -- warhead between two rocket chambers; f -- rocket chamber between two warheads.

The design layout of the RDIT for an unguided rocket depends on the purpose and intended range of flight of the missile. NRS's of land rocket artillery are calculated for a relatively short range of fire and for this reason single-chamber RDIT's are most frequently used in them.

In Figure 1.31 we show the arrangement of antitank missiles (2). In the rocket chamber there is a thin-walled charge of solid fuel. The

time of combustion of the rocket is fractions of a second, and for this reason the charge burns primarily during the period of movement of the NRS in the tube of the guiding release apparatus. The diameter of the casing of the engine is less than the diameter of the warhead of the NRS.

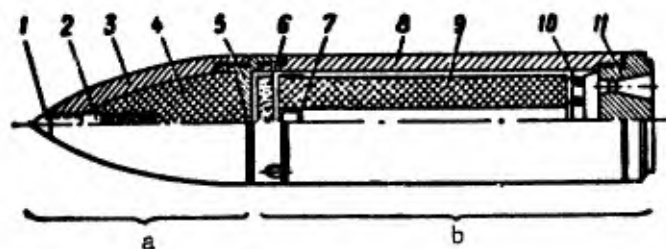


Figure 1.29. Sample design of present-day rocket missile for field artillery: a -- warhead; b -- rocket part: 1 -- detonator; 2 -- supplementary detonator; 3 -- casing of warhead; 4 -- explosive charge; 5 -- partition; 6 -- igniter with electrical ignition system; 7 -- forward frame for fastening together igniter and charge; 8 -- casing of rocket chamber; 9 -- solid fuel charge; 10 -- diaphragm; 11 -- cone block.

Aviation NRS's have an arrangement analogous to that of the missiles of surface rocket artillery (Figure 1.32) and are stabilized during flight by tail groups. In Figure 1.32 we show the structural assembly of a tail stabilizer in the form of a group which opens out.

In order to improve the clustering of fall, an apparatus is provided in the structural layout of RDTT's for unguided RS's which ensures rotation of the rocket around its longitudinal axis. In the "Honest John" unguided single-stage ballistic rocket (Figure 1.33) small RDTT's are placed behind the warhead at a certain angle to the axis, intended to rotate the rocket slowly around the axis of symmetry.

Beside usual NRS's stabilized in flight by means of tail groups, there are turbojet missiles (TRS's), in which stabilization in flight is effected by virtue of rotation of the missile around its longitudinal axis (Figure 1.29). Rotation of the TRS is created as a result of the issuance of gases through diagonally positioned cones set in the base of the rocket chamber (19).

Type layouts of solid-fuel rocket engines for unguided missiles are illustrated in Figures 1.34 and 1.35 (10).

A number of RDTT layouts are used at present for unguided RS's. The simplest in arrangement is the layout of an engine having a free-inserted charge (Figure 1.34).

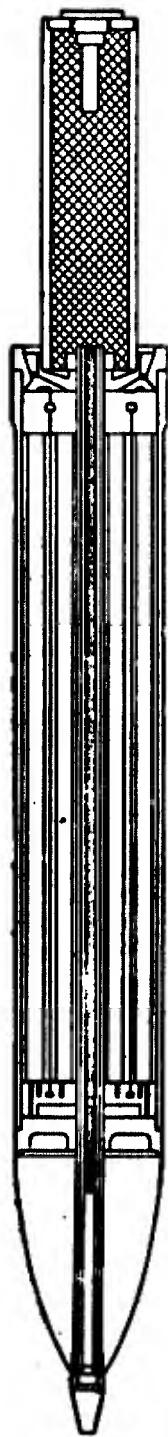


Figure 1.30. Design of turbojet unguided missile.

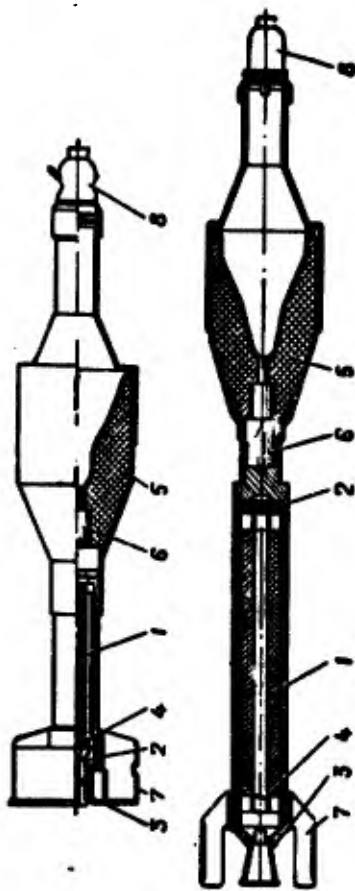


Figure 1.31. Layouts of antitank rockets: 1 -- rocket chamber with charge of solid fuel; 2 -- igniter; 3 -- cone; 4 -- diaphragm; 5 -- warhead with cumulative recess; 6 -- base detonator; 7 -- stabilizer; 8 -- point detonator.

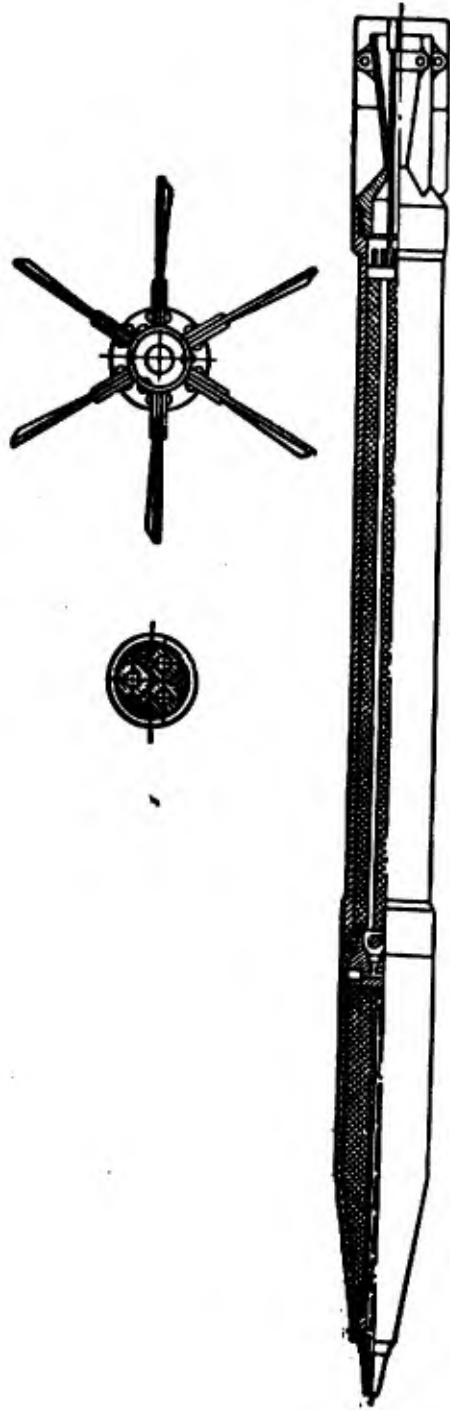


Figure 1.32. Rocket unguided missile of "air-to-air" class with opening tail group.

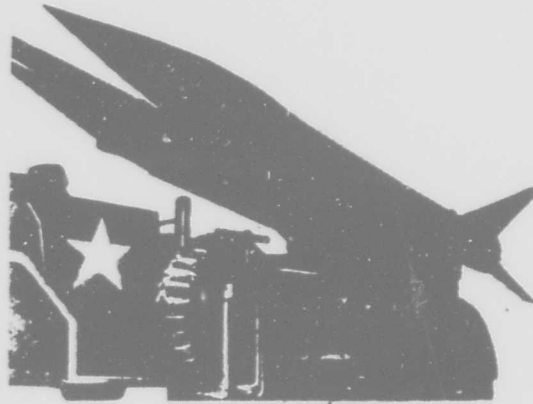


Figure 1.33. "Honest John" unguided rocket missile of "surface-to-surface" class.

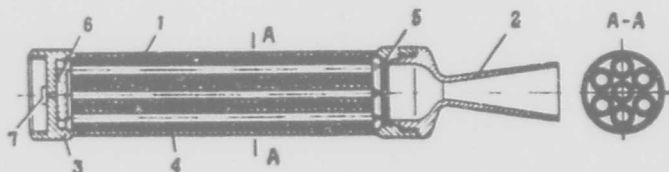


Figure 1.34. Layout of installation of RDIT with free-inserted charge of solid fuel: 1 -- casing of rocket chamber; 2 -- cone; 3 -- forward cap; 4 -- charge of solid fuel; 5 -- diaphragm; 6 -- igniter; 7 -- cartridge igniter.

The main elements of the engine are the combustion chamber, 1, in which the solid-fuel charge 4 is located; the cone block 2; the forward cap 3; the ignition apparatus 6; and the diaphragm 5, preventing the ejection of the burners of the solid fuel charge through the cone.

Along with the main elements of the design layout which have been referred to, there may also be preventer valves for emergency release of pressure, cassettes for burners, charge holders, catches on the exterior surface of the charge where the charge lies against the walls of the combustion chamber, cone stoppers to seal the engine and other parts. In these engines ballistite solid fuels are used -- nitroglycerine powders. Charges of this type of fuel in the form of cylindrical single-channel and multiple-channel burners are inserted freely in the combustion chamber. With this sort of loading of the chamber the products of combustion of the fuel touch the casing along its whole inner surface, which leads to intense heating up of the casing and reduction of the strength characteristics of the material. In connection with this supplementary difficulties associated with protecting the chamber against heating arise.

Solid-fuel rocket engines made in this way had relatively high weight, and the design quality coefficient,  $\alpha$ , came to a considerable amount, 0.8-1.5 (20). An engine having a free-inserted charge is simple in loading and checking, convenient in use.

In Figure 1.35 we show diagrammatically a variant of the engine, in which the charge, jacketed on the outside, is free-inserted into the combustion chamber. The absence of intensive convective heat exchange between gases and the combustion chamber protect the walls of the casing of the engine from substantial heating up during the process of combustion of the charge. The combustion chamber consists of a cylindrical tube, a rearward cap, and the entrance part of the cone. The structural units are put together so as to overlap (telescopic assembly) and are connected with bolts and anchor nuts, and also by welding and threading. The charge 4, jacketed on its faces and surface, is centered in the chamber by means of small supports, 5, of noninflammable material. The annular gap, 6, between the charge and the inner surface of the heat insulation of the combustion chamber amounts to a few millimeters (16). The forward face of the charge is held in place by the holder, 7, with a packing, 8, of layered plastic. During combustion of the charge gases pass through openings, 9, in the packing, 8; they create a counterpressure which protects the charge against breaking up. The rear face of the charge rests in a cone of glass plastic, 10, which simultaneously serves as a heat insulator. The rubber obturator, 11, in an annular groove in the support cone wards off transverse flow of gas in the annular gap, creating an annular dead zone around the charge. The stationary gas zone protects the wall of the chamber against intensive convective heating up (16). The basic design deficiency of this layout is the substantial increase in weight of the design on account of increased internal diameter of the combustion chamber, brought about by the presence of the gap between the charge and the casing. The size of the gap depends upon the thickness of the jacketing of the charge and of the heat-insulating covering of the chamber; production tolerances in the manufacture of the charge and chamber, and thermic expansion of the charge and chamber.

In RDIT designs carried out according to the free-inserted charge system there is a diaphragm which keeps the charge in the rocket chamber until it is completely burned up.

Diaphragms are made of steel with a carbon content of about 0.3 percent, of heat-resistant steel having a small chromium content, and also of various brands of plastic.

Depending on geometrical shape, diaphragms are multi-annular (Figure 1.36), mono-annular with ribs, grating, disc, lobed, sectoral, and pierced (18). The form and dimensions of diaphragms of present-day NRS's are determined by the design of the solid fuel charge and the cone block, and also by the time of functioning and the purpose of the RDIT. The flow of gas through the diaphragm assembly is characterized by maximum turbulization of flow and is accompanied by throttling of gas, formation of eddies, and exaggerated drop in pressure.

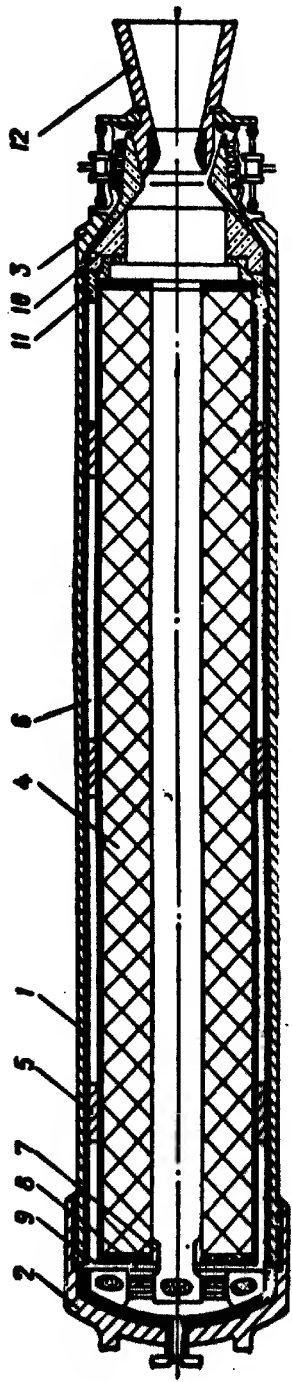


Figure 1.35. Layout of RDTT with free-inserted jacketed charge: 1 -- rocket chamber; 2 -- forward cap; 3 -- cone cap; 4 -- charge of solid fuel; 5 -- inserts to center charge in chamber; 6 -- annular gap between charge and interior surface of heat insulation; 7 -- holder for front face of charge; 8 -- packing; 9 -- openings in packing; 10 -- support cone of plastic; 11 -- rubber obturator; 12 -- cone.

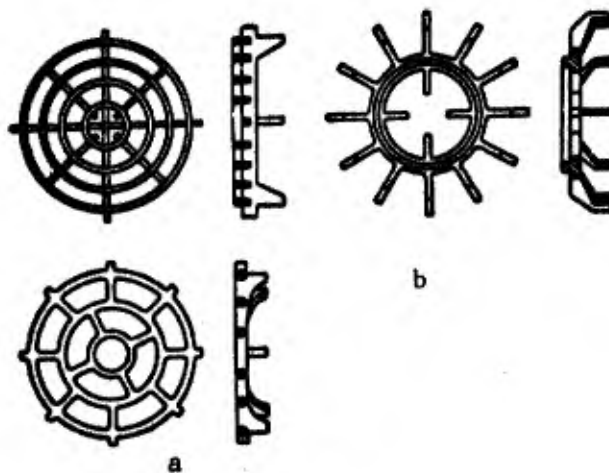


Figure 1.36. Diaphragm Designs for Solid Fuel Rocket Engines  
 a) Multiannular diaphragm for multiburner charges; b) Monoannular diaphragm without peripheral ring for single burner charges.

#### BIBLIOGRAPHY

1. Questions in Rocket Technology, No 6, 1964; Nos 1, 2, 1965, "Mir" Publishing House

Aviation and Astronautics, No 4, 1965, "Krasnaya Zvezda" Publishing House.

Goncharenko, M. N., Rockets and Antimissile Problems, DOSAAF Publishing House, Moscow, 1962.

Tatarchenko, A. E., Guided Missiles and Rockets, DOSAAF Publishing House, Moscow, 1962.

Paushkin, Ya. M., The Chemistry of Reactive Fuels, Publishing House of the Academy of Sciences of the USSR, Moscow, 1962.

Aviation Week, Vol 82, No 12, 15, 1965.

Missiles and Rockets, Vol 16, No 15, 1965.

Electronic News, Vol 10, No 482, 1965.

2. Feodos'yev, V. I., Sinyarev, G. B., Introduction Into Rocket Technology, Oborongiz Publishing House, 1960.

3. Shapiro, Ya. M., Mazing, G. Yu., Prudnikov, N. Ye., Theory of the Solid-Fuel Rocket Engine, Voenizdat Publishing House of the Defense Ministry of the USSR, Moscow, 1966.

4. Missiles and Rockets, 21/XII, 1964, page 16; Aviation Week, 1964, 22/VI, Vol 80, No 2p; Missile Space Daily, 1964, 16/VII, Vol 8, No 11.
5. Interavia, 1965, III, Vol 20, No 3, page 388.  
Missiles Space Daily, 1965, 13/IV, Vol 12, No 32, page 251.  
Interavia Air Letter, 1965, 8/III, No 5701, page 5.  
Astronautics and Aeronautics, 1964, X, Vol 2, No 10, page 94.
6. Boyd, A. B., Byorke /Bjorke?/, V. M., Medford, J. E., "Problems in Designing Large-Dimensional Rocket Engines," Investigation of Solid-Fuel Rocket Engines, edited by M. Summerfield, Foreign Literature Publishing House, Moscow, 1963.
7. Questions in Rocket Technology, No 6, 1963, "Mir" Publishing House.
8. Astronautics and Rocket Dynamics, VINITI of the Academy of Sciences of the USSR Publishing House and GNTK, No 18, 1961; Questions of Rocket Technology, No 6, 1964, "Mir" Publishing House, Moscow; Astronautics and Rocket Dynamics, (express information), No 7, 1964.
9. Morris, E. E., "Glass Cases for the Biggest Solids," Astronautics and Aeronautics, 1964, 2, No 7, 23-38.
10. US Patent, Class 60-35, No 3103784, published 15 November 1960; Class 60-35.55, No 3140584.
11. US Patent, Class 60-35.6, No 3115746, published 18 July 1960.
12. Missile Space Daily, 1965, II, No 27, 217 (English-language).
13. Aviation Week, 1964, 14.XII, Vol 81, No 24, 25.  
Missiles and Rockets, 1964, 21/XII, Vol 5, No 25.
14. Orlov, B. V., Mazing, G. Yu., Thermodynamic and Ballistic Bases for Design of Solid Fuel Rocket Engines, "Mashinostroyeniye" Publishing House, 1964.
15. Pao, Most Recent Achievements in Contouring Rocket Cones, National Engineering Science Company, Pasadena, California.
16. Barrer, M., Jaumotte, A., Bebec, B. F., Vandenkerrkkoove, Zh., Rocket Engines, Oborongiz Publishing House, 1962.

17. Lyapunov, B. V., The Rocket, Voenizdat Publishing House of the Defense Ministry of the USSR, 1960.

18. Kurov, V. D., Dolzhanskiy, Yu. M., Fundamentals of Designing Powder Rockets, Oborongiz Publishing House, 1961.

19. Serebryakov, M. Ye., Internal Ballistics of Barreled Systems and Powder Rockets, Oborongiz Publishing House, 1962.

20. Rozhkov, V. V., Solid Fuel Rocket Engines, Moscow, Voenizdat Publishing House, 1963.

## CHAPTER II. BASIC RELATIONS OF THE INTERNAL BALLISTICS OF GUIDED ROCKETS

### 2.1. The Rocket as a Variable Mass Body

In classical mechanics based on the laws of Newton the mass of a moving body is regarded as a constant quantity. But in practice one must examine problems regarding the movement of a body the mass of which is constantly changing with the passage of time as the result of the separation from it or association with it of material particles. Such a body is called a body of variable mass. Let us examine questions in the mechanics of a variable-mass body as they relate to the dynamics of a rocket.

Let us encompass a rocket with a control surface  $\Sigma$ , passing over the external surface of the rocket casing and over the outlet section of the cone, AA' (Figure 2.1).

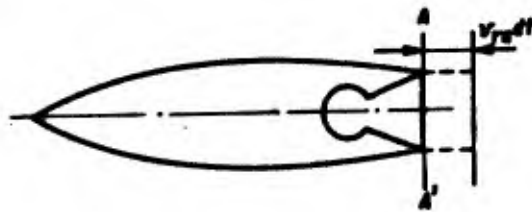


Figure 2.1. The rocket as a variable-mass body.

We shall consider all material points which are within the control surface referred to at a moment in time  $t$  as pertaining to a "variable-mass body" -- the rocket. In order to be able to consider the rocket as a constant-mass body at a time  $dt$  and apply to it the usual relations of Newtonian mechanics we further take under consideration a deformed control surface  $\Sigma_1$ . The latter is distinguished from the surface  $\Sigma$  in that part of it running through the outlet section AA' moves over time  $dt$  along the flow by an amount  $v_{ra}dt$ , where  $v_{ra}$  is the velocity of the

gas relative to the casing of the rocket and the index  $\underline{a}$  corresponds to the outlet section of the cone. Thus mass remains constant within the control surface  $\Sigma_1$  over time  $\underline{dt}$ .

From here on we shall examine three fields:

Field I comprises the solid bodies within the control surface, to the exclusion of the gases which are in the rocket chamber. Thus we shall assign to field I the casing of the rocket, and solid or liquid fuel. We shall assign to the casing of the rocket and designate by  $M_k$  the mass of the bodies which at an instant of time  $\underline{t}$  are in field I.

Field II comprises the gases which are in the rocket chamber ahead of the outlet section AA'. We designate the mass of these gases by  $\underline{m}$ .

Field III back of the outlet section of the cone contains a mass of gases which flow out of the chamber over time  $\underline{dt}$ . The mass of these gases is equal to  $\mu dt = -dm$ , where  $\mu$  is the discharge of the mass of the gases flowing out over one second.

Let us write an equation for the amount of movement of the rocket. At a moment of time  $\underline{t}$  within the control surface in fields I and II we have the mass of the rocket  $M_k + m$ . This same mass, at a moment of time  $t + dt$ , lies within the control surface  $\Sigma_1$ , in fields I, II, and III. The amount of movement of the system in a moment of time  $\underline{t}$  is equal to

$$\bar{Q} = M_k \bar{v}_{kc} + \bar{q},$$

where  $\bar{v}_{kc}$  is the velocity of the center of mass of the body,  
 $\bar{q}$  is the amount of movement of the gases.

For a moment of time  $t + dt$  we get

$$\bar{Q} + d\bar{Q} = [M_k - (\mu + d\mu) dt] (\bar{v}_{kc} + d\bar{v}_{kc}) + \bar{q} + d\bar{q} + \mu dt \cdot \bar{u}, \quad (2.1)$$

where  $\bar{u}$  is the absolute velocity of the outward flow of gases in the outlet section of the cone.

By means of the quantity  $d\mu$  we take into account the circumstance that the feed of fuel into the chamber per second may differ from the discharge of the gases flowing out.

From equation (2.1), eliminating the quantities  $(\mu + d\mu) dt \cdot d\bar{v}_{kc}$ ,  $d\mu \cdot dt \cdot \bar{v}_{kc}$  in view of their smallness, we get

$$d\bar{Q} = M_k d\bar{v}_{kc} + d\bar{q} + \mu (\bar{u} - \bar{v}_{kc}) dt.$$

We divide by  $dt$  and, taking into account the fact that  $\bar{u} - \bar{v}_{kc} = \bar{v}_{ra}$  where  $\bar{v}_{ra}$  is the velocity of outward flow of the gases relative to the system of coordinates associated with the casing of the rocket, we get\*

$$\frac{d\bar{Q}}{dt} = M_k \frac{d\bar{v}_{kc}}{dt} + \frac{d\bar{q}}{dt} + \mu \bar{v}_{ra} = \bar{\Phi}, \quad (2.2)$$

where  $\bar{\Phi}$  is the principal vector of the external forces operating upon the rocket. The quantity  $\frac{d\bar{q}}{dt}$  characterizes the change in the amount of movement of the gases in the chamber.

Let us examine the elementary mass of the gases in the chamber between sections  $x$  and  $x + dx$  (Figure 2.2). The elementary amount of movement is

$$\delta\bar{q} = \delta m \cdot \bar{v}_{ms} \quad (2.3)$$

where  $\bar{v}_{ms}$  is the velocity of the gases relative to the stationary metering system.

Differentiating expression (2.3) in time and shifting to the mobile system of coordinates associated with the casing, we have

$$\frac{d\delta\bar{q}}{dt} = \delta m \cdot \frac{d\bar{v}_{ms}}{dt} = dm (\bar{w}_e + \bar{w}_r + \bar{w}_{rop}). \quad (2.4)$$

Integrating expression (2.4) along the chamber to the outlet section, we get

$$\frac{d\bar{q}}{dt} = \int (\bar{w}_e + \bar{w}_r + \bar{w}_{rop}) dm.$$

Since acceleration  $w_e = w_{chamber}$  does not change along the cone, the first term assumes the form

$$\int \bar{w}_e dm = \bar{w}_{kc} m = m \frac{d\bar{v}_{kc}}{dt}.$$

---

\* One ought to take into account the fact that the velocity of flow relative to the casing differs from the velocity of flow relative to the center of mass of the rocket by the amount of the velocity of movement of the center of mass of the rocket relative to its casing. For a V-2 rocket this last velocity comes to 0.001 percent of the quantity  $v_{ra}$ .

The second term --

$$\int \bar{w} dm = \int \frac{d\bar{v}_r}{dt} dm = \frac{d}{dt} \bar{q}_r$$

where  $\bar{q}_r$  is the quantity of movement of gases in the chamber relative to the casing of the rocket.

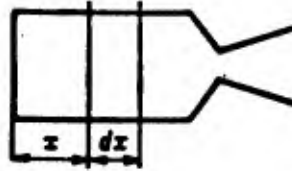


Figure 2.2. Quantity of movement of gases in chamber.

The third term --

$$\int \bar{w}_{\text{Cor}} dm = -\bar{F}_{\text{Cor}}$$

where  $F_{\text{Cor}}$  is the Coriolis inertial force which appears upon oscillation of the rocket.

Thus

$$\frac{d\bar{q}}{dt} = m \frac{d\bar{v}_{\text{xc}}}{dt} + \frac{d\bar{q}_r}{dt} - \bar{F}_{\text{Cor}}$$

Inserting the expression thus secured in expression (2.2), we have

$$(M_k + m) \frac{d\bar{v}_{\text{xc}}}{dt} = -\frac{d\bar{q}_r}{dt} + \bar{F}_{\text{Cor}} + \bar{\Phi} - \mu \bar{v}_{\text{ra}}$$

or, designating  $\underline{M}$  as equal to  $M_k + m$ ,

$$M \frac{d\bar{v}_{\text{xc}}}{dt} = \bar{\Phi} - \mu \bar{v}_{\text{ra}} - \frac{d\bar{q}_r}{dt} + \bar{F}_{\text{Cor}} \quad (2.5)$$

The main vector of the external forces is determined from the expression

$$\bar{\Phi} = M\bar{g} + \bar{F}_{\text{Am}} + \bar{F}_{\text{TP}} \quad (2.6)$$

where  $M\bar{g}$  is the weight of the rocket;

$\bar{F}_{\text{fric}}$  is the main vector of tangential forces of friction resistance;

$\bar{F}_{\text{press}}$  is the main vector of external pressure forces.

$$\bar{F}_{\text{press}} = \iint_S (p - p_H) \bar{n} ds, \quad (2.7)$$

where  $p$  is the pressure upon the surface of the rocket;

$p_H$  is the atmospheric pressure at the height of flight;

$\bar{n}$  is the unit vector of the normal to the elementary surface  $ds$ ;  
 $S$  is the entire external surface.

The pressure of gases in the outlet cross-section of the cone of the working engine does not depend upon the character of the flowing around the rocket on the part of the external stream and is determined entirely by the parameters of the rocket engine. For this reason it is well, in expression (2.7), to isolate from the field of integration  $S$  the outlet cross-section of the cone  $s_a$

$$\bar{F}_{\text{press}} = \iint_S (p - p_H) \bar{n} ds + \iint_{s_a} (p - p_H) \bar{n} ds.$$

Thus

$$\bar{F}_{\text{press}} + \bar{F}_{\text{sp}} = \bar{R} + (p_a - p_H) s_a \bar{n}_a \quad (2.8)$$

where  $p_a$  is the pressure of gases in the outlet cross-section;

$\bar{n}_a$  is the unit vector of the normal of this section;

$\bar{R}$  is the main vector of aerodynamic forces.

Expression (2.6) assumes the form

$$\bar{\Phi} = M\bar{g} + \bar{R} + (p_a - p_H) s_a \bar{n}_a \quad (2.9)$$

The equation for movement of the rocket is written as follows:

$$M \frac{d\bar{v}_{\text{cs}}}{dt} = M\bar{g} - \mu \bar{v}_{\text{rs}} + (p_a - p_H) s_a \bar{n}_a + \bar{R} - \frac{d\bar{q}_r}{dt} + \bar{F}_{\text{sof}}$$

The expression

$$-\mu \bar{v}_{\text{rs}} + (p_a - p_H) s_a \bar{n}_a = \bar{P} \quad (2.10)$$

is called the reactive force. The term  $\frac{d\bar{q}_r}{dt}$  may be regarded as a correction to the reactive force depending upon alteration in the parameters

of the flow of gases in the chamber with the passage of time. With a stabilized process in the chamber of the engine  $q_r$  is a constant, and  $\frac{dq_r}{dt}$  equals zero. Let us evaluate  $\frac{dq_r}{dt}$  in the general case.

Let us examine the elementary volume of gases in the chamber  $sdx$ , where  $s$  is the area of the cross-section of the chamber. The quantity of movement of gases in this elementary volume is

$$dq_r = sdx \cdot \rho v, = \mu dx,$$

where  $\rho$  is the mass density of the gas.

Integrating along the chamber to the outlet cross-section of the cone we get

$$q_r = \mu l,$$

whence

$$\dot{q}_r = \dot{\mu} l.$$

The discharge of gases per second is proportional to the pressure of gases in the chamber. Let us examine such a process which has not stabilized itself, when the pressure in the chamber and consequently the discharge per second double in one second. When this happens, taking  $\underline{dt}$  as equal to 1, we get

$$\dot{q} \sim q = \mu l.$$

Let us compare these quantities with the basic term in the expression for reactive force,  $\mu v_{ra}$ . We secure

$$\frac{\mu l}{\mu v_{ra}} = \frac{l}{v_{ra}}.$$

For a V-2 rocket

$$\frac{l}{v_{ra}} \sim \frac{2,5}{2000} = 1,25 \cdot 10^{-3} \approx 0,1\%.$$

Let us evaluate the magnitude of the Coriolis inertial force. Let the rocket oscillate around an axis perpendicular to the axis of its symmetry, with an angular velocity  $\varphi$ . For an elementary mass of gas  $dm = s\rho dx$  the Coriolis force is equal to

$$dF_{\text{Cor}} = 2dm \cdot v_{ra} \dot{\varphi} = 2s\rho dx \cdot v_{ra} \dot{\varphi} = 2\mu \dot{\varphi} dx.$$

Integrating along the chamber we get

$$F_{\text{top}} = 2\mu\dot{\varphi}l.$$

Let the oscillation of the rocket take place according to the formula

$$\varphi = A \cos \omega t.$$

Then

$$\dot{\varphi} = -A\omega \sin \omega t, \\ |\dot{\varphi}_{\text{max}}| \approx A\omega.$$

For a V-2 rocket the amplitude of oscillation  $A$  is about  $2^\circ$ , and the frequency  $\omega \approx 1$  Hz. Under these circumstances  $\dot{\varphi}_{\text{max}} \approx 0,035$ . The length of the chamber,  $l$ , is about 2 meters. The discharge of mass per second,  $\mu$ , is about 15 kilogram-seconds per meter. Under these circumstances we have

$$(F_{\text{top}})_{\text{max}} = 2\mu\dot{\varphi}_{\text{max}} \cdot l = 2 \cdot 15 \cdot 0,035 \cdot 2 \approx 2 \text{ kg}$$

with a rocket weight of approximately 13,000 kilograms and a reactive force of about 25,000 kilograms.

From the evaluations set forth it is apparent that in studying the movement of a rocket one may discard the terms covering the Coriolis inertial force and the alteration in the amount of movement of gases in the chamber.

When this is done the equation of movement of the center of mass of the rocket assumes the following form:

$$M(t) \frac{d\bar{v}_{\text{rc}}}{dt} = M(t) \bar{g} + \bar{R} + \bar{P},$$

where

$$\bar{P} = \mu \bar{v}_{\text{re}} + (p_a - p_H) s_a \bar{n}_a.$$

Projecting the last expression in a direction opposite to the escape of gases we get

$$P = \frac{G_{\text{ext}}}{g} v_{\text{re}} + (p_a - p_H) F_a \quad (2.11)$$

where

$$F_a = s_a \cdot G_{\text{ext}} = gA.$$

## 2.2. The Gravitational Field of the Earth

The resultant of the force of the earth's attraction and the force of inertia of transfer movement from the rotation of the earth are called the force of gravity.

Let us examine a material point P with a mass  $m = 1$ , located outside the space occupied by the earth. The force of attraction of this point by any particle of the earth is determined by the law of universal gravitation

$$F = f \frac{M}{r^2}.$$

where  $M$  is the mass of the particle of the earth,  
 $r$  is its distance from the point attracted  
 $f$  is the constant of universal gravitation.

The power function of this force is determined from the expression

$$\Pi = \frac{fM}{r}.$$

Let us recall a property of the power function: projections of the force upon the axis of the coordinates are equal to partial derivatives from the power function along the corresponding coordinates. Examining axis  $r$  directed toward the point attracted as being one of the axes of the coordinates, we secure

$$F_r = \frac{\partial \Pi}{\partial r} = - \frac{fM}{r^2}.$$

The Newton potential of the earth is secured by totaling the power functions of all particles of the earth

$$\Pi = f \int \frac{dM}{r}.$$

This potential depends upon the shape, dimensions, and distribution of the masses of the earth.

In first approximation one may regard the earth as being of spherical shape, in which density at all points depends only upon their distance to the center of the sphere. In this case one can show that a body attracts an exterior point as though its entire mass were concentrated in the center of the sphere (2).

In Figure 2.3  $R_0$  is the radius of the earth, P is the point attracted, and  $r_0$  is its distance to the center of the earth (0). Let us

construct two cones with half-angles  $\varphi$  and  $\varphi + d\varphi$ , having a common apex at the center of the sphere, and let us produce two concentric surfaces by means of radii  $R$  and  $R + dR$ . The mass of the elementary volume of a body delimited by the surfaces referred to is equal to

$$dM = \rho 2\pi R^2 \sin \varphi \cdot dR \cdot d\varphi,$$

where  $\rho = \rho(R)$ , the density in the component under examination.

Under these circumstances the value of the Newton potential of the earth is determined by means of the expression

$$\Pi = f \int \frac{dM}{r} = 2\pi f \int_0^{R_0} \rho(R) R^2 dR \int_0^\pi \frac{\sin \varphi}{r} d\varphi, \quad (2.12)$$

where  $r$  is the distance of point  $P$  to the isolated volume of the body.

Taking as our point of departure

$$\begin{aligned} r^2 &= R^2 + r_0^2 - 2Rr_0 \cos \varphi, \\ r dr &= Rr_0 \sin \varphi d\varphi, \end{aligned}$$

we introduce a variable of integration of  $r$  in place of  $\varphi$ . Thereupon

$$\Pi = \frac{2\pi f}{r_0} \int_0^{R_0} \rho(R) R dR \int_{r_0-R}^{r_0+R} dr = \frac{4\pi f}{r_0} \int_0^{R_0} \rho R^2 dR.$$

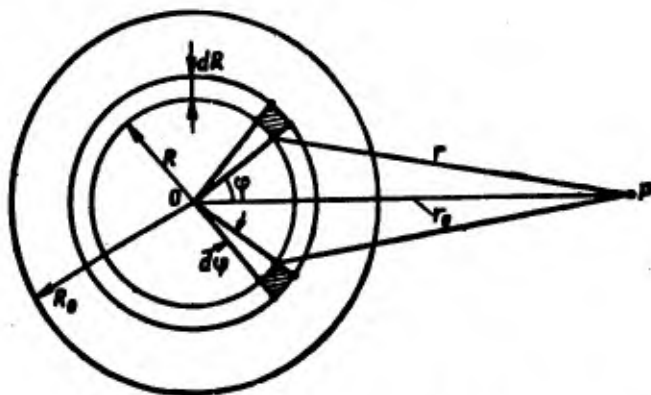


Figure 2.3. Gravitational field of the Earth.

Taking into account the fact that with the assumptions indicated the mass of the earth is

$$M = 4\pi \int_0^{R_0} \rho R^2 dR,$$

we get

$$\Pi = f \frac{M}{r_0}.$$

Just such an expression for the potential is secured in the event that we predicate that the entire of the mass of the earth is concentrated at its center.

Omitting the index 0 alongside  $r$  and designating  $fM$  by  $k^2$ , we secure in first approximation an expression for the force of attraction by the earth of a particle having mass  $m$

$$F = \frac{k^2 m}{r^2}.$$

The acceleration  $g$  communicated by this force to the particle attracted is equal to

$$g = \frac{k^2}{r^2}.$$

The last expression can be used for determination of the constant  $k^2$  for acceleration of the force of attraction of the earth  $g_0$  upon its surface

$$k^2 = g_0 R_0^2$$

The numerical value of the constant  $k^2$  may be taken as

$$k^2 = 3,986 \cdot 10^{14} \frac{M^2}{\text{сек}^2} \quad (k = 1,9965 \cdot 10^7).$$

In determining the potential of the earth in second approximation, taking into account the oblate shape of the earth the figure thereof is replaced by the spheroid of F. N. Krasovskiy. When this is done, with a precision to small quantities of the first order relative to  $\frac{1}{r}$  the expression for the potential of the earth assumes the form

$$\Pi = \frac{fM}{r} + \frac{f}{2r^3} (C - A) (1 - 3 \sin^2 \lambda), \quad (2.13)$$

where  $\lambda$  is the breadth of the point attracted;  
 $C$  is the moment of inertia relative to the earth's axis of rotation;  
 $A = B$  is the moment of inertia relative to the equatorial axis.

The second term in expression (2.13) is a quantity of the first order of smallness as compared with the first term.

Inasmuch as the distribution of the masses of the earth is unknown, in order to determine the coefficients in expression (2.13) it is necessary to take advantage of the results of measurement of the acceleration of the force of gravity on the surface of the earth, and also the results of observations of the flights of satellites. In the study (1), on the basis of generalization of the investigations referred to, the following relation is proposed for the potential of the earth:

$$\Pi = \frac{K^2}{r} \left[ 1 + \frac{J}{3} \left( \frac{a}{r} \right)^2 (1 - 3 \sin^2 \lambda) + \frac{H}{5} \left( \frac{a}{r} \right)^3 (3 \sin \lambda - 5 \sin^3 \lambda) + \frac{K}{30} \left( \frac{a}{r} \right)^4 (3 - 30 \sin^2 \lambda + 35 \sin^4 \lambda) \right], \quad (2.14)$$

where  $\lambda$  is the geocentric breadth;  
 $a$  is the length of the equatorial radius.

The values of the geocentric constants are:

$$a = 6,378,145 \cdot 10^3 \pm 11 \text{ m};$$

$$k = 1,996,5015 \cdot 10^7 \pm 111 \frac{\text{m}^2/\text{s}^2}{\text{cm}^2};$$

$$J = (1623,41 \pm 4) \cdot 10^{-6};$$

$$H = (6,04 \pm 0,73) \cdot 10^{-6};$$

$$K = (6,37 \pm 0,23) \cdot 10^{-6}.$$

The third term in expression (2.14) contains  $\sin \lambda$  in odd multiples and characterizes a certain breakdown of symmetry in the north-south direction (pear-like form of the earth).

Let us evaluate the magnitude of the second term in the expression for the potential of the earth, taking  $r$  as 7,000 kilometers =  $7 \cdot 10^6$  meters. We get

$$\frac{J}{3} \left( \frac{a}{r} \right)^2 = \frac{1623 \cdot 10^{-6}}{3} \left( \frac{6,378}{7,0} \right)^2 \approx 0,45 \cdot 10^{-3}.$$

At the equator  $\sin \lambda$  equals zero, and the correction to the first term turns out to be about 0.045 percent. At the pole  $1 - 3 \sin^2 \lambda = -2$ , and the correction proves to be about 0.9 percent.

In study of the movement of a body relative to the earth it is also necessary to take into account the inertial force of transfer movement and the Coriolis inertial force (Figure 2.4).

The centrifugal inertial transfer force operating on point P is equal to

$$F_{\text{sep}} = m r \omega^2 \cos \lambda$$

The potential of this force is equal to

$$\Pi_{\text{sep}} = \frac{m}{2} r^2 \omega^2 \cos^2 \lambda$$

The projection of force  $F_{\text{trans}}$  in the direction of the radius of the vector of point P is equal to

$$(F_{\text{sep}})_r = m \frac{\partial \Pi_{\text{sep}}}{\partial r} = m r \omega^2 \cos^2 \lambda$$

The projection of this force upon the tangent to the coordinate line of the spherical coordinate  $\lambda$  is equal to

$$(F_{\text{sep}})_\lambda = \frac{m}{r} \frac{\partial \Pi_{\text{sep}}}{\partial \lambda} = - m r^2 \cos \lambda \sin \lambda. \quad (2.15)$$

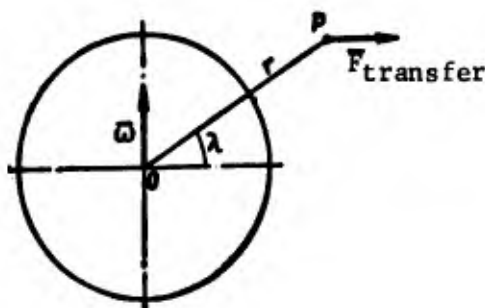


Figure 2.4. Centrifugal inertial force of the earth.

The force of gravity is the resultant of the force of terrestrial attraction and the force of inertia of transfer movement from the rotation of the earth. The potential of the force of gravity is

$$\Pi_{\text{gravity}} = \Pi + \Pi_{\text{transfer}}$$

Let us evaluate the greatest magnitude of force  $F_{\text{trans}}$  relative to the basic force of gravity of the earth.

The angular velocity of rotation of the earth is

$$\omega = \frac{2\pi}{86164} = 7,292 \cdot 10^{-5} \frac{1}{\text{сек}}$$

Then

$$\frac{F_{\text{sep}}}{F} \approx m r \omega^2 : \frac{m k^2}{r^3} = \frac{\omega^2 r^4}{k^2} = \frac{7,292^2 \cdot 10^{-10}}{1,996^2 \cdot 10^{14}} r^4 \approx 13,7 \cdot 10^{-24} r^4.$$

Taking for a satellite  $r = 7 \cdot 10^6$  meters, we get

$$\frac{F_{\text{sep}}}{F} = 13,7 \cdot 10^{-24} \cdot 343 \cdot 10^{16} \approx 0,0047.$$

The acceleration of the force of gravity upon the surface of the earth,  $g_0$ , changes with latitude both as a result of the compression of the spheroid and as a result of change in centrifugal acceleration from the rotation of the earth as latitude changes.

The Coriolis inertial force  $F_{\text{Cor}}$  is determined from the expression

$$\vec{F}_{\text{Cor}} = 2m\vec{v}_r \times \vec{\omega}. \quad (2.16)$$

where  $\vec{v}_r$  is the velocity of a body relative to the system of coordinates associated with the earth.

The maximum amount of acceleration of this force is

$$(a_{\text{Cor}})_{\text{max}} = 2v_r \omega.$$

Let us evaluate the relation

$$\frac{a_{\text{Cor}}}{g_0} = \frac{2\omega v_r}{g_0} = \frac{2 \cdot 7,292 \cdot 10^{-5}}{9,8} v_r = 1,48 \cdot 10^{-5} v_r.$$

At a velocity of body 1,000 meters per second we get  $\frac{a_{\text{Cor}}}{g_0} = 1,48 \cdot 10^{-2}$ , or 1.5 percent. With initial space speed of rocket this ratio reaches 12 percent.

### 2.3. The Terrestrial Atmosphere

The parameters of the terrestrial atmosphere (density  $\rho$ , temperature  $T$ , and pressure  $p$ ) enter into expressions for aerodynamic and reactive forces and moments and directly affect the flight of rockets. From the expression for reactive force

$$P = \frac{G_{\text{ext}}}{g} v_{re} + F_a (p_0 - p_H)$$

it is apparent that as atmospheric pressure falls off the thrust of the engine increases, i.e., thrust increases with increase of altitude.

In the expression for any resistance (2.20)

$$X = \frac{\rho v^2}{2} S c_x \left( \frac{v}{a} \right)$$

the mass density of the air,  $\rho$ , enters directly, and temperature  $T$  does so in the expression for the speed of sound

$$a = \sqrt{\kappa g R T} \quad (2.17)$$

The character of alteration in meteorological parameters with altitude depends on the general state of the weather and varies for various parts of the earth and different seasons. For this reason in order to simplify ballistic calculations some mean experimental or standard relations of meteorological factors to altitude are set up. These standard data are used for calculations associated with the ballistic designing of rockets. They are furthermore used for compiling firing tables. The influence of change in meteorological parameters upon deviation of the elements of trajectories is taken into account through special methods (the theory of corrections).

The three basic meteorological parameters  $\rho$ ,  $p$ , and  $T$ , are linked by an equation of the form

$$p = \rho R T. \quad (2.18)$$

It is further possible to establish a relationship between pressure and temperature by considering the vertical equilibrium of the atmosphere, in which connection the weight of a given column of air is equilibrated by the difference of pressures in its upper and lower sections.

Let us isolate (Figure 2.5) at an altitude  $y$  a layer of air having a base area  $s$  and a height  $dy$ . The weight of a given volume of air is equal to  $g \rho s dy$ , and the forces of pressure upon the lower and the upper sections are equal to  $p s$  and  $(p + dp)s$  respectively. Setting up an equation of vertical equilibrium we get

$$dp = -g \rho dy,$$

and on the basis of the equation of state we have

$$\frac{dp}{p} = -\frac{1}{R} \frac{dy}{T},$$

whence

$$p = p_0 e^{-\frac{1}{R} \int_0^y \frac{dy}{T}} \quad (2.19)$$

If we take into account alteration in the acceleration of the force of gravity with altitude, the weight of the elementary volume of air at altitude  $y$  is determined from the expression

$$g_0 \frac{r_0^2}{(r_0 + y)^2} \rho s dy.$$

where  $r_0$  and  $g_0$  correspond to sea level.

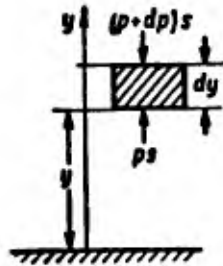


Figure 2.5. Vertical equilibrium of the atmosphere.

When this is done, expression (2.19) assumes the following form:

$$p = p_0 e^{-\frac{1}{k} \int_0^y (1 + \frac{y}{r_0})^{-2} dy}$$

In order to calculate the integral in expression (2.19) one must know the relation  $T(y)$ . If this relation and the pressure  $p_0$  at the surface of the earth are known, it is possible to calculate the pressure  $p$  at any altitude. Knowing  $p$  and  $T$ , one can calculate the density from expression (2.18). Thus we can regard temperature  $T$  as a basic meteorological parameter, the law for the alteration of which with alteration of altitude determines the character of change in other meteorological parameters.

In artillery practice the following standard values are adopted for meteorological parameters at sea level:

$$T_0 = 288^\circ \text{ K}; p_0 = 750 \text{ mm of mercury column.}$$

In addition one takes into account 50 percent humidity of air as an introduction of virtual temperature  $\tau$ , determined from the expression

$$\tau = \frac{T}{1 - \frac{3}{8} \frac{e}{p}},$$

where  $e$  is the pressure of water vapors.

$$\text{Here } \tau_0 = 288,9^\circ \text{ K}, \rho_0 = 0,123 \text{ kilogram} \cdot \text{sec}^2/\text{m}^4.$$

As a standard function  $\tau(y)$  one adopts the relation proposed by Professor D. A. Ventsel.

For  $y < 9300 \text{ m}$  one adopts a falling off of temperature with altitude having a constant gradient  $G$ :

$$\tau = 288,9 - Gy,$$

where

$$G = 6,328 \frac{0}{\text{K.M}} = 0,006328 \frac{0}{\text{m}}.$$

For altitudes from 9,300 to 12,000 meters the gradient falls off linearly from 0.006328 to zero. Under these circumstances we get

$$\tau = 230,0 - 0,006328(y - 9300) - 1,172 \cdot 10^{-6}(y - 9300)^2.$$

For altitudes greater than 12,000 meters the temperature is taken as being constant and equal to  $\tau = 221.5$ .

The value for the pressure is determined according to formula (2.19).

At present international standard atmosphere (MSA) is widely used, its characteristics are as follows:

$$T_0 = 288^\circ \text{ K}; p_0 = 760 \text{ mm of mercury column}; \rho_0 = 0.125 \text{ kg} \cdot \text{sec}^2/\text{m}^4.$$

For altitudes up to 11,000 meters:

$$T = T_0 - 0,0065y.$$

Under these circumstances one can secure from expressions (2.18), (2.19) the following:

$$p = p_0 \left(1 - \frac{y}{44300}\right)^{5,256};$$

$$\rho = \rho_0 \left(1 - \frac{y}{44300}\right)^{4,256}.$$

For altitudes from 11,000 to 20,000 meters one assumes a constant temperature  $T = 216.5^\circ \text{ K}$  ( $- 56.5^\circ \text{ C}$ ).

The character of alterations in meteorological parameters at altitudes exceeding 30 kilometers is very complicated. Reliable experimental data on this subject have been received only in recent times as a result of sounding the atmosphere with meteorological rockets and artificial satellites of the earth. According to these data, starting at an altitude of 30 kilometers the temperature rises, reaching a maximum value of  $+ 50^\circ \text{ C}$  at an altitude of about 50 kilometers. Further outward the temperature again declines, reaching a minimum at an altitude of about 80 kilometers. From there on an uninterrupted rise in temperature takes place.

In the table of Annex 1, borrowed from study (4), we set forth values for temperature, pressure, and density for altitudes up to 100 kilometers. For altitudes up to 20 kilometers these values correspond to the international standard atmosphere.

#### 2.4. Aerodynamic Forces and Moments

During motion in air there appears on the surface of a rocket an uneven distribution of forces of normal pressure and of forces of tangential stresses determined by the viscosity of the medium. The direction of the tangential stresses coincides with the direction of the velocity of the flow at the part of the surface of the rocket which is under examination. The forces referred to, in their totality, create an aggregate aerodynamic force  $\bar{R}$  (the main vector) and an aggregate moment  $\bar{M}$  (the main moment).

In order to describe aerodynamic forces and moments we select a velocity system of coordinates having its origin at the center of mass of the rocket,  $C$ . We shall suppose that the axis of the rocket is inclined at an angle  $\alpha$ , called the angle of attack, from the vector of the velocity  $\bar{v}$  of its center of mass. In the plane of the angle of attack we direct axis  $Cx$  in the direction of the vector of velocity  $\bar{v}$  and the axis  $Cy$  along a perpendicular from axis  $Cx$  in the direction of the inclination of the axis of the rocket. The axis  $Cz$  is directed so that the system  $Cxyz$  is a rectangular system of coordinates.

For the components of the aerodynamic force  $\bar{R}$  and of the aerodynamic moment  $\bar{M}$  along the axes of the coordinates the following symbols and names are adopted:

$X = - R_x$  -- frontal resistance

$Y = R_y$  -- lift force

$Z = R_z$  -- flank force

$M_x$  -- moment of banking

$M_y$  -- moment of yaw

$M_z$  -- moment of pitch

From here on we shall examine primarily the case where the plane of the angle of attack coincides with the plane of symmetry of the rocket and where the system of forces is symmetrical relative to this plane (Figure 2.6).

In this case  $Z = 0$ ,  $M_x = 0$ , and  $M_y = 0$ . The expression for aerodynamic forces and moments takes on the following form:

$$X = -\frac{\rho v^2}{2} S c_x \quad (2.20)$$

$$Y = \frac{\rho v^2}{2} S c_r \quad (2.21)$$

$$M_z = \frac{\rho v^2}{2} S L m_r \quad (2.22)$$

where  $\rho$  is the mass density of the air;  
 $v$  is the velocity of the center of mass of the rocket;  
 $S$  is the area of cross-section of the rocket ("middle" area);  
 $L$  is the representative length of the rocket (ordinarily taken to be its length).

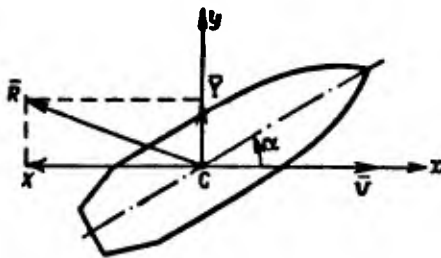


Figure 2.6. Aerodynamic forces.

Taking as point of departure the similarity theory in aerodynamics it proves to be the case that the aerodynamic coefficients  $c_x$ ,  $c_y$ , and  $m_z$  depend not only on the shape of the rocket and its orientation relative to the flow, but also on two basic parameters:

the Reynolds figure

$$Re = \frac{\rho v L}{\mu} \quad (2.23)$$

and the Mach figure

$$M = \frac{v}{a}, \quad (2.24)$$

where  $\mu$  is the coefficient of viscosity of the air;  
 $a$  is the velocity of sound in the air flow bathing the rocket.

Inasmuch as with the assumptions under examination the system of aerodynamic sources is a plane system, it can be reduced to a single force lying in the plane of the angle of attack. The point P of intersection of the line of operation of this force with the axis of the rocket is called the center of pressure. In rockets equipped with stabilizing tail groups ordinarily the center of pressure is located behind the center of mass; in this case the moment M is the stabilizing moment. In rockets without tail groups as a rule the center of pressure is ahead of

the center of weight. In this case the rocket is statically unstable and it is stabilized by the steering organs (gas rudders, turning jets, etc.) or by communicating to the rocket greater angular velocity of rotation around its axis of symmetry.

It is not difficult to find the relation between the moment  $M_z$ , the components of the aerodynamic force  $X$ ,  $Y$ , and the distance  $\Delta L = CP$  between the center of pressure and the center of mass of the rocket (Figure 2.7):

$$M_z = Y\Delta L \cos \alpha + X\Delta L \sin \alpha \quad (2.25)$$

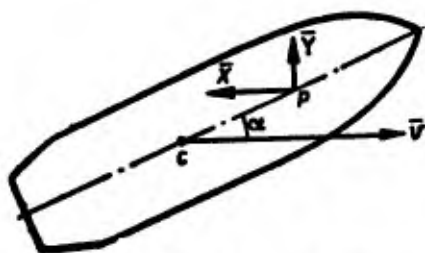


Figure 2.7. Center of pressure.

The relation between the aerodynamic coefficients  $c_x$ ,  $c_y$ , and  $m_z$  assumes the following form on the basis of expressions (2.20)-(2.25):

$$m_z = \frac{\Delta L}{L} (c_y \cos \alpha + c_x \sin \alpha). \quad (2.26)$$

### Frontal Resistance

Frontal resistance depends on the form of the body, the Mach number ( $M$ ), the Reynolds number ( $Re$ ), and the angle of attack ( $\alpha$ ). With low angles of attack and great velocities of flight, characteristic of ballistic rockets of the "surface-to-surface" class, the first two factors are determining. In Figure 2.8 we show curves for relationship of  $c_x$  to  $M$  and  $\alpha$  for the V-2 rocket.

For values of  $M < 0,7 + 0,8$  one may practically regard  $c_x$  as not dependent on velocity. In the range of velocities around the speed of sound a sharp rise in  $c_x(M)$  takes place, with ensuing smooth decline of this function. At high speeds above that of light ( $M$  more than 5) the function  $c_x(M)$  becomes practically constant.

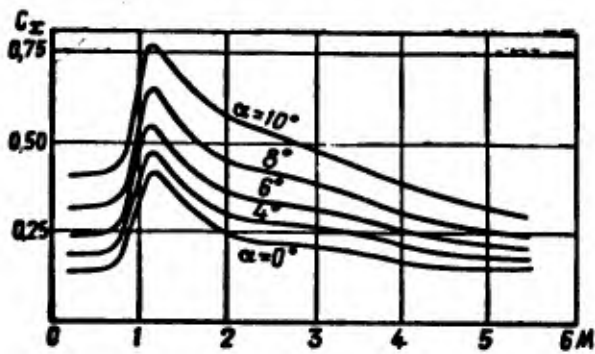


Figure 2.8. Dependence of frontal resistance on angle of attack  $\alpha$  and Mach number  $M$ .

In Figure 2.9 we present typical curves for the function  $c_x(M)$  with zero angle of attack for artillery shells and rockets.

Curve 1 corresponds to the Siacci law, secured by processing results of tests with shells having an over-all length up to 4 calibers and a nose of ogival form with a length of 1-1.3 calibers.

Curve 2 corresponds to shells of improved shape, having a more acute nose part of length about 2.5 calibers and a tail part in the form of a truncated cone, with an over-all length of shell about 5 calibers. For comparison the  $c_x$  curve of the V-2 rocket is also presented (Curve 3).

In view of the fact that there are not many shapes of artillery shells, and that determining the relation  $c_x(M)$  and figuring out ballistic tables is hard work, standard functions for air resistance  $(c_x)_{\text{stand}}$  have been established, among which are these: the Siacci law (Italy), the Havre law (France), the Mayevski-Zabudski law, the 1930 law, and the 1943 law (USSR).

When standard  $(c_x)_{\text{stand}}$  functions are used it is assumed that the function of air resistance of a concrete shell  $c_x$  can be determined approximately from the expression

$$c_x = i(c_x)_{\text{st.}}$$

where  $i$  is a constant -- the coefficient of the form of the shell.

The assumption of the constancy of the coefficient of form is not a strict one, and accordingly for precise calculations and particularly for guided rockets individual  $c_x$  functions are used which are determined for each rocket according to the data of aerodynamic calculations and

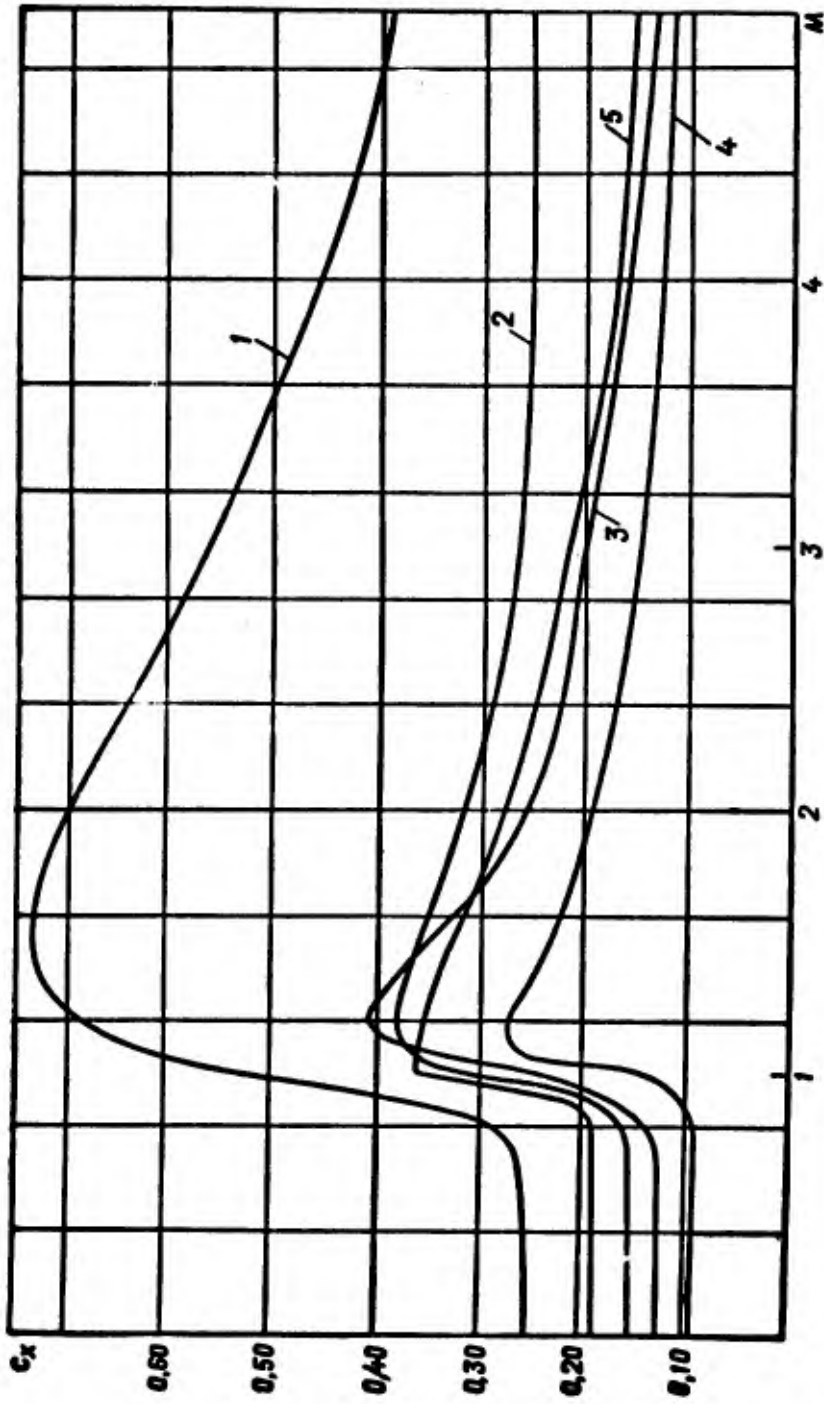


Figure 2.9. Reference  $c_x$  functions: 1 -- Siacci function; 2 -- function of 1943; 3 --  $c_x$  of V-2 rocket; 4 --  $c_x$  of Table 2.1; 5 -- function of 1930.

experiments. Standard  $c_x$  functions with constancy of the coefficient of form assumed are used basically with application to artillery shells.

Such an assumption can also be regarded as acceptable for engineering ballistic calculations associated with the evaluation of the ballistic parameters of rockets being designed (ballistic designing).

For approximate calculations presented in this book the standard  $c_x$  function presented in Table 2.1 and illustrated in Figure 2.9 (Curve 4) has been adopted.

Table 2.1

M	$c_x$	M	$c_x$	M	$c_x$
0,00	0,1020	1,00	0,1450	2,40	0,1710
0,10	0,1010	1,02	0,1780	2,50	0,1665
0,20	0,1000	1,04	0,2000	2,60	0,1620
0,30	0,0990	1,06	0,2320	2,70	0,1585
0,40	0,0980	1,08	0,2660	2,80	0,1545
0,50	0,0970	1,10	0,2730	2,90	0,1510
0,60	0,0960	1,12	0,2760	3,00	0,1495
0,62	0,0958	1,14	0,2770	3,10	0,1465
0,64	0,0956	1,16	0,2764	3,20	0,1435
0,66	0,0954	1,18	0,2760	3,30	0,1420
0,68	0,0952	1,20	0,2744	3,40	0,1400
0,70	0,0950	1,22	0,2720	3,50	0,1385
0,72	0,0940	1,24	0,2660	3,60	0,1360
0,74	0,0946	1,26	0,2620	3,70	0,1340
0,76	0,0944	1,28	0,2570	3,80	0,1324
0,78	0,0948	1,30	0,2530	3,90	0,1310
0,80	0,0954	1,40	0,2370	4,00	0,1294
0,82	0,0960	1,50	0,2250	4,10	0,1278
0,84	0,0968	1,60	0,2150	4,20	0,1262
0,86	0,0976	1,70	0,2070	4,30	0,1250
0,88	0,0986	1,80	0,2010	4,40	0,1240
0,90	0,1000	1,90	0,1950	4,50	0,1230
0,92	0,1018	2,00	0,1900	4,60	0,1220
0,94	0,1038	2,10	0,1845	4,70	0,1210
0,96	0,1060	2,20	0,1800	4,80	0,1200
0,98	0,1130	2,30	0,1750	4,90	0,1190
				5,00	0,1180

In order to calculate the coefficient of form of a given rocket it is sufficient to determine experimentally or through computation the values of  $c_x$  for a number of values of the M number and average the quantity

$$i = \left| \frac{c_x}{(c_x)_{\text{ст}}} \right|_{\text{ср}}$$

### Approximate Method of Calculating Frontal Resistance (5)

The frontal resistance of a rocket has a substantial effect upon the trajectory and range of its flight.

Precise determination of the coefficient of frontal resistance  $c_x$  calls for laborious computations and experiments, the methods for carrying out which are considered in courses of aerodynamics. Below we set forth formulae which make it possible to evaluate approximately the amount of frontal resistance of a rocket without tail group which is being designed, at velocities of flight about the speed of sound, and also the magnitude of the coefficient of form of the rocket, relative to the standard selected.

Frontal resistance of a rocket without tail group may be broken down into the following components:

- wave resistance of the nose part  $(c_x)_r$ ;
- wave resistance of the tail cone  $(c_x)_{tc}$ ;
- friction resistance  $(c_x)_{fr}$ ;
- bottom resistance  $(c_x)_b$ .

The aggregate coefficient of frontal resistance for the passive part of the trajectory is determined from the expression

$$c_x = (c_x)_r + (c_x)_{tc} + (c_x)_{fr} + (c_x)_b.$$

For the active part of the trajectory the last component is eliminated, since pressure in the outlet section of the cone of the engine is considered in the expression for reactive force.

#### Wave Resistance of the Nose Part $(c_x)_r$

Wave resistance under supersonic bathing of the nose part is brought about by the appearance of a nose shock wave, back of which a zone of heightened pressure springs up on the surface of the body. Wave resistance of the nose part reaches 50 percent, or more, of the aggregate resistance of the rocket. The proportionate part of this resistance rises with increase of the  $M$  number.

For a conical nose part the value of  $(c_x)_r$  may be calculated according to the formula

$$(c_x)_{r. \text{ con}} = (0,0016 + 0,002M^{-2}) (\beta_n^\circ)^{1,7}, \quad (2.27)$$

where  $\beta_n^\circ$  is the half-angle of the cone in degrees.

For an ogival nose part the generatrix for which is the arc of a circle:

$$(c_x)_{n \text{ og}} = \frac{0,08(15,5 + M)}{3 + M} \tilde{\rho}_n \quad (2.28)$$

where  $\tilde{\rho}_n = (c_x)_{\text{nose cone}}$  is calculated for angle  $\beta$  of taper of the tip of the nose part.

For a nose part having a parabolic generatrix

$$(c_x)_{n \text{ par}} = \frac{0,3}{\lambda_r^2} \cdot \frac{1 + 2M}{\sqrt{M^2 - 1}}, \quad (2.29)$$

where  $\lambda_r$  is the length of the nose part in calibers.

#### Wave Resistance of the Tail Cone

$(c_x)_{tc}$  is determined from the expression

$$(c_x)_{t.c.} = 0,002 (0,8 + M^{-2}) (\beta_{t.c.})^{1,7} \sqrt{1 - \tilde{S}_b}, \quad (2.30)$$

where  $S_b = \frac{S_{\text{base}}}{S_{\text{mid}}}$ .

#### Bottom Resistance

$(c_x)_b$  is determined from the expression

$$(c_x)_b = 1,14 K_1 (2 - K_1) M^{-2} \tilde{S}_b, \quad (2.31)$$

where  $K_1 = M \frac{\tilde{S}_b}{\lambda}$ ;

$\lambda$  is the length of the rocket in calibers.

At very great rocket speeds one may consider that a vacuum forms in the bottom part. Then

$$(c_x)_b = \frac{2}{KM^2} \tilde{S}_b. \quad (2.32)$$

### Friction Resistance

Approximate determination of friction resistance is carried out according to formulas for resistance of a streamlined blade  $c_f$ . The coefficient of friction resistance of the blade may be determined from the formula

$$c_f = \frac{0,032}{Re^{0,4}} (1 + 0,12M^2)^{-\frac{1}{3}} \quad (2.33)$$

with Reynolds numbers within limits  $2 \cdot 10^6 - 10^{10}$  and according to the formula

$$c_f = \frac{1,32}{\sqrt{Re}} (1 + 0,03M^2)^{-\frac{1}{3}} \quad (2.34)$$

for Reynolds numbers less than  $10^6$ .

The coefficient of friction resistance of the casing of the rocket is determined from the formula

$$(c_x)_{fr} = c_f \frac{S_{fr}}{S_{mid}} \quad (2.35)$$

where  $S_{fr}$  is the flanking surface of the casing (without the area of the bottom).

The coefficient of viscosity forming part of the expression for the Reynolds number, is determined according to the Sutherland formula

$$\mu = 1,82 \cdot 10^{-4} \left( \frac{T}{288} \right)^{3/2} \frac{383}{110 + T} \quad (2.36)$$

Calculating the aggregate coefficient of frontal resistance  $c_x$  for a number of values of the Mach number, one can determine the coefficient of form relative to the selected pattern of function  $c_x$ .

Example:

To determine the aerodynamic coefficient  $c_x$  for the following conditions:

Caliber  $D = 1.65$  m. Length in calibers: nose part  $\lambda_r = 3.16$ , cylindrical part  $\lambda_{cyl} = 3.0$ , tail cone  $\lambda_{tc} = 2.0$ , entire casing  $\lambda = 8.16$ . Relative diameter of bottom  $D_b = D_b : D = 0.675$ . Nose part is of parabolic form. Altitude of flight  $y$  is 6,000 meters, velocity of rocket  $v$  is 845 meters per second.

Solution:

According to the table of Annex 1 for altitude  $y$  equals 6,000 m, we find

$$\frac{p}{p_0} = H(y) = 0,523; \quad \rho = 0,123 \cdot 0,523 = 0,0643;$$

$$\sqrt{\frac{T_0}{T}} = 1,066; \quad T = \frac{288}{1,066^2} = 257^\circ \text{ K.}$$

The speed of sound is

$$a = a_0 \sqrt{\frac{T}{T_0}} = \frac{340}{1,066} = 320 \text{ m/sec.}$$

The Mach number if  $M = 845/1,066 = 320$  meters per second.

The coefficient of viscosity  $\mu$  determined by formula (2.36) is

$$\mu = 1,82 \cdot 10^{-6} \left( \frac{257}{288} \right)^{3/2} \frac{388}{110 + 257} = 1,62 \cdot 10^{-6}.$$

We determine the coefficient of wave resistance of the nose part  $(c_x)_n$  according to the formula

$$(c_x)_n = \frac{0,3}{\lambda^2} \cdot \frac{1 + 2M}{\sqrt{M^2 - 1}} = \frac{0,3}{3,16^2} \frac{1 + 2 \cdot 2,64}{\sqrt{2,64^2 - 1}} = 0,078.$$

We determine the coefficient of wave resistance of the tail cone  $(c_x)_{tc}$  according to formula (2.30).

We determine in advance the angle of the tail cone  $(c_x)_{tc}$

$$\begin{aligned} \operatorname{tg} \beta &= \frac{1}{2\lambda_n} (1 - \bar{D}_n) = \frac{1}{2 \cdot 2} (1 - 0,675) = 0,081; \\ \beta^\circ &= 4,63^\circ; \quad \bar{S}_n = \bar{D}_n^2 = 0,455. \end{aligned}$$

According to formula (2.30) we have

$$(c_x)_{tc} = 0,002 (0,8 + 2,64^{-2}) \cdot 1,63^{1,7} \sqrt{1 - 0,455} = 0,019.$$

We determine the coefficient of bottom resistance according to formula (2.31). We have

$$\begin{aligned} K_1 &= M \frac{\bar{S}_n}{\lambda} = 2,64 \frac{0,455}{8,16} = 0,147. \\ (c_r)_n &= 1,14 \cdot K_1 (2 - K_1) M^{-2} \bar{S}_n = 1,14 \cdot 0,147 \cdot 1,853 \cdot 2,64^{-2} \cdot 0,455 = 0,020. \end{aligned}$$

In order to determine friction resistance, we first calculate the Reynolds number (2.23)

$$Re = \frac{\rho v L}{\mu} = \frac{0,0643 \cdot 845 \cdot 8,16 \cdot 1,65}{1,62 \cdot 10^{-6}} = 4,55 \cdot 10^7.$$

According to formula (2.33) we have

$$c_f = \frac{0,032}{(4,55 \cdot 10^7)^{0,145}} (1 + 0,12 \cdot 2,64^3)^{-\frac{1}{2}} = 0,00182$$

In order to determine approximately the flank surface of the rocket, we substitute for it the surface of a cylinder of length  $L$ , whereupon:

$$\frac{S_{\text{TP}}}{S_{\text{MNA}}} = \frac{4L}{D} = 4\lambda = 32,6;$$

$$(c_r)_{\text{TP}} = c_f \frac{S_{\text{TP}}}{S_{\text{MNA}}} = 0,00182 \cdot 32,6 = 0,059.$$

We determine the aggregate coefficient of frontal resistance

$$c_r = (c_r)_r + (c_r)_{\text{z.k.}} + (c_{\text{z.k.}}) + (c_r)_{\text{TP}} = 0,078 + 0,019 + 0,020 + 0,059 = 0,176.$$

Frontal resistance is determined from the expression

$$X = \frac{\rho v^2}{2} S c_r = \frac{0,0643 \cdot 845^2}{2} \frac{\pi}{4} 1,65^2 \cdot 0,176 = 8600 \text{ кг.}$$

### Lifting Force

Lifting force is determined from expression (2.21)

$$Y = \frac{\rho v^2}{2} S c_y$$

With alpha less than  $5^\circ$  the relation of the aerodynamic coefficient  $c_y$  to the angle of attack is linear and is characterized by the graph Figure 2.10.

The expression for lifting force may be written in the form

$$Y = \frac{\rho v^2}{2} S c_{y,\alpha}^z = Y^z \alpha, \quad (2.37)$$

where the coefficient  $c_{y,\alpha}^z$  may be regarded as depending only on the M number.

Experiments and calculations show that the coefficient  $c_{y,\alpha}^z$  for rockets with tail groups is considerably higher than  $c_{y,\alpha}^z$  in rockets without them. A graph for the relation of  $c_y$  to the M number and to the angle of attack for the V-2 rocket is shown in Figure 2.11.

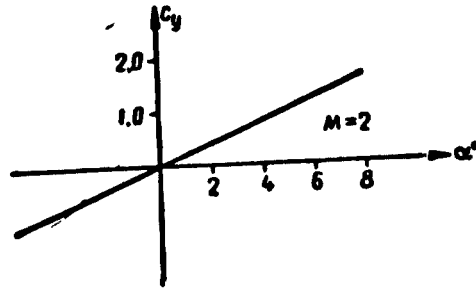


Figure 2.10. Relation of coefficient of lifting force  $\overline{[lift\ coefficient]}$  to angle of attack.

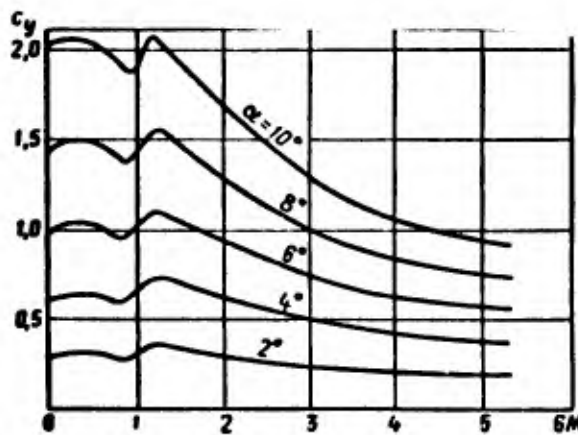


Figure 2.11. Relation of  $c_y$  coefficient to alpha and to M.

### The Aerodynamic Moment $M_z$

Aerodynamic moment is determined according to formula (2.22)

$$M_z = \frac{\rho v^2}{2} S L m_z \quad (2.38)$$

where the aerodynamic coefficient  $m_z$  depends upon the M number and the angle of attack  $\alpha$ . A graph for the relation of  $m_z$  to the angle of attack for a statically stable (tail grouped) and unstable (without tail group) rocket is shown in Figure 2.12. For the unstable rocket (curve 1) the sign of  $m_z$  coincides with the sign of the angle of attack and the aerodynamic moment seeks to overturn the rocket. In this case the moment  $M_z$  is called a tilting moment. Curve 2 corresponds to a statically stable rocket. In this case the moment is called a stabilizing one.

With small angles of attack one may presume a linear relation of  $M_z$  to the angle of attack. From here on we shall write the expression for the aerodynamic moment in the following form:

where the plus sign corresponds to the statically unstable, and the minus sign to the stable, rocket.

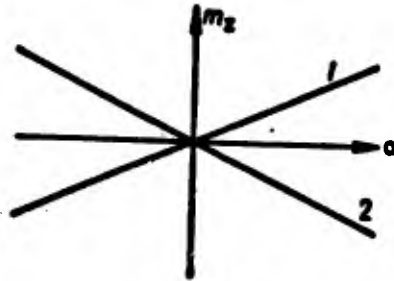


Figure 2.12. The aerodynamic coefficient  $m_z$  for a rocket without tail group (1) and with (2).

In this connection we shall assume  $m_z$  is positive. With small angles of attack, from expression (2.26) we secure the following relationship between the aerodynamic coefficients  $m_z^a$ ,  $c_y^a$  and  $c_x$ :

$$m_z^a = \frac{\Delta L}{L} (c_y^a + c_x). \quad (2.39)$$

#### Damping Moment

Under real conditions of flight the axis of a rocket oscillates relative to the vector of velocity of the center of mass of the rocket, and the angle of attack  $\alpha$  hovers around zero. The presence of an angular velocity  $\Omega = \dot{\varphi}$  of rotation of the axis of the rocket in the plane of the angle of attack gives rise to a supplementary aerodynamic moment, called the damping moment. Theory and experience show that the damping moment is determined by means of the expression:

$$M_d = -\rho v S L^2 \Omega m_d, \quad (2.40)$$

where  $m_d$  is the coefficient of damping moment. The minus sign shows that the moment seeks to reduce the angular velocity of rotation of the axis of the rocket.

#### 2.5. The Trajectory of Movement of a Guided Ballistic Rocket. The Parts of the Trajectory

The start of "ground-to-ground" class rockets intended for great ranges of flight is undertaken with the rocket in vertical position. Turning of the axis of the rocket for flight along a given trajectory is brought about by a program mechanism which constitutes one of the units of the rocket system. The power elements turning the rocket are

gas rudders, turning engines, and other apparatus which incline the main vector of reactive forces away from the axis of the rocket and create a reactive moment relative to the axis, and perpendicular to it. It is customary to call the movement of a rocket under the operation of the forces contemplated a program or undisturbed movement. In calculating the undisturbed movement of a rocket one takes into account its weight, and also the reactive and aerodynamic forces and moments, the nominal values of which are determined in advance on the basis of computations and of laboratory and flight experiments.

Under real conditions of flight the rocket will be subject to the operation of chance, or disturbing, forces and moments, the nominal values of which are determined in advance on the basis of computations and of laboratory and flight experiments.

Under real conditions of flight the rocket will be subject to the operation of chance, or disturbing, forces and moments, not taken into account during calculation of the undisturbed movement. Among these are, for example, chance forces evoked by fluctuation of the parameters of the rocket engine and of the meteorological parameters of the atmosphere (temperature, density, wind).

Under the operation of chance forces the rocket carries out so-called disturbed movement. In order that disturbed movement of the rocket may not differ greatly from its calculated disturbed movement, among the instrumental equipment there is an automatic device for stabilizing the rocket, constituting one of the basic units of the system for directing its flight. The movement of a stabilized rocket takes place in such fashion that the parameters of disturbed movement fluctuate around the parameters of undisturbed movement, deviating from them only slightly.

The requirements imposed upon precision and completeness of the taking into account of forces operating upon a rocket in its flight, and upon the precision of the actual ballistic calculations, depend upon the purpose of the rockets. Calculations intended for prior working out of the parameters of the real flight to a target or to orbit must be carried out with the greatest possible accuracy.

Substantially less severe requirements are imposed upon the accuracy of engineering calculations intended for determination of the ballistic parameters of rockets being designed and for evaluation of their dependence on design characteristics of rockets (thrust of engine, all units of structure and fuel, etc.).

We shall in fact examine such calculations below.

In studying undisturbed movement of a rocket without taking into account the influence of the rotation of the earth and the influence of

wind the trajectory of movement of the center of mass of a rocket is regarded as being a plane curve.\*

In the plane of flight of the rocket we draw the axis  $Ox$  horizontal to the point of start in the direction of the flight, the axis  $Oy$  vertically upward (Figure 2.13). At any given moment of time  $t$  the center of mass of the rocket is at some point  $M$  of the trajectory; the vector of velocity  $v$  is inclined to the horizon at an angle  $\theta$ . The axis of the rocket forms with the vector of velocity  $v$  the angle of attack  $\alpha$ , and with the plane of the horizon the angle of pitch  $\varphi = \alpha + \theta$ .

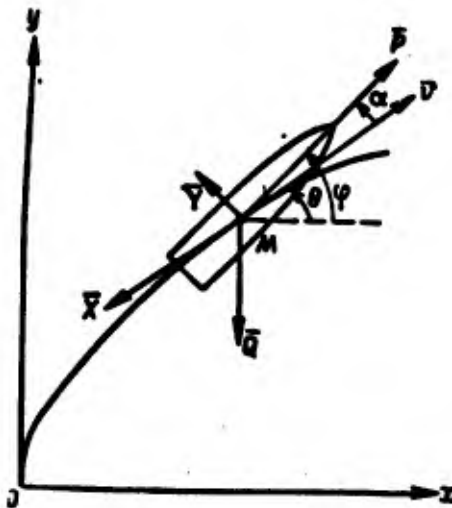


Figure 2.13. Diagram of forces operating upon rocket in active part of trajectory.

According to the character of the forces operating on the rocket the trajectory of the movement of its center of mass is divided into two fundamental sections: the active part of flight of the rocket with the rocket engine working, and the passive part of the flight after the engine cuts out. In connection with the methods of calculation which are examined below, we shall divide the trajectory into smaller sections (Figure 2.14), namely:

- an initial section OA, the vertical, active section;
- a curvilinear section AB, of turning of the rocket with respect to angle of pitch;
- a final, inclined active section BK, with approximately constant angle of pitch;

\* The effect of the rotation of the earth upon the flight of a rocket is examined in 2.15.

-- an initial passive section of flight of rocket  $KK_1$ , over which air resistance is not insignificant;

-- an airless passive section  $K_1C_1$  (on account of the great rarification of the atmosphere in this section one may disregard air resistance and calculate the elements of the trajectory according to the formulas of elliptical theory);

-- a final passive section  $C_1C$ , of return of the rocket into the dense strata of the atmosphere and of sharp braking of velocity.

## 2.6. The Equation for Motion of the Rocket in the Active Part of the Trajectory

In studying the undisturbed movement of a rocket in the active section of the trajectory we shall take into account:

-- the weight of the rocket  $Q(t) = m(t)g$ ;

-- the reactive force (thrust)  $P = \frac{G_{\text{ex}}}{g} v_{\text{ra}} + F_a(p_a - p_H)$ ;

-- the frontal resistance  $X = \frac{\rho v^2}{2} S c_x$ ;

-- the lifting force  $Y = Y^a = \frac{\rho v^2}{2} S c_y^a \cdot a$ ;

-- the static aerodynamic moment  $M_s = \pm M_s^a \cdot a \pm \frac{\rho v^2}{2} S L m_s^a \cdot a$ ;

-- the damping moment  $M_d = -\rho v S L^2 m_d \dot{\phi} = -M_d^a \cdot \dot{\phi}$ ;

-- the lifting, directing force of the steering organs  $Y_{st} = Y_{st}^a \cdot \delta$ ,

where  $\delta$  is the angle of inclination of the rudders (turning engines) from neutral position;

-- the moment of steering force relative to the center of mass of the rocket is determined from the expression  $M_{st} = -h Y_{st}^a \cdot \delta$  (the minus sign shows that upon turning of the rudders counterclockwise, the moment  $M_{st}$  produces a turn of the rocket clockwise).

Let us set up equations for the movement of a rocket, taking into account the forces and moments listed above. We shall project the acceleration of the center of mass of the rocket on a tangent and normal to its trajectory.

The equation for movement relative to the tangent assumes the following form:

$$m(t)\dot{v} = P \cos \alpha - X - m(t)g \sin \theta - Y_{ynp} \sin \alpha \quad (2.41)$$

Considering that normal acceleration  $w_n = \frac{v^2}{\rho} = v^2 \frac{d\theta}{dS} = v\dot{\theta}$ , we get the equation for movement relative to the normal:

$$m(t)v\dot{\theta} = P \sin \alpha + Y^s \cdot \alpha - m(t)g \cos \theta + Y_{ynp} \cos \alpha \quad (2.42)$$

The equation for rotatory movement of the rocket around its center of mass assumes the form:

$$A\ddot{\varphi} = \pm M_x^s \alpha - M_x^i \dot{\varphi} - Y_{ynp}^s \delta h, \quad (2.43)$$

where A is the equatorial moment of inertia of the rocket.

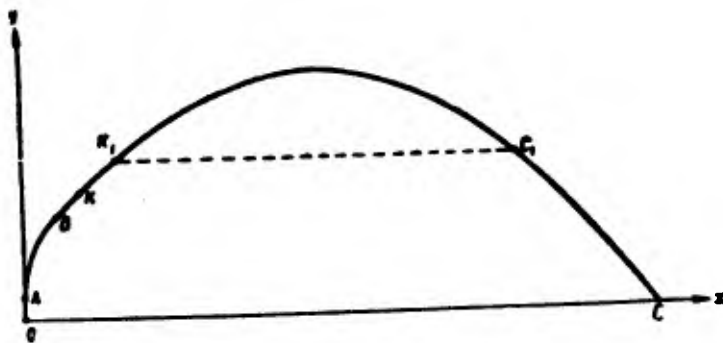


Figure 2.14. Division of trajectory of rocket into sections.

To these equations we must add kinematic equations determining the center of mass of the rocket:

$$\begin{aligned} \dot{x} &= v \cos \theta, \\ \dot{y} &= v \sin \theta \end{aligned}$$

and the equation

$$\varphi(t) = \varphi_{\text{prog}}(t),$$

determining the program value of the angle of pitch, given by the program mechanism of the steering system and carried out by the power organs of the steering system.

For rockets of "ground-to-ground" class the values of the angle of attack alpha do not exceed a few degrees. Under these circumstances sin alpha do not exceed a few degrees. Under these circumstances sin alpha is about equal to alpha and cosine alpha is about equal to 1. In expression (2.41) the component  $Y_{st} \sin \alpha \approx Y_{st}^s \cdot \delta \cdot \alpha$  may be eliminated as a quantity of the second order of smallness. When this is done we secure the following system of equations determining the movement of the rocket:

$$\dot{v} = \frac{P-X}{m(t)} - g \sin \theta; \quad (2.44)$$

$$\dot{\theta} = -\frac{g \cos \theta}{v} + \frac{P+Y^a}{vm(t)} \alpha + \frac{Y_{st}^a}{vm(t)} \delta; \quad (2.45)$$

$$A\ddot{\varphi} = \pm M_2^a \cdot \alpha - M_1^a \cdot \dot{\varphi} - hY_{st}^a \cdot \delta; \quad (2.46)$$

$$\varphi(t) = \varphi_{\text{prog}}(t); \quad (2.47)$$

$$\dot{x} = v \cos \theta; \quad (2.48)$$

$$\dot{y} = v \sin \theta; \quad (2.49)$$

$$\varphi = \alpha + \theta. \quad (2.50)$$

In all, we get seven equations for determination of seven functions which are sought,  $v, \theta, \alpha, \varphi, x, y, \delta$ .

The initial conditions are:

$$\text{with } t_0 = 0; v_0 = 0; \theta_0 = \varphi_0 = \frac{\pi}{2}; x_0 = 0; y_0 = 0; \alpha_0 = 0.$$

Integration of equations (2.44) to (2.50) is carried out by one of the methods for numerical integration of differential equations, using electronic computers.

Let us examine the system of the simplest method of numerical integration -- the Euler method. Equations (2.44)-(2.50) may be given the following general form:

$$\begin{aligned} \dot{v} &= f_1(t, y, v, \theta); \\ \dot{\theta} &= f_2(t, y, v, \theta, \alpha, \delta); \\ \dot{\delta} &= f_3(t, y, v, \alpha, \varphi, \ddot{\varphi}); \\ \varphi &= \varphi_{\text{prog}}(t); \\ \dot{x} &= f_4(v, \theta); \\ \dot{y} &= f_5(v, \theta); \\ \alpha &= \varphi - \theta \end{aligned}$$

At the initial moment with vertical start we have:

$$t_0 = 0; x_0 = 0; y_0 = 0; v_0 = 0; \theta_0 = \frac{\pi}{2};$$

$$\alpha_0 = 0; \delta_0 = 0; \varphi_0 = \theta_0 = \frac{\pi}{2}.$$

Taking as point of departure the initial conditions, we find the values  $v_0, \theta_0, x_0, y_0$ . In the section of vertical start  $\dot{\varphi}_0$  and  $\ddot{\varphi}_0$  are equal to zero.

We select an interval (spacing) small enough so that the derivatives  $v, \theta, x, y$  over this interval may be regarded as being constant and equal to their initial values. When this is done we get for the end of the interval

$$t_1 = t_0 + \Delta t;$$

$$v_1 = v_0 \Delta t;$$

$$\theta_1 = \frac{\pi}{2};$$

$$y_1 = y_0 \Delta t;$$

$$\varphi_1 = \frac{\pi}{2}.$$

The quantities  $x, \alpha$  and  $\delta$  retain zero values over the entire vertical part of the trajectory.

Substituting the values  $v_1, \theta_1, y_1, \varphi_1$  in equations (2.44)-(2.50), we get the values of the derivatives  $\dot{v}_1, \dot{\theta}_1, \dot{y}_1$ , and analogously to the foregoing, we get the values of the functions we are seeking when  $t = t_2 = t_1 + \Delta t$ .

On the curvilinear part of the trajectory  $\dot{\varphi}$  and  $\ddot{\varphi}$  are found by numerical differentiation as functions of  $\varphi(t)$ ,  $\alpha$  is determined from equation (2.50),  $\delta$  is determined from equation (2.46). Integration of the derivatives via sequential addition of increments of the functions sought is carried out up to the end of the active section.

The system of numerical integration according to the Euler method which has just been examined boils down essentially to breaking down the functions sought into Taylor series and retaining the terms of first order relative to the interval  $\Delta t$ . Such a method of calculation is exact only with a very small interval of integration  $\Delta t$ . In practice methods of calculation are used in which terms of an expansion (or final remainders) of a higher order are used. Among these are the Adams-Krylov method, the Runge-Kitt method, and others, which are set forth in special manuals.

In Figure 2.15 we show the elements of the active section of the trajectory of a V-2 rocket. One must devote attention to the course of the alteration in frontal resistance  $X$  along the trajectory. As a consequence of increase in velocity, the frontal resistance rises sharply to begin with. From there on reduction in the density of the air with altitude becomes a determining factor, and later a maximum is achieved, about 5,000 kg, frontal resistance steadily declines.

Let us examine the character of change in the angle of attack in the active part of the trajectory, taking equation (2.45) as point of departure. For approximate calculations one may eliminate from it the last term on the right-hand side. When this is done, taking into account that along the trajectory angle  $\theta$  is such that  $\dot{\theta} = -|\dot{\theta}|$ , we get

$$\alpha = \frac{m}{P + Y^\alpha} (g \cos \theta - v|\dot{\theta}|). \quad (2.51)$$

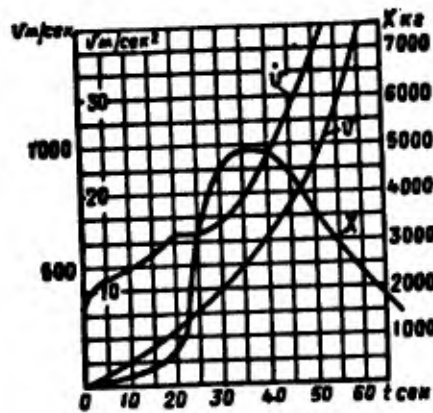


Figure 2.15. Elements of active trajectory of V-2 rocket.

On the first vertical section of the trajectory

$$\theta = \frac{\pi}{2}, \quad |\dot{\theta}| = 0$$

Under these circumstances  $\alpha = 0$ . The axis of the rocket and the vector of velocity coincide.

At the beginning of the curvilinear section the angle  $\theta$  is close in magnitude to  $\pi/2$  and one may adopt  $\cos \theta \approx 0$ .

Under these circumstances

$$\alpha \approx - \frac{mv |\dot{\theta}|}{P + Y^\alpha} < 0.$$

The nose part of the rocket inclines away from the vector of velocity of the rocket downward (in the direction of movement of the rocket).

In the inclined rectilinear section  $|\dot{\theta}| = 0$ ; here we get

$$\alpha = \frac{mg \cos \theta}{P + Y^\alpha} > 0.$$

The nose part of the rocket inclines upward from the direction of the vector of velocity.

A graph of change in the angle of attack along the active section of the trajectory for the V-2 rocket is shown in Figure 2.16.



Figure 2.16. Change in angle of attack along active section of trajectory.

2.7. Approximate Calculation of Elements of Active Section of Trajectory by the Method of Successive Integration

For approximate calculations of the active section of trajectories, considering the small size of the angle of attack  $\alpha$ , we take  $\theta \approx \varphi$ . When this is done we can consider as given the program of change in the angle  $\theta$  of incline of the vector of velocity to the horizon

$$\theta(t) = \theta_{ap}(t) \approx \varphi_{np}(t)$$

and the equations which determine movement of the center of mass of the rocket can be integrated independently of equation (2.46).

The equations for movement of the center of mass of the rocket assume the following form:

$$\dot{v} = \frac{P - X}{m(t)} - g \sin \theta; \quad (2.52)$$

$$\dot{y} = v \sin \theta; \quad (2.53)$$

$$\dot{x} = v \cos \theta; \quad (2.54)$$

$$\theta = \theta_{ap}(t),$$

where

$$\begin{aligned} P &= \frac{U_{cen} v_{ra}}{g} + F_a(p_a - p_{H0}) = \\ &= \frac{Q_{cen} v_{ra}}{g} + F_a(p_a - p_{H0}) + F_a(p_{H0} - p_H) = P_0 + F_a(p_{H0} - p_H). \end{aligned}$$

We introduce the notation

$$\kappa(y) = \frac{p_H}{p_{H0}},$$

where the function  $\kappa(y)$  determines the law of change of atmospheric pressure with altitude which has been adopted as standard. Taking into account the expression for the Mach figure  $M = v/a$ , and that for the velocity of sound

$$a^2 = \frac{kp}{\rho} = kgRT$$

and designating  $K = \frac{kpH_0}{2}$ ,

we can write:

$$P = P_0 + F_a p_{H_0} [1 - \pi(y)]; \quad (2.55)$$

$$X = t \frac{v^2}{2} S c_x = iKS\pi(y) M^2 c_x(M). \quad (2.56)$$

The weight of the rocket at any moment of time is determined from the expression

$$Q = Q_0 - G_{cen} t = Q_0 (1 - \mu),$$

where  $\mu = \frac{G_{cen} t}{Q_0}$ .

Equation (2.52) may be transcribed in the form

$$\frac{Q_0(1-\mu)}{g} \dot{v} = P_0 + F_a p_{H_0} [1 - \pi(y)] - iKS\pi(y) M^2 c_x - Q_0(1-\mu) \sin \theta$$

or

$$\frac{Q_0}{gP_0} \dot{v} = \frac{1}{1-\mu} + \frac{F_a p_{H_0}}{P_0} \cdot \frac{1-\pi(y)}{1-\mu} - \frac{iKS\pi(y)}{P_0(1-\mu)} M^2 c_x - \frac{Q_0}{P_0} \sin \theta. \quad (2.57)$$

Let us proceed from the independent variable  $t$  to the variable  $\mu$ . Here

$$\dot{v} = \frac{dv}{d\mu} \dot{\mu} = \frac{dv}{d\mu} \cdot \frac{G_{cen}}{Q_0}$$

and the left-hand part of equation (2.57) assumes the form

$$\frac{Q_0}{gP_0} \dot{v} = \frac{G_{cen}}{gP_0} \cdot \frac{dv}{d\mu}$$

From here on we shall designate by an apostrophe (') the derivative from  $\mu$ .

Starting with the expression

$$P_0 = \frac{G_{cen}}{g} u_0 = G_{cen} J_{10}$$

(where  $u_e$  is the effective velocity of escape) and introducing into the consideration the dimensionless velocity of the rocket  $w$ , determined from the expression  $w = v/u_e$ , we get equation (2.57) in the following form:

$$w' = \frac{1}{1-\mu} - \frac{1}{\eta} \sin \theta + A \frac{1-\pi(y)}{1-\mu} - B \frac{\pi(y) M^2 c_x}{1-\mu}, \quad (2.58)$$

where

$$A = \frac{F_{a0} H_0}{P_0}; \quad (2.59)$$

$$B = \frac{K S}{P_0}; \quad (2.60)$$

$$\eta = \frac{P_0}{Q_0}. \quad (2.61)$$

Equations (2.53) and (2.54) assume the form:

$$y' = Dw \sin \theta; \quad (2.62)$$

$$x' = Dw \cos \theta, \quad (2.63)$$

where

$$D = \frac{u_e^2}{g \eta} = \frac{g H_0}{\eta}. \quad (2.64)$$

Let us examine the right-hand part of equation (2.58). The first term characterizes the thrust of the rocket at the ground, the second the force of gravity. Basically these terms determine the maximum velocity of the rocket, and will be taken into account in first approximation from here on. The third and fourth terms, characterizing change in thrust with altitude, and air resistance, will be regarded as correction terms and will be taken into account in second approximation.

#### Solution of the First Approximation

Integrating equation (2.58) in first approximation and taking  $\mu = 0; w = 0$  for the moment of start we secure

$$w = \ln \frac{1}{1-\mu} - \frac{1}{\eta} \int_0^\mu \sin \theta d\mu. \quad (2.65)$$

Inasmuch as the relative consumption  $\mu$  is a known function of time, the program value  $\theta = \theta_{np}(t)$  may be regarded as a known function of  $\mu$ .

Indicating

$$U_1(\mu) = \ln \frac{1}{1-\mu}; \quad (2.66)$$

$$U_2(\mu) = \int_0^\mu \sin \theta d\mu, \quad (2.67)$$

we get a solution for velocity in first approximation in the form

$$\tilde{v} = \frac{\tilde{v}}{u_0} = U_1(\mu) - \frac{1}{\eta} U_2(\mu). \quad (2.68)$$

We shall designate the solution in first approximation by means of the symbol ( $\sim$ ).

In the table of Annex 2 values are given for the function which  $\theta(\mu)$  correspond to the program of the V-2 rocket. We shall adopt this function as typical from here on.

Values of  $U_1(\mu)$  and  $U_2(\mu)$  are set forth in the same table.

Maximum velocity of the rocket is determined according to formula (2.68), starting from the value

$$v_{max} = \frac{w_{TOT}}{Q_0}.$$

For determination of the x, y coordinates of the center of mass of the rocket it is necessary to integrate equations (2.62) and (2.63) taking expression (2.68) into account. In doing this we secure:

$$\tilde{y} = D \left[ U_2(\mu) - \frac{1}{\eta} U_1(\mu) \right]; \quad (2.69)$$

$$\tilde{x} = D \left[ U_1(\mu) - \frac{1}{\eta} U_2(\mu) \right], \quad (2.70)$$

where

$$U_3(\mu) = \int_0^\mu U_1 \cdot \sin \theta d\mu; \quad (2.71)$$

$$U_4(\mu) = \int_0^\mu U_2 \sin \theta d\mu; \quad (2.72)$$

$$U_5(\mu) = \int_0^\mu U_1 \cos \theta d\mu; \quad (2.73)$$

$$U_6(\mu) = \int_0^\mu U_2 \cos \theta d\mu. \quad (2.74)$$

The values  $U_3--U_6$  are given in the tables in Annex 2. We may remark that the functions  $U_3--U_6$  may be regarded as depending upon one argument of  $\mu$  if one starts from the type program  $\theta_{np}(\mu)$ . It is not difficult to see that

$$U_4(\mu) = \frac{1}{2} [U_3(\mu)]^2.$$

### Solution of the Second Approximation

Integration of equation (2.58) in section approximation is carried out taking into account the terms characterizing change of thrust with altitude, and frontal resistance. In this process we secure:

$$w = U_1(\mu) - \frac{1}{\eta} U_3(\mu) + A \int_0^{\mu} \frac{1 - \pi(y)}{1 - \mu} d\mu - B \int_0^{\mu} \frac{\pi(y) M^2 c_x}{1 - \mu} d\mu$$

or

$$w = U_1(\mu) - \frac{1}{\eta} U_3(\mu) + A\Phi_1(\mu, u_e, \eta) - B\Phi_2(\mu, u_e, \eta),$$

where

$$\Phi_1(\mu, u_e, \eta) = \int_0^{\mu} \frac{1 - \pi(y)}{1 - \tilde{\mu}} d\mu; \quad (2.75)$$

$$\Phi_2(\mu, u_e, \eta) = \int_0^{\mu} \frac{\pi(y) M^2 c_x}{1 - \mu} d\mu. \quad (2.76)$$

In the expression under the integral for  $\Phi_1$ ,  $\pi(y)$  enters, characterizing the change of atmospheric pressure with altitude. In addition, in the expression for  $\Phi_2$  there enters

$$M = \frac{v}{a} \text{ и } c_x(M),$$

depending on the velocity of the rocket  $v$  and upon the speed of sound  $a$ , which changes with altitude. Inasmuch as the terms containing  $\Phi_1$  and  $\Phi_2$  assume the role of corrections to the basic terms, in figuring them out one can take into account the values  $v$  and  $a$  from the solution for the first approximation. From expressions (2.68) and (2.69) it is apparent that

$$\tilde{y} = f(\mu, \eta, D) = \varphi_1(\mu, \eta, u_e);$$

$$\tilde{v} = \varphi_2(\mu, \eta, u_e).$$

Thus the functions  $\Phi_1$  and  $\Phi_2$  depend on two further parameters:  $\eta$  and  $u_e$ . In figuring out the functions  $\Phi_2$  the type function  $c_x(M)$  set forth in Table 2.1 has been adopted. The distinction between the concrete function  $c_x$  of a given object and the type function may be taken into account through the magnitude of a coefficient of form  $i$  forming part of expression (2.60) for parameter B.

Integrating equations (2.62) and (2.63) in second approximation, we secure

$$y = D \left( \mu_0 - \frac{1}{\eta} \mu_1 \right) + A\Phi_1 - B\Phi_2;$$

$$x = D \left( \mu_1 - \frac{1}{\eta} \mu_0 \right) + A\Phi_2 - B\Phi_1.$$

where

$$\Phi_1 = D \int_0^{\mu} \Phi_1 \sin \theta d\mu; \quad (2.77)$$

$$\Phi_2 = D \int_0^{\mu} \Phi_2 \sin \theta d\mu; \quad (2.78)$$

$$\Phi_3 = D \int_0^{\mu} \Phi_1 \cos \theta d\mu; \quad (2.79)$$

$$\Phi_4 = D \int_0^{\mu} \Phi_2 \cos \theta d\mu. \quad (2.80)$$

In view of the fact that upon calculating the coordinates of points of the active section of the trajectory the required accuracy is relatively less than the accuracy for calculating velocity, from here on we shall start from the approximate relations:

$$y = \bar{y} \frac{w}{w}; \quad x = \bar{x} \frac{w}{w}$$

The type program  $\theta_{np}$  adopted in setting up the tables for the function  $\mu_2(\mu)$  and set forth in Annex 2 corresponds to the value of the angle  $\theta$  on the final rectilinear portion of the active section of the trajectory ( $\theta_k = 42^\circ 50'$ ). Under real conditions the angle is selected by starting from the requirements of securing maximum range and minimum spread in the passive section of the trajectory, and it can vary within considerable limits.

Change in velocity  $v_k$  depending on change in angle  $\theta_k$  can be determined approximately if one assumes that the entire active part of the trajectory turns in its plane as a solid both at an angle  $\delta\theta_k$ . In this case, differentiating expression (2.68) according to parameter  $\theta$  and taking into account the fact that for any point on the trajectory  $\delta\theta = \delta\theta_k$ , we secure

$$\delta w = -\frac{1}{\eta} \delta U_3(\mu) = -\frac{1}{\eta} \delta \theta_k \int_0^{\theta} \cos \theta d\mu$$

or finally

$$\delta w = -\frac{1}{\eta} U_7(\mu) \delta \theta_k, \quad (2.81)$$

where

$$U_7(\mu) = \int_0^{\theta} \cos \theta d\mu. \quad (2.82)$$

Finally the system of approximate calculation of the elements of the active section of the trajectory assumes the following form.

First approximation:

$$\begin{aligned} \tilde{w} = \frac{\tilde{v}}{u_0} &= U_1 - \frac{1}{\eta} U_2; \\ \tilde{y} &= D \left[ U_3 - \frac{1}{\eta} U_4 \right]; \\ \tilde{x} &= D \left[ U_5 - \frac{1}{\eta} U_6 \right], \end{aligned}$$

where

$$D = \frac{u_0^2}{g\eta}; \quad \eta = \frac{P_0}{Q_0}.$$

The functions  $U_1-U_6$  are determined from the table of Annex 2.

Second approximation:

$$\begin{aligned} w &= \tilde{w} + A\Phi_1(\mu, u_0, \eta) - B\Phi_2(\mu, u_0, \eta); \\ y &= \tilde{y} \frac{w}{\tilde{w}}; \\ x &= \tilde{x} \frac{w}{\tilde{w}}, \end{aligned}$$

where

$$A = \frac{F_a P_{H0}}{P_0}; \quad B = \frac{IKS}{P_0} = 7140 \frac{IS}{P_0}.$$

Analysis of graphs of function  $\Phi_1$  shows that it depends only slightly on  $u_e$  and  $\eta$  and may be expressed by the interpolational formula

$$\Phi_1 = \frac{\mu^2 (1 - 0,7\mu)}{1,05 - \mu} \quad (2.83)$$

Graphs for function  $\Phi_2(\mu, u_e, \eta)$  are given in Annex 3.

Let us examine an example of the calculation of the elements of the active section of the trajectory for the following characteristics of rocket:

Caliber  $D = 1.65 \text{ m}$  ( $S = 2.14 \text{ m}^2$ )

Initial weight of rocket  $Q_0 = 13,300 \text{ kg}$

Thrust of rocket at ground  $P_0 = 26,600 \text{ kg}$

Weight of burning fuel  $w_{\text{ron}} = 8650 \text{ kg}$

Area of outlet cross-section of cone  $F_a = 0.43 \text{ m}^2$

Effective velocity of escape  $u_e = 1,920 \text{ m/sec}$

Coefficient of form of rocket, adjusted to function  $c_x$  set forth in Table 2.2,  $i = 1.4$

Coefficient of power armament  $\eta = \frac{P_0}{Q_0} = 2$

Normal atmospheric pressure at ground  $p_{\text{norm}} = 1.02 \text{ kg/cm}^2$

Calculation of constant parameters:

$$A = \frac{F_a p_{\text{H0}}}{P_0} = \frac{0,43 \cdot 1,02 \cdot 10^4}{26600} = 0,165.$$

$$B = K \frac{iS}{P_0} = 7140 \frac{1,4 \cdot 2,14}{26600} = 0,802.$$

$$D = \frac{u_e^2}{g\eta} = \frac{1920^2}{9,81 \cdot 2} = 1,88 \cdot 10^5.$$

We determine the maximum velocity of the rocket and the coordinates of the end of the active section of the trajectory upon consumption of the fuel  $w_{\text{ron}} = 8700 \text{ kg}$ .

In this connection

$$\mu = \mu_x = \frac{w_{\text{ron}}}{Q_0} = \frac{8650}{13300} = 0,65.$$

We determine the values of functions  $U_1 - U_6$  according to the tables of Annex 2:

$$\begin{aligned} U_1 &= 1,0499; & U_2 &= 0,5412; & U_3 &= 0,2127; \\ U_4 &= 0,1464; & U_5 &= 0,1793; & U_6 &= 0,1162. \end{aligned}$$

Calculation of the first approximation:

$$\tilde{w} = \Pi_1 - \frac{1}{\eta} \Pi_2 = 1,0499 - 0,5 \cdot 0,5412 = 0,7793;$$

$$\tilde{v} = \tilde{w} \cdot u_0 = 0,7793 \cdot 1920 = 1493 \text{ м/сек};$$

$$\tilde{y} = D \left[ \Pi_3 - \frac{1}{\eta} \Pi_4 \right] = 1,88 \cdot 10^4 [0,2127 - 0,5 \cdot 0,1464] = 26230 \text{ м};$$

$$\tilde{x} = D \left[ \Pi_5 - \frac{1}{\eta} \Pi_6 \right] = 1,88 \cdot 10^4 [0,1793 - 0,5 \cdot 0,1162] = 22790 \text{ м}.$$

Calculation of the second approximation:

According to formula (2.57) we find that

$$\Phi_1 = \frac{0,65^2 (1 - 0,7 \cdot 0,65)}{1,05 - 0,65} = 0,575.$$

From the graph for functions  $\Phi_2$  we find  $\Phi_2 = 0,137$ .

We calculate the second approximation:

$$w = \tilde{w} + A\Phi_1 - B\Phi_2 = 0,7793 + 0,165 \cdot 0,575 - 0,802 \cdot 0,137 = 0,7643;$$

$$v = w \cdot u_0 = 0,7643 \cdot 1920 = 1468 \text{ м/сек};$$

$$y = \tilde{y} \frac{w}{\tilde{w}} = 26230 \frac{0,7643}{0,7793} = 25720 \text{ м};$$

$$x = \tilde{x} \frac{w}{\tilde{w}} = 22790 \frac{0,7643}{0,7793} = 22360 \text{ м}.$$

## 2.8. Calculation of the Initial Passive Section of the Trajectory, by Arcs

If the end of the active section of the trajectory lies at a great altitude, where air resistance may be disregarded, the passive section of the trajectory is calculated according to formulas for elliptical trajectories in a vacuum. But if the end of the active section lies at a relatively low altitude, the initial portion of the passive section is calculated while taking into account air resistance.

We write the acceleration of the force of frontal resistance in the form

$$J_R = \frac{1g}{Q_n} \frac{\rho v^2}{2} S C_x \quad (2.84)$$

Substituting the caliber for the area of the middle

$$S = \frac{\pi D^2}{4}$$

and replacing the density of the air  $\rho$  by the function  $H(y)$

$$\rho = \rho_0 H(y),$$

we get

$$J_R = 4.74 \cdot 10^{-4} c H(y) v^2 c_x,$$

where

$$c = \frac{ID^2}{Q_x} 1000$$

the magnitude of the ballistic coefficient adopted in ballistics.

From here on we shall introduce the quantity  $c_1 = 4.74 \cdot 10^{-4} c$ .

The equations for movement of the rocket assume the form:

$$\dot{v} = -c_1 H(y) v^2 c_x - g \sin \theta;$$

$$\dot{\theta} = -\frac{g \cos \theta}{v};$$

$$\dot{y} = v \sin \theta;$$

$$\dot{x} = v \cos \theta.$$

From here on it will be convenient to change over to the independent variable  $y$ . When we do this the equations for movement take on the following form:

$$v' = -\frac{c_1 H(y) v c_x}{\sin \theta} - \frac{g}{v}; \quad (2.85)$$

$$v' = -\frac{g}{v^2 \operatorname{tg} \theta}; \quad (2.86)$$

$$x' = \frac{1}{\operatorname{tg} \theta}. \quad (2.87)$$

Let us expand  $v$ ,  $\theta$ , and  $x$  in series by stages  $\Delta y$  and let us preserve the first stages of these quantities:

$$v = v_x - \left( \frac{c_1 H v c_x}{\sin \theta} + \frac{g}{v} \right)_{c_p} \Delta y \quad (2.88)$$

$$\theta = \theta_x - \left( \frac{g}{v^2 \operatorname{tg} \theta} \right)_{c_p} \Delta y; \quad (2.89)$$

$$x = x_k + \frac{1}{\operatorname{tg} \theta_{cp}} \Delta y, \quad (2.90)$$

where  $\Delta y = y - y_k$ .

Calculation according to formulas (2.88)-(2.90) is carried out through two approximations. In the first approximation the mean values  $y$ ,  $v$ , and  $\theta$  are taken as being equal to the values of these quantities at the start of the portion being examined.

In the second approximation we take it that:

$$v_{cp} = \frac{v_k + v}{2}; \quad \theta_{cp} = \frac{\theta_k + \theta}{2}; \quad y_{cp} = \frac{y_k + y}{2}.$$

Comparison of calculations by the method indicated with calculations by the numerical integration method shows that for  $\Delta y > 5 \text{ km}$  more accurate results are found in this case, if  $y_{\text{mean}}$  is determined as a mean integral from the expression

$$H(y_{cp}) = \frac{1}{\Delta y} \int_{y_k}^y H(y) dy = \frac{1}{\Delta y} [H_1(y_k) - H_1(y)], \quad (2.91)$$

where

$$H_1(y) = \int_y^h H(y) dy,$$

$h$  is a value of  $y$  sufficiently great for one to take  $H(h) = 0$ .

The values  $H_1(y)$  are given in Table 2.2, for which  $h = 50 \text{ km}$  has been adopted.

Let us examine the case where the end of the active section of the trajectory is at altitude  $y_k = 10 \text{ km}$ .

Under these circumstances  $v_k = 2,000$  meters per second,  $\theta_k = 40^\circ$ ,  $Q_k = 4,000 \text{ kg}$ ,  $D = 1.65$  meters,  $i = 1.07$ , whereupon

$$c_1 = 4,74 \cdot 10^{-4} c = 0,474 \cdot 1,07 \frac{1,65^3}{4000} = 0,345 \cdot 10^{-4}.$$

The Mach number is determined from the expression

$$M = \frac{v}{a} = \frac{v}{a_{H_0}} \frac{a_{H_0}}{a} = \frac{v}{340} \sqrt{\frac{T_{H_0}}{T}}$$

Table 2.2

$y_{km}$	$H_1(y)$	$\Delta$	$10^{-5} \cdot H_2(y)$	$\Delta$	$10^{-9} \cdot H_3(y)$	$\Delta$
50	0		0			
45	4		0			
40	15		1			
35	38		2			
30	89	16	5	0	0	1
29	105	18	5	1	1	0
28	123	21	6	1	1	1
27	144	25	8	1	2	1
26	169	30	9	2	3	1
25	199	34	11	2	4	1
24	233	40	13	2	5	1
23	273	47	15	3	6	2
22	320	55	18	4	8	2
21	375	64	22	4	10	2
20	439	76	26	5	12	3
19	515	88	31	5	15	4
18	603	103	36	7	19	3
17	706	120	43	7	22	5
16	826	141	50	9	27	5
15	967	164	59	11	32	7
14	1131	192	70	12	39	7
13	1323	225	82	14	46	9
12	1548	262	96	17	55	11
11	1810	302	113	20	66	12
10	2112	344	133	22	78	15
9	2456	388	155	26	93	16
8	2844	438	181	27	109	20
7	3282	494	208	35	129	22
6	3776	554	243	41	151	27
5	4330	620	284	56	178	31
4	4950	693	330	61	209	36
3	5643	771	391	60	245	42
2	6414	856	451	68	287	48
1	7270	950	519	78	335	56
0	8220		597		391	

The index "H0" corresponds to normal conditions at the ground. Like  $H(y)$ ,  $\sqrt{T_{H0}:T}$  is determined according to the table of Annex 1. For altitude  $y_k = 10$  km we have

$$M_x = \frac{v_x}{340} \sqrt{\frac{T_{H0}}{T}} = \frac{2000}{340} 1,118 = 6,56$$

The value of  $c_x$  is determined according to Table 2.1. For values of  $M > 5$  we take  $c_x$  as a constant equal to 0.115.

In Table 2.3 there are set forth the results of calculation of the passive section of the trajectory for altitudes in the 10-30 km interval by the method of numerical integration. The  $x$  coordinate is figured from the end of the active section.

For comparison we calculate by the approximate method set forth above the values for  $v$ ,  $\theta$ ,  $x$  for  $y = 20$  km, taking as starting point the values of these quantities for  $y = 10$  km.

Table 2.3

$y_{км}$	$v$	$\theta^\circ$	$x$	$y_{км}$	$v$	$\theta^\circ$	$x$
10	2000	40,00	0	20	1750	37,96	12323
11	1958	39,83	1194	21	1737	37,72	13609
12	1921	39,65	2397	22	1725	37,48	14906
13	1889	39,46	3606	23	1714	37,23	16216
14	1862	39,27	4821	24	1704	36,98	17538
15	1837	39,07	6046	25	1694	36,72	18872
16	1815	38,86	7282	26	1685	36,46	20218
17	1796	38,64	8528	27	1676	36,19	21579
18	1779	38,42	9783	28	1668	35,92	22953
19	1764	38,19	11048	29	1660	35,64	24341
20	1750	37,96	12323	30	1652	35,36	25745

Calculation of first approximation:

We determine  $H(y_{\text{mean}})$  from expression (2.91), having determined  $H_1(y)$  from Table 2.2:

$$H(y_{\text{cp}}) = \frac{1}{\Delta y} [H_1(10) - H_1(20)] = \frac{2112 - 439}{10000} = 0,167.$$

We calculate  $\Delta v$  according to formula (2.88):

$$\Delta \tilde{v} = - \left( \frac{c_1 H_{\text{cp}} v_{\text{к}} c_x}{\sin \theta_{\text{к}}} + \frac{g}{v_{\text{к}}} \right) \Delta y = - \left( \frac{0,345 \cdot 10^{-3} \cdot 0,167 \cdot 2000 \cdot 0,115}{0,643} + \frac{9,81}{2000} \right) 10000 = -256;$$

$$\tilde{v} = 2000 - 256 = 1744 \text{ м/сек};$$

$$\tilde{v}_{\text{cp}} = \frac{v_{\text{к}} + \tilde{v}}{2} = 1872 \text{ м/сек}.$$

According to formula (2.89) we have:

$$\Delta \theta^\circ = -\Delta \theta \frac{180}{\pi} = -\frac{180}{\pi} \frac{g}{v_{\text{cp}}^2 \lg \theta_{\text{cp}}} \Delta y.$$

or

$$\Delta \theta^\circ = -\frac{562 \Delta y}{v_{\text{cp}}^2 \lg \theta_{\text{cp}}} = -\frac{562 \cdot 10000}{1872^2 \cdot 0,839} = -1,91^\circ;$$

$$\tilde{\theta} = 40,00^\circ - 1,91^\circ = 38,09^\circ = 38^\circ 5';$$

$$\theta_{\text{cp}} = 39^\circ 2'$$

We designate the value of the first approximation by means of the symbol ( $\sim$ ).

Calculation of the second approximation:

$$\Delta v = - \left( \frac{c_1 H_{cp} v_{cp} c_x}{\sin \theta_{cp}} + \frac{g}{v_{cp}} \right) \Delta y =$$

$$= - \left( \frac{0,345 \cdot 10^{-1} \cdot 0,167 \cdot 1872 \cdot 0,115}{0,630} + \frac{9,81}{1872} \right) 10000 = -250 \text{ м/сек};$$

$$v = 1750 \text{ м/сек}; v_{cp} = 1875 \text{ м/сек};$$

$$\Delta \theta = - \frac{562 \cdot \Delta y}{v_{cp}^2 \operatorname{tg} \theta} = - \frac{562 \cdot 10000}{1875^2 \cdot 0,810} = -1,98^\circ;$$

$$\theta_1 = 38,02^\circ = 38^\circ 1'.$$

We determine from the expression:

$$\Delta x = \frac{\Delta y}{\operatorname{tg} \theta_{cp}} = \frac{10000}{0,810} = 12350 \text{ м}.$$

Analogous calculations by the approximate method are carried out for the section of the trajectory from  $y = 15$  km to  $y = 25$  km and from  $y = 15$  km to  $y = 30$  km. Comparative results of calculations by the method of numerical integration and the approximate method are set forth in Table 2.4.

Table 2.4

Интервалы высот, км (1)	$v_0$	$\theta_0$	$x_0$	Метод расчета (2)	$v$	$\theta$	$x$
10—20	2000	40°0'	0	(3) Первое приближение	1744	38°5'	—
				(4) Второе приближение	1750	38°1'	12350
				(5) Численное интегрирование	1750	37°58'	12323
15—25	1837	39°4'	6046	(3) Первое приближение	1694	36°51'	—
				(4) Второе приближение	1693	36°46'	18860
				(5) Численное интегрирование	1694	36°43'	18872
15—30	1837	39°4'	6046	(3) Первое приближение	1653	35°41'	—
				(4) Второе приближение	1651	35°26'	25764
				(5) Численное интегрирование	1652	35°20'	25745

Key: 1 -- Intervals of altitude      4 -- Second approximation  
 2 -- Method of calculation      5 -- Numerical integration  
 3 -- First approximation

2.9. Movement of the Rocket on the Passive Airless Section of the Trajectory in the Central Field of the Earth's Attraction

Assuming that for altitudes  $y$  greater than  $h$  air resistance may be disregarded, we shall examine the movement of the rocket in the central field of attraction outside a sphere of radius  $r_0 = R + h$ , where  $R$  is the radius of the earth (Figure 2.17). In doing so we shall take into account change in the magnitude of acceleration of the gravitational attraction of the earth for the central field of attraction

$$g = g_0 \frac{r_0^2}{r^2} \quad (2.92)$$

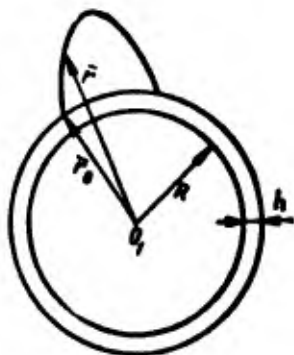


Figure 2.17. Diagram of elliptical trajectory.

In the present section we shall examine the movement of the rocket relative to a nonrotating earth. In this case it is not necessary to consider the centrifugal force of inertia from the translational movement of the earth. We examine inclusion of the rotation of the earth in 2.15.

The position of a moving material point relative to the center of the earth will be determined in polar coordinates. In Figure 2.18  $\vec{O_1O} = \vec{r}_0$ , the radius-vector of the initial point, and  $\vec{O_1M} = \vec{r}$ , the radius-vector of any point on the trajectory,  $\eta$  is the polar angle measured relative to an axis the position of which we shall define below,  $\theta$  is the angle of inclination of the vector of velocity to the local horizon of the moving point (a plane perpendicular to the radius-vector  $\vec{r}$ ).

For derivation of the equation of the trajectory we shall make use of the theorem of kinetic moment and the theorem of the kinetic energy of a point.

The theorem of kinetic moment:

According to this theorem, a derivative according to time from the moment of the quantity of movement of a point relative to some center is equal to the moment of the force operating on the point relative to the same center. In the present case, applying this theorem relative to the center of the earth  $O_1$ , we get

$$\frac{d}{dt} \bar{m}_0 (m\bar{v}) = \bar{m}_0 (\bar{F})$$

or

$$\frac{d}{dt} (\bar{r} \times m\bar{v}) = \bar{r} \times \bar{F}.$$

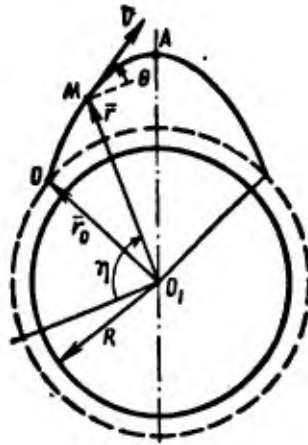


Figure 2.18. Polar coordinates of the points of an elliptical trajectory.

For the central force of attraction of the earth we have  $\bar{r} \times \bar{F} = 0$ , whence:

$$\begin{aligned} \bar{r} \times m\bar{v} &= \text{const}; \\ r\dot{\theta} \cos \theta &= \text{const}. \end{aligned} \quad (2.93)$$

The constituent of the velocity which is perpendicular to the radius-vector is equal to

$$v_{\perp} = r\dot{\theta} = v \cos \theta. \quad (2.94)$$

From expressions (2.93) and (2.94) we have

$$r^2 \dot{\theta} = c = \text{const}. \quad (2.95)$$

The constant  $c$  is found from the initial conditions. At the initial point  $O$  we have

$$c = r_0^2 \dot{\theta}_0 = r_0 v_0 \cos \theta_0. \quad (2.96)$$

For a geometrical interpretation of expression (2.96) let us examine an elementary triangle  $MM_1O_1$  (Figure 2.19). The area of this triangle is equal to

$$d\sigma = \frac{1}{2} h \dot{dS} = \frac{1}{2} r \cos \theta \cdot v dt = \frac{1}{2} r^2 \dot{\eta} dt.$$

Taking into account expression (2.95) we get

$$\frac{d\sigma}{dt} = \frac{1}{2} c = \text{const},$$

$$\Delta\sigma = \frac{1}{2} c \Delta t.$$

The last relation expresses the law of preservation of areas. Upon movement under the operation of a central force the radius-vector of a moving point describes equal areas in equal intervals of time.

The theorem of kinetic energy:

From the equation for movement relative to a tangent

$$m\dot{v} = -mg \sin \theta$$

and expression (2.92), considering that

$$\sin \theta = \frac{v_r}{v} = \frac{\dot{r}}{v} = \frac{dr}{dS},$$

we get:

$$\dot{v} = -g_0 \frac{r_0^2}{r^2} \frac{dr}{dS};$$

$$v dS = v dv = -g_0 r_0^2 \frac{dr}{r^2}.$$

Integrating within limits from the initial to any chosen point of the trajectory we get

$$v^2 = v_0^2 - 2g_0 r_0^2 \left( \frac{1}{r_0} - \frac{1}{r} \right). \quad (2.97)$$

In the event of vertical flight the maximum altitude is found from the condition  $v = 0$ .

Under these circumstances we have

$$v_0^2 = 2g_0 r_0^2 \left( \frac{1}{r_0} - \frac{1}{r_{\max}} \right) = 2g_0 r_0 \left( 1 - \frac{r_0}{r_{\max}} \right). \quad (2.98)$$

From here on it is convenient to introduce into the consideration the parameter of velocity  $v$ , determined from the expression

$$v = \frac{v_0^2}{g_0 r_0}. \quad (2.99)$$

When we do this expression (2.98) assumes the form

$$v = 2 \left( 1 - \frac{r_0}{r_{\max}} \right).$$

In order that a material point may infinitely recede from the earth, overcoming the "gravitational armor," it is necessary to start from a condition  $r_{\max} = \text{infinity}$ , whence  $v = 2$ . Here  $v_0^2 = 2g_0 r_0$ .

For values  $g_0 = 9.81$  meters per second per second,  $r_0 = 6,371 \cdot 10^6$  m, we secure

$$v_0 = \sqrt{2 \cdot 9.81 \cdot 6,371 \cdot 10^6} = 11200 \text{ m/sec}$$

This is the so-called second cosmic velocity necessary so that a body, overcoming the attraction of the earth, may be converted into an artificial planet of the solar system.

The first cosmic velocity corresponds to  $v = 1$ ; here

$$v_0 = \sqrt{g_0 r_0} = \sqrt{9.81 \cdot 6,371 \cdot 10^6} = 7900 \text{ m/sec}$$

When this velocity is reached the body becomes an artificial satellite of the earth.

The equation of trajectory:

In equations for the constituents of velocity  $v_r = \dot{r}$  and  $v_\theta = r\dot{\eta}$ , we shall transfer to the independent variable  $\eta$ , designating by an apostrophe the derivative according to  $\eta$ .

We furthermore take into account expression (2.95). In doing so we get:

$$v_r = \dot{r} = r' \frac{c}{r^2};$$

$$v_\theta = r\dot{\eta} = \frac{c}{r};$$

$$v^2 = v_r^2 + v_\theta^2 = r'^2 \frac{c^2}{r^4} + \frac{c^2}{r^2}.$$

Designating

$$p = \frac{c}{r},$$

we get

$$v^2 = \dot{\rho}^2 + \rho^2.$$

When this is done expression (2.97) assumes the form

$$\dot{\rho}^2 + \rho^2 = v_0^2 - 2g_0 r_0 + 2g_0 r_0^2 \frac{1}{r}. \quad (2.100)$$

Designating:

$$q = v_0^2 - 2g_0 r_0; \quad (2.101)$$

$$d = \frac{g_0 r_0^2}{c}; \quad (2.102)$$

$$b^2 = q + d^2, \quad (2.103)$$

we get:

$$\rho^2 = b^2 - (\rho - d)^2;$$

$$d\eta = \frac{d\rho}{\sqrt{b^2 - (\rho - d)^2}},$$

whence

$$\eta = - \arccos \frac{\rho - d}{b} + \alpha$$

Substituting the value  $\rho = \frac{c}{r}$ , we get

$$\frac{1}{r} = \frac{b}{c} \cos(\eta - \alpha) + \frac{d}{c} = \frac{d}{c} \left[ 1 + \frac{b}{d} \cos(\eta - \alpha) \right], \quad (2.104)$$

$$r = \frac{\frac{c}{d}}{1 + \frac{b}{d} \cos(\eta - \alpha)}.$$

From analytical geometry we know the equation of a conic section in polar coordinates (ellipse, parabola, hyperbola):

$$r = \frac{p}{1 + e \cos(\eta - \alpha)}, \quad (2.105)$$

where p is the parameter, e the eccentricity.

Comparing expressions (2.104) and (2.105) we see that formula (2.105) is the equation for the movement of a material point in the field of gravitation of the earth. Here:

$$p = \frac{c}{d} = \frac{c^2}{2v_0^2},$$

$$e = \frac{b}{a} = \sqrt{1 + \frac{\eta}{d^2}}$$

Taking into account expressions (2.96), (2.101)-(2.103), and (2.99) we have:

$$p = vr_0 \cos^2 \theta_0 \quad (2.106)$$

$$e = \sqrt{1 - v(2-v) \cos^2 \theta_0} \quad (2.107)$$

Now we shall determine the arbitrary constant  $\alpha$  and at the same time define the position of the axis from which the polar angle  $\eta$  is measured.

We write an equation for  $\operatorname{tg} \theta$  :

$$\operatorname{tg} \theta = \frac{v_r}{v_\theta} = \frac{\dot{r}}{r\dot{\eta}} = \frac{r'}{r}$$

Taking the logarithm and differentiating expression (2.105) we have

$$\frac{r'}{r} = \frac{e \sin(\eta - \alpha)}{1 + e \cos(\eta - \alpha)} = \operatorname{tg} \theta \quad (2.108)$$

Let us select the axis for measurement of angle  $\eta$  so that it will pass from the center of the earth to an apex (point A in Figure 2.18) which is one of the apexes of an ellipse. Since at the apex of the trajectory  $\theta_A = 0$ , then from expression (2.108), considering that  $\eta_A = 0$ , we learn that  $\sin \alpha = 0$ , which corresponds to a value  $\alpha = 0$  or  $\alpha = \pi$ . In order to refine  $\alpha$  we apply expression (2.105) to the point of take-off, assuming that  $0 < \theta < \frac{\pi}{2}$ ; when this is done  $\operatorname{tg} \theta > 0$ , and it follows from

expression (2.108) that with a positive value of eccentricity one must assume that  $\alpha = \pi$ .

Finally we secure an equation for trajectory in the form

$$r = \frac{p}{1 - e \cos \eta} \quad (2.109)$$

Investigation of the character of the trajectory:

From the expression for eccentricity (2.107) it is apparent that:

with  $v < 2$ ;  $e < 1$ ; the trajectory is an ellipse;  
 with  $v = 2$ ;  $e = 1$ ; the trajectory is a parabola;  
 with  $v > 2$ ;  $e > 1$ ; the trajectory is a hyperbola;  
 with  $v = 1$  и  $\theta_0 = 0$ ;  $e = 0$ ; the trajectory is a circle.

The last case corresponds to the movement of a satellite in a circular orbit. Under these circumstances it is assumed that the satellite is released in horizontal direction with initial velocity  $v_0 = \sqrt{g_0 r_0}$  ( $v = 1$ ).

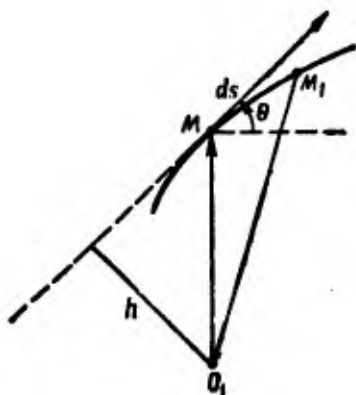


Figure 2.19. Law on the preservation of space.

With  $v < 1$  the trajectory is also an ellipse. But with this, the trajectory will not be a closed curve, since on its course the material point will collide with the surface of the earth. Thus the case  $v < 1$  corresponds to the flight of a rocket of "ground-to-ground" class.

#### 2.10. Range of Flight of a Rocket. The Angle of Greatest Range. Height of Trajectory

At a selected direction of axis of reading angle  $\eta$  the initial point of a trajectory is characterized by polar coordinates  $(r_0; -\beta)$ , and the point of fall by coordinates  $(r_0; \beta)$ , where  $2\beta$  is the angular range of flight (Figure 2.20). The range of flight read off on the curvilinear surface of a sphere of radius  $r_0$  is determined from the expression

$$L = 2\beta r_0 \quad (2.110)$$

The value of  $\beta$  is found from expression (2.109) with the substitution  $\eta = \beta$  and  $r = r_0$ . With this we secure

$$\cos \beta = \frac{r_0 - p}{r_0^2} = \frac{1 - v \cos^2 \theta_0}{\sqrt{1 - v(2 - v) \cos^2 \theta_0}} \quad (2.111)$$

With relatively short ranges (around 200 km) the angle  $\beta < 1^\circ$ . In this case an error in magnitude of  $\cos \beta$  by one unit in the fifth place brings about an error in quantity  $\beta$ , and consequently also in the range, of about 3 percent. For this reason it is convenient to transform expression (2.111) in such fashion that angle  $\beta$  enters beneath the tg or sin sign. We have



$$\operatorname{tg} \theta_0^* = \sqrt{1-v}. \quad (2.114)$$

We shall recall that upon movement of a material point in a constant gravitational field the trajectory is a parabola and the range, determined from the expression

$$X = \frac{v_0 \sin 2\theta_0}{g},$$

reaches its maximum at  $\theta_0 = 45^\circ$  for any values of  $v_0$ . Expression (2.114) shows that upon movement in a variable central gravitational field the value  $\theta_0^*$  corresponding to greatest range depends on velocity or on  $v$ . At sufficiently low velocities ( $v \rightarrow 0$ )  $\theta_0^* \rightarrow 45^\circ$ . With  $v=1$  we get  $\theta_0^* = 0$ , i.e., the greatest range is secured when the vector of initial velocity is horizontal. In this connection it is apparent from expression (2.111) that  $\beta^* = \frac{\pi}{2}$

$$L = 2\beta^* r_0 = \pi r_0$$

The greatest range of flight with  $v=1$  is found to be equal to half the circumference of the earth. Taking into account the possibility of releasing the rocket in opposite directions, we reach the conclusion that with  $v=1$ ;  $v_0 = \sqrt{g_0 r_0}$ , i.e., upon attainment of first cosmic velocity and with a value  $\theta_0 = 0$ , which corresponds to horizontal direction of the vector  $v_0$ , the rocket can reach any point of the earth. Let us note, however, that angle  $\theta^* = 0$ , ensuring with  $v=1$  the maximum range of flight, is associated with great spread of fall points, since a small deviation of angle  $\theta_0$  from the optimum  $\theta_0^* = 0$  brings about great alteration of range.

In conclusion let us recall that the value  $r_0$  forming part of expressions (2.110) and (2.113) for range of flight corresponds to a radius of a sphere outside of which air resistance may be disregarded

$$r_0 = R + h.$$

When this is true

$$g_0 = 9,81 \frac{R^2}{(R+h)^2}.$$

Height of trajectory:

The greatest height of trajectory can be found from the condition  $\beta = 0$ . In this case we get from expression (2.109):

$$r_{\max} = \frac{p}{1-e};$$

$$Y = y_{\max} = r_{\max} - r_0$$

Substituting the values  $\underline{p}$  and  $\underline{e}$  from expressions (2.106) and (2.107), we secure

$$Y = y_{max} = \frac{w_0 \cos^2 \theta_0}{1 - \sqrt{1 - v(2-v) \cos^2 \theta_0}} - r_0$$

After some transformations we secure

$$Y = \frac{r_0 v \sin^2 \theta_0}{\sqrt{1 - v(2-v) \cos^2 \theta_0} + (1-v)}. \quad (2.115)$$

For the example examined above

$$e = \sqrt{1 - v(2-v) \cos^2 \theta_0} = \sqrt{1 - 0,064 \cdot 1,936 \cdot 0,5} = 0,9685;$$

$$Y = \frac{6,371 \cdot 10^8 \cdot 0,064 \cdot 0,5}{0,9685 + 0,936} = 107 \cdot 10^3 \text{ m}$$

Limit expressions for range  $L$  and altitude  $Y$  with small  $v$  :

From the examples examined we see that small values of  $v$  and  $\beta$  ( $v \approx 0,06$ ,  $\beta \approx 0,03$ ) correspond to ranges of approximately 400 km. Under these circumstances one can disregard in formulas (2.112) and (2.113) the squares of these quantities and substitute

Here we secure:

$$\beta = \frac{v \cos \theta_0 \sin \theta_0}{1 - v \cos^2 \theta_0}.$$

$$L = 2r_0 \beta = \frac{2r_0 v \cos \theta_0 \sin \theta_0}{1 - v \cos^2 \theta_0}.$$

Taking into account the expression

$$v = \frac{v_0^2}{g r_0},$$

we get

$$L = \frac{v_0^2 \sin 2\theta_0}{g_0} \cdot \frac{1}{(1 - v \cos^2 \theta_0)}. \quad (2.116)$$

Disregarding  $v$  in comparison with unity, we secure a familiar expression for range in a constant gravitational field

$$X = \frac{v_0^2 \sin 2\theta_0}{g_0}. \quad (2.117)$$

The quantity  $(1 - v \cos^2 \theta_0)^{-1}$  may be regarded as a correction multiplier for nonhomogeneity of the gravitational field. For the example under examination

The range in the central field of attraction of the earth for the example being examined exceeds by 3.2 percent the range corresponding to a homogeneous gravitational field calculated according to formula (2.117) of the parabolic theory.

For height of trajectory, assuming smallness of  $\nu$ , one can analogously secure from expression (2.115)

$$Y = \frac{v_0^2 \sin^2 \theta_0}{2g_0} \cdot \frac{1}{1 - \frac{\nu}{2} (1 + \cos^2 \theta_0)} \quad (2.118)$$

in place of the expression

$$Y = \frac{v_0^2 \sin^2 \theta_0}{2g_0}$$

from the parabolic theory.

Formulas (2.116)-(2.118) make it possible to evaluate the error of the parabolic theory.

With  $\theta_0 = 45^\circ$   $\cos^2 \theta_0 = 0,5$  and the relative error in the amount of range is

$$\frac{\Delta X}{X} = \frac{\nu}{2}$$

Taking as the magnitude of relative error about 1 percent we secure  $\nu \approx 0,02$ . Having written expression (2.117) for  $\theta_0 = 45^\circ$  in the form  $X = r_0 \nu$ , we secure

$$X = 6,371 \cdot 10^6 \cdot 0,02 = 0,127 \cdot 10^6 \text{ m} = 127 \text{ km.}$$

For range  $X < 127 \text{ km}$  the error of the parabolic theory does not exceed 1 percent.

### 2.11. Time of Flight

For calculation of time of flight we shall start from the law of preservation of area (2.96)

$$r^2 \dot{\eta} = c = r_0 v_0 \cos \theta_0$$

whence

$$dt = \frac{r^2}{c} d\eta$$

Expressing  $r$  by means of  $\eta$  from expression (2.109) we get

$$dt = \frac{r^2}{c} \cdot \frac{d\eta}{(1 - e \cos \eta)^2} \quad (2.119)$$

With the reading of angles  $\eta$  from the axis running through the apex of the trajectory that we have already selected, for determination of the total time of flight one must integrate expression (2.119) at the left from zero to  $T$  and at the right from  $\eta = -\beta$  to  $\eta = +\beta$ . Taking into account the symmetry of the trajectory relative to the axis corresponding to  $\eta = 0$ , we can write

$$T = \frac{2r^2}{c} \int_0^{\beta} \frac{d\eta}{(1 - e \cos \eta)^2} \quad (2.120)$$

For integration of expression (2.120) we introduce the substitution

$$x = \operatorname{tg} \frac{\eta}{2}.$$

Doing so, we secure

$$T = \frac{2r^2}{c} \int_0^x \frac{2(1+x^2) dx}{[1 - e + (1+e)x^2]^2}.$$

The last expression, through substitution

$$\operatorname{tg} \frac{E}{2} = \sqrt{\frac{1+e}{1-e}} x$$

after some transformations is converted into the form

$$T = \frac{2r^2}{c} \cdot \frac{1}{(1-e^2)^{3/2}} \int_0^E (1 + e \cos E) dE \quad (2.121)$$

or

$$T = \frac{2r^2}{c(1-e^2)^{3/2}} (E + e \sin E).$$

Substituting the values  $c$  and  $p$  from expressions (2.96) and (2.106) we secure

$$T = \frac{2v_0^3 \cos^3 \theta_0}{c^2 (1-e^2)^{3/2}} (E + e \sin E).$$

On the basis of expression (2.107) we secure finally

$$T = \frac{2}{(2-\nu)^{1/2}} \sqrt{\frac{r_0}{g_0}} (E + e \sin E), \quad (2.122)$$

where

$$E = 2 \operatorname{arc} \operatorname{tg} \left( \sqrt{\frac{1+e}{1-e}} \operatorname{tg} \frac{\theta}{2} \right),$$

$$\nu = \frac{v_0^2}{g_0 r_0}$$

For the example examined in 2.10,  $v_0 = 2,000$  meters per second;  
 $\theta_0 = 45^\circ$ ;  $\nu = 0,064$ ;  $e = 0,9685$ ;  $\beta = 0,03304$ ;  $E = 14^\circ 52' = 0,2596$  rad.

Here we get

$$T = \frac{2}{(2-0,064)^{1/2}} \sqrt{\frac{6,371 \cdot 10^6}{9,81}} (0,2596 + 0,9685 \cdot 0,2567) = 304 \text{ sec.}$$

## 2.12. Calculation of the Final Section of the Trajectory

Let the point  $C_1$  be the end of the airless passive section of the trajectory and the beginning of the final section of re-entry of the rocket or of its last stage into the dense layers of the atmosphere. We shall designate the point of fall by the letter C.

For calculation of the final section of the trajectory one can make use of the method of calculating trajectory by arcs, set forth in 2.8. When this is done one must bear in mind the fact that in this section  $\theta < 0$  and  $\Delta y < 0$  and take into account the signs of these quantities in formulas (2.88)-(2.90). But one can refrain from dividing the final section into parts and secure relations for direct calculation of the elements of the point of fall, taking into account the character of change in the elements of the trajectory in its final section.

In Table 2.5 there are set forth the results of computations of the final section of a trajectory by arcs with the initial values:  
 $y_1 = 30,000$  meters;  $v_1 = 1,652$  meters;  $|\theta_1| = 35,34^\circ$ ;  $x_1 = 0$ .

The range  $x$  is measured from the start of the final section.

In the last line we have set forth the values of the elements of a trajectory as calculated according to formulas of the parabolic theory of the movement of a material point outside the atmosphere in a constant gravitational field.

From analysis of the results set forth in the table it is apparent that although air resistance reduces the velocity of fall by 710 meters

per second, or by 39 percent, the horizontal range of the final section declines only by 1.2 percent. The angle of fall also changes very little.

Table 2.5

$y$ км	$v$	$ \theta^\circ $	$x$	Remarks
30	1652	35,34	0	
25	1670	36,74	6873	
20	1674	38,05	13413	
15	1649	39,33	19659	
10	1568	40,63	25624	
5	1404	42,08	31303	
0	1110	43,98	36665	
0	1822	42,28	37120	In vacuum

We shall make use of the last circumstance and we shall secure an approximate method of calculating the elements of the point of fall without having recourse to calculating by arcs. In doing this we shall seek values of the elements of the point of fall  $\theta$  and  $x$  in the form of corrections to the values corresponding to the elements computed according to the formulas of the parabolic theory.

We introduce the designations:

$$u = v \cos \theta; p = \operatorname{tg} |\theta|.$$

The elements of the trajectory in vacuum (parabolic theory) will be indicated by the sign ( $\sim$ ).

Taking altitude  $y$  as an independent variable, we can write differential equations of movement in the following form:

$$\frac{du}{dy} = \frac{c_1 c_2 H(y) u}{\sin |\theta|}; \quad (2.123)$$

$$\frac{dp}{dy} = -\frac{g}{pu^2}; \quad (2.124)$$

$$\frac{dx}{dy} = -\frac{1}{p}. \quad (2.125)$$

It is necessary to consider that in the final section  $dy < 0$ .

With movement in vacuum we secure:

from equation (2.123)

$$\dot{u} = u_1 = \text{const}, \quad (2.126)$$

from equation (2.124)

$$\bar{p}^2 = p_1^2 + \frac{2g}{\bar{u}^2} (y_1 - y), \quad (2.127)$$

from equations (2.124) and (2.125)

$$\frac{dx}{dp} = \frac{u^2}{g}, \quad (2.128)$$

whence

$$\bar{x} = \frac{\bar{u}^2}{g} (\bar{p} - p_1). \quad (2.129)$$

Substituting the value  $\frac{\bar{u}^2}{g}$  from expression (2.127), we secure

$$\bar{x} = \frac{2(y_1 - y)}{\bar{p} + p_1}. \quad (2.130)$$

For the point of fall we secure:

$$\begin{aligned} \bar{u}_c &= u_1 = \text{const}; \\ \bar{p}_c^2 &= p_1^2 + \frac{2g}{u_1^2} y_1; \end{aligned} \quad (2.131)$$

$$\bar{x}_c = \frac{2y_1}{\bar{p}_c + p_1}. \quad (2.132)$$

Let us examine the final section of the trajectory in air. From equation (2.123) we have

$$\ln \frac{u}{u_1} = \int_{y_1}^y \frac{c_x c_x}{\sin|\theta|} H(y) dy.$$

With great velocities of re-entry of the rocket into the dense layers of the atmosphere  $c_x$  may be secured as a constant or as a quantity undergoing little change. The greater the velocity of flight, the less is the change in angle  $\theta$ . Bringing  $c_x$  and  $\sin|\theta|$  at mean value from beneath the integral sign and designating

$$c = \frac{c_x c_x}{\sin|\theta|_{cp}}, \quad (2.133)$$

we secure

$$\ln \frac{u}{u_1} = c \int_{y_1}^y H(y) dy. \quad (2.134)$$

We introduce the designation

$$H_1(y) = \int_{y_1}^y H(y) dy, \quad (2.135)$$

where  $h$  is a sufficiently high value of  $y$  so that one can secure  $H(y) = H(h) = 0$ .

When this is done we secure

$$\ln \frac{u}{u_1} = -c [H_1(y) - H_1(y_1)] = -c \Delta H_1,$$

whence

$$u = u_1 e^{-c \Delta H_1}. \quad (2.136)$$

The values of the functions  $H_1(y)$  are given in Table 2.2 for  $h = 50$  km. For the point of fall we have  $H_1(y_c) = H_1(0) = 8,220$  m.

With things thus we secure

$$u_c = u_1 e^{-c \Delta H_1} = u_1 e^{-c(8220 - H_1(y,1))}. \quad (2.137)$$

For calculation of  $\rho = \operatorname{tg} |\theta|$  we rewrite equation (2.124) in the form

$$\frac{d\pi}{dy} = -\frac{2g}{u^2}, \quad (2.138)$$

where  $\pi = \rho^2$ .

We introduce the designations:

$$\pi = \tilde{\pi} + \delta\pi;$$

$$u = \tilde{u} + \delta u,$$

where the sign ( $\sim$ ) indicates quantities corresponding to the trajectory in vacuum.

In this connection we get

$$\frac{d(\tilde{\pi} + \delta\pi)}{dy} = -\frac{2g}{(\tilde{u} + \delta u)^2} = -\frac{2g}{\tilde{u}^2} + \frac{4g\delta u}{\tilde{u}^3} + O(\delta u^2),$$

where  $O(\delta u^2)$  is a quantity of the second, or greater, order of smallness relative to  $\delta u$ .

Retaining the quantities of first order of smallness and taking into account equation (2.138), we get

$$\frac{d(\delta\pi)}{dy} = \frac{4g}{u^2} \frac{\delta u}{u}. \quad (2.139)$$

From expression (2.136) we have

$$\frac{u}{u_1} = \frac{u}{\bar{u}} = \frac{\bar{u} + \delta u}{\bar{u}} = e^{-c\Delta H_1}$$

or

$$1 + \frac{\delta u}{\bar{u}} = 1 - c\Delta H_1 + \frac{c^2}{2} (\Delta H_1)^2 + \dots$$

Eliminating the quantities greater than the first order of smallness, we secure

$$\frac{\delta u}{\bar{u}} = -c\Delta H_1.$$

Substituting the last expression in equation (2.139), integrating within corresponding limits, and considering that with  $y = y_1$ ,  $\delta u = 0$ ,  $\delta\pi = 0$ , we get

$$\delta\pi = -\frac{4gc}{u_1^2} \int_{y_1}^y \Delta H_1 dy = -\frac{4gc}{u_1^2} \int_{y_1}^y [H_1(y) - H_1(y_1)] dy. \quad (2.140)$$

We introduce the function  $H_2(y)$  determined by the expression

$$H_2(y) = \int_y^y H_1(y) dy.$$

Expression (2.140) assumes the form

$$\delta\pi = \frac{4gc}{u_1^2} [H_2(y) - H_2(y_1) - (y_1 - y)H_1(y_1)].$$

Calculations show that one may retain within the brackets only the first term. If this is done we have

$$\delta\pi = \frac{4g}{u_1^2} cH_2(y) \quad (2.141)$$

or for the point of fall

$$\delta\pi_c = \frac{4g}{u_1^2} cH_2(0), \quad (2.142)$$

$$p_c^2 = p_1^2 + \frac{2g}{u_1^2} y_1 + \frac{4g}{u_1^2} cH_2(0). \quad (2.143)$$

From Table 2.2 we find  $H_2(0)$  to be  $= 597 \cdot 10^5 \text{ m}^2$ .

We compute the correction in range.

From equation (2.125) through substitution

$$\begin{aligned} x &= \bar{x} + \delta x, \\ p &= \bar{p} + \delta p \end{aligned}$$

and linearization of equation (2.123) we secure

$$\frac{d(\delta x)}{dy} = \frac{\delta p}{\bar{p}^2} = \frac{\delta\pi}{2\bar{p}^3}.$$

Substituting the value  $\delta\pi$  from expression (2.141) we secure

$$\begin{aligned} \frac{d(\delta x)}{dy} &= \frac{2gc}{u_1^2 \bar{p}^3} H_2(y); \\ \delta x &= \frac{2gc}{u_1^2} \int_{y_1}^y \frac{H_2(y)}{\bar{p}^3} dy = \frac{2gc}{u_1^2 \bar{p}_{cp}^3} \int_{y_1}^y H_2(y) dy. \end{aligned} \quad (2.144)$$

We introduce the function  $H_3(y)$ , determined from the expression

$$H_3(y) = \int_y^h H_2(y) dy.$$

By doing this we secure

$$\delta x = - \frac{2gc}{u_1^2 \bar{p}_{cp}^3} [H_3(y) - H_3(y_1)].$$

From Table 2.2 it is apparent that the second term within the brackets may be eliminated. When this is done we secure for the point of fall

$$\delta x_c = - \frac{2gc}{u_1^2 \bar{p}_{cp}^3} H_3(0). \quad (2.145)$$

From Table 2.2 we find that  $H_3(0)$  is  $= 391 \cdot 10^9$  cubic meters.

Example

At an altitude of 30 km the parameters of the final section of the trajectory are  $v_1 = 1,652$  meters per second;  $\theta_1 = 35^\circ 20'$ ;  $c_1 c_x = 0,397 \cdot 10^{-4}$ .

One is to determine the elements of the point of fall  $\theta_c$ ,  $x_c$ ,  $v_c$ . First we determine according to the formulas of the parabolic theory (2.131) and (2.132):

$$\begin{aligned} \tilde{u}_c &= u_1 = v_1 \cos \theta_1 = 1348 \text{ м/сек}; \\ \tilde{\rho}_c^2 &= \rho_1^2 + \frac{2g}{u_1^2} y_1 = \text{tg}^2 35^\circ 20' + \frac{2 \cdot 9,81}{1348^2} 30000 = 0,8264; \\ \tilde{\rho}_c &= 0,9090; \quad |\tilde{\theta}_c| = 42^\circ 16'; \end{aligned}$$

$$\begin{aligned} \tilde{x}_c &= \frac{2y_1}{\rho_1 + \tilde{\rho}_c} = \frac{2 \cdot 30000}{0,7089 + 0,9090} = 37120 \text{ м}; \\ |\tilde{\theta}_{cp}| &= \frac{42^\circ 16' + 35^\circ 20'}{2} = 38^\circ 48'. \end{aligned}$$

We turn to calculation of the corrections  $\delta x_c$ ,  $\delta \rho_c$  to the elements  $\tilde{x}_c$ ,  $\tilde{\rho}_c$  of the parabolic trajectory. We have

$$c = \frac{c_1 c_x}{\sin |\tilde{\theta}_{cp}|} = \frac{0,397 \cdot 10^{-4}}{0,6266} = 0,645 \cdot 10^{-4}.$$

From Table 2.2 we find that  $H_1(0)$  is  $= 8,220$ ;  $H_2(0) = 597 \cdot 10^5$ ;  $H_3(0) = 0,645 \cdot 10^{-4}$ .

According to formula (2.145) we find:

$$\begin{aligned} \delta x_c &= -\frac{2gc}{u_1^2 \tilde{\rho}_c^3} H_3(0) = -\frac{2g \cdot 0,645 \cdot 10^{-4} \cdot 391 \cdot 10^9}{1348^2 \cdot \text{tg}^3 38^\circ 48'} = -525 \text{ м}; \\ x_c &= \tilde{x}_c + \delta x_c = 37120 - 525 = 36595 \text{ м}. \end{aligned}$$

According to formula (2.142) we find:

$$\begin{aligned} \delta \rho_c &= \delta(\rho_c^2) = \frac{4gc}{u_1^2} H_2(0) = \frac{4 \cdot 9,81}{1348^2} 0,645 \cdot 10^{-4} \cdot 597 \cdot 10^5 = 0,0830; \\ \rho_c^2 &= \tilde{\rho}_c^2 + \delta(\rho_c^2) = 0,8264 + 0,0830 = 0,9094; \\ \rho_c &= 0,954, \quad |\theta_c| = 43^\circ 40'. \end{aligned}$$

We compute the velocity of fall  $v_c$ .

According to formula (2.136) we find

$$\frac{u_c}{u_1} = e^{-c[8220 - H_1(y_1)]},$$

$$c[8220 - H_1(y_1)] = 0,645 \cdot 10^{-4} (8220 - 89) = 0,518;$$

$$u_c = u_1 \cdot e^{-0,518} = 1348 \cdot 0,596 = 803 \text{ м/сек};$$

$$v_c = \frac{u_c}{\cos \theta_c} = \frac{803}{\cos 43^\circ 40'} = \frac{803}{0,723} = 1110 \text{ м/сек}.$$

In Table 2.6 a comparison of the results secured with the results of computations according to the method of arcs and according to the formulas of the parabolic theory is given.

Table 2.6

<u>Method of Computation</u>	<u><math>x_c</math></u>	<u><math> \theta_c </math></u>	<u><math>v_c</math></u>
Method of corrections to the parabolic theory	36,595	43°41'	1,110
Method of arcs (6 segments)	36,655	43°59'	1,110
Parabolic theory	37,120	42°17'	1,822

### 2.13. Over-All Computation of the Elements of the Trajectory. The Method of Fictitious Initial Conditions

In 2.7-2.12 we examined methods for the calculation of separate sections of the trajectory of rockets.

"Butting together" these sections is made more complicated through the fact that the elliptical passive section is calculated in polar coordinates, and the remaining sections in Descartes coordinates. But one can simplify over-all computation of the elements of a trajectory, in particular the elements of the point of fall, if one applies the method of fictitious initial conditions, the essence of which boils down to what follows:

Let us say that as a result of calculation of the first passive section we have determined the values of the elements of point  $M_1$  ( $v_1$ ,  $\theta_1$ ,  $y_1$ ,  $x_1$ ), the end of this section. If taking point  $M_1$  as the initial point we integrate the equation for movement backward without taking air resistance into account, for an altitude  $y = 0$  we shall secure a fictitious point of fly-out  $F$  and its initial parameters  $v_f$ ,  $\theta_f$ ,  $x_f$ , which we shall call the fictitious initial conditions (Figure 2.21). By making use of these initial conditions one can calculate, according to the formulas of the elliptical theory, the elements of the point of fall, and one can introduce the necessary corrections by means of the methods examined below.

In order to determine the values  $v_f$ ,  $\theta_f$ , and  $x_f$  one can use the formulas of the parabolic theory. From the conditions of the preservation of kinetic energy we have directly

$$v_{\phi}^2 = v_1^2 + 2gy.$$

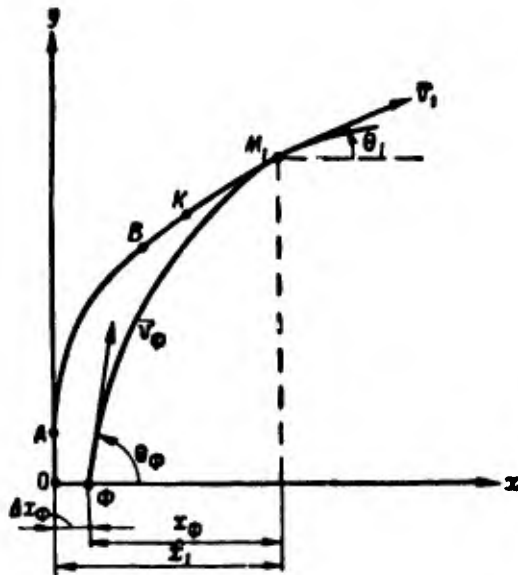


Figure 2.21. Method of fictitious initial conditions.  $\phi = f$ (ictitious).

From the conditions of constancy of the horizontal component of velocity

$$u_1 = v_1 \cos \theta_1 = u_{\phi} = v_{\phi} \cos \theta_{\phi}$$

we get

$$\cos \theta_{\phi} = \frac{v_1 \cos \theta_1}{v_{\phi}}.$$

From the familiar expression

$$\operatorname{tg} \theta_1 = \operatorname{tg} \theta_{\phi} - \frac{gx_{\phi}}{u^2}$$

we secure

$$x_{\phi} = (\operatorname{tg} \theta_{\phi} - \operatorname{tg} \theta_1) \frac{u_1^2}{g}.$$

From here on it is convenient to deal with the quantity

$$\Delta x_{\phi} = x_1 - x_{\phi}$$

characterizing the deflection of the fictitious origin of the coordinates from the point of fly-out of the rocket.

By taking advantage of the values secured for  $v_f$  and  $\theta_f$  one can determine the range  $L = X_{e1}$  according to the formulas of the elliptical theory, and as measured off along the spherical surface of the earth (2.10). It is further necessary to take into account the reduction of range over the final section  $C_1C$  where the rocket enters the dense strata of the atmosphere. This correction can be calculated according to formula (2.145)

$$\delta x_c = - \frac{2gc}{v_1^2 r_{cp}} H_3(0),$$

where

$$c = \frac{c_1 c_r}{\sin |\theta_{cp}|};$$

$$|\theta_{cp}| = \frac{1}{2} (\theta_0 + \theta_1),$$

$H_3(0) = 381 \cdot 10^9$  is determined according to Table 2.2.

An example for calculation of  $\delta x_c$  is set forth in 2.12.

The full range of flight of the rocket is determined from the expression

$$X = X_{sa} + \Delta X_0 - |\delta x_c|.$$

If it is necessary to refine further the values of  $\theta_c$  and  $v_c$  taking into account the air resistance in the final section of the rocket's entry into the dense strata of the atmosphere, one can use the method examined in 2.12.

#### 2.14 Trajectory of Flight of an Earth Satellite

Let us take as the initial point of the trajectory of the center of mass of the satellite some point A at an altitude  $h$  above the surface of the earth. Let the velocity  $v_A$  be directed horizontally ( $\theta_A = 0$ ). The initial value of the radius-vector of the point  $r_A = r_0 = R + h$ , where  $R$  is the radius of the earth. Let us draw a polar axis from the center of the earth to point A, considered as the initial point. When this is done the initial conditions have the form:

$$\eta = 0; \quad r = r_0; \quad v = v_0; \quad \theta = \theta_0 = 0.$$

From equation (2.105), in which  $\alpha$  is an arbitrary constant, we secure  $\sin \alpha = 0$ . From expressions (2.106) and (2.107), considering that  $\sin \theta_0 = 0$ , we secure

$$p = r_0^2, \tag{2.146}$$

$$e = \sqrt{1 - v(2 - v)} = \pm(v - 1). \quad (2.147)$$

The plus or minus sign is selected so that  $e > 0$ . Let  $v > 1$ ; then  $e = v - 1$  and equation (2.105) assumes the form

$$r = \frac{vr_0}{1 + (v - 1)\cos(\eta - \alpha)}.$$

Substituting the initial conditions  $r = r_0$ ,  $\eta_0 = 0$ , we secure  $\cos \alpha = 1$ .

Considering the fact that  $\sin \alpha = 0$ , we secure  $\alpha = 0$ , and expression (2.105) assumes the form

$$r = \frac{vr_0}{1 + (v - 1)\cos \eta}. \quad (2.148)$$

With  $e = 1 - v$  and  $\alpha = \pi$  equation (2.105) assumes the form

$$r = \frac{r_0 v}{1 - (1 - v)\cos \eta}. \quad (2.149)$$

Let us examine some cases of the movement of an earth satellite.

1.  $v < 1$

Here  $e = 1 - v < 1$ . The trajectory is an ellipse. The initial point A is one of the vertices of the ellipse. The other vertex is on a continuation of the straight line AC (Figure 2.22). Its distance from the center of the earth is determined from the expression

$$r_B = \frac{r_0 v}{1 - (1 - v)\cos \pi} = \frac{vr_0}{2 - v} < r_0$$

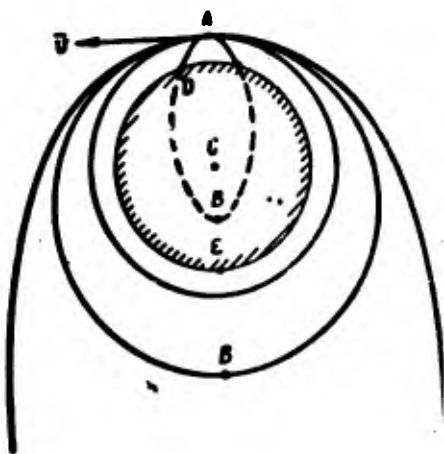


Figure 2.22. Trajectories of earth satellites.

Thus the initial point A is the more distant from the center of gravitational pull and is called the apogee. The opposite point, B (the closer to the center of gravitational pull of the point), is called the perigee.

In this connection it is apparent from Figure 2.22 that the section of the trajectory AD up to encounter with the surface of the earth is the real section.

In the extreme case, when  $r_B = R$ , the elliptical orbit will touch the surface of the earth at the point of the perigee (in the absence of air resistance).

2.  $v = 1$

In this case  $v_0 = \sqrt{g_0 r_0}$  becomes equal to first cosmic velocity. The equation for the trajectory assumes the form  $r = r_0$ . The satellite moves on a circular orbit.

3.  $2 > v > 1$

In this case the equation for the trajectory is determined by expression (2.148).

For the vertices A and B of the ellipse we secure ( $\eta = 0$  and  $\eta = \pi$ )

$$r_A = r_0; \quad r_B = \frac{r_0 v^2}{2 - v^2} > r_0$$

The initial point A is the one closer to the center of gravitational pull of the point and is called the perigee, and point B is the apogee.

As velocity increases the position of the perigee remains the same, and the apogee point becomes more and more distant from the center of gravitational pull.

4.  $v \geq 2$

With  $v = 2$ ;  $v_0 = \sqrt{2g_0 r_0}$  second cosmic velocity is achieved. Under these circumstances one gets

$$e = 1; \quad r_B = \frac{r_0 v^2}{2 - v^2} = \infty.$$

The point, moving on an open curve (a parabola), departs into infinity.

With  $v > 2$   $e > 1$  the trajectory of the point is a hyperbola.

In conclusion we may remark that the conclusions regarding the infinite removal of a moving point from the earth with  $v > 2$  were reached without taking into account the gravitational field of the sun. Actually when a body attains second cosmic speed in departing from the earth, it becomes an artificial planet of the solar system. When a body departs from the earth to a distance of a million kilometers the attraction of the sun becomes predominant.

The period of revolution of a satellite around the earth can be calculated by taking as point of departure (2.96)

$$\frac{ds}{dt} = \frac{1}{2} c = \frac{1}{2} r_0 v_0 \cos \theta_0,$$

whence

$$dt = \frac{2}{c} ds.$$

Examining a full revolution around the earth in an elliptical orbit we get

$$T = \frac{2}{c} \sigma,$$

where  $\sigma$  is the area of the ellipse, determined from the expression  $\sigma = \pi ab$  ( $a$  and  $b$  are the large and the small half-axes of the ellipse).

From analytic geometry we are aware that

$$a = \frac{p}{1-e^2};$$

$$b = \frac{p}{\sqrt{1-e^2}}.$$

Thus we have

$$T = \frac{2\pi a^2 \sqrt{1-e^2}}{c} = \frac{2\pi \sqrt{p}}{c} a^{3/2}. \quad (2.150)$$

During movement on a circular orbit  $v = 1$ ;  $e = 0$ ;  $a = b = r_0$ ;  $c = v_0^2$ .

Under these circumstances

$$T = \frac{2\pi r_0}{v_0}.$$

Expressing  $v_0$  through the parameter of velocity  $v = 1$  we secure

$$T = 2\pi \sqrt{\frac{r_0}{g_0}}$$

Example

At an altitude of 300 km:

$$g_0 = 9,81 \frac{R^2}{(R+h)^2} = 9,81 \frac{6,371^2}{6,671^2} = 8,93 \text{ м/сек}^2$$

$$T = 2\pi \sqrt{\frac{r_0}{g_0}} = 2\pi \sqrt{\frac{6,671 \cdot 10^6}{8,93}} = 5140 \text{ сек} = 90,7 \text{ мин.}$$

Let us examine the case where at the same altitude  $h = 300$  km, the parameter of velocity  $v = 1,1$ .

Here we have  $r_0 = 6,671 \cdot 10^6$ ,  $g_0 = 8,93$ ,  $v = 1,1$ , so:

$$v_0 = \sqrt{v g_0 r_0} = \sqrt{1,1 \cdot 8,93 \cdot 6,671 \cdot 10^6} = 8100 \text{ м/сек.}$$

With  $\theta_0 = 0$

$$\begin{aligned} e &= v - 1 = 0,1; \\ p &= v r_0 = 1,1 \cdot 6,671 \cdot 10^6 = 7,341 \cdot 10^6. \end{aligned}$$

Altitude of perigee

$$r_A = r_0 = 6,671 \cdot 10^6 \text{ м.}$$

Altitude of apogee

$$r_B = r_0 \frac{v}{2-v} = 8,16 \cdot 10^6 \text{ м.}$$

Major half-axis

$$a = \frac{r_A + r_B}{2} = 7,42 \cdot 10^6 \text{ м.}$$

Furthermore

$$c = r_0 v_0 = r_0 \sqrt{g_0 v r_0}.$$

Substituting the values of  $c$  and  $p$  in expression (2.150), we secure

$$T = \frac{2\pi}{r_0 \sqrt{g_0}} a^{3/2},$$

or

$$T = 2\pi \frac{(7.42 \cdot 10^4)^2}{6.671 \cdot 10^{-8} \cdot \sqrt{8.93}} = 6380 \text{ сек} = 106,2 \text{ мин.}$$

## 2.15. The Trajectory of Movement of a Satellite Relative to a Rotating Earth

The relationships examined above, for the movement of a material point in the field of terrestrial gravity, correspond to a system of coordinates associated with a nonrotating earth. In order to take into account the effect of rotation of the earth one must contemplate a system of coordinates associated with the rotating earth.

In this process, beside the force of gravitational attraction of the earth one must consider also the force of inertia of migratory motion and the Coriolis inertia force. But in studying the movement of a point in the central field of gravity of the rotating earth a different method is customarily applied; its substance is set forth below:

Let us examine the spherical surface associated with the earth and running through the origin of the elliptical section of the trajectory in a vacuum; the center of the sphere is to correspond with the center of the earth. From here on we shall call this sphere the moving sphere. The radius of the moving sphere is  $r_0$ . The position of the initial point relative to the moving sphere will be defined by breadth  $\lambda_0$ , and length  $\phi_0$ . In addition to the moving sphere we shall also consider a stationary sphere which coincides with the moving sphere at the initial moment of time.

In Figure 2.23 in the plane of the drawing we show the curvature of the meridian of the initial point. Let us project an axis  $Oz$  in the direction of the vertical to the initial point, an axis  $Ox$  in the horizontal plane to the north, an axis  $Oy$  to the west. Let us call the plane running through the vertical and through the vector  $\bar{v}_{or}$  of initial velocity relative to the earth the plane of departure. In this plane we project axis  $Ox_1$  horizontally in the direction of flight and the axis  $Oy_1$  to the left. The angle  $\alpha$ , laid off from the plane of the meridian to the plane of departure, will be called the azimuth of the plane of departure. We shall be studying movement of a material point relative to the stationary sphere. On this account when we examine the initial conditions of flight we must consider, in addition to the initial velocity  $\bar{v}_{or}$  relative to the earth, also the migratory velocity of the initial point as it moves along with the earth. As may easily be seen, this velocity is

$$\bar{v}_{or} = r_0 \omega \cos \lambda \quad (2.151)$$

and is directed inversely to the direction of axis  $y$ .

The absolute initial velocity  $(\bar{v}_0)_{ss}$  is determined from the expression

$$\bar{v}_0_{ss} = \bar{v}_{or} + \bar{v}_{or}$$

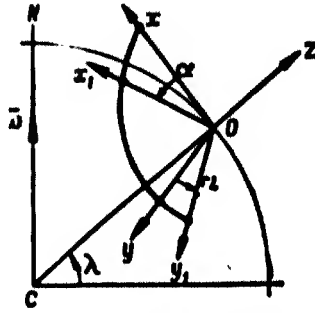


Figure 2.23. System of coordinates associated with the rotating earth.

Projecting this equality upon the stationary axes of coordinates and dropping off the index ab we get (Figure 2.24):

$$\begin{aligned} v_{0x} &= v_{0r} \cos \theta_0 \cos \alpha; \\ v_{0y} &= v_{0r} \cos \theta_0 \sin \alpha - r_0 \omega \cos \lambda; \\ v_{0z} &= v_{0r} \sin \theta_0. \end{aligned} \quad (2.152)$$

Examining the horizontal projection of the vector of absolute velocity we see that

$$\operatorname{tg} \alpha_1 = \frac{v_{0y}}{v_{0x}} = \frac{v_{0r} \cos \theta_0 \sin \alpha - r_0 \omega \cos \lambda}{v_{0r} \cos \theta_0 \cos \alpha}, \quad (2.153)$$

where  $\alpha_1$  is the azimuth of the plane of departure in absolute motion.

The angle  $\theta_{01}$ , formed by the vector of absolute velocity with the horizon of the initial point, is found from the expression

$$\operatorname{tg} \theta_{01} = \frac{v_{0z}}{\sqrt{v_{0x}^2 + v_{0y}^2}}. \quad (2.154)$$

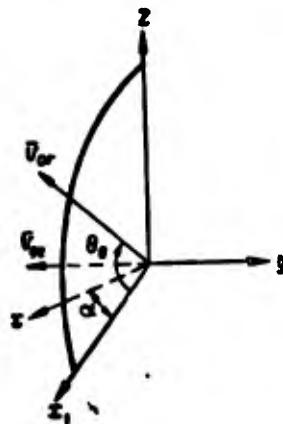


Figure 2.24. Vector Components of the Initial Speed Taking into Account Earth's Rotation

Thus the vector  $\vec{v}_0$  of absolute motion will be determined both as regards module and as regards direction ( $\theta_0$  and  $\alpha_1$ ). Knowing the initial conditions of flight, one can determine, via familiar formulas of the elliptical theory, the trajectory of flight in polar coordinates  $\eta, r$  relative to the stationary sphere. For the point of fall  $\eta = 2\beta$ .

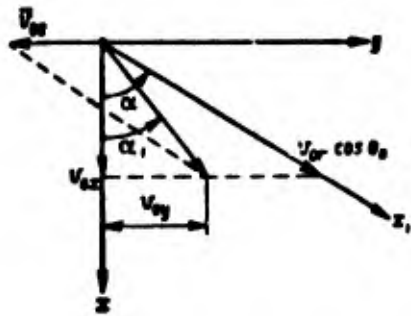


Figure 2.25. Azimuth of fire, taking into account the rotation of the earth.

Making use of spherical trigonometry formulas, one can express the geodesic coordinates of an arbitrary point,  $\lambda$  and  $\phi$ , through the parameter  $\eta$  of the elliptical trajectory and the azimuth  $\alpha_1$ , determined from expression (2.153) (Figure 2.26).

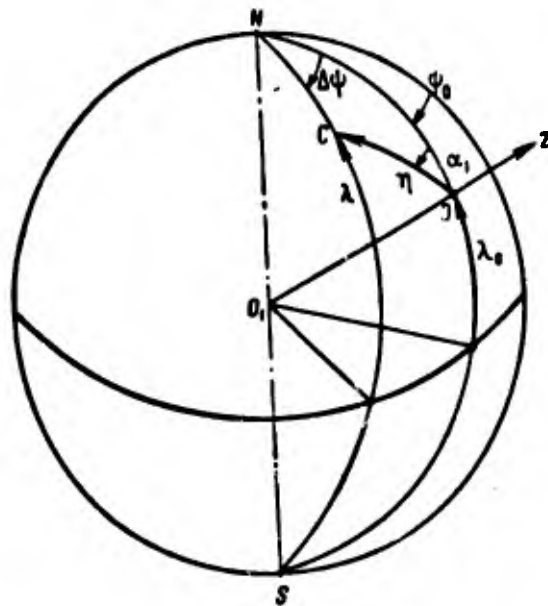


Figure 2.26. Geodesic coordinates of a rocket.

Let us recall some basic relationships in spherical trigonometry.

If  $a, b, c$  (Figure 2.27) are the sides of a spherical triangle and  $\alpha, \beta, \gamma$  are the angles opposite the corresponding sides, then

$$\frac{\sin a}{\sin \alpha} = \frac{\sin b}{\sin \beta} = \frac{\sin c}{\sin \gamma} \text{ (the sine formula);} \quad (2.155)$$

$$\cos a = \cos b \cdot \cos c + \sin b \cdot \sin c \cdot \cos \alpha \text{ (the cosine formula).} \quad (2.156)$$

Examining Figures 2.26 and 2.27 we see that

$$a = 90^\circ - \lambda; \quad b = 90^\circ - \lambda_0; \quad c = \eta;$$

$$\alpha = \alpha_1; \quad \gamma = \psi - \psi_0 = \Delta\psi.$$

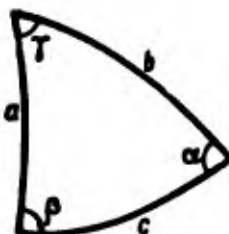


Figure 2.27. A spherical triangle.

Thus from expression (2.156) we have

$$\sin \lambda = \sin \lambda_0 \cos \gamma + \cos \lambda_0 \sin \gamma \cos \alpha_1. \quad (2.157)$$

Having determined  $\lambda$ , let us find according to formula (2.155)

$$\frac{\cos \lambda}{\sin \alpha_1} = \frac{\sin \eta}{\sin \Delta\psi}. \quad (2.158)$$

Having determined  $\Delta\psi$  from the last expression, let us find the value

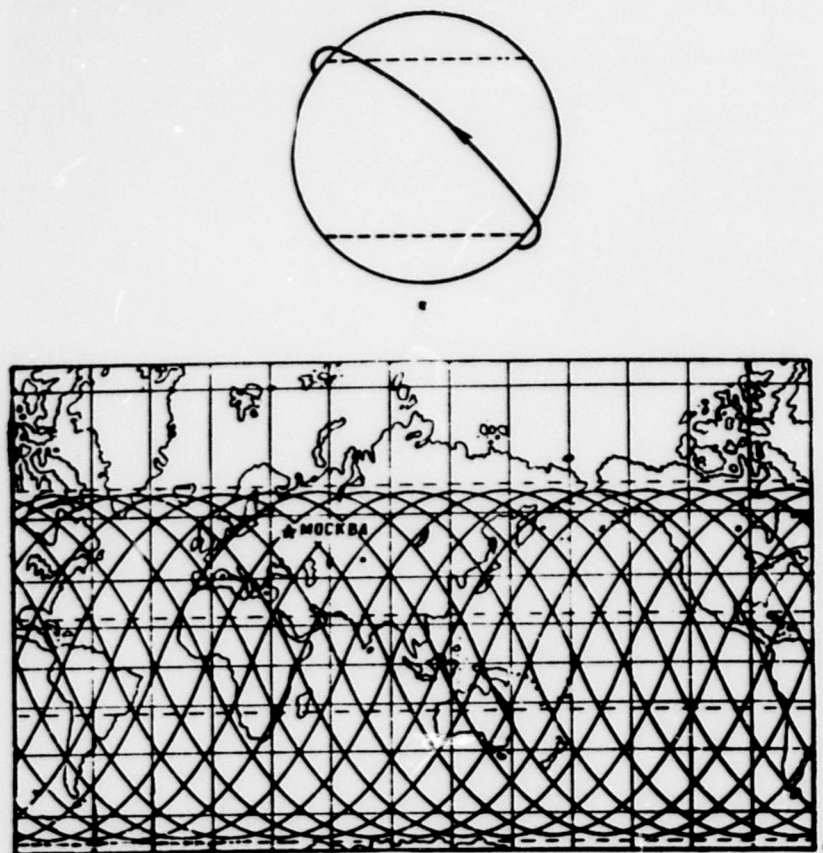
$$\psi = \psi_0 + \Delta\psi.$$

Thus we shall determine the spherical coordinates  $r, \lambda, \phi$ , for an arbitrary point of the elliptical trajectory relative to a stationary sphere, corresponding to the position of the earth at the initial moment. In order to secure the coordinates of the point of the trajectory relative to a rotating earth it suffices to take into account the angle of rotation of the earth over time  $t$  of the flight of the material point. In doing this it is apparent that the rotation of the mobile sphere relative to a stationary one does not bring about change in the radius-vector of point  $\underline{r}$  and of the latitude  $\lambda$ . As regards longitude, this changes to the amount  $\delta\phi = \omega t$ , where  $\omega$  is the angular velocity of rotation of the

earth =  $7.292 \cdot 10^{-5}$  1/sec. Finally, we secure, for an arbitrary point of the trajectory

$$\psi = \psi_0 + \Delta\psi + \omega t.$$

In Figure 2.28 we show the general aspect of the trajectory of an earth satellite relative to a stationary and to the rotating earth.



6

Figure 2.28. Trajectory of motion of a satellite: a -- relative to non-rotating earth; b -- relative to rotating earth.

#### BIBLIOGRAPHY

1. Westrom, J. B., "Trajectory Constants," Symposium "Space Trajectories," Foreign Literature Publishing House, Moscow, 1963.

2. Pogorelov, D. A., Theory of Kepler Motions of Flying Apparatus, State Physics and Mathematics Literature Publishing House, Moscow, 1961.
3. Lakhtin, L. M., Free Motion in the Field of the Terrestrial Spheroid, State Physics and Mathematics Literature Publishing House, Moscow, 1963.
4. Feodosiyev, V. I., Sinyarev, G. B., Introduction to Rocket Technics, Oborongiz Publishing House, 1960.
5. Krasnov, N. F., The Aerodynamics of Rotational Bodies, "Mashinostroyeniye" Publishing House, Moscow, 1964.

## CHAPTER III. BALLISTIC DESIGNING OF GUIDED ROCKETS

### 3.1. Statement of the Problem

Working out a rocket constitutes a most laborious process, and it covers the following stages (1):

- working out the tactical technological requirements in the light of investigation of operations;
- preliminary draft designing;
- preparing working designs for the rocket (working designing);
- preparing and testing models and full-size examples.

In execution of the first stage, initial data for designing the rocket are first developed and then handed over to the construction designers (1):

- requisite range of flight  $X_3$ ;
- requisite probability of hitting target;
- requisite useful load;
- requirements as to economics of production;
- conditions of organization of military supply and servicing.

Designing a rocket commences with selection of the general design scheme, the fuel, and the materials for the main structural units. Before proceeding to preparation of the preliminary draft design for the rocket as a whole and working out of the design for its individual units, one must at least approximately determine the weight, dimensional, and thrust characteristics of the rocket. Approximate calculation of these characteristics in the initial stage of designing is called ballistic designing.

The aim of ballistic designing is to determine the basic design parameters of the optimum ballistic pattern which, ensuring required range with required useful load, will have the lowest start weight with the fuel and materials characteristics adopted.

With minimum weight and over-all dimensions of a rocket, its use is simplified; the weight, over-all dimensions, and output of its power units and lifting and transport devices are reduced; and the maneuverability of the rocket complex is enhanced. With reduction of weight of the rocket, fuel supply and expenditure of materials are diminished, and expenses on preparation for construction are lowered. Consequently one may assume that in first approximation the minimum of start weight for a rocket, with required range and weight of useful fuel and other circumstances being equal (guidance method selected, characteristics of guidance system) provides the minimum of material expenditure in carrying out the military task. At the same time, the requirement of minimum start weight is distinguished by simple analytical expression, which in fact makes possible its use as the basic criterion for optimum results in carrying out the design treatment.

The aim of ballistic designing and the part it plays within the field of over-all rocket designing determine the applicability of one sort of computational method or another, and the requirements imposed upon precision of resolution. In the ballistic designing stage one need not take into account all factors affecting the start weight of the rocket. Only the most essential are examined. At this stage of designing there is no need to achieve a great precision in determining the characteristics of the rocket, as they will alter and become refined in subsequent stages of designing. The methods of ballistic designing should be rather simple and -- the main thing -- they should ensure convenience of analysis of the influence of individual design parameters upon the characteristics of the rocket.

The methods system of ballistic calculation set forth in Chapter II makes it possible to present the range of a single-stage guided rocket having vertical start as a function of six parameters. In order to express these parameters in the form most convenient for the purposes of ballistic designing we transform the coefficients of equation (2.75).

Inasmuch as

$$P_0 = f(\lambda_a) p_0 F_a - p_{H0} F_a = F_a p_0 \left[ f(\lambda_a) - \frac{p_{H0}}{p_0} \right], \quad (3.1)$$

where  $f(\lambda_a) = (1 + \lambda_a^2) \left( 1 - \frac{k-1}{k+1} \lambda_a^2 \right)^{\frac{1}{k-1}}$  -- is the tabular gasodynamic function (see (2));

$p_0$  is the pressure in the chamber;

$\lambda_a$  is the nondimensional velocity in the outlet cross-section of the cone, determined by the relation  $F_a/F_{Cr}$ ,

then the coefficient A may be presented in the form

$$A = \frac{p_{H0} F_a}{p_0} = \frac{p_{H0}}{p_0} \frac{1}{\left[ f(\lambda_a) - \frac{p_{H0}}{p_0} \right]} \quad (3.2)$$

The coefficient B may be transformed as follows:

$$B = \frac{7140iS_m}{p_0} = \frac{7140iS_m}{\eta Q_0} = \frac{7140i}{\eta \Pi_0} \quad (3.3)$$

where  $Q_0$  is the start weight of the rocket;  
 $\Pi_0 = \frac{Q_0}{S}$  is the initial transverse load.

When this is done maximum range may be presented in the form

$$X_{max} = f(J_{10}, \mu_k, \eta_0, \Pi_0, p_0, \lambda_a). \quad (3.4)$$

We may note that with selected fuel characteristics, pressure in engine  $p_0$ , and expansion of cone  $F_a/F_{cr}$ , which is to say with  $\lambda_a$  given, the amount of unit impulse at the ground,  $J_{10}$ , is unequivocally determined. Consequently, with values of  $\eta_0$ ,  $\Pi_0$ ,  $p_0$  and  $\lambda_a$ , the value of  $\mu_k$  which corresponds to them for a given range. From here on, in examining treatment of the problem of ballistic designing we shall assume that the relationship  $\mu_k = f(X_m, \eta_0, \Pi_0, p_0, \lambda_a)$  is given. From here on we shall call the parameters  $\eta_0$ ,  $\Pi_0$ ,  $p_0$  and  $\lambda_a$  project parameters. We shall call the values of the project parameters that ensure minimum start weight of the rocket with the fuel and materials characteristics selected optimum values.

In this chapter we examine in general form the problem of the ballistic designing of a single-stage guided solid-fuel rocket. The methods system for solution of this problem comprises the following basic steps:

- utilization of the relationships connecting the weight of the rocket with the parameters of the motive assembly;
- calculation of the start weight of a rocket for a set range of fire, with fixed values for the project parameters;
- analysis of the influence of each of the project parameters upon the start weight of the rocket; selection of optimum value of project parameters;
- determination of basic construction design parameters of the optimum ballistic variant.

The use of electronic computers substantially expands the potentialities of ballistic designing, making it possible to carry out computations for a large number of variants having various combinations of project parameters.

### 3.2. Weight Equation of Single-Stage Ballistic Rocket.

The start weight of the rocket is

$$Q_0 = q_{nn} + q_{ny} + q_{oy} + q_{ky} + q_{ao} + q_{kc} + q_a + q_c + q_{tp} + \omega, \quad (3.5)$$

where  $q_{nn} = q_{ul}$  is the weight of the useful load (warhead, scientific investigation apparatus, etc.);

$q_{ny} = q_{fg}$  is the weight of the apparatus for flight guidance of the rocket;

$q_{oy} = q_{go}$  is the weight of the executant guidance organs and power transmissions (gasodynamic rudders, vernier engines, turning jets, rudder machines, and power assemblies);

$q_{ky} = q_{se}$  is the weight of the section casings carrying the useful load and the guidance apparatus;

$q_{ao} = q_{ao}$  is the weight of the aerodynamic organs (stabilizers, aerodynamic rudders, wings used in rockets having intermediate ballistics);

$q_{kc} = q_{cc}$  is the weight of the connection and commutation units (fastening units and parts, cables and air conduits of guidance system);

$q_a = q_{cap}$  is the weight of the forward cap of the engine;

$q_c = q_{cone}$  is the weight of the cone unit;

$q_{tp} = q_{tr}$  is the weight of the cylindrical part of the engine;

$\omega$  is the weight of the rocket charge.

Such a breakdown is arbitrary, but this has no effect upon the approach to solution of the problem of ballistic designing.

The weight equation must be transformed in such fashion as to secure the simplest possible relationships connecting the start weight of the rocket with the parameters of the motive apparatus, and through these, with the project parameters examined above. Similar relationships have been proposed by various authors (3, 6, 8). Essentially these relationships are based upon elementary theoretical considerations. But as statistical data secured from analyses of designs that have been worked out are accumulated, similar methods systems may be reinforced through the use of experimental statistical coefficients and formulas.

Let us unite in a first group the weights of useful load, guidance apparatus on board, and the sections of the casing. The weight of the useful load is the initial characteristic in designing. One can assume the weight of the apparatus and the casing sections as being designated or selected independently of the start weight of the rocket. Let us call the sum of the weights of the first group the adduced weight of useful load:

$$q'_{nn} = q_{nn} + q_{ny} + q_{ky}. \quad (3.6)$$

From here on we shall regard the adduced weight of useful load as a known quantity.

We shall assign to a second group the units the weight of which may be assumed in first approximation to rise proportionately with the start weight of the rocket:

$$q_{oy} + q_k + q_{so} = (\bar{q}_{oy} + \bar{q}_k + \bar{q}_{so}) Q_0 \quad (3.7)$$

where  $\bar{q}_{oy}$ ,  $\bar{q}_k$ , and  $\bar{q}_{so}$  are weight coefficients determined as mean statistical quantities according to data on analogous models and on developed design treatments.

For brevity's sake let us designate:

$$\bar{k} = \bar{q}_{oy} + \bar{q}_{kc} + \bar{q}_{so}. \quad (3.8)$$

A third group brings together the weight of the units of the motive apparatus.

Let us introduce the designation:

$$\alpha = \frac{q_{rp} + q_A + q_c}{\omega} = \frac{q_{xy}}{\omega}, \quad (3.9)$$

where  $q_{xy}$  is the weight of the motive apparatus structure.

The quantity  $\alpha$  characterizes the weight ideality of the engine design, for which reason it is called the engine coefficient.

Sometimes in computations the coefficient  $\beta = 1 + \alpha$  is used in place of the coefficient  $\alpha$ .

The weight of the fuel may be presented in the form:

$$\omega = \omega_{ps} + \omega_{rs} + \omega_{as} + \omega_{so}$$

where  $\omega_{ps}$  is the working supply of fuel;  
 $\omega_{rs}$  is the reserve supply;  
 $\omega_{as}$  is the prestart supply;  
 $\omega_{so}$  is the weight of degressive residues.

The reserve supply of fuel is selected so as to be such that the engine cuts off from the automatic guidance system at a certain range, and with firing at limit range.

The prestart supply constitutes the weight of fuel burned after the igniter commences to operate and up to the attainment of thrust equal to the weight of the rocket.

The residues of fuel which burn degressively after consumption of the basic mass of fuel are considered lost for the working process of a solid-fuel engine. The presence of degressive residues can be occasioned

by the form of the charge (for example, with a channel of star-shaped section) or by difference in vaulting (elliptical or conical character of channel, eccentricity of channel relative to diameter of rocket chamber).

In amount these components differ substantially from one another. For a solid-fuel rocket engine the time of getting under way amounts, depending on caliber, to some hundredths to tenths of a second, as a consequence of which the third component represents an infinitesimal quantity which can be disregarded in ballistic designing. The second and fourth components are more considerable, but they too represent a relatively small proportion of the working supply of fuel. The quantity of these components can be refined in the stage of preliminary draft designing. In ballistic designing they can be taken into account through a correctional coefficient  $k_w$ , selected on the basis of processing statistical data for examples close in characteristics.

Thus:

$$\omega = k_w \omega_{ps},$$

in which connection

$$\mu_k = \frac{\omega_{ps}}{Q_0} = \frac{\omega}{k_w Q_0} = \frac{\mu_k}{k_w}.$$

Making use of the designations adopted, we secure

$$Q_0 = q'_{nn} + \bar{k}Q_0 + (1 + \alpha)\omega, \quad (3.10)$$

whence

$$\frac{q'_{nn}}{Q_0} = 1 - (1 + \alpha)\mu_k - \bar{k}, \quad (3.11a)$$

or

$$\frac{q'_{nn}}{Q_0} = 1 - \beta\mu_k - \bar{k}. \quad (3.11b)$$

The ratio  $q'_{nn}/Q_0$  may be called the design-weight ideality coefficient of the rocket. One can take this criterion as a guide in comparing, for a given range, models that differ as regards start weight and weight of useful load.

With given adduced weight of useful load, if the characteristics  $\beta$  and  $\bar{k}$  are known the start weight of a rocket for a given range is defined as

$$Q_0 = \frac{q'_{nn}}{1 - \beta\mu_k - \bar{k}}. \quad (3.12)$$

It should be emphasized that in equation (3.12), as in subsequent operations associated with its transformation, the value  $\mu_k$  is introduced; it represents the ratio of the total weight of the charge to the start weight of the rocket. This value is  $k_0$  times greater than that which ensures a given range of fire, and it is secured by ballistic computation.

### 3.3. The Weight Coefficient of a Solid-Fuel Rocket Engine

Let us consider what the weight of the basic units of the solid-fuel motive apparatus depends upon.

The weight of the cylindrical portion of the casing (the tube) can be represented as the sum of the weights of the container envelope and of the heat insulation covering or the adhesion layer  $q_{\text{тн}}$ . The container envelope is made of high-strength material and is the element of the structure that takes up internal and external loads. In determination of the thickness of the container envelope,  $\Delta_k$ , at the ballistic designing stage we shall start from its loading with internal pressure alone, regarding it as a thin-walled endless tube. Then

$$\Delta_k = \frac{p_m D_H}{2\sigma_B}, \quad (3.13)$$

where  $D_H$  is the caliber of the engine

$p_m$  is the computed pressure;

$\sigma_B$  is the strength limit of the envelope material.

Inasmuch as with present-day use in rocket technics of materials having high strength characteristics the thickness of the envelope constitutes an inconsiderable portion of the caliber of the engine, in determining the weight of the envelope one may start from a very simple relation:

$$q_{\text{тн}} = \pi D_H \Delta_k \gamma_k k_L L, \quad (3.14)$$

where  $\gamma_k$  is the unit weight of the envelope material;

$L$  is the length of the charge;

$k_L$  is the coefficient covering the difference between the lengths of the charge and the chamber.

Inasmuch as the relative thickness of the envelope

$$\bar{\Delta}_k = \frac{\Delta_k}{D_H} = \frac{p_m}{2\sigma_B},$$

we may write

$$q_{\text{тн}} = \pi D_H^2 \bar{\Delta}_k \gamma_k k_L L. \quad (3.15)$$

A layer of heat-protective covering is applied to the inner surface of the casing of the solid-fuel rocket engine. The thickness of this

layer is selected in correspondence with the heat-exchange conditions in the section in question and with the thermophysical characteristics of the covering material adopted. In the section of the casing protected by the charge attached to it the thickness of this layer is slight and in large-caliber examples it comes to a few millimeters (in the solid-fuel engine of the "Minuteman" rocket it is 5 millimeters).

When slotted charges are used or ones with conical burning faces, some part of the internal cylindrical surface of the casing comes into contact with hot gases from the start of combustion of the charge onward. As the charge burns the contact surface enlarges. These sections of the casing need reinforced heat protection. The thickness of the covering in these sections may reach some tens of millimeters.

The temperature of the products of fuel combustion has a substantial influence on the thickness of the heat insulation covering (this ratio is close to linear); so do the solid particles found among the combustion products, and the chemically aggressive components. Computation of heat-protective coverings for solid-fuel rocket engines are examined in studies (8, 18).

In order to ensure adhesion (bonding) of fuel to the inner surface of the casing, an adhesion layer the thickness of which is determined by technological considerations is applied to the latter.

The weight of these coatings may be computed as

$$q_{\tau n} = \pi D_n \Delta_n \gamma_n l.$$

If one assumes the thickness of the coating over the length of the cylindrical part of the casing to be a constant, equal to some mean value, we get

$$q_{\tau n} = \pi D_n \cdot \Delta_n \gamma_n k_L L. \quad (3.16)$$

The weight of the cylindrical section of the casing is

$$q_{\tau} = q_{\tau k} + q_{\tau n} = \pi D_n \Delta_n k_L L \left( \gamma_k + \gamma_n \frac{\Delta_n}{\Delta_k} \right). \quad (3.17)$$

Let us designate

$$\gamma_{np} = \gamma_k + \gamma_n \frac{\Delta_n}{\Delta_k}$$

and let us call this quantity the adduced unit weight of the envelope. In the ballistic designing stage the ratio  $\frac{\Delta_n}{\Delta_k}$  is selected on the basis of statistical analysis of designs processed earlier.

Equation (3.17) is transcribed in the following form:

$$q_r = \gamma_{np} \pi D_n^2 \Delta_n k_L L. \quad (3.18)$$

The weight of the jet cone can also be represented in the form of the sum of the weights of the container envelope and the heat insulation material:

$$q_c = q_{cx} + q_{c.n} \quad (3.19)$$

The thickness of the carrier envelope loaded with low pressure and protected from the action of high temperatures is ordinarily selected with construction considerations in mind (i.e., hardness considerations and those relating to the attachment to it of the organs for guiding the thrust vector). If one assumes the thickness of the container envelope to be proportional to the diameter of the given section of the cone, its weight may be represented in the form

$$q_{cx} = \int_0^L \gamma_k \pi D^2 \bar{\Delta}_k dl. \quad (3.20)$$

Inasmuch as  $dl = 1/2 dD |\operatorname{ctg} \alpha|$  (see Figure 3.1), we secure

$$q_{cx} = \int_{D_{cr}}^{D_a} \gamma_k \pi D^2 \bar{\Delta}_k |\operatorname{ctg} \alpha| dD. \quad (3.21)$$

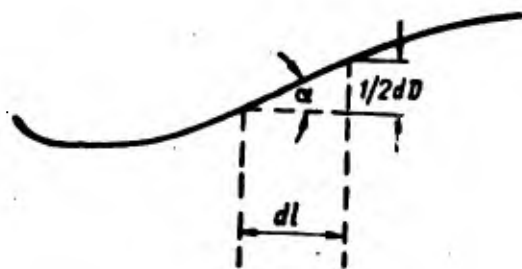


Figure 3.1. Elements of cone contour.

With a given profile  $\alpha = f(D)$  the weight of the cone envelope for a fixed ratio  $D_a/D_{cr}$  may be represented in a general form associating its amount with some characteristic diameter, for which it is well to select  $D_{cr}$ . Then

$$q_{cx} = k_{cx} D_{cr}^3, \quad (3.22)$$

or

$$q_{cx} = k_{cx} F_{np}^3. \quad (3.23)$$

Inasmuch as the thrust of the engine is proportional to the area of the critical section of the cone, one may write

$$q_{cr} = k_{cr} P^{3/2}. \quad (3.24)$$

Coatings are ordinarily applied over the entire length of the cone of a solid-fuel rocket engine having long working time. Various plastics can be used for protection of the inlet and outlet funnels of the cone. In the area of the critical cross-section of the cone an insert of refractory erosion-resistant material (graphite, molybdenum, tungsten) is positioned. If in first approximation we assume that the thickness of the heat-protective elements of the cone is proportional to the time of operation of the engine  $\tau$ , the over-all weight of these elements is expressed by the relationship

$$q_{cr} = \int_{D_{cr}}^{D_a} \gamma_n \pi D k_\tau \tau |\operatorname{ctg} \alpha| dD. \quad (3.25)$$

Carrying out transformations analogous to those examined in the foregoing case we secure

$$q_{cr} = k_{cr} F_{cr} \tau. \quad (3.26)$$

Assuming  $F_{cr} \sim P$ , we secure

$$q_{cr} = k_{cr} P \tau = k_{cr} I, \quad (3.27)$$

where  $I$  is the over-all impulse of thrust.

The total weight of the cone comes to

$$q_c = k_{cr} P^{3/2} + k_{cr} I. \quad (3.28)$$

For engines having long working time the second term may prove determinative. Thus Vandenberg (2) considers that the weight of the cone is approximately proportional to the over-all impulse, i.e.,

$$q_c \approx k_c I.$$

On the basis of analysis of designs examined he suggests taking  $k_c$  as more or less equal to  $2.5 \cdot 10^{-4}$ . If  $I$  is taken in kilogram times seconds, then with this coefficient the weight of the cone is secured in kilograms. According to data in the literature (4, 5), for some of the most recent solid-fuel rocket engine designs one gets

$$k_c = (0.9 - 1.2) 10^{-4}.$$

The relationships secured for  $q_{cr}$  and  $q_{cn}$  are correct, strictly speaking for geometrically similar cones, i.e., ones having equal  $D_a/D_{cr}$

ratios. Let us see how the coefficients  $q_{ck}$  and  $q_{cn}$  will change as this relationship changes. Augmentation of the weight of the carrier envelope of the jet as the area of the outlet cross-section increases may be presented as

$$\Delta q_{ck} = \gamma_k \bar{\Delta}_k \Delta S,$$

where  $\Delta S$  is the augmentation of the surface of the cone which corresponds to augmentation of  $\Delta F_a$ .

But

$$\Delta S = \Delta F_a \cdot \text{ctg } \bar{\alpha}_a,$$

where  $\bar{\alpha}_a$  is the mean angle of conicity of the cone for the outlet portion.

In turn,

$$\Delta F_a = F_{kp} \cdot \Delta \left( \frac{F_a}{F_{kp}} \right).$$

Accordingly:

$$\Delta q_{ck} = \gamma_k \bar{\Delta}_k \text{ctg } \bar{\alpha}_a F_{kp} \Delta \left( \frac{F_a}{F_{kp}} \right). \quad (3.29)$$

From expression (3.23) we secure

$$\Delta q_{ck} = F_{kp}^{3/2} \Delta k_{ck}. \quad (3.29a)$$

Equating the right-hand parts of equations (3.29) and (3.29a), we find that

$$\Delta k_{ck} = \frac{\gamma_k \bar{\Delta}_k \text{ctg } \bar{\alpha}_a}{F_{kp}^{1/2}} \Delta \left( \frac{F_a}{F_{kp}} \right).$$

Carrying out analogous transformations, we secure

$$\Delta q_{cn} = \gamma_n k_n F_{kp} \text{ctg } \bar{\alpha}_0 \Delta \left( \frac{F_a}{F_{kp}} \right),$$

whence

$$\Delta k_{cn} = \gamma_n k_n \cdot \text{ctg } \bar{\alpha}_0 \Delta \left( \frac{F_a}{F_{kp}} \right).$$

The cap of the casing is of spherical or elliptical shape. The thickness of the spherical cap should theoretically be equal to half the thickness of the cylindrical envelope of the casing. Actually the effective thickness of the cap, by virtue of the placement of various supports and fastenings, will be considerably greater. The weight of the strong part  $q_{cc}$  [weight, cap of casing] for a rocket of a given class may,

evidently, be assumed to be proportionate to the area of the mid-section of the rocket:

$$q_{AK} = k_{AK} \frac{\pi D_n^2}{4}. \quad (3.30)$$

A considerable part of the weight of the caps, particularly the cone one, consists of the weight of the heat-protective coating. Thus, for example, for the cone cap of the engine of the first stage of the "Minuteman" rocket the thickness of the glass-plastic coating exceeds 50 millimeters. In order to determine the weight of these coatings one may make use of a relation analogous to relation (3.26):

$$q_{AK} = k_{AK} \frac{\pi D_n^2}{4} \tau. \quad (3.31)$$

Accordingly:

$$q_A = \frac{\pi D_n^2}{4} (k_{AK} + k_{AK} \tau). \quad (3.32)$$

The weight of the rocket charge is expressed by the formula

$$w_r = \delta \frac{\pi D_n^2}{4} \varphi \epsilon L, \quad (3.33)$$

where  $\delta$  is the specific weight of the fuel;

$\epsilon$  is the coefficient of the extent to which the area of the cross section of the chamber is filled with the charge,  $\epsilon = \frac{S_r}{F_n}$ ;

$\varphi$  is a coefficient covering the difference between the area of the chamber and the mid-section of the rocket

$$\varphi = \frac{F_n}{F_n} = \left(1 - 2 \frac{\Delta_n + \Delta_k}{D_n}\right)^2. \quad (3.34)$$

When the charge consists of sections having substantially varying values of  $\epsilon$  (as, for example, a slotted charge), in examining relation (3.33) one should have in mind the corrected value

$$\epsilon = \frac{\epsilon_1 L_1 + \epsilon_2 L_2}{L_1 + L_2} = \epsilon_{\text{cor}}$$

where  $\epsilon_1$  and  $\epsilon_2$  are values of  $\epsilon$  for individual sections of the charge;  $L_1$  and  $L_2$  are the lengths of these sections.

Substituting the values derived for the weight of individual elements of the engine, in the initial equation (3.9), after contraction we have

$$\alpha = \frac{k_{2k} + 4\gamma_{np}k_L\bar{J}_kL}{\delta\varphi_eL} + \frac{k_cI + k_{2k}\tau S_M}{\omega}. \quad (3.35)$$

Inasmuch as  $\tau = I/P$  and  $\omega = I/J_{icp}$  we secure

$$\alpha = \frac{k_{2k} + 4\gamma_{np}k_L\bar{J}_kL}{\delta\varphi_eL} + J_{icp} \left( k_c + k_{2k} \frac{S_M}{P} \right). \quad (3.36)$$

After dividing both arms of the equation (3.33) by the area of the mid-section of the rocket and after having replaced  $\omega$  with the product  $\mu_k Q_0$ , we find that

$$\frac{\mu_k Q_0}{S_M} = \delta\varphi_eL, \quad (3.37)$$

or

$$\mu_k \Pi_0 = \delta\varphi_eL, \quad (3.38)$$

whence

$$e = \frac{\mu_k \Pi_0}{\delta\varphi_eL}; \quad (3.39)$$

$$eL = \frac{\mu_k \Pi_0}{\delta\varphi_e}. \quad (3.40)$$

We shall substitute:

$$\frac{S_M}{P} = \frac{S_M}{\eta Q_0} = \frac{1}{\eta \Pi_0}. \quad (3.41)$$

Substituting expressions (3.40) and (3.41) into expression (3.36), we secure.

$$\alpha = \frac{k_{2k} + 4\gamma_{np}k_L\bar{J}_kL}{\mu_k \Pi_0} + J_{icp} \left( k_c + k_{2k} \frac{1}{\eta \Pi_0} \right). \quad (3.42)$$

The weight summary of the 15 KS 25,000 (4), set forth below, may give some idea of the distribution of weight for a low-thrust engine among its basic elements.

The weight coefficient of an engine depends upon the selection of thrust parameters, the characteristics of the structural and heat-insulation materials used, and the design configuration of the individual units of the engine assembly.

With increase in the dimensions of an engine the value of  $\alpha$  declines. For present-day large engines in single-stage rockets  $\alpha = 0.1$  to 0.08 (5, 15).

One can decrease the weight coefficient of an engine by:

- reducing the working pressure in the engine;
- using fuels having a low temperature ratio, thermostarting the engine, or regulating the cone with a view to diminishing the pressure-temperature ratio;
- making the casing of the engine of materials having high unit strength;
- increasing the density of the charging.

As the computed pressure is decreased and the unit strength of the rocket chamber is increased, the part played by heat-insulating coatings, the caps, and the cone in the weight balance rises.

Even in an engine of relatively small dimensions, as will be seen from the table presented, the weight of heat insulation and the cone make up about 25 percent of the weight of the engine structure. For various modifications of the "Polaris" rocket in the first-stage engine the overall weight of the caps and the cone block, according to the data of Table 3.1, makes up from 30 to 44 percent of the weight of the casing without heat insulation. In this connection the design refinement of the cones of solid-fuel rocket engines and the use of the most efficient heat-insulating materials take on significance.

Table 3.1

<u>Element</u>	<u>Weight,</u> <u>kg</u>	<u>Characteristics</u> <u>of Engine</u>	<u>Value of</u> <u>Characteristic</u> <u>With <math>T^{\circ} = + 21^{\circ} C</math></u>
Casing	171	Mean pressure	61.5 kg/cm <sup>2</sup>
Heat insulation	32		
Fuel	800	Burning time of charge	12.7 sec
Igniter	2		
Cone	21	Mean thrust	12,110 kg
Total	1,026	Unit impulse	219.8 sec

#### 3.4. Relationship Between Admissible Changes in Unit Impulse and Weight of Engine Structure for Given Velocity of Rocket at End of Active Section

In designing a rocket it is necessary to take into account the factors which on the one hand increase unit impulse and on the other hand raise the weight of the engine structure. Let us enumerate the basic factors among these.

1. Temperature of burning of fuel charge. Use of fuels having a high combustion temperature in the engine is the basic way of increasing the unit impulse of a solid-fuel rocket engine. But under these circumstances the need for heavier heat-insulation coatings, and for the use of special measures for protection of the cone against heat, as a result of increase in its weight, also increase (18).

2. Working pressure in the engine. As pressure increases, the  $p_a/p_0$  ratio rises, which leads to increase of  $I_1$ , and at the same time the thickness of the walls of the engine casing mounts.

3. The  $F_a/F_{cr}$  ratio. As the outlet cross-section of the cone and the  $F_a/F_{cr}$  ratio rise, the mean value for  $l_{icp}$  in the active section also increases (up to a certain limit). At the same time the weight of the cone increases.

In order to find a solution which will ensure maximum advantage in the weight of the rocket when the factors listed are taken into account, it is necessary to establish an equivalent for changes in unit impulse and the weight of the engine structure vis-à-vis maximum velocity of the rocket.

In determining this equivalent we shall assume that the parameters  $\eta_0$  and  $\Pi_0$  are given. For ballistic parameters at the end of the active section of the trajectory which will ensure a given range of fire, the following condition must be met:

$$dV_k = 0 \quad du_e \cdot k + u_e \cdot dw_k = dl_{10} \cdot g \cdot w_k + gl_{10} \cdot dw_k$$

whence

$$\frac{dl_{10}}{l_{10}} = - \frac{dw_k}{w_k} \quad (3.43)$$

From formula (2.75)

$$dw_k = d[U_1(\mu_k)] - \frac{1}{\eta} d[U_2(\mu_k)] + d[A\Phi_1(\mu_k, l_{10}, \eta)] - B \cdot d[\Phi_2(\mu_k, l_{10}, \eta)] \quad (3.44)$$

Inasmuch as the third and fourth terms of expression (3.44) represent only a small part of the sum of the first two, in a majority of cases not exceeding 1-2 percent, their differentials may be regarded as quantities of the second order of smallness. Dropping these components out in the expression for  $w_k$ , and their differentials in the expression for  $dw_k$ , we secure a simplified equation

\* To simplify the computation we take  $k_e$  as being equal to 1.

$$\frac{dI_{10}}{I_{10}} = - \frac{d[U_1(\mu)] - \frac{1}{\eta} d[U_2(\mu)]}{U_1(\mu) - \frac{1}{\eta} U_2(\mu)} \quad (3.55)$$

We should note that the function  $U_2(\mu)$  approximates a linear ratio with great precision

$$U_2(\mu) = a + b\mu,$$

where  $a = 0.1$ ,  $b = 0.689$ .

Making use of this approximation we secure:

$$d[U_1(\mu)] = \frac{d\mu}{1-\mu};$$

$$d[U_2(\mu)] = b d\mu.$$

The equation assumes the form

$$\frac{dI_{10}}{I_{10}} = - \frac{\frac{1}{1-\mu} - \frac{b}{\eta}}{\ln \frac{1}{1-\mu} - \frac{a+b\mu}{\eta}} d\mu \quad (3.56)$$

Considering the fuel weight,  $\omega = \mu Q_0$ , as a constant we secure

$$d\mu \cdot Q_0 + dQ_0 \cdot \mu = 0. \quad (3.57)$$

Since what we are examining is change in the weight of the rocket by virtue of the weight of the engine structure, then

$$dQ_0 = dq_{xy}$$

Consequently

$$d\mu = - \frac{\mu \cdot dq_{xy}}{Q_0} \quad (3.58)$$

Substituting expression (3.58) into equation (3.56), we secure

$$- \frac{dq_{xy}}{Q_0} = \frac{\ln \frac{1}{1-\mu} - \frac{a+b\mu}{\eta}}{1 - \frac{b}{\eta}(1-\mu)} \frac{1-\mu}{\mu} \frac{dI_{10}}{I_{10}}.$$

Multiplying both arms of the equation by the ratio  $\frac{Q_0}{q_{xy}}$ :

$$\frac{dq_{AY}}{q_{AY}} = \frac{\ln \frac{1}{1-\mu} - \frac{a+b\mu}{\eta}}{1 - \frac{b}{\eta}(1-\mu)} \frac{Q_0(1-\mu)}{q_{AY}\mu} \frac{dl_{10}}{l_{10}}. \quad (3.59)$$

Hence the percentage change in the weight of the engine structure which is equivalent to a 1 percent change in unit impulse is equal to

$$D = \frac{\ln \frac{1}{1-\mu} - \frac{a+b\mu}{\eta}}{1 - \frac{b}{\eta}(1-\mu)} \frac{Q_0}{q_{AY}} \frac{1-\mu}{\mu}$$

or, since  $Q_0(1-\mu) = q_n$  (the passive weight of the rocket),

$$D = \frac{\ln \frac{1}{1-\mu} - \frac{a+b\mu}{\eta}}{1 - \frac{b}{\eta}(1-\mu)} \frac{q_n}{q_{AY}} \frac{1}{\mu}. \quad (3.60a)$$

Considering that  $q_{AY} = Q_0\mu\alpha$ , this expression may also be presented in the form

$$D = \frac{\ln \frac{1}{1-\mu} - \frac{a+b\mu}{\eta}}{1 - \frac{b}{\eta}(1-\mu)} \frac{1-\mu}{\alpha\mu^2}. \quad (3.60b)$$

From the relationships examined it follows that increase in the weight of the solid-fuel rocket engine structure is expedient if, with a weight increase of D percent, the unit impulse rises by no less than 1 percent; and on the other hand, reduction of engine weight by virtue of diminution of unit impulse attains its goal if with reduction of weight by D percent the unit impulse falls off by no more than 1 percent.

In Figure 3.2 there is set forth a graph for the dependence of  $\alpha D$  upon  $\mu_k$ , computed for  $\eta = 2, 4, 6$  according to formula (3.60b). In order to determine the value of D from it, one must know the weight coefficient  $\alpha$ . At present values of  $\alpha$  from 0.08 to 0.1 are achieved in single-stage solid-fuel rocket engines and in the first stage of multiple-stage ones (5). Under these circumstances, for  $\eta = 4-6$  according to the graph and for the range of  $\mu_k$  under examination the characteristic  $D = 3-18$ .

With rise in  $\mu_k$  the ratio  $q_n/q_{AY}$  declines, i.e., the share of the weight of the engine structure in the passive weight of the rocket mounts. The rocket becomes more sensitive to relative change in weight of the engine structure, for which reason the quantity D also declines with increase of  $\mu_k$ . For models of more up-to-date design of engine (low  $\alpha$ ) the D characteristic is greater than for models having high  $\alpha$ . This is explained by the fact that decrease of  $\alpha$  with values of  $\mu_k$  equal leads

to decrease in the proportion of the weight of the engine structure to the weight of the rocket, which lowers the sensitivity of the rocket to change in the weight of the engine structure. Increase in thrust-weight ratio within limits  $\eta < \eta_{\text{opt}}$  (cf. 3.6) also leads to increase in D. Heightening thrust-weight ratio is equivalent, from the standpoint of ensuring a given rocket speed, to reduction of  $\mu_{\text{K}}$ , i.e., to increase of the passive weight of the rocket, which in turn is accompanied by reduction of sensitivity to change in weight of the engine structure.

### 3.5. Determination of Basic Dimensions of Charge

The selection of basic dimensions of charge is limited by the existence of a certain value for the loading criterion which characterizes the threshold for normal functioning of the charge. The basic dimensions of the charge should be coordinated with each other and with the interior dimensions of the engine in such fashion that the value of the loading parameter ensured thereby shall be less than the limit admissible one.

In domestic literature (6, 7, 8), use is customarily made of the loading parameter  $\alpha$ , proposed by Professor Yu. A. Pobedonostsev as a criterion for the combustion stability of the charge. There exists a certain maximum admissible value  $\alpha_{\text{np}}$ , upon exceeding which anomalous combustion of charge commences, accompanied by sharp reduction of unit impulse and sometimes passing over into spasmodic combustion with complete extinguishment. The value  $\alpha_{\text{np}}$  depends essentially upon the level of working pressure in the engine, the initial temperature of the charge, the brand of fuel, and some design peculiarities of the charge. In Figure 3.3 we present a graph associating the magnitude of the limit value  $\alpha_{\text{np}}$  with the working pressure in the engine, secured for one of the recipes for ballistic fuel (7). Each of the curves on the graph, constructed for a specific value for the initial temperature of the charges, limits at the bottom the field of pressures which ensure stable combustion. Obviously the value for  $\alpha_{\text{np}}$  chosen in designing should lie within this field.

Let us examine some studies of foreign investigators on this question. Wimpress (9), examining the planning of engines for ballistic fuel, shows that at high values for the  $F_{\text{kp}}/F_{\text{cb}}$  ratio pressure in the chamber becomes decidedly sensitive to change in the dimensions of the chamber

and the fuel. Basing himself upon experimental data, he asserts that for a charge in the shape of a cylindrical single-channel burner of JPN fuel with an initial temperature of  $54^{\circ}\text{C}$  the  $F_{\text{kp}}/F_{\text{cb}}$  ratio should not exceed 0.5. He represents this ratio in the form  $\frac{F_{\text{np}}}{F_{\text{cb}}} = \frac{S}{F_{\text{cb}}} : \frac{S}{F_{\text{np}}}$ . Inasmuch as

the magnitude of the divisor is limited, Wimpress considers that in planning a charge the principle part is played by the quantity  $K_1 = S/F_{\text{cb}}$ , which is identical with  $\alpha$ .

Bedevant (10) recommends that in planning a charge one start from the amount of admissible internal compression  $K_1$ , which by definition corresponds with our  $\alpha$  parameter.

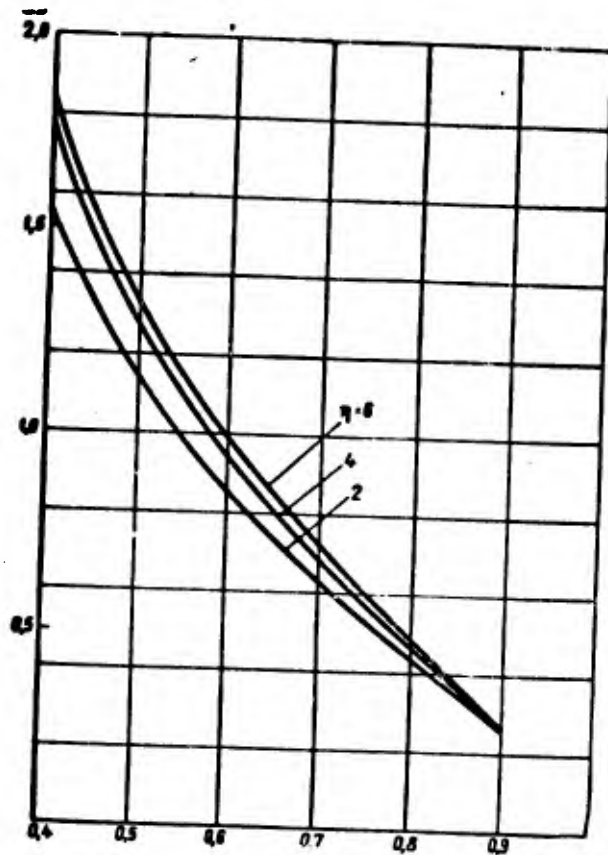


Figure 3.2. Dependence of  $aD$  characteristic upon relative supply of fuel and initial thrust-weight ratio  $\eta$ .

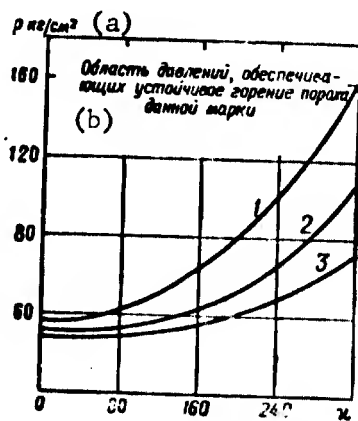


Figure 3.3. Dependence of minimum admissible pressure upon  $x$  for one of the ballistic fuels: 1 -- initial temperature of charge ( $T_H$ ) -  $20^\circ\text{C}$ ; 2 -- initial temperature of charge +  $20^\circ\text{C}$ ; 3 -- initial temperature of charge +  $60^\circ\text{C}$ . a --  $\text{kg}/\text{cm}^2$ ; b -- Field of pressures ensuring stable combustion of powder of a given brand.

Vandenkerkhove (2), Bartley and Mills (11), propose that in planning a solid-fuel rocket engine charge use be made of a graph of the relationship associating pressure in the forward part of the engine  $K_s = \frac{S}{F_{sp}}$  and  $H = \frac{l}{T} = \frac{F_{cs}}{F_{sp}}$ . In Figure 3.4 we show such a graph, constructed for one

of the mixed fuels according to data secured from stand tests of a solid-fuel rocket engine (11). It is not difficult to note that since  $K_s \cdot l = x$ , this graph admits of transposition into coordinates with  $p_{0x} = f\left(\frac{S}{F_{sp}}, x\right)$ .

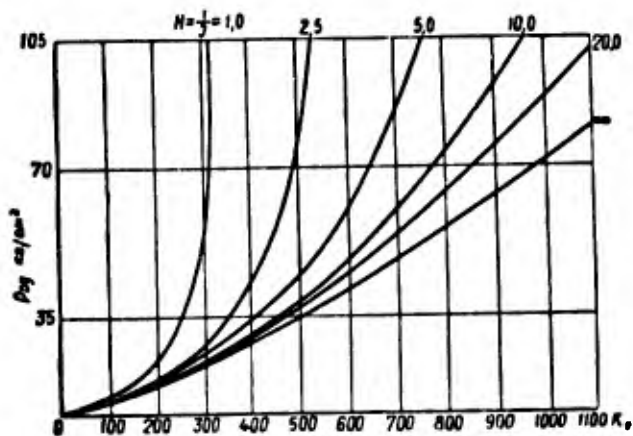


Figure 3.4. Relationship of pressure in forward part of engine to  $K$  and  $H$  for one of the mixed fuels ( $u_{10} = 0.38$  cm/sec,  $v = 0.25$ ,  $T_H = +20^\circ$  C).

Thus in all cases the criteria determining the selection of the geometry of the charge are two simplexes:  $x = \frac{S}{F_{cs}}$  and  $\frac{S}{F_{sp}}$ , the latter of which, with given characteristics of fuel, determines the mean level of working pressure in the engine.

In selecting the magnitude of the  $x$  parameter in computing a charge, one should bear the following circumstances in mind. On the one hand, as  $x$  rises (within the limits of the field of stable combustion of the charge) the density of loading increases. On the other hand, with rise of  $x$  the drop in pressure along the length of the charge rises, which with a given mean pressure in the engine leads to increase of pressure at the forward cap of the engine at the initial moment of combustion of the charge. With a certain value of  $x$  there commences, and with further increase therein there is augmented, an erosive combustion of fuel accompanied with rise in pressure in the initial section of the pressure curve. This leads to increase in maximum pressure at the forward cap, in accordance with which the computed pressure determining the thickness of the wall of the rocket chamber is in fact selected. Obviously the optimum will be a value for  $x$  which ensures sufficiently high density of loading

with a relatively low computed pressure. A final judgment on the optimum character of selection of  $\alpha$  may be formed upon the basis of computations of the weight of the rocket performed with various arbitrarily selected given values of  $\alpha$ .

The difficulties associated with erosive combustion and with great falls in pressures along the length of the rocket chamber are eliminated if one uses a charge with face burning. In addition a charge burning from the face ensures maximum possible density of loading.

But the deficiencies present in a charge with face burning block its use in ballistic rockets. With face burning, as fuel is consumed more and more new sections of the casing surface are laid bare and come into contact with burning gases. As a consequence of this, for the heat protection of the casing, and in particular for parts of the chamber facing the cone, a sufficiently thick and heavy heat insulation is required. In this respect the face charge is the antipode of a charge attached to the walls and burning from within, which ensures optimum resolution of the heat protection problem.

In addition, with face burning of charges of present-day fuels it is difficult to ensure a thrust-weight ratio such as is indispensable for a guided ballistic rocket.

The thrust provided with face burning may be calculated as

$$P = I_0 G = I_0 \delta S_f u.$$

The thrust-weight ratio ensured thereby is

$$\eta = \frac{P}{Q_0} = \frac{I_0 \delta S_f u}{\Pi_0 F_m}.$$

Adopting in first approximation an area of charge face equal to the area of the midship section, we secure

$$\eta \approx \frac{I_0 \delta u}{\Pi_0},$$

whence the necessary speed of combustion of fuel is equal to  $u = \frac{\eta \Pi_0}{I_0 \delta}$ .

Adopting  $\Pi_0 = 8000 \text{ kg/m}^2$ ,  $I_{10} = 230 \text{ kg} \cdot \text{sec/kg}$ ,  $\delta = 1700 \text{ kg/m}^3$ , we secure

$$u = \eta \frac{8000}{230 \cdot 1700} = 0,02\eta \text{ m/sec}$$

With  $\eta = 3-6$ , the requisite speed of face burning of charge comes to

$$u = 60-120 \text{ mm/sec},$$

which is beyond the limits of the potentialities of present-day solid fuels.

The relationships associated with the basic dimensions of the charge and the chamber with  $x = x_{np}$  have each their individual expression for each of the forms of charges. This limits the general character of a solution of the problem of ballistic planning, associating it with a specific form of charge, something which, strictly speaking, runs counter to the very formulation of the problem, which calls for the finding of optimum values for plan parameters and optimum forms and dimensions of charge. From this there arises a need for a generalized relationship, suitable for charges of any shape, and conjoined by a single feature most essential from the standpoint of their geometry. In planning a solid-fuel rocket engine, in most cases departure is from the requirement for constant thrust, which in its turn calls for constancy of the surface of the charge during combustion. With the condition  $S = \text{const}$  maintained independently of the shape of the charge, the following system of equations may be used for determination of the coefficient of charging:

$$\epsilon = \delta S e_1; \quad (3.61)$$

$$\epsilon = \delta L e F_x; \quad (3.62)$$

$$x = \frac{S}{F_x(1-\epsilon)}, \quad (3.63)$$

where  $e_1$  is the thickness of the vault which is burning.

Solution of this system leads to the expression

$$\epsilon = \frac{x e_1}{x e_1 + L}, \quad (3.64)$$

whence

$$L = x e_1 \frac{1-\epsilon}{\epsilon}. \quad (3.65)$$

If in formula (3.65) we insert in place of  $\epsilon$  its value from expression (3.39), we secure

$$L = \frac{x e_1}{\frac{x e_1 \delta \varphi}{\mu_x \Pi_0} - 1}. \quad (3.66)$$

We establish the relationship between the thickness of the burning vault and the initial thrust-weight ratio:

$$\eta_0 = \frac{P_0}{Q_0} = \frac{I_{10} G}{Q_0}.$$

Inasmuch as with constant expenditure of fuel:

$$G = \frac{w}{\tau};$$

$$\tau = \frac{e_1}{u_{cp}},$$

where  $u_{cp}$  is the speed of combustion of the fuel with the mean pressure in the engine adopted,

$$\eta_0 = \frac{I_{10} w u_{cp}}{Q_0 e_1}. \quad (3.67)$$

Since  $w/Q_0 = \mu_k$ , we secure

$$\eta_0 = \frac{I_{10} \mu_k u_{cp}}{e_1}, \quad (3.68)$$

whence

$$e_1 = \frac{I_{10} \mu_k u_{cp}}{\eta_0}. \quad (3.69)$$

Substituting expression (3.69) into expression (3.66), we secure

$$L = \frac{\mu_k}{\frac{\delta \varphi}{\Pi_0} - \frac{\eta_0}{\mu_k I_{10} u_{cp}}}. \quad (3.70)$$

### 3.6. Dependence of Start Weight of Rocket Upon Initial Thrust-Weight Ratio

Let us examine the way change in initial thrust-weight ratio of a rocket influences the amount of velocity it achieves at the end of the active section of the trajectory.

With increase in thrust-weight ratio losses of velocity  $\Delta v_g$ , associated with the operation of the force of gravity over the time the engine operates, expressed by the second term of formula (2.75), decline. In graph 3.5 we present computed values for this quantity, related to velocities  $v_u$  computed according to the Tsiolkovskiy formula. As will be seen from the graph, with low thrust-weight ratio ( $\eta < 2$ ) the magnitude of these losses depending on  $\mu_k$  may come to 15 to 36 percent of the maximum possible velocity of the rocket. With increase in thrust-weight ratio the magnitude of these losses falls off, and with  $\eta = 6-8$  it comes to 4-12 percent of  $v_u$ . Further increase in thrust-weight ratio leads to insubstantial change in these losses.

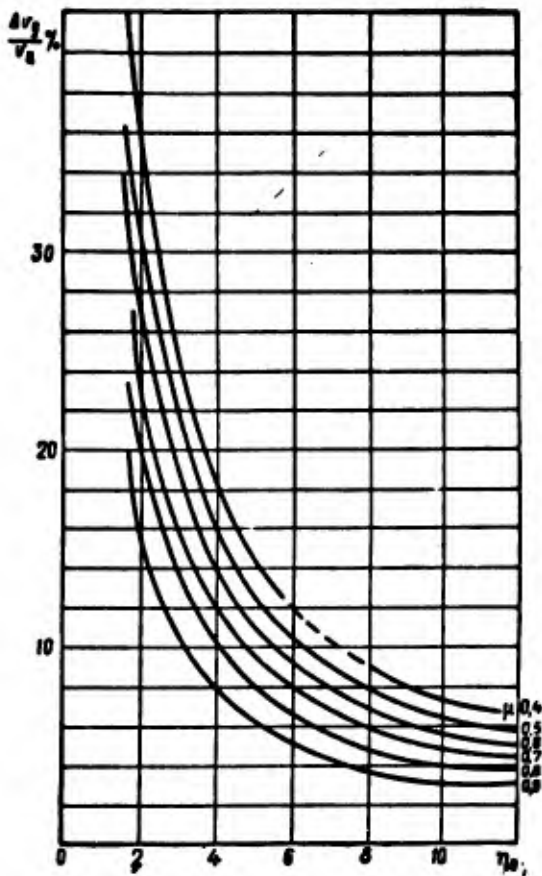


Figure 3.5. Change in loss in velocity of rocket occasioned by operation of force of gravity, with increase in initial thrust-weight ratio  $\eta_0$ . Losses are expressed in percentages of velocity, computed by the Tsiolkovskiy formula for  $\mu_x = 0.4-0.9$ .

Simultaneously with increase in thrust-weight ratio an abbreviation of the length of the active section takes place. High speeds of flight are achieved in the lower, dense strata of the atmosphere, as a consequence of which losses in velocity occasioned by the operation of frontal resistance mount. In the third term of expression (2.75), determining the amount of loss of velocity from frontal resistance, the parameter  $\eta$  enters into the denominator of coefficient B, and also as the argument of function  $\Phi_2$ . With increase in thrust-weight ratio this component grows. Thus, for example, with  $I_{10} = 230$  sec,  $\Pi_0 = 10000$  kg/m<sup>2</sup>,  $\mu_x = 0.7$  with change in thrust-weight ratio from 2.5 to 6 the magnitude of these losses, related to maximum possible velocity  $v_n$ , changes from 3.7 to 6.4 percent. As computations show, the relative magnitude of these losses with  $\Pi_0 > 8000$  kg/m<sup>2</sup> is relatively slight; with  $\eta < 6$  it does not exceed 7-8 percent.

With reduction of the altitude of the active section the mean-trajectory value of the unit impulse declines, and consequently the correction for velocity occasioned by the increase of thrust with altitude is reduced (the third component in formula 2.75).

With this sort of character of change in the individual components of expression (2.75) there must exist some value  $\eta_{vm}$  which ensures, with given values for  $\mu_k$ ,  $\Pi_0$ ,  $\rho_0$  and  $\lambda_a$ , the greatest velocity for the rocket at the end of the active section of the trajectory. Displacement from the value  $\eta_{vm}$  in the direction of less thrust-weight ratio leads to falling-off in velocity by virtue of increase in  $\Delta v_g$ . Exceeding the value  $\eta_{vm}$  increases losses in velocity by virtue of frontal resistance forces and reduction of the mid-trajectory value of the unit impulse. But one should note within the limits of increase of  $\eta$  which are of practical interest, reduction in the velocity of the rocket with  $\eta > \eta_{vm}$  proves to be insubstantial. The maximum of range, which is determined, not only by the amount of velocity of the rocket at the end of the active section, but also by the coordinates of that point, should correspond to  $\eta_{xm} < \eta_{vm}$ .

Obviously if one starts with a given range of flight of rocket, a minimum value for  $\mu_k$  will correspond to the value  $\eta_{xm}$ . In view of the transcendent character of the relationships associating maximum range with the project parameter  $\eta$ , analytical solution of the equation

$$\frac{d\mu_k}{d\eta} = 0$$

with  $X = X_3$  cannot be brought about, and the precise value of  $\eta_{xm}$  can be determined only by checking over a large number of ballistic variants.

But the influence of the thrust-weight ratio upon the start weight of a rocket is not limited by the quantity  $\mu_k$  necessary to ensure a set range  $X_3$ . It also becomes manifest in change of the weight coefficient of the engine,  $\alpha$ . Increase in thrust-weight ratio with fixed level of mean pressure in the engine for a given fuel calls for reduction of the thickness of the burning valut, which reduces the density of loading, and consequently increases the quantity,  $\alpha$ . For this reason the optimum thrust-weight ratio, at which minimum start weight of the rocket is ensured, should be determined according to the minimum of the product of  $(1+\alpha)\mu_k$ , i.e., from the condition

$$\frac{d\alpha}{d\eta} \mu_k + (1+\alpha) \frac{d\mu_k}{d\eta} = 0. \quad (3.71)$$

From equation (3.42)

$$\frac{d\alpha}{d\eta} = \frac{4\gamma_{sp} k_L \bar{\delta}_k}{\mu_k \Pi_0} \frac{dL}{d\eta} - \frac{l_1 c p k_{AM}}{\Pi_0 \eta^2}. \quad (3.72)$$

In order to determine the derivative  $\frac{dL}{d\eta}$  we make use of formula (3.70), from which

$$\frac{dL}{d\eta} = \frac{\mu_{K1}}{\pi J_{10} \mu_{cp}} \frac{1}{\left( \frac{\delta \varphi}{\Pi_0} - \frac{\eta_0}{\pi J_{10} \mu_{cp}} \right)^2}. \quad (3.73)$$

Substituting expression (3.73) into expression (3.72) we secure

$$\frac{d\alpha}{d\eta} = \frac{4\gamma_{np} k_L \bar{\Delta}_K}{\pi J_{10} \mu_{cp} \Pi_0} \frac{1}{\left( \frac{\delta \varphi}{\Pi_0} - \frac{\eta}{\pi J_{10} \mu_{cp}} \right)^2} - \frac{l_{1cp} k_{2K}}{\Pi_0 \eta^2}. \quad (3.74)$$

The first term in the right-hand arm of equation (3.74) expresses increase in the coefficient  $\alpha$  with a rise in thrust-weight ratio  $\eta$  by virtue of increased weight of rocket chamber. The second term expresses reduction of coefficient  $\alpha$  by virtue of lightening of heat protection of the cone as engine working time declines. The structure of equation (3.74) points toward the existence of a maximum of  $\alpha$  in accordance with  $\eta$ , but such a maximum is not of practical interest, because by view of the smallness of the second term, in the real range of change of  $\eta$  one will always note an increase in  $\alpha$  with increase in thrust-weight ratio.

If on the basis of ballistic computations we construct a relationship  $\mu_{K1} = f(\eta)$  with  $X = X_3$  and if from it we determine the value of  $\frac{d\mu}{d\eta}$ , it will be possible, making use of expression (3.74), to determine from equation (3.71) the optimum value for thrust-weight ratio, which with other parameters fixed will determine the minimum start weight of a rocket for a set range.

The existence of a dependence of  $\alpha$  upon  $\eta$  leads to the fact that the value of the thrust-weight ratio which at given  $\Pi_0$ ,  $l_{10}$ ,  $\lambda_a$  will ensure minimum start weight of the rocket will be displaced to the left of the optimum value  $\eta_{xm}$  determined only through solution of external ballistics.

Let us note that in the field of low thrust-weight relationships the weight characteristics of a solid-fuel rocket engine depend relatively slightly upon the magnitude of  $\eta$ , something which makes it possible to adopt relatively high values of thrust for solid-fuel rockets.

### 3.7. Selection of Initial Transverse Loading.

The influence of  $\Pi_0$  upon the start weight of a rocket may become manifest in the magnitude of  $\alpha$ , and also in the magnitude of the weight coefficient of the engine  $\alpha$ .

Change in the requisite value of  $\mu_K$  of a rocket for a set range with change in  $\Pi_0$  is associated with losses of velocity on account of frontal resistance during the active section of the trajectory. Turning to the relationship (2.75), one can follow the way the quantity  $\underline{w}$  changes with change in  $\Pi_0$  and with fixed values for  $\eta$ ,  $\mu_K$ ,  $l_{10}$  and  $\rho_0$ . In Figure 3.6 we show a graph of  $w = f(\Pi_0)$ , which we have constructed in accordance

with data secured by computation according to formula (2.75), for two thrust-weight ratio values. As will be seen from the graph, the influence of  $\Pi_0$  upon the amount of the velocity at the end of the active section of the trajectory is substantially pronounced only at low values of  $\Pi_0$  (in the case examined, with  $\Pi_0 < 5000 \text{ kg/m}^2$ ). With values of  $\Pi_0 > 8000 \text{ kg/m}^2$  the quantity  $\underline{w}$  changes very little. Thus, with  $\eta = 2,5$  changes of from 8,000 to 12,000  $\text{kg/m}^2$  increases  $\underline{w}$  by less than 2 percent. With rise in thrust-weight ratio the relative change in  $\underline{w}$  provoked by increase in rises because with increase of  $\eta$  the latitude of the active section declines and great velocities are reached by the rocket in the lower, denser strata of the atmosphere, in view of which the part played by aerodynamic resistance rises and the sensitivity of velocity to change in the area of the midship section is heightened. But even with  $\eta = 6$ , in the range of changes of  $\Pi_0$  examined the relative change in  $\underline{w}$  comes to 3 percent in all. Consequently, with  $\Pi_0 > 8000 \text{ kg/m}^2$  maximum velocity at the end of the active section depends but little upon initial transverse loading of the rocket.

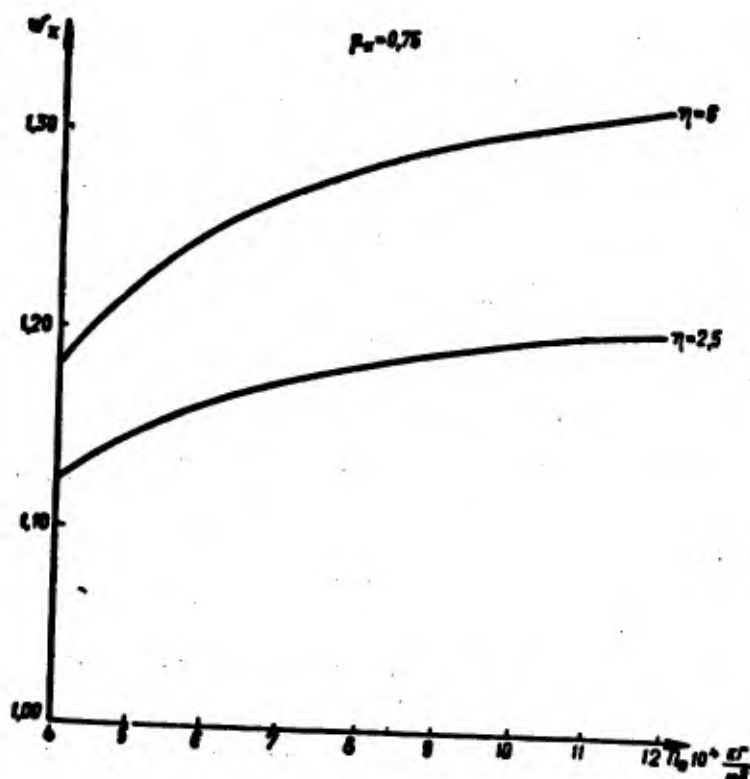


Figure 3.6. Change in relative velocity of rocket at end of active section of trajectory with rise in initial transverse loading  $\Pi_0$  for a thrust-weight ratio  $\eta_0 = 2,5$ ;  $\eta_0 = 6$ .

Obviously, turning to the condition  $\underline{w} = \text{const}$ , which corresponds to the requirement that a set range of fire be ensured, analogous conclusions may be reached with regard to change in  $\mu_k$  evoked by change in  $\Pi_0$ . Thus one can assume that with values of  $\Pi_0 > 8000 \text{ kg/m}^2$  this parameter will exhibit no substantial effect upon  $\mu_k$ .

Let us examine the influence of  $\Pi_0$  upon the weight coefficient of the engine,  $\alpha$ . We determine from equation (3.42) the extreme of  $\alpha$  according to  $\Pi_0$ , taking into account expression (3.70)

$$\frac{d\alpha}{d\Pi_0} = -\frac{k_{\Delta K}}{\nu_K \Pi_0^2} + 4\gamma_{np} k_L \bar{\Delta}_K \frac{\eta}{\kappa J_{10} \mu_{cp}} \frac{1}{\left(\delta\varphi - \frac{\eta \Pi_0}{\kappa J_{10} \mu_{cp}}\right)^2} - \frac{I_{1cp} k_{\Delta K}}{\eta \Pi_0^2} = 0. \quad (3.75)$$

We introduce the designation

$$B = \sqrt{\frac{4\gamma_{np} k_L \bar{\Delta}_K \eta}{\kappa J_{10} \mu_{cp}} \frac{1}{\frac{k_{\Delta K}}{\nu_K} + \frac{I_{1cp} k_{\Delta K}}{\eta}}}. \quad (3.76)$$

Solving equation (3.75) relative to  $\Pi_0$  and making use of expression (3.76), we secure

$$\Pi_{opt} = \frac{\delta\varphi}{B + \frac{\eta}{\kappa J_{10} \mu_{cp}}}. \quad (3.77)$$

Expression (3.77) determines the optimum value for the initial transverse loading at which minimum value of weight coefficient of engine,  $\alpha$ , is achieved.

In accordance with formula (3.77), the optimum value of  $\Pi_0$  rises with increase in the unit weight of the fuel, with increase in the  $\kappa J_{10} \mu_{cp}$  complex, and also with reduction in thrust-weight ratio  $\eta$ .

Let us examine the physical meaning of the existence of this optimum. Increase in  $\Pi_0$  is associated with increase in  $L_p$  -- the length of the rocket, and consequently with lengthening of the engine and charge. According to relationship (3.64), with lengthening of the charge while value of the parameter of loading  $\kappa$  remains fixed the quantity  $\epsilon$  declines, i.e., the extent of filling of the chamber with fuel declines, something which of itself must lead to increase of the relative weight of the structure, i.e., to increase of  $\alpha$ . Simultaneously with increase of  $\Pi_0$  the caliber of the rocket  $D_H$  decreases. If one starts from the necessity of positioning in the chamber approximately one and the same quantity of fuel, the length of the chamber, determined without taking into account reduction in the density of charging, must rise proportionately with  $\Pi_0$ . The perimeter of the chamber declines proportionately to  $1/\sqrt{\Pi_0}$ . Consequently, the weight of the chamber with a constant given volume must rise proportionately to  $\sqrt{\Pi_0}$ . But with reduction of the midship section of the rocket the weight of the caps of the rocket engine declines. Thus with short charges the coefficient  $\alpha$  increases on account of increasing weight of caps, with long charges on account of reduction

in density of charging and increasing weight of cylindrical envelope of casing. This in fact conditions the existence of an optimum extension of the engine in length and of the value of  $\Pi_{0\text{opt}}$  associated with it.

The higher the value of the weight coefficients of the forward and cone caps  $\kappa_{\text{дк}}$ ,  $\kappa_{\text{сн}}$  and  $\kappa_{\text{дк}}$ , the less (in accordance with expression 3.76) is the value of complex  $\beta$ , and the greater is the value of  $\Pi_{0\text{opt}}$  determined according to formula (3.77). Thus with a heavier construction of caps the optimum  $\Pi_0$  is displaced in the direction of longer charges, and, conversely, with light construction it is displaced into the field of short charges, for which a higher density of charging is ensured.

In accordance with formula (3.77) the  $\frac{\pi J_{10} \mu_{\text{ср}}}{\eta}$  complex has a considerable influence upon the magnitude of the optimum value for  $\Pi_0$ .

Let us transcribe formula (3.64) in the form

$$\alpha = \frac{1}{\frac{L}{\mu_{\text{с1}}} + 1}. \quad (3.78)$$

Substituting here the value  $e_1$  from expression (3.69), we secure

$$\frac{1 + \frac{\pi J_{10} \mu_{\text{ср}} / \eta}{k_7}}{1} = \alpha \quad (3.79)$$

Thus the complex examined, with  $L$  and  $\mu_{\text{с}}$  given, determines the density of charging. With increase of this complex the density of charging rises, something which, in accordance with equation (3.77), leads to displacement of the optimum value for  $\alpha$  in the direction of longer charges.

In final selection of the  $\Pi_0$  value it is necessary to take into account the convenience of using and firing the rocket. If in planning one sets oneself a high value of  $\Pi_0$ , the rocket may turn out to be excessively long, something which will make its transport and setting up on the launch apparatus difficult. Such a rocket will possess a great equatorial moment of inertia, which will make steering its flight difficult and will occasion high transverse overloading upon in effecting turning movements during the active section of the trajectory.

In Table 3.2 we set forth the values of  $\Pi_0$  which we have computed for solid-fuel rockets in accordance with the data set forth in 1.1.

Table 3.2

Rocket	Sergeant	Pershing	Polaris	Minuteman
$\Pi_0 \left[ \frac{\kappa \Gamma}{x^2} \right]$	9,250	5,780	8,600	10,400

3.8. Connection Between the  $x$  Parameter and the Pressure in the Forward Part of the Engine (Taking Erosive Combustion Into Account)

In order to make the computations associated with determination of the optimum  $x$  value, it is necessary to know the relationship between the  $x$  parameter and pressure in the forward part of the engine. The experimental graph presented in Figure 3.4 (11) is a graphic representation of this relationship. Analytical solution of this problem is considered in the studies (2, 9, 11).

The solution set forth below is based upon the utilization of tables of gasodynamic functions, and is for this reason methodologically the most convenient one.

Let us examine the change in basic gasodynamic parameters along the lengths of charges burning from the flank surface, with a free area of transverse section which is constant throughout the length of the charge (cf. Figure 3.7). For a channel of constant section the full flow of the impulse is constant, i.e.,

$$v \cdot G/g + pF = \text{const} = I_p. \quad (3.80)$$

In the initial section of the channel, with  $v = 0$ ,

$$I_p = p_{0x} \cdot F_x. \quad (3.81)$$

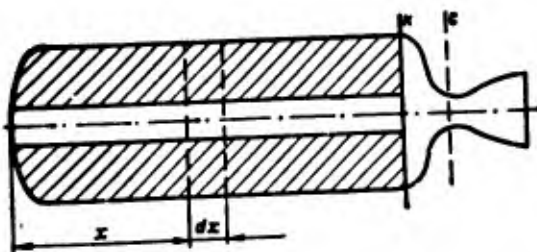


Figure 3.7. Diagram of geometry of a rocket chamber.

For an arbitrary section

$$\frac{G}{g} v + pF = \frac{pF}{r(\lambda)} = \text{const}, \quad (3.82)$$

where

$$r(\lambda) = \frac{1 - \frac{k-1}{k+1} \lambda^2}{1 + \lambda^2}; \quad (3.83)$$

$\lambda = v/a_{kp}$  -- the nondimensional velocity;

$$a_{kp} = \sqrt{\frac{2k}{k+1} gRT_0},$$

$k$  is the index of the adiabatic curve;

$R$  is the gas constant;

$T_0$  is the braking temperature of the products of combustion of the solid fuel.

Equation (3.83) does not take into account the forces of friction of the gas flow upon the surface of the charge. In the estimation of some investigators (11), with Reynolds numbers characteristic for the flow of a gas along a charge ( $Re \approx 10^6$ ), for the initial period of combustion of the charge losses from friction come to not more than 2-5 percent of the falling off in pressure along the charge, associated with the flow of the mass of gases.

From equations (3.82) and (3.83) it follows that static pressure along the channel changes as does

$$p = p_{01} \cdot r(\lambda). \quad (3.84)$$

With burning on the face surface facing the forward cap (Figure 3.8) the initial section of the channel may be regarded as the final section of a fictitious channel having a flank surface equal to the area of the face  $S_T$ :

where  $l_\phi$  is the length of the fictitious section;  
 $\Pi_r$  is the perimeter of combustion.

Hence

$$l_\phi \Pi_r = S_T, \quad (3.85)$$

$$l_\phi = \frac{S_T}{\Pi_r}.$$

In order to associate change in the parameters of flow in the channel with the afflux of gas by reason of combustion of the fuel, we divide the elementary sector of combustion by an extent  $dx$  (Figure 3.7). Change in output through the transverse section of the channel in the sector  $dx$  is equal to the gas afflux in this sector:

$$dG = \delta \Pi_r u_{10} f(p) \varphi(\lambda) dx, \quad (3.86)$$

where  $u_{10}$  is the unit velocity of fuel combustion;

$f(p)$  is a function expressing the relationship of combustion velocity to pressure;

$\varphi(\lambda)$  is a function expressing the relationship of combustion velocity to velocity of the gas flow passing around it.

The general expression for output of gases may be presented in the form

$$G = g_p F v = \frac{p}{RT} F v. \quad (3.87)$$

Substituting the value  $p$  from expression (3.84) and taking the temperature of the gas through the length of the chamber as constant, equal to the braking temperature (this is in fact the temperature of the fuel combustion), we secure

$$G = \frac{p_{0k}}{RT_0} F a_{kp} \lambda r(\lambda). \quad (3.88)$$

Differentiating expression (3.87), we find that

$$dG = \frac{p_{0k}}{RT_0} F a_{kp} \left\{ r(\lambda) + \lambda \frac{d[r(\lambda)]}{d\lambda} \right\} d\lambda. \quad (3.89)$$

Equating the right-hand arms of equations (3.88) and (3.89), we secure the basic equation for determination of the parameters of the flow along the length of the charge

$$\frac{p_{0k}}{RT_0} F a_{kp} \left\{ r(\lambda) + \lambda \frac{d}{d\lambda} [r(\lambda)] \right\} d\lambda = \delta \Pi_r u_{10} f(p) \varphi(v) dx. \quad (3.90)$$

In order to simplify the solution without substantially diminishing its accuracy, with values of  $\lambda < 0,5$  one can make use, in place of the relationship (3.83), of a simpler formula

$$r(\lambda) = 1 - \lambda^2. \quad (3.91)$$

Approximate and exact values of the function  $r(\lambda)$  for  $k = 1.25$  are set forth in Table 3.3.

In accordance with Table 3.3, with values  $\lambda < 0,4$ ;  $k = 1,1-1,25$  the error of the approximation  $\Delta$  remains less than 1 percent, and only with  $\lambda = 0,50-0,55$  does it rise sharply to 3-6 percent.

The dependence of the speed of burning of a solid rocket fuel upon pressure is called the law of fuel combustion. On the basis of a great deal of experimental material various formulas expressing this dependence have been proposed. In the internal ballistics of the solid-fuel rocket engine the following are the most frequently used:

-- the graduated law of combustion, applied within the range of pressures running up to approximately 70 kg/cm<sup>2</sup>:

$$\begin{aligned} u &= u_{10} p^n; \\ f(p) &= p^n; \end{aligned} \quad (3.92)$$

-- the linear law of combustion, applied in the pressure range from 30 to 120 kg/cm<sup>2</sup>:

$$u = u_{10}(1 + bp).$$

Table 3.3

$\lambda$	0,1	0,2	0,3	0,4	0,50	0,55
$r(\lambda)(3,91)$	0,99	0,96	0,91	0,84	0,75	0,6975
$r(\lambda)(3,83)$	0,9891	0,9572	0,9083	0,8467	0,7778	0,7419
$\Delta\%$	+0,09	+0,28	+0,19	-0,79	-3,57	-5,97

At present the Summerfield law finds widespread use; it covers a wide range of pressures (from 1 to 100 kg/cm<sup>2</sup>):

$$u = \frac{ap}{1 + bp^{1/2}}.$$

Upon movement of the gas flow along the surface of combustion of the charge, the speed of burning of fuel increases. The increase in speed of combustion is occasioned by the effort of conveying heat from the gas to the fuel in the presence of turbulization of the gas flow in the neighborhood of the surface of the charge. In the literature this phenomenon is called erosive combustion. A number of investigators have indicated the existence of some threshold speed of flow, starting from which the influence of the bathing of the surface with gases becomes manifest upon the speed of burning of the fuel. Relative change in the speed of fuel combustion is customarily expressed by the relation

$$\varphi(v) = \frac{u_{1v}}{u_{10}} = 1 + k_\lambda(\lambda - \lambda_{np}), \quad (3.93)$$

where  $k_\lambda$  is an erosion constant which is characteristic of the fuel;  
 $\lambda_{np}$  is the threshold value of nondimensional speed, starting with which erosive combustion commences to become manifest.

With  $\lambda < \lambda_{np}$   $\varphi(v) = 1$ .

Substituting expressions (3.91), (3.92), and (3.93) in equation (3.90) we secure

$$\begin{aligned} & \frac{p_{0\lambda} F a_{np}}{RT_0} (1 - 3\lambda^2) d\lambda = \\ & = \delta \Pi_r u_{10} p_{0\lambda}^* (1 - \lambda^2)^* [1 + k_\lambda (\lambda - \lambda_{np})] dx. \end{aligned} \quad (3.94)$$

To simplify computation it is logical to adopt

$$[r(\lambda)]^* = (1 - \lambda^2)^* = 1 - v\lambda^2. \quad (3.95)$$

One may judge of the greatest amount of error introduced by this change into the real range of change of  $\lambda$  according to the data of Table 3.4, computed for  $\lambda_\kappa = 0,5$ .

Table 3.4

$v$	0,2	0,3	0,5	0,7
$[r(\lambda)]^*$	0,951	0,927	0,882	0,838
$1 - v\lambda^2$	0,950	0,925	0,875	0,825
$\Delta\%$	0,1	0,2	0,8	1,6

Dividing the variables and integrating, we secure

$$\int_{\lambda_{np}}^{\lambda} \frac{1 - 3\lambda^2}{(1 - k_\lambda \lambda_{np} + k\lambda)(1 - v\lambda^2)} d\lambda = \frac{\delta \Pi_r u_{10} RT}{F a_{np} p_{0\lambda}^{1-v}} (x - x_{np}), \quad (3.96)$$

where  $x_{np}$  is a coordinate of the section at which nondimensional speed attains a value of  $\lambda_{np}$ .

For the sector  $x < x_{np}$  equation (3.94) assumes the form

$$\frac{p_{0\lambda} F a_{np}}{RT} \frac{1 - 3\lambda^2}{1 - v\lambda^2} d\lambda = \delta \Pi_r u_{10} p_{0\lambda}^* dx, \quad (3.97)$$

whence, after integrating, we secure

$$\int_0^{\lambda_{np}} \frac{1 - 3\lambda^2}{1 - v\lambda^2} d\lambda = \frac{\delta u_{10} RT}{a_{np} p_{0\lambda}^{1-v}} \frac{\Pi_r x_{np}}{F}. \quad (3.98)$$

Determining from equation (3.98) the value  $x_{np}$  and substituting it in expression (3.96) we secure

$$\int_{\lambda_{np}}^{\lambda} \frac{1-3\lambda^2}{(1-k_\lambda(\lambda-\lambda_{np}))(1-v\lambda^2)} d\lambda + \int_{\lambda}^{\lambda^*} \frac{1-3\lambda^2}{1-v\lambda^2} d\lambda = \frac{\partial u_{10} \Pi_r RT}{Fa_{np} \rho_{ox}^{1-v}} x. \quad (3.99)$$

The left-hand part of the equation constitutes a function of  $\lambda$ ,  $\lambda_{np}$ ,  $k_\lambda$  and  $v$ . An analytical expression of this function can be secured through integration:

$$\begin{aligned} \Phi(\lambda, k_\lambda, \lambda_{np}, v) = & \frac{3}{v} \lambda_{np} - \frac{3-v}{2v\sqrt{v}} \ln \frac{1/\sqrt{v} + \lambda_{np}}{1/\sqrt{v} - \lambda_{np}} + \\ & + \frac{3}{vk_\lambda} \ln [1 + k_\lambda(\lambda - \lambda_{np})] + \frac{v-3}{v^2} \frac{1}{k_\lambda^2/v - (1 - k_\lambda \lambda_{np})^2} \times \\ & \times \left\{ k_\lambda \ln [1 + k_\lambda(\lambda - \lambda_{np})] - \frac{k_\lambda}{2} \ln \frac{1-v\lambda^2}{1-v\lambda_{np}^2} - \right. \\ & \left. - \frac{1-k_\lambda \lambda_{np}}{2} \sqrt{v} \ln \left( \frac{1/\sqrt{v} + \lambda}{1/\sqrt{v} - \lambda} \frac{1/\sqrt{v} - \lambda_{np}}{1/\sqrt{v} + \lambda_{np}} \right) \right\}. \end{aligned} \quad (3.100)$$

A graph for the function  $\Phi(\lambda, k_\lambda, \lambda_{np}, v)$  for  $\lambda_{np} = 0.15$ ,  $k_\lambda = 1.0 \div 5.0$ ,  $v = 0.3-0.7$  is set forth in Figure 3.9.

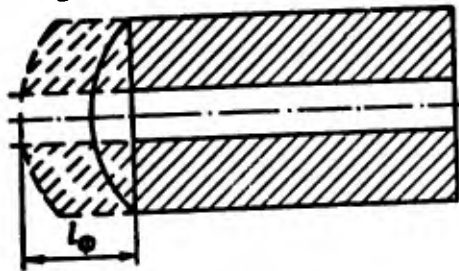


Figure 3.8. Adduction of the area of the burning face toward the supplementary fictitious channel.

Let us note that  $\Pi_r x/F$  is nothing other than the  $x$  criterion of Yu. A. Pobedonostsev.

Thus:

$$\Phi(\lambda, k_\lambda, \lambda_{np}, v) = \frac{\partial u_{10} x}{\rho_{ox}^{1-v}} \sqrt{\frac{k+1}{2gk}} \sqrt{RT_0} \quad (3.101)$$

Let us determine the complete falling-off in pressure over the channel of the chamber from the cap to the critical cross-section.

For the channel of the charge

$$\Delta p_k = p_{ox} - p_k = p_{ox} [1 - r(\lambda_k)] \quad (3.102)$$

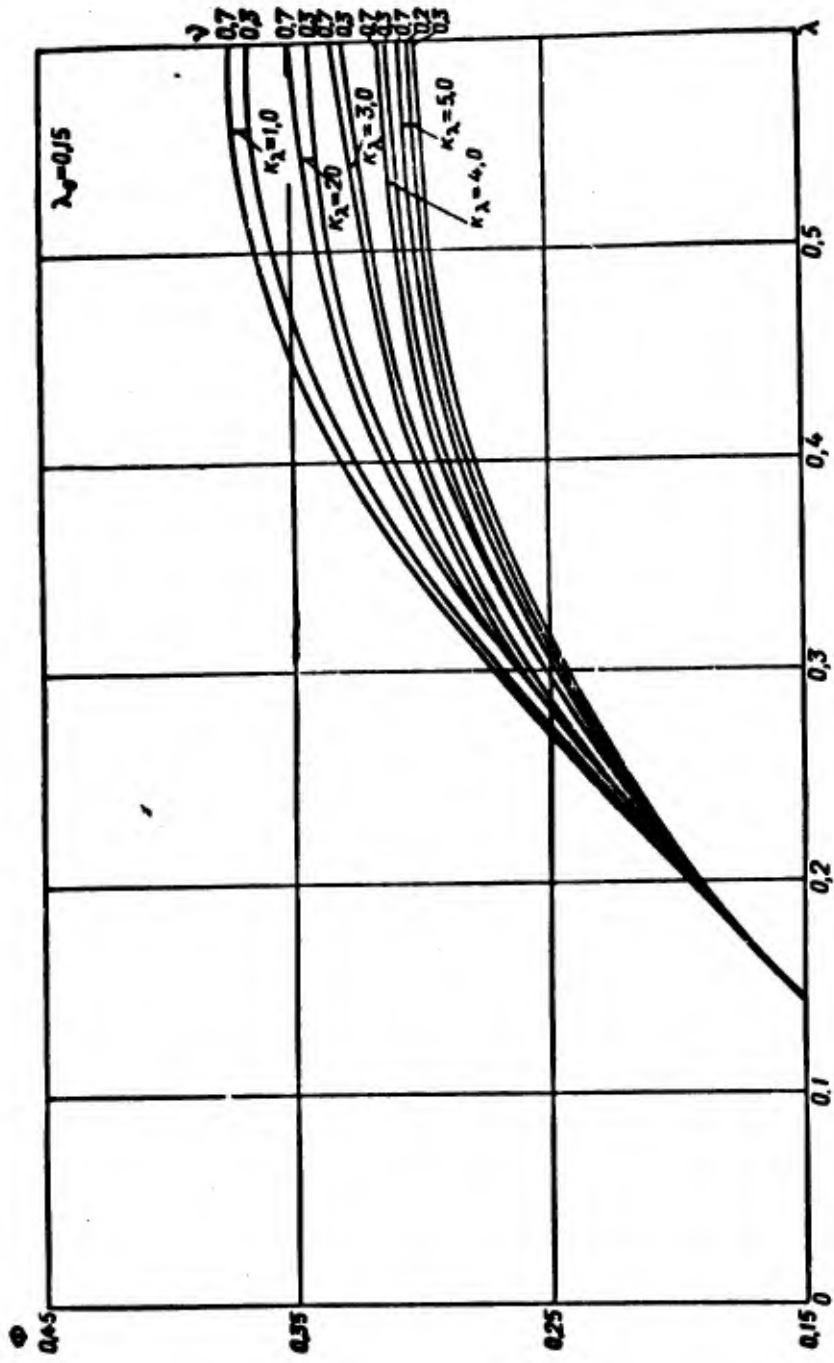


Figure 3.9. Dependence of function  $\Phi(\lambda, \kappa\lambda, \lambda_{sp}, \nu)$  upon  $\lambda$  for  $\kappa\lambda = 1.0-5.0$ ,  $\nu = 0.3-0.7$ ,  $\lambda_{sp} = 0.15$ .

or, making use of expression (3.91), we secure

$$\Delta p_x = p_{0x} \lambda_x^2. \quad (3.103)$$

The falling off in pressure in the precone space may be approximately evaluated on the basis of general hydraulics relationships:

$$\Delta p_c = \xi \frac{\rho v^2}{2},$$

where  $\xi$  is a coefficient of hydraulic losses.

Let us examine the case of a multiple-cone bloc (Figure 3.10), where basic losses of pressure are occasioned by the shock of the gas jet issuing from the channel into the cone cap. According to Idelchik (12) upon the issuance of the flow from the conduits and channels onto the baffle the magnitude of the coefficient of hydraulic losses is determined by the relative distance from the outlet cross-section of the tube to the baffle. Experimental values of this coefficient are set forth in Table 3.5 (12).

Table 3.5

$h/d$	0,5	0,6	0,7	1,0
$\xi$	1,37	1,20	1,11	1,00

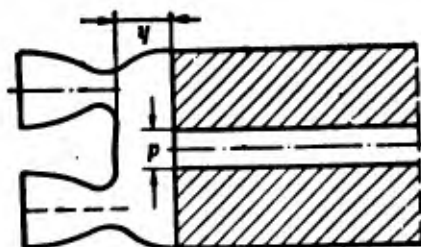


Figure 3.10. Diagram of cone portion of engine.

Expressing density through static pressure in the outlet cross-section of the channel, and velocity in this cross-section through  $\lambda_x a_{HP}$ , we secure:

$$\Delta p_c = \frac{p_x}{gRT_x} \frac{2gk}{k+1} RT_x \xi \frac{\lambda_x^2}{2} = \frac{k\xi}{k+1} p_x \lambda_x^2. \quad (3.104)$$

or

$$\Delta p_c = \frac{k\xi}{k+1} p_{0x} f(\lambda_x) \lambda_x^2. \quad (3.105)$$

Full pressure in the outlet cross-section of the channel is expressed as

$$p_{0K} = \frac{p_K}{\pi(\lambda_K)} = \frac{p_{0K} r(\lambda_K)}{\pi(\lambda_K)}, \quad (3.106)$$

where

$$\pi(\lambda_K) = \left(1 - \frac{k-1}{k+1} \lambda_K^2\right)^{\frac{k}{k-1}}$$

The coefficient of restoration of full pressure for the channel consists of

$$\sigma_K = \frac{p_{0K}}{p_{0K}} = \frac{r(\lambda_K)}{\pi(\lambda_K)}. \quad (3.107)$$

Losses of full pressure prove quantitatively to be substantially less than the falling off of static pressures,  $\Delta p_K$ . The relative magnitudes of these characteristics, computed with  $k = 1.25$  for various values of  $\lambda_K$ , are set forth in Table 3.6.

Table 3.6

$\lambda_K$	0,2	0,3	0,4	0,5
$\Delta p_K/p_{0K}$	0,04	0,09	0,16	0,25
$1-\sigma_K$	0,025	0,045	0,072	0,105

The coefficient of restoration of full pressure for the precone space is equal to

$$\sigma_c = \frac{p_{0K} - \Delta p_c}{p_{0K}} = 1 - \frac{\Delta p_c}{p_{0K}}, \quad (3.108)$$

or after substituting expression (3.105)

$$\sigma_c = 1 - \frac{k\varepsilon}{k+1} \lambda_K^2 \pi(\lambda_K). \quad (3.109)$$

In engineering computations over the range  $\lambda_K < 0,5$  one can, with a sufficient degree of accuracy, adopt

$$\varepsilon \pi(\lambda_K) = 1.$$

The coefficient of restoration of full pressure for the entire gasodynamic stretch of the chamber is

$$(\gamma) \lambda^2 \frac{1+\gamma}{2\gamma} - \frac{(\gamma) \lambda^2}{(\gamma) \lambda} = \sigma_{\text{oc}} = \sigma_{\text{oc}} \quad (3.110)$$

This coefficient makes it possible to express full pressure of the gas flow at entrance into the cone as

$$\rho_{\text{oc}} \quad (3.111)$$

hence

$$\frac{\rho_{\text{oc}}}{\rho_{\text{oc}}} = \frac{1}{\sigma_{\text{oc}}} = \frac{\pi(\lambda_{\text{K}})}{r(\lambda_{\text{K}})} \frac{1}{1 - \frac{\xi k}{k+1} \lambda_{\text{K}}^2 \pi(\lambda_{\text{K}})} \quad (3.112)$$

The expression secured establishes a connection between the non-dimensional speed at the end of the channel and the relation of full pressure at the forward end of the engine to that ahead of the cone.

The aggregate falling off in static pressure for the entire gasodynamic stretch of the chamber is

$$\sum \Delta p = \Delta p_{\text{K}} + \Delta p_{\text{c}} = \rho_{\text{oc}} \lambda_{\text{K}}^2 \left[ 1 + \frac{\xi k}{k+1} r(\lambda_{\text{K}}) \right] \quad (3.113)$$

The relationship between the nondimensional speed  $\lambda_{\text{K}}$  and the relation of the area of the cross-section of the channel to the area of the critical cross-section of the cone may be established from the equation of continuity for these cross-sections:

$$\rho_{\text{oc}} F_{\text{K}} q(\lambda_{\text{K}}) = \rho_{\text{oc}} \sigma_{\text{c}} F_{\text{Kp}} \varphi_{\text{c}}$$

whence

$$\frac{F_{\text{K}}}{F_{\text{Kp}}} = \frac{\sigma_{\text{c}} \varphi_{\text{c}}}{q(\lambda_{\text{K}})} = \frac{\varphi_{\text{c}}}{q(\lambda_{\text{K}})} \left[ 1 - \frac{\xi k}{k+1} \lambda_{\text{K}}^2 \pi(\lambda_{\text{K}}) \right] \quad (3.114)$$

In Table 3.7 we set forth  $F_{\text{K}}/F_{\text{Kp}}$  ratios corresponding to various values of  $\lambda_{\text{K}}$  with  $k = 1.25$ ,  $\xi = 1$ ,  $\varphi_{\text{c}} = 1$ .

Table 3.7

$\lambda_{\text{K}}$	0,2	0,3	0,4	0,5	0,6
$F_{\text{K}}/F_{\text{Kp}}$	3,15	2,05	1,54	1,225	1,025

If one starts from a given geometry of engine, after having determined according to the  $F_{\text{K}}/F_{\text{Kp}}$  relation the magnitude of  $\lambda_{\text{K}}$ , and then according to it the value of the function  $\Phi(\lambda, k, \lambda_0, \nu)$ , one can compute  $\rho_{\text{oc}}$  in accordance with relationship (3.101):

$$p_{0\lambda} = \left[ \frac{\delta u_{10} x}{\Phi(\lambda, k_\lambda, \lambda_{op}, \nu)} \sqrt{\frac{k+1}{2gk} R T_0} \right]^{\frac{1}{1-\nu}}. \quad (3.115)$$

On the basis of the relation secured it is also possible to determine the relationship of the maximum value  $p_{0\lambda \max}$ , corresponding to the erosion peak of pressure, to the mean value of  $p_{0\lambda \text{cp}}$ , which can be assumed to be associated with mean values of  $x$  and of  $\Phi(\lambda)$  over the time of the charge's burning:

$$\frac{p_{0\lambda \max}}{p_{0\lambda \text{cp}}} = \left[ \frac{x_{\max} \Phi(\lambda_{k \text{cp}})}{x_{\text{cp}} \Phi(\lambda_{k \max})} \right]^{\frac{1}{1-\nu}}.$$

The quantity  $x_{\text{cp}} = \frac{x_{\max} + x_{\min}}{2}$  may be substituted in the form

$$x_{\text{cp}} = \frac{x_{\max}}{2} \left( 1 + \frac{F_{k \min}}{F_{k \max}} \right),$$

where  $F_{k \min}$  is the minimum cross-section of channel, in accordance with which  $x_{\max}$ , corresponding with the start of the burn, is computed;

$F_{k \max}$  is the maximum cross-section of the channel at the end of the burn; assumed to be equal to the area of the chamber.

The value of function  $\Phi(\lambda_{k \text{cp}})$  is determined in accordance with  $\lambda_k$ , figured for the  $F_{k \text{cp}}/F_{kp}$  ratio, where  $F_{k \text{cp}} = \frac{F_{k \min} + F_{k \max}}{2}$ .

Inasmuch as

$$F_{k \min} = F_{k \max} (1 - \epsilon),$$

then

$$x_{\text{cp}} = x_{\max} \left( 1 - \frac{\epsilon}{2} \right)$$

and

$$F_{k \text{cp}} = F_{k \max} \left( 1 - \frac{\epsilon}{2} \right).$$

The relations we have introduced make it possible to determine, with given geometry of engine and of charge ( $F_k, F_{kp}, x$ ), the gasodynamic and ballistic parameters ( $p_{0\lambda}, \lambda_k, p_{0\lambda}/p_{0c}$ ) and to compute the geometry of charge and engine ( $F_k, F_{kp}, x$ ) which will ensure prescribed values for  $p_{0\lambda}$  and  $p_{0\lambda}/p_{0c}$ .

For ballistic planning the problem of the second type offers the greatest interest. A possible scheme for solution consists of the following:

1. We set ourselves a series of arbitrary values of  $\lambda_K$ , for which  $\rho_{0K}$  is determined for given values of  $K$ ,  $\xi$  and  $\rho_{0c}$  according to formula (3.112).

2. With given characteristics of fuel  $v$ ,  $k_\lambda$ ,  $\lambda_0$  we determine the function  $\Phi(\lambda, k_\lambda, \lambda_0, v)$ , and then through formula (3.101) we compute the value of  $x$ .

We utilize the values secured for  $x$  and  $\rho_{0K}$  in computing the weight characteristics of the rocket.

We have examined the case where the cross-section of the channel is constant over the length of the charge. Erosion burning of fuel and the "foaming" of pressure associated with it can be avoided if one makes the cross-section of the channel with enlargement in the direction of the cone. But this is bound up with reduction of density of charging and with variety of vaulting over the length of the charge. More complicated conditions of flow arise with the use of sectional charges, when sectors of the channel having small cross-section alternate with gaps between individual sections. In the intersectional gaps supplementary hydraulic losses arise which are occasioned by the formation of eddies and by sudden compression of the stream upon entry into the channel of the following section. The character of change in pressure along the channel of a sectional charge is set forth in a graph (Figure 3.11), which is computed for the solid-fuel rocket engine of the "Titan" ZS rocket (15). The value of the parameter  $x$  for this engine, computed with the faces taken into account, is equal to approximately 90. The relation of the mean area of the channel to the area of the critical cross-section of the cone is approximately 1.3. Maximum falling off of full pressure over the length of the engine is 12 percent.

### 3.9. Selection of Optimum Values of Working Pressure and of the Loading Parameter

Let us examine the basic consequences of increasing the working pressure in a solid-fuel rocket engine.

1. Increase of unit impulse. As we are aware, unit impulse for conditions at the surface of the earth is sensitive to change in pressure with  $p < 70 \text{ kg/cm}^2$  and practically does not depend upon pressure with  $p > 120\text{-}150 \text{ kg/cm}^2$ .

In computing discharge ( $p_0 = p_H$ ) at the surface of the earth the relative change in unit impulse can be presented in first approximation through the following table (13):

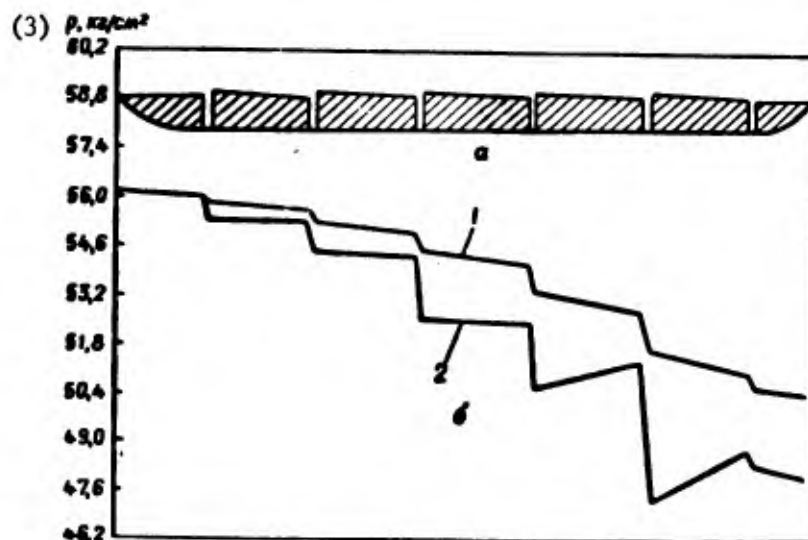


Figure 3.11. Change of pressure along sectional charge: a -- profile of charge; b -- graph of change of pressure; 1 -- braking pressure; 2 -- static pressure; 3 --  $p$ ,  $\text{kg}/\text{cm}^2$ .

Table 3.8

$p_0 \text{ kg/cm}^2$	21	28	35	42	49	56	63	70	77	84
$\bar{I}_1 = \frac{I_1}{(I_1)_{p_0}}$	0,88	0,92	0,93	0,95	0,96	0,98	0,99	1,00	1,02	1,025

Obviously in order to heighten the amount of unit impulse, working pressure -- as may be seen from the table -- should logically be increased within limits running up to approximately  $70 \text{ kg}/\text{cm}^2$ .

2. Increase of speed of burning of fuel. If the thrust-weight ratio  $\eta$  is given, increase in speed of burning of fuel makes it possible to augment the thickness of the burning vault, which, in harmony with the relations examined above, leads to increase of the density of charging.

3. Increase of the weight of the structure of the engine. The rise in computed pressure occasioned by increase of working pressure in the engine leads to thickening of the carrier wall of the rocket chamber. This thickening, and the increase in weight associated with it, are proportional to the computed pressure. With increase of working pressure proportional to  $p^{0.8}$  the coefficient of heat surrender from gases to the internal surface of the engine rises. Inasmuch as the time of burning of the charge changes proportionally to  $1/p^*$ , where as a rule  $v < 0,8$ , on the

whole with increase of pressure the total amount of heat transmitted to the surface of the rocket chamber goes up. Consequently with increase of pressure requisite weight of heat-protective coatings of the engine should mount.

Thus the influence of change in working pressure is manifested in directions contrary as regards their results. This in fact occasions the existence of an optimum value of working pressure, at which lightness of engine structure is linked with high value of unit impulse and great density of charging, something which ensures minimum start weight of rocket for a set range.

One can select the optimum pressure only with application to a concrete motive apparatus layout, with fuel, materials, and other planning parameters given for it. In selecting  $p_0$ , with cognizance of the conjoint influence of pressure upon the magnitude of unit impulse and upon the weight of the engine structure, one can adopt as guide the relations set forth in 3.4.

Selection of the optimum value for the parameter of charging is associated with selection of working pressure in the engine. With rise of  $x$  the area of the free cross-section of the chamber diminishes. On the one hand this leads to rise in density of charging, i.e., to reduction of the weight coefficient of the engine,  $\alpha$ . On the other hand, under these circumstances the erosion effect of the burning of the fuel increases and the falling off in pressure over the length of the charge in the precone space is heightened. Inasmuch as in determining the thickness of the carrier envelope of the envelope computed pressure must be set using the highest pressure at the forward cap as one's starting point, increase of  $x$  must lead to augmentation of the weight of the engine structure. Hence in each individual case it is possible to determine an optimum value of  $x$  which will ensure sufficiently great density of charging with the least possible increase in computed pressure and which will be associated with a specific working (mean indicator) pressure in the engine. As a result of analysis we find the optimum combination of  $p$ ,  $x$ , which will make it possible to secure the least weight for the product.

### 3.10. Selection of Optimum Degree of Expansion of Cone

Unit impulse of engine attains its maximum amount with computed discharge regime when the gases in the cone expand to the pressure of the surrounding environment. But with change in altitude of flight of the rocket atmospheric pressure changes and the regime for gas discharge from the cone diverges considerably from the computed regime.

If the cone operates at computed regime at the surface of the earth, then as the rocket rises it will work at an incomplete expansion regime, and conversely, if the cone of the engine is computed for high altitudes, then at low altitudes it will work at an overexpansion regime with considerable losses of unit impulse.

To start with, let us examine the question of the optimum degree of expansion of the cone, without touching upon the influence of this factor on the weight of the motive apparatus. With given values for  $\mu_k$ ,  $\eta$  and  $\Pi_0$  the condition for maximum velocity of rocket with varying expansion of cone is written as

$$\frac{dv_k}{d\lambda_a} = \frac{dI_{10}}{d\lambda_a} gw + \frac{dw}{d\lambda_a} gI_{10} = 0. \quad (3.116)$$

Here the nondimensional speed of the gas flow at the outlet cross-section of the cone,  $\lambda_a$ , is adopted as the characteristic for expansion of the cone.

Analytical solution of equation (3.116) is impossible in view of the transcendent character of the relationship of  $w$  to  $\lambda_a$ , inasmuch as  $\lambda_a$  forms part of the functions  $\Phi_1(\mu_k, I_{10})$  and  $\Phi_2(\mu_k, I_{10}, \eta)$  via the quantity  $I_{10}$ . Setting ourselves arbitrary values of  $\lambda_a$ , we can compute for them values of  $I_{10}$  and  $w$ ; then, having constructed a graph  $v = gI_{10}w$ , we can determine the maximum. In Table 3.9 we give the results of such a computation carried out for  $\mu_k = 0,6$ ,  $\Pi_0 = 8000 \text{ kg/m}^2$ ,  $p_0 = 40 \text{ kg/cm}^2$ , and for the value of the unit impulse with  $p_a = p_H = 1 \text{ kg/cm}^2$ ,  $I_{10} = 235 \text{ kg}\cdot\text{sec/kg}$ . Maximum speed is ensured with  $\lambda_a = 2,3$ .

Table 3.9

$\lambda_a$	2,17	2,3	2,5	2,6
$I_{10}$ , sec	235	229,6	170,7	46,7
$w$	0,810	0,8909	1,0723	3,187
$v_k$ , m/sec	1863	2007	1796	1459
$p_a$ , kg/cm <sup>2</sup>	0,985	0,475	0,106	0,038

The values  $I_{10}$  and  $p_a$  are computed without taking into account the breaking away of the marginal stratum from the wall of the cone. In order to determine the point of breaking away, use is frequently made of a simplified criterion proposed by Summerfield. According to Summerfield, for conical jets with a half-span angle of approximately  $15^\circ$  with  $\rho_0/\rho_H > 16$  the danger of breaking away arises at a calculated value of  $\rho_a/\rho_H < 0,4$ . According to data secured for large rocket cones, the breaking away sets in at  $p_a/p_H$  equal to approximately 0,296 (3). Consequently, the point of the maximum as determined by us lies above the point of possible breaking away of the marginal stratum, and consequently the computations carried out maintain their validity for the field  $\lambda_a < 2,37$  (corresponding to  $\rho_a/\rho_H \approx 0,3$ ).

In selecting the optimum degree of expansion of cone it is also necessary to take into account the engine structure's becoming heavier as the  $F_a/F_{kp}$  ratio increases.\* As a consequence of this the true optimum  $\lambda_a$  is

\* See 3.3.

displaced toward the left, in the direction of less expansion, relative to the value which was determined on the basis of maximum speed without taking change in weight into account. Selection of height of cone depends in considerable degree upon pressure in the engine, upon relative supply of fuel, and upon thrust-weight ratio. With increase of relative supply of fuel and with reduction of thrust-weight ratio, when the extent of the active section of the trajectory increases, the optimum is shifted in the direction of great expansions.

For the engine of the first stage of the "Minuteman" rocket the  $F_a/F_{kp}$  ratio comes to approximately 8 (14).

Of late, in rocket technics abroad, a cone having a central body in which, at the supersonic section of flow, an internal expansion of flow to a pressure equal to the pressure of the surrounding environment is becoming widespread. The free surface of the gas stream bathing the central body adapts itself to surrounding circumstances constantly as altitude of the flight changes. Thus a cone with central body both may be regarded as a self-regulating apparatus ensuring computed discharge at exit from the cone.

With a ratio of pressures  $p_0/p_H$  lower than the computed one, i.e., the one at which the extreme characteristic of the expanding flow passes through the nozzle of the central body, for a cone having a central body higher unit impulse values are ensured than for a cone having internal expansion operating on an over-expansion regime.

In addition, the use of a cone with a central body makes it possible to decrease the over-all length of the rocket engine. It should be noted, however, that the use of a cone having a central body in a solid-fuel rocket engine is associated with certain difficulties, first and foremost with the problem of the erosion resistance of the material in the neighborhood of the critical cross-section.

### 3.11. Determination of Basic Characteristics of Rocket

The task of ballistic planning is to seek out the basic characteristics of the optimum design variant having a given useful load, such as to ensure a given range of fire with minimum start weight. In the course of ballistic planning values for project parameters that will guarantee optimum solution of this problem should be set up. Under earlier headings we have examined the approach to the determination of the optimum value for each of the project parameters on the condition that the values of the remaining parameters remain fixed. In reality, in order to solve the problem it is necessary to examine a multiplicity of variants having various combinations of  $\eta_0$ ,  $\Pi_0$ ,  $\rho_0$ ,  $\lambda_0$ , and to select the one for which the start weight proves to be the least. Frequently the selection of optimum values of project parameters is limited by the real potentialities of the solid-fuel rocket engine and by supplementary requirements imposed upon the model. Thus, for example, optimum thrust-weight ratio at an acceptable

level of pressure in the engine becomes impossible by reason of the non-existence of fuels having the requisite burning speed. The selection of transverse loading is often limited by the length of model admissible under use conditions.

Let us write out the relationships we have secured that are intended for computation of the basic characteristics of a rocket with given values for project parameters:

$$Q_0 = \frac{q_{\text{нн}}}{1 - (1 + \alpha)\mu_{\text{к}} - k}; \quad (3.12)$$

$$\alpha = \frac{k_{\text{нн}}}{\mu_{\text{к}}\Pi_0} + 4\gamma_{\text{нр}}k_L\bar{\Delta}_{\text{к}} \frac{l}{\delta\varphi - \frac{\eta_0\Pi_0}{\pi I_{10}u_{\text{ср}}}} + I_{1\text{ср}} \left( k_c + \frac{k_{\text{нн}}}{\eta\Pi_0} \right). \quad (3.42)$$

Relation (3.42) makes it possible, with given values for  $\mu_{\text{к}}$ ,  $\Pi_0$ ,  $I_{10}$ ,  $I_{1\text{ср}}$  and with set characteristics of fuel and construction materials, to determine the weight coefficient of a rocket, and then, making use of this, to compute the start weight of the rocket in accordance with formula (3.12).

The area of the midship cross-section of the rocket is determined thus:

$$S_{\text{н}} = \frac{\pi D_{\text{н}}^2}{4} = \frac{Q_0}{\Pi_0};$$

the fuel weight:

$$G = k_{\text{с}}\mu_{\text{к}}Q_0;$$

the length of the charge

$$L = \frac{l}{\frac{\delta}{\Pi_0\mu_{\text{к}}} - \frac{\eta}{\pi I_{10}\mu_{\text{к}}u_{\text{ср}}}}.$$

#### BIBLIOGRAPHY

1. Bonnie, E. A., Zukrow, M. J., Besserer, K. U., Basic Planning of Guided Missiles; Aerodynamics; Jet Engines; Construction and Computation Practice, Fizmatgiz Publishing House, 1960.

2. Abramovich, G. N., Applied Gas Dynamics, Gosteortekhnizdat Publishing House, 1953.

3. Barrere, M., Jomotte, A., Bebel, B. F., Vandekerkhove, G., Rocket Engines, Oborongiz Publishing House, 1962.
4. Cameron, J. R., "Programs on Rocket Propulsion at Carde," Canadian Aeronautics and Space Journal, Vol 9, No 1, 1963.
5. Maxwell, W., Young, G., "Large Solid-Fuel Rocket Engines," Problems in Rocket Technics, No 1, 1962.
6. Danning, J. E., "Optimum Dimensions of Rocket Engine," Problems in Rocket Technics, No 1, 1962.
7. Kurov, V. D., Dolzhanskiy, Yu. M., Fundamentals of Planning Powder-Propelled Rocket Missiles, Oborongiz Publishing House, 1961.
8. Orlov, B. V., Mazing, G. Yu., Thermodynamic and Ballistic Bases of Planning Solid-Fuel Rocket Engines, Oborongiz Publishing House, 1964.
9. Wimpres, R. N., Internal Ballistics of Powder-Propelled Rockets, Foreign Literature Publishing House, 1952.
10. Bedevant, V., "Most Advantageous Shapes of Solid Fuel Charges," Problems in Rocket Technics, No 6, 1959.
11. Bartley, Ch. E., Mills, M. M., "Solid-Fuel Rocket Engines," Jet Engines, symposium of translations under editorship of N. G. Dubrovskiy, Voenizdat Publishing House, 1962.
12. Idelchik, I. Ye., Manual on Hydraulic Resistances, Gosenergoizdat Publishing House, 1960.
13. Besserer, K. U., Engineering Manual on Guided Missiles, Voenizdat Publishing House, 1962.
14. "The Boeing Firm's 'Minuteman' Intercontinental Ballistic Missile," Problems in Rocket Technics, No 6, 1963.
15. Working Out of Heavy Solid-Fuel Rocket Engines in the US (survey), Problems in Rocket Technics, No 3, 1966.
16. Working Out of the Rocket Carrier "Titan-3" in the US (survey), Problems in Rocket Technics, No 11, 1964.
17. Hitch, Ch., and Mackin, R., Military Economics in the Atomic Age, 1964.
18. Shapiro, Ya. M., Mazing, G. Yu., Prudnikov, N. Ye., Theory of the Rocket Engine for Solid Fuel, Voenizdat Publishing House, 1966.

## CHAPTER IV. SOLID-FUEL ROCKET ENGINE STRENGTH COMPUTATION

### 4.1. Working Loads, Computed Cases, and Peculiarities of Computation for Strength of Engines

One of the basic problems in planning solid-fuel rockets is determination of the strength of the units of the rocket.

In strength computations on a solid-fuel rocket it is necessary to take into account all possible loading cases (in transport, in servicing, in storage, at start, in flight) both of the structure as a whole and of its individual assemblies.

The most substantial working loads operating upon a rocket in the process of its transportation and storage are static weight loads, vibrations, and overloads under different conditions of use. Transport and storage conditions depend on the type of the rocket, its over-all dimensions, and the character of its use. For example, for aviation rockets one of the computation cases is suspension of the rocket upon the carrier plane, and in storage of rockets on shipboard loading regimes will be determined basically by vibrations (1).

For rockets the start of which takes place from stationary apparatus, the computations for strength will include the overloads which the rocket undergoes when the launch apparatus is fed and shifted. If the rocket must be on the launch table for a prolonged period and has an engine of large dimensions with solid fuel, working loads will be the loads from the weight and internal loads. Computation of elastic-plastic deformations in the charge will occupy a special place in this case (5.8).

At the moment of the actual launch there are taken into account in strength computations vibrations, the character of the rise in pressure in the rocket chamber, and also inertial loads as the rocket gathers speed, which depend upon the weight and the character of motion of the rocket along the launch apparatus.

In flight the basic working loads are excess pressure in the rocket chamber; inertial loads upon construction units; aerodynamic forces and moments distributed upon the carrying surfaces and the casing, and also the effects of aeroelasticity (flutter); loads from guidance organs in the form of reactions developing at points where transmitting mechanisms are fastened to the casing, and also dynamic loads transmitted to arresting devices when rudders are shifted; loads upon the separation of launch engines, the separation of stages, the cutting off of thrust, and the braking of the ballistic warhead in the dense strata of the atmosphere.

The operational regime of a solid-fuel rocket engine, the internal conditions during use, launch, and military application are different for each type of rocket. On this account establishment of computation cases is carried out in correspondence with concrete conditions for a specific design of rocket.

Methods and procedures of computing rockets for strength against the operation of the static and dynamic loads listed above are examined in specialized literature.

While a solid-fuel engine is operating the walls of the rocket chamber experience a temperature reaction on the part of the gases. The temperature of the gases in the chamber reaches 3,000-3,500° C. In order to create an efficient design for a solid-fuel guided rocket reliable heat insulation of the walls of the casing is indispensable. Heat insulation makes it possible to reduce the temperature of the surface of the engine walls to 300-800° C. At these temperatures the materials of the casing of the rocket preserve sufficiently high mechanical properties.

Computations of the units of a solid-fuel rocket engine for strength under high temperature reaction are associated with great difficulties. This is explained by the fact that, aside from the actual circumstance that temperature stresses occasioned by the unevenness of the field arise, it is necessary to take into account change in the mechanical characteristics of the material. With rise in temperature the limit of viscosity of the material sometimes rises somewhat to begin with, then falls off, and the limit of strength falls off even more rapidly.

The very short interval of time for the operation of the engine (a maximum of about two minutes) and the conditions associated therewith, of almost instantaneous application of working loads, require one to take into account not only the influence of high temperatures, but also those of elevated rates of deformation of materials (2).

In Figure 4.1 we show the influence of temperature and of the rate of deformation on the tensile strength of annealed low-carbon steel, which has at room temperature  $\sigma_B = 6240 \text{ kg/cm}^2$  and  $\delta = 28,4$  percent (3), according to data from the experiments of Inouye (Japan).

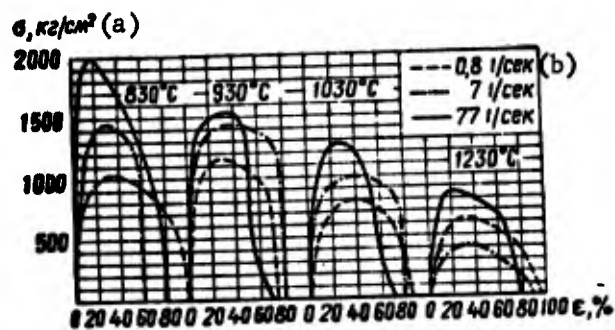


Figure 4.1. Influence of temperature and speed of deformation on mechanical characteristics of materials  $\sigma = f(\epsilon)$ . a -- kg/cm<sup>2</sup>; b -- seconds.

Tenacity diagrams (Figure 4.2) secured at various fixed speeds of deformation show that the sections of elastic deformations coincide, and that the rectilinear section reflecting the plastic range of deformations is the higher, the greater is the speed of deformation.

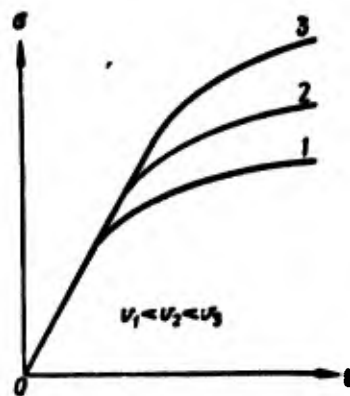


Figure 4.2. Diagram of tenacity secured for various fixed speeds of deformation.

One must also take into account the fact that in the process of manufacture, technological checking, and operating regime, the structural units of a solid-fuel rocket engine are subjected to repeated reactions from force and temperature loadings. Repeated loading of the elements of an engine working in elastic-plastic ranges has an influence upon the mechanical properties of the material.

One should note that preventative plastic deformation of one indicator worsens the resistance of the material relative to subsequent plastic deformation of another indicator. This phenomenon is defined as the Bauschinger effect.

In connection with the fact that stresses perceptibly exceeding the limit of elasticity develop in the units of a solid-fuel rocket engine, strength calculations should be carried out in the plastic range.

In calculating for structures which operate under circumstances of a complicated stressed state it is indispensable to know the functional relationship of the intensity of the stressed state  $\sigma_1$  to the intensity of the deformed state  $\epsilon_1$ . Numerous tests show that any compound spatial stressed state, independently of whether the range under examination is in a state of elastic or of plastic deformations, can be reduced to simple stretching of a bar (4). In order to determine the quantity  $\epsilon_1$  according to the magnitude of one of the parameters, for example the quantity  $\sigma_1$ , one can make use of customary tenacity diagrams for  $\sigma \approx \epsilon$ .

In connection with the fact that all the peculiarities examined above are important in setting permissible stresses, those of them (as, for example, the influence of the speed of deformation, the Bauschinger effect, et al.) the influence of which cannot be determined analytically in the making of strength calculations, must be taken into account in determining the amount of strength reserve.

The basic carrier part of the solid-fuel rocket engine is the rocket chamber, which is under the effect of excess pressure of gases. But calculation of the casing of a solid-fuel rocket engine for strength must be carried out not according to the amount of excess pressure, but upon the computed pressure ( $p_{pac}$ ).

The magnitude of computed pressure is determined according to the formula

$$p_{pac} = k_1 k_2 p_{max},$$

where  $k_1$  is a coefficient taking into account the admissible amount of maximum pressure variation in solid fuel from various lots;

$k_2$  is a coefficient taking into account backfiring of pressure upon ignition of charge;

$p_{max}$  is maximum pressure at greatest initial absolute temperature set for the engine.

The coefficient for the strength reserve is determined in a check computation evaluating the true stressed state of the structure.

The amount of the loads taken up by the casing of the engine depends on the positioning of the units transmitting thrust force to the rocket. Let us examine two of the most widespread ways of fastening the engine to the rocket (Figure 4.3).

In the first case the fastening links (brackets or supports) are set up along the casing giving form to the combustion chamber, at points close to the forward cap and to the cone block. Sometimes fastening units are set up at three or even four points.

This method of fastening is used in the "Aerojet" engine (Figure 4.4).

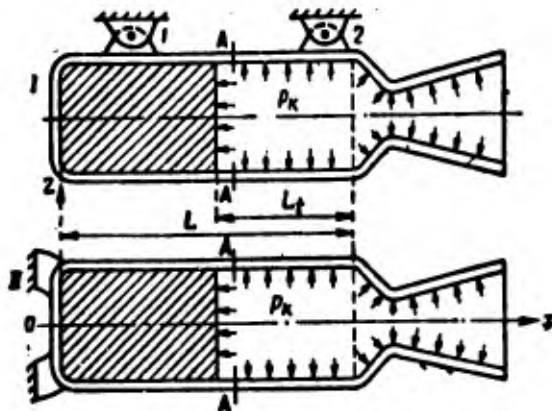


Figure 4.3. Diagram of fastening of engine to casing of rocket: 1 -- Fastening links set up on cylindrical part of rocket chamber; 2 -- Fastening lines set up on forward cap of rocket chamber.

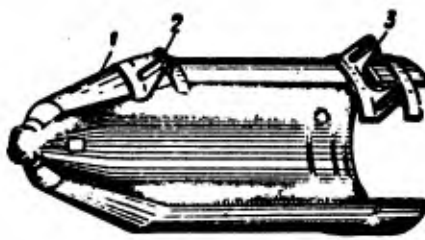


Figure 4.4. Casing of engine with fastening units set up on cylindrical part of rocket chamber: 1 -- Rocket chamber; 2 -- Forward fastening brackets; 3 -- Rearward fastening brackets.

In the second case (Figure 4.3) the fastening units are set up on the forward cap of the combustion chamber (2).

Let us determine the axial force which will be operating, during the period the engine is working, at section AA of the casing of the combustion chamber, in which the charge is firmly fastened at the side wall.

#### First Method of Fastening Engine

Let us adopt the following assumptions:

1. Cross-section AA is at a distance from fastening units 1 and 2 which is greater than the zone of extent of local flexure (of marginal effect).
2. We shall disregard the operation of the moment of flexure which is a consequence of reactions in the supports.

The assumptions made make it possible, in order to simplify the problem, to substitute provisionally for the effect of the reaction in the supports the effect of the evenly distributed loads  $q_1$  (Figure 4.5) and  $q_2$ , directed along the generatrices of the external surface of the casing of the combustion chamber. These loads are applied to circumferences lying in planes which run respectively through the axes of fastening units 1 and 2 and perpendicular to the axis of the engine. Actually with such placement no moments of flexure will develop in the section AA.

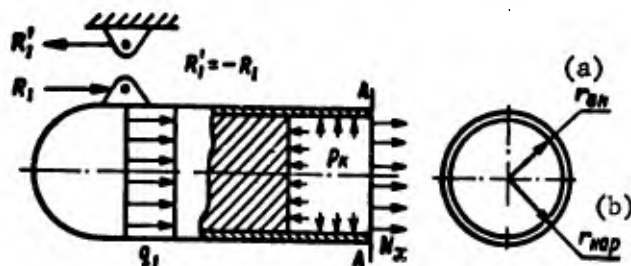


Figure 4.5. Calculation diagram for determination of reaction in fastening units. a --  $r_{\text{interior}}$ ; b --  $r_{\text{exterior}}$ .

If we designate by  $R_I$  and  $R_{II}$  the reactions in the supports for support 1 and 2 respectively, then it will be possible to write

$$R_I = 2\pi r_{\text{in}} q_1 \text{ and } R_{II} = 2\pi r_{\text{in}} q_2$$

The reactions in supports 1 and 2 can in first approximation be regarded as equal to each other; then

$$R_I = R_{II}; \quad q_1 = q_2 = \frac{P - (Q_{\text{c. s.}} + \omega_t) \cdot n}{4\pi r_{\text{in}}}, \quad (4.1)$$

where  $P$  is the thrust of the engine;

$R_I = R_{II}$  are the reactions in supports 1 and 2 respectively;

$Q_{\text{c. s.}}$  is the weight of the engine without fuel;

$\omega_t$  is the weight of the fuel at the moment of time  $t$  after launch of the rocket;

$n$  is the coefficient of overload;

$r_{\text{in}}$  is the external radius of the casing of the combustion chamber.

$$\omega_t = \omega - G \cdot t \dots, \quad (4.2)$$

where  $\omega$  is the weight of fuel with  $t = 0$ ;

$G$  is the expenditure of products of combustion over a unit of time.

Let us write an equation of equilibrium for the parts of the rocket chamber located to the left of section AA (Figures 4.3 and 4.5):

$$p_k \pi r_{BH}^2 = \frac{P - (Q_{k. \lambda} + \omega_l) n}{2} + N_x^I \cdot 2\pi r_{cp} \quad (4.3)$$

whence

$$N_x^I = \frac{2p_k \pi r_{BH}^2 - P + (Q_{k. \lambda} + \omega_l) n}{4\pi r_{cp}}, \quad (4.4)$$

where

$$r_{cp} = \frac{r_{BH} + r_H}{2}$$

$r_{BH}$  is the interior radius of the casing of the combustion chamber;  
 $p_k$  is the pressure in the combustion chamber;  
 $N_x^I$  is the unit meridional effort (2).

#### Second Method of Fastening

In this case thrust is transmitted via fastening units located on the forward cap (2). Analogously to the first example, we shall write an equation of equilibrium for the left-hand part of the combustion chamber:

$$p_k \pi r_{BH}^2 = P - (Q_{k. \lambda} + \omega_l) n + N_x^{II} 2\pi r_{cp} \quad (4.5)$$

whence

$$N_x^{II} = \frac{p_k \pi r_{BH}^2 - P + (Q_{k. \lambda} + \omega_l) n}{2\pi r_{cp}}. \quad (4.6)$$

The second method of fastening is used for the majority of designs of rocket engines using solid fuel.

#### 4.2. Calculating the Casing of the Engine for Strength

A rocket chamber consists of a cylindrical thin-walled envelope within which hot gas under elevated pressure is contained. To calculate for strength a distinction should be made between long and short cylindrical envelopes. The combustion chamber of a solid-fuel rocket engine may be referred to the class of long cylindrical envelopes. An envelope may be regarded as long if it satisfies the following inequality (5):

$$L \geq 2.4 \sqrt{R\delta}, \quad (4.7)$$

where  $L$  is the length of the envelope;  
 $R$  is the internal radius;  
 $\delta$  is the thickness of the wall.

As an example confirming the correctness of the inequality (4.7) for casings of rocket engines, we may make use of the results of calculation of the optimum variant of a solid-fuel rocket engine having a pressure in the chamber of 120 kg/cm<sup>2</sup>, set forth in study (6). Engines with

such pressure must have the following optimum geometrical dimensions: length of combustion chamber 133 centimeters; internal radius about 12.0 centimeters.

The casing of the rocket chamber of such an engine, made of steel having an admissible stretch  $\sigma = 7500 \text{ kg/cm}^2$ , has a wall thickness of about 2 millimeters. Hence, in accordance with condition (4.7), we have

$$133 > 2,4 \sqrt{12 \cdot 0,2} = 3,84.$$

Having secured confirmation of the fact that the casing of the rocket engine falls among the type of long envelopes, in calculating the casing for strength we may disregard the influence of loads, applied to one margin, upon the stress state at the other margin (5).

Inasmuch as the relative thickness of the walls of the combustion chamber is small, in the case examined being, for example, 0.2/12 or about 0.01, the requisite precision of calculation makes it possible to consider the module of elasticity (if the material of the casing lies within the zone of elastic deformations) and the coefficient of linear expansion of the material of the envelope as constant quantities, equal to their mean value within the interval of the temperatures of the external and the internal surfaces of the envelope.

Further it may be assumed that temperature through the thickness of the wall changes in linear fashion from the value  $T_B$  on the internal surface of the envelope to the value  $T_H$  on the external one.

For such an envelope, heated to an uneven extent at various points of its thickness and under the action of pressure  $p$  and axial force  $N_x$ , shifting of points of the median surface ( $W_x$ ) will be characterized by the following differential equation (4):

$$D \frac{d^4 W}{dx^4} + \frac{E_{cp} b}{R^3} W = -p + \mu \frac{N_x}{R} - \frac{\alpha_{cp} E_{cp} b}{R} T_0 + \frac{D(1+\mu)\alpha_{cp}}{b} \cdot \frac{d^2(\Delta T)}{dx^2}, \quad (4.8)$$

where  $D = \frac{E_{cp} b^3}{12(1-\mu^2)}$  is the cylindrical rigidity,  $\text{kg} \cdot \text{cm}$ ;

$E_{cp}$  is the module of elasticity of the material on the median surface,  $\text{kg/cm}^2$ ;

$\mu$  is the Poisson coefficient;

$p$  is the internal pressure,  $\text{kg/cm}^2$ ;

$R$  is the radius of the median surface,  $\text{cm}$ ;

$\alpha$  is the coefficient of linear expansion,  $1/^\circ\text{C}$ ;

$T_0 = \frac{T_H + T_B}{2}$  is the temperature of the median surface of the envelope

in degrees;

$\Delta T = T_u - T_i$  is the difference between the temperatures of the external and internal surfaces of the envelope in degrees.

In the general case  $T_0$  and  $\Delta T$  are variable along the length of the envelope. In a transverse section of the envelope (Figure 4.6) (a section perpendicular to the axis) the following operate, per unit of length (4):

-- shearing force in kg/cm

$$Q = -D \left[ \frac{d^2 W}{dx^2} - \frac{1 + \mu}{\delta} \alpha_{cp} \frac{d(\Delta T)}{dx} \right] = \frac{dM_x}{dx}; \quad (4.9)$$

-- moment of flexure in kg·cm/cm

$$M_x = -D \left[ \frac{d^2 W}{dx^2} - (1 + \mu) \alpha_{cp} \frac{\Delta T}{\delta} \right]. \quad (4.10)$$

In longitudinal section (a section passing through the axis) the following operate upon a unit of length (4):

-- stretching force in kg/cm

$$N_y = \mu N_x - \frac{E_{cp} \delta W}{R} - \alpha_{cp} E_{cp} \delta T_0; \quad (4.11)$$

-- moment of flexure in kg·cm/cm

$$M_y = -D \left[ \mu \frac{d^2 W}{dx^2} - (1 + \mu) \alpha_{cp} \frac{\Delta T}{\delta} \right]. \quad (4.12)$$

Knowing the internal force factors  $Q$ ,  $M_x$ ,  $M_y$ ,  $N_y$ , one can reckon the stresses developing in the casing of the combustion chamber. In an arbitrary stratum of the wall of the combustion chamber, distant by an amount  $z$  from the median surface, tangential and normal stresses develop. The tangential stresses develop under the operation of the shearing force  $Q$ , and for their distribution through the thickness of the envelope,  $\delta$ , one can have recourse to the parabolic law (4, 5):

$$\tau = \frac{Q}{\delta} \left( \frac{3}{2} - \frac{6z^2}{\delta^2} \right). \quad (4.13)$$

Generally speaking, tangential stresses in a section of the envelope are ordinarily slight and they may be disregarded.

Normal stresses, evoked by the operation of longitudinal efforts and moments of flexure, are substantially greater than tangential stresses, and for an arbitrary stratum of the envelope they can be reckoned according to the formula:

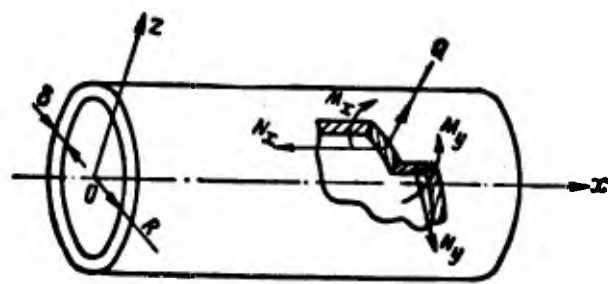


Figure 4.6.

$$\sigma_x = \frac{N_x}{\delta} - \frac{12M_x}{\delta^3} z; \quad \sigma_y = \frac{N_y}{\delta} - \frac{12M_y}{\delta^3} z. \quad (4.14)$$

The value  $N_x$  for the two methods of attaching the engine to the rocket can be determined according to formulas (4.4) and (4.6).

The amount of the maximum tangential stress is as a rule considerably less than the maximum normal stress. For this reason the most heavily stressed points will always be external or internal points of the wall, at which normal stresses are reckoned according to the formulas (4):

$$(\sigma_x)_{\max} = \frac{N_x}{\delta} \pm \frac{6M_x}{\delta^3}; \quad (\sigma_y)_{\max} = \frac{N_y}{\delta} \pm \frac{6M_y}{\delta^3}. \quad (4.15)$$

Thus it is apparent that for determination of the over-all bearing capacity of the casing of the combustion chamber it is necessary to find function  $W(x)$ . In study (4) there is set forth an approximate solution of equation (4.8), the general integral of which will be an expression of the form

$$W(x) = e^{-kx} (c_1 \cdot \sin kx + c_2 \cdot \cos kx) - \frac{\rho R^3}{E_{cp} \delta} \left( 1 - \mu \frac{N_x}{\rho R} \right) - R\alpha_{cp} T_0. \quad (4.16)$$

where  $k = \sqrt[4]{\frac{3(1-\mu^2)}{\delta^3 R^2}}$  is a parameter depending upon the dimensions of the envelope.

The last two terms of the function  $W(x)$  constitute a partial solution of equation (4.8). Thus, for example, with interior pressure  $p$  constant over the length and with absence of temperature stresses this partial solution has the form (5):

$$W_1(x) = \frac{\rho R^3}{E_{cp} \delta}. \quad (4.18)$$

The values of the coefficients  $c_1$  and  $c_2$  are found from the limit conditions. With  $x = 0$

$$\left. \begin{aligned} W(0) &= -R\alpha_{cp} T_0 \\ W'(0) &= 0 \end{aligned} \right\} \quad (4.19)$$

Substituting the value  $W(0)$  in equation (4.16) we secure

$$c_1 = \frac{\rho R^3}{E_{cp} \delta} \left( 1 - \mu \frac{N_x}{\rho R} \right). \quad (4.20)$$

If we differentiate equation (4.16) through for  $x$  and substitute the value  $W'(0)$  from the system (4.19), we secure

$$c_1 = c_2 = \frac{\rho R^2}{E_{cp} \delta} \left( 1 - \mu \frac{N_x}{\rho R} \right). \quad (4.21)$$

Now, substituting the values  $c_1$  and  $c_2$  respectively from equations (4.20) and (4.21) in equation (4.16), we secure a solution of differential equation (4.8):

$$W(x) = \frac{\rho R^2}{E_{cp} \delta} \left( 1 - \mu \frac{N_x}{\rho R} \right) [e^{-kx} (\cos kx + \sin kx) - 1] - R \alpha_{cp} T_0 \quad (4.22)$$

For determination of internal force factors  $Q(x)$ ,  $M_x(x)$ ,  $N_y(x)$ , and  $M_y(x)$  we find the first, second, and third derivatives of the function  $W(x)$ :

$$W'(x) = \frac{\rho R^2}{E_{cp} \delta} \left( 1 - \mu \frac{N_x}{\rho R} \right) [e^{-kx} \cdot k (-\sin kx + \cos kx - \cos kx - \sin kx)] = -2k \frac{\rho R^2}{E_{cp} \delta} \left( 1 - \frac{N_x}{\rho R} \mu \right) e^{-kx} \cdot \sin kx, \quad (4.23)$$

$$W''(x) = -2k \frac{\rho R^2}{E_{cp} \delta} \left( 1 - \mu \frac{N_x}{\rho R} \right) [e^{-kx} k \cos kx - k e^{-kx} \sin kx] = -2k^2 \frac{\rho R^2}{E_{cp} \delta} \left( 1 - \mu \frac{N_x}{\rho R} \right) (\cos kx - \sin kx) e^{-kx}, \quad (4.24)$$

$$W'''(x) = -2k^2 \frac{\rho R^2}{E_{cp} \delta} \left( 1 - \mu \frac{N_x}{\rho R} \right) [e^{-kx} (\cos kx - \sin kx) + k e^{-kx} (-\sin kx - \cos kx)] = -4k^2 \frac{\rho R^2}{E_{cp} \delta} \left( 1 - \mu \frac{N_x}{\rho R} \right) e^{-kx} \cdot \cos kx. \quad (4.25)$$

After substituting the values  $W(x)$ ,  $W'(x)$ ,  $W''(x)$ , and  $W'''(x)$  secured from equations (4.22), (4.23), (4.24), and (4.25) respectively in equations (4.9), (4.10), (4.11), and (4.12) and after simple transformations we secure:

$$Q(x) = -\frac{\rho}{k} \left( 1 - \mu \frac{N_x}{\rho R} \right) e^{-kx} \cos kx, \quad (4.26)$$

$$M(x) = \frac{\rho}{2k^2} \left( 1 - \mu \frac{N_x}{\rho R} \right) e^{-kx} (\cos kx - \sin kx) + \frac{E_{cp} \alpha_{cp} \Delta T_0^2}{12(1-\mu)}; \quad (4.27)$$

$$N_y = \mu N_x - \rho R \left( 1 - \mu \frac{N_x}{\rho R} \right) [e^{-kx} (\cos kx + \sin kx)]; \quad (4.28)$$

$$M_y = \frac{\rho}{2k^2} \mu \left( 1 - \mu \frac{N_x}{\rho R} \right) e^{-kx} (\cos kx - \sin kx) + \frac{E_{cp} \alpha_{cp} \Delta T_0^2}{12(1-\mu)}. \quad (4.29)$$

Now we shall determine computational formulas for figuring out internal force factors for two characteristic sections.

1. We shall examine a section of the combustion chamber located around the forward cap or around the cone block (at the entrance into the cone). The origin of the coordinates is located in the section referred to above, i.e.,  $x = 0$ ; then:

$$\left. \begin{aligned} Q(0) &= -\frac{\rho}{k} \left(1 - \mu \frac{N_x}{\rho R}\right); \\ M_x(0) &= \frac{\rho}{2k^2} \left(1 - \mu \frac{N_x}{\rho R}\right) + \frac{E_{cp} \cdot a_{cp} \cdot \Delta T \delta^2}{12(1-\mu)}; \\ N_y(0) &= \mu N_x; \\ M_y(0) &= \frac{\rho}{2k^2} \mu \left(1 - \mu \frac{N_x}{\rho R}\right) + \frac{E_{cp} \cdot a_{cp} \cdot \Delta T \delta^2}{12(1-\mu)}. \end{aligned} \right\} \quad (4.30)$$

2. For a section located in the middle part (as regards length) of the combustion chamber, i.e., with  $x = \frac{L_k}{2}$ , in the system of coordinates adopted in the first case we shall have:

$$\left. \begin{aligned} Q\left(\frac{L_k}{2}\right) &= -\frac{\rho}{k} \left(1 - \mu \frac{N_x}{\rho R}\right) e^{-k \frac{L_k}{2}} \cdot \cos k \frac{L_k}{2}; \\ M_x\left(\frac{L_k}{2}\right) &= \frac{\rho}{2k^2} \left(1 - \mu \frac{N_x}{\rho R}\right) e^{-k \frac{L_k}{2}} \left(\cos k \frac{L_k}{2} - \sin k \frac{L_k}{2}\right) + \\ &\quad + \frac{E_{cp} \cdot a_{cp} \cdot \Delta T \delta^2}{12(1-\mu)}; \\ N_y\left(\frac{L_k}{2}\right) &= \mu N_x - \rho R \left(1 - \mu \frac{N_x}{\rho R}\right) \left[ e^{-k \frac{L_k}{2}} \cos k \frac{L_k}{2} + \sin k \frac{L_k}{2} \right]; \\ M_y\left(\frac{L_k}{2}\right) &= \frac{\rho}{2k^2} \mu \left(1 - \mu \frac{N_x}{\rho R}\right) e^{-k \frac{L_k}{2}} \left(\cos k \frac{L_k}{2} - \sin k \frac{L_k}{2}\right) + \\ &\quad + \frac{E_{cp} \cdot a_{cp} \cdot \Delta T \delta^2}{12(1-\mu)}. \end{aligned} \right\} \quad (4.31)$$

We make use of formulas (4.30) and (4.31) for calculation of a casing the material of which in the calculated case does not depart from the zone of plastic deformations. But, as was shown in 4.1, the casing of the combustion chamber of a solid-fuel rocket engine frequently works under circumstances of elastic-plastic deformations. In the case of elastic-plastic deformations the connection between deformations and stress can be presented in the form (4):

$$\begin{aligned} \epsilon_x &= E_c(\epsilon_x; z) [\epsilon_x - \alpha(z) T(z)]; \\ \epsilon_y &= E_c(\epsilon_y; z) [\epsilon_y - \alpha(z) T(z)]; \end{aligned} \quad (4.32)$$

where  $E_c = \frac{E_1}{\nu_1}$  is the secant module of elasticity;

$\alpha$  is the coefficient of linear expansion.

Actually, let us suppose that  $\epsilon_{xn}$  and  $\epsilon_{yn}$  are the full relative elongations at a point on the casing of the combustion chamber, occasioned by loads  $p_i$ ,  $N_x$ , and  $T$ . Then the relative elongations occasioned only by  $p_i$  and  $N_x$  can be presented in the following form:

$$\begin{aligned} \epsilon_x &= \epsilon_{xn} - \epsilon_p; \\ \epsilon_y &= \epsilon_{yn} - \epsilon_p. \end{aligned} \quad (4.33)$$

We multiply the left and right-hand arms of the system of equations (4.33) by  $E_c$ , and we get equation (4.32).

Let us examine the condition of equilibrium for an element of the envelope having central angle  $d\varphi$  (Figure 4.7). Pressure  $p_i$  operates upon the internal surface of the element of the envelope:

$$p_i R = \int_{-\frac{1}{2}}^{+\frac{1}{2}} \sigma_y \cdot dz. \quad (4.34)$$

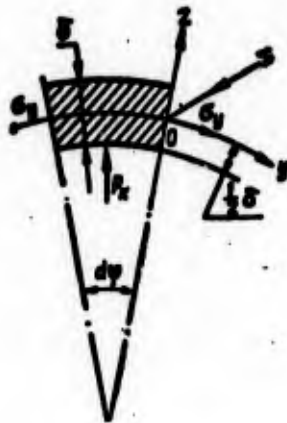


Figure 4.7. Element of envelope having central angle  $d\varphi$ .

The amount of unit force  $N_x$  can be determined as follows:

$$N_x = \int_{-\frac{b}{2}}^{+\frac{b}{2}} \sigma_x dz. \quad (4.35)$$

Let us substitute, in the equations (4.34) and (4.35) which we have secured, respectively the values  $\sigma_y$  and  $\sigma_x$  from the system of equations (4.32). Without committing any great error -- as the envelope is a thin-walled one -- we can consider  $\sigma_{xn}$  and  $\sigma_{yn}$  as not depending on  $z$ , and we solve the resultant equations relative to  $\sigma_y$  and  $\sigma_x$  (4):

$$\left. \begin{aligned} \sigma_y &= \frac{\rho_1 R + \int_{-\frac{b}{2}}^{+\frac{b}{2}} E_c(z) T(z) dz}{\int_{-\frac{b}{2}}^{+\frac{b}{2}} E_c dz}; \\ \sigma_x &= \frac{N_x + \int_{-\frac{b}{2}}^{+\frac{b}{2}} E_c(z) T(z) dz}{\int_{-\frac{b}{2}}^{+\frac{b}{2}} E_c dz}. \end{aligned} \right\} \quad (4.36)$$

It is impossible to determine the values of  $\sigma_y$  and  $\sigma_x$  from expressions (4.36), since the secant module  $E_c$  which forms part of the right-hand arm of the formulas is a function of  $\sigma_x$  and  $\sigma_y$ .

Expressions (4.36) can be considerably simplified if one assumes that the coefficient of linear expansion  $\alpha$  and the secant module of elasticity  $E_c$  do not depend on  $z$ , and that temperature changes in linear fashion, i.e.,

$$T(z) = T_0 + \frac{\Delta T}{b} z. \quad (4.37)$$

Then

$$\left. \begin{aligned} \sigma_y &= \frac{\rho R}{E_c b} + \alpha(T_0); \\ \sigma_x &= \frac{N_x}{E_c b} + \alpha(T_0). \end{aligned} \right\} \quad (4.38)$$

If we now substitute the values of  $\sigma_x$  and  $\sigma_y$  from expressions (4.38) in formula (4.32) we secure:

$$\sigma_y = \frac{PR}{b} + E_c \alpha T_0 - E_c \alpha \left( T_0 + \frac{\Delta T}{b} z \right) = \frac{PR}{b} + \alpha \frac{\Delta T}{b} z E_c;$$

$$\sigma_x = \frac{NR}{b} + E_c \alpha T_0 - E_c \alpha \left[ T_0 + \frac{\Delta T}{b} z \right] = \frac{NR}{b} + \alpha \frac{\Delta T}{b} z E_c,$$

where  $z$  varies from  $-\frac{b}{2}$  to  $+\frac{b}{2}$ .

$\sigma_x$  and  $\sigma_y$  have maximum values with  $z = \frac{b}{2}$ :

$$\sigma_{x \max} = \frac{NR}{b} + \alpha \frac{\Delta T}{2} E_c;$$

$$\sigma_{y \max} = \frac{PR}{b} + \alpha \frac{\Delta T}{2} E_c. \quad (4.39)$$

The system of equations (4.39) can be solved by the method of successive approximations (4). For example, as first approximation one can adopt the values of  $\sigma_x$  and  $\sigma_y$  determined in accordance with formulas (4.15). Knowing the values of  $\sigma_x$  and  $\sigma_y$ , one can determine the value of the intensity of the stressed state  $\sigma_1$ :

$$\sigma_1 = \sqrt{\sigma_x^2 - \sigma_x \sigma_y + \sigma_y^2}. \quad (4.40)$$

In accordance with the magnitude of  $\sigma_1$  we find from the corresponding diagram of stretching or elongation the value of the intensity of the deformed state  $\epsilon_1$ . The value of  $\epsilon_1$  can also be figured out according to the formula (4):

$$\epsilon_1 = \frac{2}{\sqrt{3}} \sqrt{\sigma_x^2 + \sigma_x \sigma_y + \sigma_y^2}. \quad (4.41)$$

for which we determine in advance, in correspondence with the values  $\sigma_x$  and  $\sigma_y$ , the values  $\epsilon_x$  and  $\epsilon_y$ .

Further, we find the value of the secant module of elasticity  $E_c = \frac{\sigma_1}{\epsilon_1}$  and substitute it in formula (4.39) in order to determine the values  $\sigma_x$  and  $\sigma_y$  in second approximation. The approximations must be continued until the differences between the preceding and the following approximations satisfies the required precision of calculation. After this, one can determine the stress sought in accordance with formulas (4.39).

Thus, in order to determine stresses sought we must know the parameters of the nonstationary temperature field. The function  $T(z)$ , determining the distribution of temperature within the wall depending on current values of  $z$ , does not alter in linear fashion. Questions of distribution of temperature in the wall are examined in greater detail in courses of heat transfer.

#### 4.3. Evaluation of the Reliability of the Structure of Large Solid-Fuel Rocket Engines

By the reliability of a system we understand the capacity of the system to carry out assigned functions under specific conditions of use and over the course of specific time.

In the working process of creating solid-fuel rocket engines two methods of calculating the reliability of the system have become highly developed: determination of the characteristics of reliability based upon utilization of experimental statistical data, and upon nonstatistical criteria of reliability.

The statistical method of analysis of distribution curves, used for evaluation of the reliability of a solid-fuel rocket engine, is based upon derivations of the theory of probability and mathematical statistics. This method is applicable under circumstances where a large cycle of single-type stand and flight tests are carried out. For this reason the accumulation of statistical information regarding the operation of an engine, and regarding the strength of the casing of a solid-fuel rocket engine and its individual elements are of decisive significance for evaluation of the reliability of the structure of a solid-fuel rocket engine.

Qualitative results of the carrying out of a program of flight tests on large rocket engines are presented in a graph (Figure 4.8); they show that for intercontinental ballistic rockets and for rockets to launch artificial earth satellites reliability is a function of the number of tests. This function rises asymptotically with increase of the number of tests from a relatively small initial value (7, 8). Inasmuch as the enormous expense of testing large rocket engines will limit the number of possible flight tests, the amount of reliability of systems must be taken from the initial field of these curves. In this field solid-fuel rocket engines prove to be systems of high reliability (9). This is confirmed by the comparative reliability data set forth in Table 4.1 (7, 8), based solely on study of the work of the engines to the exclusion of disturbance during work by the guidance systems, and for purely hypothetical values for the reliability of the individual stages of the rocket. It is also assumed that breakdowns in ignition of engines occasion just such failures as does burning-through of the combustion chamber.

A deficiency of the statistical method in evaluating the strength and reliability of the structure of a solid-fuel rocket engine with the requisite credibility of 90-95 percent is the need for carrying out a

large number of tests, even for medium reliability values. For example, for the NOVA carrier rocket the reliability of each engine in the packet must come to 99 percent (10). In order to secure 95 percent credibility, it is necessary to carry out no-fail fire tests on 295 engines, which is too expensive and takes a great deal of time.



Figure 4.8. Dependence of reliability factor on number of flight tests in process of working through. a -- Reliability of power apparatus; b -- RDTT [solid-fuel rocket engine]; c -- ZhRD [liquid-fuel rocket engine?] with displacer system of fuel feed; d -- ZhRD with turbine-pump system of fuel feed.

Table 4.1

<u>Reliability of Individual Stage</u>	<u>Type of Engine</u>	<u>Number of Stages</u>	<u>Total Reliability</u>
0.8	Liquid	3	0.512
0.8	Liquid	4	0.410
0.98	Solid fuel	4	0.922

Of late the methods system of prognosis of reliability in planning engines has assumed great importance (10, 11). The reliability of an engine is expressed as the product of the reliability of structure  $R_K$  and the reliability of operational capability  $R_p$ .

#### Evaluation of Reliability of Structure

Reliability of structure may be regarded as the probability of successful (without disassembly) work on the part of the basic structural units of the engine apparatus under circumstances where force loads of the surrounding milieu are operating. The method for evaluation of the probability of failure or reliability of the structure is set forth in study (11). The methods system for prior calculation of reliability is based upon two fundamental assumptions.

1. It is considered that all types and causes of failures leading to destruction of an engine are known (11). For this reason it is possible to make use of the data from preceding programs of developing solid-fuel rocket engines and to select coefficients for reserve strength so as to ensure reliable operation under circumstances which have earlier led to failure.

2. The distribution of stress in elements from the operation of surrounding circumstances and of admissible stress for the material of the element are subject to the normal law of distribution of random quantities, in which connection their mean values  $\bar{x}$  and their dispersion are known. In Figure 4.9 there are set forth functions of distribution of stresses.

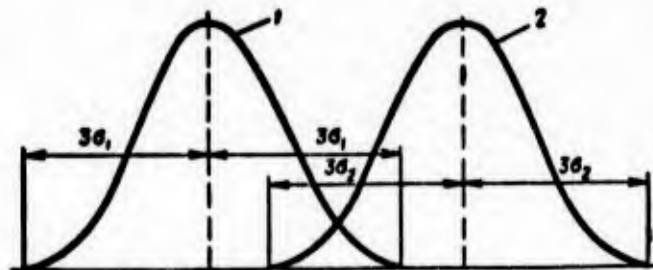


Figure 4.9. Functions of normal distribution of stresses: 1 -- Function of distribution of operative stress; 2 -- Function of distribution of admissible stress.

For prognosis of reliability of structure the solid-fuel rocket engine is broken down into a series of basic sub-systems (Figure 4.10) and detailed analysis of the possible types of failures is carried out. All independent and reciprocally linked causes of failure are tabulated.

Let  $x_1$  be a stress which arises in an element of the structure from an external reaction of specified intensity  $E$ ;  $x_2$  -- the admissible stress for the material of the element. If  $x = x_2 - x_1 > 0$ , a failure in work will not occur.

Inasmuch as  $E$  is a variable quantity, the mean value (the mathematical expectancy) for  $\bar{x}$  is equal to

$$\bar{x} = \bar{x}_2 - \bar{x}_1. \quad (4.42)$$

Analogously the mean-square dispersion of  $\underline{x}$  is equal to

$$\sigma_x = \sqrt{\sigma_2^2 + \sigma_1^2}. \quad (4.43)$$

The law of distribution of probability of  $\underline{x}$  is written in the form

$$y = \frac{1}{\sqrt{2\pi\sigma_x}} \cdot e^{-\left[\frac{(x-\bar{x})^2}{2\sigma_x^2}\right]} \quad (4.44)$$

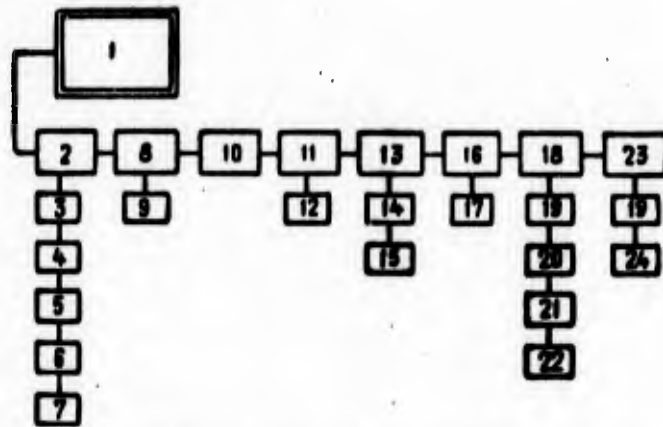


Figure 4.10. Basic subsystems of solid-fuel rocket engine: 1 -- the solid-fuel rocket engine; 2 -- casing; 3 -- rocket chamber; 4 -- forward cap; 5 -- rearward cap; 6 -- forward "skirt"; 7 -- rearward "skirt"; 8 -- armor; 9 -- elements; 10 -- insulation; 11 -- fuel; 12 -- components; 13 -- cone or jet; 14 -- conical part of jet; 15 -- insert in critical cross-section of cone; 16 -- system for guidance of vector of thrust; 17 -- guidance organs; 18 -- ignition system; 19 -- ignition charge; 20 -- envelope of igniter; 21 -- safety apparatus; 22 -- igniter; 23 -- destruct system; 24 -- electric fuse.

The probability of nonfailure will be equal to

$$P(x > 0) = \frac{1}{\sqrt{2\pi\sigma_x}} \int_0^{\infty} e^{-\left[\frac{(x-\bar{x})^2}{2\sigma_x^2}\right]} \quad (4.45)$$

Introduction of the substitution

$$z = -\frac{(x-\bar{x})}{\sigma_x} \quad (4.46)$$

makes it possible to express the probability of nonfailure with the help of the function  $\Phi\left(\frac{\bar{x}}{\sigma_x}\right)$ , the value of which can be secured from existing tables (12).

Then

$$P(x > 0) = \frac{1}{\sqrt{2\pi}} \int_{-\infty}^{\frac{\bar{x}}{\sigma_r}} e^{-\frac{z^2}{2}} dz = \Phi\left(\frac{\bar{x}}{\sigma_r}\right). \quad (4.47)$$

Next the coefficient for reserve strength is introduced:

$$k = \frac{\bar{x}_2 - 3\sigma_2}{x_1 + 3\sigma_1} \quad (4.48)$$

as are the coefficients for variation of operative and admissible stresses (a and b), determined by the relations:

$$a = \frac{3\sigma_1}{x_1}; \quad (4.49)$$

$$b = \frac{3\sigma_2}{x_2}. \quad (4.50)$$

After transformation formula (4.48) takes on the form

$$k = \frac{\bar{x}_2(1-b)}{x_1(1+a)}. \quad (4.51)$$

Then the relation  $\frac{\bar{x}}{\sigma_r}$  may be expressed through K, a, and b, making use of formulas (4.42) and (4.43):

$$\frac{\bar{x}}{\sigma_r} = \frac{\bar{x}_2 - \bar{x}_1}{\sqrt{\sigma_2^2 + \sigma_1^2}} = \frac{\bar{x}_1 \left( k \frac{1+a}{1-b} - 1 \right)}{\frac{\bar{x}_1}{3} \sqrt{a^2 + k^2 b^2} \frac{(1+a)^2}{(1-b)^2}} = 3 \frac{k \frac{1+a}{1-b} - 1}{\sqrt{a^2 + k^2 b^2} \left( \frac{1+a}{1-b} \right)^2}. \quad (4.52)$$

An approximate solution can be secured in the event only nominal values for the quantities  $\bar{x}_1$  and  $\bar{x}_2$  are used, i.e., when  $K = \frac{\bar{x}_2}{x_1}$ .

Expression 4.52 assumes a simplified form

$$\frac{\bar{x}}{\sigma_r} = 3 \frac{K-1}{\sqrt{a^2 + b^2 K^2}}. \quad (4.53)$$

The function  $\Phi\left(\frac{\bar{x}}{\sigma_r}\right)$  is found for each basic subsystem from the tables in accordance with the values figures out for  $\frac{\bar{x}}{\sigma_r}$ .

For each type of failure, it is necessary to set up corresponding values for a, b, and k(K) in evaluating reliability.

The results are summarized in Table 4.2, in the last column of which the probability of nonfailure working while under the operation of the surrounding milieu is entered.

Table 4.2

Type of Failures	$k$	$a$	$b$	$\Phi(\cdot)$	$P$
1	$k_1$	$a_1$	$b_1$	$\Phi_1(\cdot)$	$P_1$
2	$k_2$	$a_2$	$b_2$	$\Phi_2(\cdot)$	$P_2$
$\vdots$	$\vdots$	$\vdots$	$\vdots$	$\vdots$	$\vdots$
$n$	$k_n$	$a_n$	$b_n$	$\Phi_n(\cdot)$	$P_n$

Taking into account the fact that the types of failures are independent quantities, and that some elements of the structure may have a number of causes of failures, the probability of what the first system will not show will be presented by the product

$$P \text{ (subsystem)} = P_a \cdot P_b \cdot P_c \dots$$

The value of the reliability of the structure of a solid-fuel rocket engine will be expressed as the product of the resultant probabilities of nonfailure operation for each of the subsystems (10, 11):

$$R_x = P_1 \cdot P_2 \cdot P_3 \dots P_n$$

In Figures 4.11 and 4.12 we set forth the dependence of reliability upon the coefficient of variation for various values of  $\underline{k}$ ,  $\underline{K}$ ,  $\underline{a}$ , and  $\underline{b}$  (10, 11).

Example 1. Let us determine the probability of bursting of the casing of a solid-fuel rocket engine under working conditions, with the following basic data. Calculated working pressure in the combustion chamber is  $p_{\text{max}} = 42 \frac{\text{kg}}{\text{cm}^2}$ . Pressure by reason of change in speed of burning

of solid fuel can reach  $2.52 \text{ kg/cm}^2$  (amount of normal dispersion). Casing of engine is made of steel having a tensile strength of  $12,500 \text{ kg/cm}^2$ . Magnitude of normal dispersion of indicated strength of material is  $120 \text{ kg/cm}^2$ . Coefficient of reserve strength  $K = 1.25$  from calculation at limit load.

Solution. From analysis of possible anomalies in the working of a solid-fuel rocket engine we reach the conclusion that the basic cause

of bursting of the casing is breakage of the binding ring (hoop). We determine in accordance with formulas (4.49) and (4.50) the coefficients of variation of operative loads and admissible loads for the material:

$$a = 3 \frac{\sigma_1}{x_1} = 3 \cdot \frac{2,52}{42} = 0,181;$$

$$b = 3 \frac{\sigma_2}{x_2} = 3 \cdot \frac{120}{12500} = 0,0288.$$

Making use of formula (4.53) we find that

$$\frac{\bar{x}}{\sigma_x} = 3 \cdot \frac{K-1}{(a^2 + b^2 K^2)^{\frac{1}{2}}} = 3 \cdot \frac{1,25-1}{(0,181^2 + 0,0288^2 \cdot 1,25^2)^{\frac{1}{2}}} = 3,51.$$

The table value of function  $\Phi$  (3.51) = 0.9996. Consequently, the reliability of breakage of the binding ring (hoop) under working conditions is equal to 0.04 percent.

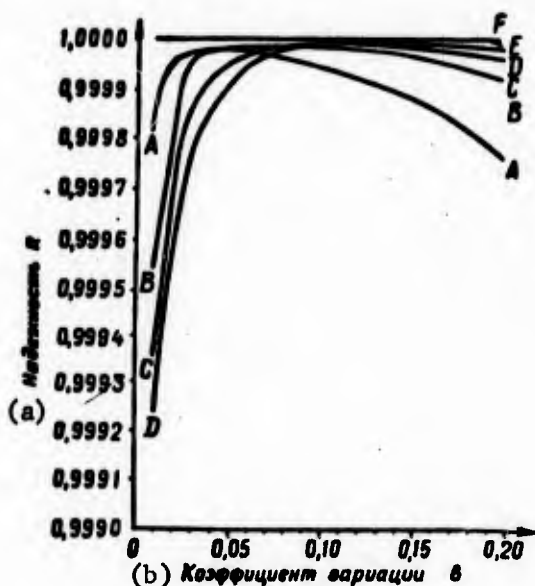


Figure 4.11. Dependence of reliability R upon coefficient of variation  $b$  ( $0,01 < b < 0,20$ ):

A -  $\kappa=1$ ,  $a=0,05$ ; B -  $\kappa=1$ ,  $a=0,10$ ; C -  $\kappa=1$ ,  $a=0,15$ ;  
D -  $\kappa=1$ ,  $a=0,20$ ; E -  $\kappa=1,1$ ,  $0,01 < a < 0,2$ ; F -  $\kappa=1,1$ ,  
 $0,01 < a, b < 0,2$

a -- Reliability, R; b -- Coefficient of variation, B.

The methods system for prior calculation of reliability which we have examined makes it possible to carry out reliability analysis for the material of the structure and facilitates careful selection of material. The possibility of considerable increase in the relationship of normal dispersion to nominal amount of strength of material is of great

importance. On this account, this circumstance must indispensably be taken into account upon the use of new materials appearing in rocket building and having higher strength characteristics. As an example we shall set forth the calculation of probability of nonfailure operation of the individual elements with various values for the coefficient  $\underline{b}$ .

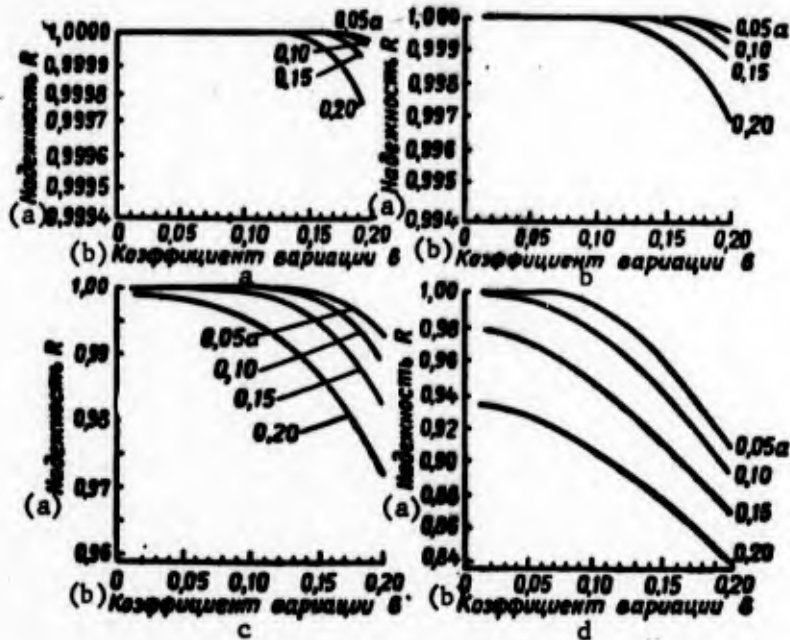


Figure 4.12. Dependence of reliability  $R$  upon coefficient of variation  $\underline{b}$  with use of nominal values for magnitude of  $K$ : a --  $K = 1.4$ ; b --  $K = 1.3$ ; c --  $K = 1.2$ ; d --  $K = 1.1$ .  
a -- Reliability,  $R$ ; b -- Coefficient of variation,  $B$ .

**Example 2.** The elements of the structure of a solid-fuel rocket engine are made of different materials A and B. The coefficient of reserve strength for both materials,  $K$ , is 1.25. (From calculation of nominal values for stresses.)

Let coefficient  $\underline{a}$  be 15 percent for both materials. We shall take the coefficient of variation of admissible stresses ( $\underline{v}$ ) for material A as being 5 percent, and for material B as being 20 percent. We shall determine the reliability of the material of the structure.

**Solution.** Making use of equation (4.53) for the solution, we secure:

$$\left(\frac{\bar{x}}{\sigma_x}\right)_A = 3 \frac{K-1}{\sqrt{a^2 + \mu K^2}} = 3 \frac{1.25-1}{\sqrt{0.15^2 + 0.05^2 \cdot 1.25^2}} = 4.61;$$

$$\left(\frac{\bar{x}}{\sigma_x}\right)_B = 3 \frac{K-1}{\sqrt{a^2 + \mu K^2}} = 3 \frac{1.25-1}{\sqrt{0.15^2 + 0.2^2 \cdot 1.25^2}} = 2.69.$$

Then for  $\left(\frac{\bar{x}}{\sigma}\right)_A = 4.61$  the table value of reliability  $\Phi(4.61)$  is equal to

$$P_A = 0.9999,$$

for  $\left(\frac{\bar{x}}{\sigma}\right)_B = 2.69$  the table value of reliability  $\Phi(2.69)$  is equal to

$$P_B = 0.9962.$$

The difference in the reliability of the two elements, depending on the characteristics of the materials, is relatively slight. But in complicated systems even a slight reduction in reliability of elements may considerably affect the reliability of the system. Let us note that the requisite reliability of structure can be secured upon changing the coefficient for reserve strength  $K$ . The methods system for prior calculation of reliability which we have examined makes it possible to introduce necessary changes into the characteristics of reliability in order to ensure an assigned reliability of successful working on the part of a solid-fuel rocket engine.

#### Evaluation of Exploitational Reliability

By exploitational reliability (reliability of working capability) we mean the probability of reliable working of an engine within assigned limits of working characteristics. The fire testing of a real engine is imitated with the help of a programmed computing apparatus modeling the processes of the internal ballistics of a solid-fuel rocket engine. Computation of the characteristics of an engine is based upon utilization of the probability properties of the input parameters. Knowing the technical requirements imposed upon the working of the engine, one can carry out evaluation of reliability in accordance with the quantity of computations on the modeling machine (imitation of starts) in which the engine has been working within the assigned limits (11). The program computing set-up for computation of the reliability in use is made identical to the program in accordance with which prior checking of the correctness of the design of the charge of solid fuel and evaluation of the operation of the engine up to launch has been carried out (11). This is apparent also from a partial listing of the basic input parameters:

- $k$  -- relation of unit heat capacities of basic components of fuel;
- $A$  -- coefficient of consumption, or coefficient of discharge of gases;
- $u_1$  -- unit speed of combustion in exponential law of combustion ( $u = u_1 \cdot \rho^v$ );
- $v$  -- index of degree in law of combustion;
- $\epsilon$  -- coefficient of increase in speed of combustion of fuel on account of heat action of gas flow upon intensivity of combustion of charge;
- $\rho$  -- density of solid fuel;
- $T_R^0$  -- temperature of gases in rocket chamber;
- $F_{out1}$  -- area of outlet cross-section of cone;
- angle of half-span of cone of jet;

$K_p$  -- effective coefficient of thrust;  
 $F_{cr} \tau$  -- change in area of critical cross-section of cone depending on time of operation of engine.

To this listing some further input data, making it possible to determine the form of the burner of solid fuel as a function of time, are added:

$I/t$  -- mean amount of thrust;  
 $p_k$  -- pressure in forward part of combustion chamber of engine;  
 $p_{k\tau}$  -- pressure in chamber at conclusion of engine's work;  
 $F_{cbk}/F_{kp}$  -- relation of area of transverse cross-section of chamber for free passage of gas flow to area of critical cross-section of cone;  
 $S$  -- complete surface of combustion of burner of solid fuel;  
 $P$  -- thrust;  
 $I$  -- complete impulse;  
 $I_1$  -- unit (specific) impulse;  
 $\tau$  -- time of working of engine.

In order to investigate the influence of dispersion of input variables upon the characteristic of the engine the method of statistical trials (the Monte Carlo method) is used (8, 11). It is also assumed that the majority of input parameters are subject to the normal law of distribution. The use of the method of statistical trials gives just the same evaluation of reliability as does that for experimental launches, in view of the relation of the number of successful launches to the number of modeled launches. Such an evaluation of the reliability of a real engine with the help of a modeling set-up is sufficiently objective, as is confirmed by comparison of previously computed and of experimental characteristics (Table 4.3).

Comparison of Computed and Experimental Characteristics of Solid-Fuel Rocket Engine\*

<u>Ballistic Characteristics</u>	<u>Variance Relative to Normal Value, %</u>
Mean thrust	0.9
Total impulse	2.1
Time of working of engine	4.7

\* Secured as result of 20 modeled launches.

The accuracy of the evaluation is affected by the degree of independence of the input parameters and the character of the correspondence of the modeled launch to the actual one. Refinement of modeling of the real process will follow the course of improvement in the imitation of shorter intervals of time of the ignition of the charge of solid fuel and further approximation of the process of the burning of solid fuel taking into account the heat reaction of the gas flow upon the speed of

combustion of the charge. The introduction of variables subjected to the law of normal distribution of random quantities makes it possible to evaluate the conjoint influence of random change in these variables upon the basic parameters determining the working capability of a solid-fuel rocket engine.

In conclusion we should note that computation in accordance with the methods system of prognosis of reliability determines the reliability of some ideal plan for a solid-fuel rocket engine. Reduction of reliability in the process of production and in use is possible.

#### BIBLIOGRAPHY

1. Bonni, E. A., Zukrou, M. J., Besserer, K. U., Designing and Computation Practice, State Publishing House for Physical and Mathematical Literature, Moscow, 1960.
2. Feodos'yev, V. I., Strength of Heat-Stressed Units of Liquid-Fuel Rocket Engines, Oborongiz Publishing House, 1963.
3. Ilyushin, A. A., Resistance of Materials, Fizmatgiz Publishing House, 1959.
4. Bezukhov, N. I., Bazhanov, V. L., Goldenblat, I. A., Nikolayenko, N. A., Sinyukov, A. M., Computations for Strength, Resistance, and Oscillation Under Circumstances of High Temperatures, Mashinostroyeniye Publishing House, 1965.
5. Birger, I. A., Schorr, B. F., Shneiderovitch, R. M., Strength Calculations on Machine Parts, Mashgiz Publishing House, 1959.
6. Barrere, M., Jomotte, A., Bebek, B. F., Vandekerkhove, J., Rocket Engines, Oborongiz Publishing House, 1962.
7. Space Technics, "Nauka," 1964.
8. Lipov, Lloyd, "Evaluation of Reliability of Large Rocket Engines Using Solid Fuel in Process of Their Development," Problems of Rocket Technics, No 1, 1964.
9. "Solid Fuel Rocket Engines (Survey)," Problems in Rocket Technics, No 6, 1964.
10. Astronautics and Rocket Dynamics, No 2, 1965.
11. Klueger, Paul, American Rocket Company (preprints), 1963, No 2755, pages 1-10. Express information of Astronautics and Rocket Dynamics, No 48, 1965.

12. Gnedenko, B. V., Course in Theory of Probability, State Publishing House for Physical and Mathematical Literature, 1961.

## CHAPTER V. STRENGTH OF CHARGES OF SOLID ROCKET FUEL

### 5.1. Working Characteristics and Character of Deformation of Solid-Fuel Rocket Charges

Solid fuels must be distinguished not only by high energy, ballistic, and technological properties, but also by high strength characteristics. The mechanical properties of a fuel must be such that fuel charges resist developing stresses without breaking. In this connection there must be no sloughing off of the charge from the interior surface of the combustion chamber, no appearing of cracks or fractures. In addition, the hardness of the fuel must be sufficient for the assigned law of change in surface should be complied with in the combustion process. The fuel should possess a modicum of elastic properties, since otherwise local deformations may exceed the admissible amount, which will lead to explosion of the rocket engine.

During the period the rocket engine is working the solid fuel is under the action of inertial forces and gas pressures in the combustion chamber. These forces provoke deformation of the charge, the character of which depends on the geometrical and mechanical properties of the fuel burners and the method of the fastening of the charge in the chamber.

In rocket engines with burners inserted loose in the chamber and supported in the chamber only at parts of their surface, under the action of the loads referred to the fuel is subjected to longitudinal compression and to stretching in transverse direction (Figure 5.1). At the end of the engine's work the tubular charge becomes very delicate and with insufficient strength of the charge the burner may lose longitudinal stability. Breakage of the charge may also take place in the event that local stresses exceed the limit of elasticity. At high initial temperatures the fuel becomes soft. In order that the burner may not crumple and split, the fuel must be characterized by a high permissible stress value. In checking computation the true magnitude of bearing stress in the face part of the burner and the size of the bearing surface are taken into account; they are found from the condition

$$F_{\text{cm}} = \frac{G \cdot n}{\sigma_{\text{cm}}}$$

where  $n$  is the coefficient of overload, equal to the relationship of maximum acceleration of the rocket to acceleration of the force of gravity;

$G$  is the weight of the charge of solid fuel;

$\sigma_{\text{cm}}$  is the permissible stress of the burner of solid fuel under warping at a charge temperature of  $+ 50^{\circ} \text{C}$ .

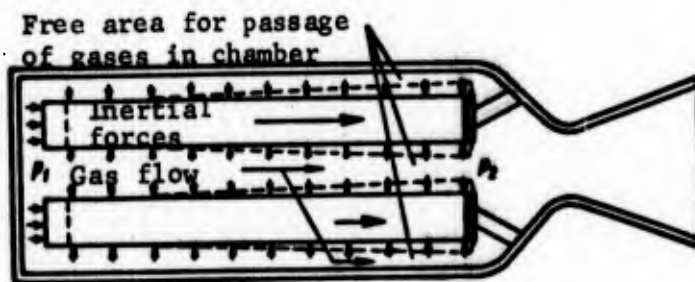


Figure 5.1. Diagram of stresses and character of deformations of a charge of solid fuel placed loose in the combustion chamber and resting upon the diaphragm.

A face-burning charge is stressed by forces running in contrary directions (Figure 5.2) (pressure forces  $p_{\text{cham}} \cdot F_{\text{cham}}$  and inertial forces). In flight the inertial forces will be less than the pressure forces. Under the pressure of the gases in the chamber the burner may considerably reduce in length. But if the fuel burner is enclosed in an elastic envelope, loosely lying against the walls of the chamber (a jacket), the forces of pressure in the chamber will operate as a hydrostatic load, accompanied by small deformation and very little reduction of the volume of the burner (2).

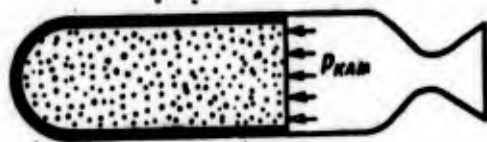


Figure 5.2. Diagram of solid-fuel rocket engine with face-burning charge.

In rocket engines having charges that burn on the inward surface (Figure 5.3) pressure is transmitted via the fuel to the walls of the combustion chamber. Under the operation of forces from the falling off of pressure along the chamber and from acceleration, the charge strives to move toward the cone (Figure 5.4). Forces operating counter to displacement of the charge are the forces connecting the fuel to the walls of the combustion chamber (adhesion forces), and also the internal attachment forces of the fuel. Dangerous dislocation forces are ordinarily the stresses arising in points where the fuel is cemented to the envelope.

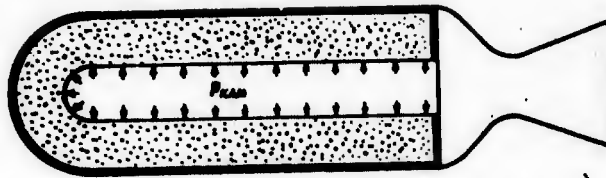


Figure 5.3. Diagram of solid-fuel rocket engine with charge which burns internally.

In solid-fuel rocket engines of large dimensions the substantial loads operating on the solid fuel charge are loads from weight and from inertial forces, which at the moment of launch and during flight of the rocket provoke a perceptible axial slippage of the burner (Figure 5.4), leading to reduction of the area of the channel for the exit of gases.

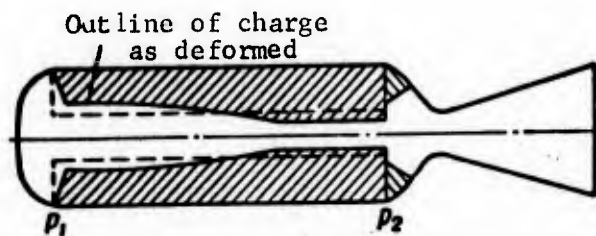


Figure 5.4. Character of deformations in a charge of solid fuel firmly fastened to the interior surface of the combustion chamber.

Computations show (4) that for a single-channel charge having a relative thickness of vault of 50 percent, with a hard casing and a firm fastening of the face of the charge, the magnitude of relative decrease in area of the channel  $F_{kan}$  at the cone face has proved to be equal to

$$\frac{\Delta F}{F_{kan}} \approx 40 \frac{\rho R n}{E}, \quad (5.1)$$

Where  $E$  is the module of elasticity (Young);

$R$  is the exterior radius of the burner of the equivalent tubular charge;

$\rho$  is the specific weight of the fuel charge.

For charges having relatively great diameter the maximum value of relative change in the passage cross-section will be approximately 10 per cent per 1 g (6).

Depending on the working regime of the engine, requirements imposed upon the mechanical properties of the fuel may be different. In the solid-fuel rocket engine of the first stage of a rocket, when the charge is subjected to short-term operation of inertial forces, clogging in the chamber does not occur (unless it has not taken place in advance

under the effects of weight and upon assembly of the rocket), since the speed of combustion of the solid fuel is ordinarily greater than the speed of creepage. The second stage of a rocket is subjected to the action of acceleration over a longer period. For this reason it is logical to select a charge having a harder module, great relaxation time, or a channel expanding toward the outlet.

## 5.2. Mechanical Properties of Solid Rocket Fuels

In Table 5.1 we set forth some mechanical characteristics of ballistic fuels.

Table 5.1. Typical Mechanical and Thermophysical Properties of Solid Ballistic Fuels (1)

<u>Characteristic</u>	<u>Denomination</u>	<u>Amount</u>
Module of elasticity at 20° C	E, kg/cm <sup>2</sup>	1,000-3,000
Module of elasticity at 50° C	E, kg/cm <sup>2</sup>	200-1,000
Poisson coefficient	$\mu$	0.35-0.5
Coefficient of linear thermic expansion	$\frac{1}{K}$	1.2 · 10 <sup>-4</sup> - 2.0 · 10 <sup>-4</sup>

Solid ballistic fuel may be regarded as an absolutely elastic and isotropic material. At positive temperatures such a fuel is characterized by a glass-like (hard) state of material. At negative temperatures it becomes friable. In Figures 5.5, 5.6, and 5.7 there are set forth curves indicating the influence of temperature upon the mechanical characteristics of ballistic fuels, and also the results of experiments (5) to determine critical stresses upon loss of longitudinal stability of burners of 25-millimeter diameter having no channels. The indicated dependences are in qualitative agreement with computations carried out according to the familiar Euler formula for critical stress:

$$\sigma = \frac{\pi^2 E}{\left(\frac{L}{r_1}\right)^2}, \quad (5.2)$$

where E is the module of elasticity of a solid fuel;

L is the adduced length of the burner;

r<sub>1</sub> is the radius of inertia of the transverse section of the burner.

Let us examine limit deformation of a tubular charge (Figure 5.1) from the standpoint of maximum permissible crumpling of the charge to an extent leading to coverage of free openings for passage of gases, which in the last analysis leads to breakage or destruction of the charge. A force P<sub>1</sub>, arising as a result of the falling off of pressure along the length of the burners, operates on a charge in the form of tubular burners:

$$P_1 = (p_1 - p_2) S_T \quad (5.3)$$

where  $p_1$  and  $p_2$  are the pressure of gases respectively at the forward and the rearward ends of the charge;

$S_T$  is the area of the faces of the charge.

In addition, an inertial force  $P_2$  from longitudinal acceleration of the rocket operates upon the charge:

$$P_2 = \sigma \cdot n \quad (5.4)$$

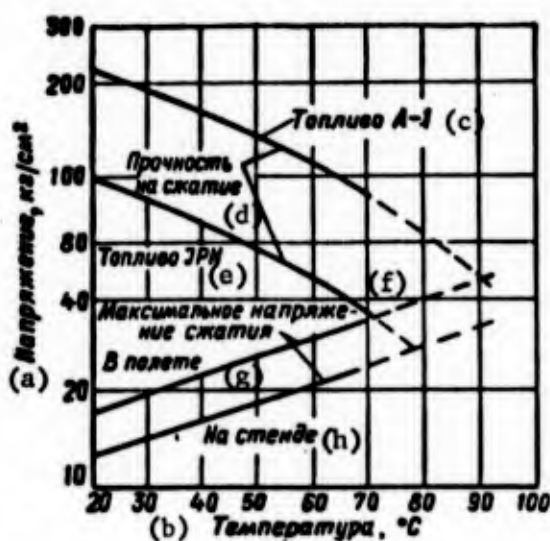


Figure 5.5. Compression strength and maximum compression stress for a burner of ballistic fuel. a -- Stress,  $\text{kg/cm}^2$ ; b -- temperature,  $^{\circ}\text{C}$ ; c -- Fuel A-1; d -- Compression strength; e -- Fuel JPN; f -- Maximum compression stress; g -- In flight; h -- On stand.

Under the action of these forces and in consequence of the relatively low module of elasticity of solid fuel, particularly at high temperatures, the charge is deformed (Figure 5.1) and thereby the free area for passage of gases in the chamber is reduced.

The expression for axial stress  $\sigma$ , arising at the end of the charge next to the diaphragm, can be written as follows:

$$\sigma = (p_1 - p_2) + L \rho_T j \quad (5.5)$$

where  $L$  is the length of the charge;

$\rho_T$  is the mass density of the fuel;

$j$  is the longitudinal acceleration of the rocket.

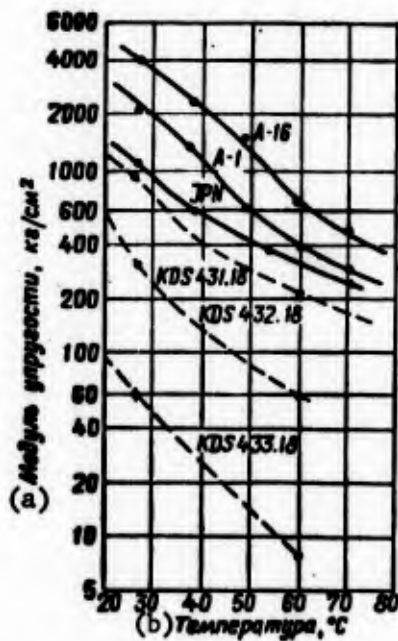


Figure 5.6. Dependence of module of elasticity upon temperature for various brands of solid fuel: KDS -- brand of fuel possessing low mechanical strength, specially prepared for experimental purposes. a -- Module of elasticity,  $\text{gk/cm}^2$ ; b -- Temperature,  $^{\circ}\text{C}$ .

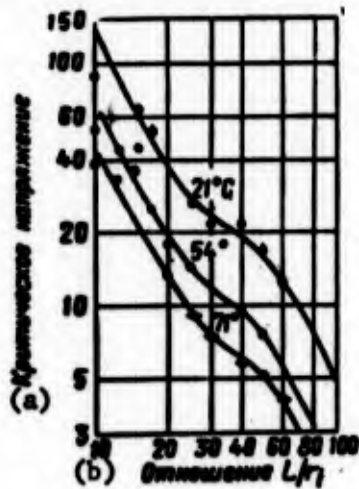


Figure 5.7. Strength of burner of JPN solid fuel under longitudinal flexure. a -- Critical stress; b --  $L/r_1$  ratio.

The dependence of the area of transverse section of the charge,  $S$ , upon the magnitude of stress is expressed by the formula (2)

$$S_T = S_{T_0} \left( 1 + 2 \frac{\mu}{E} \sigma \right), \quad (5.6)$$

where  $S_{T_0}$  is the initial area of the transverse section of the charge;  
 $\mu$  is the Poisson coefficient;  
 $E$  is the module of elasticity.

Taking into account heat expansion of the burner of the fuel, we convert formula (5.6) to the following form:

$$S_T = S_{T_0} [1 + 2\alpha(T_0 - T)] \left( 1 + 2 \frac{\mu}{E} \sigma \right), \quad (5.7)$$

where  $\alpha$  is the coefficient of linear thermic expansion of the fuel;  
 $T_0$  is the initial temperature of the fuel;  
 $T$  is the standard temperature of the fuel, equal to 15° C.

Bearing in mind the relationship

$$F_{CB} = F_{KAM} - S_T; \quad F_{CB_0} = F_{KAM} - S_{T_0} \quad (5.8)$$

where  $F_{CB}$  is the area for passage of gases in the chamber;  
 $F_{CB_0}$  is the initial area for passage of gases in the chamber;  
 $F_{cham}$  is the area of transverse section of the chamber, and taking  $F_{cham}$  as more or less equal to  $2S_{T_0}$ , one can transform equation (5.6) as follows:

$$\frac{\sigma}{\sigma_0} = \frac{1}{2\mu} \cdot \frac{E}{\sigma_0} \left[ 1 - \frac{F_{CB}}{F_{CB_0}} \right], \quad (5.9)$$

where  $\sigma_0$  is the stress in the charge up to start of work of engine.

Possessing data regarding the dependence of falling off in pressure (or, which is the same thing, regarding  $\sigma$  in the fuel) upon the amount of free passage section, one can show diagrammatically (Figure 5.8) the influence of the module of elasticity of fuel upon the character of deformation in the charge.

In the region of Point A (the stable field) deformations of the charge  $\left( \frac{\sigma}{\sigma_0} \right)$  correspond to stresses which have been evoked by the gas flow on account of falling off in pressure, and these stresses will be less than the permissible elastic stresses which take place under circumstances of reduced area of channels. In the region of Point B (unstable field) displacement to the right leads to reduction of area for passage of gases in the chamber and to increase of pressure, as a result of which destruction of the charge takes place.

Equations (5.8) and (5.9), upon substitution therein of internal ballistics characteristics, make it possible to determine, taking into

account the deformation of the charge, the relation  $F_{crit}/F_{CB}$  as it depends upon the module of elasticity  $E$ . In Figure 5.9 this dependence is presented on the basis of results of the calculation of a tubular charge made of ballistic fuel (1). When the module of elasticity  $E$  is sufficiently high, deformations of the charge practically do not take place and the quantity  $F_{crit}/F_{CB}$  differs little from its initial value. Reduction of the module of elasticity of the fuel leads to rise in the ratio  $F_{crit}/F_{CB}$  and with  $E = E_{min}$  (Point M) a limit of stability which is determined by the condition

$$\frac{d\left(\frac{F_{crit}}{F_{CB}}\right)}{dE} = \infty.$$

curve located higher than Point M describes a process corresponding to increase of pressure, when the input of gases coming from the hot surfaces of the charge will be greater than the output of gases through the free area of the transverse section of the chamber, something which in the last analysis will lead to explosion of the engine.

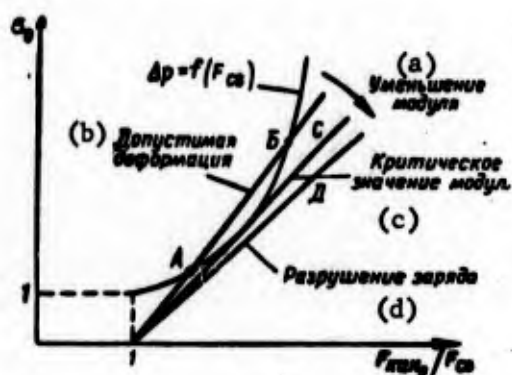


Figure 5.8. Diagrammatic drawing of change of stresses in a charge of solid fuel as they depend upon the amount of free area for passage of gases ( $F_{CB}$ ). a -- Reduction of module; b -- Permissible deformation; c -- Critical value of module; d -- Destruction of charge.

In analysis of the mechanical properties of mixed fuels a series of substantial assumptions are adopted, the main one of which is that of regarding the fuel as an isotropic and homogeneous material, possessing linear viscous-elastic properties, i.e., when deformations remain proportionate to loads, even though both parameters may change over time.

At the same time one should take into account the fact that although the particles of the oxidizer are moistened (enveloped) by the hot polymer binder, there is nevertheless a faint interaction between the oxidizer and the binder. For this reason the mechanical properties of a mixed fuel are almost completely determined by the physical properties of the combustible. In Table 5.2 there are set forth data regarding the limit of strength of some combustible binders.

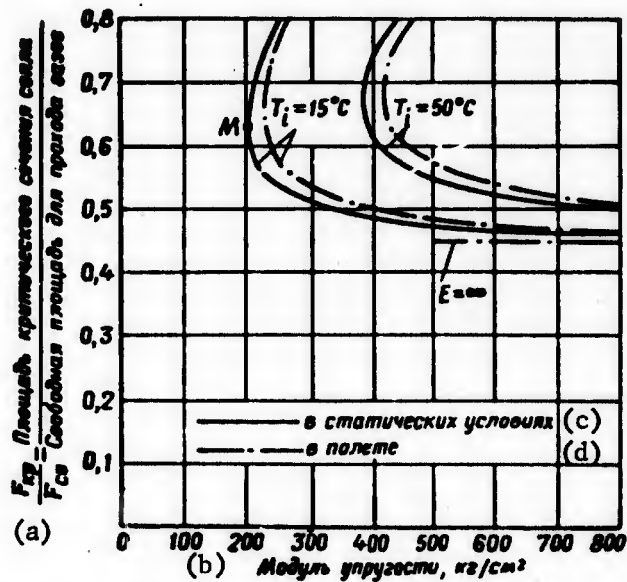


Figure 5.9. Dependence of ratio  $F_{crit}/F_{CB}$  upon amount of module of elasticity of a tubular charge of solid fuel of JPN brand. a -- Area of critical section of cone/Free area for passage of gases; b -- Module of elasticity,  $kg/cm^2$ ; c -- Under static circumstances; d -- In flight.

Table 5.2. Strength Characteristics of Combustible Binders of Solid Fuels (7)

<u>Plastic Resins Possessing Casting Properties</u>	<u>Limit of Breaking Strength in Vulcanized Form Without Additives, <math>kg/cm^2</math></u>
Epoxide resins	28-914
Epoxy-polysulphides	70-703
Phenolic resins	280-492
Polyethers	422-703
Polyethylenes	105-387
Polyurethanes	211-281
Vinyls	70-633

In Figure 5.10 we set forth data on the strength of a fuel in dependence upon the percentage content of binder in the fuel. Obviously breakage strength is approximately proportionate to combustible binder content.

In Table 5.3 we set forth approximate values for some characteristics of mixed fuels.

The mechanical characteristics of viscous-elastic fuels depend markedly upon temperature and speed of deformation.

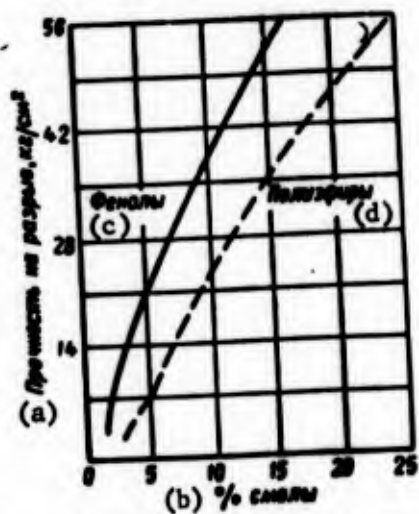


Figure 5.10. Influence of percentage content of combustible binder components upon amount of strength in mixed fuels. a -- Breaking strength,  $\text{kg}/\text{cm}^2$ ; b -- % resins; c -- Phenols; d -- Polyethers.

Table 5.3. Typical Mechanical and Thermophysical Properties of Mixed Solid Fuels (1)

<u>Characteristic</u>	<u>Designation</u>	<u>Quantity</u>
Module of elasticity at $-40^\circ\text{C}$	$E, \text{kg}/\text{cm}^2$	1,000-2,000
Module of elasticity at $+15^\circ\text{C}$	$E, \text{kg}/\text{cm}^2$	100-200
Module of elasticity at $+41^\circ\text{C}$	$E, \text{kg}/\text{cm}^2$	50-100
Poisson coefficient	$\mu$	0.35-0.50
Coefficient of linear thermic expansion	$\alpha_{\text{TK}}$	$0.5 \cdot 10^{-4}$
		$1.5 \cdot 10^{-4}$

In figure 5.11 we set forth diagrams of elongation of an elastic highly-filled mixed fuel at various temperatures. At the temperature of brittleness, equal to approximately  $-25^\circ\text{C}$ , the fuel, altering its elastic-plastic properties, loses the capacity for any considerable elongation, which is characteristic for higher temperatures. At temperatures lower than that of glass transition,  $T_{\text{glass}}^0$ , the fuel becomes brittle.

Inclusion of the time parameter (the rheological factor) in investigating the dependence of deformations upon stresses makes strength calculation considerably more complicated. But even a simplified physical picture, showing the influence of speed of elongating effort upon the mechanical characteristics of a fuel, will be useful for understanding of the causes of defects in fuel. Dependence of elongations upon temperature at various speeds of application of elongating effort is illustrated by the curves presented in Figure 5.12. From this it is apparent that the greater the speed of application of elongating effort,

the higher the temperature at which the friability state sets in. Consequently, at the moment of ignition rapid application of load is dangerous with low initial temperatures of fuel (4).

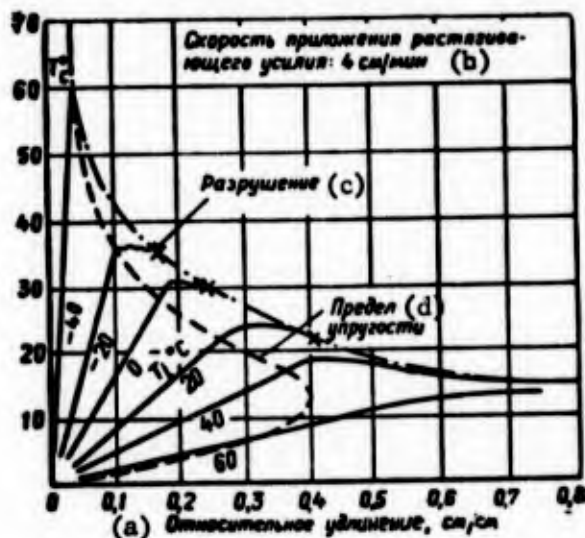


Figure 5.11. Typical diagrams of elongation of elastic mixed fuels. a -- Relative elongation, cm/cm; b -- Speed of application of elongating force, 4 cm per minute; c -- Destruction; d -- Limit of elasticity.



Figure 5.12. Dependence of elongations corresponding to maximum permissible stresses in elastic mixed fuel upon temperature at various speeds of application of elongating effort. a -- Relative elongation at maximum permissible stress; b -- Temperature, °C; c -- Speed of application of elongating effort: 0.0025 cm/min; d -- 25 cm/min; e -- 2,500 cm/min.

In qualitative examination of deformation of a burner as it depends upon speed of deformation the following observation may be made. To begin with, with rise of deformation, the values of the limit stress, like those of limit deformation, rise monotonically. But this increase continues up

to a certain critical speed of deformation, the magnitude of which will be determined by the physical properties of the fuel (for example, by temperature). Then with further increase of speed of deformation one observes a reduction of the values of limit stresses and deformations. This is confirmed by the graph presented in Figure 5.13, secured by Smith for pure rubber (3).

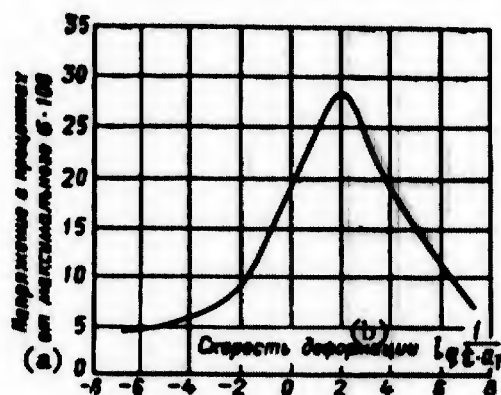


Figure 5.13. Characteristic profile of curve showing dependence of limit stresses upon speed of deformation, with elongation along a single axis:  $\dot{\epsilon}$  -- speed of deformation;  $a_T$  -- temperature parameter. a -- Stress in percent of maximum,  $\sigma \cdot 100$ ; b -- Speed of deformation.

The relationship given as existing between limit deformations and speed of deformation was established in testing examples for monaxial deformation. Examples were carried through to destruction at various constant speeds of deformation.

At the same time it has been established theoretically and experimentally (3) that it is possible to associate the critical speed of deformation (or the time of destruction at a constant speed of deformation) with temperature, namely:

$$\lg a_T = \lg \frac{t}{t_0} = - \frac{k_1 (T - T_{\text{стекл}})}{k_2 + (T - T_{\text{стекл}})} \quad (5.11)$$

where  $a_T$  is the temperature parameter;

$t_T$  is the time of observing a given phenomenon at absolute temperature;

$t_0$  is the time with initial temperature  $T_0$ ;

$T_{\text{стекл}}$  is the temperature at which the module is equal to the module of a glass-like body (lower than this temperature the material is essentially friable);

$k_1, k_2$  may be regarded as universal empirical constants for many polymers.

In the analysis of elastic deformations and stresses of solid fuel charges a considerable part is played by the Poisson coefficient (5.9). The ratio of transverse deformation to longitudinal deformation is not constant, but is a function of time or of deformation, and it depends both on the viscous-elastic properties of the fuel and upon the conditions of loading. As a result of analysis carried out on various elastic-compressible media it has been shown (6) that the Poisson coefficient is a rising function of time or of deformation (Figure 5.14).

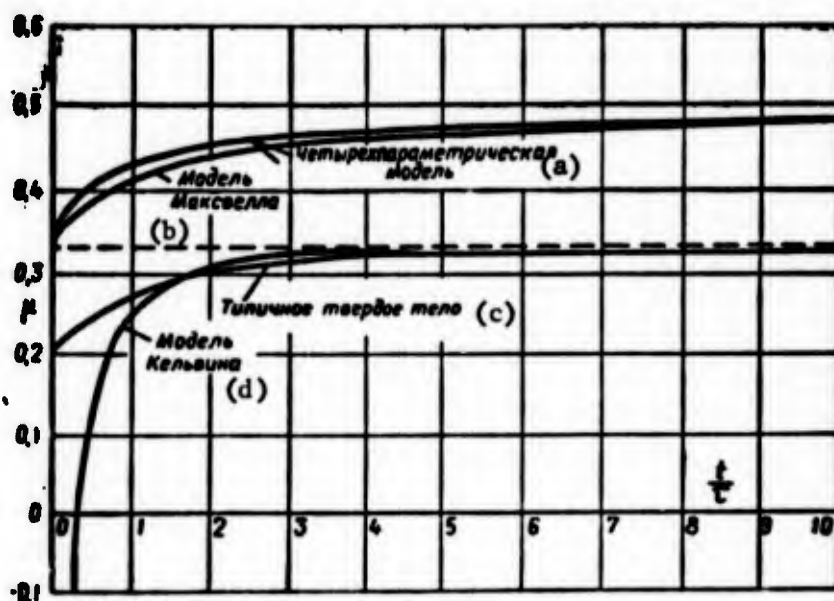


Figure 5.14. The Poisson coefficient,  $\mu$ , as a function of time,  $\mu \left( \frac{t}{\tau} \right)$ , for various viscous-elastic media subjected to elastic compression at a constant speed of stress ( $\dot{\sigma} = c$ ):  $\tau$  is a quantity characterizing the mechanical properties of the fuel. a -- Four-parameter model; b -- Maxwell model; c -- Typical solid body; d -- Kelvin model.

### 5.3. The Strength Criterion

Independently of the degree to which success is encountered in carrying out analysis of elastic or nonelastic deformations, analysis of strength cannot be completed until a strength criterion is established. At present the conditions under which destruction of elastic-plastic materials, among which are solid fuels, take place have been insufficiently studied.

For the field of elastic deformations one can make use of customary strength theories and one can adopt as the criterion of strength either maximum normal deformation, or shear deformation.

In the elastic-plastic field one can make use (3), for the strength criterion, of maximum normal deformation, as the occurrence of destruction as encountered in mixed-fuel rocket engines depends much more markedly upon deformation than upon stress.

Let us examine the possibility of utilizing as a strength criterion the amount of maximum octahedral shear deformation, and let us establish a connection between three-dimensional and one-dimensional failure. The maximum octahedral shear deformation  $\gamma_{\text{Oct}}$  is associated with specific energy of shape formation  $\mathfrak{D}_\phi$ , which is determined as follows in its general form:

$$\begin{aligned} \mathfrak{D}_\phi &= \frac{1}{12G} [(\sigma_x - \sigma_y)^2 + (\sigma_y - \sigma_z)^2 + (\sigma_z - \sigma_x)^2 + 6(\tau_{xy}^2 + \tau_{yz}^2 + \tau_{zx}^2)] = \\ &= \frac{1}{12G} [(\sigma_1 - \sigma_2)^2 + (\sigma_2 - \sigma_3)^2 + (\sigma_3 - \sigma_1)^2], \end{aligned} \quad (5.12)$$

where  $\sigma_1, \sigma_2, \sigma_3$  are the principal stresses,  
 $G = \frac{E}{2(1+\mu)}$  is the module of elasticity of second type.

Octahedral tangential stresses may be expressed through principal stresses and principal deformations:

$$\begin{aligned} \tau_{\text{Oct}} &= \frac{1}{3} \sqrt{(\sigma_1 - \sigma_2)^2 + (\sigma_2 - \sigma_3)^2 + (\sigma_3 - \sigma_1)^2} = \\ &= \frac{2}{3} G \sqrt{(\epsilon_1 - \epsilon_2)^2 + (\epsilon_2 - \epsilon_3)^2 + (\epsilon_3 - \epsilon_1)^2}. \end{aligned} \quad (5.13)$$

After insertion of formula (5.13) into formula (5.12), the expression of the energy of shape alteration assumes the form:

$$\mathfrak{D}_\phi = \frac{G}{3} [(\epsilon_1 - \epsilon_2)^2 + (\epsilon_2 - \epsilon_3)^2 + (\epsilon_3 - \epsilon_1)^2]. \quad (5.14)$$

Applying to equation (5.13) the Guk  $\overline{\text{Hook}}$  law, we secure

$$\tau_{\text{Oct}} = \frac{2}{3} \sqrt{(\epsilon_1 - \epsilon_2)^2 + (\epsilon_2 - \epsilon_3)^2 + (\epsilon_3 - \epsilon_1)^2}. \quad (5.15)$$

Now, substituting expression (5.15) in expression (5.14), we can express  $\mathfrak{D}_\phi$  in terms of  $\tau_{\text{Oct}}$ :

$$\mathfrak{D}_\phi = \frac{3 \cdot G}{4} \tau_{\text{Oct}}^2 \quad (5.16)$$

In computing the charge of solid fuel for strength it is advisable to make use of principal cylindrical deformations  $\epsilon_r, \epsilon_\theta,$  and  $\epsilon_z$ .

Then expression (5.15) can be transcribed in the form:

$$\gamma_{\text{OCT}} = \frac{2}{3} \sqrt{(\epsilon_r - \epsilon_\theta)^2 + (\epsilon_\theta - \epsilon_z)^2 + (\epsilon_z - \epsilon_r)^2}. \quad (5.15')$$

Now let us examine a one-dimensional trial (Figure 5.15), for which we have

$$\epsilon_r = \epsilon_\theta = -\mu \epsilon_z.$$

Substituting the last expression in formula (5.15') we secure:

$$\gamma_{\text{OCT}} = \frac{2}{3} \sqrt{2} (1 + \mu) \epsilon_z. \quad (5.16')$$

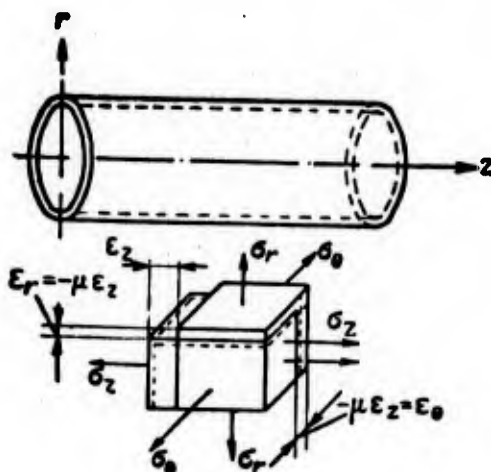


Figure 5.15. Diagram of distribution of principal stresses and principal deformations in one-dimensional stress.

If we now designate limit deformation by  $\epsilon_{\text{failure}}$ , then at the moment of failure in the case under examination

$$\epsilon_z = \epsilon_{\text{failure}}$$

Then from expression (5.16') we find that

$$\sigma_{\text{failure}} = \frac{3\sqrt{2}}{4(1+\mu)} \gamma_{\text{OCT}} \quad (5.17)$$

Inasmuch as the quantity  $\gamma_{\text{OCT}}$  is invariant relative to transformation of coordinates, the value  $\epsilon_{\text{failure}}$ , at which the quantity  $\gamma_{\text{OCT}}$  attains critical magnitude, will be equal to

$$\epsilon_{\text{pass}} = \frac{1}{\sqrt{2} (1 + \mu)} \sqrt{(\epsilon_r - \epsilon_\theta)^2 + (\epsilon_\theta - \epsilon_z)^2 + (\epsilon_z - \epsilon_r)^2} \quad (5.18)$$

In plane deformation of a tubular charge  $\epsilon_z = 0$ . Then expression (5.18) assumes the form

$$\epsilon_{\text{pass}} = \frac{1}{\sqrt{2} (1 + \mu)} \sqrt{(\epsilon_r - \epsilon_\theta)^2 + \epsilon_\theta^2 + \epsilon_r^2}. \quad (5.19)$$

Let us examine, as an example, the stress in a charging having a star-shaped channel at the moment of ignition. The dangerous section will be the star-shaped points, for which, from the law of stress-deformation with plane deformation, we have (4):

$$\epsilon_r = \frac{1 + \mu}{E} [(1 - \mu) \sigma_r - \mu \sigma_\theta]; \quad (5.20)$$

$$\epsilon_\theta = \frac{1 + \mu}{E} [(1 - \mu) \sigma_\theta - \mu \sigma_r]. \quad (5.21)$$

For uncompressed fuel ( $\mu = 0,5$ )  $\epsilon_r = \epsilon_\theta$ ; then

$$\epsilon_{\text{pass}} = \frac{2\sqrt{3}}{3} \epsilon'_\theta \approx 1,15 \epsilon'_\theta$$

where  $\epsilon'_\theta$  is the permissible annular deformation at the ends of the rays of the star-shaped channel in the burner.

Thus on the basis of the criterion selected it is necessary that for the given type of fuel permissible deformation on the rays of the star come to approximately 85 percent of the limit deformation measured during elongation tests (4).

#### 5.4. Calculating of a Solid Fuel Charge for Strength During Working of Rocket Engine

For the sake of simplicity of computation we carry out an analysis of stresses and deformations set up in a cylindrical single-channel burner firmly fastened to the wall of the chamber, under the influence of internal pressure evenly applied in all directions (Figure 5.16). We disregard axial acceleration and falling off of pressure over the length of the burner during its combustion.

In addition, in order to simplify we assume that the chamber and the burner are subject to the laws of ideal elasticity (the nonlinear effects provoked by plasticity are insignificant), the burner is long enough so that in accordance with the Sen-Venan [St.-Venant?] principle and effect can be disregarded, and that any transverse section perpendicular to the axis of the chamber will remain plane under the operation of stress upon the burner (longitudinal stress does not depend upon radius).

The burner is subjected to the operation of internal pressure  $p_i$ , which is equal to effective pressure within the interior channel and external effective pressure  $p_b$ , occasioned by the presence of a thin-walled chamber.

The stresses developing in the solid fuel charge can be expressed through effective pressures with the help of the Lyame [Lame?] formulas for thin-wall tubes. In the case of a plane problem, at all points of the charge radial and tangential stresses will operate (3):

$$\sigma_r = \frac{p_i r_1^2 - p_o r_2^2}{r_2^2 - r_1^2} + \frac{(p_o - p_i) r_1^2 r_2^2}{r^2 (r_2^2 - r_1^2)}; \quad (5.22)$$

$$\sigma_\theta = \frac{p_i r_1^2 - p_o r_2^2}{r_2^2 - r_1^2} - \frac{(p_o - p_i) r_1^2 r_2^2}{r^2 (r_2^2 - r_1^2)}; \quad (5.23)$$

where  $r$  is the current radius;

$p_i$  is the internal effective pressure operating on the burner;

$p_o$  is the external effective pressure operating on the burner.

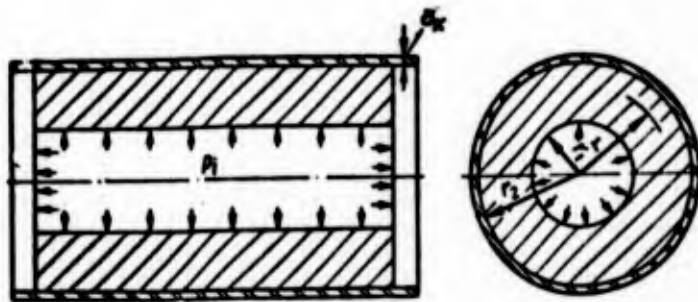


Figure 5.16. As regards question of strength calculation for a charge under influence of internal pressure.

If the charge burns, for example, upon its inward surfaces, then

$$p_i = p_{\text{cham}} - p_a;$$

where  $p_{\text{cham}}$  is the absolute pressure in the chamber,  
 $p_a$  is atmospheric pressure.

We shall note that the sum  $\sigma_r + \sigma_\theta$  for all points of the charge must be constant:

$$\sigma_r + \sigma_\theta = 2 \frac{p_i r_1^2 - p_o r_2^2}{r_2^2 - r_1^2}. \quad (5.24)$$

Introducing into the Lyame formulas the nondimensional parameters

$$m = \frac{r_1}{r_2} \quad \text{and} \quad \rho = \frac{r_1}{r},$$

we secure:

$$\sigma_r = \frac{m^2 p_i - p_a}{1 - m^2} + \frac{p^2 (p_a - p_i)}{1 - m^2}; \quad (5.25)$$

$$\sigma_\theta = \frac{m^2 p_i - p_a}{1 - m^2} - \frac{p^2 (p_a - p_i)}{1 - m^2}. \quad (5.26)$$

From analysis of formulas (5.25) and (5.26) one may conclude that in calculating a charge for strength, when the inequality  $p_i > p_a$  holds good, tangential stresses  $\sigma_\theta$  are of decisive significance; they achieve their maximum value on the internal surface of the channel of the burner with  $p_B = 0$ :

$$\sigma_{\theta_{\max}} = \frac{m^2 + p^2}{1 - m^2} p_i. \quad (5.27)$$

Inasmuch as in the scheme of computation adopted  $m < p < 1$ , radial stresses  $\sigma_r$  always manifest themselves as compressive, and tangential stresses  $\sigma_\theta$  as elongative. In practice the quantity  $m$  can vary within limits between 0 and 1, whereupon  $\sigma_\theta$  will vary from  $p^2 p_i$  to infinity. On this account, in order to avoid great elongative stresses, one should not choose an amount for the parameter  $m$  which is lower than 0.5 or 0.6, or (which is the same thing) the relative thickness of the vault of the charge, fastened to the walls of the chamber, should not exceed approximately 0.5-0.4 (1).

Assuming an ideal fastening together of the chamber and the burner one can take as being equal upon the fastening surface ( $r = r_2$ ) the tangential and axial deformations in the burner and in the chamber ( $\epsilon_{\theta r} = \epsilon_{\theta k}$ ):

$$\epsilon_\theta = \frac{1}{E} [\sigma_\theta - \mu(\sigma_r + \sigma_\theta)] = \frac{1}{E_k} [\sigma_{\theta k} - \mu_k(\sigma_{rk} + \sigma_{\theta k})]; \quad (5.28)$$

$$\epsilon_r = \frac{1}{E} [\sigma_r - \mu(\sigma_r + \sigma_\theta)] = \frac{1}{E_k} [\sigma_{rk} - \mu_k(\sigma_{rk} + \sigma_{\theta k})]. \quad (5.29)$$

where  $E$  and  $E_k$  are the modules of elasticity of the fuel and the chamber, respectively;

and  $\mu$  and  $\mu_k$  are the Poisson coefficients of the burner and the casing.

If one regards the material of the chamber as absolutely rigid with  $r = r_2$ , then equations (5.28) and (5.29) assume the form:

$$\epsilon_\theta = \frac{1}{E} [\sigma_\theta - \mu(\sigma_r + \sigma_\theta)] = 0; \quad (5.30)$$

$$\epsilon_r = \frac{1}{E} [\sigma_r - \mu(\sigma_r + \sigma_\theta)] = 0. \quad (5.31)$$

Eliminating  $\sigma_r$  from expressions (5.30) and (5.31), we secure (1):

$$\sigma_t - \mu(\sigma_r + \sigma_t) = 0. \quad (5.32)$$

The value of effective external pressure can be determined if one substitutes in equation (5.32) the values for  $\sigma_r$  and  $\sigma_t$  secured from formulas (5.26) and (5.25), under the condition that  $\rho = m$ :

$$\sigma_r = -p_0$$

$$\sigma_t = \frac{2m^2 p_t - (1 + m^2) p_0}{1 - m^2},$$

whereupon

$$p_0 = \frac{2m^2(1 - \mu)}{1 + m^2 - 2\mu} p_t. \quad (5.33)$$

Now, substituting the  $p_0$  values in the Lyame formulas one can determine the values of tangential and radial stresses as functions of the parameters  $m$ ,  $\rho$ , and  $\mu$ . With  $m = 0$  maximum tangential stress,  $(\sigma_t)_{\max}$ , becomes equal to effective pressure in the chamber; such an amount is inadmissible for elastic and soft fuels used in charges fastened to the walls of the chamber. The Poisson coefficient,  $\mu$ , exercises marked influence upon the amount of stresses in the burner. If the fuel constitutes an almost incompressible resin-like material ( $\mu = 0,5$ ), then at elevated temperatures tangential deformations become insignificant. But if the fuel is sensitive to deformations, it is desirable to make the relative rigidities of the chamber and of the burner itself such that the fuel shall not deform. In this case we proceed to the scheme of the rocket engine having a loosely inserted charge, where passage of gases to the outward surface of the burner is ensured and the solid fuel burner finds itself amid circumstances of evenly applied hydrostatic pressure ( $\sigma_r = \sigma_t = p_{\text{cham}}$ ).

##### 5.5. Analysis of Concentrations of Stresses in Solid Fuel Charge Having Compound Perforations of the Internal Channel of the Burner

Up to this point in our computations we have examined charges of simple configuration in the form of thin-walled cylinders. In reality burners of solid fuel have considerably more complicated shapes, for example a burner having a star-shaped channel or a burner profiled internally (Figure 5.17). In burners having a compound geometrical shape, around the angles stresses concentrate which reduce the strength of the charge under the action of force or temperature factors upon the burner. Real stresses at the points of the star in the channel of a burner exceed by several times the stresses developing in a simple thin-walled cylinder.

Special experiments (1, 3) upon thin-walled cylinders having symmetrical interior cut-outs of various depths, breadths, and shapes have made it possible, applying the method of photoelasticity, to study the influence of the geometrical shape of the interior channel of the burner upon the concentration in the charge of stresses occasioned by the pressure of gases in the combustion chamber.

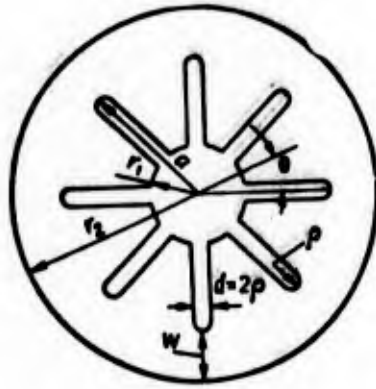


Figure 5.17. Typical model of charge having profiles (slots).

As an index of concentration of stresses the coefficient of concentration of stresses  $K_i$  is adopted (3), which may be defined as

$$K_i = \frac{\sigma_\theta - \sigma_r}{\sigma_{\theta_0} - \sigma_{r_0}}, \quad (5.34)$$

where  $\sigma_\theta$  and  $\sigma_r$  are the actual amounts of tangential and radial stresses;  $\sigma_{\theta_0}$  and  $\sigma_{r_0}$  are the stresses which would develop in an equivalent charge in the shape of a thick-walled cylinder.

In Figure 5.18 we present computational graphs of coefficients of concentration of stresses from internal pressure in investigating burners having internal slots. It is apparent from the graph that one can reduce the concentration of stresses in the burner with profiles by reducing the thickness of the vault and increasing the radii of curvature in the profiles.

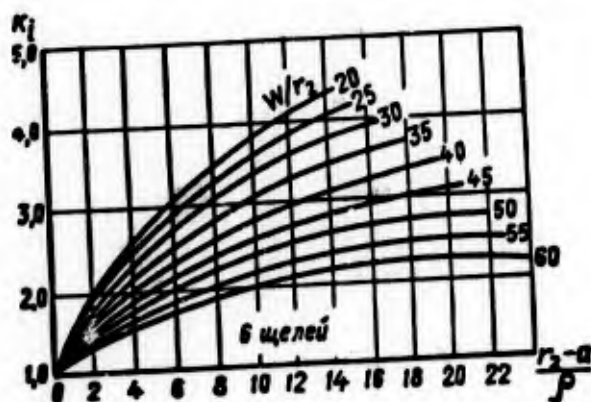


Figure 5.18. Dependence of coefficient of concentration of stresses upon geometrical dimensions of burner.

Large experiments have been carried out (1, 3) upon photoelastic models in order to investigate the field of stresses in charges having a star-shaped internal channel of various configurations, stressed with pressure on the external surface. Making use of the conclusions of the method of photoelasticity, the coefficient of concentration of stresses  $K_i$  can be defined experimentally as the relationship of the actual number of bands at the point examined to the number which would exist in an equivalent thick-walled cylinder with the same falling off in pressures ( $p_{ext} = p_{int}$ ). In Figure 5.19 we show a typical photoelastic model of a charge. The isochromatic bands are secured as a result of imitation of interior pressure. Data from experiments show that one can also reduce the concentration of stresses in the fuel burner, taking into account the recommendations made earlier, if one increases the relative thickness of the vault and the number of rays of the star with values of  $W$  and of  $\alpha$  given, having increased the angle of the aperture of a ray of the star and the breadth of the slot of the ray of the star.



Figure 5.19. Typical aspect of photoelastic model of solid fuel charge having star-shaped channel.

In precise strength computations of solid fuel charges one must take into account not only the thermic and mechanical stresses referred to above, but also the phenomenon of relaxation, and likewise stress allowing for the viscous-elastic properties of the fuel.

#### 5.6. Strength Calculation of Rocket Charge Allowing for Elastic-Plastic Deformations and Rheological Properties of Solid Fuel

For the case of thick-walled cylindrical burners, one can secure from the general theory of elasticity analytical expressions and relatively simple solutions. The strength of charges having a compound shape of channel can be evaluated with the help of data relative to the strength of a simple charge, taking the coefficient of concentration of stresses into account.

But for precise computation of solid fuel charges for strength it is not possible to apply the usual methods of elastic analysis, because a solid fuel is characterized by a potentially nonlinear elastic-plasticity, and plastic elastic deformations thereof are time (rheological) processes.

In a solid fuel two characteristic deformations,  $\epsilon$  and  $\tau$ , take place. In this connection deformation  $\epsilon$  relates to elongation or compression

$$\epsilon = E\epsilon \tag{5.35}$$

where E is the Young module.

Deformation  $\tau$  relates to shear or torsion, and in unidimensional form it is written as follows:

$$\tau = G\gamma \tag{5.36'}$$

where G is the module of shear.

It has been established in special experiments (3) that the distribution of stresses in an isotropic incompressible elastic-plastic medium coincides with the distribution of stresses in an elastic medium, if the limit conditions are applied only one the stresses. Making use of a mathematical apparatus of operational calculus, a method for figuring out elastic-plastic stresses and dislocations was worked out for many problems (3).

Without going into detailed analysis we may remark that for figuring out stresses and deformations direct methods of investigating a broad class of elastic-plastic problems are applicable if what is involved is a fuel characterized by approximately linear plasticity.

In order to set up equations associating the stresses and deformations in solid fuels one must apply the classical method of presenting the material in the form of mechanical models consisting of elementary springs and dampers. The model is composed of springs and dampers in such fashion that as a whole it reproduces, under loads, the behavior of a solid fuel.

The simplest model is the linear spring (the Guk [Hook?] model), which affords a direct proportionality between stress and deformation (Figure 5.20). The constant of the spring is an analog of the Young model. Another simple model is the unit damper (the Newton model) (Figure 5.21), which is characterized by proportionality between stress and speed of deformation. A natural generalization of these very simple models would be a model consisting of a spring and a damper. If one joins the spring and the damper in parallel fashion (Figure 5.22), one will get a model known as the Voit [Voigt?] model (stresses are

superimposed). With sequential connection of the spring and the model we secure the Maxwell model (deformations are superimposed) (Figure 5.23). In many problems one may expect that the Voigt and Maxwell models will give a good approximation to the real reaction of a fuel with small deformations over a limited interval of time.

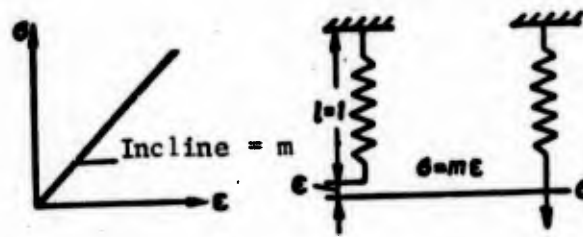


Figure 5.20. Single-element Guk Hook? model.

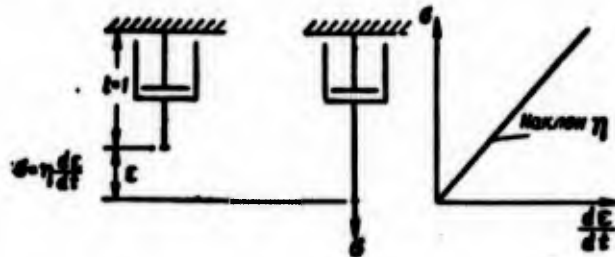


Figure 5.21. Single-element Newton model.

With the help of the Voigt model (Figure 5.22), in the investigation of creep under constant load the following equation was secured (3, 4, 6):

$$\epsilon(t) = \frac{\sigma_0}{m} \left[ 1 - e^{-\frac{t}{\tau}} \right] \text{ for } 0 < t < t_0 \quad (5.36)$$

where  $\sigma_0$  is the stress corresponding to constant load;  
t is time;

$$\tau = \frac{\eta}{m}$$

$\eta$  and  $m$  are the constants of the damper and the spring.

With very high values of time  $\epsilon(t)$  static deformation is approached. Such behavior of a material is called creep (retarded deformation).

The process of relaxation (weakening of stresses or restoration of initial form after cutting off of operation of load), according to the same model (Figure 5.22), is described by equations of the form

$$\sigma = 0; \epsilon(t) = \epsilon_1 e^{-\frac{t-t_1}{\tau}} \text{ for } t > t_1, \quad (5.37)$$

where  $\epsilon_1$  is deformation at moment of removal of load;  
 $t_1$  is time at moment of removal of load.

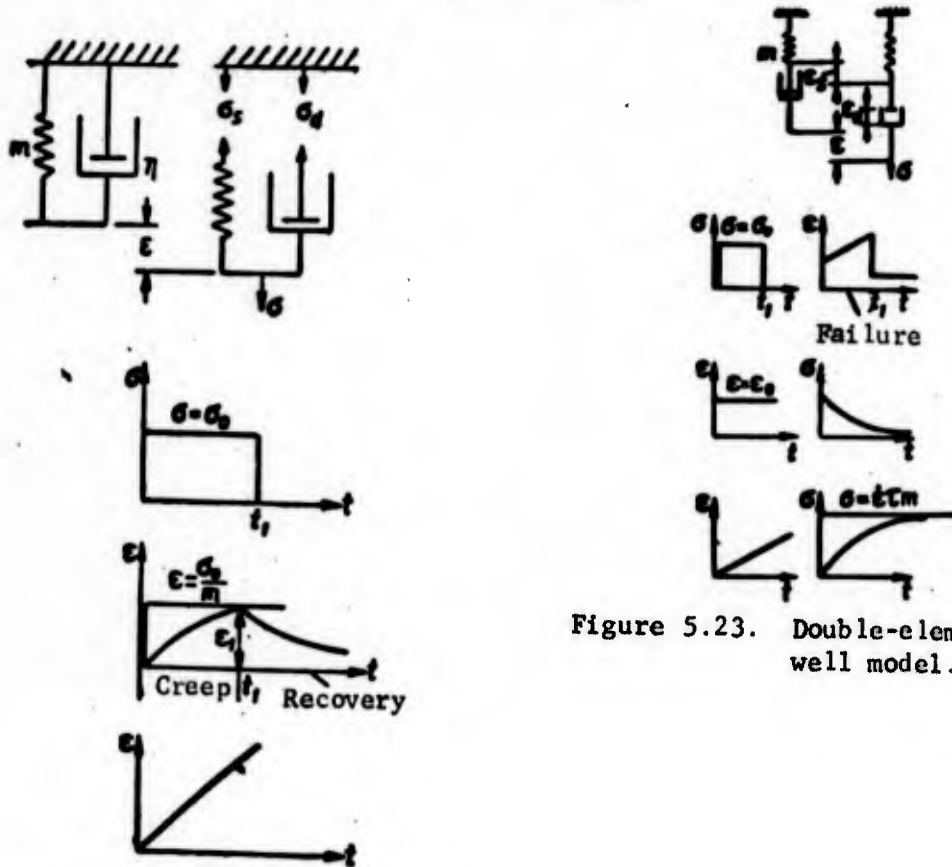


Figure 5.22. Double-element Voigt model.

But if on the Voigt model we model through the processes taking place with constant speed of deformation  $\dot{\epsilon}$ , these processes can be described by the following equations:

$$\begin{aligned} \dot{\epsilon} &= \dot{\epsilon}; \\ \sigma &= \dot{\epsilon} m \left( t + \frac{\eta}{m} \right), \end{aligned} \quad (5.38)$$

where  $\dot{\epsilon} = \frac{d\epsilon}{dt}$  is the speed of deformation.

With the help of the Maxwell model it is also possible to model creep under constant load.

In this case the processes are described by the following equations:

$$\sigma = \sigma_0; \quad \epsilon(t) = \frac{\sigma_0}{m} \left( 1 + \frac{t}{\tau} \right) \quad \text{for } 0 < t < t_0 \quad (5.39)$$

and after removal of load

$$\sigma = 0; \quad \epsilon(t) = \frac{\sigma_0}{m} \frac{t_0}{\tau} \quad \text{for } t > t_0 \quad (5.40)$$

The processes taking place with constant speed of deformation can be modeled according to the same scheme (Figure 5.23) and can be described by equations of the form

$$\begin{aligned} \sigma &= \sigma_0; \\ \epsilon &= \sigma_0 m \left( 1 - e^{-\frac{t}{\tau}} \right) \end{aligned} \quad (5.41)$$

The processes of relaxation on the Maxwell model (Figure 5.23) are described by the equation ( $\dot{\epsilon} = \dot{\epsilon}_0$ ):

$$\sigma(t) = \sigma_0 m e^{-\frac{t}{\tau}} \quad \text{for } t > 0.$$

If necessary, one can model with three- and four-element models (Figure 5.24). But practically speaking, calculations with such models present great difficulties and can be carried out only for burners having a very simple geometrical shape. As a rule, in calculations models are used which constitute a maximum of two elements.

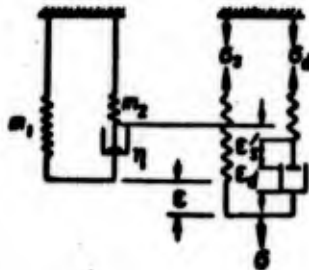


Figure 5.24. Three-element mechanical model representing reaction of material under shear.

Let us determine the elastic-plastic deformations under the operation of pressure upon an infinitely long tubular cylindrical burner enclosed in an elastic envelope.

The solution in the elastic field of deformations for an incompressible fuel ( $\mu=0,5$ ) and in the presence of a thin envelope under the action of internal pressure in projections of stresses has the form (3):

$$\begin{aligned} \sigma_r &= - \frac{\left(\frac{r_2}{r}\right)^2 - 1 + \frac{1/2}{(1-\mu_k^2)} \cdot \frac{\delta_k \cdot E_k}{r_2 E}}{\left(\frac{r_2}{r_1}\right)^2 - 1 + \frac{1/2}{(1-\mu_k^2)} \cdot \frac{\delta_k E_k}{r_2 E}} \cdot p_i \\ \sigma_\theta &= \frac{\left(\frac{r_2}{r}\right)^2 + 1 - \frac{1/2}{(1-\mu_k^2)} \cdot \frac{\delta_k E_k}{r_2 E}}{\left(\frac{r_2}{r_1}\right)^2 - 1 + \frac{1/2}{(1-\mu_k^2)} \cdot \frac{\delta_k E_k}{r_2 E}} \cdot p_i \\ \sigma_z &= \frac{1 - \frac{1/2}{(1-\mu_k^2)} \cdot \frac{\delta_k \cdot E_k}{r_2 \cdot E}}{\left(\frac{r_2}{r_1}\right)^2 - 1 + \frac{3}{2(1-\mu_k^2)} \cdot \frac{\delta_k E_k}{r_2 E}} p_i \end{aligned} \quad (5.42)$$

where  $E$  and  $\mu$  are the Young module and the Poisson coefficient for the fuel;

$E_k$  and  $\mu_k$  are the Young module and the Poisson coefficient for the material of the chamber;

$\delta_k$  is the thickness of the chamber wall.

We represent an isotropic elastic-plastic material with the help of the Voigt model. Then the lag in shear with time can be written as follows:

$$\tau_{ij} = \eta \left( \frac{d\gamma_{ij}}{dt} \right) + G \gamma_{ij} \quad (i \neq j) \quad (5.43)$$

Applying the Laplace transformation to equation (5.43) for initial conditions, we secure

$$\bar{\tau}_{ij} = (\eta p + G) \bar{\gamma}_{ij} \quad (5.44)$$

From the theory of elasticity for incompressible materials it follows that

$$\tau_{ij} = G \gamma_{ij} = \frac{E}{3} \gamma_{ij} \quad (5.45)$$

From equations (5.44) and (5.45) we secure the value of the equivalent module of elasticity

$$E(p) \rightarrow 3(\eta p + G) \quad (5.46')$$

Substituting the module determined by the operator expression (5.46') in each of the initial equations for elastic deformation, we find the corresponding elastic-plastic deformations (3):

$$\bar{\sigma}\left(\frac{r}{r_1}\right) = - \frac{\left[\pm \left(\frac{r_2}{r}\right)^2 - 1\right] (\eta p + G) + \frac{\delta_{\kappa} E_{\kappa}}{2(1-\nu_{\kappa}^2)} r_2}{\left[\left(\frac{r_2}{r_1}\right)^2 - 1\right] (\eta p + G) + \frac{\delta_{\kappa} E_{\kappa}}{2(1-\nu_{\kappa}^2)} r_2} \bar{p}_i(p), \quad (5.46)$$

where the upper sign corresponds to  $\sigma_r$ , and the lower sign to  $\sigma_{\theta}$ .

Assuming  $\bar{p}_i = \frac{p_i}{p}$ , the transformed equation (5.46) will assume the form

$$\bar{\sigma}\left(\frac{r}{r_1}\right) = K \frac{(p + a_0)}{p \left(p + \frac{1}{\tau}\right)}, \quad (5.47)$$

where

$$K = - \frac{\pm \left(\frac{r_2}{r}\right)^2 - 1}{\left(\frac{r_2}{r_1}\right)^2 - 1} p_i; \quad (5.48)$$

$$a_0 = \frac{\left[\pm \left(\frac{r_2}{r}\right)^2 - 1\right] G + \frac{\delta_{\kappa} E_{\kappa}}{2(1-\nu_{\kappa}^2)} r_2}{\left[\pm \left(\frac{r_2}{r}\right)^2 - 1\right] \eta}; \quad (5.49)$$

$$\frac{1}{\tau} = \frac{\left[\left(\frac{r_2}{r_1}\right)^2 - 1\right] G + \frac{\delta_{\kappa} E_{\kappa}}{2(1-\nu_{\kappa}^2)} r_2}{\left[\left(\frac{r_2}{r_1}\right)^2 - 1\right] \eta}. \quad (5.50)$$

Making the inverse Laplace transformation, we secure an expression for physical stresses allowing for the rheological properties of a solid fuel

$$\sigma\left(\frac{r}{r_1}\right) = K \tau \left[ a_0 - \left(a_0 - \frac{1}{\tau}\right) e^{-\frac{t}{\tau}} \right], \quad (5.51)$$

where  $\tau$  is time;

$\eta$  and  $\underline{m}$  are coefficients of the model, determined experimentally.

For the case where  $r = r_2$ , pressure between the burner and the envelope is damped down with constant time  $\tau$ , and stresses can be determined according to the formula

$$\frac{\sigma_r(r_2)}{p_i} = - \frac{1 - e^{-\frac{t}{\tau}}}{1 + 2(1 - \mu_k^2) \left( \frac{r_2^2}{r_1^2} - 1 \right) \left( \frac{r_2 E}{3b_k E_k} \right)} \quad (5.52)$$

Thus stresses in a charge depend on the elastic-plastic constants  $E$  and  $G$ , which form part of formula (5.52) and of the expression for time  $\tau$ . At the same time, the influence of speed ( $\eta$ ) is allowed for only in expression (5.50), written for time of relaxation  $\tau$ .

It is also appropriate to note that with a rigid envelope  $E_k \rightarrow \infty$ ,  $\tau^{-1} \rightarrow \infty$ , and  $\sigma_r(r_2) \rightarrow -p_i$ .

Finally, calculation of a stressed-deformed charge with allowance for the rheological properties of a solid fuel is carried out according to the formulas (3):

$$\frac{\sigma_\theta(r_1)}{p_i} = \frac{\left( \frac{r_2^2}{r_1^2} + 1 \right) E - \frac{3b_k E_k}{2(1 - \mu_k^2) r_2} \left( 1 - e^{-\frac{t}{\tau}} \right) + \frac{\frac{r_2^2}{r_1^2} + 1}{\frac{r_2^2}{r_1^2} - 1} e^{-\frac{t}{\tau}}}{\left( \frac{r_2^2}{r_1^2} - 1 \right) + \frac{3b_k E_k}{2(1 - \mu_k^2) r_2} E} \quad (5.53)$$

$$\frac{\sigma_r(r_1)}{p_i} = 1;$$

$$\frac{E \cdot \dot{\sigma}_\theta(r_1)}{p_i} = \frac{3 \frac{r_2^2}{r_1^2}}{\left( \frac{r_2^2}{r_1^2} - 1 \right) + \frac{3b_k E_k}{2(1 - \mu_k^2) r_2} E} \left[ 1 + \frac{\frac{3b_k E_k}{2(1 - \mu_k^2) E r_2}}{\frac{r_2^2}{r_1^2} - 1} e^{-\frac{t}{\tau}} \right]$$

Differentiating, we secure the speed of deformation

$$\dot{\sigma}_r = \frac{d}{dt} \sigma_\theta(r_1),$$

whereupon

$$\frac{E}{p_i} \dot{\sigma}_\theta(r_1) = - \frac{3 \frac{r_2^2}{r_1^2} \frac{b_k E_k}{2(1 - \mu_k^2)} r_2 \cdot e^{-\frac{t}{\tau}}}{\left( \frac{r_2^2}{r_1^2} - 1 \right) \cdot \tau} \quad (5.53')$$

Making use of the Smith curve (Figure 5.13) and the relationships secured, we can determine the reserve of strength of a solid fuel charge.

5.7. Taking Temperature Stresses Into Account in Calculating a Solid Fuel Charge for Strength

In the majority of cases rocket engines on solid fuel are subject to the action of the temperature of the surrounding environment during prolonged storage. The action of temperature stresses is more strongly marked upon charges fastened to the envelope than upon charges loosely placed in the combustion chamber.

In order to study thermic stresses we shall make the following assumptions:

1. In its initial state the engine with the fuel charge cast into it is free of thermic stresses and deformations.
2. Distribution of temperature is symmetrical relative to the axis and does not depend upon the axial coordinate  $z$ .
3. The module of elasticity, the coefficient of linear expansion  $\alpha$ , and the Poisson coefficient do not depend upon temperature.
4. Upon examination the charge is assumed to be pretty long, so that in accordance with the St. Venant principle one may disregard end effects.

The general expressions for radial, tangential, and axial stresses in a charge of solid fuel firmly fastened to a thin elastic envelope may be written as follows (3):

$$\sigma_r = -p' \frac{1 - \left(\frac{r_1}{r}\right)^2}{1 - \left(\frac{r_1}{r_2}\right)^2}; \quad (5.54)$$

$$\sigma_\theta = -p' \frac{1 + \left(\frac{r_1}{r}\right)^2}{1 - \left(\frac{r_1}{r_2}\right)^2}; \quad (5.55)$$

$$\sigma_z = -p' \frac{1}{1 - \left(\frac{r_1}{r_2}\right)^2}. \quad (5.56)$$

where

$$p' = \frac{(\alpha - \alpha_2) E \cdot T^0}{\frac{3r_1^2}{2(r_2^2 - r_1^2)} + (1 - \nu_2^2) \frac{r_2 E}{4r_2 E_2}}. \quad (5.57)$$

Examining the picture of elastic-plastic shear with the help of the Maxwell model and assuming a linear law of temperature change for the charge over time ( $T^0 = k't$ ), we can secure final computation formulas for stresses in the charge under the operation of temperature stresses and taking into account the rheological properties of a solid fuel:

$$\sigma_r(t) = -k \frac{\left(1 - \frac{r_1^2}{r^2}\right) \left(1 - e^{-\frac{t}{\tau}}\right)}{\alpha \left(1 - \frac{r_1^2}{r_2^2}\right)}; \quad (5.58)$$

$$\sigma_\theta(t) = -\frac{k \left(1 + \frac{r_1^2}{r^2}\right) \left(1 - e^{-\frac{t}{\tau}}\right)}{\alpha \left(1 - \frac{r_1^2}{r_2^2}\right)}; \quad (5.59)$$

$$\sigma_z(t) = -\frac{k}{\alpha \left(1 - \frac{r_1^2}{r_2^2}\right)} \left(1 - e^{-\frac{t}{\tau}}\right), \quad (5.60')$$

where

$$k = \frac{(\sigma - \sigma_w) G \cdot h}{\frac{r_1^2}{2(r_2^2 - r_1^2)} + (1 - \nu_w) \frac{r_2 G}{4\alpha E_s}}. \quad (5.60)$$

These equations show the exponential character of the rise in stresses in all directions, something which corresponds with the proposed Maxwell mechanical model, which absorbs the energy of deformation.

#### 5.8. Calculating Elastic-Plastic Deformations in a Solid Fuel Charge Under the Effect of Weight

The tangents of shear stress from the actual weight of a cylindrical single-channel burner, set up in vertical position and supported by an elastic envelope, are determined (disregarding margin effects) by the equation

$$\tau_{rz}(r) = -\frac{M}{2} \left( r - \frac{r_1^2}{r} \right). \quad (5.61)$$

To these stresses there corresponds a coincident dislocation (dislocation at the point where the burner is fastened to the envelope is equal to zero), expressed by the formula

$$W_r = -\frac{\rho g}{2G} \left( r_2^2 \ln \frac{r_2}{r} - \frac{r_2^2 - r^2}{2} \right). \quad (5.62)$$

Let us present the characteristics of the material by means of a mechanical three-element elastic-plastic model (Figure 5.24). Assuming that when the burner is set up in vertical position weight rises in a sharp jump, and considering that  $\mu = 0,5$ , the final expression for determination of axial slippage assumes the following form:

$$W(t) = -\frac{\rho g r_1^2}{4m_1} \left\{ 2 \ln \frac{r_2}{r} - \left( \frac{r_2}{r_1} \right)^2 \left[ 1 - \left( \frac{r}{r_2} \right)^2 \right] \right\} \times \quad (5.63)$$

$$\times \frac{1 + \left( \frac{m_2}{m_1} \right) - \left( \frac{m_2}{m_1} \right) e^{-\frac{t}{\tau_1}}}{1 + \left( \frac{m_2}{m_1} \right)},$$

where  $\tau_1 = \eta \left( \frac{1}{m_1} + \frac{1}{m_2} \right)$  is the constant of time for constant stress;

$\eta$ ,  $m_1$  and  $m_2$  are the coefficients of the damper and the two springs.

With large values for  $t$  deformation approaches the elastic and depends upon the constant shear module of the material ( $m_1$  or  $m_2$ ).

#### BIBLIOGRAPHY

1. Barrere, M., Jomotte, A., et al., Rocket Engines, Oborongiz Publishing House, 1962.
2. Bartley, Ch. E., Mills, M. M., Jet Engines, Voenizdat Publishing House, 1962.
3. Williams, "The Strain Analysis of Solid Propellant Rocket Grains," IAS Paper, No 59-110, 1959.
4. Williams, M. L., "Influence of Mechanical Properties Upon Design of Solid Fuel Engines," Investigation of Solid-Fuel Rocket Engines, Publishing House for Foreign Literature, 1963.
5. Wimpres, R. N., Internal Ballistic of Solid-Fuel Rockets, McGraw-Hill Book Company, New York, 1950.
6. Friedenthal, A., Henry, L., "The Poisson Coefficient in Fuels Having Linear Viscous-Elasticity," Investigation of Solid-Fuel Rocket Engines, Publishing House for Foreign Literature, 1963.
7. Zachringer, A. I., Solid Propellants Rockets, ARG, Wyandotte, Michigan, 1958.

## CHAPTER VI. EXECUTANT ORGANS FOR GUIDANCE OF A ROCKET HAVING SOLID-FUEL ENGINE

The executant organs of guidance of a rocket are intended to regulate the thrust vector of a solid-fuel rocket engine in flight as regards amount and direction.

### 6.1. Regulation of Thrust in Amount

Studies (1, 6) describe mechanical means for prelaunch adjustment of an engine to receive a constant amount of thrust when solid fuel charges having various initial temperatures are used. In flight the system for regulating the amount of thrust of a solid-fuel rocket engine must:

- change thrust over time in accordance with a set program;
- maintain the necessary amount of thrust independently of random factors (for example, chance alterations in speed of fuel combustion and surface of charge, erosion of cone, and the like) provoking alteration therein (3);
- cut off working of engine upon achievement of velocity assigned for rocket.

Regulation of the amount of thrust of a solid-fuel rocket engine may be achieved through appropriate selection of the characteristics of a solid fuel and the geometry of a charge.

The simplest principle for alteration of thrust over time is the two-stage principle, corresponding to the launch and route regimes of a solid-fuel rocket engine.

In Figure 6.1a we show transverse sections of two possible variants of the solid-fuel rocket engine, in which a two-stage principle of thrust change is put into effect. In the launch regime the engine develops high thrust in relatively brief time and communicates to the rocket the velocity necessary for flight and maneuver (4). In the route regime, for which

long time of engine work at low thrust is characteristic, the rocket receives supplementary velocity or retains the velocity achieved at the start of the launch sector (Figure 6.1b).

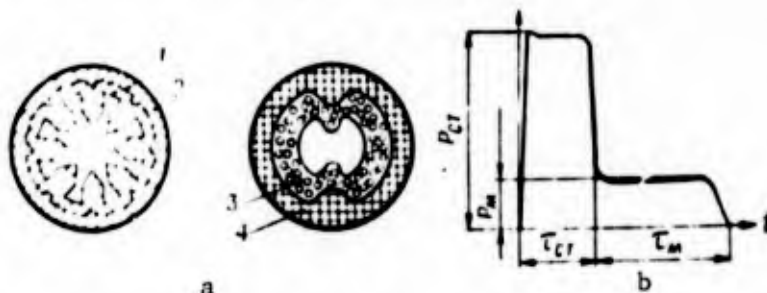


Figure 6.1. Various shapes of solid fuel charges providing two-stage principle of thrust change: a -- transverse sections of two possible variants of solid-fuel rocket engine; b -- diagram of two-stage principle of thrust change: 1 -- combustion surface for launch stage; 2 -- combustion surface for route stage; 3 -- rapid-burning fuel for launch stage; 4 -- slow-burning fuel for route stage.

Uninterrupted regulation of amount of thrust of a solid-fuel rocket engine in flight is a more complicated design problem. For this purpose schemes having self-regulating cones may be used. An acceleration integrator, which sends signals to the executant organs in accordance with the amount of metered accelerations, can serve as a monitor for the regulating system; the organs change the magnitude of the critical cross-section of the cone (5).

One of the well-known methods for regulating thrust as regards amount in a solid-fuel rocket engine is the use of a cone having a contoured spindle (Figure 6.2). In the combustion chamber there is placed at the critical cross-section of the engine cone a spindle (a choke) which can move along the longitudinal axis of the engine by means of a hydraulic drive. As the spindle changes position it changes the area of the critical section of the cone depending upon pressure in the chamber. In order to cut off the engine the spindle is drawn into the chamber to the maximum extent. In this case the area of critical section of the cone is considerably augmented, the pressure falls off sharply, and the engine stops working. During the carrying out of experimental investigations a solid fuel rocket engine was turned on six times at intervals of 10 minutes and each time it worked for 3-4 seconds (6). By means of this method of regulation it is only possible to lower the amount of spread of thrust. In addition, regulation of thrust based upon alteration only of the area of critical cross-section of the cone alone becomes ineffective (4) when fuels having  $v \rightarrow 0$  are used. In all cases the cone, the contoured spindle, and other elements of the regulating mechanism must be made of heat-resistant materials with the use of heat insulants. In some cases constant cooling of the regulating apparatus is required.

Among new regulation methods we have: 1) regulation of thrust by letting gas pass through or by leading it aside from the cone block; 2) reaction on the process of combustion of solid fuel by sound vibrations generated in the solid-fuel rocket engine combustion chamber; 3) regulation by changing the delivery of the liquid component in combined (hybrid) engines using solid fuel (3).

Among promising methods for regulating thrust as regards amount there are the nonmechanical methods of changing the area of the critical cross-section by blowing\* auxiliary gas at high velocity into the critical section of the cone (7). Such cones may be called cones with gasodynamically variable critical cross-section area (Figure 6.3). If auxiliary gas is blown into the critical section of the cone (or near it) annularly, then this flow will, as it were, move the basic flow of outward-flowing gases toward the axis and will thus reduce the area of the critical section of the cone. The blowing may take place through a narrow fissure or through a series of apertures located around the critical cross-section. Reduction of the area of critical cross-section by virtue of the blowing in of gas leads to considerable increase of pressure in the combustion chamber, of mass delivery, and of thrust.

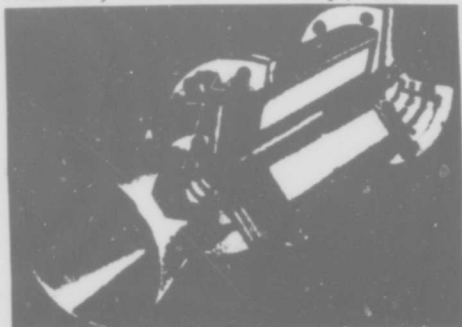


Figure 6.2. A solid-fuel rocket engine with regulated thrust.

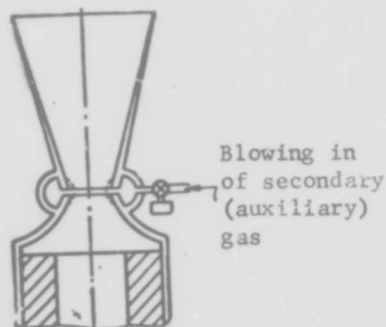


Figure 6.3. Diagram of cone with critical cross-section susceptible of regulation.

For approximate analysis of the effect of changing the area of the critical cross-section of the cone we apply the gas balance equation (1)

$$u_1 p_1^* \gamma \cdot S = \left( \frac{2}{k+1} \right)^{\frac{k+1}{2(k-1)}} \sqrt{\frac{g \cdot k}{R}} \frac{p_1 F_{kp}}{\sqrt{T_0}} \quad (6.1)$$

In study (1) it is shown that for the stage principle of velocity of combustion a relationship of the following form is correct:

$$p_k \approx (F_{kp})^{-\frac{1}{1-\gamma}} \quad (6.2)$$

\* In foreign literature the process of blowing gas into the critical section of the cone is called secondary ejection.

Then, taking into account expression (6.2), the right-hand arm of equation (6.1) can be written as follows:

$$G_{\text{con}} \approx F_{\text{sp}} \rho_x \approx (F_{\text{sp}})^{-\frac{1}{\gamma}} \quad (6.3)$$

For determination of the thrust of the engine we have the formula

$$P = \frac{G}{g} u_e + F_a (p_a - p_H) \quad (6.4)$$

In the thrust equation the quantities  $p_H$  and  $F_a$  do not depend upon change in the area of the critical cross-section of the cone, and the value of the effective speed of outward flow of gas from the cone,  $u_e$ , changes little as  $F_{kp}$  changes, this latter change being occasioned by the blowing in of auxiliary gas. For this reason in first approximation one can write equation (6.4) in the following form:

$$P \approx \left[ (F_{\text{sp}})^{-\frac{1}{\gamma}} \cdot u_e + \frac{p_a}{p_x} F_a (F_{\text{sp}})^{-\frac{1}{\gamma}} - p_H F_a \right] \quad (6.5)$$

If one designates with the index 0 the terms of the equation which relate to equilibrated flow at initial area of critical section of cone  $F_{kp0}$ , and leaves the index off those terms which relate to equilibrated flow at altered area  $F_{kp}$ , one gets the final expression (1, 7)

$$\frac{P}{P_0} = \frac{G_{p_x} u_e \left( \frac{F_{\text{sp}}}{F_{\text{sp}_0}} \right)^{-\frac{1}{\gamma}} + \frac{p_a}{p_x} F_a \rho_x \left( \frac{F_{\text{sp}}}{F_{\text{sp}_0}} \right)^{-\frac{1}{\gamma}} - p_H F_a}{G_{\text{con}} u_e + \frac{p_a}{p_x} \cdot p_x F_a - p_H F_a} \quad (6.6)$$

Upon blowing of gas into the cone with reduction of critical section, when the index of degree in the combustion principle,  $\nu$ , is less than 1 the pressure in the rocket chamber increases (6.2). In correspondence with this, the amount of mass discharge per second rises, which is confirmed by equation (6.3). The results of theoretical analysis are found to be in agreement with experimental data secured in study (7). In a cone the degree of expansion of which was made equal to  $\frac{p_x}{p_a} = 15$ ,

blowing in of air in order to regulate thrust as regards quantity was carried out on an experimental rocket engine. In order to supply auxiliary air at low temperature in the critical section of the cone an annular fissure was made (Figure 6.4). The breadth of the fissure was changed with the help of gaskets. In Figure 6.5 we show the dependence of change of discharge of basic flow upon discharge of auxiliary air blown in ( $G_{p2}$ ). With increase of discharge of air blown in ( $G_{p2}$ ) the discharge of the basic flow increases considerably, and consequently the

thrust of the engine rises in accordance with equation (6.4). Of practical interest are the results of experiments showing the dependence of the discharge of the basic flow upon the pressure of the gases of the flow blown in at various breadths of fissure (Figure 6.6). With the help of this graph it is possible to determine pressure of air blown in for a given change in discharge of basic flow.

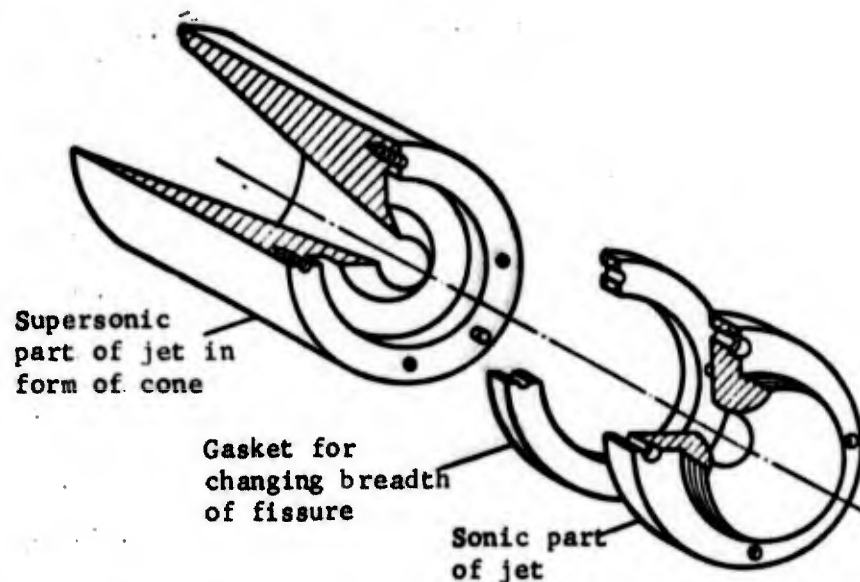


Figure 6.4. Diagram of experimental cone.

Inasmuch as pressure of secondary gas blown in cannot exceed the pressure of the basic flow, the actual combustion chamber of a solid-fuel rocket engine might serve as an auxiliary source of feed. But use of gas from the combustion chamber for secondary blowing in of gas would, as a consequence of its high temperature, complicate the cooling of the cone at its critical cross-section. But the use of cold gas, kept in a reservoir, for the secondary injection will cool the cone.

## 6.2. Interception of Thrust

Interception of thrust, as one of the forms of regulating thrust, is being more and more used in the design of ballistic and space rockets, and also in other jet flight apparatus, the flight trajectories of which must be exactly adjusted.

In order to guide exactly the range of flight of a ballistic rocket it is necessary to regulate the time duration of the operation of the solid-fuel rocket engine's thrust. As an interception (cut-off) monitor of the thrust of an engine at the requisite moment one can use a hydrosopic acceleration integrator.

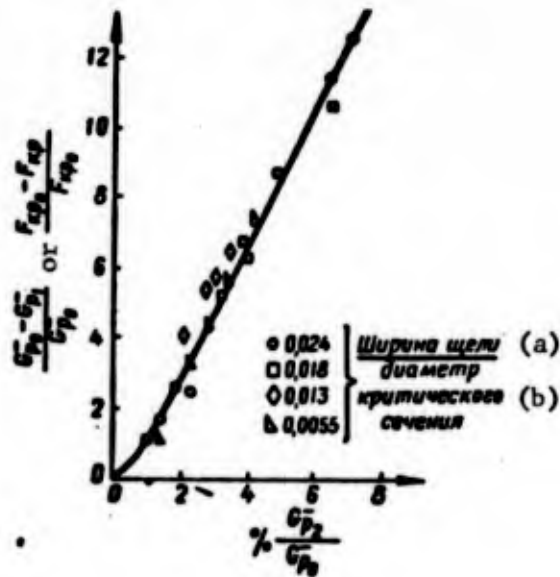


Figure 6.5. Change of discharge of basic flow in relation to discharge of auxiliary gas blown in:  $G_{p2}$  -- discharge of gas blown in;  $G_{p0}$  -- discharge of basic flow. a -- Breadth of fissure; b -- Diameter of critical cross-section.

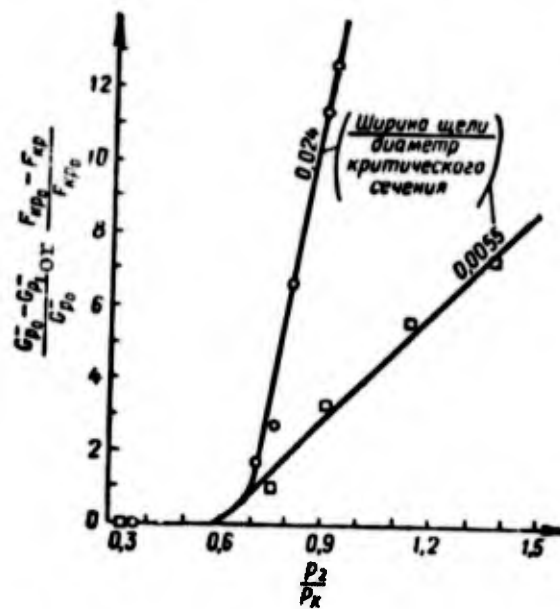


Figure 6.6.

Let us examine some design systems for controlling the range of a rocket's flight. In Figure 6.7 we represent a rocket bundle in the middle of which the rocket's warhead is located. When an assigned speed is reached the working engines separate from the warhead and, increasing their velocity in consequence of reduction of load, move away from the warhead of the rocket, which continues to move along the program trajectory (8). The time of operation of thrust in a solid-fuel rocket engine can also be regulated either by creating a counterthrust, or by cutting off the combustion of the charge completely. In Figure 6.8 we show a design diagram for cutting off thrust through extinction of the flame and complete cessation of the combustion of the charge (9). Experiments carried out with solid-fuel rocket engines the charges of which weighed about one ton have shown that to extinguish the flame of combustion of the charge in question about 11.0 liters of water were required (20). For complete assurance of thrust cut-off, at the moment of cut-off supplementary apertures in the forward part of the chamber open, as a result of which pressure in the rocket chamber falls.

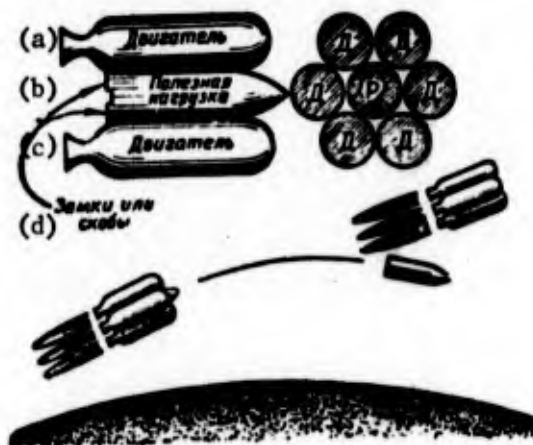


Figure 6.7. Diagram of control of range of flight of rocket. a -- Engine; b -- Useful load; c -- Engine; d -- Locks or clamps.

The most widespread method of cutting off thrust is reversal of thrust (creation of counterthrust). In the engine of the second stage of the "Polaris" rocket cut-off of thrust occurs as a result of the opening of four reverse cones which are turned forward. The falling off of pressure in the engine is combined with equilibration of thrust by the counterthrust of the supplementary cones (Figure 6.9). The operation of thrust is cut short in 50 milliseconds, which makes it possible to control the final velocity of the rocket with a precision of 10 meters per second (3). More severe requirements are imposed for the thrust cut-off system in the monoblock "Bead or Bid Package No 6" [??] solid-fuel rocket engine. Fall of thrust by 50 percent in a given experimental engine must occur within 5 milliseconds after the system has been turned on (11).

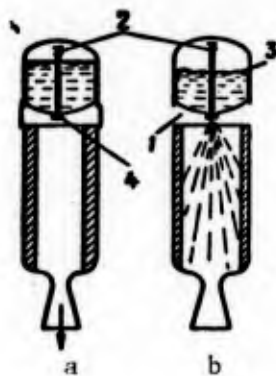


Figure 6.8. Design diagram of thrust cut-off: a -- Engine before thrust cut-off; b -- Engine at moment of thrust cut-off; 1 -- aperture for creation of counterthrust; 2 -- return channel; 3 -- rubber sack; 4 -- stopper with breakable diaphragm.

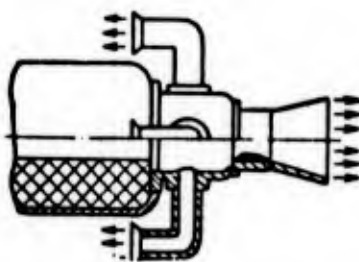


Figure 6.9. Reverse jets for cutting off thrust.

The time of the system's operation (Figure 6.10) is characterized by an amount of pressure gradient  $dp/dt$ , directly associated with the assigned principle of opening apertures in order to reverse thrust. From the equation for the balance of matter in a solid-fuel rocket engine during work (12) an expression has been secured which characterizes the dependence of the area of opening of the apertures for reversing thrust upon time:

$$t - t_{\text{pes}} = \frac{V_{\text{своб.}}}{f \cdot s (F_{\text{сп}} + F_{\text{pes}}) (1 - \nu)} \ln \frac{1 - \left[ \frac{F_{\text{сп}}}{F_{\text{сп}} + F_{\text{pes}}} \right]}{\left( \frac{p}{p_{\text{pes}}} \right)^{1-\nu} - \left[ \frac{F_{\text{сп}}}{F_{\text{сп}} + F_{\text{pes}}} \right]}, \quad (6.7)$$

where  $t_{\text{rev}}$  is the time of opening the apertures for reversing thrust;

$V_{\text{free}}$  is the free volume of the chamber, equal to the initial free volume plus the volume becoming free through the part of the fuel consumed, at the moment when reversing of thrust commences;

$f = RT_0$  is the power of the solid fuel;

$s$  is the coefficient of discharge.

From equation (6.7) one can secure a graphic dependency of change in pressure in the chamber upon time after commencement of reversing of thrust for various values of the area of the apertures opened (Figure 6.11). In study (12) there is adduced an example of the figuring out of the principle of opening apertures for reversing thrust by the method explained. To begin with, for an engine having given parameters an experimental dependence of change in pressure in the chamber upon time after the cut-off signal is obtained. In accordance with this experimentally determined dependence it is calculated that the effective opening of the reverse thrust apertures is achieved approximately 45 milliseconds after the signal, and complete opening after 160 milliseconds (12).

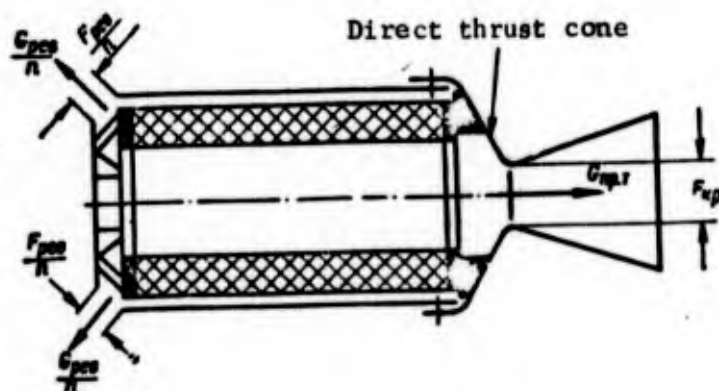


Figure 6.10. Regarding cut-off of thrust in a solid-fuel rocket engine:  $F_{rev}$  -- area of all opened critical apertures for reversing thrust;  $n$  -- number of apertures.

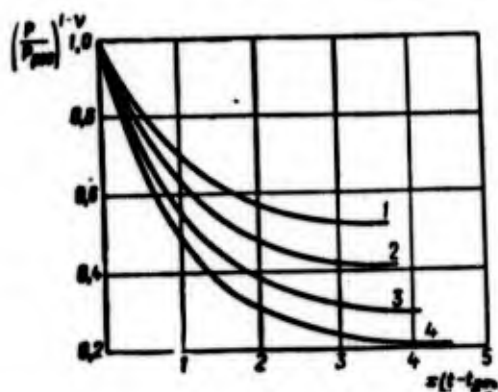


Figure 6.11. Calculated dependence of pressure in chamber upon time after commencement of gas flow through thrust reversal apertures:

$$1 - \frac{F_{rev}}{F_{rev} + F_{dir}} = 0.5; \quad 2 - \frac{F_{rev}}{F_{rev} + F_{dir}} = 0.4$$

$$3 - \frac{F_{rev}}{F_{rev} + F_{dir}} = 0.3; \quad 4 - \frac{F_{rev}}{F_{rev} + F_{dir}} = 0.2$$

$p$  -- pressure in chamber in process of reversing thrust;  $p_{rev} = p_k$  -- pressure in chamber at moment of opening of thrust reversal apertures.

Thrust of a solid-fuel rocket engine can be reduced to zero by breaking off combustion of the engine's charge, which is achieved by lowering pressure in the engine. Rapid lowering of pressure in the combustion chamber can be secured by opening an outlet aperture in the chamber -- for example, by separating the rearward cap of the engine together with the cone (Figure 6.12a) or by opening supplementary radial openings (Figure 6.12b). Tests carried out under stand conditions have shown that the arrangement for "radial cast-off" of pressure illustrated in Figure 6.12a creates at the moment of separating the cone block an increase of thrust amounting to 4-6 times (9). Despite the fact that the peak of thrust is brief in time, it is still undesirable since it diminishes the reliability of the apparatus on board. This can be avoided by using "radial cast-off" of pressure (Figure 6.12b). Such an arrangement for cutting off pressure partially balances the direct thrust created by the cone of the engine.

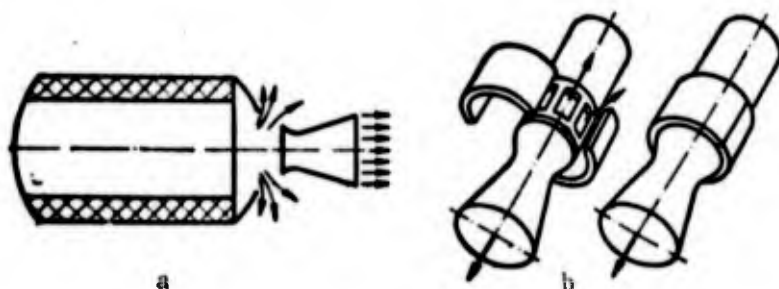


Figure 6.12. Possible methods of reducing pressure in combustion chamber:  
 a -- "axial cast-off" system for reducing pressure in engine;  
 b -- "radial cast-off" system.

The influence of rapid reduction of pressure upon combustion of solid fuel has been investigated under laboratory conditions on a device of "combustion interrupter" type (3). Tests have shown that the basic influence upon interruption of combustion with sudden fall of pressure is exercised by the speed with which pressure is reduced. Complete cutting off of the combustion process was observed only at a particular value for rapidity in fall of pressure, which in study (3) is called the critical value  $(dp/dt)_{cr}$ .

The quantity  $(dp/dt)_{cr}$  is determined by the composition of the fuel and the working pressure in the chamber of the engine.

For a mixed fuel the minimum value of rapidity of reduction of pressure in the chamber which will ensure definitive cutting off of combustion was equal to 5,200 atm/sec with an initial pressure in the chamber of 38 ata. The higher the working pressure in the engine, the greater the rapidity of reduction of pressure that is necessary for reliable extinguishment of the charge. The quantity  $(dp/dt)_{cr}$  changes in linear fashion with increase of pressure in the chamber.

### 6.3. Regulating the Vector of Thrust as Regards Direction

Modern ballistic and space rockets need uninterrupted regulation of the vector of thrust as regards direction in order to guide flight in carrying out a program.

The rocket can carry out a command maneuver relative to the axes of pitch, yaw, and bank if a force is applied to the rocket which is directed at a certain angle relative to the position of the tangent to the trajectory. The constituent of this force, directed along the normal to the trajectory, is called the control constituent. A complex of apparatus and devices for measurement of deviations of the actual movement of the rocket from the required direction of flight, the formulation of an appropriate signal, and the creation, with the help of the guidance organs, of a steering force, forms part of the system for controlling a rocket engine.

Depending on the nature of the forces taking part in control of the rocket's movement, the guidance organs can be divided into three types: aerodynamic, gasodynamic, and combined (14). The aerodynamic guidance organs (rudders, wings, stabilizers, ailerons, interceptors) create steering force only during flight under atmospheric conditions, by virtue of turning the vector of aerodynamic forces. The gasodynamic guidance organs constitute a complex of devices regulating the vector of thrust as regards direction. Combined guidance organs for creating steering force make use of aerodynamic forces and thrust.

Among the basic executant guidance organs of a solid-fuel rocket one may mention: gas rudders, obliquely cut cones, annular gas rudders, deflectors, rotating cones, turning engines, and apparatus for gasodynamic guidance of the vector of thrust by means of secondary injection of gas or injection of liquids in the supersonic part of the cone.

Gas rudders. As far back as the start of the 20th century the father of astronautics K. E. Tsiolkovskiy anticipated the possibility of steering a rocket by means of rudders located in the stream of outward-flowing gases. In the K. E. Tsiolkovskiy home museum at Kaluga there is a diagram drawing "Turning of a Rocket by Explosion With Inclination of Rudder" (15). This diagram of K. E. Tsiolkovskiy affords a prototype of gas-jet apparatus for steering the flight of present-day rockets.

Possible layouts of finned gas-jet rudders are shown in Figure 6.13. The following operate on a gas rudder located in the flow of gases issuing from the cone of an engine:

-- frontal force

$$X_{r,p} = c_{x,r,p} \frac{\rho v^2}{2} S,$$

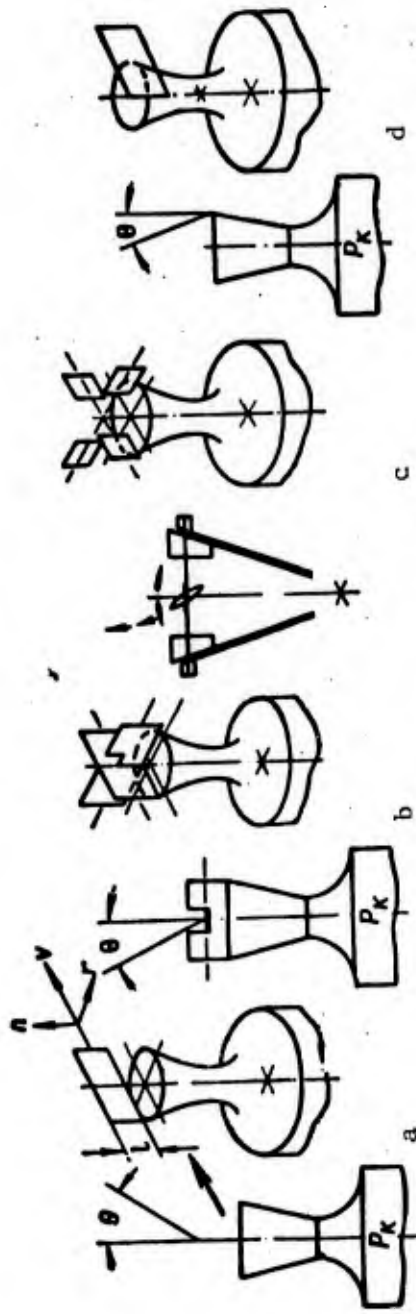


Figure 6.13. Various shapes of gas-jet rudders: a -- central gas rudder; b -- for intersecting rudders; c -- gas rudders set on the periphery of the outlet cross-section of the cone; d -- rudder set on the edge of the stream.

-- lifting force or flank thrust  $Y_{r.p.} = c_{y,r.p.} \frac{\rho v^2}{2} S;$

-- gasodynamic moment  $M_{r.p.} = c_{m,r.p.} \frac{\rho v^2}{2} S \cdot l,$

where  $v$  is the speed of flow bathing the rudder;  
 $\rho$  is the density of gas in flow;  
 $S$  is the characteristic area of rudder;  
 $l$  is the characteristic length of rudder.

The forming of steering flank force by turning one of the horizontal gas rudders to an angle  $\theta$  is graphically presented in Figure 6.14. If a force  $Y_{r.p.}$  is applied to the center of mass of a rocket, then a moment made up of the pair of forces  $Y_{r.p.}$  and  $Y'_{r.p.}$  will turn the rocket around the center of mass (CM) to a certain angle of attack,  $\alpha$ . This will lead to the development of lifting force  $Y$  applied to the rocket at the center of mass. The difference between the forces  $Y - Y'_{r.p.}$  will constitute the magnitude of the steering force under the action of which the center of mass of the rocket will commence to deviate in the direction of the operation of the steering force (16, 17).

The angle of turning of rudders in the flow varies within limits of  $\pm 25^\circ$  for long-range ballistic rockets. This leads to a state of affairs where the forces operating on a rudder vary within broad limits. In Figure 6.15 we set forth the results of experiments in determining the flank thrust of a gas rudder (18). Experimental investigations show that flank thrust upon changing the inclination of a gas rudder is subject to an approximately linear law. The difference between the axial thrust of a free stream and the axial thrust of an inclined stream is equivalent to the frontal resistance of the rudder. Measurements have shown that for all types of rudders the magnitude of losses comes on the average to 60 percent of the flank thrust secured.

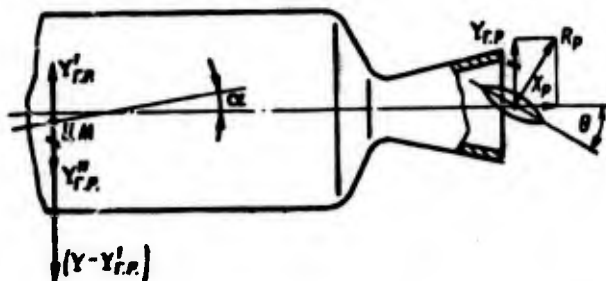


Figure 6.14. Regarding the question of formation of steering force with a gas rudder.

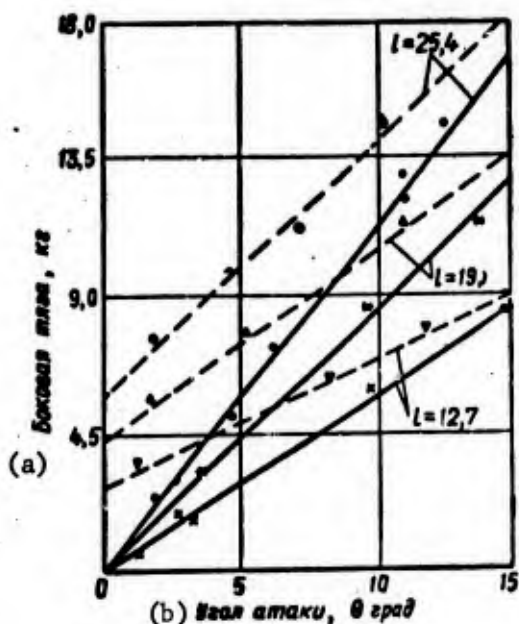


Figure 6.15. Experimental data on determination of flank thrust of gas rudders ( $p_K = 50 \text{ kg/cm}^2$ ):

- change of flank thrust with change of angle of attack of central gas rudder ( $r = 0$ );
- change of flank thrust with change of angle of attack of displaced gas rudder (the rudder is located at a distance of  $r = 8.6 \text{ mm}$  from the axis of the stream.
- a -- Flank thrust, kg; b -- Angle of attack,  $\theta$  degrees.

In multiple-chamber engines gas rudders can be set up in neutral position between chambers. In this case the gas rudders will be under the action of the gas flow only when the rudders are turned.

Cone with inclined section. Deflection of the stream in a cone having an oblique section (Figure 6.16) leads to formation of flank force. Effective transverse expansion of the stream in cones of such design can be created in the presence of elevated pressure at the cone section as compared with the atmospheric pressure. The results of experiments are set forth in the graph (Figure 6.17). A cone cut off at an angle of  $30^\circ$  deflects the stream by  $4^\circ$ . In this connection the flank thrust secured is equal to the flank thrust of an ordinary gas rudder set at a  $6^\circ$  attack angle (18).

A more effective design of cone for controlling the vector of thrust in flight is a cone with a cut cylindrical adapter (Figure 6.16b). The experimental data shown in graph (Figure 6.18) show that with increase of the length of the adapter flank thrust increases, at first in linear fashion, and achieves its maximum magnitude when the adapter catches in its entirety the stream flowing from the cone.

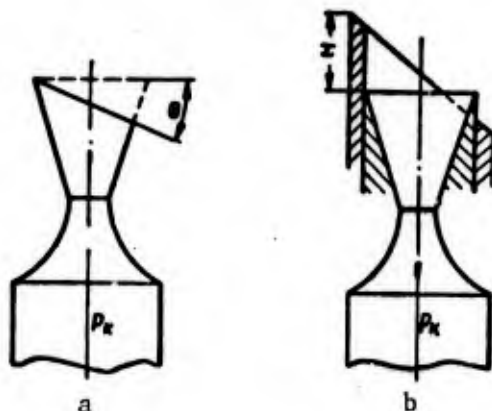


Figure 6.16. Cone with oblique section.

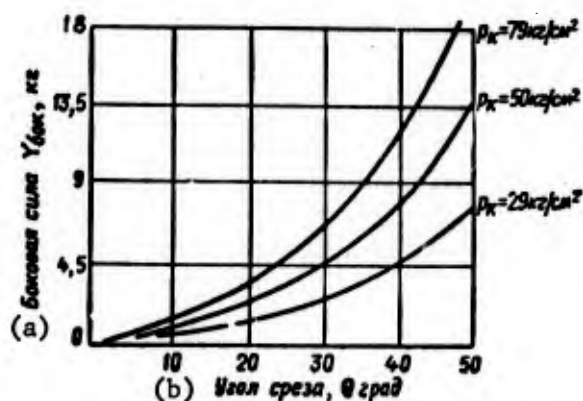


Figure 6.17. Dependence of flank thrust upon angle of section of cone at various pressures in rocket chamber. a -- Flank thrust,  $Y_{flank}$ , kg; b -- Angle of section,  $\theta$  degrees.

Losses of axial thrust occasioned by the presence of an inclined flow are insignificant, and come to about 2.5 percent of full thrust (18).

Cylindrical turning adapter. In this system for controlling the vector of thrust the same principle of deflection of the jet stream by means of a rudder apparatus is used and in the application of gas rudders. But the advantage of this executant organ of control as compared with gas rudders is the fact that a cylindrical turning adapter reacts with streams of gases only during the time a command signal for the creation of a flanking vector of thrust is in operation (Figure 6.19).

Turning around its transverse axis, the cylindrical adapter or curved vane rudder creates a flank force the magnitude of which depends on the angle of turning and the length of the adapter (Figures 6.20, 6.21) (18). With turning to one and the same angle the executant organ for steering a rocket which is in the form of a cylindrical adapter gives

a greater magnitude of thrust than does a gas rudder. The maximum flank thrust corresponds to a length of cylindrical adapter equal to approximately three calibers of the critical section of the cone. A deficiency of this apparatus is the great quantity of hinge moment.

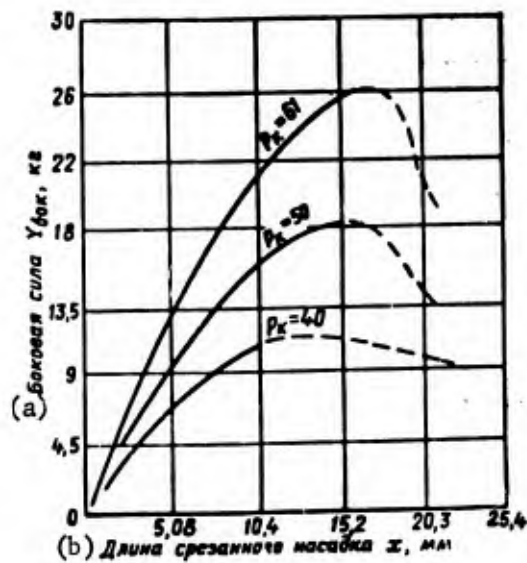


Figure 6.18. Dependence of flank force upon length of adapter with oblique section, under various pressures in the rocket chamber.  
 a -- Flank thrust,  $Y_{flank}$ , kg; b -- Length of cut adapter,  $x$ , mm.

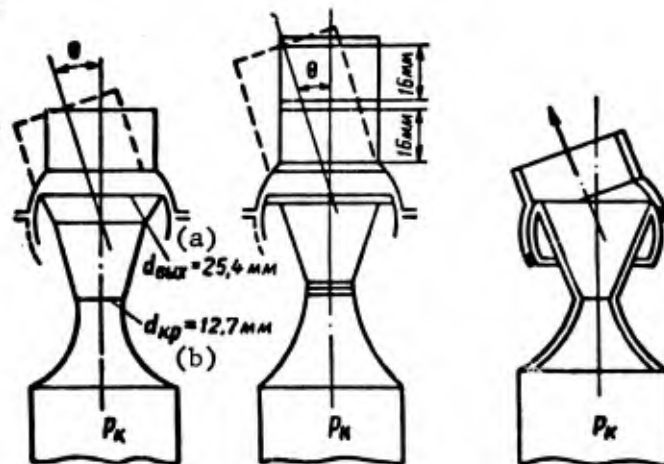


Figure 6.19. Cylindrical turning adapter for control of vector of thrust.  
 a -- Outlet diameter; b -- Critical diameter.

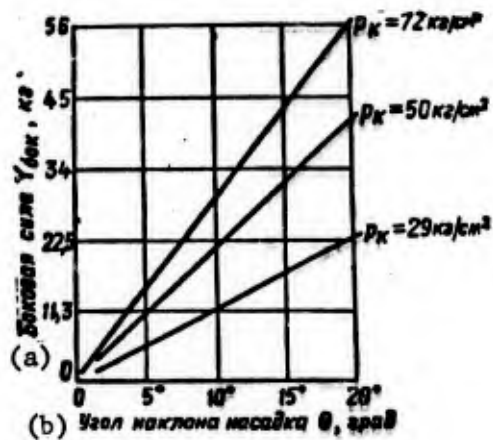


Figure 6.20. Dependence of flank thrust upon angle of turning of cylindrical adapter (according to experimental data). a -- Flank thrust,  $Y_{flank}$ , kg; b -- Angle of turning of adapter,  $\theta$  degrees.

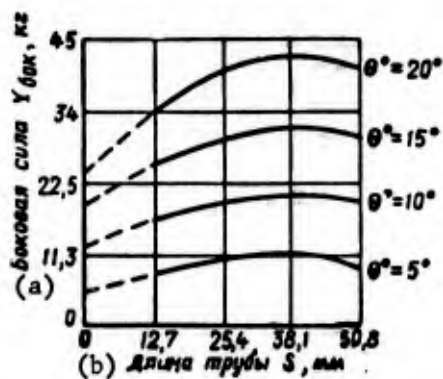


Figure 6.21. Dependence of flank thrust upon length of cylindrical adapter (according to experimental data). a -- Flank thrust,  $Y_{flank}$ , kg; b -- Length of tube,  $S$ , mm.

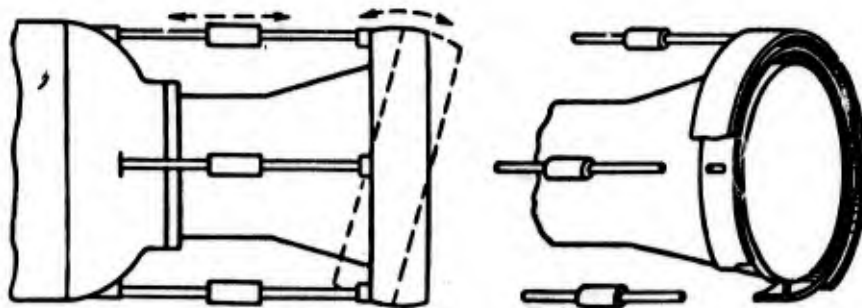


Figure 6.22. Deflector for regulating vector of thrust as regards direction.

The application of deflectors as executant organs for gasodynamic guidance of a rocket is a further development of the designs for cylindrical turning adapters. The deflector (Figure 6.22) consists of a spherical polished ring which turns on hinge supports and is introduced into the gas flow where, deflecting the flow, it thereby changes the direction of the vector of thrust. In order to turn flow and create flank forces a relatively low hinge moment is required, which is an advantage in such a design of rudder. From the literature we are aware that deflectors are set up on each of the four cones of the first stages of the "Polaris A-1" and "Polaris A-2" rockets.

Turning engines and cones. One can steer a rocket by turning the combustion chamber of the engine (Figure 6.23). The magnitude of the constituent of thrust  $P \cdot \sin \theta$  used for turning will depend on the angle of turn  $\theta$ . Inasmuch as ordinarily the angle of turning the chamber,  $\theta$ , is small, the steering force changes approximately according to the linear relation.

$$Y_{ynp} = P \sin \theta \approx P\theta.$$

The loss of thrust,  $X_{ynp}$ , will be a very small quantity, and its value is determined from the expression

$$X_{ynp} = P - P \cos \theta = P(1 - \cos \theta) \approx P \frac{\theta^2}{2}.$$

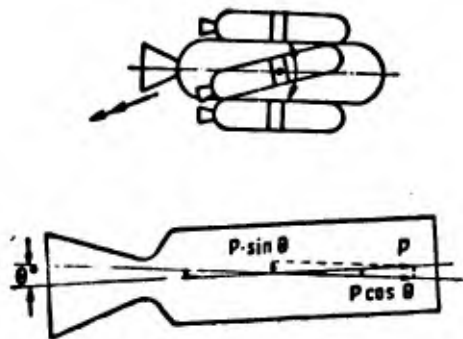


Figure 6.23. Steering flight of rocket by means of turning engine combustion chamber.

Deflection from the trajectory of flight by reason of pitch and yaw are detected through gyroscopes. Signals from the gyroscope are transmitted through an amplifier and the guidance chain to servomechanisms which turn the combustion chamber, set up in its universal-joint suspension.

Direction of thrust force can be controlled by turning small universal-joint-suspended engines (Figure 6.23). In the scheme of guidance by means of flank engines, when the vector of velocity of the rocket

coincides with the assigned direction the flow of gases from each flank engine is identical. Upon deflection of the rocket from the assigned trajectory, a gyroscope gives a signal to special mechanisms which turn the necessary flank engines. The flows of gases issuing from the turned engines create a force which turns the rocket relative to its center of gravity. After the axis of the rocket coincides with the assigned direction of flight, the gyroscope breaks the circuit of excitation of the electromagnet and special apparatus return the flank engines to their initial position.

In solving the problem of regulating the direction of thrust turning cones are often used which have low weight and slow losses of axial thrust when the direction of actual thrust force is deflected from the axis of the rocket (19). The "Minuteman" rocket may serve as an example of such a system. On each stage of the rocket there is a set of four turning cones, the deflection of which to the requisite angle is carried out by corresponding hydraulic circuits. In Figure 6.24 we set forth the system of operation of the turning cones for guidance of the flight of the "Minuteman" rocket. Control with respect to angle of pitch is carried out by turning two cones upward or downward (a); maneuvers with respect to angle of yaw (on the course) are carried out by turning both cones located in the vertical plane to one side or the other (b); control as regards angle of bank is carried out by turning the cones located in the horizontal plane in different directions (c). The cone (Figure 6.25) consists of a stationary part 1, an annular turning gasket 2, and a turning part 3, which can deflect on hinge-pins 4 to an angle of up to  $8^\circ$ .

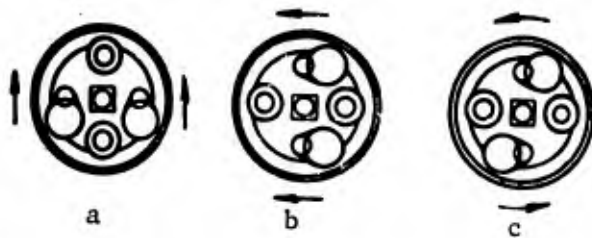


Figure 6.24. System of operation of turning cones for guidance of rocket flight.

Evaluation of the magnitude of hinge moments of such a design of cones was carried out through the testing of an experimental rocket engine having a thrust of 3.2 tons with a pressure of  $35 \text{ kg/cm}^2$  in the chamber. Turning the cone for deflection of the thrust vector by  $10^\circ$  was accomplished with a maximum torque of 2 kg.m (20).

In the engine group of the accelerator of the "Nova" rocket a cone with universal joint suspension is used (Figure 6.26). Ordinarily such a cone is fastened to the universal joint apparatus with hinges at two points. In the plane perpendicular to this suspension the ring of the universal joint suspension is hinge-fastened to the casing of the engine.

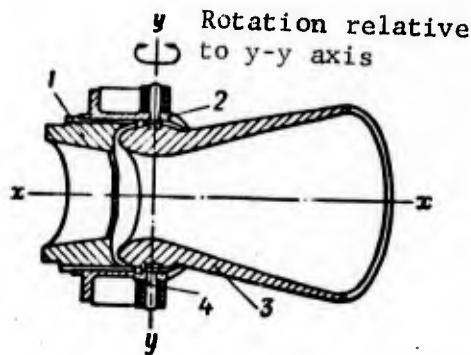


Figure 6.25. Diagram of turning cone.



Figure 6.26. Turning cone with universal joint suspension. a -- Turning relative to y-y axis relative to ring of universal joint suspension; b -- Turning relative to x-x axis of the ring of the universal joint suspension with respect to stationary casing.

Control of turning cones is accomplished via pneumatic and hydraulic conduits. In Figure 6.27 we set forth a diagram of a pneumatic servosystem using hot gas. A powder pressure accumulator (PAD) is used as a source of the working medium for the servosystem. In order to prevent clogging of the system there are fine filters in the structure of the servosystem (21).

In the diagram on Figure 6.28 we show the apparatus of a turning cone with syphon bellows packing. Flexible metallic syphon connecting the cone to the engine constitutes a movable gas packing.

The area of stationary gas around the throat of the cone preserves the delicate syphon from heating up from the combustion products of the fuel (9, 22).

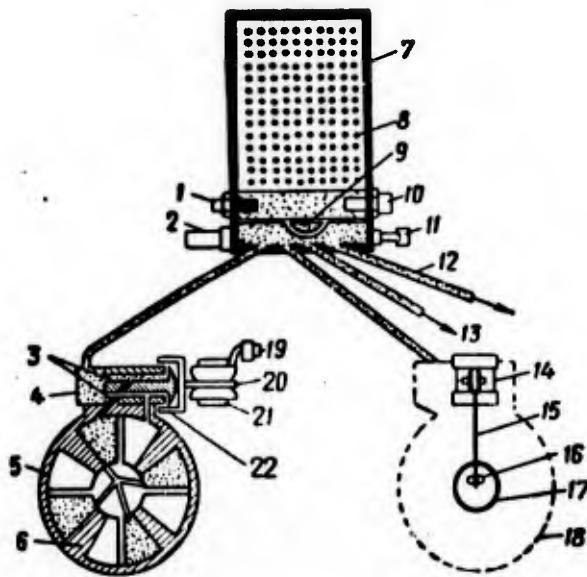


Figure 6.27. Diagram of pneumatic servosystem for turning executant control organs of rocket: 1 -- thermocouple (when necessary to use ignition signal); 2 -- pressure regulating valve; 3 -- constant throttles; 4 -- receiver filter; 5 -- unit-cast rubber packing; 6 -- four-bladed turning rudder machine using hot gas (quadrant); 7 -- generator for gas; 8 -- powder pressure accumulator (PAD); 9 -- filter and packing for protection from moisture; 10 -- igniter; 11 -- removable plug for ground inspection; 12 and 13 -- supplying of gas to rudder machine; 14 -- electromechanical transformer; 15 -- return link spring; 16 -- slotted guiding connections; 17 -- output shaft; 18 -- rudder machine (seen from behind); 19 -- guidance signal; 20 -- fastening of return link spring; 21 -- electromechanical transformer; 22 -- baffle.

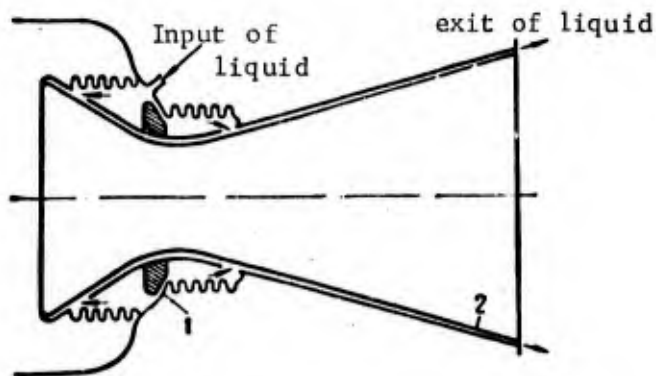


Figure 6.28. Diagram of turning cone with sylphon packing: 1 -- flexible sylphon; 2 -- area beyond skirt.

#### 6.4. Controlling the Vector of Thrust by Injecting Gas or by Injecting\* Liquid Into the Postcritical Part of the Cone

From the materials published in the foreign press it is apparent that the working out of methods to create flank thrust is at present one of the most difficult and important problems engineers encounter in planning large solid-fuel engines (23).

At present great attention is being devoted to the method of controlling the thrust vector through blowing in gas or injecting liquid into the cone of a rocket engine. When this method is applied there is no contact between the moving units and the gases flowing out of the cone. The gas or liquid introduced into the cone deflects the basic flow, creating flank force which is used for control of the rocket.

In this connection two types of systems for supplying working medium are being examined: that with blowing-in of hot gas, and the system of injecting a liquid. Each system, for purposes of regulating thrust vector, requires an additional quantity of working medium used in the rocket, at the cost of reducing the amount of useful load. In tests carried out in order to give effect to the method under examination the following are used as working media: hot gas, gaseous nitrogen, liquid nitrogen, liquid hydrogen, water, and freon-12.

When hot gas is blown in it is supplied from an auxiliary gas generator or is taken from the basic combustion chamber. Then this gas enters the postcritical part of the cone via regulating channels. The "Thiocol" firm has worked out a system for admitting hot gases with a thrust of 2,270 kilograms from the engine combustion chamber into the postcritical part of the cone. Tests of this system of supply have shown reliable working over a time of 50 seconds on the part of a needle valve made of porous materials saturated with copper and cooled by exudation. The discharge of gases through the valve did not exceed 3 percent of the maximum discharge from the basic combustion chamber. The weight of the conduit mechanism and valve are less than 1.8 kilograms (24).

The use of freon somewhat facilitates the problem of supplying gas, but it requires auxiliary tanks, in which the freon is under helium or nitrogen pressure.

Physical scheme of process. The flow of liquid or gas introduced into the supersonic part of the cone interacts with the supersonic flow of gaseous products of combustion of the fuel and, constituting a barrier to the basic flow, it brakes this flow. Thus in the cone there are created conditions leading to the constitution of a sharp jump in the compression arising upon the interaction of the supersonic flow with the barrier (transverse flow) in the form of the stream introduced. The flow

---

\* In some sources the processes of blowing in gases and injecting a liquid are called injection, the working medium an injectant, and the supply system the injector.

introduced, deviating from its initial direction, runs down along the flow to the cut-off of the cone, mixing with the basic flow (Figure 6.20).

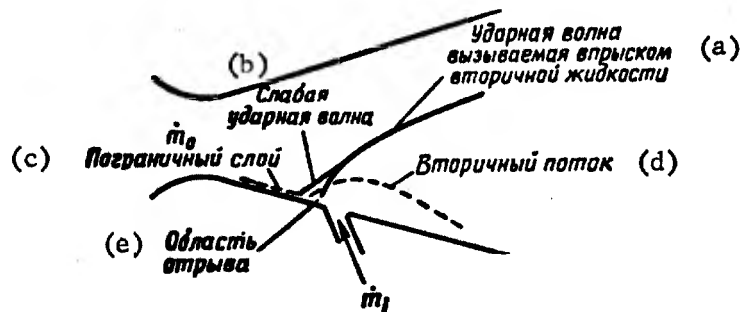


Figure 6.29. Elements of physical scheme of process in cone upon blowing of gas into postcritical part of cone. a -- Shock wave provoked by injection of secondary liquid; b -- Weak shock wave; c --  $m_0$ , limit stratum; d -- Secondary flow; e -- Break-off area.

At the same time, as silhouette photographs of the process show (23), an interaction takes place between the curvilinear shock wave developing and the limit stratum, which leads to breaking off of the secondary flow from the wall upon which the injection aperture is located. Position of the point of break-off from the limits of the break-off zone and of the mixing stratum depends on the discharge of the introduced component (and consequently upon pressure) and upon the Mach number in the cross-section of the injection. After the mixing of the gases they expand isentropically to a static pressure equal to the static pressure of an undisturbed supersonic flow. After the jump in compression the velocity of the gas falls off sharply, and pressure rises. When this happens pressure on the wall of the cone below the injection point along the flow proves to be greater than in the event no injection had occurred. This circumstance leads to the development of a flank force  $Y_{flank}$  the magnitude of which is equal to the sum of all forces from the diversion of pressure operating on the wall of the cone after the jump in compression.

The shape of the shock wave. In all experiments (23) the shock waves forming upon the injection of gas or liquid, independently of the physical properties of the component introduced, are analogous in shape to those presented in Figure 6.29. The inclination of the shock wave in any section increases with increase of the discharge of the component introduced and declines with diminution of the Mach number at the cross-section of introduction. In some combinations of introduced component and of positioning of the aperture for introduction the shock wave falls upon the opposite wall of the cone and is reflected from it. This is most frequently observed when the point of injection is located close to the critical cross-section of the cone, or the discharge of the component introduced is too great. In this case, the specific flank thrust related to a unit of mass discharge of the component introduced falls off. The

effectiveness of creation of flank thrust also declines in the presence of a blurred contour of shock wave is present and there are high discharges of the component introduced, when the system of jumps commences to diffuse radially. In both cases disturbances of pressure go beyond the limits of the plane normal to the plane of injection.

Various approximate methods for theoretical investigation of the processes of injecting gas or liquid into the cone are examined in the literature (25, 26).

Experimental investigation of flank forces (23) arising upon introduction of secondary liquid into engine cone. Tests have been carried out with solid-fuel rocket engines the charges of which consisted of mixed fuel composed of polyurethane and ammonium perchlorate. In operation of the engine 590-680 kilograms of thrust were developed in 8 seconds. Experimental cones were made in the form of cones having a gas expansion rate of 25:1. Depending on the placement of the aperture for introduction of the component, the character of the interaction of the induced shock wave with the opposite wall of the cone changed. The induced jump does not hit the opposite wall of the cone when there is a cone expansion rate ( $\epsilon_1$ ) of 9.9 at the point of introduction of the component. The jump falls and is reflected from the opposite wall when  $\epsilon_1 = 2.65$ . The angle, defined by the opposite wall and a line connecting the point of injection with the point of reflection, determining the level of pressure on the opposite wall is equal to approximately  $53^\circ$ .

Freon-12, water, and gaseous nitrogen were used as working media for introduction into the postcritical section of the cone. The ratio of weight discharges of injected substance and basic flow fell within limits from 0.039 to 0.118. Pressure measured along the wall of the cone ran from 0.07 to 1 kilogram/square centimeter.

In Figures 6.30 and 6.31 we show typical pressure profiles along the surface of a cone, secured for identical  $\epsilon_1$  upon introduction of freon-12 and  $N_2$  through drainage apertures located in one quadrant of a conical jet. Comparison of the pressure profiles shows a substantial rise in positive pressure over the pressure of an undisturbed flow in the field back of the point of introduction of nitrogen relative to the direction of the flow. The relatively high characteristic of gaseous nitrogen as compared with the characteristic of freon-12 is partially explained through the fact that nitrogen is already in gaseous state and the amount of movement of the nitrogen stream is considerably greater than that of the freon-12 stream at identical mass discharges of flow.

As the pressure profiles show, the basic part of the flank force is reflected lower along the flow than the point of injection and is to be explained by disturbances in the distribution of pressure on the wall of the cone.

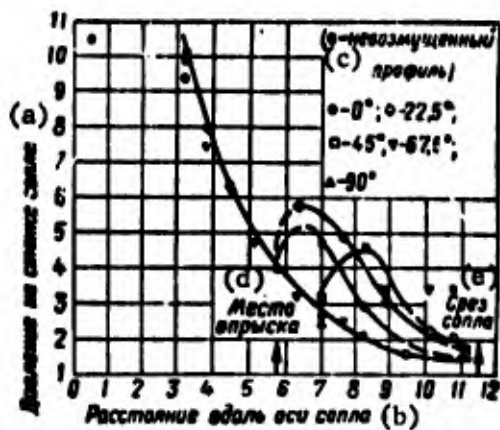


Figure 6.30. Typical pressure profiles along surface of cone upon injection of freon-12:

$$p_k = 20,3 \frac{\text{кг}}{\text{см}^2}; \quad p_{\text{торм}} = 70 \frac{\text{кг}}{\text{см}^2}; \quad \frac{p_{\text{торм}}}{p_k} = 3,46;$$

$$\frac{Q_{\text{сек1}}}{Q_{\text{сек0}}} = 0,20; \quad \sigma_i = 9,90; \quad d_i = 2,03 \text{ мм.}$$

a -- Pressure upon wall of cone; b -- Distance along axis of cone; c -- o -- undisturbed profile; d -- Point of injection; e -- Cut-off of cone.

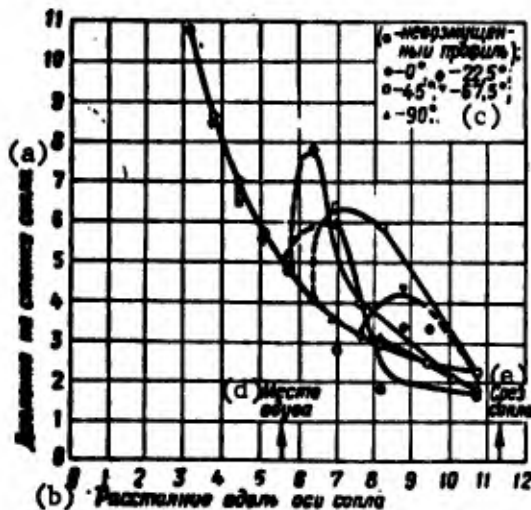


Figure 6.31. Typical pressure profiles along surface upon cone upon injection of gaseous nitrogen:

$$p_k = 26,3 \frac{\text{кг}}{\text{см}^2}; \quad p_{\text{торм}} = 76,9 \frac{\text{кг}}{\text{см}^2}; \quad \frac{p_{\text{торм}}}{p_k} = 2,11;$$

$$\frac{Q_{\text{сек1}}}{Q_{\text{сек0}}} = 0,042; \quad \sigma_i = 9,9; \quad d_i = 3,3 \text{ мм.}$$

a -- Pressure upon wall of cone; b -- Distance along axis of cone; c -- o -- undisturbed profile; d -- Point of injection; e -- Cut-off of cone.

In Table 6.1 we present experimental data on aggregate force, and these are compared with data secured in the measuring of thrust on a six-component stand.

Table 6.1. Comparative Thrust Characteristics of Solid-Fuel Rocket Engine Upon Injection of Freon-12 in Supersonic Part of Cone

(1) Величины, полученные на основании измерений профиля давления *						Величины, полученные экстраполяцией данных по замеру боковой тяги	
$\alpha^\circ$	(6) $\frac{G_l}{G_0}$	(3) $P'_{бок}$	(5) $P_{бок}$	(4) $\frac{\Delta P_{осев}}{P_{бок}}$	(4) $\frac{\Delta P_{осев}}{P_{осев}}$	(5) $P_{бок}$	(6) $\frac{G_l}{G_0}$
(7)	(6)	(5) $P_{осев}$	(5) $P_{осев}$	(5) $P_{бок}$	(5) $P_{осев}$	(5) $P_{осев}$	(6)
0°	0,08	0,0216	0,0233	0,305	0,071	0,0253	0,08
40°	0,103	0,363	0,0387	0,393	0,0152	0,043	0,103

- Key: 1 -- Quantities secured on basis of measurements of pressure profiles\*
- 2 -- Quantities secured by extrapolation of data on measurement of flank thrust
- 3 -- Part of flank force determined by redistribution of pressure on wall of cone, in kg  $P'_{бок}$
- 4 -- Increment in amount of axial force by virtue of operation of secondary flow, in kg  $\Delta P_{осев}$
- 5 -- Axial and flank thrusts, kg  $P_{осев}$  и  $P_{бок}$
- 6 -- Weight discharges of injected liquid and basic flow  $G_l$  и  $G_0$
- 7 -- Angle of injection of liquid relative to normal to wall of cone, positive in direction upward along flow  $\alpha$
- \* -- Secured by integrating pressure profile and impulse as measured in the process of injecting liquid.

The arising of flank forces upon the injection of liquid or gas into the postcritical part of the cone provokes increase of the axial thrust of an engine. The axial augmentation of thrust has a tendency toward direct proportionality with the discharge of the secondary flow. For given discharges of secondary components and for a selected shape of cone, the augmentation in axial thrust force comes approximately to 1/3 of the flank thrust developing in this connection.

In Figure 6.32 we show the influence of discharge of freon-12 upon the magnitude of specific impulse. Extrapolation of experimental data coincides pretty well with the computed value for effective unit impulse of the secondary liquid, equal to 156 kilograms · second/kilogram, the theoretical computation of which is carried out in study (27).

In the literature schemes for blowing gases taken off the combustion chamber into the postcritical part of a fixed cone partially embedded

in the casing are described (Figure 6.33). The cone can be embedded in the casing to the extent of 30-80 percent of its length, depending on the design of the engine. In tests of solid-fuel rocket engines at a thrust of 7.7 T over 70 seconds and with a pressure of 50 atmospheres in the chamber, the vector of thrust by virtue of the injection of gases into the postcritical part of the cone inclined by  $3^\circ$  in two planes (18). Injection of gas into the cone was carried out through two needle valves, the axes of which were at a  $90^\circ$  angle to each other. The needle was made of porous tungsten saturated with copper. As the valve operated the copper boiled out of the pores, ensuring elimination of heat.

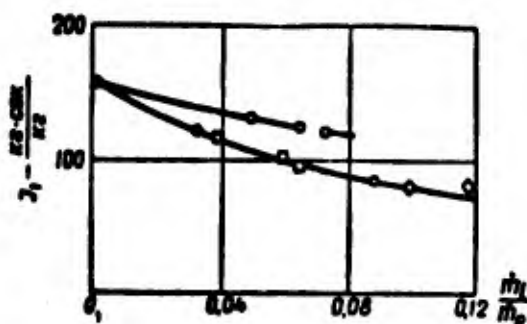


Figure 6.32. Influence of discharge of freon-12 upon magnitude of specific impulse:  $J_1$  -- effective specific impulse of secondary injected liquid.

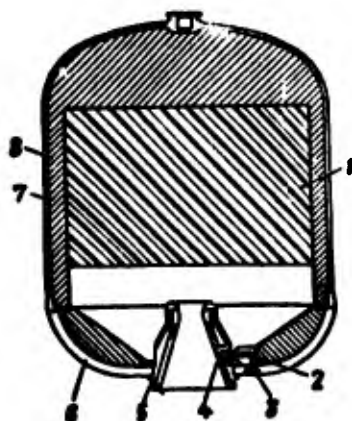


Figure 6.33. Diagram of solid-fuel rocket engine with cone partly embedded in casing: 1 -- Solid fuel charge; 2 -- needle of valve; 3 -- valve for injection of gases from rocket chamber into postcritical part of cone; 4 -- nozzle for injection of gases; 6 -- lower cap of casing of engine; 7 -- rocket chamber; 8 -- heat insulation.

## BIBLIOGRAPHY

1. Shapiro, Ya. M., Mazing, G. Yu., Prudnikov, N. Ye., Theory of the Solid-Fuel Rocket Engine, Voenizdat Publishing House, 1966.
2. Kurov, V. D., Dolzhanskiy, Yu. M., Basic Planning of Powder Rocket Missiles, Oborongiz Publishing House, 1961.
3. Orlov, B. V., Mazing, G. Yu., Thermodynamic and Ballistic Fundamentals of Planning Solid-Fuel Rocket Engines, Mashinostroyeniye Publishing House, 1964.
4. Barrere, M., Jomotte, A., Bebek, B. F., Vandekerkhove, G., Rocket Engines, Oborongiz Publishing House, 1962.
5. Gates, I., and Pinto S., Solid Rocket Engines Thrust Control, ASME Preprint No 59T, March-April 1959.
6. Aviation Week, 1964, 30 November, Vol 81, No 22, page 58; Missiles Space Daily, 1964, 18 February, Vol 10, No 12.
7. Gleg, U., Zumwalt, and William, N., Cone With Secondary Ejection for Regulation of Thrust as Regards Amount, in Solid-Fuel Rockets, Baylor University, 24 January 1962.
8. Space Technics, under editorship of G. Seifert, "Nauka," 1964.
9. Pirs, "Some Methods of Regulating Solid-Fuel Rocket Engine Thrust," Problems in Rocket Technics, No 6, 1962.
10. Chemical Engineering, Vol 71, No 18, 26 (31 August 1964); No 16, No 38.
11. Aviation Week, 4 November 1964, Vol 81, No 18, pages 64-65.
12. Kalt, "Use of Data of Ballistic Tests for Evaluation of System of Cutting Off Thrust of Engine Working on Solid Fuel," Rocket Technics, No 1, 1961.
13. Siplach, "Influence of Rapid Reduction of Pressure Upon Combustion of Solid Fuel," Rocket Technics, Vol 31, No 11, 1961.
14. Dmitriyevskiy, A. A., Koshevoy, V. N., Basic Theory of Rocket Flight, Voenizdat Publishing House, 1964.
15. Guide to K. E. Tsiolkovskiy Home-Museum, Kaluga Book Publishing House, 1961.

16. Panichkin, I. A., Korshun, V. I., Gas Dynamics, Dom Tekhniki Publishing House, 1963.
17. Bonni, E. A., Zukrow, J., Besserer, K. U., Aerodynamics. Jet Engines. Design and Computation Practice, Fizmatgiz Publishing House, 1960.
18. Frazer and Rowe, "Deflection of the Supersonic Stream," Journal of the Royal Aeronautical Society, January, No 565, 1958.
19. Moak, "System for Guiding Thrust Vector of Rocket Engines Using Solid Fuel," Problems in Rocket Technics, No 10, 1962.
20. Aeroplane, 20 January 1961.
21. Delson, G., Space-Aeronautics, 32, No 3, 46-48 (1959); Mensi and Berk, "Sources of Feed for Small Rockets," Problems in Rocket Technics, "Mir" Publishing House, Moscow, No 3, 1961; Lazo, "Hot-Gas Resistance-Type Servosystems," Problems in Rocket Technics, No 11, 1962.
22. Missiles Space Daily, 20 January 1965, No 13, Vol II, page 101.
23. Newton, Jr., Spade, "Investigation of Interaction of Basic Flow in Rocket Engines With Secondary Flow Created in Order to Control Vector of Thrust," Rocket Technics, No 8, 1962.
24. Missile Space Daily, Vol 12, No 09, 15 March 1965, page 86.
25. Sya, Seifert, Caramcetti, "Shock Waves Provoked by Injection of Secondary Fluid," Rocket Technics and Astronautics, No 5, No 11, 1963.
26. Krasnov, N. F., Aerodynamics of Bodies of Rotation, Mashinostroyeniye Publishing House, 1964.
27. Walker, Szandor, "Influence of Properties of Liquids on Effectiveness of System for Control of Thrust Vector Through Injection of Liquid," Problems of Rocket Technics, No 4, 1965.
28. Aviation Week, 21 June 1965, Vol 82, No 25, pages 91-93; Astronautics and Aeronautics, October 1964, No 10, page 86.
29. Hauck, Geyer, "Systems for Controlling Thrust Vector Through Secondary Injection," Problems in Rocket Technics, No 11, 1963.

## CHAPTER VII. MOTION OF THE CENTER OF MASS OF AN UNGUIDED ROCKET

### 7.1. Equations for the Motion of an Unguided Rocket Over the Active Part of Its Trajectory

The launch of unguided rockets is carried out from rocket launch stands set on an incline. During the time of its motion along the guides the rocket takes on a relatively low velocity necessary for its stable flight in the active part of its trajectory.

The altitude of the active part of the trajectory of an unguided rocket does not exceed 1-2 kilometers. Under these circumstances for approximate calculations one may leave out of account change in the thrust of the engine with altitude. From here on we shall write the expression for reactive force in the following form:

$$P = \frac{G_{\text{ext}}}{g} u_e = \frac{u_e v_c}{g}, \quad (7.1)$$

where  $u_e$  is the effective speed of outward flow.

By means of this quantity we take into account not only the actual characteristics of the engine itself, but also the influence of external atmospheric pressure upon the amount of the engine's thrust.

Into the expression for frontal resistance

$$X = \frac{\rho v^2}{2} S c_x \left( \frac{v}{a} \right) \quad (7.2)$$

we introduce the function  $F(v)$ , customarily applied in the ballistics of unguided missiles and determined from the relationship

$$F(v) = \frac{\pi}{8000} \rho v^2 c_x = 4,74 \cdot 10^{-4} v^2 c_x$$

Hereupon expression 7.2 assumes the form  $X = \frac{1D^2}{g} 1000H(y)F(v)$ ,

where  $H(y) = \frac{p}{\rho}$  -- a function allowing for change in the density of air with altitude.

In view of the slight altitude of the active part of the trajectory it is ordinarily assumed that

$$H(y) \approx H(y_{cp}) \approx H\left(\frac{1}{2} y_r\right).$$

Let us write an equation for motion of the center of mass of a rocket relative to the tangent

$$m(t) \dot{v} = - \frac{ID^2}{g} 1000H(y) F(v) - m(t) g \sin \theta. \quad (7.3)$$

With the introduction of substitutions:

$$\mu = \frac{Q_{cos \theta}}{Q_0} = \frac{a_r}{a_0} t; \quad (7.4)$$

$$m = m_0 (1 - \mu) = \frac{Q_0}{g} (1 - \mu) \quad (7.5)$$

equation (7.3) is brought to the form

$$\dot{v} = \frac{P}{m_0} \frac{1}{1 - \mu} - cH(y) \frac{F(v)}{1 - \mu} - g \sin \theta. \quad (7.6)$$

Let us write another equation, for motion relative to the normal

$$\dot{\theta} = - \frac{g \cos \theta}{v} \quad (7.7)$$

and the kinematic equations

$$\dot{x} = v \cos \theta; \quad (7.8)$$

$$\dot{y} = v \sin \theta. \quad (7.9)$$

Equations (7.6)-(7.9) define the motion of the rocket on the active section of the trajectory. The initial conditions corresponding to the moment the rocket leaves the guides have the following form:

$$\text{with } t = t_0; x_0 = 0; y_0 = 0; v = v_0; \theta = \theta_0$$

In order to determine velocity  $v_0$  it is necessary to examine separately the motion of the rocket along the guides. Acceleration of motion of the rocket among the guides will be determined from the expression

$$\dot{v} = j = \frac{P}{m_0} - g \sin \theta_0 \quad (7.10)$$

If one can assume that  $\underline{m}$  is a constant and  $\underline{P}$  is a constant, then  $\underline{j}$  is a constant and the velocity at which the rocket leaves the guides will be determined from expression

$$v_0 = \sqrt{2js_0} \quad (7.11)$$

where  $s_0$  is the course of the rocket's motion along the guide.

The time of motion along the guide is determined from the expression

$$t_0 = \sqrt{\frac{2s_0}{j}} \quad (7.12)$$

But the assumption regarding constancy of engine thrust for the initial period of its working can in some cases lead to considerable errors. In this case it is necessary to integrate the motion of the rocket along the guides while taking the curve  $P(t)$  into account. It is also not difficult to determine the initial velocity  $v_0$  experimentally.

Ordinarily in study of the motion of the rocket beyond the guides it is assumed that  $P = P_{cp} = \text{constant}$ . But if the character of the curve  $P(t)$  is such that the mean value for thrust  $P_{cp}$  upon motion along the guides and beyond them is substantially different, then it is useful to introduce the concept of a fictitious length of guides,  $s_0 \text{ fict}$ . This length is determined from the condition of securing the real amount of  $v_0$  for a value of  $P_{cp}$  corresponding to flight of the rockets beyond the guides. The value  $s_0 \text{ fict}$  can be secured from formula (7.11)

$$v_0 = \sqrt{2js_{0p}}$$

whence

$$s_{0p} = \frac{v_0^2}{2j} = \frac{v_0^2}{2 \left[ \frac{P_{cp}}{m} - g \sin \theta_0 \right]}$$

## 7.2. Integration of Equations for Motion of Rocket in Active Section of Trajectory, in First Approximation

Equations (7.6)-(7.9) can be integrated exactly only by one of the methods for numerical integration of differential equations. In first approximation, let us examine the method for determining the elements of the trajectory of motion of a rocket without taking air resistance into account. In addition, let us replace angle  $\theta$  in equation (7.6) by its mean value along the active trajectory  $\theta_{cp} = \frac{\theta_0 + \theta_1}{2}$  or by its initial value  $\theta_0$ .

Equation (7.6) assumes the following form:

$$d\mathbf{v} = \frac{P}{m_0} \cdot \frac{dt}{1-\mu} - g \sin \theta_{cp} dt.$$

Taking into account expressions (7.1) and (7.4) and designating  $g \sin \theta_{cp}$  as  $g_1$ , we secure

$$d\mathbf{v} = u_0 \frac{d\mu}{1-\mu} - g_1 dt. \quad (7.13)$$

Integrating from the start of motion of the rocket to an arbitrary moment in time, we secure the Tsiolkovskiy formula with the weight of the rocket taken into consideration

$$\tilde{\mathbf{v}} = u_0 \ln \frac{1}{1-\mu} - g_1 t = u_0 U_1(\mu) - g_1 t. \quad (7.14)$$

By the wave sign ( $\sim$ ) we indicate the magnitude of the first approximation. The values of  $U_1(\mu)$  are given in Annex 2.

The velocity of the rocket at the end of the active section of the trajectory is determined from the expression

$$\tilde{\mathbf{v}}_r = u_0 U_1(\mu_r) - g_1 \tau,$$

where  $\tau$  is the full time of the engine's working;

$$\mu_r = \frac{m_r}{Q_0}.$$

We find the length of the arc of the trajectory from the expression

$$\tilde{s} = \int_0^t v dt = u_0 \int_0^{\mu} \ln \frac{1}{1-\mu} dt - g_1 \frac{t^2}{2}.$$

Substituting  $dt$  from expression (7.4)

$$dt = \frac{Q_0 \tau}{u_r} d\mu, \quad (7.15)$$

we secure

$$\tilde{s} = \frac{u_0 Q_0 \tau}{u_r} \int_0^{\mu} \ln \frac{1}{1-\mu} d\mu - g_1 \frac{t^2}{2}.$$

We introduce the designation

$$K_1(\mu) = \int_0^{\mu} \ln \frac{1}{1-\mu} d\mu = (1-\mu) \ln(1-\mu) + \mu$$

By doing this we secure

$$\bar{s} = \frac{u_c Q_0 s}{a_T} K_1(\mu) - \frac{g t^2}{2}. \quad (7.16)$$

Values for the function  $K_1(\mu)$  are given in Table 7.1.

Table 7.1

$\mu$	$K_1(\mu)$	$K_2(\mu)$	$\mu$	$K_1(\mu)$	$K_2(\mu)$	$\mu$	$K_1(\mu)$	$K_2(\mu)$
0,010	0,00005	0,0000	0,090	0,0042	2,159	0,30	0,0503	3,254
0,011	0,00006	0,0945	0,095	0,0047	2,210	0,31	0,0539	3,282
0,012	0,00007	0,0181	0,100	0,0051	2,259	0,32	0,0577	3,308
0,013	0,00008	0,2604	0,105	0,0057	2,305	0,33	0,0617	3,334
0,014	0,00010	0,3340	0,110	0,0062	2,349	0,34	0,0658	3,358
0,015	0,00011	0,4026	0,115	0,0069	2,391	0,35	0,0700	3,382
0,016	0,00013	0,4668	0,120	0,0075	2,431	0,36	0,0744	3,405
0,017	0,00015	0,5271	0,125	0,0082	2,470	0,37	0,0789	3,427
0,018	0,00016	0,5838	0,130	0,0088	2,506	0,38	0,0836	3,448
0,019	0,00018	0,6373	0,135	0,0096	2,541	0,39	0,0885	3,468
0,020	0,00020	0,6881	0,140	0,0103	2,575	0,40	0,0935	3,488
0,021	0,00022	0,7364	0,145	0,0110	2,608	0,41	0,0987	3,508
0,022	0,00024	0,7825	0,150	0,0119	2,639	0,42	0,1041	3,526
0,023	0,00027	0,8265	0,155	0,0127	2,669	0,43	0,1096	3,544
0,024	0,00029	0,8686	0,160	0,0135	2,699	0,44	0,1153	3,562
0,025	0,00032	0,9089	0,165	0,0144	2,727	0,45	0,1212	3,579
0,026	0,00034	0,9477	0,170	0,0154	2,754	0,46	0,1273	3,595
0,027	0,00037	0,9849	0,175	0,0163	2,780	0,47	0,1335	3,611
0,028	0,00040	1,020	0,180	0,0172	2,806	0,48	0,1400	3,627
0,029	0,00042	1,055	0,185	0,0183	2,831	0,49	0,1466	3,642
0,030	0,00045	1,088	0,190	0,0193	2,855	0,50	0,1534	3,657
0,035	0,00065	1,241	0,195	0,0204	2,878	0,52	0,1677	3,685
0,040	0,00083	1,372	0,20	0,0215	2,901	0,54	0,1828	3,711
0,045	0,00107	1,488	0,21	0,0238	2,945	0,56	0,1988	3,736
0,050	0,00126	1,591	0,22	0,0262	2,986	0,58	0,2156	3,760
0,055	0,00151	1,684	0,23	0,0287	3,025	0,60	0,2335	3,782
0,060	0,0018	1,769	0,24	0,0315	3,063	0,62	0,2523	3,804
0,065	0,0022	1,846	0,25	0,0342	3,098	0,64	0,2722	3,824
0,070	0,0025	1,917	0,26	0,0372	3,132	0,66	0,2932	3,843
0,075	0,0029	1,984	0,27	0,0403	3,165	0,68	0,3154	3,861
0,080	0,0033	2,046	0,28	0,0435	3,196	0,70	0,3612	3,878
0,085	0,0038	2,104	0,29	0,0468	3,226			

In order to determine the angle  $\theta$ , of incline of the vector of velocity to the horizon, we integrate expression (7.7) through:

$$\int_{t_0}^t \frac{dt}{\cos \theta} = -g \int_{t_0}^t \frac{dt}{v},$$

where  $t_0$  is the moment at which the rocket departs from the guides.

In determining angle  $\theta$  we shall disregard, in the expression for velocity (7.14), the second term of the right-hand part. In doing this, with expression (7.15) taken into account, we secure

$$\int_{\theta_0}^{\theta} \frac{d\theta}{\cos \theta} = - \frac{g Q_0 \tau}{u_r u_T} \int_{\mu_0}^{\mu} \frac{d\mu}{\ln \frac{1}{1-\mu}}. \quad (7.17)$$

We introduce the designations:

$$\xi(\theta) = \int_{\theta}^{\theta_0} \frac{d\theta}{\cos \theta} = \ln \operatorname{tg} \left( \frac{\theta}{2} + \frac{\pi}{4} \right);$$

$$K_2(\mu) = \int_{\mu}^{\mu_0} \frac{d\mu}{\ln \frac{1}{1-\mu}}.$$

From this we get

$$\begin{aligned} \xi(\theta) - \xi(\theta_0) &= - \frac{g Q_0 \tau}{u_r u_T} [K_2(\mu) - K_2(\mu_0)] = \\ &= - \frac{1}{3} [K_2(\mu) - K_2(\mu_0)]. \end{aligned} \quad (7.18)$$

The values for function  $K_2(\mu)$  are given in Table 7.1. The value of  $\mu_0$  is determined from expression (7.4)

$$\mu_0 = \frac{Q_{cp}}{Q_0} t_0 = \frac{u_T}{Q_0 \tau} t_0$$

and  $t_0$  is determined according to formula (7.12).

When change of angle  $\theta$  is slight, the left-hand arm of equation (7.17) may be calculated from the expression

$$\int_{\theta_0}^{\theta} \frac{d\theta}{\cos \theta} = \frac{\Delta \theta}{\cos \theta_{cp}} \approx \frac{\Delta \theta}{\cos \theta_0},$$

whereupon expression (7.18) assumes the form

$$\Delta \theta = - \frac{g Q_0 \tau \cos \theta_{cp}}{u_r u_T} [K_2(\mu) - K_2(\mu_0)]. \quad (7.19)$$

For the end of the active part we secure

$$\bar{\theta}_2 = \theta_0 - \frac{g Q_0 \tau \cos \theta_{cp}}{u_r u_T} [K_2(\mu_2) - K_2(\mu_0)].$$

Example. Let us calculate in first approximation the elements of the end of the active section of the trajectory of a rocket, characterized by the following parameters:

$D = 200 \text{ mm}$ ;  $Q_0 = 200 \text{ kg}$ ;  $w_r = 96 \text{ kg}$ ;  $\tau = 3.0 \text{ sec}$ ;  $u_e = 2,000 \text{ m/sec}$ ;  $\theta_0 = 45^\circ$ .

The length of the run of the rocket along the guides is  $L = s_0 = 7.8 \text{ meters}$ .

We determine the parameter  $\mu_r$  :

$$\mu_r = \frac{w_r}{Q_0} = \frac{96}{200} = 0,48.$$

We determine the thrust of the rocket, which we assume to be constant:

$$P = \frac{w_r u_e}{g \tau} = \frac{96 \cdot 2000}{9,81 \cdot 3} = 6520 \text{ kg}$$

We determine the initial acceleration of the rocket

$$j_0 = \frac{P_g}{Q_0} - g \sin \theta_0 = \frac{6520 \cdot 9,81}{200} - 9,81 \cdot 0,707 = 313 \text{ m/sec}^2$$

We determine the velocity  $v_0$  for the departure of the rocket from the guides:

$$v_0 = \sqrt{2jL} = \sqrt{2 \cdot 313 \cdot 7,8} = 70 \text{ m/sec}$$

We determine the time of motion along the guides:

$$t_0 = \sqrt{\frac{2L}{j_0}} = \sqrt{\frac{2 \cdot 7,8}{313}} = 0,224 \text{ sec}$$

We determine the initial relative expenditure of fuel:

$$\mu_0 = \frac{w_r}{Q_0 \tau} t_0 = \frac{96 \cdot 0,224}{200 \cdot 3} = 0,036.$$

We determine in accordance with formula (7.19) the change in angle  $\theta$  :

$$\Delta \theta = \frac{g Q_0 \tau \cos \theta_0}{w_r u_e} [K_1(\mu_r) - K_1(\mu_0)] = \frac{9,81 \cdot 200 \cdot 3 \cdot 0,707}{96 \cdot 2000} (3,627 - 1,254) = 5,15 \cdot 10^{-3} \text{ radians} = 2,95^\circ;$$

$$\tilde{\theta}_r = \theta_0 - \Delta \theta = 45^\circ - 2,95^\circ = 42,05^\circ;$$

$$\theta_{cp} = \theta_0 - \frac{\Delta \theta}{2} = 43,52^\circ.$$

We determine velocity at the end of the active section:

$$\bar{v}_x = a_0 \mu_1(\mu) - g \sin \theta_{cp} \cdot \tau = 2000 \cdot 0,654 - 9,81 \cdot 0,689 \cdot 3 = 1288 \text{ m/sec}$$

We determine the length of the active section,  $s_k$  according to formula (7.16):

$$\bar{s}_x = \frac{a_0 Q_0 \tau}{a_1} K_1(\mu_x) - \frac{g \sin \theta_{cp} \cdot \tau^2}{2} = \frac{2000 \cdot 200 \cdot 3}{96} \cdot 0,140 - \frac{9,81 \cdot 0,689 \cdot 3^2}{2} = 1720 \text{ m.}$$

We determine the height of the active section:

$$\bar{h}_x = \bar{s}_x \sin \theta_{cp} = 1720 \cdot 0,689 = 1185 \text{ m.}$$

### 7.3. Allowing for Air Resistance

In calculating the velocity of the rocket in second approximation we shall take into account additionally the air resistance. In doing this we secure from expression (7.6), taking expression (7.15) into account:

$$d\bar{v} = a_0 \frac{d\mu}{1-\mu} - g_1 dt - aF(\bar{v}) \frac{d\mu}{1-\mu}, \quad (7.20)$$

where

$$a = \frac{cH(\bar{v}_{sp}) Q_0 \tau}{a_1}.$$

Integrating within appropriate limits, we secure:

$$\bar{v} = a_0 \ln \frac{1}{1-\mu} - g_1 t - a \int \frac{F(\bar{v}) d\mu}{1-\mu}. \quad (7.21)$$

We express by  $\frac{d\mu}{1-\mu}$ , on the basis of expression (7.20) the multiplier forming part of the right-hand arm of the last equation; under these circumstances

$$d\bar{v} = \frac{d\mu}{1-\mu} \left[ a_0 - g_1 (1-\mu) \frac{dt}{d\mu} - aF(\bar{v}) \right].$$

Taking expression (7.15) into account and designating

$$g_1 \frac{dt}{d\mu} = \frac{g_1 Q_0 \tau}{a_1} = \beta, \quad (7.22)$$

we secure

$$\frac{d\mu}{1-\mu} = \frac{d\bar{v}}{a_0 \left[ 1 - \frac{aF(\bar{v}) + \beta(1-\mu)}{a_0} \right]}.$$

The integral in expression (7.21) assumes the form

$$\alpha \int_0^v F(v) \frac{d\mu}{1-\mu} = \frac{\alpha}{u_e} \int_0^v \frac{F(v) dv}{1 - \frac{\alpha F(v) + \beta(1-\mu)}{u_e}} \quad (7.23)$$

The quantity

$$\frac{\alpha F(v) + \beta(1-\mu)}{u_e} = \epsilon,$$

expressing the ratio of the weight of the rocket and frontal resistance to engine thrust can be regarded as a quantity of the first order of smallness. Eliminating small quantities higher than the first order, we can write

$$\frac{1}{1-\epsilon} = 1 + \epsilon + O(\epsilon^2) \approx 1 + \epsilon$$

When this is done expression (7.23) assumes the form

$$\begin{aligned} \alpha \int_0^v F(v) \frac{d\mu}{1-\mu} &= \frac{\alpha}{u_e} \int_0^v \left[ 1 + \frac{\alpha}{u_e} F(v) + \frac{\beta(1-\mu)}{u_e} \right] F(v) dv = \\ &= \frac{\alpha}{u_e} \int_0^v F(v) dv + \frac{\alpha^2}{u_e^2} \int_0^v [F(v)]^2 dv + \frac{\alpha\beta(1-\mu)_{cp}}{u_e^2} \int_0^v F(v) dv. \end{aligned} \quad (7.24)$$

We may note that expression (7.23) is a quantity of the first order of smallness relative to the first term of the right-hand arm of expression (7.21). For this reason, eliminating the quantity  $\epsilon^2$  in expression (7.23), we essentially disregard a quantity of the third order of smallness relative to the velocity of the rocket.

From expressions (7.21) and (7.24) we secure

$$v = u_e \ln \frac{1}{1-\mu} - g_1 t - \frac{\alpha}{u_e} \int_0^v F(v) dv - \frac{\alpha^2}{u_e^2} \int_0^v [F(v)]^2 dv - \frac{\alpha\beta(1-\mu)_{cp}}{u_e^2} \int_0^v F(v) dv.$$

In the last term of the right-hand arm  $(1-\mu)$  is taken out in its mean value.

We introduce the designations:

$$\bar{v} = u_e \ln \frac{1}{1-\mu} - g_1 t; \quad (7.25)$$

$$L_1(v) = \int_0^v F(v) dv, \quad (7.26)$$

$$L_2(v) = \int_0^v [F(v)]^2 dv. \quad (7.27)$$

Under these circumstances we secure

$$v = \bar{v} - \frac{a}{a_v} \left[ 1 + \frac{p}{a_v} (1-p)_{cp} \right] L_1(v) - \frac{a^2}{a_v^2} L_2(v).$$

The functions  $L_1(v)$  and  $L_2(v)$  are figured out conformably to the "1930 law of air resistance" (1) (Figure 2.9).

Taking expression (7.22) into account we secure

$$\frac{p}{a_v} (1-p)_{cp} = \frac{g Q_0}{a_v \cdot a_v} (1-p)_{cp} = \frac{g \sin \theta_{cp}}{a_v a_v} Q_0 (1-p)_{cp} = \frac{Q_{cp} \cdot \sin \theta_{cp}}{p},$$

where

$$Q_{cp} = Q_0 + \frac{a}{g}.$$

Finally the expression for velocity assumes the following form\*:

$$v = \bar{v} - \frac{a}{a_v} \left( 1 + \frac{Q_{cp} \sin \theta_{cp}}{p} \right) L_1(v) - \frac{a^2}{a_v^2} L_2(v). \quad (7.28)$$

\* The functions  $L_1(v_{Tg})$  and  $L_2(v_{Tg})$  are introduced in study (1) as functions of the velocity according to Tsiolkovskiy

$$v_{Tg} = a_v \ln \frac{1}{1-p}.$$

The values for  $L_1(v)$  and  $L_2(v)$  are given in Table 7.2.

Equation (7.28) contains only one unknown,  $v$ , which must be determined by trial and error, as the velocity falls under the sign of two tabulated functions. In practice proceeding in the following fashion may be recommended. Let us designate the right-hand arm of equation (7.28) by  $f(v)$ , whereupon we secure

$$\Delta v = f(v) - v = 0. \quad (7.29)$$

Let us assign ourselves three values of velocity, with  $v_1 = \bar{v}$ ,  $v_2$  and  $v_3$  less than  $\bar{v}$  by 5 percent and by 10 percent. The values for velocity are rounded off in such fashion as to spare oneself interpolation in

determining the table values  $L_1(v)$  and  $L_2(v)$ . Having determined the value  $\Delta v$ , we construct a graph for the dependence of  $\Delta v$  upon  $v_1$  and we find the value of  $v$  at which  $\Delta v=0$ . This will give us the value for velocity which is being sought.

Table 7.2

$v$	$10^{-3}L_1(v)$	$10^{-6}L_2(v)$	$v$	$10^{-3}L_1(v)$	$10^{-6}L_2(v)$	$v$	$10^{-3}L_1(v)$	$10^{-6}L_2(v)$
100	0,029	0,00002	550	8,12	0,244	1000	41,23	2,804
110	0,039	0,00002	560	8,58	0,265	1010	42,26	2,910
120	0,050	0,00004	570	9,04	0,287	1020	43,29	3,017
130	0,064	0,00006	580	9,52	0,309	1030	44,34	3,128
140	0,080	0,00008	590	10,01	0,333	1040	45,40	3,240
150	0,098	0,00012	600	10,51	0,358	1050	46,48	3,356
160	0,119	0,00016	610	11,02	0,384	1060	47,56	3,474
170	0,143	0,00022	620	11,55	0,420	1070	48,66	3,595
180	0,170	0,00029	630	12,08	0,441	1080	49,78	3,719
190	0,200	0,00038	640	12,63	0,471	1090	50,90	3,846
200	0,233	0,00049	650	13,20	0,503	1100	52,04	3,975
210	0,270	0,00063	660	13,78	0,537	1110	53,19	4,107
220	0,310	0,00079	670	14,37	0,572	1120	54,35	4,242
230	0,355	0,00099	680	14,98	0,609	1130	55,53	4,381
240	0,403	0,0012	690	15,60	0,648	1140	56,72	4,522
250	0,456	0,0015	700	16,24	0,688	1150	57,92	4,66
260	0,513	0,0018	710	16,89	0,731	1160	59,13	4,813
270	0,574	0,0022	720	17,56	0,775	1170	60,35	4,963
280	0,640	0,0026	730	18,24	0,821	1180	61,60	5,116
290	0,712	0,0032	740	18,93	0,869	1190	62,85	5,272
300	0,791	0,0038	750	19,63	0,919	1200	64,11	5,432
310	0,881	0,0046	760	20,35	0,970	1210	65,38	5,594
320	0,990	0,0057	770	21,08	1,028	1220	66,67	5,760
330	1,12	0,0075	780	21,82	1,078	1230	67,97	5,929
340	1,29	0,0104	790	22,58	1,135	1240	69,28	6,110
350	1,49	0,0144	800	23,34	1,194	1250	70,61	6,277
360	1,71	0,0190	810	24,12	1,254	1260	71,94	6,456
370	1,93	0,0242	820	24,91	1,317	1270	73,29	6,638
380	2,17	0,0300	830	25,71	1,381	1280	74,66	6,823
390	2,42	0,0363	840	26,52	1,447	1290	76,03	7,012
400	2,69	0,0433	850	27,35	1,516	1300	77,42	7,205
410	2,97	0,0510	860	28,19	1,586	1310	78,82	7,401
420	3,26	0,0594	870	29,04	1,658	1320	80,23	7,600
430	3,56	0,0685	880	29,90	1,733	1330	81,66	7,803
440	3,87	0,0784	890	30,78	1,809	1340	83,09	8,010
450	4,20	0,0890	900	31,67	1,888	1350	84,54	8,220
460	4,54	0,100	910	32,57	1,969	1360	86,01	8,434
470	4,89	0,113	920	33,48	2,053	1370	87,48	8,651
480	5,25	0,126	930	34,41	2,138	1380	88,97	8,873
490	5,63	0,140	940	35,34	2,226	1390	90,47	9,093
500	6,01	0,155	950	36,29	2,316	1400	91,98	9,326
510	6,41	0,171	960	37,26	2,409	1410	93,50	9,559
520	6,82	0,188	970	38,23	2,504	1420	95,04	9,795
530	7,25	0,206	980	39,22	2,602	1430	96,59	10,03
540	7,68	0,224	990	40,22	2,702	1440	98,15	10,28

Example. Let us calculate the velocity of a rocket at the end of the active section for the example examined in first approximation in 7.2. In this example the velocity  $\check{v}$  was determined without allowing for air resistance ( $\check{v} = 1,288$ ).

Let the coefficient of the shape of the rocket,  $\underline{i}$ , be 1.75 under the "1930 resistance law."

According to Table 1 of the annex we find

$$H(y_{cp}) = H\left(\frac{1}{2} \bar{y}_x\right) = H(593) = 0,944.$$

We determine

$$\frac{a}{u_r} = \frac{cQ_0 c H(y_{cp})}{u_r u_r} = \frac{i D^2 \cdot 10^3 H(y_{cp}) c}{u_r u_r} = \frac{1,75 \cdot 0,2^2 \cdot 10^3 \cdot 0,944 \cdot 3}{96 \cdot 2000} = 1,032 \cdot 10^{-3}.$$

We compute

$$\frac{Q_{cp} \sin \theta_{cp}}{P} = \frac{(200 - 0,5 \cdot 96) \cdot 0,689}{6520} = 0,0160.$$

Expression (7.29) assumes the form

$$\Delta v = 1288 - 1,032 \cdot 10^{-3} \cdot 1,016 L_1(v) - 1,032^2 \cdot 10^{-6} L_2(v) - v = 0$$

or finally

$$\Delta v = 1288 - 1,05 \cdot 10^{-3} L_1(v) - 1,068 \cdot 10^{-6} L_2(v) - v = 0.$$

Solving this equation by trial and error, we select in accordance with what has been said above three values for  $v_1$ , and from Table 7.2 we determine  $L_1$  and  $L_2$ :

$v_1$	$L_1 \cdot 10^{-3}$	$L_2 \cdot 10^{-6}$	$1,05 \cdot 10^{-3} L_1$	$1,068 \cdot 10^{-6} L_2$
1280	74,66	6,823	78,5	7,3
1220	66,67	5,760	70,1	6,1
1160	59,13	4,813	62,1	5,2

We compute the values of  $\Delta v_1$  :

$$\Delta v_1 = 1288 - 78,5 - 7,3 - 1280 = -78;$$

$$\Delta v_2 = 1288 - 70,1 - 6,1 - 1220 = -8;$$

$$\Delta v_3 = 1288 - 62,1 - 5,2 - 1160 = +61.$$

We enter the values secured for  $\Delta v = f(v_1)$  on the graph Figure 7.1 and we find the value of  $v_1$  to be 1,213, with  $\Delta v = 0$ .

Finally we get  $v_k = 1,213$  meters per second.

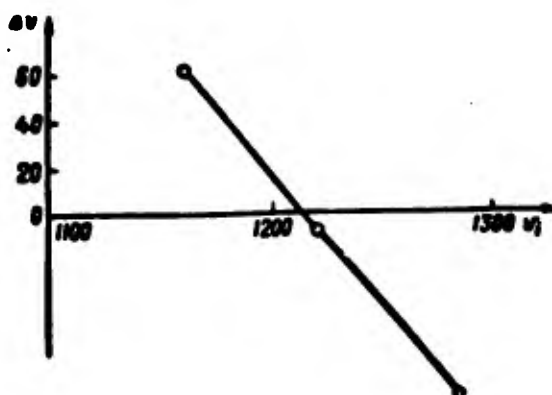


Figure 7.1. Graphical solution of equation (7.28).

### Calculating the Length of the Arc

In 7.2 we got a relationship (7.16) for determination of the length of the arc  $s_k$  without taking air resistance into account. Let us examine a methods system for taking air resistance into account in computing the length of the arc. In doing this we take it that the coordinates of the end of the active section can be determined with precision relative to the lesser precision of the computation of velocity. Let us write the corrections which take into account the influence of air resistance in the form:

$$\Delta v_R = \bar{v} - v,$$

$$\Delta s_R = \bar{s} - s.$$

Calculations show that one may approximately regard acceleration of the force of air resistance upon the active section of the trajectory as being proportional to the square of the time of flight:

$$j_R \approx kv^2.$$

Hence it follows that

$$\Delta v_R = \frac{kv^2}{3}; \quad \Delta s_R = \frac{kv^2}{12} = \frac{\Delta v_R^2}{4} = \frac{(\bar{v} - v)^2}{4} t. \quad (7.30)$$

Finally for the end of the active section we secure

$$\Delta s_{R2} = \frac{\bar{v} - v_R}{4} \tau = \frac{\Delta v_R}{4} \tau,$$

where  $\Delta v_R$  is determined from expression (7.28).

For the example considered above we have

$$\Delta v_{\text{air}} = \frac{1200 - 1213}{4} \cdot 3 = 96 \text{ m,}$$

whence

$$v_2 = \bar{v}_2 - 96 = 1730 - 96 = 1634 \text{ m.}$$

### Calculating the Angle $\theta_2$

For angle  $\theta$  we secure from expression (7.7)

$$\int \frac{dv}{v} = -g \int dt.$$

The substitution under the integral sign of velocity  $v$  by velocity according to the Tsiolkovskiy formula

$$v = v_0 \ln \frac{1}{1-p} = v_0 I_0(p)$$

led to formula (7.19), in which the influence of the weight of the rocket and of air resistance was not taken into account. In order to allow approximately for these factors we write the expression for velocity in the following form:

$$v = v_0 I_0(p) - g t - \Delta v_{\text{air}} \quad (7.31)$$

where  $\Delta v_{\text{air}}$  is determined from expression (7.30), in which connection the coefficient  $b$  is determined from expression

$$b = \frac{2bv_0}{g}.$$

Thus for an arbitrary moment of time we have

$$\Delta v_{\text{air}} = \frac{bv_0}{g} \cdot t^2$$

and expression (7.31) assumes the following form:

$$v = v_0 - g t - t^2 = v_0 \left( 1 - \frac{g t + t^2}{v_0} \right), \quad (7.32)$$

where

$$t = \frac{bv_0}{g}.$$

Regarding

$$\frac{E^2 + r^2}{v_a}$$

as a quantity of the first order of smallness, we transform the integral

$$I = \int_0^l \frac{dt}{v} = \int_0^l \frac{dt}{v_a \left(1 - \frac{E^2 + r^2}{v_a^2}\right)} \approx \int_0^l \frac{1}{v_a} \left(1 + \frac{E^2 + r^2}{v_a^2}\right) dt$$

or

$$I = \int_0^l \frac{dt}{v_a} + \int_0^l \frac{E^2 + r^2}{v_a^3} dt.$$

The first term was taken into account in deriving formula (7.19). The correction to this formula assumes the form

$$\delta(\Delta\theta) = g \cos \theta_{sp} \int_0^l \frac{E^2 + r^2}{v_a^3} dt. \quad (7.33)$$

Let us replace  $v_{T_0}$  with its approximated expression

$$v_a = s_1 \ln \frac{1}{1-p} \approx s_1 p = s_1 \frac{Q_0^2}{Q_0^2} t.$$

When this is done expression (7.33) assumes the form

$$\delta(\Delta\theta) = \frac{g \cos \theta_{sp} Q_0^2}{s_1^3} \int_0^l \left(\frac{E^2}{t^2} + r^2\right) dt. \quad (7.34)$$

For the end of the active section we get

$$\delta(\Delta\theta) = A \left[ E_1 \ln \frac{s}{l_0} + \frac{r^2}{2} (r^2 - \theta) \right],$$

where

$$A = \frac{g Q_0^2}{s_1^3} \cos \theta_{sp}. \quad (7.35)$$

For the example we have been examining

$$\frac{Q_0^2}{s_1^3} = \frac{200 \cdot 3}{2000 \cdot 98} = \frac{1}{330};$$

$$A = \frac{g \cos \theta_{cp}}{320^2} = \frac{9,81 \cdot \cos 43^{\circ}31'}{320^2} = 0,693 \cdot 10^{-4};$$

$$g_1 \ln \frac{v}{v_0} = g \sin \theta_{cp} \cdot \ln \frac{3}{0,224} = 9,81 \cdot 0,689 \cdot 2,303 \cdot \lg 13,35 = 17,5;$$

$$r = \frac{\Delta v_{cp}}{g} = \frac{75}{27} = 2,78;$$

$$\frac{r}{2} (v^2 - v_0^2) = \frac{2,78}{2} (9 - 0,224^2) = 12,4;$$

$$\delta(\Delta\theta) = 0,693 \cdot 10^{-4} (17,5 + 12,4) = 20,7 \cdot 10^{-4} \text{ rad} = 0,12^{\circ}.$$

We get

$$\delta(\Delta\theta) = 0,12^{\circ} = 7,2'.$$

Taking this correction into account we secure:

$$\Delta\theta = 2,95 + 0,12 = 3,07^{\circ} = 3^{\circ}04';$$

$$\theta_x = \theta_0 - \Delta\theta = 45^{\circ} - 3,07^{\circ} = 41,93^{\circ} = 41^{\circ}56'.$$

After refining the values  $s_k$  and  $\theta_x$  we determine the values for the coordinates of the end of the active section from expressions

$$\begin{aligned} x_x &= s_x \cos \theta_{cp}; \\ y_x &= s_x \sin \theta_{cp}. \end{aligned}$$

For the example being examined we have:

$$\theta_{cp} = \theta_0 - \frac{1}{2} \Delta\theta = 45^{\circ} - 1,54^{\circ} = 43,46^{\circ} = 43^{\circ}28';$$

$$x_x = 1624 \cdot \cos 43^{\circ}28' = 1180 \text{ m};$$

$$y_x = 1624 \cdot \sin 43^{\circ}28' = 1120 \text{ m}.$$

#### 7.4. Determining the Full Range of Flight of the Rocket

In order to determine the full range of flight of the rocket one must calculate the elements of the passive section of the trajectory. For this purpose one can make use of equations (7.6)-(7.9), taking  $P = 0$  and  $\mu = \mu_x = \frac{g_1}{Q_0}$  in them and taking into account in explicit form the

change in the density of the air and in the speed of sound with altitude. In ballistics the following system of differential equations of motions, with independence of the variable  $x$ , is the generally used (2):

$$\frac{dv}{dt} = -cH_0(y)O(v); \quad (7.36)$$

$$\frac{dp}{dx} = -\frac{g}{u^2}; \quad (7.37)$$

$$\frac{dy}{dx} = p; \quad (7.38)$$

$$\frac{dt}{dx} = \frac{1}{u}. \quad (7.39)$$

In these equations:

$$\begin{aligned} p &= \operatorname{tg} \theta; \\ c &= \frac{1D^2 10^8}{Q_r}; \\ u &= v \cos \theta; \\ G(v_r) &= \frac{F(v_r)}{v_r}; \\ v_r &= v \sqrt{\frac{T_0}{T}}; \\ H_r(y) &= H(y) \sqrt{\frac{T}{T_0}}. \end{aligned}$$

Equations (7.36)-(7.39) are integrated numerically with initial conditions corresponding to the end of the active section of the trajectory.

No approximate methods exist which might enable one to integrate with acceptable accuracy the equations for the motion of a rocket on the passive section of the trajectory.

It is possible, however, to make use of ballistic tables (collections) drawn up for artillery shells, in which values for the elements of the point of fall  $\underline{X}$ ,  $v_c$ ,  $\theta_c$ , and  $\underline{T}$  and for the height of trajectory  $\underline{Y}$  as they depend upon the three initial parameters  $\underline{c}$ ,  $v_0$ , and  $\theta_0$  (2). As applied to the passive section of the trajectory of a rocket the initial values will be:  $c_k$ ,  $v_k$ , and  $\theta_k$ , where

$$c_k = cH(y_k).$$

In this connection one must recall that the initial values of the tables:  $\underline{X}$ ,  $v_c$ ,  $\theta_c$ ,  $\underline{T}$  -- will correspond in this case not to the point of fall  $C'$ , but to the point  $\underline{C}$  where the trajectory intersects with the horizon of the end of the active section of the trajectory (Figure 7.2).

In order to determine the elements of the point of fall, it is necessary in addition to calculate the section of the trajectory  $CC'$ .

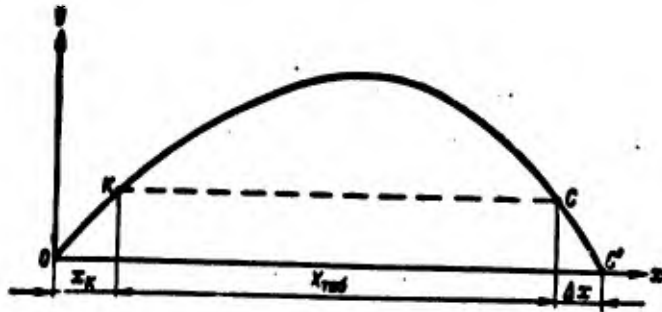


Figure 7.2. Constituents of full range.

Inasmuch as the extent of this section is not great, the elements of the point of fall can be calculated in accordance with approximate formulas secured by expansion in series of the functions  $\underline{v}$ ,  $\theta$ , and  $\underline{y}$  over the stages  $\Delta x = x_c - x_e$ . For the  $\underline{y}$  ordinates we secure the following relationship:

$$y_K = \Delta x \operatorname{tg} |\theta_c| + \frac{g \Delta x^2}{2v_c^2 \cos^2 \theta_c} + \frac{g \Delta x^2 c}{3v_c^3 \cos^3 \theta_c} O(v_c).$$

The last term in the right-hand arm can ordinarily be disregarded, and the quantity  $\Delta x$  can be determined from the expression

$$\Delta x = -\frac{A \operatorname{tg} |\theta_c|}{2} + \sqrt{\frac{A^2 \operatorname{tg}^2 \theta_c}{4} + A y_K}, \quad (7.40)$$

where

$$A = \frac{2v_c \cos^3 \theta_c}{g}.$$

The full range of the rocket will be determined from the expression

$$X_{\text{total}} = x_K + X_{\text{tab}} + \Delta x,$$

where  $X_{\text{tab}}$  is determined in accordance with the ballistic collection and  $\Delta x$  in accordance with formula (7.40).

#### BIBLIOGRAPHY

1. Gantmacher, F. R., and Levin, L. M., Theory of Flight of Unguided Rockets, Fizmatgiz Publishing House, 1959.
2. Shapiro, Ya. M., External Ballistics, Oborongiz Publishing House, 1946.

## CHAPTER VIII. PLANE OSCILLATIONS AND DISPERSION OF FINNED UNGUIDED ROCKETS

### 8.1. Factors Determining Dispersion of Unguided Rockets

Dispersion of unguided rockets considerably exceeds dispersion of artillery shells in fire over an identical range. This relates particularly to flank dispersion. It is customary to evaluate dispersion in fire by the magnitudes of probable or mean deflections of shells in a flank direction ( $B_b$ ) and in range ( $B_d$ ). A central strip of the ellipse of dispersion having a breadth of  $2B_d$  will contain 50 percent of all falls. The same applies to the central strip of an ellipse of dispersion having a length of  $2B_b$ .

If the quantities  $B_b$  and  $B_d$  relate to range of fire, then the dispersion of artillery shells can as a mean be characterized by the quantities:

$$\frac{B_b}{X} \approx \frac{1}{200}; \quad \frac{B_d}{X} \approx \frac{1}{250}$$

Unguided rockets used during World War II are characterized by the mean values:

$$\frac{B_b}{X} \approx \frac{1}{50}; \quad \frac{B_d}{X} \approx \frac{1}{50}$$

at maximum range of fire. The causes of the considerable augmentation in dispersion of unguided rockets as compared with artillery shells will be analyzed on the basis of the example of unguided finned rockets. The departure of an artillery shell from the bore of a gun is accompanied by initial disturbances occasioning oscillation of the axis of the projectile having a maximum amplitude of 5 percent. These oscillations provoke the appearance of a flank aerodynamic force inclining the vector of initial velocity from the plane of fire. The initial disturbances referred to are a random character and together with aiming errors they produce flank dispersion of shells. But the mean magnitude of angular deflection of the

vector of velocity comes to very little (approximately 1/2000), which produces small flank dispersion of artillery shells. The motion of unguided rockets along the guides is also accompanied by initial disturbances producing oscillation of the axis of the rocket with an amplitude of the same order as in artillery shells. But in this case the oscillations of the axis of the rocket provoke the appearance not only of flank aerodynamic force, but also of a flank constituent reactive force. The latter exceeds by many times the flank aerodynamic force, something which leads to substantial increase in the angular deflection of the vector of velocity. An important factor which increases the dispersion of unguided rockets is the presence of eccentricity of the reactive force. With ideal symmetry of the rocket the vector of the reactive force is directed along the axis of the rocket. Under real circumstances a skewing of the reactive force develops, and the line of its operation deflects from the center of mass of the rocket by a quantity  $\Delta$ , called the eccentricity of reactive force. The moment  $M_r$  of reactive force, evoked by this eccentricity, relative to the center of mass of the rocket increases the oscillation of the axis of the rocket and as a consequence, the angular dispersion of the rocket.

In addition to eccentricity of reactive force, disturbances upon the departure of the rocket from the guide, provoked by imprecision in the manufacture of the latter and by vibrations of the launch stand as the rocket moves along the guide, also influence the angular dispersion of rockets. The factors referred to provoke initial oscillations of the axis of the rocket upon its departing from the guide, and these are characterized by an angle  $\varphi_0$  between the axis of the rocket and the undisturbed position of the axis of the guide, and also by angular velocity  $\dot{\varphi}_0$ .

In addition to the disturbance factors referred to above, the force of gravity affects the deflection of the vector of velocity. But considering that the operation of the force of gravity is of a systematic character and does not in practice affect the dispersion of rockets, we shall examine from here on plane oscillations of rockets without taking this force into account. In particular, it is possible to examine plane oscillations of a rocket in the horizontal plane which arise through the undisturbed position of the axis of the guide.

## 8.2. Motion of the Rocket Along the Guide

During the time of motion along the guiding launch apparatus the rocket takes on a velocity  $v_0$  necessary for its stable flight over the active part of the trajectory. In this connection it is desirable that the design of guides should make it possible to reduce to a minimum the disturbance factors which provoke deflection of the rocket from the axis of the guide ( $\varphi_0$ ) and appearance of an angular velocity ( $\dot{\varphi}_0$ ) of rotation of the rocket about an axis perpendicular to the axis of symmetry of the rocket. The quantities  $\varphi_0$  and  $\dot{\varphi}_0$  (along with the moment from the eccentricity of the reactive force) are the initial disturbances which determine oscillation of the rocket on the active section of the trajectory, and dispersion of rockets. The design of the guides may be in the form of

tubes, chutes, or runners, along which the guiding slides of the rocket run. Launch apparatus may be of two types as regards the character of the connection between the rocket and the guide. One may refer to apparatus of the first type the guide runner, to which the rocket is hung by two slides. After the first slide comes free, the head part of the rocket is in a position to drop, turning around the rear slide (Figure 8.1). When this occurs point X of contact of the rocket with the guide, remaining stationary relative to the rocket, slides relative to the guide. One may include with the same type also a guide along which a rocket moves, contacting it with two cylindrical centering bands. After the first centering band departs, contact with the guide takes place at a single point, stationary relative to the rocket (Figure 8.2).

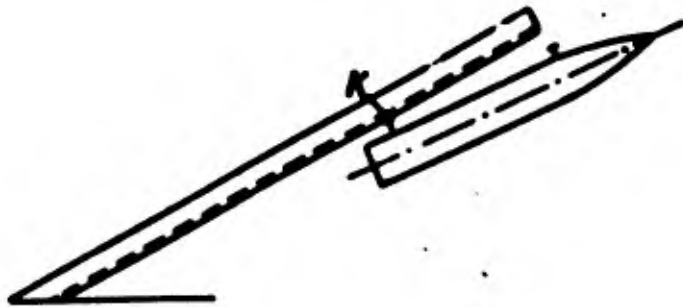


Figure 8.1. Diagram of suspension of rocket to guide of first type.

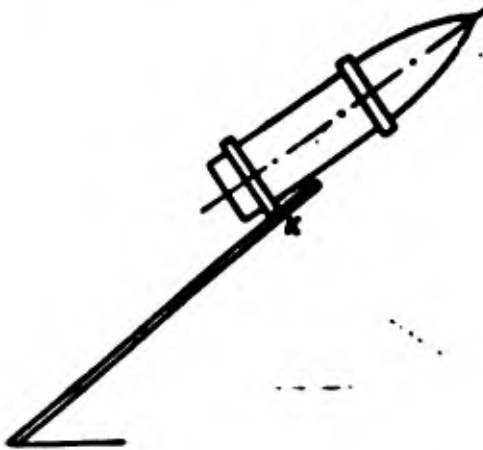


Figure 8.2. Contact of rocket with guide via centering bands.

An apparatus of the second type is the guide along which the rocket moves sliding on the cylindrical part of its body without protruding parts. After the center of gravity of the rocket passes the forward section of the guide the head part of the rocket commences to drop. When this occurs rotation of the rocket takes place around the point of contact, stationary relative to the guide (Figure 8.3). Launch apparatus of the first type are the more widespread.

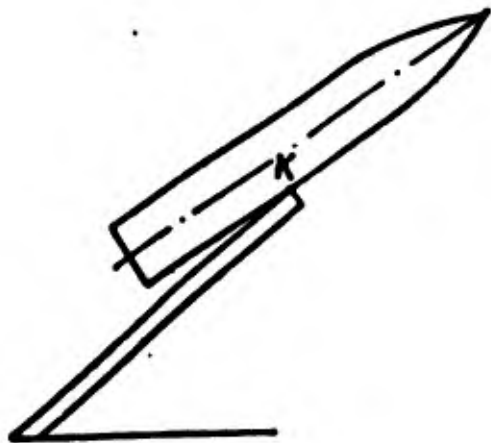


Figure 8.3. Diagram of guide of second type.

Launch Apparatus of the First Type

Let us examine the motion of a rocket along the guide of a launch apparatus of the first type, after the forward contact has been freed.

In Figure 8.4 C is the center of mass of the rocket; K is the point of contact between the rocket and the guide, which for simplicity's sake we shall assume to be lying on the axis of the rocket. We project axis Kx parallel to the axis of the guide, and axis Ky perpendicular to it. We designate by  $\theta_0$  the angle of inclination of the guide to the horizon, and by  $\varphi$  the angle of inclination of the axis of the rocket to the Kx axis. We designate  $l$  as equal to KC.

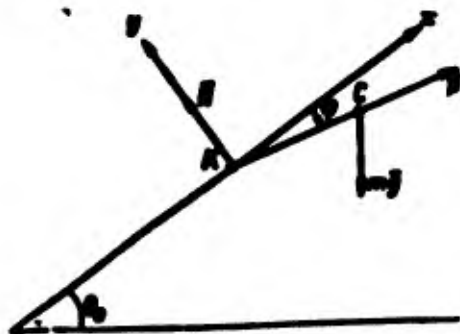


Figure 8.4. Motion of rocket relative to guide of first type.

Let us write equations for motion of the center of mass of the rocket:

$$m\ddot{x}_c = P \cos \varphi - mg \sin \theta_0; \quad (8.1)$$

$$m\ddot{y}_c = N - P \sin \varphi - mg \cos \theta_0. \quad (8.2)$$

where  $N$  is the reaction on the part of the guide at the point of contact.

We shall consider mass  $\underline{m}$  and thrust  $\underline{P}$  as being constant.

Let us write an equation for rotation of the rocket around its center of mass. In doing this we shall take into account the moment of reaction,  $N$ , and the moment from the eccentricity of reactive force,  $M_\Delta$ .

The equation will assume the following form:

$$A\ddot{\varphi} = M_\Delta + Nl \cos \varphi, \quad (8.3)$$

where  $A$  is the equatorial moment of inertia of the rocket;  
 $\underline{l}$  is the distance from the center of mass of the rocket to the rear slide.

From here on, considering the smallness of the angle  $\varphi$ , we shall adopt

$$\sin \varphi \approx \varphi; \quad \cos \varphi \approx 1.$$

In addition, we shall exclude the reaction from equations (8.2) and (8.3). When this is done we secure the following equations:

$$\ddot{x}_c = \frac{P}{m} - g \sin \theta_0 = f; \quad (8.4)$$

$$A\ddot{\varphi} = M_\Delta + lP\varphi + mgl \cos \theta_0 + lm\ddot{y}_c. \quad (8.5)$$

For an ideally rectilinear and stationary guide we have:

$$y_h = 0; \quad y_c = -l\varphi.$$

Taking into account possible curvature of the guide and vibration of the launch apparatus, let us write an expression for  $y_c$  in the form

$$y_c = y_h - l\varphi, \quad (8.6)$$

where  $y_h = y_h(t)$  will be regarded as a function determined experimentally or theoretically with the design and dynamic characteristics of the launch apparatus taken as point of departure. From equations (8.5) and (8.6) we secure

$$(A + ml^2)\ddot{\varphi} = lP\varphi + mgl \cos \theta_0 + M_\Delta + lm\ddot{y}_h \quad (8.7)$$

or finally

$$\ddot{\varphi} - \lambda^2\varphi = f(t), \quad (8.8)$$

where

$$\lambda^2 = \frac{lp}{A + ml^2}; \quad (8.9)$$

$$f(t) = \frac{1}{A + ml^2} [mgl \cos \theta_0 + M_\lambda + lm\ddot{y}_k]. \quad (8.10)$$

If the function  $y_K = y_K(t)$  is known, then by double differentiation it is possible to determine  $\ddot{y}_K$ , and the right-hand arm of equation (8.8) will be a known function of time. At the same time, equation (8.4) makes it possible to determine the relationship

$$x_c(t) = \frac{1}{2} \beta^2$$

and the value  $t_0$  corresponding to the end of the period of motion of the rocket along the guide.

The solution of equation (8.8) without the right-hand arm has the form

$$\varphi = c_1 e^{\lambda t} + c_2 e^{-\lambda t}.$$

Applying the methods of variation of an arbitrary constant, we secure for the nonhomogeneous equation (8.8) the following relationship:

$$\varphi = c_1 e^{\lambda t} + c_2 e^{-\lambda t} + \frac{e^{\lambda t}}{2\lambda} \int_0^t e^{-\lambda t} f(t) dt - \frac{e^{-\lambda t}}{2\lambda} \int_0^t e^{\lambda t} f(t) dt. \quad (8.11)$$

Let us examine the particular case of the motion of a rocket in a stationary rectilinear guide without taking into account the moment provoked by eccentricity of the reactive force. In this case

$$\begin{aligned} M_\lambda &= 0; \quad \ddot{y}_k = 0; \\ f(t) &= \frac{mgl \cos \theta_0}{A + ml^2} = \text{const} = B. \end{aligned} \quad (8.12)$$

From equation (8.11) we secure

$$\varphi = c_1 e^{\lambda t} + c_2 e^{-\lambda t} + \frac{B}{\lambda^2} (\text{ch } \lambda t - 1). \quad (8.13)$$

We shall start from the following initial conditions for the instant when the forward slide departs from the guides:

$$t_1 = 0; \quad \varphi_1 = 0; \quad \dot{\varphi}_1 = 0.$$

Under these circumstances it is not difficult to secure arbitrary constants  $c_1 = 0$ ;  $c_2 = 0$ , and expression (8.13) assumes the form

$$\varphi = \frac{B}{\lambda^2} (\operatorname{ch} \lambda t - 1).$$

Substituting the values  $B$  and  $\lambda$  from expressions (8.9) and (8.12), we secure

$$\varphi = \frac{mg \cos \theta_0}{P} (\operatorname{ch} \lambda t - 1). \quad (8.14)$$

Differentiating the last expression, we secure a relationship for angular velocity  $\dot{\varphi}$  of rotation of the axis of the rocket

$$\dot{\varphi} = \frac{mg \cos \theta_0}{P} \lambda \operatorname{sh} \lambda t. \quad (8.15)$$

In expressions (8.14) and (8.15) time was counted from the instant the forward slide left the guide. If the time count is from the start of motion of the rocket, it is necessary to replace  $t$  by  $t - t_1$ , where  $t_1$  is the interval of time from the start of motion of the rocket to the instant the first slide is freed. For the instant  $t_0$  of cessation of the connection of the rocket with the guide we get:

$$\varphi_0 = \frac{mg \cos \theta_0}{P} [\operatorname{ch} \lambda (t_0 - t_1) - 1]; \quad (8.16)$$

$$\dot{\varphi}_0 = \frac{mg \cos \theta_0}{P} \lambda \operatorname{sh} \lambda (t_0 - t_1). \quad (8.17)$$

The values  $t_0$  and  $t_1$  are determined from the expressions

$$t_0 = \sqrt{\frac{2x_0}{j}}; \quad t_1 = \sqrt{\frac{2x_1}{j}},$$

where  $x_1$  and  $x_0$  are the displacement of the center of mass of the rocket up to the freeing of the forward and of the rearward slides respectively:

$$j = \frac{P}{m} - g \cos \theta_0$$

At the instant  $t_0$  the constituent of the velocity of the center of mass of the rocket along axis  $y$  is equal to

$$-y_0 = b \dot{\varphi}_0$$

and the vector of velocity will turn over an angle  $\Delta \theta$ , determined from the expression

$$\operatorname{tg} \Delta \theta \approx \Delta \theta = \frac{b \dot{\varphi}_0}{v_0}.$$

Under these circumstances the angle of attack  $\alpha_0$ , formed by the axis of the rocket with the vector of velocity  $\bar{v}_0$ , will be determined from the expression  $\alpha_0 = \varphi_0 - \Delta\theta_0$ .

Example. The characteristics of the rocket and the guide are determined by the following parameters:  $Q = 194$  kg;  $P = 3,040$  kg;  $l = 1$  m;  $x_1 = 1.5$  m;  $x_0 = 2.8$  m;  $A = 14$  kg  $\cdot$  m  $\cdot$  sec<sup>2</sup>;  $j = 152$  m/sec<sup>2</sup>.

We determine

$$\lambda = \sqrt{\frac{Pl}{A + ml^2}} = \sqrt{\frac{3040 \cdot 1}{14 + \frac{194}{9,81} \cdot 1}} = 9,5 \text{ 1/sec};$$

$$t_0 = \sqrt{\frac{2x_0}{j}} = \sqrt{\frac{2 \cdot 2,8}{152}} = 0,192 \text{ sec};$$

$$t_1 = \sqrt{\frac{2x_1}{j}} = \sqrt{\frac{2 \cdot 1,5}{152}} = 0,140 \text{ sec};$$

$$t_0 - t_1 = 0,052 \text{ sec};$$

$$\lambda(t_0 - t_1) = 9,5 \cdot 0,052 = 0,495;$$

$$\text{ch } \lambda(t_0 - t_1) = 1,125;$$

$$\text{sh } \lambda(t_0 - t_1) = 0,515;$$

$$\varphi_0 = \frac{Q \cos \theta_0}{P} [\text{ch } \lambda(t_0 - t_1) - 1] = \frac{194 \cdot 0,707}{3040} \cdot 0,125 = 0,0056 \text{ radians} = 0,032^\circ = 19';$$

$$\dot{\varphi}_0 = \frac{Q \cos \theta_0}{P} \lambda \text{sh } \lambda(t_0 - t_1) = \frac{194 \cdot 0,707}{3040} \cdot 9,5 \cdot 0,515 = 0,312 \text{ 1/sec};$$

$$\Delta\theta_0 = \frac{\dot{\varphi}_0}{v_0} = \frac{\dot{\varphi}_0}{jt_0} = \frac{1 \cdot 0,312}{152 \cdot 0,192} = 0,0107 \text{ radians} = 0,006^\circ = 3,6';$$

$$\alpha_0 = \varphi_0 - \Delta\theta_0 = 0,032 - 0,006 = 0,026^\circ = 15,4'.$$

#### Launch Apparatus of Second Type

In launch apparatus of the second type the point of contact remains stationary relative to the guide. In this case the distance from the center of gravity of the rocket to the point of contact is equal to  $x_c - x_c'$ , where  $x_c'$  is the course of the center of mass of the rocket from the start of its motion and up to its passing the end of the guide. In equation (8.3) it is necessary to replace  $l$  with  $x_c - x_c'$ . After eliminating reaction in the contact and substituting

$$y_c = y_h - (x_c - x_c') \varphi$$

we secure an equation for angle  $\varphi$  in the form

$$\frac{A + m(x_c - x_c')^2}{x_c - x_c'} \ddot{\varphi} = \frac{M_\Delta}{x_c - x_c'} - 2m\dot{x}_c\dot{\varphi} + mg \cos \theta_0 + mg\varphi \sin \theta_0 \quad (8.18)$$

where  $x_c$  and  $\dot{x}_c$  are determined from equation (8.4).

\* Equation (8.18) can be integrated numerically.

In the case where  $M_\Delta = 0$ , from evaluation of the coefficients of equations (8.7) and (8.18) it follows that turning of the rocket,  $\varphi_0$ , under operation of the force of gravity is less for launch apparatus of the second type as compared with this quantity for launch apparatus of the first type.

### 8.3. Differential Equations of Plane Oscillation of the Rocket in the Active Part of the Trajectory

In formulating equations of plane oscillations of a rocket we shall consider

- reactive force  $P$ ;
- frontal resistance  $X = \frac{\rho v^2}{2} S c_x$ ;
- lifting (flank) aerodynamic force  $Y = \frac{\rho v^2}{2} S c_y \alpha$ ;
- aerodynamic stabilizing moment  $M_\Delta = -\frac{\rho v^2}{2} S L m_\Delta^* \alpha$ ;
- aerodynamic damping moment  $M_D = -\rho v S L^2 m_D^* \dot{\varphi}$ ;
- the moment  $M_\Delta = P_\Delta$ , provoked by eccentricity of reactive force.

In the expressions derived  $\varphi$  is the angle of turning of the axis of the rocket from the axis of undisturbed position of the vector of initial velocity;  $\alpha$  is the angle of attack. From here on we shall further introduce into our examination the angle  $\psi$  of deflection of the vector of velocity from its initial undisturbed position. Between angles  $\varphi$ ,  $\psi$ , and  $\alpha$  an obvious relationship exists (Figure 8.5):

$$\varphi = \psi + \alpha$$

The differential equations for motion of the rocket have the following form:

$$m\dot{v} = P \cos \alpha - X; \quad (8.19)$$

$$m v \dot{\psi} = P \sin \alpha - Y; \quad (8.20)$$

$$A \ddot{\varphi} = M + M_\Delta + M_D. \quad (8.21)$$



Figure 8.5. The angle determining oscillation of a rocket.

From here on we shall assume that  $\alpha$  is a small quantity, so that

$$\cos \alpha \approx 1; \quad \sin \alpha \approx \alpha.$$

The fundamental investigations carried out in study (1) show that the basic factors determining oscillation of the axis of a rocket are reactive force  $P$ , moment  $M_x$  and stabilizing aerodynamic moment  $M_z$ . The remaining forces entering into equations (8.19)-(8.21) are of secondary significance. From here on we shall examine oscillations of the axis of a rocket under the operation of the basic forces referred to. In this connection equations (8.19)-(8.21) assume the form:

$$\dot{v} = \frac{P}{m} = b, \quad (8.22)$$

$$\dot{\psi} = \frac{P\alpha}{mv} = \frac{b}{v} \alpha; \quad (8.23)$$

$$\ddot{\psi} = \frac{P\Delta}{A} - \frac{\rho v^2}{2A} S L m_z^2 \cdot \alpha = a - \sigma^2 v^2 \alpha, \quad (8.24)$$

where

$$\frac{P}{m} = b; \quad \frac{m\Delta}{A} = a; \quad \sigma^2 = \frac{\rho S L m_z^2}{2A}.$$

In study (1) it is shown that in investigation of oscillation of the axis of a rocket and of angular deflection of the vector of velocity it is possible to adopt coefficients  $a$ ,  $b$ , and  $\sigma$  as constants.

Considering that  $\varphi = \psi + \alpha$  we transform equation (8.24):

$$\ddot{\alpha} = a - \sigma^2 v^2 \alpha - \ddot{\psi}.$$

The quantity  $\ddot{\psi}$  is determined from equations (8.22) and (8.23):

$$\ddot{\psi} = -\frac{b}{v^2} \dot{v} \alpha + \frac{b}{v} \dot{\alpha} = -\frac{b^2}{v^2} \alpha + \frac{b}{v} \dot{\alpha}$$

When this is done equation (8.24) assumes the form

$$\ddot{a} + \frac{b}{v} \dot{a} + \left( v^2 - \frac{b^2}{v^2} \right) a = ha. \quad (8.25)$$

#### 8.4. Oscillation of a Rocket in the Presence of Eccentricity of Reactive Force

We shall examine the oscillation of a rocket in the presence of only one disturbance fact -- eccentricity of the reactive force  $\Delta$ , forming part of the right-hand arm of equation (8.25). In this connection it is assumed that initial disturbances upon the departure of the rocket from the guide are absent, and equations (8.23)-(8.25) are to be integrated with initial conditions:

$$t = t_0; \quad v = v_0; \quad a_0 = 0; \quad \dot{a}_0 = 0; \quad \psi_0 = 0.$$

For integration of equation (8.25) it is convenient to shift to the independent variable

$$x = as,$$

where  $\underline{s}$  is the length of the arc of the trajectory of the center of mass of the rocket. We introduce the substitutions:

$$y = \frac{v}{a} \alpha; \quad z = \frac{v}{a} \psi.$$

It is not difficult to see that  $\underline{x}$ ,  $\underline{y}$  and  $\underline{z}$  are nondimensional quantities. From the expressions:

$$\frac{dy}{dx} = \frac{1}{a} \cdot \frac{da}{ds} = \frac{1}{av} \dot{a};$$

$$\dot{a} = av y'_x;$$

$$\ddot{a} = a \dot{v} y'_x + av y''_x \cdot \dot{x} = av y'_x + av^2 y''_x,$$

substituting the values  $\dot{a}$  and  $\ddot{a}$  in expression (8.25) and considering that with constancy of acceleration  $\underline{b}$

$$v = \sqrt{2bs} = \sqrt{\frac{2bx}{a}},$$

we shall secure equations (8.23) and (8.25) in the following form:

$$y''_x + \frac{1}{x} y'_x + \left( 1 - \frac{1}{4x^2} \right) y = \frac{1}{2x}, \quad (8.26)$$

$$z'_x = \frac{1}{2x} y. \quad (8.27)$$

From here on we shall distinguish with an apostrophe (') the derivative in accordance with  $x$ . Every differential equation of the form

$$y' + f(x)y' + \varphi(x)y = 0$$

may be reduced to a two-term form through substitution

$$y = ue^{-\frac{1}{2} \int f(x) dx}$$

In the present case this substitution has the form\*

$$y = \frac{u}{\sqrt{x}}. \quad (8.28)$$

Substitution into equation (8.26) the values  $y$ ,  $y'$ , and  $y''$ , we secure after simple transformations

$$u'' + u = \frac{1}{2\sqrt{x}}. \quad (8.29)$$

The integral of the homogeneous equation

$$u'' + u = 0 \quad (8.30)$$

has the form

$$u = c_1 \cos x + c_2 \sin x. \quad (8.31)$$

Applying the method of variation of arbitrary constants, we secure the following differential equations for  $c_1$  and  $c_2$ :

$$\begin{aligned} c_1' \cos x + c_2' \sin x &= 0; \\ -c_1' \sin x + c_2' \cos x &= \frac{1}{2\sqrt{x}}. \end{aligned}$$

Determining the values  $c_1'$  and  $c_2'$ , we shall secure:

$$\begin{aligned} c_1' &= -\frac{\sin x}{2\sqrt{x}}; \quad c_2' = \frac{\cos x}{2\sqrt{x}}; \\ c_1 &= -\int_{x_0}^x \frac{\sin x}{2\sqrt{x}} dx + c_{10}; \quad c_2 = \int_{x_0}^x \frac{\cos x}{2\sqrt{x}} dx + c_{20}. \end{aligned}$$

---

\* This substitution is distinguished only as regards the constants from the substitution  $u = v_a$ , first introduced in study (1).

Substituting the values  $c_1$  and  $c_2$  into equation (8.31) and taking into account substitution (8.28) and the initial conditions  $x = x_0$ ,  $y_0 = 0$ , and  $y'_0 = 0$ , we shall secure

$$y = -\frac{\cos x}{2\sqrt{x}} \int_{x_0}^x \frac{\sin x}{\sqrt{x}} dx + \frac{\sin x}{2\sqrt{x}} \int_{x_0}^x \frac{\cos x}{\sqrt{x}} dx \quad (8.32)$$

Introducing the Frenelle integral, determined by the equations

$$s(x) = \frac{1}{\sqrt{2x}} \int_0^x \frac{\sin x}{\sqrt{x}} dx, \quad (8.33)$$

$$c(x) = \frac{1}{\sqrt{2x}} \int_0^x \frac{\cos x}{\sqrt{x}} dx, \quad (8.34)$$

and designating for brevity's sake

$$C = c(x); \quad C_0 = c(x_0); \quad C'_0 = c(x) - c(x_0);$$

$$S = s(x); \quad S_0 = s(x_0); \quad S'_0 = s(x) - s(x_0),$$

we shall secure equation (8.32) in the form

$$y = \sqrt{\frac{x}{2}} \left( \frac{\sin x}{\sqrt{x}} C'_0 - \frac{\cos x}{\sqrt{x}} S'_0 \right). \quad (8.35)$$

The substitution

$$y = \frac{e}{a} \alpha = -\frac{eA}{m\Delta} \alpha$$

reduces expression (8.35) to the form

$$\alpha = \frac{m\Delta}{eA} \sqrt{\frac{x}{2}} \left( \frac{\sin x}{\sqrt{x}} C'_0 - \frac{\cos x}{\sqrt{x}} S'_0 \right). \quad (8.36)$$

Expression (8.36) makes it possible to determine the angle of attack for any value  $x = es$ , if the parameters of the rocket  $e$ ,  $A$ ,  $m$  and the eccentricity of the reactive force  $\Delta$  are known.

Values for the Frenelle integrals  $c(x)$  and  $s(x)$  are given in Table 8.1. Graphs of these functions are shown in Figure 8.6.

In order to determine the deflection of the vector of velocity  $\phi$ , one must substitute in equation (8.27) the value  $y$  from equation (8.35). On doing this we secure

Table 8.1. Frenelle Integrals

$x$	$s(x)$	$c(x)$	$x$	$s(x)$	$c(x)$	$x$	$s(x)$	$c(x)$
0,1	0,0084	0,2521	5,1	0,4492	0,3343	10,1	0,6011	0,4268
2	0,0237	0,3554	2	0,4333	0,3418	2	0,5928	0,4174
3	0,0431	0,4331	3	0,4183	0,3507	3	0,5836	0,4090
4	0,0665	0,4966	4	0,4045	0,3610	4	0,5737	0,4015
5	0,0924	0,5502	5	0,3918	0,3724	5	0,5632	0,3951
6	0,1205	0,5962	6	0,3805	0,3850	6	0,5521	0,3898
7	0,1504	0,6356	7	0,3706	0,3985	7	0,5406	0,3857
8	0,1818	0,6693	8	0,3621	0,4129	8	0,5288	0,3827
9	0,2143	0,6979	9	0,3552	0,4278	9	0,5168	0,3809
1,0	0,2476	0,7217	6,0	0,3499	0,4433	11,0	0,5048	0,3804
1	0,2813	0,7410	1	0,3461	0,4591	1	0,4928	0,3810
2	0,3153	0,7563	2	0,3440	0,4750	2	0,4810	0,3829
3	0,3491	0,7676	3	0,3434	0,4909	3	0,4695	0,3859
4	0,3826	0,7751	4	0,3445	0,5067	4	0,4584	0,3900
5	0,4155	0,7791	5	0,3471	0,5220	5	0,4478	0,3952
6	0,4475	0,7798	6	0,3512	0,5372	6	0,4378	0,4013
7	0,4785	0,7773	7	0,3568	0,5517	7	0,4286	0,4084
8	0,5081	0,7719	8	0,3637	0,5654	8	0,4201	0,4164
9	0,5363	0,7639	9	0,3718	0,5782	9	0,4125	0,4251
2,0	0,5629	0,7533	7,0	0,3812	0,5901	12,0	0,4059	0,4346
1	0,5876	0,7405	1	0,3916	0,6009	1	0,4014	0,4446
2	0,6103	0,7256	2	0,4030	0,6106	2	0,3955	0,4550
3	0,6310	0,7089	3	0,4152	0,6190	3	0,3920	0,4658
4	0,6496	0,6906	4	0,4281	0,6261	4	0,3895	0,4769
5	0,6658	0,6710	5	0,4415	0,6319	5	0,3882	0,4882
6	0,6797	0,6503	6	0,4553	0,6362	6	0,3880	0,4994
7	0,6913	0,6287	7	0,4695	0,6391	7	0,3890	0,5106
8	0,7005	0,6064	8	0,4837	0,6406	8	0,3910	0,5216
9	0,7073	0,5838	9	0,4979	0,6407	9	0,3941	0,5322
3,0	0,7117	0,5610	8,0	0,5120	0,6393	13,0	0,3933	0,5425
1	0,7138	0,5383	1	0,5258	0,6366	1	0,4034	0,5523
2	0,7136	0,5158	2	0,5392	0,6325	2	0,4095	0,5615
3	0,7112	0,4938	3	0,5520	0,6271	3	0,4164	0,5700
4	0,7067	0,4725	4	0,5641	0,6206	4	0,4241	0,5777
5	0,7002	0,4521	5	0,5755	0,6129	5	0,4325	0,5846
6	0,6918	0,4326	6	0,5859	0,6041	6	0,4415	0,5906
7	0,6816	0,4144	7	0,5954	0,5944	7	0,4510	0,5956
8	0,6699	0,3975	8	0,6038	0,5839	8	0,4610	0,5997
9	0,6566	0,3821	9	0,6111	0,5727	9	0,4713	0,6027
4,0	0,6421	0,3682	9,0	0,6172	0,5608	14,0	0,4818	0,6047
1	0,6265	0,3560	1	0,6220	0,5485	1	0,4924	0,6057
2	0,6099	0,3456	2	0,6256	0,5358	2	0,5030	0,6055
3	0,5926	0,3369	3	0,6279	0,5229	3	0,5135	0,6043
4	0,5748	0,3302	4	0,6289	0,5099	4	0,5236	0,6021
5	0,5565	0,3253	5	0,6286	0,4969	5	0,5337	0,5989
6	0,5380	0,3222	6	0,6270	0,4841	6	0,5433	0,5947
7	0,5196	0,3211	7	0,6241	0,4716	7	0,5524	0,5896
8	0,5013	0,3218	8	0,6200	0,4595	8	0,5609	0,5836
9	0,4834	0,3242	9	0,6148	0,4480	9	0,5687	0,5768
5,0	0,4659	0,3285	10,0	0,6084	0,4370	15,0	0,5758	0,5693

$$s = \frac{1}{2} \int_{x_0}^x \frac{y dx}{x} = \sqrt{\frac{\pi}{2}} \int_{x_0}^x \left( \frac{\sin x}{2x\sqrt{x}} C_0^2 - \frac{\cos x}{2x\sqrt{x}} S_0^2 \right) dx$$

Integrating termwise, we have

$$\begin{aligned} s = & \frac{1}{2} \sqrt{\frac{\pi}{2}} \int_{x_0}^x (\sin x \cdot C_0^2 - \cos x S_0^2) \frac{dx}{x\sqrt{x}} = \\ & -\frac{1}{2} \sqrt{\frac{\pi}{2}} \left\{ - \left[ \frac{2}{\sqrt{x}} (\sin x \cdot C_0^2 - \cos x \cdot S_0^2) \right]_{x_0}^x + \right. \\ & \left. + 2 \int_{x_0}^x \frac{1}{\sqrt{x}} [(\cos x \cdot C_0^2 + \sin x \cdot S_0^2) dx + \sin x dC_0^2 - \cos x dS_0^2] \right\}. \end{aligned} \quad (8.37)$$

On the basis of expressions (8.33) and (8.34) we have

$$\sin x dC_0^2 - \cos x dS_0^2 = 0$$

and

$$\frac{2}{\sqrt{x}} (\cos x C_0^2 + \sin x S_0^2) dx = \sqrt{2x} d[(C_0^2)^2 + (S_0^2)^2].$$

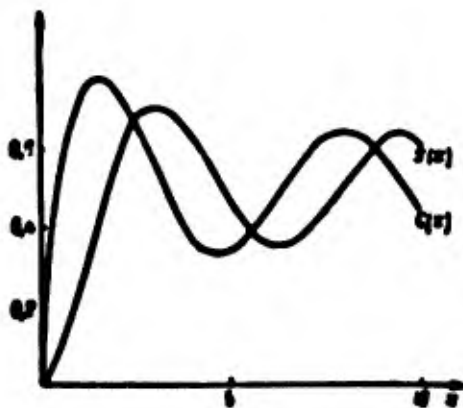


Figure 8.6. Frenelle integrals.

After some transformations expression (8.37) assumes the form

$$s_{\Delta} = \frac{\pi}{2} [(C_0^2)^2 + (S_0^2)^2] + \sqrt{\frac{\pi}{2x}} (S_0^2 \cos x - C_0^2 \sin x). \quad (8.38)$$

The index  $\Delta$  emphasizes the fact that the disturbance influence of the eccentricity of reactive force has been taken into account.

Taking into account the expression

$$s_{\Delta} = \frac{v}{g} \psi_{\Delta} = \frac{eA}{2g} \psi_{\Delta},$$

we secure finally

$$\psi_{\Delta} = \frac{\Delta m}{eA} \left\{ \frac{v}{2} [(C_0^2)' + (S_0^2)'] + \sqrt{\frac{v}{2x}} (S_0^2 \cos x - C_0^2 \sin x) \right\}. \quad (8.39)$$

Formula (8.39) makes it possible to reckon the deflection  $\psi_{\Delta}$  of the vector of velocity  $\bar{v}$  from its initial undisturbed position, as provoked by the influence of the eccentricity of the reactive force.

With angle of departure  $\theta_0$  and with the condition that eccentricity  $\Delta$  is perpendicular to the plane of fire, angular deflection of the latter is equal to  $\frac{\psi_{\Delta}}{\cos \theta_0}$ . If  $X$  is the full range of fire, the flank deflection of the point of fall  $\Delta z$  will be determined from expression

$$\Delta z = \frac{\psi_{\Delta}}{\cos \theta_0} X. \quad (8.40)$$

Inasmuch as eccentricity  $\Delta$  is a random quantity, we can examine a probable magnitude  $B_{\Delta}$  of eccentricity perpendicular to the plane of fire. Substituting in formulas (8.39) and (8.40)  $\Delta$  by  $B_{\Delta}$ , we secure the probable magnitude of angular deflection  $B_{\psi_{\Delta}}$  from expression (8.39) and the probable magnitude of flank dispersion from expression

$$B\Delta z = \frac{B_{\Delta}}{\cos \theta_0} X. \quad (8.41)$$

**Example.** Let us examine a rocket the characteristics of which are as follows:  $Q = 42.5$  kg;  $m_p = 7.2$  kg;  $Q_{cp} = Q - 0.25 m_p = 40.7$  kg;  $m_{cp} = 4.14$ ;  $s_0 = 5$  m;  $s = 148$  m;  $e = 0.0845$  1/M;  $A = 0.5$  kg · m/sec<sup>2</sup>. We shall examine the case where  $\Delta = 1$  mm =  $10^{-3}$  m.

We compute:

$$x = es = 0,0845 \cdot 150 = 12,50;$$

$$x_0 = e s_0 = 0,0845 \cdot 5 = 0,422.$$

From the table of Frenelle integrals we find:

$$c(x) = 0,4882; \quad c(x_0) = 0,5091; \quad C_0^2 = -0,1208;$$

$$s(x) = 0,3882; \quad s(x_0) = 0,0720; \quad S_0^2 = 0,3162;$$

$$\sin x = \sin 12,5 = \sin 1,99\pi = -\sin 0,01\pi = -0,0317;$$

$$\cos x = \cos 0,01\pi = 0,9985 \approx 1.$$

We substitute into expression (8.39):

$$\psi_{\Delta} = \frac{10^{-3} \cdot 4,14}{0,5 \cdot 0,0845} \left[ \frac{\pi}{2} (0,1209^{\circ} + 0,3162^{\circ}) - \sqrt{\frac{\pi}{2 \cdot 12,5}} (1 \cdot 0,3162 - 0,0317 \cdot 0,1209) \right] = 0,029 \text{ rad} = 1,66^{\circ} = 1^{\circ}40'.$$

Assuming that the angle of departure  $\theta_0 = 45^{\circ}$ , the probable magnitude of eccentricity  $B_{\Delta} = 0,5 \text{ mm}$ , and the full range of fire  $X = 10 \text{ km}$ , we secure the probable magnitude of flank dispersion from the expression

$$B\sigma = \frac{B_{\psi_{\Delta}}}{\cos \theta_0} X = \frac{0,5 \cdot 0,029}{0,707} 10000 = 200 \text{ m},$$

whence

$$\frac{B\sigma}{X} = \frac{1}{50}.$$

### 8.5. The Critical Section of the Trajectory

The character of change in angles  $\alpha$  and  $\phi$  along the trajectory depending on the flank eccentricity of reactive force for a typical unguided finned rocket are shown in Figure 8.7.

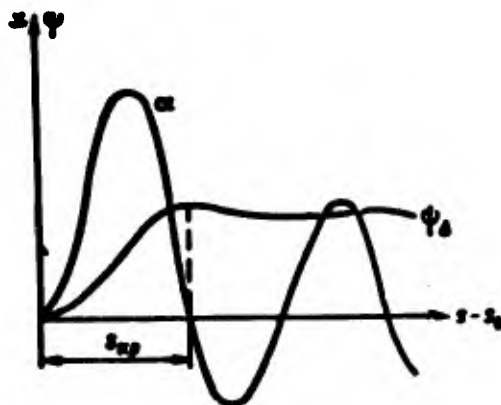


Figure 8.7. Oscillation of angles  $\alpha$  and  $\phi$  in the presence of eccentricity.

From examination of the graphs in Figure 8.7, it is apparent that the change in angle  $\alpha$  bears the character of diminishing oscillations. The length of the trajectory corresponding to the first half-wave of the oscillation of angle  $\phi$  is called the critical section of the trajectory. We shall designate the nondimensional length of the critical section as  $x_{cr} = s_{cr}$ . The first maximum of angle  $\phi$  corresponds to the value

$x = x_{cr}$ . Under these circumstances angle  $\alpha = 0$ , which follows directly from equation (8.23), since with  $\alpha = 0$  we secure  $\dot{\phi} = 0$ , corresponding to the condition of the extreme of function  $\phi(t)$ . The extent of the critical section comes to one-third of the active section of the trajectory. From what has been said it follows that the forming of the angular deflection of the vector of velocity, and consequently also of the angular dispersion, takes place basically in the critical section. At the beginning of this section the velocity of the rocket is low, and consequently the stabilizing aerodynamic moment is low. Under these circumstances, under the operation of moment from the eccentricity of reactive force a considerable deflection of the axis takes place and the flank constituent of reactive force increases, which leads to deflection of the vector of velocity. Subsequently increase of stabilizing moment approximately balances the influence of eccentricity of reactive force, and change in angle  $\phi$  possesses the character of small oscillations. The circumstance that with  $x > x_{cr}$  angle  $\phi_{\Delta}$  changes little makes it possible to simplify computation of the quantity  $\phi_{\Delta}$ , taking in place of  $x = x_k$ , corresponding to the end of the active section, the quantity  $x_{cr}$ . It is not difficult to show that the quantity  $x_{cr}$  depends only upon  $x_0$ . For this reason formula (8.38) can be replaced by a dependence in the form  $z_{\Delta} = f(x_0)$ . For  $z_{\Delta}$  the following interpolating formula may be proposed:

$$z_{\Delta} = \frac{0,2}{0,3 + x_0}, \quad (8.42)$$

whence

$$\psi_{\Delta} = \frac{\Delta m}{A_0} z_{\Delta} = \frac{\Delta m}{A_0} \cdot \frac{0,2}{0,3 + x_0}.$$

For the example examined above we have

$$\psi_{\Delta} = \frac{10^{-3} \cdot 4,14 \cdot 0,2}{0,5 \cdot 0,0845 (0,3 + 0,422)} = 0,027 \text{ radians.}$$

Formula (8.42) makes it possible to analyze directly the influence of various factors upon angular deflection  $\psi_{\Delta}$  of the vector of velocity. Considering that  $x_0 = \sigma s_0$ , where

$$\sigma = \sqrt{\frac{\rho a l m_2^a}{2A}}, \quad (8.43)$$

we come to the conclusion that the quantity  $\psi_{\Delta}$  declines: with decrease in eccentricity  $\Delta$ ; with increase of length  $s_0$  of the motion of the rocket along the guide; with increase of coefficient  $m_2^a$  of stabilizing moment, which is associated with increase of the area of the fins.

But it must be noted that increase of the length of the guides leads to substantial increase of the weight of the apparatus. Excessive increase in the area of the finds increases the sensitivity of the rocket to gusts

of wind, which may lead to increase of dispersion on the part of the rocket when the wind is gusty. Selection of design parameters of a rocket and of the launch apparatus is carried out with all the factors referred to taken into account.

### 8.6. Oscillation of a Rocket in the Presence of Initial Disturbances $\varphi_0$ and $\psi_0$

In order to study the influence of initial disturbances upon angular deflection of the axis of a rocket we shall assume that eccentricity  $\Delta$  is equal to zero. In this event it is necessary to assume in equation (8.25) that  $a = 0$ . The equations for oscillations of the axis of the rocket assume the following form:

$$\ddot{\alpha} + \frac{b}{\sigma} \dot{\alpha} + \left( \sigma^2 \omega^2 - \frac{b^2}{4\sigma^2} \right) \alpha = 0, \quad (8.44)$$

$$\dot{\psi} = \frac{b}{\sigma} \alpha \quad (8.45)$$

Shifting to the independent variable  $x = \sigma s$  makes it possible to transform the last equations into the following form:

$$\alpha'' + \frac{1}{x} \alpha' + \left( 1 - \frac{1}{4x^2} \right) \alpha = 0, \quad (8.46)$$

$$\psi' = \frac{1}{x} \alpha, \quad (8.47)$$

where the derivative according to  $x$  is designated by an apostrophe. Integration of the homogeneous equation (8.46) with the substitution

$$\alpha = \frac{\beta}{\sqrt{x}}$$

makes it possible to secure the general integral

$$\alpha = c_1 \frac{\cos x}{\sqrt{x}} + c_2 \frac{\sin x}{\sqrt{x}}, \quad (8.48)$$

where  $c_1$  and  $c_2$  are determined from the initial conditions. Let us examine separately the influences of initial disturbances  $\varphi_0$  and  $\psi_0$ .

The initial conditions are

$$\varphi_0 = 0 \quad \text{and} \quad \psi_0 \neq 0.$$

Let us express the initial conditions for  $\alpha$  and  $\dot{\psi}$  through the initial conditions for  $\varphi$ .

From expression

$$\eta_0 = \epsilon + \phi_0 = 0,$$

considering that

$$\dot{\phi} = \int \frac{a_n}{v} dt,$$

we have directly  $\dot{\phi}_0 = 0$  under any initial conditions for  $\epsilon$ . In this event, from the condition  $\eta_0 = 0$  it follows that  $\epsilon_0 = 0$ .

Furthermore, from the expression  $\dot{\eta}_0 = \dot{\epsilon}_0 + \dot{\phi}_0$ , taking into account the fact that

$$\dot{\eta}_0 = \frac{b}{a_0} \epsilon_0 = 0,$$

we secure the initial conditions for equations (8.46), (8.47) in the following form: with  $t = t_0$ ;  $x = x_0$ ;  $\epsilon_0 = 0$ ;  $\dot{\epsilon}_0 \neq 0$ ;  $\phi_0 = 0$ .

Starting from these initial conditions, we secure:

$$\epsilon_1 = -\dot{\epsilon}_0 \sqrt{x_0} \sin x_0;$$

$$\epsilon_2 = \dot{\epsilon}_0 \sqrt{x_0} \cos x_0,$$

and the expression for angle of attack  $\epsilon$  assumes the following form:

$$\epsilon = \dot{\epsilon}_0 \sqrt{x_0} \left( \cos x_0 \frac{\sin x}{\sqrt{x}} - \sin x_0 \frac{\cos x}{\sqrt{x}} \right). \quad (8.49)$$

Considering that

$$\dot{\epsilon}_0 = \dot{\epsilon}_0 \frac{1}{x_0} = \frac{\dot{\epsilon}_0}{\sqrt{2bx_0}},$$

we shall finally secure

$$\epsilon = \frac{\dot{\epsilon}_0}{\sqrt{2bx_0}} \frac{\sin(x-x_0)}{\sqrt{x}}. \quad (8.50)$$

The relationship secured makes it possible to determine the oscillation of the angle of attack depending on the nondimensional length of the arc of the trajectory  $\underline{x}$ . In order to determine the angle  $\phi$  of deflection of the vector of velocity, it is necessary to substitute the value secured for  $\epsilon$  in equation (8.47). On doing this we shall secure

$$\phi = \frac{a_0}{2\sqrt{2k}} \int_{x_0}^x \frac{\sin(x-x_0)}{x\sqrt{x}} dx$$

Integrating partially and considering that

$$\int_{x_0}^x \frac{\sin x dx}{x\sqrt{x}} = - \left[ \frac{2 \sin x}{\sqrt{x}} \right]_{x_0}^x + 2\sqrt{2k} C_0^2;$$

$$\int_{x_0}^x \frac{\cos x dx}{x\sqrt{x}} = - \left[ \frac{2 \cos x}{\sqrt{x}} \right]_{x_0}^x - 2\sqrt{2k} S_0^2.$$

after some transformations we shall secure

$$\phi_0 = \frac{a_0}{\sqrt{2k}} \left[ \sqrt{k} (\cos x_0 C_0^2 - \sin x_0 S_0^2) - \frac{\sin(x-x_0)}{\sqrt{x_0}} \right]. \quad (8.51)$$

The initial conditions are  $\varphi_0 \neq 0$ ;  $\dot{\varphi}_0 = 0$ .

We shall find the initial conditions for  $s$  and  $\phi$  by taking into account the fact that

$$\phi_0 = 0; \quad \dot{\phi}_0 = -\frac{b}{2k} a_0$$

In doing this we secure from the expression  $\varphi = s + \phi$ :

$$a_0 = -\dot{\phi}_0;$$

$$a_0' = -\dot{\phi}_0' = -\frac{b}{2k} a_0.$$

Finally, we secure the following initial conditions:

$$\text{with } t = t_0; \quad x = x_0; \quad a_0 = \varphi_0; \quad a_0' = -\frac{1}{2k} a_0; \quad \phi_0 = 0.$$

Determining the arbitrary constants in equation (8.48) and considering that

$$a_0' + \frac{1}{2k} a_0 = \varphi_0' = 0,$$

we secure

$$c_1 = a_0 \sqrt{x_0} \cos x_0;$$

$$c_2 = a_0 \sqrt{x_0} \sin x_0.$$

then the expression for the angle of attack assumes the following form:

$$\alpha = \alpha_0 \sqrt{\frac{x_0}{x}} \cos(x - x_0) \quad (8.52)$$

Substituting the value secured for  $\alpha$  into equation (8.47) we secure:

$$\dot{\phi} = \frac{\alpha_0 \sqrt{x_0}}{x} \int_{x_0}^x \frac{\cos(x - x_0)}{x \sqrt{x}} dx$$

Integrating termwise and considering that  $\phi_0 = \alpha_0$  we secure, after simple transformations,

$$\dot{\phi}_0 = \alpha_0 \left[ 1 - \sqrt{\frac{x_0}{x}} \cos(x - x_0) + \sqrt{2\pi x_0} (\sin x_0 C_1^* - \cos x_0 S_1^*) \right] \quad (8.53)$$

Formulas (8.51) and (8.52) make it possible to determine the angular deflections of the vector of velocity provoked by the initial disturbances  $\alpha_0$  and  $\phi_0$ . Typical graphs for changes in angles  $\alpha$  and  $\dot{\phi}$  are shown in Figures 8.8 and 8.9.

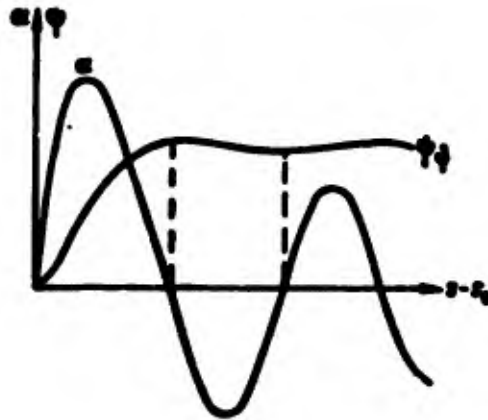


Figure 8.8. Oscillation of angles  $\alpha$  and  $\dot{\phi}$  with disturbance  $\phi_0$ .

From examination of these graphs it is apparent that a substantial rise in angle  $\dot{\phi}$  takes place only in the critical section of the trajectory. From there on, change in angle  $\dot{\phi}$  possesses the character of small oscillations. This makes it possible to simplify computation of angle  $\dot{\phi}_k$  for the end of the active section, substituting  $x_k = x_{cr}$ . As has already been shown in 8.5,  $x_{cr}$  is a function of  $x_0$ , for which reason one can regard  $\dot{\phi}_k$  as a function of  $x_0$ . Computations which have been carried out permit one to recommend the following formulas of interpolation in order to determine  $\dot{\phi}_k$  and  $\dot{\phi}_0$ :

$$\dot{\phi}_k = \frac{\dot{\phi}_0}{\sqrt{x_0}} \frac{0.6}{1 + 2x_0}; \quad (8.54)$$

$$\psi_{\infty} = \varphi_0 \frac{0,5}{0,7 + x_0} \quad (8.55)$$

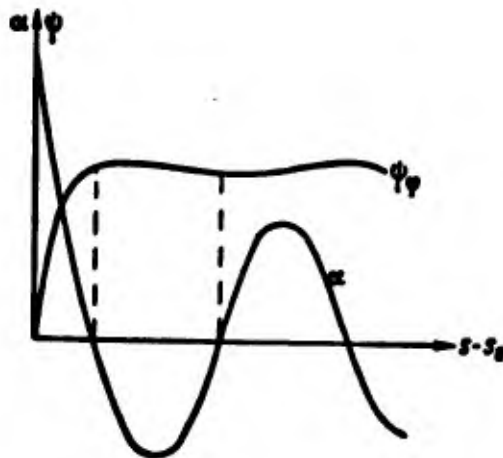


Figure 8.9. Oscillation of angles  $\alpha$  and  $\phi$  with disturbance  $\varphi_0$ .

For the example examined in 8.4 we have  $x_0 = 0.422$ ;  $b = 408 \text{ m/sec}^2$ ;  $\bullet = 0.0845 \text{ 1/m}$ .

Taking  $\varphi_0 = 0.002 \text{ rad}$ ,  $\dot{\varphi}_0 = 0.1 \text{ 1/sec}$ , we secure:

$$\psi_{\infty} = \frac{0,1}{\sqrt{408 \cdot 0,0845}} \cdot \frac{0,6}{1 + 2 \cdot 0,422} = 0,0055 \text{ radians};$$

$$\psi_{\infty} = \frac{0,002 \cdot 0,5}{0,7 + 0,422} = 0,0009 \text{ radians}.$$

In conclusion we may note that the relationships secured in 8.4-8.6, determining the oscillation of the axis of the rocket and of the vector of velocity in the plane perpendicular to the plane of fire can also be applied for the case of application of the axis of the rocket in the plane of fire. This is explained by the fact that the weight of the rocket has practically no effect upon oscillations of the axis of the rocket provoked by random disturbance factors.

### 8.7. Axial Rotation of Finned Rockets

In the flight of nonrotating rockets the flank moment provoked by eccentricity of reactive force retains its position stationary in space, which leads to considerable deflection of the vector of velocity. In order to reduce the influence of eccentricity of reactive force upon the dispersion of finned rockets they are given a slow axial rotation which periodically alters the direction of flank moment  $M_1$  and substantially reduces the angular deflection of the vector of velocity and the dispersion of the rockets. It has been said earlier that the disturbance effect of

eccentricity of reactive force takes place basically in the critical section of the trajectory. For this reason it is necessary that the rocket should complete several rotations around its axis in this initial part of the trajectory.

In this event angular velocity of the rocket proves to be relatively slight, tens of times less than the angular velocity necessary for gyroscopic stability of finless missiles and rockets. Finned rockets to which a slight rotation is communicated to reduce their dispersion are called rotating rockets.

For a rotating rocket the differential equation of oscillation of the axis of the rocket assumes the following form:

$$\ddot{\alpha} + \frac{b}{v} \dot{\alpha} + \left( \sigma^2 v^2 - \frac{b^2}{v^2} \right) \alpha = ba \cos \theta, \quad (8.56)$$

where  $\theta$  is the angle of turning of the plane of eccentricity. This equation is distinguished from expression (8.25) only through the presence of the multiplier  $\cos \theta$  in the right-hand arm. Integration of equation (8.56) together with equation (8.23) makes it possible to determine the deflection of the axis of a rotating rocket in the presence of eccentricity.

Computations show (2) that rotation reduces dispersion occasioned by eccentricity, proportionally to the number of rotations of the rocket in the critical section. But excessive increase of the angular velocity of a rocket increases initial disturbances upon the rocket's leaving the guide,  $\varphi_0$  and  $\varphi_0$ , which in the last analysis increases dispersion. This circumstance must be taken into account in selecting an optimum rotation for the rocket.

The most efficient method of a rocket's rotation is a method in which the rocket receives rotation in the launch apparatus itself, which is provided with spiral guides. The rocket rotates with constant angular velocity after its departure from the launch apparatus. In the event of reactive rotation of the rocket the rotational moment  $M_p$  can be determined from the expression

$$M_p = PR \sin \gamma,$$

where  $R$  is the radius of a circumference running through the centers of the outlet sections of inclined cones;

$\gamma$  is the angle of inclination of the cone to the plane of an angular section running through the critical section of the cone.

The equation for rotation of the axis of the rocket has the following form:

$$C \frac{d\gamma}{dt} = C\ddot{\theta} = PR \sin \gamma, \quad (8.57)$$

where  $\theta$  is the angle of the rocket's turning;  
 $r$  is the angular velocity of the rocket;  
 $C$  is the polar moment of inertia of the rocket.

Taking into account the equation of forward motion

$$m\dot{v} = P \cos \gamma,$$

one can write equation (8.57) thus:

$$dr = k dv, \quad (8.58)$$

where

$$k = \frac{Rm}{C} \operatorname{tg} \gamma.$$

If the rocket rotates in the launch apparatus, then, integrating equation (8.58) on the left from zero to  $\underline{r}$  and on the right from zero to  $\underline{v}$ , we shall secure:

$$\begin{aligned} \theta &= r = kv = ks, \\ \theta &= ks \end{aligned}$$

If the rocket commences to rotate only after departure from the launch apparatus, then, taking as limits of integration to the left from zero to  $\underline{r}$  and on the right from  $v_0$  to  $\underline{v}$ , we secure:

$$\begin{aligned} r &= k(v - v_0); \\ \theta &= k(s - s_0) - kv_0(t - t_0). \end{aligned} \quad (8.59)$$

Considering that:

$$v_0 = bt_0; \quad s = \frac{bt_0^2}{2}.$$

we secure expression (8.59) in the following form:

$$\theta = \frac{kb}{2} (t - t_0)^2 = k(Vs - Vs_0)^2. \quad (8.60)$$

Setting ourselves a number of rotations of the rocket  $\underline{n}$  in the critical section and determining the length of the critical section  $S_{cr}$ , we secure the expression

$$k = \frac{2n\pi}{(Vs_{cr} - Vs_0)^2} = \frac{Rm \operatorname{tg} \gamma}{C}, \quad (8.61)$$

from which we shall find the necessary angle of inclination of the cones. In the case where the rocket rotates by means of spiral guides on the

launch apparatus, the angular velocity of the rocket at the moment of its departure from the launch apparatus will be determined from the expression

$$\omega_0 = \frac{2n_0 \lg \beta}{D}, \quad (8.62)$$

where  $\beta$  is the angle of incline of the spiral line;  
 $D$  is the diameter of a cylinder corresponding to this spiral line.

The angular velocity  $\omega_0$  remains practically constant in the critical section of the trajectory. Under these circumstances

$$\theta_{sp} = 2\pi n_{sp} = \omega_0 (t_{sp} - t_0) = r_0 \sqrt{\frac{2}{b}} (V_{s_{sp}} - V_{s_0}). \quad (8.63)$$

The last expression, together with formula (8.52), makes it possible to determine the angle of incline of the spiral line which will ensure the necessary number of rotations  $n_{cr}$  in the critical section of the trajectory.

#### 8.8. Influence of Wind on the Flight of Finned Rockets

Let us examine the influence of a flank wind  $W_z$  blowing to the right, i.e., in the direction of axis  $z$  (Figure 8.10). Let us introduce a movable system of coordinates moving progressively with velocity  $\bar{W}_z$  in the direction of the wind. Relative to this system the velocity of the wind is equal to zero. In doing this one must take into account the fact that the initial velocity of the rocket relative to a stationary system of coordinates ( $\bar{v}_0$ ) will differ from initial velocity  $\bar{v}_{0r}$  relative to the movable system by the amount of the translational velocity  $\bar{v}_{0e} = \bar{W}_z$ :

$$\bar{v}_0 = \bar{v}_{0r} - \bar{W}_z, \quad (8.64)$$

Projecting the last equation upon the axis of the coordinates, we secure:

$$(v_{0r})_x = v_0 \cos \theta_0;$$

$$(v_{0r})_y = v_0 \sin \theta_0;$$

$$(v_{0r})_z = -W_z.$$

In the movable system of coordinates the plane of departure inclines to the left at angle  $\phi_1$  determined from the expression

$$\lg \phi_1 = - \frac{W_z}{v_0 \cos \theta_0}. \quad (8.65)$$

and flank deflection of the rocket will be found from the expression

$$s_r = x \lg \phi_1 = - \frac{x W_z}{v_0 \cos \theta_0}.$$

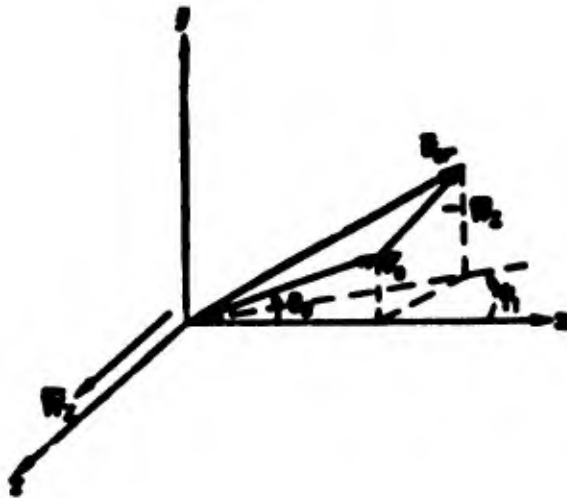


Figure 8.10. Influence of wind on flight of rocket.

Shifting to the stationary system of coordinates,

$$s = s_0 + W_2 t,$$

where  $W_2 t$  is the displacement of the movable system over the time of motion of the rocket.

Carrying out a number of transformations, we shall secure

$$s = W_2 \left( t - \frac{s}{u_0 \cos \theta_0} \right). \quad (8.66)$$

The flank velocity of the rocket will be determined from the expression

$$\dot{s} = W_2 \left( 1 - \frac{\dot{s}}{u_0 \cos \theta_0} \right). \quad (8.67)$$

For angular deflection of the plane of fire we shall secure the expression

$$\phi_2 \approx \lg \phi_1 = \frac{\dot{s}}{s} = W_2 \left( \frac{1}{u} - \frac{1}{u_0} \right), \quad (8.68)$$

where  $u = \dot{x}$  is the horizontal projection of velocity.

Relations (8.66)-(8.68) are secured irrespectively of the system of forces operating upon the rocket, and for this reason are correct for the active and the passive sections of the trajectory, and also for artillery shells. Let us note, however, that for artillery shells  $u < u_0$ ,  $\phi_2 > 0$ , and consequently a shell deflects in the direction of the wind. For the active part of the trajectory of a rocket we have  $u > u_0$ , for which reason the rocket deflects against the wind. This circumstance was noted for the first time and explained by K. I. Konstantinov (3).

A flank wind, deflecting the tail group in its direction, turns the head part of a rocket against the wind, as a result of which the flank constituent of reactive force deflects the vector of velocity of the rocket against the wind.

In deriving equation (8.68) we did not take into account the fact that in a movable system of coordinates the vector of initial velocity is rotating at an angle  $\phi_1$ , and the axis of the rocket coincides with the undisturbed position of the axis of the guide. Under these conditions, in the movable system of counting at the initial moment  $t_0$  the axis of the rocket deflects from the vector  $\vec{v}_0$  or wind the wind at an angle  $\varphi_0$  determined from the expression

$$\tan \varphi_0 = \frac{W_x}{v_0}$$

The presence of an initial disturbance  $\varphi_0$  will provoke angular deflection of the vector of velocity  $\psi_0^*$ , determined by means of expressions (8.53) or (8.55). Designating  $\psi_0^* = \frac{\psi_0^*}{v_0}$ , we secure

$$\psi_0^* = \psi_0^* \cdot v_0 = \psi_0^* \cdot \frac{W_x}{v_0}$$

Supplementary deflection  $\psi_1$  of the plane of departure, provoked by angle  $\psi_0^*$ , is determined from the expression

$$\psi_1 = \frac{\psi_0^*}{\cos \theta_0} = \psi_0^* \frac{W_x}{v_0 \cos \theta_0}$$

Over-all deflection  $\psi_w$  of the plane of fire will be secured from the expression  $\psi_w = \psi_1 + \psi_0$ , or

$$\psi_w = -W_x \left( \frac{1 - \psi_0^*}{v_0} - \frac{1}{v_1} \right)$$

For the end of the active section taking  $\cos \theta_1 = \cos \theta_0$ , we shall finally secure

$$\psi_w = -\frac{W_x}{\cos \theta_0} \left( \frac{1 - \psi_0^*}{v_0} - \frac{1}{v_1} \right) \quad (8.69)$$

We shall find the deflection of the point of fall of the rocket from the expression

$$z_w = \psi_w \cdot X = -\frac{W_x}{\cos \theta_0} \left( \frac{1 - \psi_0^*}{v_0} - \frac{1}{v_1} \right) X \quad (8.70)$$

In the case of a longitudinal wind  $W_x$ , as it is not difficult to show, formula (8.69) assumes the form

$$\Delta\theta_{\psi} = W_z \sin \theta_0 \left( \frac{1 - \dot{\psi}_{\psi_0}}{v_0} - \frac{1}{v_k} \right), \quad (8.71)$$

where  $\Delta\theta_{\psi}$  is the change of angle  $\theta_k$  at the end of the active section of the trajectory provoked by the longitudinal wind. In this event with  $W_z > 0$ ,  $\Delta\theta_{\psi} > 0$ . We may note that for the passive section of the trajectory formula (8.66) remains correct. In this connection, taking the start of the count as being the end of the active section of the trajectory, we secure for the point of fall

$$s_{\text{acc}} = W_z \left( T_{\text{acc}} - \frac{X_{\text{acc}}}{v_0 \cos \theta_0} \right). \quad (8.72)$$

Example. For the example examined in 8.6 we have  $\epsilon_0 = \epsilon_{\psi_0} = 0.423$ . We shall furthermore take  $v_0 = 60$  m/sec;  $v_k = 400$  m/sec;  $\theta_0 = 45^\circ$ ; full range  $X = 8,000$  m; full time of flight  $T = 42$  sec;  $W_z = 5$  m/sec. According to formula (8.55) we secure

$$\dot{\psi}_{\psi_0} = \frac{\dot{\psi}_{\psi_0}}{v_0} = \frac{0.5}{0.7 + 0.423} = 0.455.$$

According to formula (8.69) we have

$$\psi_{\psi} = -\frac{5}{0.707} \left( \frac{0.545}{60} - \frac{1}{400} \right) = -0.046.$$

The deflection at the point of fall, provoked by the influence of a flank wind in the active section, will be determined from the expression

$$s_{\psi} = -X\psi_{\psi} = -8000 \cdot 0.046 = -367 \text{ m}$$

Assuming that an equal wind  $W_z = 5$  m/sec is blowing in the passive section of the trajectory, and taking  $T_{\text{pas}} \approx T$ ,  $X_{\text{pas}} \approx X$ ,  $\theta = \theta_0$ , we secure from expression (8.72)

$$s_{\text{acc}} = 5 \left( 42 - \frac{8000}{400 \cdot 0.707} \right) = 69 \text{ m}$$

The over-all deflection is

$$s = s_{\psi} + s_{\text{acc}} = -367 + 69 = -298 \text{ m}$$

From the example examined it is apparent that the influence of wind in the active section of the trajectory is decisive. Inasmuch as in the terrestrial strata of the atmosphere wind is often of an intermittent character, this must have an effect upon the dispersion of rockets. If one examines the probable deviation of the wind from its mean value  $B_W$  and assumes  $B_W = 1$  m/sec, then for the example examined we secure a corresponding amount of flank dispersion evoked by wind  $(B\delta)_{\psi} = \frac{367}{3} \approx 122$  meters.

#### BIBLIOGRAPHY

1. Gantmacher, F. R., and Levin, L. M., Theory of Flight of Un-guided Rockets, Fizmatgiz Publishing House, Moscow, 1959.
2. Davis, L., Follin, D., Blanter, L., External Ballistics of Rockets, Voenizdat Publishing House, 1961.
3. Konstantinov, K. I., Concerning Military Rockets, St. Petersburg, 1956.

## CHAPTER IX. ROTATORY MOTION OF TURBOJET MISSILES

### 9.1. Drawing up Differential Equations for Motion of a Rocket

In the flight of a finless rocket static aerodynamic moment is a tilting moment, and the stability of the rocket is ensured by virtue of the gyroscopic effect of its rotation. Rotation of the rocket commences on the launch apparatus (tube) in such fashion that upon leaving the tube the rocket is already stable. The angular velocity of the rocket's own rotation is determined from the relationship (8.58)

$$\omega = \frac{R \sin \gamma}{C} v. \quad (9.1)$$

Initial disturbances of the axis of the rocket produce its oscillations, precession, and nutation, and the appearance of flank constituents of reactive force. The last provoke angular deflections of velocity which are the basic factor determining the flank dispersion of rotating rockets.

In studying the rotatory motion of turbojet missiles we shall consider:

-- reactive force  $P = mb$ , where  $b$  is the acceleration of the center of mass of the rocket;

-- reactive rotatory moment

$$M_p = P \cdot R \sin \gamma; \quad (9.2)$$

-- aerodynamic tilting moment

$$M_a = \frac{\rho v^2}{2} S L m^2 \cdot \alpha. \quad (9.3)$$

We do not take the force of gravity into account, for reasons indicated in 8.1.

In order to determine the position of the vector of velocity and of the axis of the rocket we must select a system of coordinates 0123, in which axis 03 lines along the direction of the vector  $\vec{v}_0$ , axis 01 lies in the plane of fire, and axis 02 is perpendicular to it (Figure 9.1). The disturbed direction of the vector of velocity is determined by the angles  $\phi_1$  and  $\phi_2$ , and the disturbed direction of the axis of the rocket by the angles  $\varphi_1$  and  $\varphi_2$ .

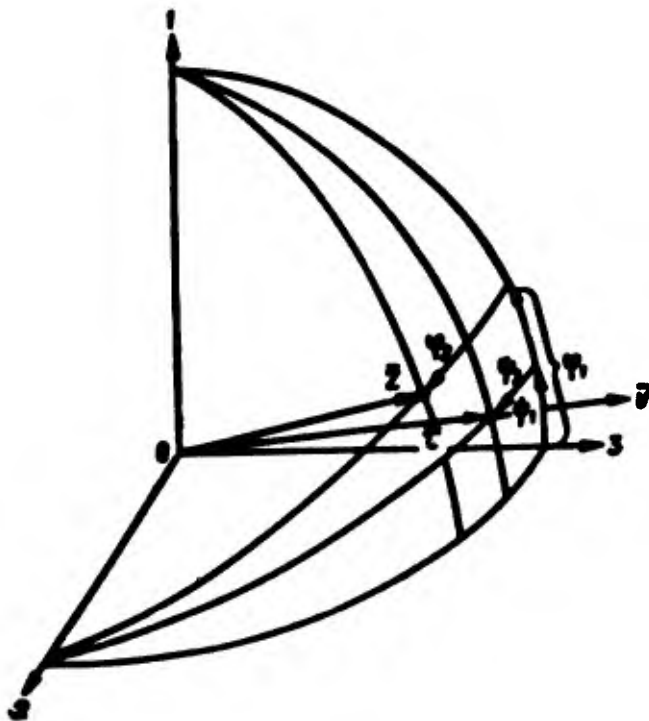


Figure 9.1. Diagram of constituents of the angle of pitch and of the angle of attack.

From here on we shall examine the angles  $\varphi_1$ ,  $\varphi_2$ ,  $\phi_1$ ,  $\phi_2$  and their derivatives as quantities of the first order of smallness and we shall disregard quantities having smaller orders of smallness. We shall introduce the designations:

$$\begin{aligned} \alpha_1 &= \varphi_1 - \phi_1, \\ \alpha_2 &= \varphi_2 - \phi_2. \end{aligned} \quad (9.4)$$

where  $\alpha_1$  and  $\alpha_2$  are the constituents of the angle of attack. Thus we indicate vertical deflections by index 1 and flank deflections by index 2. We shall introduce into the consideration the unit vector of the tangent  $\vec{\tau}$  and the unit vector of the axis of the rocket  $\vec{z}$ . It is not difficult to see that with a precision up to small quantities of the first order:

$$\begin{aligned} \tau_1 = \dot{\phi}; \quad \tau_2 = \dot{\psi}; \quad \tau_3 = 1; \\ Z_1 = \tau_1; \quad Z_2 = \tau_2; \quad Z_3 = 1. \end{aligned} \quad (9.5)$$

We shall write the equations for motion of the center of mass of the rocket in the following form:

$$\begin{aligned} \ddot{\phi} &= b, \\ \ddot{\psi}_1 &= \frac{b}{\sigma} \tau_1, \\ \ddot{\psi}_2 &= \frac{b}{\sigma} \tau_2. \end{aligned} \quad (9.6)$$

We shall write the equation for rotation of the axis of the rocket in vector form:

$$\dot{\bar{L}} = \sum \bar{M} = \bar{M}_p + \bar{M}_s, \quad (9.7)$$

where  $\bar{L}$  is the kinetic moment of the rocket, which we shall write in the following form:

$$\bar{L} = A\bar{\omega} + Cr\dot{Z},$$

where  $A$  is the equatorial moment of inertia;

$C$  is the polar moment of inertia;

$\bar{\omega}$  is the angular velocity of rotation of the rocket around an axis perpendicular to it.

It is easy to see that the vectors  $\bar{\omega}$ ,  $\dot{Z}$ , and  $\dot{\bar{L}}$  are reciprocally perpendicular (Figure 9.2); under these circumstances the following relation holds good:

$$\bar{\omega} = \dot{Z} \times \dot{\bar{L}}$$

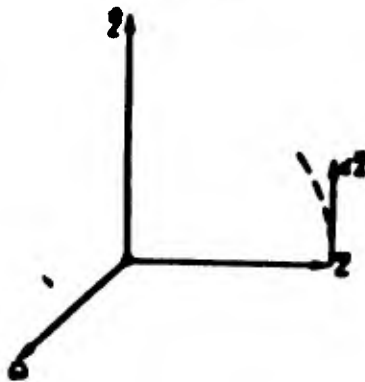


Figure 9.2. Angular velocity  $\bar{\omega}$  of axis of rocket.

The expression for kinetic moment assumes the form

$$\bar{L} = A\dot{Z} \times \dot{\bar{L}} + Cr\dot{Z}$$

Differentiating the last expression and substituting in equation (9.7), we secure

$$A\ddot{Z} < \ddot{Z} + Cr\dot{Z} + CrZ = \Sigma \bar{M} \quad (9.8)$$

We shall write the equation for axial reactive moment in vector form

$$\bar{M}_p = PR \sin \gamma \bar{Z}.$$

One can write equation (9.3) for tilting aerodynamic moment thus:

$$\bar{M}_z = \frac{\rho^2}{2} SLm_z^2 \bar{i} \times \bar{Z}.$$

It is true that

$$|\bar{i} \times \bar{Z}| = \sin(\bar{i}, \bar{Z}) = \sin \alpha \approx \alpha,$$

in which connection the vector  $\bar{i} \times \bar{Z}$  is directed perpendicularly to the plane of the angle of attack so that the moment  $\bar{M}_z$  augments this angle.

Substituting the values  $\bar{M}_p$  and  $\bar{M}_z$  into expression (9.8) we secure

$$A\ddot{Z} \times \ddot{Z} + Cr\dot{Z} + CrZ = \frac{\rho^2}{2} SLm_z^2 \bar{i} \times \bar{Z} + PR \sin \gamma \cdot \bar{Z}. \quad (9.9)$$

The last terms in both arms of the equation (9.9) are contracted on the basis of the equation for axial rotation of the rocket

$$Cr = M_p = PR \sin \gamma. \quad (9.10)$$

Taking expression (9.1) into account as well, we secure equation (9.9) in the following form:

$$\ddot{Z} \times \ddot{Z} + 2\lambda v \dot{Z} = \beta v^2 \bar{i} \times \bar{Z}, \quad (9.11)$$

where

$$\lambda = \frac{Rm}{2A} \operatorname{tg} \gamma, \quad (9.12)$$

$$\beta = \frac{\rho SLm_z^2}{2A}. \quad (9.13)$$

Equation (9.11) constitutes a differential equation for rotatory motion of the axis of the rocket in vector form. Expressing the vector derivatives through determinants and segregating projections on axes 01 and 02, we secure Table 9.1.

Table 9.1

Vector	Projection on Axes		
	$u_1$	$u_2$	$u_3$
$\epsilon$	$\psi_1$	$\psi_2$	1
$Z$	$\varphi_1$	$\varphi_2$	1
$\dot{Z}$	$\dot{\varphi}_1$	$\dot{\varphi}_2$	0
$\ddot{Z}$	$\ddot{\varphi}_1$	$\ddot{\varphi}_2$	0
$Z \times \ddot{Z}$	$Z_2 \ddot{Z}_1 - Z_1 \ddot{Z}_2 = -\ddot{\varphi}_2$	$Z_2 \ddot{Z}_1 - Z_1 \ddot{Z}_2 = \ddot{\varphi}_1$	
$\bar{\epsilon} \times Z$	$\epsilon_2 Z_1 - \epsilon_1 Z_2 = \psi_2 - \varphi_2 = -a_2$	$\epsilon_2 Z_1 - \epsilon_1 Z_2 = \varphi_1 - \psi_1 = a_1$	

The equations for oscillation of the axis of the rocket assume the following form:

$$-\ddot{\varphi}_2 + 2\lambda\sigma\dot{\varphi}_1 + \beta\sigma^2 a_2 = 0, \quad (9.14)$$

$$\ddot{\varphi}_1 + 2\lambda\sigma\dot{\varphi}_2 - \beta\sigma^2 a_1 = 0. \quad (9.15)$$

Let us move on to the complex variables  $A$ ,  $\Phi$ , and  $\Psi$ , determined by the expressions

$$\begin{aligned} A &= a_1 + ia_2; \\ \Phi &= \varphi_1 + i\varphi_2; \\ \Psi &= \psi_1 + i\psi_2. \end{aligned}$$

Multiplying equation (9.14) by  $-t$  and adding it to equation (9.15) we secure

$$\dot{\Phi} - 2\lambda\sigma\dot{\Phi} - \beta\sigma^2 A = 0. \quad (9.16)$$

Equations (9.6) for  $\phi_1$  and  $\phi_2$  can also be written in complex form

$$\dot{\Psi} = \frac{b}{v} A. \quad (9.17)$$

We substitute in equation (9.16) the values:

$$\begin{aligned} \Phi &= \Psi + A; \\ \dot{\Phi} &= \dot{\Psi} + \dot{A} \end{aligned}$$

and we consider that

$$\dot{\Psi} = -\frac{b}{v} \dot{\Psi} + \frac{b}{v} \dot{A} = -\frac{b}{v} \dot{\Psi} + \frac{b}{v} \dot{A}.$$

Under these circumstances equation (9.16) assumes the following form:

$$\ddot{A} + \left( \frac{b}{v} - 2i\lambda v \right) \dot{A} - \left( \frac{b^2}{v^2} + 2i\lambda b + \beta v^2 \right) A = 0. \quad (9.18)$$

Equation (9.18) determines oscillation of the axis of the rocket relative to the vector of velocity.

Equation (9.17) determines oscillation of the vector of velocity.

### 9.2. Integrating the Equations for Rotatory Motion of a Rocket

In equation (9.18) we shift to the independent variable  $\underline{s}$  and introduce the substitution

$$A = \frac{u}{v},$$

whereupon

$$\dot{A} = u' - u \frac{b}{v^2};$$

$$\ddot{A} = v u'' - \frac{b}{v} u' + \frac{2b^2}{v^3} u,$$

where the derivative according to  $\underline{s}$  is marked with an apostrophe. Equation (9.18) assumes the following form:

$$u'' - 2i\lambda u' - \beta u = 0.$$

The general integral of this equation has the form

$$u = c_1 e^{k_1 s} + c_2 e^{k_2 s},$$

whence

$$A = \frac{1}{v} (c_1 e^{k_1 s} + c_2 e^{k_2 s}), \quad (9.19)$$

where

$$k_{1,2} = i\lambda (1 \pm \sqrt{\sigma}); \quad (9.20)$$

$$\sigma = \sqrt{1 - \frac{\beta}{\lambda^2}}. \quad (9.21)$$

We shall assume that as the rocket departs from the launch apparatus the following initial disturbances take place:

$$\text{with } t = t_0; \quad A = A_0; \quad \dot{A} = \dot{A}_0.$$

Determining the arbitrary constants from equation (9.19) we secure:

$$c_1 = \frac{\Lambda_0 + \left(\frac{b}{v_0} - v_0 k_2\right) \Lambda_0}{k_1 - k_2}; \quad (9.22)$$

$$c_2 = \frac{-\Lambda_0 - \left(\frac{b}{v_0} - v_0 k_1\right) \Lambda_0}{k_1 - k_2}. \quad (9.23)$$

In equation (9.19) the length of the arc  $\underline{s}$  is counted off from the instant the rocket departs from the launch tube.

Equations (9.19)-(9.23) determine the oscillations of the angle of attack which are provoked by the initial disturbances upon the departure of the rocket. In order to determine the deflection of the vector of velocity it is necessary to substitute the value  $\Lambda$  from expression (9.19) into equation (9.17).

Under these circumstances, shifting to the independent variable  $\underline{s}$  we secure:

$$\Psi' = \frac{\dot{\Psi}}{v} = \frac{b}{v^2} \Lambda = \frac{b}{v^2} (c_1 e^{k_1 s} + c_2 e^{k_2 s}).$$

Integrating within appropriate limits and substituting the values  $k_{1,2}$ , we secure

$$\Psi = bc_1 \int_0^s \frac{e^{k_1(1+\sqrt{G})s}}{v^2} ds + bc_2 \int_0^s \frac{e^{k_2(1-\sqrt{G})s}}{v^2} ds. \quad (9.24)$$

In expression (9.24) let us shift to the variable of integration  $\xi$ , determined from the expression  $\xi = \frac{v}{v_0}$ .

Here, considering that

$$\begin{aligned} v &= \sqrt{2b(s + s_0)}; \\ v_0 &= \sqrt{2bs_0}, \end{aligned}$$

we have:

$$\xi = \sqrt{1 + \frac{s}{s_0}}; \quad \frac{s}{s_0} = \xi^2 - 1. \quad (9.25)$$

Equation (9.24) assumes the following form:

$$\Psi = \frac{c_1}{v_0} \int_1^\xi \frac{e^{km(\xi^2-1)}}{\xi^2} d\xi + \frac{c_2}{v_0} \int_1^\xi \frac{e^{km(\xi^2-1)}}{\xi^2} d\xi,$$

where

$$\begin{aligned} n &= \lambda s_0 (1 + \sqrt{\sigma}); \\ m &= \lambda s_0 (1 - \sqrt{\sigma}). \end{aligned} \quad (9.26)$$

Considering that

$$\int_0^{\xi} \frac{e^{i k (\xi^2 - 1)}}{\xi^2} d\xi = \int_0^{\xi} \frac{\cos k (\xi^2 - 1)}{\xi^2} d\xi + i \int_0^{\xi} \frac{\sin k (\xi^2 - 1)}{\xi^2} d\xi$$

and introducing the designations:

$$\begin{aligned} f_c(k, \xi) &= \int_0^{\xi} \frac{\cos k (\xi^2 - 1)}{\xi^2} d\xi \\ f_s(k, \xi) &= \int_0^{\xi} \frac{\sin k (\xi^2 - 1)}{\xi^2} d\xi \end{aligned}$$

we finally secure

$$\Psi = \frac{c_1}{v_0} [f_c(n, \xi) + i f_s(n, \xi)] + \frac{c_2}{v_0} [f_c(m, \xi) + i f_s(m, \xi)]. \quad (9.27)$$

The functions  $f_z$  and  $f_c$  can be expressed through Frenelle integrals:

$$\begin{aligned} f_s(k, \xi) &= -\frac{\sin k (\xi^2 - 1)}{\xi} + \sqrt{2\pi k} (\cos k \cdot [c(k\xi^2) - c(k)] + \\ &\quad + \sin k \cdot [s(k\xi^2) - s(k)]); \\ f_c(k, \xi) &= 1 - \frac{\cos k (\xi^2 - 1)}{\xi} + \sqrt{2\pi k} (\sin k \cdot [c(k\xi^2) - c(k)] - \\ &\quad - \cos k \cdot [s(k\xi^2) - s(k)]). \end{aligned} \quad (9.28)$$

Expression (9.27) makes it possible to determine the deflection of the vector of velocity provoked by the initial disturbances.

Particular Case of Initial Conditions  $A_0 = 0$ ;  $\dot{A}_0 \neq 0$

This case is the most typical one for rotating shells and rockets. Here, from expressions (9.22) and (9.23), we have:

$$c_1 = \frac{\dot{A}_0}{k_1 - k_2} = \frac{\dot{A}_0}{2i\lambda \sqrt{\sigma}}; \quad c_2 = -c_1.$$

Expression (9.19) assumes the following form:

$$A = \frac{\dot{A}_0}{2\lambda v \sqrt{\sigma}} [e^{\mu(1+\sqrt{\sigma})s} - e^{\mu(1-\sqrt{\sigma})s}],$$

or

$$A = \frac{\dot{A}_0}{\lambda v \sqrt{\sigma}} \sin \lambda \sqrt{\sigma} s (\cos \lambda s + i \sin \lambda s). \quad (9.29)$$

We shall recall that A is a complex quantity determined by the expression

$$A = a_1 + i a_2,$$

whence

$$\dot{A} = \dot{a}_1 + i \dot{a}_2.$$

Let us note that disturbance  $\dot{A}_0$  can be in any plane. Let the initial disturbance (impetus) take place in the vertical plane. Here  $a_{20} = 0$  and expression (9.29) assumes the following form:

$$a_1 + i a_2 = \frac{\dot{a}_{10}}{\lambda v \sqrt{\sigma}} \sin \lambda \sqrt{\sigma} s (\cos \lambda s + i \sin \lambda s).$$

We divide the real and the imaginary arms and secure:

$$a_1 = \frac{\dot{a}_{10}}{\lambda v \sqrt{\sigma}} \sin \lambda \sqrt{\sigma} s \cdot \cos \lambda s, \quad (9.30)$$

$$a_2 = \frac{\dot{a}_{10}}{\lambda v \sqrt{\sigma}} \sin \lambda \sqrt{\sigma} s \cdot \sin \lambda s. \quad (9.31)$$

In the expressions for  $a_1$  and  $a_2$  an augmenting velocity forms part of the denominator. This shows that oscillations of the angle of attack are diminishing in both planes.

Expression (9.27) for the angle  $\Psi$  assumes the following form:

$$\Psi_1 = \frac{\dot{a}_{10}}{2\lambda v_0 \sqrt{\sigma}} [f_c(m, \xi) - f_c(n, \xi)]; \quad (9.32)$$

$$\Psi_2 = \frac{\dot{a}_{10}}{2\lambda v_0 \sqrt{\sigma}} [f_s(n, \xi) - f_s(m, \xi)]. \quad (9.33)$$

#### The Particular Case of Initial Conditions $\Phi_0 = 0$ ; $\dot{\Phi}_0 \neq 0$

In this case the initial conditions for the angle of attack have the form (8.6):

$$A = A_0; \quad \dot{A}_0 = -\frac{b}{v_0} A_0;$$

Here we secure the following values for the arbitrary constants:

$$\begin{aligned} c_1 &= -\frac{\Lambda_0 v_0 (1 - \sqrt{\sigma})}{2\sqrt{\sigma}}; \\ c_2 &= \frac{\Lambda_0 v_0 (1 + \sqrt{\sigma})}{2\sqrt{\sigma}}. \end{aligned} \quad (9.34)$$

The expression for angle  $\Lambda$  assumes the following form:

$$\begin{aligned} \Lambda &= \frac{\Lambda_0 v_0}{v(n-m)} \left\{ n \left[ \cos m \frac{s}{s_0} + i \sin m \frac{s}{s_0} \right] - \right. \\ &\quad \left. - m \left[ \cos n \frac{s}{s_0} + i \sin n \frac{s}{s_0} \right] \right\}. \end{aligned} \quad (9.35)$$

Assuming that at the initial moment the angle of attack falls in the vertical plane, after dividing the real and the imaginary arms we secure:

$$a_1 = \frac{a_{10} v_0}{v(n-m)} \left( n \cos m \frac{s}{s_0} - m \cos n \frac{s}{s_0} \right); \quad (9.36')$$

$$a_2 = \frac{a_{10} v_0}{v(n-m)} \left( n \sin m \frac{s}{s_0} - m \sin n \frac{s}{s_0} \right). \quad (9.36)$$

The expressions for the angles  $\phi_1$  and  $\phi_2$  assume the following form:

$$\phi_1 = \frac{a_{10}}{n-m} [m f_s(n, \xi) - n f_s(m, \xi)]; \quad (9.37)$$

$$\phi_2 = \frac{a_{10}}{n-m} [n f_c(m, \xi) - m f_c(n, \xi)]. \quad (9.38)$$

We will recall that index (1) corresponds to the vertical plane.

Example. Let us compute the angular deflection, at the end of the active section of the trajectory, of the vector of velocity of a turbojet missile under the following conditions:

$$\lambda = 0,0675 \frac{1}{\mu}; \quad \beta = 0,00162; \quad \sigma = 0,8; \quad v_0 = 41,5 \frac{M}{сек}; \quad v_{\pi} = 300 \frac{M}{сек}; \quad s_0 = 2 \mu.$$

Let the initial disturbance upon departure of the rocket from the launch tube be characterized by a magnitude of angular velocity  $\dot{\alpha}_{10} = 0.1$  1/sec. The (1) index shows that the plane of rotation  $\dot{\alpha}_{10}$  coincides with the plane of fire (inclination of the head part upward). We determine in advance the values of the Frenelle integrals. We have:

$$\begin{aligned}
 n &= \lambda s_0 (1 + \sqrt{\sigma}) = 0,0675 \cdot 2 \cdot 1,8 = 0,243; \\
 m &= \lambda s_0 (1 - \sqrt{\sigma}) = 0,0675 \cdot 2 \cdot 0,2 = 0,027; \\
 \xi &= \frac{v_{\text{н}}}{v_0} = \frac{300}{41,5} = 7,23;
 \end{aligned}$$

$$\begin{aligned}
 m\xi^2 &= 1,41; \quad n\xi^2 = 12,65; \quad m(\xi^2 - 1) = 1,33; \quad n(\xi^2 - 1) = 12,4; \\
 S(m\xi^2) &= 0,386; \quad S(n\xi^2) = 0,388; \quad S(m) = 0,001; \quad S(n) = 0,032; \\
 C(m\xi^2) &= 0,776; \quad C(n\xi^2) = 0,505; \quad C(m) = 0,131; \quad C(n) = 0,391.
 \end{aligned}$$

Computing the functions  $f_S$  and  $f_C$  in accordance with formulas (9.28), we have

$$\begin{aligned}
 f_S(m, \xi) &= -\frac{\sin 1,38}{7,23} + \sqrt{2\pi \cdot 0,027} (\cos 0,027 [C(1,41) - C(0,027)] + \\
 &\quad + \sin 0,027 [S(1,41) - S(0,027)]) = 0,134.
 \end{aligned}$$

Analogously we compute:

$$f_S(n, \xi) = 0,0273; \quad f_C(m, \xi) = 0,887; \quad f_C(n, \xi) = 0,474.$$

In accordance with formulas (9.32) and (9.33) we determine:

$$\begin{aligned}
 \psi_1 &= \frac{0,1}{2 \cdot 0,0675 \cdot 41,5 \cdot 0,8} [0,887 - 0,474] = 0,0092 \text{ rad} = 0^\circ 32'; \\
 \psi_2 &= \frac{0,1}{2 \cdot 0,0675 \cdot 41,5 \cdot 0,8} [0,273 - 0,134] = 0,0031 \text{ rad} = 0^\circ 11'.
 \end{aligned}$$

Thus if a turbojet missile with the characteristics indicated receives an upward impetus upon departing from the launch tube, so that  $\dot{\alpha}_0 = 0.1$  l/sec, as a result of oscillations of the axis of the rocket the vector of velocity will incline upward at the end of the active section of the trajectory at an angle  $\psi_{1\text{н}} = 0^\circ 32'$  and to the right at an angle of  $0^\circ 11'$ . If the impulse had been to the right, the corresponding inclination of the vector of velocity would have proved to be  $0^\circ 32'$  to the right and  $0^\circ 11'$  downward.

### 9.3. The Condition of the Gyroscopic Stability of Turbojet Missiles

Inasmuch as the static aerodynamic moment operating upon a finless missile is a tilting moment, in order to avoid tilting of the missile it is necessary to communicate to it a rapid rotation around its axis of symmetry. This ensures so-called gyroscopic stability of the missile.

The relations secured in 9.2 (9.30, 9.31) for the constituents of the angle of attack show that they are expressed through trigonometric functions and are limited quantities. But this will apply only in the case where  $\sqrt{\sigma}$  is a real number, i.e., when  $\sigma > 0$ . If  $\sigma < 0$ , then expanding expression (9.19) we shall secure along with the periodic terms also constantly increasing terms which bring about constant increase in the angle of attack and in the tilting of the rocket.

From expression (9.21) we secure the following conditions of gyroscopic stability for a turbojet missile

$$\sigma = 1 - \frac{\beta}{\lambda^2} > 0.$$

Substituting the values  $\beta$  and  $\lambda$  from expressions (9.12) and (9.13), we secure

$$\frac{\beta}{\lambda^2} = \frac{2\rho S L m_2^2 A}{R^2 m^2 \operatorname{tg}^2 \gamma} < 1,$$

whence

$$\operatorname{tg} \gamma > \frac{1}{Rm} \sqrt{2\rho S m_2^2 A}. \quad (9.39)$$

The inequality secured makes it possible to determine the minimum angle of inclination of the cones which is necessary for gyroscopic stability of the rocket. In order that it may be possible to replace the inequality (9.39) with an equality it is necessary to introduce a coefficient of reserve of stability,  $a$ . Here we secure

$$\operatorname{tg} \gamma = \frac{a}{Rm} \sqrt{2\rho S m_2^2 A}. \quad (9.40)$$

In order to compute angle  $\gamma$  it is necessary to know not only the geometrical dimensions of the rocket and the equatorial moment of inertia  $A$ , but also the aerodynamic coefficient  $m_2^2$  and the coefficient of reserve of stability  $a$ , determined through experiment. In view of the limited character of these data we make use of characteristics known for artillery shells (1). Here we shall start from the form of writing the expression for tilting moment which is adopted in the ballistics of artillery shells

$$M = \frac{D^3 h}{g} 10^3 H(\gamma) v^2 K_M \cdot a, \quad (9.41)$$

where  $K_M$  is the aerodynamic coefficient of tilting moment. We shall determine the quantity  $h$  from the expression

$$h = h_1 + 0,57 h_r - 0,16 D, \quad (9.42)$$

where  $h_1$  is the distance from the center of gravity to the base of the ogival head part;

$h_r$  is the height of the head part;

$D$  is the caliber.

The values of  $K_M$  secured by D. A. Ventzel for artillery shells are set forth in Table 9.2.

Table 9.2

$v$	$10^3 K_M$	$v$	$10^3 K_M$	$v$	$10^3 K_M$
< 200	0,97	350	1,32	600	1,35
250	1,00	375	1,36	700	1,33
275	1,05	400	1,39	800	1,32
300	1,13	450	1,39	900	1,31
325	1,24	500	1,38	1000	1,30

The expression (9.40) assumes the form

$$\operatorname{tg} \gamma = 200 \frac{aD}{RQ} \sqrt{AhK_M} \quad (9.43)$$

For artillery shells it is assumed that  $a \approx 1,35$ . In nondimensional parameters the last expression can be transcribed in the following form:

$$\operatorname{tg} \gamma = 2 \frac{\tilde{a}\tilde{r}}{\tilde{R}} \sqrt{\frac{\tilde{h}K_M}{C_q}} \quad (9.44)$$

where  $\tilde{r}$  is the nondimensional radius of inertia determined from

$$\tilde{r} = \frac{r}{D} = \frac{1}{D} \sqrt{\frac{Ag}{Q}};$$

$C_q$  is the weight coefficient, defined as the relation of weight of the shell to the cube of the caliber expressed in decimeters,  $C_q = Q/D^3$ ;

The wave ( $\sim$ ) indicates the linear quantities related to the caliber  $D$ .

**Example.** Let us determine the angle of incline of a cone  $\gamma$ , necessary for stability of a rocket at the end of the active section, and defined by the following characteristics:

$$C_q = 7; \tilde{r} = 1,9; \tilde{h} = 2,0; \tilde{R} = 0,38; a = 1,35; v_x = 320 \text{ м/сек.}$$

From Table 9.2 we find that  $K_M = 1,22 \cdot 10^{-5}$ . According to formula (9.44) we determine that

$$\operatorname{tg} \gamma = 2 \frac{1,35 \cdot 1,9}{0,38} \sqrt{\frac{2,0 \cdot 1,22 \cdot 10^{-5}}{7}} = 0,252;$$

$$\gamma = 14^\circ.$$

If gyroscopic stability of a rocket at the end of the active section is assured, then practically speaking the rocket is stable also in all the active and passive sections of the trajectory.

In conclusion we may note that expression (9.42) for the quantity  $\underline{h}$ , and also the values  $K_M$  set forth in Table 9.2, are secured for artillery shells just as is the coefficient of reserve of stability. For this reason these quantities can be utilized only for rotating rockets the characteristics of which are close to the characteristics of artillery shells.

#### 9.4. Over-All Dispersion of Unguided Rockets

The character of the oscillation of unguided rockets in the active part of the trajectory determines the angular dispersion of the vector of velocity at the end of the active section. If the initial disturbances  $\varphi_0$  and  $\psi_0$  upon departure of the rocket from the guide and the eccentricity of reactive force are known, then by means of the methods set forth in Chapters VIII and IX one can compute the corresponding deflections of the vector of velocity  $\phi_{1K}$  and  $\psi_{2K}$ .

The disturbances referred to are of a random character, and for evaluation of angular dispersion  $r_\psi$  one must start from probable or mean values for the disturbances  $r_{\varphi_0}$ ,  $r_{\psi_0}$ ,  $r_\lambda$ , referred to. These quantities, and also  $r_\psi$ , can be determined experimentally through motion picture photography of the flight of a rocket on the initial section of the trajectory.

The flank dispersion of a rocket depends not only upon angular dispersion but furthermore upon the disturbance factors operating on the passive section (busts of wind, oscillation of rocket). These factors are conveniently defined by the quantity,  $r_j$ , of dispersion of flank acceleration. The corresponding flank dispersion of the point of fall is determined from the expression

$$r_{sj} = r_j \frac{T^2}{2}. \quad (9.45)$$

Inasmuch as  $r_\psi$  and  $r_j$  may be regarded as independent random quantities, the over-all flank dispersion will be determined from the expression

$$B\delta = \sqrt{r_{sj}^2 + r_\psi^2} = \sqrt{(r_\psi X)^2 + \left(r_j \frac{T^2}{2}\right)^2} \quad (9.46)$$

If  $r_\psi$  is known, then, having determined the quantity  $B\delta$  in accordance with the data from test firing, it is possible to reckon the value  $r_j$  from the expression (9.46), and to determine dispersion for various angles of departure. Dispersion in range depends not only on angular dispersion in the vertical plane,  $r_{\psi_K}$ , but also on dispersion  $r_{v_K}$  of the velocity of the rocket at the end of the active section of the trajectory  $v_K$  and upon disturbance factors operating on the passive section of the trajectory. The quantity  $r_{v_K}$  depends on the nonhomogeneity of the working of

the rocket engine. The disturbance factors operating on the passive section of the trajectory are determined basically by the nonhomogeneity of frontal resistance, which depends on tolerances in the dimension and shape of the rocket and on the character of the oscillation of the axis of the rocket. It is convenient to reduce all these factors to oscillation of the ballistic coefficient  $\underline{c}$ . Taking the three disturbance factors  $r_{\theta_0}$ ,  $r_{v_0}$ ,  $r_c$  referred to into account, it is possible to write an expression for  $B\delta$ , characterizing dispersion in range, in the following form:

$$B\delta = \sqrt{\left(r_{\theta_0} \frac{\partial X}{\partial \theta_0}\right)^2 + \left(r_{v_0} \frac{\partial X}{\partial v_0}\right)^2 + \left(r_c \frac{\partial X}{\partial c}\right)^2}, \quad (9.47)$$

where  $\frac{\partial X}{\partial \theta_0}$ ,  $\frac{\partial X}{\partial v_0}$ ,  $\frac{\partial X}{\partial c}$  are corrective coefficients determining change in range in consequence of a slight change in  $\theta_0$ ,  $v_0$  respectively.

These corrective coefficients are determined in accordance with special tables (2). For artillery shells the values  $r_{\theta_0}$ ,  $r_c$  are characterized by the following mean values:

$$r_{\theta_0} \approx 1,5 \frac{\mu}{\text{сек}}, \quad r_c \approx 1\%.$$

For rockets these quantities are regarded as the lower limit of possible dispersion of these parameters.

It should be noted that with small angles of departure the factor  $r_{\theta_0}$  is decisive and dispersion according to range is determined almost entirely by angular dispersion  $r_{\theta_0}$ .

With increase of the angle of departure the part played by this factor falls off, and it becomes minimal at  $\theta_0 = 45^\circ$ .

#### BIBLIOGRAPHY

1. Shapiro, Ya. M., External Ballistics, Oborongiz Publishing House, 1946.
2. Ventzel, D. A., Shapiro Ya. M., External Ballistics. Part III, Oborongiz Publishing House, 1939.

## CHAPTER X. BALLISTIC PLANNING OF UNGUIDED ROCKET MISSILES

### 10.1. Posing the Problem

The planning of unguided rocket missiles is done in conformity with the tactical and technical requirements examined in Chapter III. In this process, in view of the mass character of the application of this weapon, the requirements of simplicity and technological practicality of design, ready domestic availability of materials, assume front-rank importance as indispensable conditions for cheapness of manufacture and high productivity in the mass output of manufactures. The use of unguided rocket missiles in the combat dispositions of forces in immediate proximity to the enemy imposes a requirement for a high state of readiness for launch, simplicity in use, and minimum vulnerability. These requirements to a certain extent predetermine the selection of design layouts, fuels, materials, and shapes of missiles. It is necessary to reject variants which, although they ensure high ballistic characteristics in the model, nevertheless complicate production and use. All of this determines the specific character of the planning of unguided rocket missiles, which finds its reflection in the methods of ballistic planning.

The basic aim of ballistic planning consists in determining the fundamental design parameters of a missile which will ensure minimum start weight of the model for a given range with given weight of useful load, with the fuel and materials selected, and with the values for project parameters adopted ( $I_1$ ,  $\kappa$ ,  $P_m$ ,  $\sigma_B$ , etc.).

In harmony with the supplementary conditions or limitations imposed upon the solution, three basic cases are possible:

1. A missile not limited as to length of model and as to thickness of burning vault (the optimum ballistic variant).
2. A missile limited as to length.
3. A missile with an assigned time of combustion of charge.

The first case is the most characteristic for the planning of finned missiles, where the method of stabilizing the missile in flight permits any length of missile.

The second case corresponds to the planning of turbojet missiles, the stability of which in flight can be ensured only with a relative length of missile which does not exceed 7-8 calibers. This case, however, is not confined to the planning of turbojet rocket missiles; it is always used when a limitation is imposed upon the length of the model by conditions of use.

The third case becomes applicable in the planning of antitank unguided finned missiles and launch engines. In order to ensure the high grouping necessary to hit a tank, it is necessary that the combustion time of the charge be less than the time of motion of the missile in the critical section of the trajectory. It is ordinarily also required of launch engines that the attainment of set velocity of the rocket (the flight apparatus) take place in the course of an assigned time.

The solutions of problems in the ballistic planning of unguided rocket missiles set forth below are based upon a simplified method of determining maximum range of fire. In determining  $X_{\max}$  it is postulated that the rocket charge burns instantaneously, and that the angle of maximum range  $\theta_{\max}$  is equal to  $45^\circ$ . This makes it possible to consider maximum range as a function of two parameters: maximum velocity  $v_{\max}$  computed according to the Tsiolkovskiy formula, and the ballistic coefficient  $\underline{c}$ , computed for a missile with charge burned out at  $y = 0$ .

Divergence in the results of computation of range carried out by the approximative and the precise methods systems comes to 1-3 percent, which is within the limits of precision of solution for the problems of ballistic planning.

In order to explain so felicitous a coincidence of results, it is sufficient to compare the velocity of the missile for both cases (precise solution and approximative solution) at a single check point of the trajectory. We shall take as such the point A, corresponding to the end of the active section for a variant having progressive combustion of charge (the precise solution). It is obvious that beyond this point the development of the trajectory for both variants will be determined by three parameters:  $\theta_A$ ,  $\underline{c}$  and  $v_A$ . The difference in ranges for the two variants of the treatment with equal values of  $\theta_A$  and  $\underline{c}$  will be determined only by the differences in velocities at point A. For each of the variants velocity at point A can be presented in the form:

$$v_{A_1} = v_x - \Delta v_{g1} - \Delta v_{x1};$$

$$v_{A_2} = v_x - \Delta v_{g2} - \Delta v_{x2};$$

where  $v_{TS}$  is the value calculated according to the Tsiolkovskiy formula;  
 $\Delta v_g$  is the gravitational losses in the section of the trajectory  
being examined;

$\Delta v_x$  is the loss in velocity by reason of air resistance;  
the index (1) relates to the variant having instantaneous combustion  
(simplified treatment); the index (2) to the variant which takes into ac-  
count progressive combustion of charge (precise treatment).

The difference in velocities at point A, characterizing the error  
of the simplified method of solution, comes to

$$\Delta v_A = v_{A_1} - v_{A_2} = (\Delta v_{g_1} - \Delta v_{g_2}) + (\Delta v_{x_1} - \Delta v_{x_2}).$$

The mean velocity of motion of the missile in the section OA for the first  
variant comes to  $\approx v_{TS}$ , for the second variant to  $\approx v_{TS}/2$ . The times of  
motion in this section for the first and the second variants are propor-  
tionate:  $\tau_1 \approx 1/v_u$ ,  $\tau_2 \approx 2/v_u$ . For the second variant gravitational losses  
will be higher by virtue of considerably greater time of motion. Conse-  
quently:

$$\Delta v_{g_1} - \Delta v_{g_2} < 0.$$

Losses of velocity from frontal resistance, on the other hand, will  
be higher for the first variant, for which mean velocity of motion in the  
section being examined is approximately twice as great as for the second.  
Consequently:

$$\Delta v_{x_1} - \Delta v_{x_2} > 0.$$

As analysis shows, for the high thrust-weight ratios that character-  
ize unguided rocket missiles the following condition is met:

$$|\Delta v_{g_1} - \Delta v_{g_2}| \approx |\Delta v_{x_1} - \Delta v_{x_2}|.$$

Here

$$\Delta v_A \rightarrow 0$$

and

$$\Delta X_{\max} \rightarrow 0.$$

Utilization of the approximative method for determining range cuts  
down the number of project parameters and thereby considerably simplifies  
the selection of the optimum ballistic variant. The characteristics of  
this variant may then be refined on the basis of the more perfect methods  
for computing range set forth in Chapter VII.

## 10.2. The Weight Equation for an Unguided Rocket Missile

It is desirable to present the weight equation for an unguided rocket missile in the form

$$Q = q_{\text{NM}} + q_{\text{K}} + q_{\text{TP}} + w_T, \quad (10.1)$$

where  $q_{\text{K}}$  represents the over-all weight of the caps of the rocket chamber, the diaphragm and other fastening units of the charge, and the stabilizer.

We shall assume the weights of these units do not change with change in the length of the charge and that with the design layout and the material adopted they depend only on the caliber of the missile:

$$q_{\text{K}} = G_{\text{K}} D_{\text{K}}^2$$

The weight of the cylindrical part of the engine casing can be presented in the form (Figure 10.1)

$$q_{\text{TP}} = k_L L \frac{\pi}{4} [(D_{\text{H}}^2 - D_{\text{K}}^2) \gamma_{\text{H}} + (D_{\text{K}}^2 - D_{\text{H}}^2) \gamma_{\text{H}}], \quad (10.2)$$

where  $D_{\text{K}}$  is the interior diameter of the tube (the carrier unit of the structure);

$D_{\text{H}}$  is the interior diameter of the heat insulation;

$\gamma_{\text{H}}$  is the specific weight of the structural material;

$\gamma_{\text{H}}$  is the specific weight of the heat insulation;

$L$  is the length of the charge;

$k_L$  is a coefficient taking into account the amount by which the length of the chamber exceeds the length of the charge.

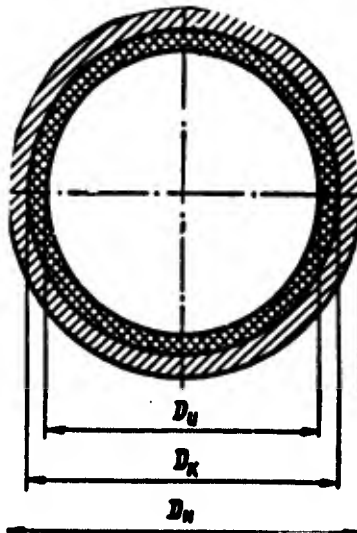


Figure 10.1. Transverse section of rocket chamber.

Let us introduce the designations:

$$B_n = \frac{D_n}{D_H}; \quad B_k = \frac{D_k}{D_H}.$$

Making use of them, we can present the relation for  $q_{TP}$  in the form

$$q_{TP} = k_L L \frac{\pi}{4} D_n^2 (1 - B_n^2) \left[ \gamma_n + B_n^2 \frac{1 - B_n^2}{1 - B_k^2} \gamma_n \right]. \quad (10.3)$$

The expression within brackets can be regarded as the adduced specific weight of the wall of the engine

$$\gamma_{np} = \gamma_n + B_n^2 \frac{1 - B_n^2}{1 - B_k^2} \gamma_n \quad (10.4)$$

consequently

$$q_{TP} = k_L L \frac{\pi}{4} D_n^2 (1 - B_n^2) \gamma_{np} \quad (10.5)$$

For an engine without heat insulation:

$$B_k = 1; \quad \gamma_{np} = \gamma_n.$$

$$D_n - D_k = \frac{p_m^i D_k}{\sigma_B}, \quad (10.6)$$

where  $p_m^i$  is the computed pressure;

$\sigma_B$  is the limit of strength of the structural material.

Having divided both arms of equation (10.6) by  $D_H$  and having solved the equation secured relative to  $B_H = D_K/D_H$ , we find that

$$B_n = \frac{\sigma_B}{\sigma_B + p_m^i}. \quad (10.7)$$

The quantity  $B_k$  is determined by the conditions of heat exchange in the chamber and by the thermophysical characteristics of the coating. In ballistic planning this quantity is assigned in approximate form, in accordance with the analogy of existing models of similar type.

The weight of the rocket charge, making use of the designations adopted (see 3.2), is expressed by the formula

$$G = \rho \frac{\pi D_n^2}{4} B_n^2 B_k^2 \sigma_B L \quad (10.8)$$

From here on we shall have to examine change of parameters of the missile with change in the length of the missile. In doing this the weight of such units of the structure as the diaphragm, the cap, and the stabilizer are conveniently conjoined in equation (10.1) with the weight of the warhead in a single term, which we shall call the adduced weight of useful load

$$q'_{\text{su}} = q_{\text{su}} + q_{\text{st}} \quad (10.9)$$

Then

$$Q = q'_{\text{su}} + k_L L \frac{\pi D_n^2}{4} (1 - B_n^2) \gamma_{\text{np}} + \delta \frac{\pi D_n^2}{4} B_n^2 B_n^2 L. \quad (10.10)$$

### 10.3. Change of Ballistic and Structural Characteristics of an Unguided Rocket Missile With Length of Charge. Condition of Maximum Range

In order to elucidate the approach to a solution of the problem posed, let us examine how ballistic and structural-weight parameters of an unguided rocket missile of assigned caliber, having assigned weight of warhead, change with change in the length of the charge (Figure 10.2).

With increase in the length of charge of a shape adopted, the surface of its combustion inevitably rises. In order that under these circumstances a permissible value for the Yu. A. Pobedonostsev parameter may be retained, it is necessary to increase correspondingly the free cross-section of the chamber, i.e., to reduce the density of the charging. The influence of this factor may become predominant at a certain length, which will lead to reduction in the weight of the charge. At the limit it is possible to conceive of a case where with very great length of charge its weight would become zero, inasmuch as with great combustion surface it is necessary to assume the entire transverse section of the chamber for passage of the gas flow. The charge is converted into a sort of parchment-thin roll with disappearing thickness of vaulting.

The weight of the cylindrical part of the chamber  $q_{\text{TP}}$  rises in linear fashion with the length of the charge. Together with it, the passive weight of the missile follows in linear relation:

$$q = q'_{\text{su}} + q_{\text{TP}}$$

It is obvious that the maximum ratio  $\omega/q$  with increase of the length of the charge is achieved earlier than the maximum of its weight, inasmuch as in the field of maximum weight of the charge with linear rise in passive weight  $q$  the ratio  $\omega/q$  will decline. Maximum velocity  $(v_m)_{\text{max}}$  coincides with maximum  $\omega/q$  ratio. This quantity represents a velocity of missile which is the maximum attainable with given caliber and useful load.

The second factor determining maximum range of the model is the ballistic coefficient  $\underline{c}$ , which changes in inverse proportion to passive

weight, and consequently to the length of the charge, which must be propitious to increase of range over the entire scope of lengths examined. Obviously maximum of range will be located to the right of maximum velocity for the model. As investigations show, for various combinations of ballistic and structural parameters the extreme of range is only insubstantially different from the range corresponding to the maximum of velocity. Consequently, taking as limit for the attainability of the range which corresponds to  $(v_m)_{max}$ , we lower to an insignificant extent the ballistic potentialities of the assigned caliber, but we link the conditional limit of range obtained in this way with a structural variant having less weight and length. We shall in fact consider such a variant the optimum ballistic solution of the problem.

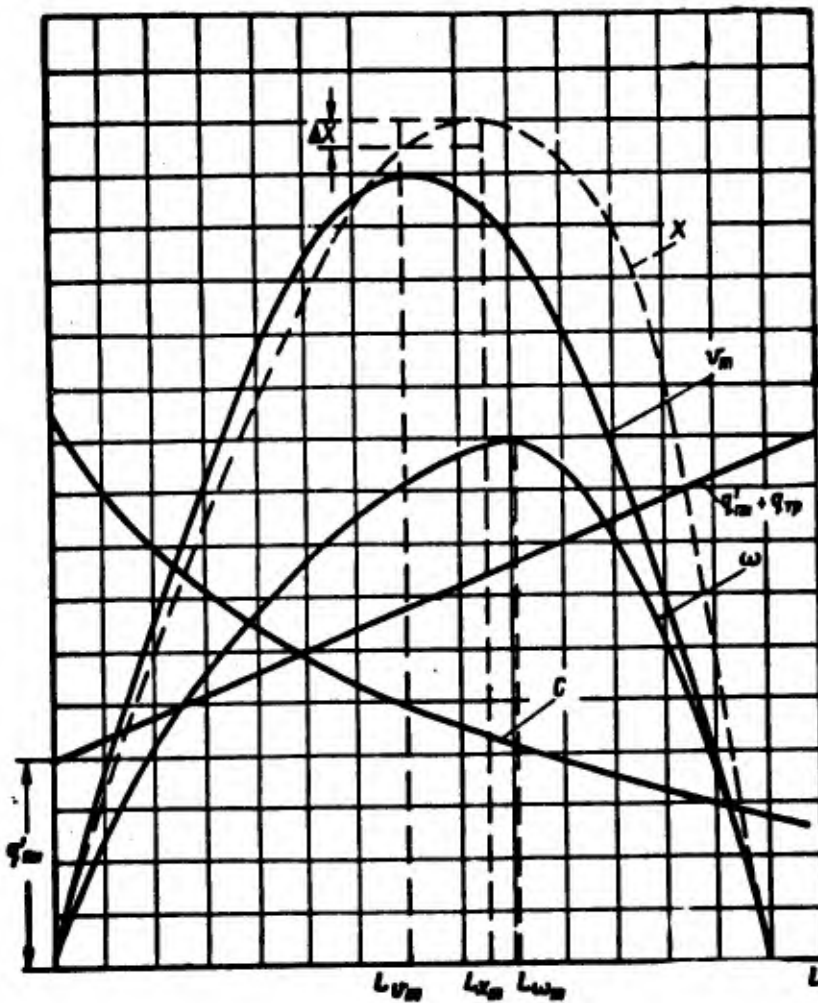


Figure 10.2. Change of weight and ballistic characteristics of unguided rocket missile with rise in length of charge.

Inasmuch as the extreme of range is attained with maximum ratio  $\omega/q$  (the Tsiolkovski number), we shall pass on to determination of this maximum.

From the weight equation for an unguided rocket missile (10.10) we secure

$$\frac{\omega}{q} = \frac{\frac{\pi D_n^2}{4} \delta B_n^2 B_n^2 L_s}{q_{\max} + \frac{\pi D_n^2}{4} \gamma_{np} (1 - B_n^2) k_L L} \quad (10.11)$$

Dividing the numerator and the denominator of the right-hand arm by the cube of the caliber, we secure

$$\frac{\omega}{q} = \frac{\frac{\pi}{4} \delta B_n^2 B_n^2 \bar{L}_s}{C'_{q_{\max}} + \frac{\pi}{4} \gamma_{np} k_L (1 - B_n^2) \bar{L}} \quad (10.12)$$

where  $\bar{L} = \frac{L}{D_n}$ ;

$$C'_{q_{\max}} = \frac{q_{\max}}{D_n^3}$$

In seeking the maximum for the  $\omega/q$  ratio it is a matter of indifference which of the two reciprocally linked quantities --  $\bar{L}$  or  $\epsilon$  -- is assumed to be the independent variable, inasmuch as the dependence of  $\bar{L}$  on  $\epsilon$  is unambiguous. In order to simplify mathematical computations it is well to take  $\epsilon$  as the independent variable. Then, differentiating expression (10.12) according to  $\epsilon$  and making the derivative equal to zero, we secure

$$C'_{q_{\max}} \frac{d\bar{L}}{d\epsilon} \epsilon + \bar{L} C'_{q_{\max}} + \frac{\pi}{4} k_L \gamma_{np} (1 - B_n^2) \bar{L}^2 = 0 \quad (10.13)$$

or

$$-\frac{\frac{d\bar{L}}{d\epsilon} \epsilon + \bar{L}}{\bar{L}^2} = \frac{\pi}{4} \frac{k_L \gamma_{np} (1 - B_n^2)}{C'_{q_{\max}}} \quad (10.14)$$

Equation (10.14) expresses in general form the condition of maximum range of an unguided rocket missile of unlimited length with a given weight of useful load. In order to secure a numerical solution, in equation (10.14) we must substitute a concrete expression of the functional relation  $\bar{L} = f(\epsilon)$  for a charge of the form adopted. Then, having solved the equation, we shall find the value of  $\epsilon_{\max}$  which determines maximum range.

#### 10.4. Connection Between Dimensions of Charge and Coefficient of Charging • for Charges of Various Shapes

The basic dimensions of a charge being planned should be harmonious among themselves and with the internal dimensions of the rocket chamber in such fashion that a charging parameter which is the lowest permissible in accordance with the conditions of stability of combustion is achieved.

Let us examine the relations which establish such a connection for some typical shapes of charges. In doing this we shall limit ourselves to shapes guaranteeing constancy of combustion surface, such as are most frequently used in unguided rocket missiles.

Inasmuch as in an unguided rocket missile both charges with loose charging of chamber and those fastened to the casing of the engine may be used, we shall examine shapes characteristic for both groups. The first group is represented by a charge of cylindrical single-channel burners, the second by a telescopic charge and a charging having a star-shaped section.

##### A. Charge Consisting of Single-Channel Cylindrical Burners

We shall introduce the designations:

- n -- number of burners;
- D -- exterior diameter of burners;
- d -- diameter of channel.

In determining the parameter  $\alpha$  for such a charge there is a difference between  $\alpha_{int}$ , calculated for conditions of combustion within the channel of the burner, and  $\alpha_{ext}$ , calculated for conditions of combustion on the exterior surface of the burners.

In this case

$$\alpha_{int} = \frac{\pi d L}{\frac{\pi}{4} d^2} = \frac{4L}{d}; \quad (10.15)$$

$$\alpha_{ext} = \frac{\pi n D L}{\frac{\pi}{4} (D^2 - n D^2)} = \frac{4n D L}{D^2 - n D^2}. \quad (10.16)$$

Some investigators (1), in planning charges of cylindrical burners, start from an equality in fallings-off of pressure for the channels and the exterior gaps of the charge. With inequality in fallings-off, at the forward cap of the engine an escape of gas from one gap to another commences, something which worsens the combustion circumstances of the charge and contributes to the appearance of anomalies in combustion. It is particularly important to fulfill this condition at the start of combustion

of the charge with minimum free section of the chamber, when the velocity of gas flows and fallings-off in pressure are greatest.

In Chapter III it was shown that there is an unambiguous connection between falling off in pressure along the burning surface of the charge and the  $x$  parameter. Consequently the requirement of equality in fallings-off which is being examined may be reduced to the requirement that

$$x_{\text{за}} = x_{\text{нап}}$$

Let us equivate the right-hand arms of equations (10.15) and (10.16) and determine

$$d = \frac{D_x^2 - nD^2}{nD}. \quad (10.17)$$

The coefficient of charging of the section of the chamber for a charge of single-channel cylindrical burners is

$$\epsilon = \frac{n(D^2 - d^2)}{D_x^2}. \quad (10.18)$$

From equation (10.18)

$$d = \sqrt{\frac{nD^2 - \epsilon D_x^2}{n}}. \quad (10.19)$$

Equating the right-hand arms of equations (10.17) and (10.18) and solving the equality secured relative to  $D$ , we secure

$$D = \frac{D_x}{\sqrt{n(2-\epsilon)}}. \quad (10.20)$$

Substituting expression (10.20) into expression (10.19), we secure

$$d = \frac{D_x(1-\epsilon)}{\sqrt{n(2-\epsilon)}} \quad (10.21)$$

or

$$d = D(1-\epsilon). \quad (10.22)$$

Substituting expression (10.21) into expression (10.15), we find

$$L = \frac{x d}{4} = \frac{x D_x (1-\epsilon)}{4 \sqrt{n(2-\epsilon)}}. \quad (10.23)$$

In order to simplify subsequent calculations we must shift to relative dimensions, dividing the values secured by the caliber of the engine. We shall secure

$$\bar{D} = \frac{D}{D_n} = \frac{B_n B_k}{\sqrt{n(2-\epsilon)}}; \quad (10.24)$$

$$\bar{d} = \frac{d}{D_n} = \frac{B_n B_k (1-\epsilon)}{\sqrt{n(2-\epsilon)}}; \quad (10.25)$$

$$\bar{L} = \frac{L}{D_n} = \frac{\epsilon B_n B_k}{4\sqrt{n}} \frac{1-\epsilon}{\sqrt{2-\epsilon}}. \quad (10.26)$$

In some cases, for example in planning short multiple-burner missiles, when falling off in pressures along the length of the charge is slight, it is well to depart from the equality of  $\epsilon_{int}$  and  $\epsilon_{ext}$ . For arbitrary relationships of  $\epsilon$  deduction of a dependency of  $D$ ,  $d$ , and  $L$  upon  $\epsilon$  differs from the one which has been examined in that a supplementary parameter  $m = \epsilon_{int}/\epsilon_{ext}$  is introduced.

With  $\epsilon_{int} = 2 \epsilon_{ext}$

$$\bar{D} = \frac{B_n B_k}{2\sqrt{n}} (1 + \epsilon); \quad (10.27)$$

$$\bar{d} = \frac{B_n B_k}{2\sqrt{n}} (1 - \epsilon); \quad (10.28)$$

$$\bar{L} = \frac{\epsilon B_n B_k}{4\sqrt{n}} (1 - \epsilon). \quad (10.29)$$

We shall designate

$$\frac{\epsilon B_n B_k}{4\sqrt{n}} = A. \quad (10.30)$$

Then for the type of charge under examination the dependence of  $\bar{L}$  upon  $\epsilon$  can be written in the general form

$$\bar{L} = A f(\epsilon);$$

for  $\epsilon_{int} = \epsilon_{ext}$

$$f(\epsilon) = \frac{1-\epsilon}{\sqrt{2-\epsilon}};$$

for  $\epsilon_{int} = 2 \epsilon_{ext}$

$$f(\epsilon) = 1 - \epsilon.$$

Graphs for the dependence of  $\epsilon$  upon  $\bar{L}$  for these two cases, constructed with various values of  $A$ , are presented in Figures 10.3 and 10.4.

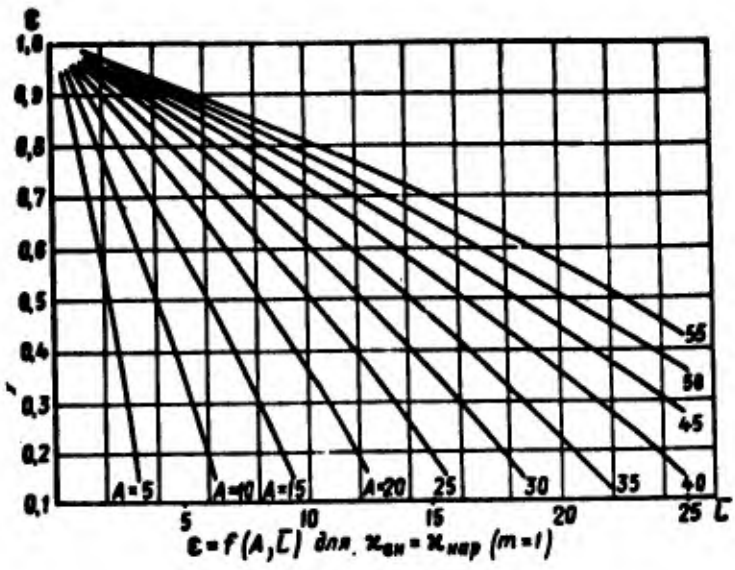


Figure 10.3. Dependence of coefficient of charging section of chamber  $\epsilon$  upon relative length  $\bar{L}$  of charge consisting of cylindrical single-channel burners, with  $\lambda_{int} = \lambda_{ext}$ .

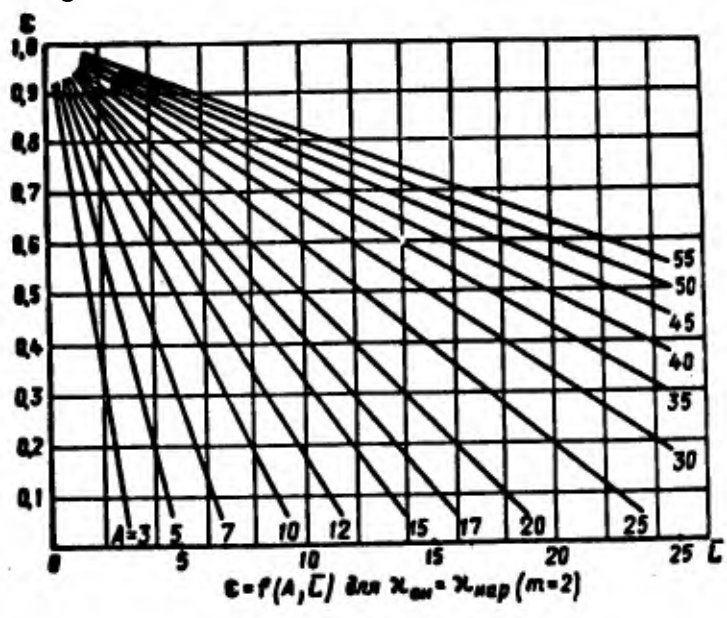


Figure 10.4. Dependence of coefficient of charging section of chamber  $\epsilon$  upon relative length  $\bar{L}$  of charge consisting of cylindrical single-channel burners, with  $\lambda_{int} = 2 \lambda_{ext}$ .

In the planning of a multiple-burner charge a supplementary condition determining the possibility of placing a charge, with the assigned number of burners and having dimensions satisfying the assigned value  $\lambda$ ,

in the rocket chamber arises. It is necessary that the ratio of the diameter of the burner to the interior diameter of the chamber not exceed the value  $\bar{D}_{np}$  corresponding to tight packing of the charge with a given value of  $\underline{n}$ , i.e.,

$$\frac{D}{D_k} < \bar{D}_{np} \quad \text{and} \quad \frac{D}{B_n B_k} < \bar{D}_{np}$$

The value  $\bar{D}_{np}$  depends only upon the number of burners  $\underline{n}$  and is determined from elementary geometrical ratios such as the nondimensional diameter  $\underline{n}$  of identical circles inscribed within a circle of given diameter  $D_k = 1$ .

Values of  $\bar{D}_{np}$  for various values of  $\underline{n}$  are set forth in Table 10.1.

Table 10.1

$n$	3	4	5	7	12	14	19	
$\bar{D}_{np}$	0,464	0,414	0,370	0,333	0,244	0,220	0,200	
$\epsilon_{np}$	$(x_{int} = x_{ext})$	0,452	0,541	0,539	0,714	0,633	0,668	0,757
	$(x_{int} = 2x_{ext})$	0,610	0,656	0,650	0,762	0,692	0,650	0,745

Substituting in equation (10.24)  $\bar{D}' B_n B_k = \bar{D}_{np}$ , we find from it the value  $\epsilon_{np}$ , corresponding to tight packing with  $x_{int} = x_{ext}$ :

$$\epsilon_{np} = 2 - \frac{1}{n \bar{D}_{np}^2}. \quad (10.31)$$

In the general case with  $x_{int} = x_{ext}$  the dependence for  $\epsilon_{np}$  takes on the form

$$\epsilon_{np} = n \left[ \bar{D}_{np}^2 - \left( \frac{1 - n \bar{D}_{np}^2}{n n \bar{D}_{np}} \right)^2 \right]. \quad (10.32)$$

From equation (10.32) for  $x_{int} = 2 x_{ext}$  we secure

$$\epsilon_{np} = 0,5 + \frac{3}{4} n \bar{D}_{np}^2 - \frac{1}{4 n \bar{D}_{np}^2}. \quad (10.33)$$

Values of  $\epsilon_{np}$  calculated in accordance with relations (10.31) and (10.33) for various values of  $\underline{n}$  are set forth in Table 10.1.

The number of burners which will ensure greatest density of packing is determined from the formula

$$n = 1 + 3(i + i^2), \quad (10.34)$$

where  $i$  is a whole number ( $i = 1, 2, 3, \dots$ ).

### B. The Telescopic Charge

The section of a telescopic charge, with basic designations, is set forth in Figure 10.5. For both elements of the charge the thickness of the burning vault must be identical. Consequently

$$\frac{D-d}{2} = \frac{D_{on}}{2},$$

whence

$$D = D_{on} + d. \quad (10.35)$$

The surface of combustion of the charge is

$$S = \pi L (D_{on} + d).$$

The area of free passage is

$$F_{co} = \frac{\pi}{4} (d^2 - D_{on}^2).$$

The Pobedonostsev parameter is defined as being

$$\alpha = \frac{S}{F_{co}} = \frac{4L}{d - D_{on}}, \quad (10.36)$$

whence

$$d - D_{on} = \frac{4L}{\alpha}. \quad (10.37)$$

The coefficient of charging of the section of the chamber with fuel is

$$\epsilon = \frac{S_T}{F_{co}} = \frac{\frac{\pi}{4} (D^2 - d^2 + D_{on}^2)}{\frac{\pi}{4} D^2} = 1 - \frac{d^2 - D_{on}^2}{D^2}. \quad (10.38)$$

Substituting into expression (10.38) expressions (10.35) and (10.37), we secure

$$\epsilon = 1 - \frac{4L}{\alpha D}. \quad (10.39)$$

Inasmuch as  $D = D_H B_H B_K$ , we secure

$$\epsilon = 1 - \frac{4\bar{L}}{\pi B_H B_K}. \quad (10.40)$$

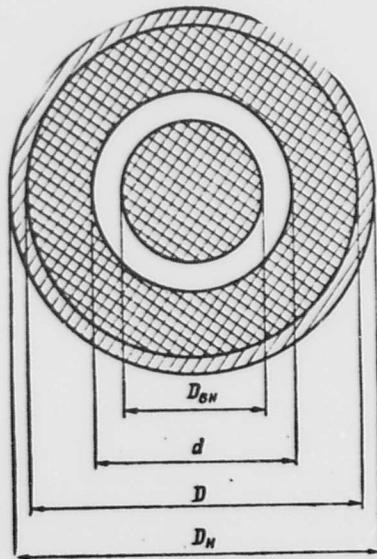


Figure 10.5. Characteristic dimensions of telescopic charge.

#### B. Charge With Channel of Star-Shaped Section

The section of a charge having characteristic dimensions is presented in Figure 10.6.

The coefficient of filling the cross-section of the chamber with the charge is expressed by the relation

$$\epsilon = 1 - \frac{4n}{\pi} \left[ \left( 0,5 - \bar{e}_1 - \bar{r} - \frac{\bar{r}}{\cos \alpha} \right)^2 \frac{\sin \frac{\pi}{n} \cos \alpha}{\sin \theta} + \bar{r}^2 (\alpha - \text{tg } \alpha) \right], \quad (10.41)$$

where  $n$  is the number of rays of the star;

$\bar{e}_1 = \frac{e_1}{D}$  is the relative thickness of the burning vault ( $D$  is the diameter of the charge);

$r, \bar{r} = \frac{r}{D}$  is the radius of rounding-off at the tip of a ray ( $D$  is the diameter of the charge);

$\alpha$  is the angle describing half the original arc of the rounding off;

$\theta$  is the angle at the tip of a projection of the charge.

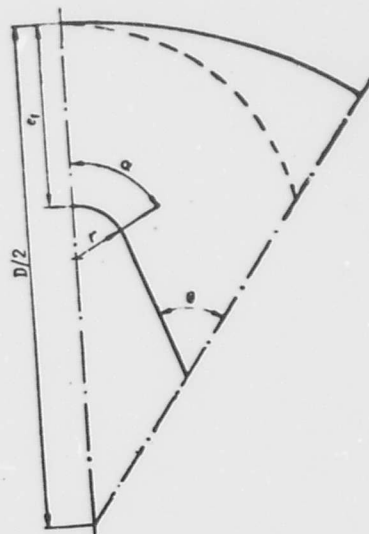


Figure 10.6. Characteristic dimensions of charge having channel of star-shaped section.

After the charge has burned out to a thickness of combustion vault  $e_1$  there remain degressively burning elements which must be regarded as lost for the working process of the engine. The degressive remnants of the charge actually constitute a supplement to the passive weight of the rocket, and in order to reduce this weight it is well to replace these elements of the charge with inserts of a light material (foam plastic) (5).

The ratio of the area of transverse section of these elements to the area of the transverse section of the chamber is called the coefficient of residue,  $\psi_k$  ;

$$\psi_k = 1 - \frac{4n}{\pi} [(\bar{r} + \bar{e}_1)^2 \varphi_1 + (\bar{r} + \bar{e}_1)(0,5 - \bar{r} - \bar{e}_1) \sin \varphi_1], \quad (10.42)$$

where

$$\varphi_1 = \frac{\pi}{n} + \arcsin \frac{(0,5 - \bar{r} - \bar{e}_1) \sin \frac{\pi}{n}}{\bar{r} + \bar{e}_1}.$$

As analysis of this shape of charge shows, for each value of  $n$  there is a unique geometrical variant which will ensure constancy of combustion surface, characterized by a definite ratio of the parameters  $\bar{e}_1$ ,  $\alpha$ , and  $\theta$  (2). The basic characteristics of these variants are presented in Table 10.2. As will be seen from the table, these variants are characterized by high values for  $\psi_k$ . The usefully exploited area of the section

of the chamber rises if a certain progressive character of combustion is assumed. In the same table there are set forth the characteristics of a charge with  $\sigma_s = 1,1$ . Increase of permissible progressive character of surface of the charge with reduction of  $\psi_k$  makes it possible to increase the thickness of the burning vault and the density of charging  $\epsilon$ .

Table 10.2

n	$\sigma_s = 1,0$			$\sigma_s = 1,1$		
	6	7	8	6	7	8
$\bar{e}_1$	0,150	0,142	0,125	0,206	0,190	0,181
$\epsilon$	0,824	0,755	0,666	0,865	0,796	0,757
$\psi_k \text{ o/n}$	15	12,7	11,7	8,8	8,3	6,9
$x/\bar{L}$	25,6	18,1	13,5	26,6	17,5	14,9

The weight of the effectively utilized charge can be computed according to the formula

$$\omega = \delta \frac{\pi D_n^2}{4} \epsilon \left(1 - \frac{\psi_k}{\epsilon}\right) L. \quad (10.43)$$

The weight of the rocket chamber, taking into account the weight of the degressive elements of the charge or their substitutes, is computed as

$$q_{\tau p} = k_L L \frac{\pi D_n^2}{4} [\gamma_{np} (1 - B_n^2) + \gamma_\psi \psi_k], \quad (10.44)$$

where  $\gamma_\psi$  is the specific weight of the fuel or filling.

This relation can be reduced to a general form if one introduces a new expression for the adduced specific weight of the wall:

$$\gamma'_{np} = \gamma_{np} + \gamma_\psi \frac{\psi_k}{1 - B_n^2}. \quad (10.45)$$

Then

$$q_{\tau p} = \gamma'_{np} \frac{\pi D_n^2}{4} k_L L (1 - B_n^2). \quad (10.46)$$

The initial value of the relative perimeter of combustion is

$$\bar{\Pi}_{r0} = \frac{\Pi_{r0}}{D} = \bar{r}\alpha + \frac{(0,5 - \bar{e}_1 - \bar{r}) \sin \frac{\pi}{n}}{\sin \theta} - \bar{r} \operatorname{ctg} \theta. \quad (10.47)$$

The parameter of charging,  $x$ , is computed as

$$x = \frac{\Pi_{ro}L}{F_{\kappa}(1-\epsilon)} = \frac{4Z\Pi_{ro}}{\pi(1-\epsilon)}, \quad (10.48)$$

hence

$$\frac{x}{L} = \frac{4\Pi_{ro}}{\pi(1-\epsilon)}. \quad (10.49)$$

Inasmuch as for a charge having a constant surface of combustion with a given number  $n$  the values  $\Pi_c$  and  $\epsilon$  are reciprocally linked and correspond to the single combination of geometrical parameters which ensure that  $\sigma=1$ , they define the single value for the nondimensional ratio  $x/\bar{L}$ . For the variants set forth in Table 10.2 the values of  $x/\bar{L}$  are given in the last graph. Making use of this relationship, with a given value for  $x$  one can determine the permissible length of the charge and its weight.

If one starts from the desired elongation of the charge  $\bar{L}$ , one can select a number of rays of the star  $n$  at which the value of  $x$  realized approaches the permissible value. Thus, in contradistinction to the charge of single-channel cylindrical burners, in the present case it is not possible to change the relative length of the charge without interruption, while preserving the number of rays and without in doing so changing the characteristics of progressivity of the charge. For this reason, determining from expression (10.49) the value of  $\epsilon$  as

$$\epsilon = 1 - \frac{4\Pi_{ro}L}{\pi x}, \quad (10.50)$$

one should note that strictly speaking with  $\sigma=1$  this formula covers the totality of individual variants which are different as to the  $n$  number.

But the relation (10.50), as also the graphs in Figure 10.7, constructed on the basis of data from Table 10.2, express a general tendency toward change of  $\epsilon$  with elongation of a charge of a given type at fixed value for  $x$ . As follows from the graph, over a pretty long range of elongations of charge with a channel of star-shaped section it is possible in first approximation to consider that the coefficient of charging  $\epsilon$  changes in linear fashion with rise in  $\bar{L}$ .

#### 10.5. Determination of Basic Design Parameters of Optimum Ballistic Model for Charge Consisting of Cylindrical Single-Channel Burners

For a charge of cylindrical single-channel burners, with  $x_{int} = x_{ext}$  we secure from formula (10.26)

$$\frac{d\bar{L}}{d\epsilon} = -\frac{x B_n B_{\kappa}}{4\sqrt{\frac{n}{2}} \sqrt{2-\epsilon}} \frac{\epsilon-3}{2(2-\epsilon)\sqrt{2-\epsilon}}. \quad (10.51)$$

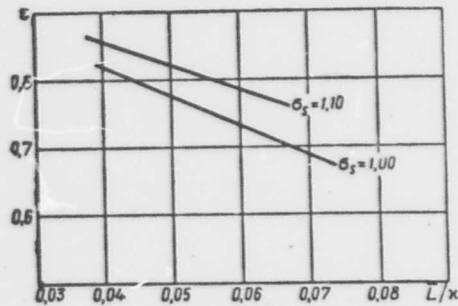


Figure 10.7. Dependence of coefficient of charging  $\epsilon$  upon  $\bar{L}/x$  for charges having channel of star-shaped section and possessing constant surface of combustion.

Substituting expressions (10.26) and (10.51) into equation (10.14) we secure

$$\frac{-3\epsilon^2 + 9\epsilon - 4}{2(1-\epsilon)^2\sqrt{2-\epsilon}} = \frac{\pi^2 \gamma_{np} k_L B_H B_K (1-B_H^2)}{16 \sqrt{n} C'_{q_{HH}}}. \quad (10.52)$$

Analytical solution of equation (10.52) relative to  $\epsilon$  proves to be too cumbersome. For this reason in order to determine  $\epsilon_{\max}$  it is well to make use of the graphic method. The left-hand arm of the equality constitutes the function  $f(\epsilon_{\max})$ .

The right-hand arm of the equality (10.52) represents a nondimensional complex made up of the project parameters and the relative weight of useful load. We shall designate it by the symbol  $N$ .

Setting oneself arbitrary values of  $\epsilon$  one can compute the values of the function  $f(\epsilon_{\max})=N$  that correspond to them. It is well to present the results of computations in coordinates  $\epsilon_{\max}=f(N)$  (Figure 10.8). In order to determine the value of  $\epsilon_{\max}$  it is necessary to compute, in accordance with given values of the project parameters for a given value  $C'_{q_{HH}}$ , the magnitude of the complex  $N$  and to enter the graph  $\epsilon_{\max}=f(N)$  or the table with it. Finding  $\epsilon_{\max}$  from the graph or from the table, one can then compute all the basic ballistic and design parameters determined by it.

Let us examine the character of the function  $\epsilon_{\max}=f(N)$ . The following equality corresponds to the condition  $N=0$ :

$$-3\epsilon^2 + 9\epsilon - 4 = 0, \quad (10.53)$$

the roots of which are equal to

$$\epsilon_1 = 2.62; \quad \epsilon_2 = 0.543.$$

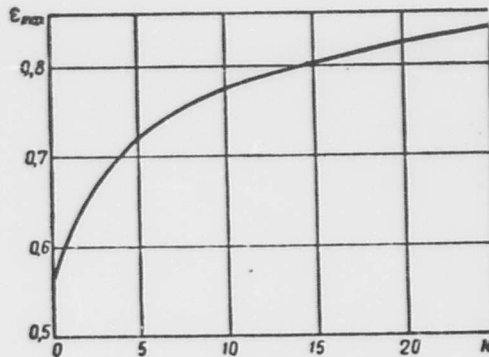


Figure 10.8. Dependence of coefficient of charging  $\epsilon_{max}$ , ensuring maximum velocity of unguided rocket missile, upon complex  $N$  with  $\epsilon_{int} = \epsilon_{ext}$ .

Inasmuch as a value  $\epsilon > 1$  is devoid of physical meaning, the only acceptable root of the equation in question, determining the initial ordinate of the graph  $\epsilon_{max} = f(N)$ , is

$$\epsilon_{max(0)} = 0,543.$$

The following equality corresponds to the condition  $N = \infty$ :

$$\sqrt{2 - \epsilon}(1 - \epsilon)^2 = 0, \quad (10.54)$$

which is satisfied with  $\epsilon_1 = 2$  and  $\epsilon_2 = 1$ .

Eliminating the first of these as contradictory to reality, we secure  $\epsilon_{max(\infty)} = 1$ . This is an asymptotic value, toward which the function  $\epsilon_{max}(N)$  trends with  $N \rightarrow \infty$ .

The condition  $N = 0$  is met with  $C'_{q_{nn}} = \infty$  or with  $B_H = 1$ . In this event the weight of the rocket chamber becomes negligibly small in comparison with the weight of useful load, in one case by virtue of infinite rise of  $q'_{nn}$ , in the other by virtue of trending of the thickness of the wall of the rocket chamber toward zero (for example by virtue of the use of material having infinitely high strength characteristics). Obviously in practice these conditions cannot be fulfilled, and the case  $N = 0$  may be regarded as only a limit toward which this complex trends for some real designs.

Let us note that equation (10.53) can be secured from the condition of maximum weight of charge.

In harmony with equation (10.8)

$$\frac{d\omega}{d\epsilon} = \frac{\pi D_H^2}{4} \delta B_H^2 B_K^2 \left( \frac{d\bar{L}}{d\epsilon} \epsilon + \bar{L} \right).$$

Making the derivative equal to zero we secure the equation

$$\frac{d\bar{L}}{d\epsilon} \epsilon + \bar{L} = 0,$$

which, after substitution of expressions (10.26) and (10.51), leads to equation (10.53).

Table 10.3

$$\epsilon_{\max} = f(N).$$

N	0,0	0,2	0,4	0,6	0,8
0	0,543	0,559	0,574	0,586	0,598
1	0,608	0,618	0,628	0,636	0,642
2	0,648	0,654	0,660	0,666	0,672
3	0,678	0,684	0,688	0,692	0,696
4	0,700	0,704	0,708	0,712	0,716
5	0,720	0,724	0,728	0,732	0,734
6	0,736	0,738	0,740	0,742	0,744
7	0,746	0,748	0,750	0,752	0,754
8	0,756	0,758	0,760	0,762	0,764
9	0,766	0,768	0,770	0,772	0,774
10	0,776	0,778	0,780	0,781	0,782
11	0,783	0,784	0,785	0,786	0,787
12	0,788	0,789	0,790	0,791	0,792
13	0,793	0,794	0,795	0,796	0,797
14	0,798	0,800	0,801	0,802	0,803
15	0,804	0,804	0,805	0,806	0,807
16	0,808	0,808	0,809	0,810	0,811
17	0,812	0,812	0,813	0,814	0,815
18	0,816	0,816	0,817	0,818	0,819
19	0,820	0,820	0,821	0,822	0,823
20	0,824	0,824	0,825	0,826	0,826
21	0,827	0,828	0,828	0,829	0,829
22	0,830	0,831	0,831	0,832	0,832
23	0,833	0,834	0,834	0,835	0,835
24	0,836	0,836	0,837	0,837	0,837

Thus with  $N = 0$  the maximum velocity of an unguided rocket missile coincides with maximum weight of rocket charge, which corresponds to the physical meaning of the condition  $N = 0$  as revealed above: for a missile in which the weight of the rocket chamber plays an insignificant part amid the passive weight, the maximum for the ratio  $\omega/q$  must approach the maximum for  $\omega$ .

Among the conditions ensuring the equality  $N = \infty$ , let us examine one:  $\alpha = \infty$ . This means that in planning a charge there are no limitations upon  $\alpha$ . In this event the maximum velocity is achieved with maximum filling of the cross-section of the chamber with fuel ( $\epsilon = 1$ ).

The real values of  $\epsilon_{\max}$  are to be found within the range

$$0,543 < \epsilon_{\max} < 1.$$

Let us examine the sequence of computation of maximum possible range of flight of an unguided rocket missile with given caliber and weight of useful load.

1. In accordance with assigned values  $q'_{\text{nh}}$ ,  $D_{\text{n}}$  and of project parameters  $\alpha$ ,  $\sigma_B$ ,  $p'_m$ ,  $\gamma_{\text{np}}$ ,  $\delta$ ,  $k_L$ , the magnitude of  $N$  is computed, in accordance with which the value of  $\epsilon_{\max}$  is determined from the graph.

2. In accordance with formulas (10.20), (10.22), and (10.23), with  $\epsilon = \epsilon_{\max}$  the basic parameters of the charge are determined.

3. In accordance with formulas (10.8) and (10.5) the weights of the charge  $\omega$  and of the rocket chamber  $q_{\text{TP}}$  are computed, and the passive weight of the missile  $q = q'_{\text{nh}} + q_{\text{TP}}$  is determined.

4. The following formula is computed:

$$v_{\max} = I_1 g \ln \left( 1 + \frac{\omega}{q} \right).$$

5. The ballistic coefficient is computed:

$$c = \frac{I D_{\text{n}}^2}{q} 10^8.$$

6. In accordance with ballistic tables for  $\theta_0 = 45^\circ$  the maximum range of fire is determined.

In accordance with the results of the computations carried out for various calibers and useful load weights, one can construct a graph for  $X_{\max} = f(D_{\text{n}}, q'_{\text{nh}})$ , with the help of which the reverse problem can be solved; to determine the caliber in accordance with given values of  $q'_{\text{nh}}$  and  $X_{\max}$ , and in accordance with it also the remaining parameters of the optimum model.

A solution analogous to the one examined may be carried out for other shapes of charge as well. For this purpose it is necessary to substitute into expression (10.14) the relationship  $L = f(\epsilon)$  pertinent to a charge of given shape.

#### 10.6. Determination of Basic Design Parameters of Optimum Ballistic Model for Charge of Any Given Shape (Generalized Graph-Analytical Method of Solution)

The method of solution examined in the preceding section is constructed upon relations suitable only for a charge of a definite shape, in

which connection even in this case the use of these relationships is limited by supplementary conditions, for example  $x_{\text{int}} = x_{\text{ext}}$ . The first deficiency of the method examined lies in this circumstance. A second and even more substantial deficiency of the method consists in the use of graphs for  $X=f(D_n, q_{\text{in}}')$  which can be computed and constructed only for a certain combination of values of project parameters. If in planning the adopted value even of only one of the project parameters proves to be different from the one for which a graph has been constructed, use thereof becomes impossible. At the same time, steady technical progress forces the designer to seek new design solutions associated with the use of new layouts, fuels, and materials, and consequently characterized by constantly changing values for project parameters.

A virtue of the method set forth is its universality, i.e., its suitability for charges of any shape, and also for any numerical values of project parameters and their combinations.

Analysis of the relationship  $\epsilon=f(\bar{L})$  for charges of varying shape shows that in the majority of cases over the range  $\bar{L}$  which is of practical interest, it can be approximated with a sufficient degree of precision through the following formula:

$$\epsilon = 1 - k_s \bar{L}. \quad (10.55)$$

The specifics of the shape of the charge and the influence of the parameter of charging are reflected in this relationship in the magnitude of the coefficient  $k_s$ .

In order to convince oneself of the correctness of formula (10.55) it suffices to return to the graphs in Figures 10.3, 10.4, and 10.7 and to formulas (10.29), (10.40), and (10.50). From the formulas referred to one secures an analytical expression for  $k_s$ :

for a charge of cylindrical single-channel burners with  $x_{\text{int}} = 2x_H$ :

$$k_s = \frac{4\sqrt{n}}{x_B B_K};$$

for a telescopic charge:

$$k_s = 4/x_B B_K;$$

for a charge having a channel of star shaped section:

$$k_s = 4\bar{\Pi}_{r0}/\pi x.$$

In the remaining cases  $k_s$  is determined from the graph for  $\epsilon=f(\bar{L})$  as the tangent of the angle of incline of the approximating straight line in the section  $\epsilon = 1,0-0,6$ .

Making use of relationship (10.55) we secure

$$\bar{L} = \frac{1-\varepsilon}{k_s}; \quad (10.56)$$

$$\frac{d\bar{L}}{d\varepsilon} = -\frac{1}{k_s}. \quad (10.57)$$

Substituting expressions (10.56) and (10.57) into the general solution (10.14) we secure

$$\frac{2\varepsilon-1}{(1-\varepsilon)^2} k_s = \frac{\pi}{4} \frac{k_L \gamma_{np} (1-B_n^2)}{C'_{q_{nn}}}. \quad (10.58)$$

Let us designate

$$\bar{N} = \frac{\pi}{4} \frac{k_L \gamma_{np} (1-B_n^2)}{C'_{q_{nn}}}. \quad (10.59)$$

Consequently

$$\bar{N} = \frac{2\varepsilon-1}{(1-\varepsilon)^2}. \quad (10.60)$$

Solving this equation relative to  $\varepsilon$  we secure

$$\varepsilon_{\max} = \frac{(1+\bar{N}) \pm \sqrt{1+\bar{N}}}{\bar{N}}. \quad (10.61)$$

Let us evaluate the error introduced by the approximation (10.55) into the solution of the problem with the greatest divergence of the relationship  $\varepsilon=f(\bar{L})$  from the linear, for a charge of cylindrical single-channel burners with  $\varepsilon_{\text{int}} = \varepsilon_{\text{ext}}$ ,  $A = 40$ .

Let us take  $N = 10$ . From the expression for  $N$  it follows that

$$\frac{\pi}{4} \frac{k_L \gamma_{np} (1-B_n^2)}{C'_{q_{nn}}} = \frac{N}{A}.$$

The complex

$$\bar{N} = \frac{\pi}{4} \frac{k_L \gamma_{np} (1-B_n^2)}{C'_{q_{nn}}} = \frac{N}{A} \frac{1}{k_s}.$$

is used in the universal solution.

From the graph (Figure 10.3) for the range  $L = 0 \div 14$ ,  $\epsilon = 1 \div 0.6$ .  
Then

$$k_s = \frac{1-0.6}{14} = 0.0296; \bar{N} = \frac{10}{40 \cdot 0.0296} = 8.45;$$

$$\epsilon_{\max} = \frac{9.45 - \sqrt{9.45}}{8.45} = 0.755.$$

According to Table (10.3) for  $N = 10$   $\epsilon_{\max} = 0.776$ .

Thus the divergence in the quantity  $\epsilon_{\max}$  for the two methods of solution comes to 2.8 percent. The divergence in the quantity  $\bar{L}_{\max}$ , calculated according to formulas (10.23) and (10.56), comes to 2.2 percent ( $\bar{L}_1 = 8.0$ ,  $\bar{L}_2 = 8.28$ ). Thus the divergence between the results of computations according to both methods lies within the limits of precision for solution of the problem.

The relative weights of the basic elements of a rocket engine will be expressed in the following fashion:

$$C_{\bullet} = \frac{\pi}{4} \delta B_n^2 B_k^2 \bar{L} = \frac{\pi}{4} \delta \frac{B_n^2 B_k^2}{k_s} (1 - \epsilon) \epsilon; \quad (10.62)$$

$$C_{q_T} = \frac{\pi}{4} \gamma_{np} (1 - B_n^2) k_L \bar{L} = \frac{\pi}{4} \gamma_{np} (1 - B_n^2) \frac{k_L}{k_s} (1 - \epsilon). \quad (10.63)$$

$C'_{q_{nn}}$  can be determined from expression (10.59)

$$C'_{q_{nn}} = \frac{\pi}{4} \frac{k_L}{k_s} \gamma_{np} (1 - B_n^2) \frac{1}{N}. \quad (10.64)$$

Making use of expressions (10.62) and (10.63) one can write

$$\frac{\omega}{q} = \frac{C_{\bullet}}{C_{q_T} + C'_{q_{nn}}} = \frac{\delta}{\gamma_{np}} \frac{B_n^2 B_k^2}{(1 - B_n^2) k_L} \frac{(1 - \epsilon) \epsilon}{(1 - \epsilon + \frac{1}{N})}. \quad (10.65)$$

Substituting expression (10.60) into expression (10.65) we secure

$$\frac{\omega}{q} = \frac{\delta}{\gamma_{np}} \frac{B_n^2 B_k^2}{(1 - B_n^2) k_L} (2\epsilon - 1). \quad (10.66)$$

The equality (10.66) can be presented in the form

$$\left( \frac{\omega}{q} \right)_{\max} = B f_1(\epsilon_{\max}), \quad (10.67)$$

where

$$B = \frac{3}{100 k_L} \frac{B_0^2 B_1^2}{1 - B_0^2}; \quad (10.68)$$

$$f_1(c_{max}) = 2c_{max} - 1. \quad (10.69)$$

The expression for the ballistic coefficient can be presented in the form

$$c = \frac{100^2 10^6}{g} = \frac{100^2 10^6}{g} \cdot \frac{g}{100^2} \quad (10.70)$$

or

$$c = \frac{100}{C_0 \cdot D_0} \frac{g}{g}. \quad (10.71)$$

In formula (10.71), in contradistinction to formula (10.70), the caliber PC is expressed in decimeters, which has in fact led to the appearance of the transitive multiplier 10.

Substituting into formula (10.71) the values for  $C_0$  and  $\frac{g}{g}$  from expressions (10.62) and (10.66) we secure

$$c = \frac{100}{\pi D_0} \frac{k_0}{k_L 100} \frac{1}{1 - B_0^2} \frac{2n - 1}{(1 - \epsilon)}. \quad (10.72)$$

From the expression for  $N$

$$D_0 = \sqrt[3]{\frac{4N g_m k_0}{\pi k_L 100 (1 - B_0^2)}}. \quad (10.73)$$

Substituting expression (10.73) into expression (10.72) we secure

$$c = \frac{100 k_0}{\pi k_L 100 (1 - B_0^2)} \sqrt[3]{\frac{\pi k_L 100 (1 - B_0^2)}{4g_m k_0}} \frac{1}{\sqrt[3]{N}} \frac{2n - 1}{(1 - \epsilon)}. \quad (10.74)$$

This relationship can be presented as follows:

$$c = \Phi \cdot f_2(c_{max}), \quad (10.75)$$

where

$$\Phi = \frac{100}{\sqrt[3]{g_m}} \left| \frac{k_0}{\pi k_L 100 (1 - B_0^2)} \right|^{1/3}; \quad (10.76)$$

$$f_2(\epsilon_{\max}) = \frac{1}{\epsilon} \sqrt[3]{\frac{(2\epsilon - 1)^2}{1 - \epsilon}}. \quad (10.77)$$

A solution of the problem can be secured with the help of the graph (Figure 10.9). In the upper left quadrant there are set forth the curves establishing a connection between range of fire, maximum velocity, and the ballistic coefficient. With the system of solution adopted one must construct these in a  $v - c$  system of coordinates. These curves are constructed for the 1943 resistance principle. Beneath these there is a graph for the relationship  $c = f(\epsilon_{\max})$  with  $\Phi = \text{constant}$ , constructed in accordance with formula (10.75). In the upper right quadrant curves for the dependence of  $v_m$  upon  $Z = \omega/q$ , as calculated from the Tsiolkovskiy formula for various values of  $I_1$ , are placed. Beneath these in the lower right quadrant curves for  $Z = f(\epsilon_{\max})$  with  $B$  constant, constructed according to formula (10.67), are set up.

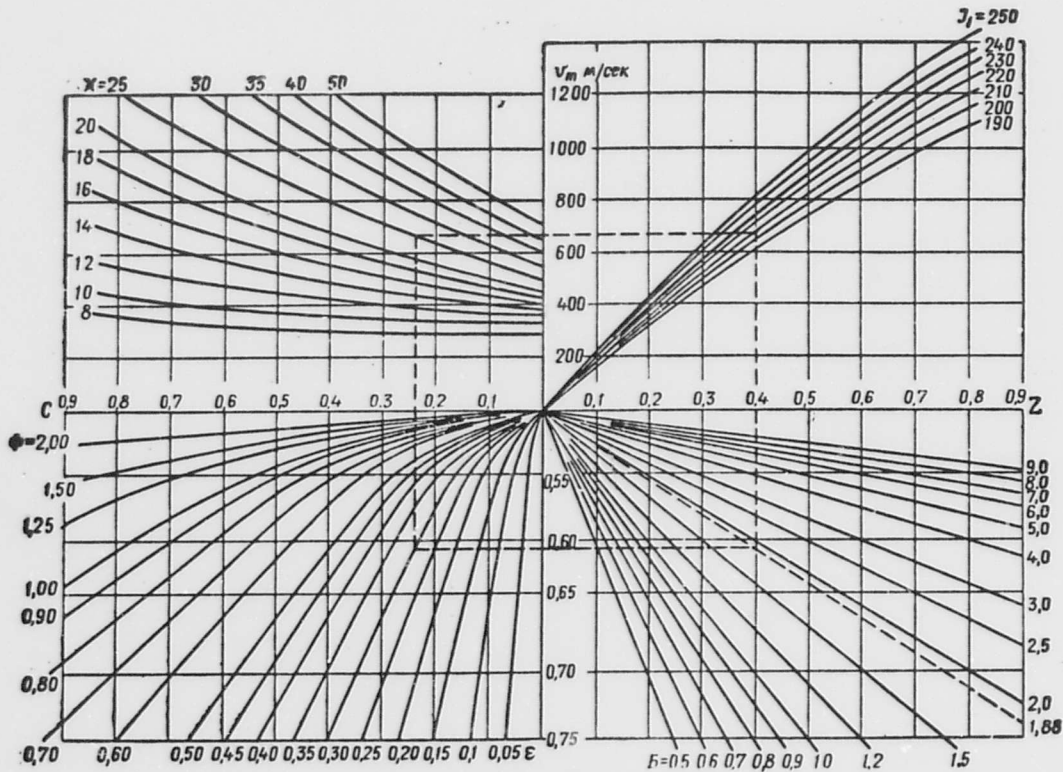


Figure 10.9. Nomogram for determination of basic parameters of optimum ballistic model.

The layout for solution of the problem is shown by dashed straight lines. It is necessary, in advance and in accordance with the values for

project parameters adopted for the solution, to figure out the values of the coefficients B and  $\Phi$  and to find the curves which correspond to them in the lower quadrants. Moving along the curve  $X = X_{\text{зад}}$  we shall be getting various values for c and Z, for which we shall find from the lower graphs, with constant B and  $\Phi$ , the values for  $\epsilon_{\text{max}1} = \varphi(c)$  and  $\epsilon_{\text{max}2} = \varphi(Z)$  that correspond to them. Obviously an equality  $\epsilon_{\text{max}1} = \epsilon_{\text{max}2}$  must correspond to the solution of the problem. Having achieved coincidence of these values and having secured in this manner the desired quantity  $\epsilon_{\text{max}}$ , and knowing also from the graphs the values for c and Z which correspond to it, we easily find all the other parameters of the optimum ballistic model. The caliber of the missile can be determined from expression (10.72):

$$D_n = \frac{40ik_s}{\pi k_{Lnp} (1 - B_n^2) c} \cdot \frac{2\epsilon - 1}{\epsilon(1 - \epsilon)}. \quad (10.78')$$

The passive weight of the missile can be defined as follows:

$$q = \frac{iD_n^2}{c} 10^3, \quad (10.79')$$

and the following can be found in accordance with the value of Z

$$\omega = Z \cdot q. \quad (10.80')$$

The full weight of the model is determined as follows:

$$Q_0 = q + \omega.$$

The basic dimensions of the missile are determined in accordance with the value found for  $\epsilon_1 = \epsilon_2 = \epsilon_{\text{max}}$ .

Thus, for example, for a charge of cylindrical single-channel burners the dimensions D, d, and L which are of interest to us can be computed in accordance with formulas (10.20), (10.22), and (10.23).

If the quantity  $k_s$ , found from the graph  $\epsilon = f(\bar{L})$ , is used in solving, in the event of need the precision of the solution can be heightened by virtue of a second approximation. In the second approximation a refined value for  $k_s$  is used; this is secured via approximation of graph  $\epsilon = f(\bar{L})$  to the straight line within a narrower field defined by the value for  $\epsilon_{\text{max}}$  from the first solution.

Example 1. To determine the basic design parameters of an optimum ballistic model for a range of 25 kilometers with adduced weight of useful load  $q'_{\text{нн}} = 250$  kg.

For computation we adopt the following project parameter values:

$$\begin{aligned}
 n &= 1; & p_m &= 200 \text{ кг/см}^2; & \sigma_B &= 3500 \text{ кг/см}^2; \\
 \gamma_{np} &= 7,82 \text{ кг/д.м}^3; & \delta &= 1,60 \text{ кг/д.м}^3; & i &= 1,3; & k_L &= 1,02; \\
 B_n &= 1; & I_1 &= 200 \frac{\text{кгсек}}{\text{кг}}; & x_{BH} &= x_H &= 170.
 \end{aligned}$$

$$\begin{aligned}
 1. \quad B_n &= \frac{\sigma_B}{\sigma_B + p_m} = \frac{3500}{3500 + 200} = 0,95. \\
 2. \quad B &= \frac{\delta}{\gamma_{np}} \frac{B_n^2}{1 - B_n^2} \frac{1}{k_L} = \frac{1,6}{7,82} \frac{0,95^2}{1 - 0,95^2} \frac{1}{1,02} = 1,88. \\
 3. \quad A &= \frac{x_B B_n}{4 \sqrt{n}} = \frac{170 \cdot 0,95}{4} = 40,4.
 \end{aligned}$$

4. From the graph in Figure 10.3 we find, in accordance with the computed value  $A = 10,4$ ,  $k_s$  as the tangent of the angle of incline of the curve  $\epsilon = f(\bar{L})$  over the section  $\epsilon = 0,8 + 0,5$ :

$$\begin{aligned}
 k_s &= \frac{\epsilon_1 - \epsilon_2}{\bar{L}_2 - \bar{L}_1} = \frac{0,8 - 0,5}{16,3 - 7,1} = 0,0326. \\
 5. \quad \Phi &= \frac{10I}{3 \sqrt{q_{BH}}} \left[ \frac{4k_s}{\pi \gamma_{np} (1 - B_n^2) k_L} \right]^{3/4} = \\
 &= \frac{10 \cdot 1,3}{3 \sqrt{250}} \left[ \frac{4 \cdot 0,0326}{\pi \cdot 7,82 (1 - 0,95^2) \cdot 1,02} \right]^{3/4} = 0,292.
 \end{aligned}$$

6. From the graph we find that equality of the values for  $\epsilon$ , determined from the left and the right portions of the graph, is ensured under the following conditions:

$$\begin{aligned}
 \epsilon_{\max} &= 0,61; & c &= 0,24; & Z &= 0,4; & v_m &= 660 \frac{\text{м}}{\text{сек}}. \\
 7. \quad D_n &= \frac{40Ik_s}{\pi k_L \gamma_{np} (1 - B_n^2) c} \cdot \frac{2\epsilon_{\max} - 1}{\epsilon_{\max} (1 - \epsilon_{\max})} = \\
 &= \frac{40 \cdot 1,3 \cdot 0,0326}{\pi \cdot 1,02 \cdot 7,82 (1 - 0,95^2) \cdot 0,24} \cdot \frac{2 \cdot 0,61 - 1}{0,61 (1 - 0,61)} = 2,68 \text{ д.м.} \\
 8. \quad q &= \frac{1D_n^2}{c} 10^3 = \frac{1,3 \cdot 0,268^2}{0,24} 10^3 = 388 \text{ кг.} \\
 9. \quad \omega &= qZ = 388 \cdot 0,4 = 155,5 \text{ кг.} \\
 10. \quad Q_0 &= \omega + q = 156 + 388 = 544 \text{ кг.} \\
 11. \quad \bar{L} &= \frac{x_B B_n}{4 \sqrt{n}} \cdot \frac{1 - \epsilon}{\sqrt{2 - \epsilon}} = \frac{170 \cdot 0,95}{4} \cdot \frac{1 - 0,61}{\sqrt{2 - 0,61}} = 13,3; \\
 &L = 13,3 \cdot 2,68 = 35,8 \text{ д.м.} \\
 12. \quad D &= \frac{D_n B_n}{\sqrt{n(2 - \epsilon)}} = \frac{2,68 \cdot 0,95}{\sqrt{2 - 0,61}} = 2,16 \text{ д.м.} \\
 13. \quad d &= D(1 - \epsilon) = 2,16 (1 - 0,61) = 0,845 \text{ д.м.}
 \end{aligned}$$

14. We check whether the assigned value for  $\alpha$  is ensured with the dimensions computed:

$$\alpha_{\text{нн}} = \frac{4L}{d} = \frac{4 \cdot 35,8}{0,845} = 170;$$

$$\alpha_{\text{нсп}} = \frac{\pi DL}{\frac{\pi}{4} (D_k^2 - D^2)} = \frac{\pi 2,16 \cdot 35,8}{\frac{\pi}{4} [(0,95 \cdot 2,68)^2 - 2,16^2]} = 172,5.$$

#### 10.7. Selection of Optimum Design Variant of Unguided Rocket Missile

At the basis of the selection of an optimum ballistic variant there lies a single criterion -- minimum launch weight; which, despite all its significance, is not all-inclusive. In practice it is sometimes well to depart a little from the optimum ballistic solution in order to meet other requirements imposed upon the model being planned. Thus, for example, in some cases the optimum ballistic variant may turn out to be excessively long, and for this reason it will be justifiable to shift to another larger caliber in order to make the model shorter at the cost of its becoming somewhat heavier.

In order to determine the basic design parameters of variants close in caliber to the optimum, one can exploit one of the properties of the coefficient  $\alpha$  for weight of the engine.

At the great elongations of the charge characteristic for the optimum ballistic variant the coefficient  $\alpha$  changes faintly with length. This conclusion can be extended to models having close relative lengths of charge and calibers as regards amount, i.e., it can be assumed that the value of  $\alpha$  found for the optimum ballistic variant can be transferred to these models as well.

In Figure 10.10 a graph is set forth which can be utilized for solution of the problem posed. The left side of the graph is filled with curves which establish the connection between range of fire and maximum velocity at various fixed values for the ballistic coefficient  $\underline{c}$ . In the right half there are curves for the dependence of  $v_m$  upon  $\mu$  at various values of unit impulse  $I_1$ . The scale for  $\mu$  is duplicated in the values of the variable  $Z = \frac{\mu}{1-\mu}$  which are linked with  $\mu$  by the ratio

$$Z = \frac{\mu}{1-\mu}.$$

Cutting through the bundle of curves in the left half of the graph with a vertical corresponding to the range assigned, we secure a number of values for  $\underline{c}$ , to each of which corresponds, at the adopted value for  $I_1$ , one definite value of  $\mu$  or  $Z$ . In other words, a number of combinations of reciprocally linked values of  $\underline{c}$  and  $Z$  (or  $\mu$ ) correspond to the assigned range. Making use of these values one must determine the design parameters of the model which will ensure them.

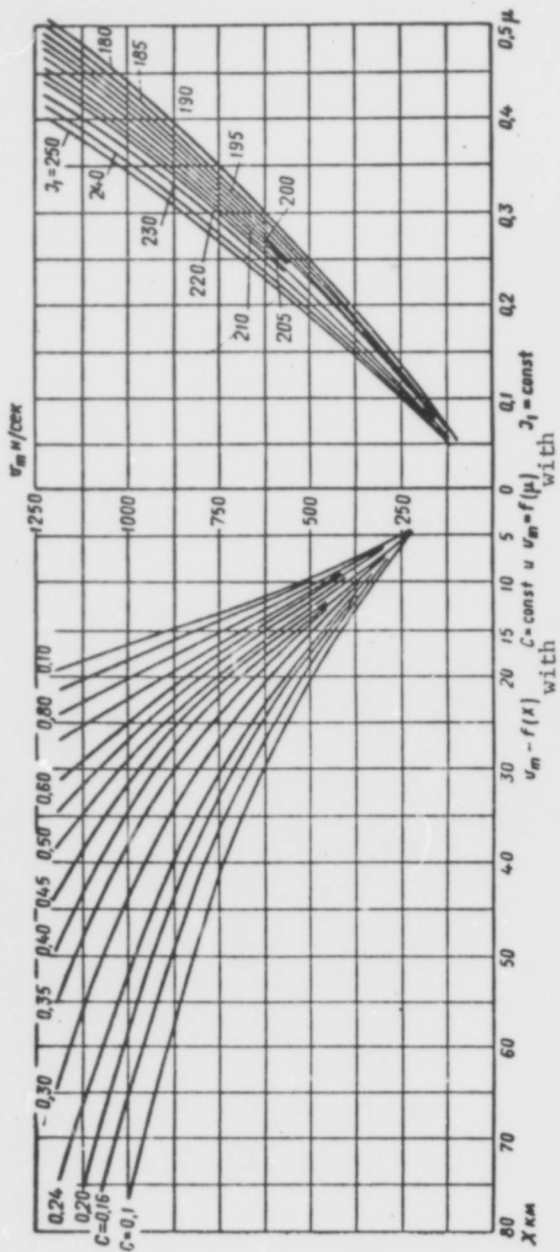


Figure 10.10. Nomogram for determining relative fuel reserve for a model having an assigned range.

With the value for  $\mu$  secured from the graph, the launch weight of the model is defined as

$$Q_0 = \frac{q_{nn}}{1 - (1 + a)\mu} = \frac{q_{nn}}{1 - \beta\mu}.$$

The weight of the charge can be defined as

$$\omega = \mu Q_0.$$

The passive weight of the charge is

$$q = Q_0(1 - \mu) = q_{nn} \frac{1 - \mu}{1 - \beta\mu}. \quad (10.78)$$

The caliber of the model is found from the expression for the ballistic coefficient:

$$D_n = \sqrt{\frac{c \cdot q}{110^3}} = \sqrt{\frac{c \cdot q_{nn}(1 - \mu)}{(1 - \beta\mu) \cdot 10^3}}. \quad (10.79)$$

In order to determine the basic linear dimensions of the charge we must make use of the graph for dependence of relative weight of a charge of the assigned type upon its relative length. The relative weight of the charge is

$$C_\omega = \frac{\omega}{D_n^3} = \delta \frac{\pi}{4} B_n^2 B_k^2 \varepsilon \bar{L}.$$

For the sake of convenience in computing we shall introduce a new characteristic

$$C'_\omega = \frac{C_\omega}{\delta \frac{\pi}{4} B_n^2 B_k^2} = \varepsilon \bar{L}. \quad (10.80)$$

As an example, there are set forth in Figures 10.11 and 10.12 graphs for the ratio  $C'_\omega = f(\bar{L})$  constructed with various values for  $A = \frac{x B_n B_k}{4 \sqrt{n}}$  for the cases  $x_{int} = x_{ext}$  and  $x_{int} = 2 x_{ext}$  for charges of cylindrical single-channel burners.

Thus, having determined the value  $C_\omega = \frac{\omega}{D_n^3}$  and having divided it by the complex  $\delta \frac{\pi}{4} B_n^2 B_k^2$  it is necessary, in accordance with the value secured for  $C'_\omega$ , to go into a graph similar to Figure 10.11, and to determine  $\bar{L}$  from it, and in accordance with  $\bar{L}$  the remaining dimensions of the charge.

After solution of the problem it is well, on the basis of the dimensions secured for the chamber and the charge, to reckon the value of

the weight characteristic of the engine,  $\beta$ , and to compare it with the value with which one started. If they diverge considerably, which is ordinarily possible only when there is a decidedly considerable deviation from the caliber of the optimum model, it is necessary to recompute all the characteristics of the missile, starting with the value secured for  $\beta$ .

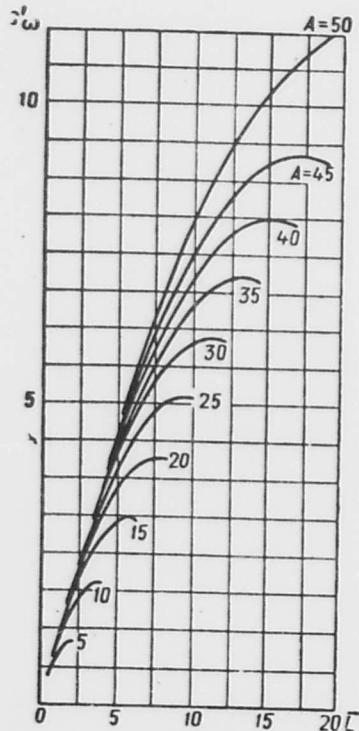


Figure 10.11. Dependence of adduced relative weight of charge  $C'_w$  consisting of single-channel cylindrical burners, upon relative length  $\bar{L}$  for  $x_{int} = x_{ext}$ .

Example 2. To compute the basic design parameters of one of the variants of a model for a range of 25 km and with weight of useful load 230 kg.

The values of the project parameters are taken to be the same as in example 1.

We shall carry out computation for the variant  $c = 0.30$ .

1. According to the graph, Figure 10.10, with a range of 25 km corresponds to this value.

2. The weight coefficient of the engine,  $\alpha$ , is determined in accordance with the data of example 1. For computation we shall take it as being  $q_K = 20$  kg. Then

$$\alpha = \frac{q_n - q_{nn} + q_K}{\omega} = \frac{388 - 250 + 20}{156} = 1,01.$$

$$3. Q_0 = \frac{q_{nn}}{1 - (1 + \alpha)\mu} = \frac{230}{1 - 2 \cdot 0,32} = 638 \text{ кг.}$$

$$4. \omega = \mu Q_0 = 0,32 \cdot 638 = 204 \text{ кг.}$$

$$5. q = Q_0(1 - \mu) = 0,68 \cdot 638 = 434 \text{ кг.}$$

$$6. D_H = \sqrt{\frac{c \cdot q}{110^3}} = \sqrt{\frac{0,30 \cdot 434}{1,3 \cdot 10^3}} = 0,307 \text{ м;}$$

$$D_H = 3,07 \text{ дм.}$$

$$7. C'_\omega = \frac{\omega}{D_H^3 \cdot \frac{\pi}{4} \cdot B_H^2} = \frac{204}{3,07^3 \cdot 1,6 \cdot \frac{\pi}{4} \cdot 0,95^2} = 6,24.$$

8. From the graph, Figure 10.11, with  $C'_\omega = 6,24$ ,  $A = 40$ ;  $\bar{L} = 8,14$ . From the graph, Figure 10.3, with  $\alpha_{int} = \alpha_{ext}$  and  $A = 40$ ,  $\alpha = 0,767$  corresponds to this value for  $\bar{L}$ .

$$9. \omega = \alpha L \frac{\pi}{4} \cdot B_H^2 \cdot D_H^3 = 0,767 \cdot 8,14 \cdot 1,6 \cdot \frac{\pi}{4} \cdot 0,95^2 \cdot 3,07^3 = 204 \text{ кг.}$$

$$10. \alpha = \frac{q - q_{nn}}{\omega} = \frac{434 - 230}{204} = 1,00.$$

Thus the value secured for  $\alpha$  corresponds to the one we were set.

We may note that for an engine having loose filling of the chamber without heat insulation the values of the coefficient  $\alpha$  are very high and come to 0.85-1.25. Thus, for example, for the "Honest John" rocket, in accordance with (1) the over-all weight comes to 2,700 kg,  $q_{nn}$  to 675 kg,  $\omega$  to 930 kg. Consequently for the engine of this rocket.

$$\alpha = \frac{Q_0 - \omega - q_{nn}}{\omega} = \frac{2700 - 930 - 675}{930} = 1,18.$$

11. Let us compare some characteristics of the model computed in this example with the characteristics of the optimum ballistic variant.

Ratio of launch weights

$$\frac{Q_0}{Q_{0 \text{ opt}}} = \frac{638}{544} = 1,175.$$

Ratio of charge lengths

$$\frac{L_{\text{opt}}}{L} = \frac{35,8}{8,14 \cdot 3,07} = 1,45.$$

Ratio of charge weights

$$\frac{\omega}{\omega_{\text{opt}}} = \frac{204}{155,5} = 1,31.$$

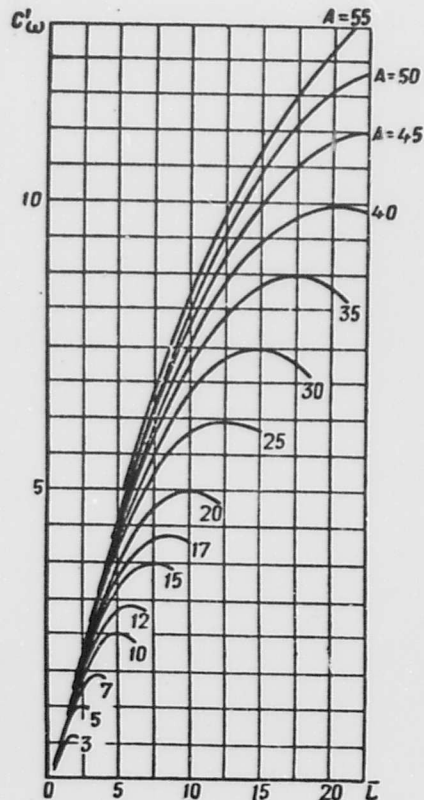


Figure 10.12. Dependence of added relative weight of charge  $C'$ , consisting of cylindrical single-channel burners, upon relative length of charge  $\bar{L}$  for  $\alpha_{\text{int}} = 2$   $\alpha_{\text{ext}}$ .

Thus increase of the caliber from 268 mm to 307 mm while preserving the assigned range of fire has led to increase of launch weight by 17.5 percent with preservation of the length of the missile, only by virtue of shortening the length of the charge (by 1.5 times) to 1 meter. But when this occurs the weight of the charge rose sharply (by 31 percent).

Similar computations carried out for various cases show that with increase of the caliber of an unguided rocket missile above that which

ensures the optimum ballistic solution and in the presence of a small departure from  $D_H \text{ opt}$  one observes a relatively slow rise in launch weight combined with substantial shortening of the length of the missile. With further increase of caliber the shortening of length becomes less and less perceptible, and the launch weight commences to rise rapidly. In each concrete case it is possible, on the basis of such computations, to establish a boundary for reasonable exceeding of  $D_H \text{ opt}$ , at which considerable shortening of the length of the model is achieved, but with only slight increase in launch weight.

#### 10.8. Peculiarities of Planning Turbojet Missiles

As has already been pointed out above, the stability in flight of turbojet missiles is ensured with a length  $\bar{L}_{\text{mis}}$  not exceeding 7-8 calibers, the length being distributed among the warhead, the cone block, and the rocket chamber. If one considers that the length of the ogival part for such missiles ordinarily comes to 1.5-2 calibers, then it will prove to be the case that no more than 4-5 calibers fall to the share of the rocket chamber. In a series of cases the relative length of the rocket chamber may prove to be substantially less than this quantity.

With such a short chamber the most acceptable charge is a multiple-burner one, ensuring short combustion time and symmetrical disposition of the mass of fuel upon consumption. With short charge combustion time the turbojet rocket missile, during the time it is moving along the guides, takes on an angular velocity of rotation sufficient to ensure its stability in the initial section of free flight. Short combustion time makes it possible to avoid burning out the critical cross-sections, which in a turbojet rocket missile are of very small diameter and as a consequence are decidedly sensitive to erosion.

At the same time, with a relatively short length a sufficiently high coefficient of charging  $\epsilon$ , not much smaller than for a single-burner missile, is ensured for the multiple-burner charge.

In planning charges for turbojet rocket missiles it is necessary to take into account that the centrifugal forces which reach their peak toward the end of combustion of the charge produce in the elements of the charge considerable stresses, which sometimes lead to their breaking down. Breakdown of remnants of the charge, accompanied by sharp increase of surface, in its turn occasions a foaming of pressures which may lead to destruction of the chamber. For this reason the brand of fuel used in a turbojet rocket missile must possess enough mechanical strength. As experience shows, some additives to the fuel reduce its friability at low temperatures -- for instance, diethylphthalate (3). Rise of pressure at the end of combustion of the charge must be taken into account in setting computed pressure, for which purpose the results of tests of turbojet rocket engines on a special stand offering the missile the ability to rotate during the test at the same speed as during flight are made use of (3).

In determining the necessary wall thickness it is necessary to take into account not only the stresses provoked in the material by pressure but also the stress arising as a result of the operation of centrifugal forces. Regarding the chamber as a thin-walled vessel and computing it only for tangential stress we secure

$$\sigma_t = \frac{\rho_m \dot{D}_n}{2\lambda} + \frac{1_n}{g} \pi^2 D_n^3 n^2 + \frac{\omega(1-\psi)}{gL} \frac{\pi d_3 n^2}{\Delta}, \quad (10.81)$$

where  $n$  is the number of revolutions achieved at a given moment of time;  
 $\psi$  is the portion of the charge which has burned up at a given moment of time;

$d_3$  is the mean diameter over which the remaining part of the charge is distributed.

Here the first term expresses stresses provoked by pressure forces, the second term the stress arising in the wall from centrifugal forces operating on the mass of the wall, and the third term stresses provoked by centrifugal forces pressing the unburned part of the charge against the interior surface of the chamber.

We shall transcribe formula (10.81) in the form

$$\sigma_t = \frac{D_n \rho_m}{2\lambda} \left[ 1 + \frac{2\gamma_{1n}}{g} \pi^2 \frac{D_n \Delta n^2}{\rho_m} + 2 \frac{\omega(1-\psi) \pi d_3 n^2}{g \rho_m L D_n} \right] \quad (10.82)$$

The expression within the square brackets may be regarded as a coefficient taking into account the operation of centrifugal forces. We shall designate it by  $k_n$ . Then the necessary wall thickness is

$$\Delta = \frac{k_n \rho_m D_n}{2\sigma_B}, \quad (10.83)$$

whence

$$B_n = \frac{\sigma_B}{\sigma_B + k_n \rho_m}. \quad (10.84)$$

Let us determine the basic design parameters of a turbojet rocket missile for a specified range of fire.

The volume occupied by the warhead for a given weight thereof can be determined approximately by starting from the mean value for the coefficient of charging  $a_n$ :

$$W_{G_n} = \frac{a_n q_{G_n}}{\gamma_{G_n}} + \frac{(1-a_n) q_{G_n}}{\gamma_n}. \quad (10.85)$$

where  $\gamma_{\text{CH}}$  and  $\gamma_{\text{M}}$  are the specific weights of the missile and of the material of the casing

The volume of the ogival part, if one starts from the proximity of its shape to the paraboloid, can be computed according to the formula

$$W_{\text{OЖ}} = \frac{\pi D_{\text{H}}^2}{6} L_{\text{OЖ}} = \frac{\pi D_{\text{H}}^3}{6} \bar{L}_{\text{OЖ}}$$

where  $L_{\text{OЖ}}$  is the length of the ogival part.

To the cylindrical part of the warhead there falls a length

$$L_{\text{H}} = \frac{W_{\delta\text{ч}} - W_{\text{OЖ}}}{\frac{\pi D_{\text{H}}^2}{4}} = \frac{4W_{\delta\text{ч}}}{\pi D_{\text{H}}^2} - \frac{2}{3} D_{\text{H}} \bar{L}_{\text{OЖ}} \quad (10.86)$$

The relative length of the warhead is

$$\bar{L}_{\delta\text{ч}} = \bar{L}_{\text{OЖ}} + \bar{L}_{\text{H}} = \frac{1}{3} \bar{L}_{\text{OЖ}} + \frac{4W_{\delta\text{ч}}}{\pi D_{\text{H}}^3} \quad (10.87)$$

Making use of formula (10.85), one can present relation (10.87) in the form

$$\bar{L}_{\delta\text{ч}} = \frac{1}{3} \bar{L}_{\text{OЖ}} + \frac{4}{\pi} C_{q\delta\text{ч}} \left[ \frac{a_{\text{H}}}{\gamma_{\text{CH}}} + \frac{1-a_{\text{H}}}{\gamma_{\text{M}}} \right], \quad (10.88)$$

where  $C_{q\delta\text{ч}} = \frac{q_{\delta\text{ч}}}{D_{\text{H}}^3}$ .

To the rocket part there remains

$$\bar{L}_{\text{P}} = \bar{L}_{\text{CH}} - \bar{L}_{\delta\text{ч}}$$

Making use of formula (10.88) we secure

$$\bar{L}_{\text{P}} = \bar{L}_{\text{CH}} - \frac{1}{3} \bar{L}_{\text{OЖ}} - \frac{4}{\pi} C_{q\delta\text{ч}} \left( \frac{a_{\text{H}}}{\gamma_{\text{CH}}} + \frac{1-a_{\text{H}}}{\gamma_{\text{M}}} \right) \quad (10.89)$$

If we designate  $\frac{4}{\pi} \left( \frac{a_{\text{H}}}{\gamma_{\text{CH}}} + \frac{1-a_{\text{H}}}{\gamma_{\text{M}}} \right) = \frac{1}{\gamma_{\Phi}}$ , we secure

$$\bar{L}_{\text{P}} = \bar{L}_{\text{CH}} - \frac{1}{3} \bar{L}_{\text{OЖ}} - \frac{C_{q\delta\text{ч}}}{\gamma_{\Phi}} \quad (10.99)$$

The relative length of the charge is determined as

$$\bar{L} = \frac{\bar{L}_{\text{P}}}{k_L}$$

In accordance with the magnitude of  $\bar{L}$  one can determine the coefficient of charging  $\epsilon$ , for this purpose making use of the graphs, Figure 10.3 or Figure 10.4, or of the relations (10.26) or (10.29).

With  $x_{int} = x_{ext}$ , from relation (10.26)

$$\epsilon = 1 - \frac{L^2}{2A^2} \pm \sqrt{\left(1 - \frac{L^2}{2A^2}\right)^2 + \left(2\frac{\bar{L}^2}{A^2} - 1\right)}, \quad (10.100)$$

and with  $x_{int} = 2 x_{ext}$

$$\epsilon = 1 - \frac{L}{A}. \quad (10.101)$$

In accordance with the quantity  $\epsilon$  one can then compute the relative weight of the charge.

In planning turbojet rocket missiles the cone block is made in the form of a cap-cone -- a solid-cast unit with jets drilled around its circumference. With such a design the weight of the cone block depends substantially on the linear dimensions of the cone, which determine the thickness of the unit. In turn, the linear dimensions of the cone for a given value  $F_{cr}$  and given  $d_a/d_{cr}$  ratio and angle of funnel  $\beta$  depend upon the number of jets. It will be necessary to consider not only our desire to reduce the weight of the cone block in selecting the number of jets, but also the possibility of placing them on a single circumference of the greatest possible diameter in order to secure the highest torque.

The maximum possible number of jets  $n_{max}$  which can be placed in a single row in a cone block having a face area  $F_M$  with an adduced over-all area of outlet cross-sections of jets  $F_a$  can be determined from the equation

$$\frac{F_M}{F_a} = \frac{n \left(1 + \frac{\pi}{n}\right)^2}{\pi^2},$$

where

$$F_a = \frac{\pi}{4} (d_a + \Delta d)^2 n; \quad F_M = \frac{\pi}{4} (D_n - \Delta d)^2.$$

Here  $\Delta d$  is the minimum permissible amount of the interval between the circumferences of the outlet cross-sections of the jets.

Minimum values for the ratio  $F_M/F_a'$  computed in accordance with this formula for various values of  $n$  are set forth in Table 10.4. In the selection of  $n$  the ratio  $F_M/F_a'$  serves as an initial quantity; here in first approximation  $F_a'$  is taken as being equal to  $F_{kp}\xi_a^2$ .

Table 10.4

$n$	10	12	14	16	18	20	22	24	28	30
$F_w/F'_a$	1,75	1,94	2,12	2,31	2,52	2,71	2,91	3,10	3,50	3,70

Let us examine the sequence of computation in determining the characteristics of a turbojet missile having a given weight of warhead and a given range of fire  $X$ .

1. With value for  $\alpha_n$  selected we determine the mean specific weight for the warhead,  $\gamma_\phi$ .
2. We set ourselves a number of calibers for the turbojet rocket missile and for each of them we determine  $C_{q64} = q_{64}/D_n^3$ .
3. For each of the variants we compute, in accordance with formula (10.89), the length of the charge,  $\bar{L}$ .
4. We determine the magnitude of coefficient  $B_H$ , setting ourselves the value of  $k_n$  from experience in working out similar objects.
5. Setting ourselves the number of burners and the value for parameter  $x$ , and making use of the value secured for  $B_H$ , for each of the variants we compute in accordance with formula (10.100) the coefficient of charging  $\epsilon$ .
6. We determine the weight of the charges in accordance with formula (10.8).
7. In accordance with formula (10.3) we compute the weights of the rocket chambers. Having determined the weights of the structural elements  $q_k = C_{q_x} D_n^3$ , we determine for each of the variants the passive weight  $q = q_k + q_{64} + q_{TP}$ .
8. In accordance with the Tsiolkovskiy formula we compute  $v_m$  for each of the variants, taking the value adopted for  $I_1$  as starting point.
9. With the adopted value for the coefficient of shape  $\underline{i}$ , we compute in accordance with  $q$  and  $D_H$  the values for the ballistic coefficient  $C$ .
10. In accordance with  $v_m$  and  $C$  with  $\theta_0 = 45^\circ$ , we compute the range of fire for each of the variants.
11. We construct a graph for  $X = f(D_H)$ , from which we determine the caliber which will ensure the range set, and we refine all the basic characteristics for this caliber.

### 10.9. Determination of Basic Design Parameters of Model Having Set Charge Combustion Time

In planning models having set charge combustion time two limit cases are possible:

1. Planning of an engine of specified caliber which at a given useful load will ensure maximum possible velocity.
2. Planning of an engine which will ensure a specified velocity with a given useful load and with least weight of its own.

In both cases the specified charge combustion time, together with the characteristics of the fuel selected and with the working pressure in the engine selected, determines the thickness of the burning vault of the fuel,  $e_1$ .

Let us examine a solution for the first case. Let us determine the optimum parameters for a model with specified thickness of burning vault  $e_1$ , parameters such as to ensure greatest velocity  $(v_m)_{\max}$  with the project parameters adopted. For this purpose we make use of equation (3.65), for a charge having a specified thickness of burning vault

$$\bar{L} = \frac{1-\epsilon}{\epsilon} \times \bar{e}_1$$

whence

$$\frac{d\bar{L}}{d\epsilon} = -\frac{1}{\epsilon^2} \times \bar{e}_1 \quad (10.102)$$

Substituting expressions (3.66) and (10.102) into expression (10.14), after elementary transformations we secure

$$\frac{\epsilon^2}{(1-\epsilon)^2} = \frac{\pi}{4} \frac{k_L \gamma_{np} (1 - B_n^2) \times \bar{e}_1}{C'_{q_{nn}}}$$

or

$$\frac{\epsilon}{1-\epsilon} = \sqrt{\frac{\pi}{4} \frac{k_L \gamma_{np} (1 - B_n^2) \times \bar{e}_1}{C'_{q_{nn}}}} \quad (10.103)$$

We carry out the substitution

$$\frac{\bar{e}_1}{C'_{q_{nn}}} = \frac{e_1 D_n^2}{q_{nn}}$$

and we designate

$$M = \sqrt{\frac{\pi D_n^2}{4 q_{nn}} \gamma_{np} (1 - B_n^2) k_L x e_1}. \quad (10.104)$$

Then

$$\epsilon_{\max} = \frac{M}{1 + M}. \quad (10.105)$$

Substituting expression (10.105) into expression (3.65) we secure

$$L_{\max} = \frac{x e_1}{M}. \quad (10.106)$$

With set caliber of engine, relations (10.104), (10.105), and (10.106) determine all the design and ballistic characteristics of a model which will ensure maximum velocity with set values for  $e_1$  and set project parameters.

Making use of the expressions secured for  $\bar{L}_{\max}$  and  $\epsilon_{\max}$  in order to determine the ratio  $\frac{\omega}{q}$ , we secure

$$\frac{\omega}{q} = \frac{\delta \frac{\pi}{4} D_n^2 B_n^2 B_n^2 \frac{x e_1}{1 + M}}{q_{nn} + \gamma_{np} \frac{\pi}{4} D_n^2 k_L (1 - B_n^2) \frac{x e_1}{M}}. \quad (10.107)$$

From expression (10.104) we find that

$$x e_1 = \frac{M^2}{\gamma_{np} \frac{\pi D_n^2}{4} \frac{k_L}{q_{nn}} (1 - B_n^2)}. \quad (10.108)$$

Dividing the numerator and the denominator of the right-hand arm of the equality (10.107) by the numerator, and utilizing the substitution of formula (10.108) we secure:

$$\frac{\omega}{q} = \frac{1}{\frac{\gamma_{np}}{\delta} \frac{1 - B_n^2}{B_n^2} k_L \left( \frac{1 + M}{M} \right)^2},$$

or

$$\frac{\omega}{q} = \frac{\delta}{\gamma_{np}} \frac{B_n^2}{1 - B_n^2} \frac{1}{k_L} \left( \frac{M}{1 + M} \right)^2. \quad (10.109)$$

Using the designations adopted in 10.6 we can transcribe this relation in the form

$$Z = B \left( \frac{M}{1+M} \right)^2. \quad (10.110)$$

In the general case the caliber is the quantity sought. A solution of the problem can be secured with the help of the graph presented in Figure 10.13. The left half of this graph is in no wise distinguished from the right-hand upper quadrant of the graph in Figure 10.10 which establishes the connection between maximum velocity, the value of  $I_1$ , and the variable  $Z = \omega/q$ . The right half of the graph expresses the dependence of  $Z$  upon  $M$  with  $B = \text{constant}$ . As a result of this, in accordance with set values for  $v_m$  and  $I_1$  and the value for  $B$  computed for the project parameters adopted, one determines the parameter  $M$ , in accordance with which the optimum caliber of the engine is then computed:

$$D_{H \text{ опт}} = \frac{M}{\sqrt{\frac{\pi}{4} \gamma_{np} (1 - B_n^2) k_{L, x e_1 / q_{n, n}}}}. \quad (10.111)$$

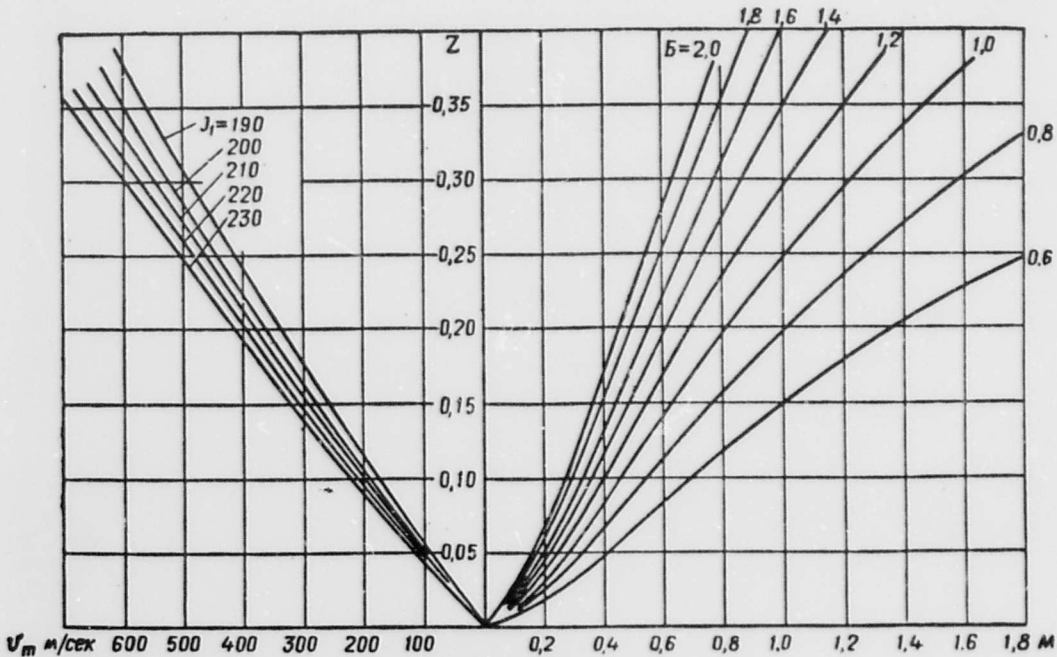


Figure 10.13. Nomogram for determination of  $M$  complex in planning an unguided rocket missile having a set fuel combustion time.

The solution we have examined, based upon a general property of charges having a constant combustion surface and a set thickness of burning vault, does not take into consideration certain specific properties of charges of individual shapes. In the case of a charge of cylindrical single-channel burners, after determining the general characteristics of the charge it is necessary in addition to solve the problem of placement of this charge in the rocket chamber of the optimum model.

Let us examine this on the example of a variant  $x_{int} = x_{ext}$ , for which  $d = D(1-\epsilon)$ ; consequently,

$$e_1 = \frac{D-d}{4} = \frac{D\epsilon}{4}.$$

Having divided both parts of the equation by the interior diameter of the chamber  $D_K = D_H B_H$ , we secure:

$$\frac{e_1}{D_H B_H} = \frac{\tilde{D}_\epsilon}{4} \quad \text{or} \quad \frac{4e_1}{D_H B_H \epsilon} = \tilde{D}. \quad (10.112)$$

In order that a charge of  $\underline{n}$  burners with set values  $e_1$  and  $D_H$  may fit in the chamber, it is necessary that the relation of the diameter of the burner to the diameter of the chamber, as determined through equation (10.112), should be no greater than  $\tilde{D}_{np}$  for a given  $\underline{n}$ . Accordingly the limit condition for fitting in the chamber proves to be the equation

$$\frac{4e_1}{D_H B_H \epsilon_{max}} = \tilde{D}_{np}. \quad (10.113)$$

Having computed the complex in the left-hand arm, one can determine from Table 10.1 the number of burners,  $\underline{n}$ , which corresponds to it.

In Figure 10.14 we set forth a graph for  $\epsilon = f(L/x e_1)$  with indication of the points corresponding to  $\epsilon_{np}$  for charges having different numbers of cylindrical single-channel burners, when  $x_{int} = x_{ext}$ .

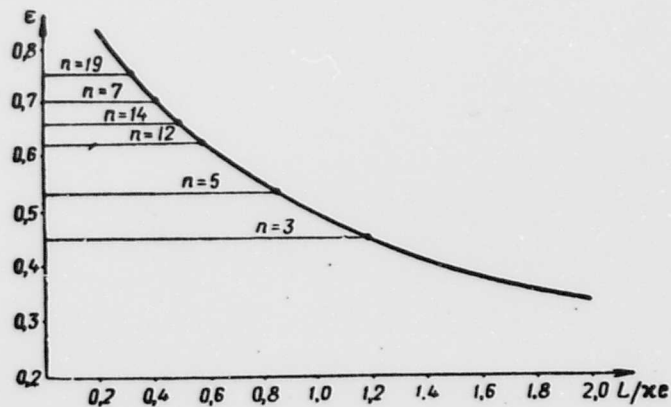


Figure 10.14. Dependence of coefficient of charging  $\epsilon$  upon  $L/x e_1$  for charges having a set thickness of burning vault.

Let us examine the solution for the second case. Let us determine the basic parameters of an engine which will ensure a specified range with least weight of its own. Obviously the minimum for the weight coefficient

$\alpha$ , secured for a set thickness of burning vault, will correspond to the requirement for least weight of engine.

In order to simplify the solution it is well to present the overall weight of the cone, caps, and diaphragm in the form

$$q_k = \Pi_k \frac{\pi D_H^2}{4}.$$

Then the expression for  $\alpha$  assumes the form

$$\alpha = \frac{q_T + q_k}{w} = \frac{\Pi_k \frac{\pi D_H^2}{4} + \gamma_{np} \frac{\pi D_H^2}{4} (1 - B_H^2) k_L \frac{1 - \epsilon}{\epsilon} x e_1}{\delta \frac{\pi D_H^2}{4} B_H^2 B_K^2 (1 - \epsilon) x e_1},$$

or

$$\alpha = \frac{\Pi_k}{\delta B_H^2 B_K^2 x e_1} \frac{1}{1 - \epsilon} + \frac{\gamma_{np}}{\delta} \frac{1 - B_H^2}{B_H^2 B_K^2} k_L \frac{1}{\epsilon}. \quad (10.114)$$

Differentiating expression (10.114) in accordance with  $\epsilon$  and equating the derivative to zero, let us solve the relation secured with reference to  $\epsilon$ :

$$\frac{\epsilon}{1 - \epsilon} = \sqrt{\frac{\gamma_{np} (1 - B_H^2) k_L x e_1}{\Pi_k}}. \quad (10.115)$$

Let us designate

$$\tilde{M} = \sqrt{\frac{\gamma_{np} (1 - B_H^2) k_L x e_1}{\Pi_k}} \quad (10.116)$$

Then the conditions ensuring optimum value for  $\alpha$  will be:

$$\epsilon = \frac{\tilde{M}}{1 + \tilde{M}}; \quad (10.117)$$

$$L = \frac{x e_1}{\tilde{M}} \quad (10.118)$$

The optimum value,  $\alpha_{min}$ , will be expressed by the relation

$$\alpha_{min} = \frac{1 + \tilde{M}}{\tilde{M}} \left[ \frac{\Pi_k \tilde{M}}{x e_1} + \gamma_{np} (1 - B_H^2) k_L \right]. \quad (10.119)$$

The weight of a charge necessary to accelerate the flight apparatus to a set velocity will be

$$\omega = \frac{q_{\text{нн}}^2}{1 - (1 + a_{\text{мин}}) \mu} \quad (10.120)$$

The caliber of the engine is equal to

$$D_{\text{н}} = \sqrt{\frac{4\omega}{\pi \delta B_{\text{н}}^2 B_{\text{к}}^2 \kappa \epsilon_1} (1 + \tilde{M})} \quad (10.121)$$

Example. To determine the characteristics of a launch engine to accelerate a flight apparatus weighing 1 ton to a velocity of 500 meters per second over a time of 2 seconds. The values of the project parameters are taken to be the same as in Example 1, 10.6. Assume  $\Pi_{\text{н}} = 4$ ,  $u_{\text{ср}} = 10$  м/сек.

1.  $\epsilon_1 = \tau u_{\text{ср}} = 2 \cdot 10 = 20$  м.м = 0,2 дм.

2.  $\tilde{M} = \sqrt{\frac{7,82(1 - 0,95^2) \cdot 1,02 \cdot 170 \cdot 0,2}{4}} = 2,617$

3.  $\epsilon = \frac{\tilde{M}}{1 + \tilde{M}} = \frac{2,617}{3,617} = 0,724$

4.  $L = \frac{170 \cdot 0,2}{2,617} = 13$  дм.

5.  $a_{\text{мин}} = \frac{1 + 2,617}{1,60 \cdot 0,95^2} \left[ \frac{4 \cdot 2,617}{170 \cdot 0,2} + 7,82(1 - 0,95^2) \cdot 1,02 \right] = 0,966$

6.  $\omega = \frac{1000 \cdot 0,225}{1 - (1 + 0,966) \cdot 0,225} = 403$  кг.

7.  $D_{\text{н}} = \sqrt{\frac{4 \cdot 403(1 + 2,617)}{\pi \cdot 1,60 \cdot 0,95^2 \cdot 170 \cdot 0,2}} = 6,132$  см.

\* It is also possible to use groups of engines, the diameter of each of which is equal to  $D_{\text{н}_i} = \frac{D_{\text{н}}}{\sqrt{m}}$ , where  $m$  is the number of engines in the group. With  $m = 4$ ,  $D_{\text{н}} = 3,066$  дм; with  $m = 6$ ,  $D_{\text{н}} = 2,51$  дм.

8. Let us examine the possibility of placing in the engine charges of single-channel cylindrical burners when the condition  $\kappa_{\text{int}} = \kappa_{\text{ext}}$  is met.

The diameter of a burner is

$$D = \frac{4\epsilon_1}{\epsilon} = \frac{4 \cdot 0,2}{0,724} = 1,108$$
 дм.

For a single engine

$$\bar{D} = \frac{D}{D_n B_n} = \frac{1,108}{6,132 \cdot 0,95} = 0,19.$$

In accordance with Table 10.1 under these circumstances it is possible to use a charge of 19 burners. For a group of 4 or 6 engines we secure a permissible number of burners per engine equal respectively to 5 and to 4.

Thus we have examined the two extreme cases. The first of these is the more characteristic for the planning of antitank unguided rocket missiles, where the caliber of the warhead is given, and the caliber of the rocket part is taken as being equal to the caliber of the warhead or as equal to a specified portion of this caliber (for example, from the condition of placement of fins which do not project beyond the caliber of the warhead). The second case is the more characteristic for the planning of launch engines, where in accordance with the conditions of placement of the launch engines on a flight apparatus rigid requirements are as a rule not imposed upon the caliber of the engine.

A common deficiency of both solutions is the fact that the parameters of the engine are determined from the conditions of an extreme which is of a very sharply inclined character for some variants. In the first case this leads to the computed variant's being secured excessively long, and for practical purposes it can be shortened without substantial reduction of the velocity of the unguided rocket missile. In the second case, on the other hand, the computed variant is sometimes secured in shortened form, and permits, in order to reduce the caliber of the engine, a certain elongation without substantial augmentation of the weight of the design.

In the computation of variants which exhibit some departure from the optimum ones as secured from solutions for the extreme cases, one must set oneself a length of charge and determine the caliber which with this length will ensure a specified velocity for the model, i.e., the required ratio  $\omega/q=Z$ .

From equation (10.11):

$$Zq'_{nn} - \delta \frac{\pi}{4} B_n^2 B_k^2 \epsilon L D_n^2 + \gamma_{np} \frac{\pi}{4} (1 - B_n^2) k_L L D_n^2 Z = 0. \quad (10.122)$$

Let us designate

$$E = \delta \frac{\pi}{4} B_n^2 B_k^2$$

$$\Gamma = \gamma_{np} \frac{\pi}{4} (1 - B_n^2) k_L$$

Substituting into expression (10.122) the value for  $\epsilon$  from expression (3.64) and solving with reference to caliber we find that:

$$D_0 = \sqrt{\frac{1}{L} \frac{q_{00}^2 Z}{E \left( \frac{1}{1 + L/\kappa_1} - \Gamma Z \right)}} \quad (10.123)$$

Example.

To determine the basic parameters of an engine for an infantry reactive grenade with the following initial data:

$$\begin{array}{lll} \dot{q}_{00} = 2 \text{ кг} & v_m = 150 \text{ м/сек} & \rho_m = 600 \text{ кг/см}^3 \\ \sigma_B = 7000 \text{ кг/см}^2 & \delta = 1,6 \text{ кг/дм}^3 & \gamma = 7,8 \text{ кг/дм}^3 \\ k_L = 1,05 & \alpha = 100 & I_1 = 200 \text{ кг сек/кг} \\ \epsilon_1 = 1,5 \text{ мм} & L = 250 \text{ мм} & \end{array}$$

1. From graph 10.13 we find, with  $I_1 = 200 \text{ кг-сек/кг}$ , that  $v_m = 150 \text{ м/сек}$ ;  $Z = 0.0792$ .

$$2. B_0 = \frac{\sigma_B}{\sigma_B + \rho_m} = \frac{7000}{7000 + 600} = 0,92.$$

$$3. E = 1,6 \frac{\pi}{4} 0,92^2 = 1,06 \text{ кг/дм}^3.$$

$$4. \Gamma = 7,8 \frac{\pi}{4} (1 - 0,92^2) 1,05 = 0,99 \text{ кг/дм}^3.$$

$$5. D_0 = \sqrt{\frac{2 \cdot 0,0792}{2,5 \cdot 1,06 \left( \frac{1}{\left( \frac{2,5}{100 \cdot 0,015} + 1 \right)} - 0,0792 \cdot 0,99 \right)}} = 0,446 \text{ дм}.$$

Let us take  $D_H = 46 \text{ мм}$ .

$$6. \bar{L} = \frac{L}{D_0} = \frac{250}{46} = 5,44.$$

$$7. \epsilon = \frac{1}{\frac{2,5}{100 \cdot 0,015} + 1} = 0,375.$$

8. For determination of a suitable number of burners we make use of formula (10.26):

$$n = \left[ \frac{\alpha B_0 (1 - \epsilon)}{4 \bar{L} \sqrt{2 - \epsilon}} \right]^2 = \left( \frac{100 \cdot 0,92}{4 \cdot 5,44} \frac{0,625}{\sqrt{1,625}} \right)^2 = 2,06^2 = 4,29.$$

Let us take  $n = 4$ .

$$9. D = D_n \frac{B_n}{\sqrt{n(2-\epsilon)}} = 46 \frac{0,92}{\sqrt{4 \cdot 1,625}} = 16,6 \text{ мм.}$$

$$10. d = D(1-\epsilon) = 16,6 \cdot 0,625 = 10,4 \text{ мм.}$$

$$\epsilon_1 = \frac{16,6 - 10,4}{4} = 1,55 \text{ мм.}$$

i.e., this corresponds to the value set.

11. Let us check whether the set value  $\alpha$  is ensured with these measurements:

$$\alpha = \frac{4Ln(D+d)}{D_n^2 - n(D-d^2)} = \frac{4 \cdot 4 \cdot 25,0 (1,66 + 1,04)}{0,92^2 \cdot 4,6^2 - 4 (1,66^2 - 1,04^2)} = 99,6.$$

12. Let us determine the weights of the individual elements:

$$\omega = \delta \cdot n \frac{\pi}{4} (D^2 - d^2) L = 1,6 \cdot 4 \frac{\pi}{4} (0,166^2 - 0,104^2) 2,5 = 0,21 \text{ кг.}$$

$$q_n = \Gamma \cdot LD_n^2 = 0,99 \cdot 2,5 \cdot 0,46^2 = 0,522 \text{ кг.}$$

$$Q_0 = q_{nn}' + q_n + \omega = 2,0 + 0,21 + 0,522 = 2,732 \text{ кг.}$$

$$Z = \frac{\omega}{Q_0 - \omega} = \frac{0,21}{2,522} = 0,083.$$

Thus the required value for Z is ensured with a reserve of 5 percent.

#### 10.10. Initial Data and Project Parameters Determining Basic Design Characteristics of an Unguided Rocket Missile

##### Weight and Over-All Dimensions of Warhead

The weight of the warhead with a set type of armament is determined in first approximation by the power of action of the missile at its target. Sometimes the weight of the armament,  $q_{CH}$ , is specified in a tactical-technical assignment in place of the weight of the warhead. One can shift from the weight of the armament to the full weight of the warhead of the missile by making use of mean statistical values for the coefficient of filling for a given type of warhead. The coefficient of filling represents the ratio of the weight of the armament of the warhead to its full weight:

$$\eta = \frac{q_{CH}}{q_{nn}} 100\%.$$

Let us indicate typical values of this coefficient for warheads of various types:

- 50-60 percent -- for warhead of high-explosive effect,
- 10-15 percent -- for warhead of fragmentation effect,
- 25-30 percent -- for warhead of fragmentation-high explosive effect.

In first approximation the weight of the warhead is determined as

$$q_{nn} = \frac{q_{cn}}{\eta} 100.$$

An important design characteristic of the warhead is the relative thickness of the walls of the casing in calibers. On the basis of literature data available (4) one can furnish orienting values of this quantity for warheads for various purposes:

high-explosive warhead	$\bar{\lambda}_{ct} = 0.023$ (M31, USSR)
fragmentation warhead	$\bar{\lambda}_{ct} = 0.1$ (M8, USSR)
fragmentation-high explosive warhead	$\bar{\lambda}_{ct} = 0.1$ (M13, USSR)

The relative weight of the warhead  $C_{q_{nn}} = \frac{q_{nn}}{D_n^3}$  can vary within pretty broad limits. It is nevertheless well to indicate the value thereof for some known examples (4):

For high-explosive effect missile	$C_{q_{nn}} = 2$ (300 mm missile, Germany)
For fragmentation effect missile	$C_{q_{nn}} = 6$ (M8, USSR)
For fragmentation-high explosive effect missile	$C_{q_{nn}} = 8$ (M13, USSR)

In using the methods of ballistic planning of an unguided rocket missile examined above, the weight of the warhead includes the weight of the cone block and the tail group. For small rocket missiles Vandenberg recommends taking the weight of the caps, the cone, and the tail group as equal to  $0.04425 R_H^3$  (1). The half-caliber of the rocket missile should be taken in centimeters; when this is done the weight of the elements indicated is secured in kilograms. This corresponds to a value of  $C_{qk} = 5.53$  kg/dm<sup>3</sup>. But as the author himself points out, the formula gives exaggerated results in a number of cases. According to the data for the M8, M13, and M31, one can take  $C_{qk}$  as being equal to 2.2 kg/dm<sup>3</sup> for finned unguided rocket missiles of medium caliber.

#### Selection of the Number of Burners

In planning unguided rocket missiles with a charge of single-channel cylindrical burners one of the project parameters is the number of burners,  $n$ . Let us examine what influence this parameter has upon the basic characteristics of an unguided rocket missile.

In Figure 10.15 we set forth graphs for maximum velocity of an unguided rocket missile computed by Professor Ya. M. Shapiro for charges having different numbers of burners at different elongations  $L$ . From the graphs it is apparent that at any elongations of the charge the greatest velocity is ensured by a single-burner charge. Comparison of the quantity  $v_m$  for various multiple-burner variants shows that with a relative length

of charge  $\bar{L}$  greater than 8 the greatest velocities are ensured by a charge of three burners, when  $\bar{L} = 5$  to 8 by a charge of four burners, and when  $\bar{L}$  is less than 5, by a charge of seven burners.

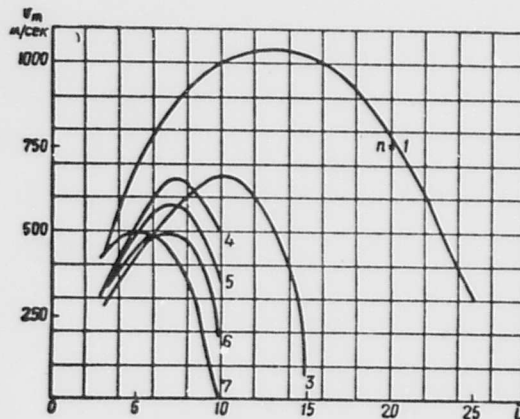


Figure 10.15. Dependence of maximum velocity of unguided rocket missile on relative length of charge for variants having different numbers of burners ( $n = 1, 3, 4, 5, 6, 7$ ).

The need for using in an unguided rocket missile a multiple-burner charge in place of a single-burner one, which in all cases ensures greatest range, is brought about first and foremost by requirements associated with grouping of fire. Above we have examined the causes calling for the use of multiple-burner charges in turbojet rocket missiles. The application of multiple-burner charges in finned unguided rocket missiles in order to increase speed of departure from the guides makes it possible to reduce the influence of a flank wind, which provokes flank dispersion of an unguided rocket missile. Upon the thrust-weight ratio of an unguided rocket missile, associated with the number of burners, depends reduction of the angle of incline of the tangent to the trajectory in the active section. In Figure 10.16 we set forth a graph for the dependence of this angle at the end of the active part --  $\theta_a$  -- upon the thrust-weight ratio, computed for  $\mu_R = 0,35$ ,  $\theta_0 = 45^\circ$  with varying lengths of guides, according to formula (7.18).

From the graph it is apparent that the steepness of the  $\theta_a = f(\eta)$  curves diminishes as thrust-weight ratio rises. With  $\eta \geq 20$  the increase in thrust-weight ratio already has little effect upon change in the angle  $\theta_a$ . With  $\eta < 12$  change in the angle of incline of the tangent to the trajectory in the active section comes to more than  $10^\circ$ .

The great steepness of the curves  $\theta_a = f(\eta)$  at low thrust-weight ratio brings about a high sensitivity of  $\theta_a$  to random changes in thrust-weight ratio brought about, for example, by scattering of thrust. In turn, scattering of the size of  $\theta_a$  brings about spread of the unguided rocket

missile as regards range. Hence arises a need for ensuring relatively high thrust-weight ratio.

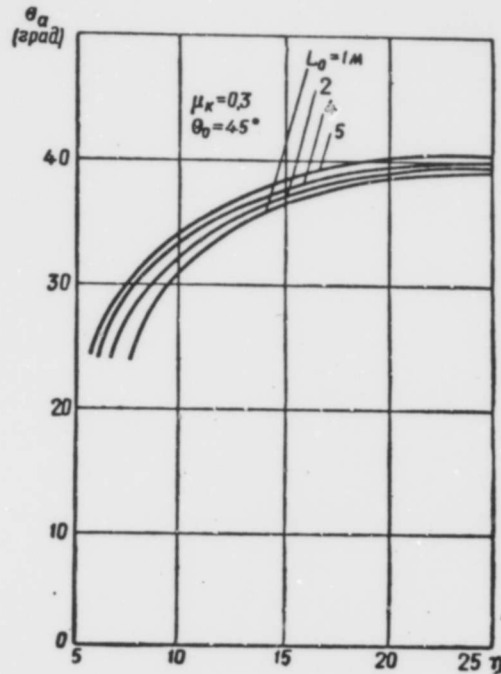


Figure 10.16. Dependence of angle of incline of tangent to trajectory of unguided rocket missile at the end of the active section,  $\theta_a$ , upon the thrust-weight ratio with different lengths of guides.

Let us note that with increase of the caliber of an unguided rocket missile one observes a tendency toward reduction of thrust-weight ratio. This is to be explained in the following fashion. With increase in the caliber of a model, while preserving geometrical similarity, the working time of the engine increases proportionately to the thickness of the burning vault, i.e., proportionately to the caliber in the first stage. The weight of the charge, as also the weight of the entire model, rises proportionately to the cube of the caliber:

$$Q_0 \sim D_n^3 \quad \omega \sim D_n^3$$

The output of products of combustion, and consequently also the thrust of the engine, change under these circumstances as

$$P = I_1 G = I_1 \frac{\omega}{\tau};$$

$$P \sim \frac{D_n^3}{D_n} = D_n^2$$

Consequently the initial thrust-weight ratio of the model must change with increase in caliber as

$$\eta = \frac{P}{Q_0} \sim \frac{D_H^2}{D_H^3}; \quad \eta \sim \frac{1}{D_H}.$$

For this reason, in order to ensure a set thrust-weight ratio in a missile of large caliber it is necessary to use charges with less relative thickness of vault  $\bar{e}_1$  than in models of small caliber, i.e., to proceed to the use of charges having a larger number of burners.

#### Thrust Diagram

Increasing the speed of an unguided rocket missile's departure from the guides by increasing the number of burners, i.e., by decreasing the thickness of the vault, is associated with falling off in the density of charging and, as a consequence, with reduction in range of fire.

It is possible to increase the speed of departure of the unguided rocket missile without reduction of the thickness of the vault of the basic charge by applying a staged thrust diagram, the upper stage of which coincides in time with the motion of the missile along the guide (7).

A staged thrust diagram can be ensured: by using a launch engine having a charge that is consumed upon the guide; a two-stage engine working successively at a launch thrust rate (on the guide) and at a route thrust rate (the free flight portion).

Questions regarding the arrangement of two-rate engines were examined in Chapter VI.

#### Computed Pressure $p_m$

In selecting the amount of maximum pressure in accordance with which the thickness of the engine wall is computed, one must take the following circumstances into account:

a) the need for ensuring stable combustion of the specific fuel for the most unfavorable temperature conditions, i.e., at the  $T_{\min}$  constituting the lower boundary of the temperature interval for which the model being worked out is intended; from this condition one selects the minimum permissible pressure  $p_{\min}$ :

b) the possibility of degressive combustion of the charge or the presence of a staged pressure diagram, characterized by the ratio between maximum and minimum pressures:  $p_{\max}/p_{\min} = \xi$ ;

c) presence of a dependence of speed of fuel combustion upon temperature, which in the case of an unregulated engine leads to rise in pressure with the temperature of the charge. This change in pressure is defined by the coefficient

$$\frac{(p_{\max})_{T_{\max}}}{(p_{\max})_{T_{\min}}} = e^{\frac{m+D}{1-\nu}(T_{\max}-T_{\min})},$$

where  $\underline{m}$  and  $D$  are the thermochemical constants of the fuel (see (6));

d) spread of magnitude of maximum pressure at the upper boundary of the temperature interval for use of the model, characterized by the coefficient  $\varphi_p$ ;

e) scattering of strength characteristics of the material and of the thickness of the wall in consequence of tolerances in the manufacture of the rocket chamber; this scattering is taken into account through the reserve strength coefficient  $\eta_p$ .

Under these circumstances computed pressure is defined as

$$p'_m = \gamma_p \varphi_p e^{\frac{m+D}{1-\nu}(T_{\max}-T_{\min})} \xi p_{\min}. \quad (10.124)$$

The magnitude of computed pressure can be reduced by using fuels which burn stably under low working pressures in the engine and which possess a low temperature dependence, and also by regulating the cone of a solid-fuel rocket engine in accordance with the temperature of the charge or by thermostating the engine.

#### The Charging Parameter $\alpha$

General considerations regarding the selection of this parameter were set forth in 3.9. They continue to be in force for unguided reactive missiles as well.

But for unguided rocket missiles, in contradistinction to guided missiles having a vertical launch, greater development of the combustion surface is characteristic; this is occasioned by the greater thrust-weight ratio necessary with an inclined launch.

For this reason the optimum value of  $\alpha$  for an unguided rocket missile is shifted in the direction of its increase so as to approach the value which determines the limit of the field of stable combustion. The selection of the  $\alpha$  parameter is inseparable from the selection of working pressure in the engine which will ensure stable combustion of the charge at minimum temperature thereof.

#### BIBLIOGRAPHY

1. Barrere, M., Jomotte, A., Bebek, B. F., Vandekerkhove, J., Rocket Engines, Oborongiz Publishing House, 1962.
2. Stone, M., "Practical Mathematical Calculation of Configuration of Charge," Problems in Rocket Technics, No 6, 1958.
3. Wimpres, R. N., Internal Ballistics of Powder Rockets, Foreign Literature Publishing House, 1952.
4. Kurov, V. D., Dolzhanskiy, Yu. M., Fundamentals of Planning Powder Rocket Missiles, Oborongiz Publishing House, 1961.
5. "The Boeing Firm's 'Minuteman' Intercontinental Ballistic Missile," Problems in Rocket Technics, No 6, 1963.
6. Shapiro, Ya. M., Mazing, G. Yu., Prudnikov, N. Ye., Theory of Solid-Fuel Rocket Engines, Voenizdat Publishing House, 1966.
7. Gantmakher, F. R., and Levin, L. M., Theory of Flight of Unguided Rockets, Fizmatgiz Publishing House, 1959.

ANNEX 1. CHANGE IN METEOROLOGICAL ELEMENTS WITH ALTITUDE

$r_m$	$\alpha (y)$	$H (y)$	$\sqrt{\frac{T_s}{T}}$	$r_m$	$\alpha (y)$	$H (y)$	$\sqrt{\frac{T_s}{T}}$
0	1,000	1,000	1,000	7600	0,367	0,433	
200	0,976	0,980		7800	0,356	0,422	1,091
400	0,953	0,960		8000	0,346	0,412	
600	0,930	0,940		8200	0,336	0,402	
800	0,907	0,921		8400	0,327	0,393	
1000	0,885	0,902	1,010	8600	0,317	0,383	
1200	0,863	0,884		8800	0,308	0,374	
1400	0,842	0,866		9000	0,299	0,365	1,104
1600	0,821	0,848		9200	0,291	0,356	
1800	0,800	0,831		9400	0,282	0,347	
2000	0,780	0,813	1,021	9600	0,274	0,339	
2200	0,761	0,796		9800	0,266	0,330	
2400	0,742	0,779		10000	0,258	0,323	1,118
2600	0,723	0,763		10200	0,250	0,314	
2800	0,705	0,747		10400	0,243	0,306	
3000	0,687	0,731	1,032	10600	0,235	0,298	
3200	0,670	0,715		10800	0,228	0,290	
3400	0,653	0,700		11000	0,221	0,282	1,133
3600	0,636	0,685		11200	0,214	0,274	
3800	0,619	0,670		11400	0,207	0,266	
4000	0,603	0,655	1,043	11600	0,201	0,258	
4200	0,587	0,641		11800	0,195	0,251	
4400	0,572	0,627		12000	0,189	0,243	1,133
4600	0,557	0,613		12200	0,183	0,236	
4800	0,542	0,600		12400	0,178	0,229	
5000	0,527	0,586	1,054	12600	0,172	0,222	
5200	0,513	0,573		12800	0,167	0,215	
5400	0,499	0,560		13000	0,162	0,208	1,133
5600	0,486	0,548		13200	0,157	0,202	
5800	0,473	0,535		13400	0,152	0,195	
6000	0,460	0,523	1,066	13600	0,148	0,189	
6200	0,448	0,511		13800	0,143	0,183	
6400	0,435	0,499		14000	0,139	0,177	1,133
6600	0,423	0,487		14200	0,135	0,172	
6800	0,412	0,476		14400	0,130	0,167	
7000	0,400	0,465	1,078	14600	0,126	0,162	
7200	0,389	0,454		14800	0,122	0,157	
7400	0,378	0,443		15000	0,118	0,152	1,133

Annex 1 (continued)

$v_m$	$z(y)$	$H(y)$	$\sqrt{\frac{T_s}{T}}$	$v_v$	$\kappa(y)$	$H(y)$	$\sqrt{\frac{T_s}{T}}$
15200	0,114	0,148		33000	0,756	$0,919 \cdot 10^{-2}$	1,102
15400	0,111	0,143		34000	0,652	0,790	1,100
15600	0,107	0,139		35000	0,563	0,679	1,098
15800	0,104	0,134		36000	0,487	0,573	1,084
16000	0,101	0,130	1,133	37000	0,423	0,485	1,071
16200	$0,980 \cdot 10^{-1}$	0,126		38000	0,369	0,413	1,058
16400	0,950	0,122		39000	0,322	0,352	1,046
16600	0,923	0,118		40000	0,283	0,302	1,034
16800	0,895	0,115		41000	0,249	0,260	1,022
17000	0,867	0,111	1,133	42000	0,219	0,224	1,011
17200	0,841	0,108		43000	0,194	0,194	1,000
17400	0,815	0,105		44000	0,172	0,168	0,999
17600	0,790	0,101		45000	0,153	0,147	0,979
17800	0,766	$0,980 \cdot 10^{-1}$		46000	0,136	0,128	0,969
18000	0,742	0,952	1,133	47000	0,122	0,112	0,960
19000	0,635	0,814	1,133	48000	0,109	$0,984 \cdot 10^{-2}$	0,951
20000	0,543	0,697	1,133	49000	$0,977 \cdot 10^{-2}$	0,865	0,942
21000	0,465	0,594	1,130	50000	0,878	0,764	0,933
22000	0,398	0,507	1,128	55000	0,508	0,473	0,963
23000	0,341	0,432	1,125	60000	0,284	0,282	0,997
24000	0,299	0,369	1,123	65000	0,152	0,163	1,034
25000	0,251	0,316	1,121	70000	$0,774 \cdot 10^{-4}$	$0,895 \cdot 10^{-4}$	1,075
26000	0,216	0,270	1,118	75000	0,372	0,468	1,122
27000	0,185	0,231	1,116	80000	0,167	0,229	1,176
28000	$0,159 \cdot 10^{-1}$	$0,198 \cdot 10^{-1}$	1,114	85000	$0,721 \cdot 10^{-4}$	$0,990 \cdot 10^{-4}$	1,176
29000	0,137	0,169	1,112	90000	0,310	0,429	1,176
30000	0,118	0,145	1,109	95000	0,134	0,185	1,176
31000	0,102	0,125	1,107	100000	$0,560 \cdot 10^{-6}$	$0,800 \cdot 10^{-6}$	1,176
32000	$0,876 \cdot 10^{-2}$	0,107	1,105				

## ANNEX 2

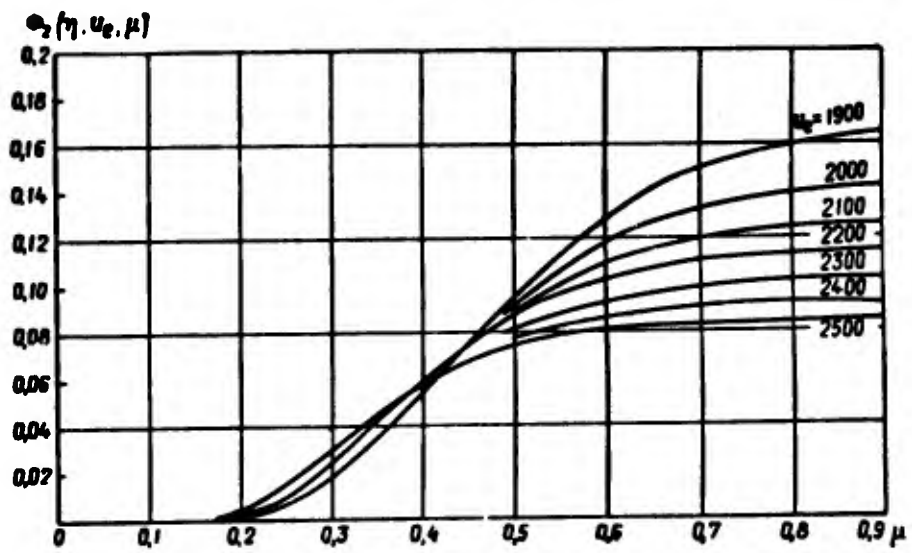
		$u_1 - u_2$		$u_3 = \frac{1}{2} (u_2)^2$			
$\rho$	$\theta^\circ$	$u_1$	$u_2$	$u_3$	$u_4$	$u_5$	$u_7$
0,01	90,00	0,0100	0,0100	0	0	0	0
2	90,00	202	200	0,0002	0	0	0
3	90,00	301	300	4	0	0	0
4	89,86	408	400	8	0	0	0
5	88,02	513	500	0,0013	0	0	0,0002
6	86,22	619	600	18	0	0	7
7	84,46	726	700	25	0,0001	0,0001	0,0015
8	82,76	834	799	33	2	2	26
9	81,09	943	898	42	3	3	40
0,10	79,51	0,1054	997	51	5	5	57
1	77,97	0,1166	0,1095	62	7	7	76
2	76,57	1279	1193	74	0,0010	9	98
3	75,30	1393	1290	87	13	0,0012	0,0122
4	74,13	1509	1386	0,0101	17	16	149
5	73,06	1625	1482	116	21	20	177
6	72,04	1743	1577	132	26	24	207
7	71,04	1863	1672	149	32	29	239
8	70,07	1984	1766	167	38	35	272
9	69,13	2107	1860	187	45	41	308
0,20	68,20	2231	1953	207	53	48	344
1	67,25	2357	2046	228	62	56	382
2	66,33	2484	2138	250	71	64	422
3	65,43	2613	2229	273	82	73	463
4	64,53	2744	2320	298	93	83	505
5	63,65	2876	2410	323	0,0105	93	549
6	62,77	3010	2499	349	119	0,0104	594
0,27	61,88	3146	2588	377	133	116	540
8	61,00	3284	2676	405	148	129	588
9	60,12	3424	2763	434	165	142	638
0,30	59,23	3566	2849	464	183	156	688
1	58,35	3710	2935	495	201	171	740
2	57,46	3856	3020	527	221	187	793
3	56,58	4004	3104	560	243	204	847
4	55,70	4154	3187	594	266	221	903
5	54,83	4307	3269	629	290	240	960
6	53,98	4462	3350	665	315	259	0,1018
7	53,14	4620	3430	701	342	279	1078
8	52,28	4780	3510	739	371	300	1138
9	51,43	4943	3589	777	401	322	1200
0,40	50,59	5108	3667	816	432	345	1263
1	49,77	5276	3744	856	466	368	1327
2	48,96	5447	3820	897	500	393	1392
3	48,14	5621	3898	938	537	419	1458
4	47,33	5798	3969	980	575	445	1525
5	46,51	5978	4042	0,1023	616	473	1594

Annex 2 (continued)

P	q	U <sub>1</sub>	U <sub>2</sub>	U <sub>3</sub>	U <sub>4</sub>	U <sub>5</sub>	U <sub>6</sub>
6	45,69	0,6162	0,4114	0,1067	0,0658	0,0501	0,1663
7	44,88	6349	4185	1112	702	530	1733
8	44,06	6539	4255	1156	748	560	1805
9	43,25	6733	4324	1202	796	591	1878
0,50	42,83	6931	4392	1249	846	623	1951
1	42,83	7133	4460	1297	897	656	2024
2	42,83	7339	4528	1346	950	688	2097
3	42,83	7550	4596	1397	0,1005	722	2170
4	42,83	7765	4664	1487	1061	756	2244
5	42,83	7985	4732	1502	1119	790	2317
0,56	42,83	8210	4800	1557	1178	824	2390
7	42,83	8440	4868	1614	1239	860	2464
8	42,83	8675	4936	1672	1302	896	2537
9	42,83	8916	5004	1732	1367	932	2610
0,60	42,83	9163	5072	1793	1433	969	2634
1	42,83	9416	5140	1856	1501	0,1007	2757
2	42,83	9676	5208	1921	1571	1044	2830
3	42,83	9943	5276	1988	1643	1083	2903
4	42,83	1,0217	5344	2057	1717	1122	2977
5	42,83	0499	5412	2127	1793	1161	3050
6	42,83	0789	5480	2199	1870	1201	3123
7	42,83	1087	5548	2274	1951	1241	3197
8	42,83	1396	5616	2350	2033	1282	3270
9	42,83	1714	5684	2429	2118	1323	3343
0,70	42,83	2042	5752	2509	2205	1365	3417
1	42,83	2381	5820	2593	2295	1408	3490
2	42,83	2732	5888	2678	2387	1450	3563
3	42,83	3096	5956	2766	2482	1494	3636
4	42,83	3473	6024	2856	2579	1538	3710
5	42,83	3865	6092	2949	2679	1582	3783
6	42,83	4274	6160	3045	2782	1627	3856
7	42,83	4699	6228	3143	2889	1672	3930
8	42,83	5144	6296	3244	2998	1718	4003
9	42,83	5609	6364	3349	3111	1764	4076
0,80	42,83	6097	6432	3457	3227	1811	4150
1	42,83	6610	6500	3568	3347	1859	4223
2	42,83	7151	6568	3683	3471	1906	4296
3	42,83	7723	6636	3801	3597	1955	4370
4	42,83	8329	6704	3924	3731	2004	4443
5	42,83	8975	6772	4051	3868	2053	4516
6	42,83	9665	6840	4182	4009	2103	4589
7	42,83	2,0406	6908	4318	4156	2153	4663
8	42,83	1206	6976	4460	4308	2204	4736
9	42,83	2077	7044	4607	4467	2255	4809
0,90	42,83	3030	7112	4760	4633	2307	4883

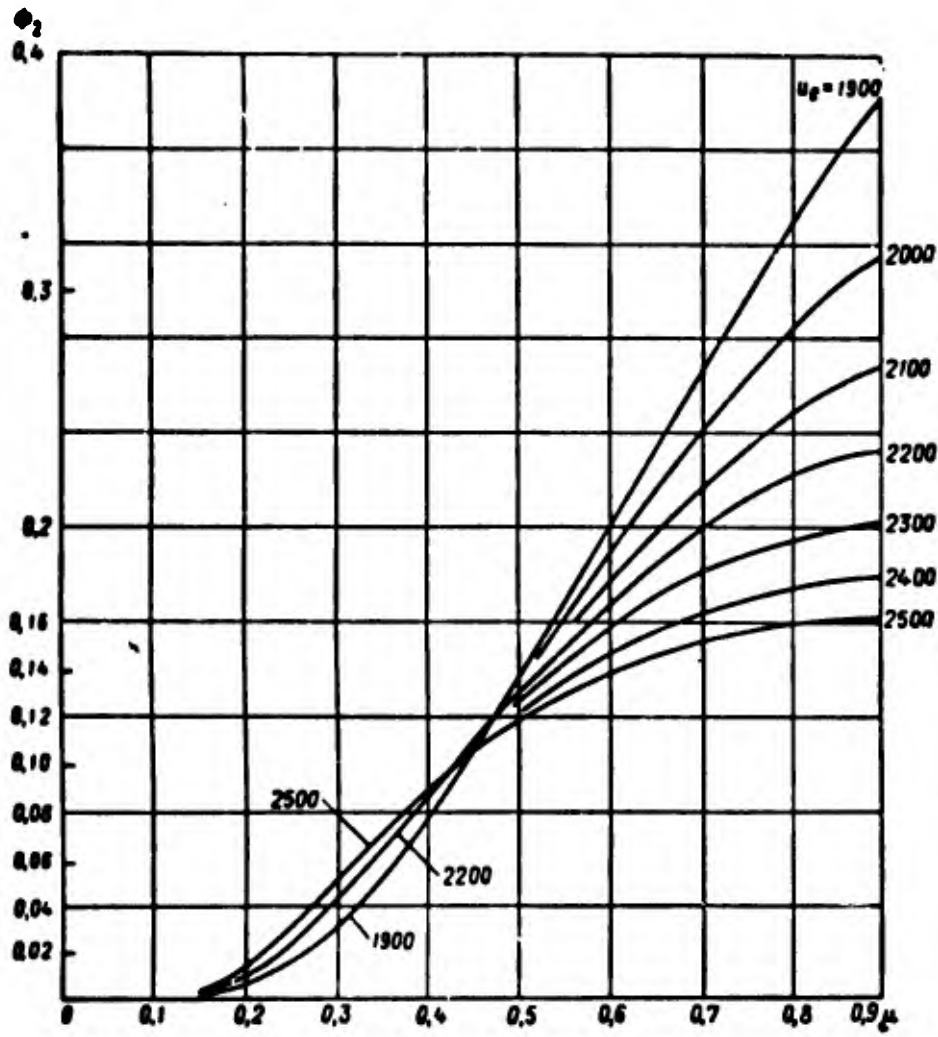
ANNEX 3. GRAPHS FOR FUNCTION  $\phi_2(\eta, u_0, \mu)$  FOR CHAPTER II

$\eta = 2$



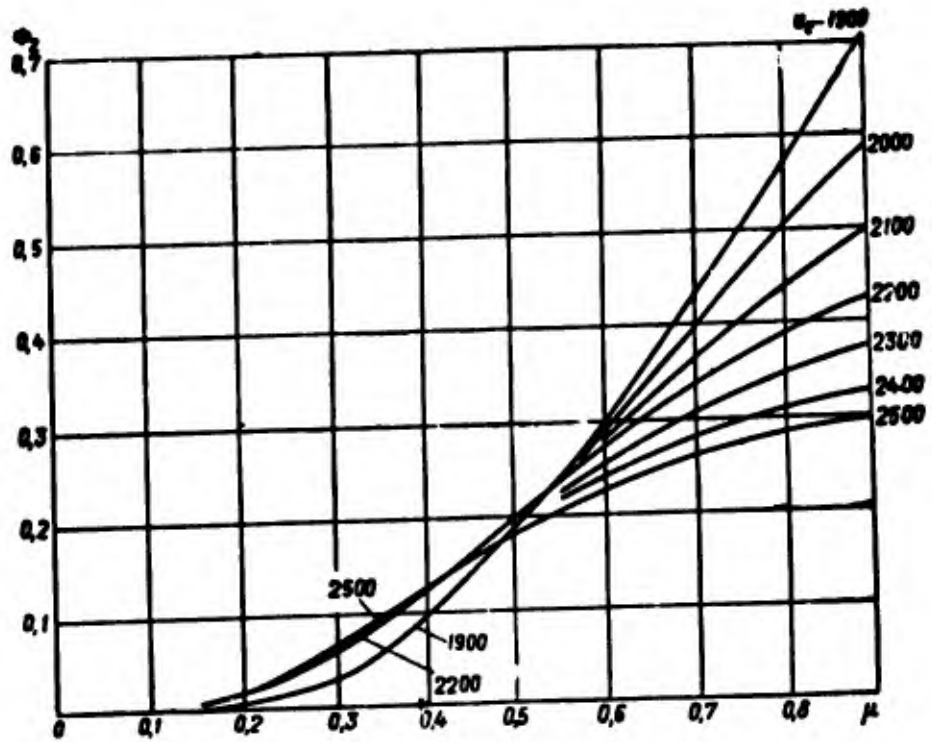
Annex 3 (continued)

$\eta = 8$



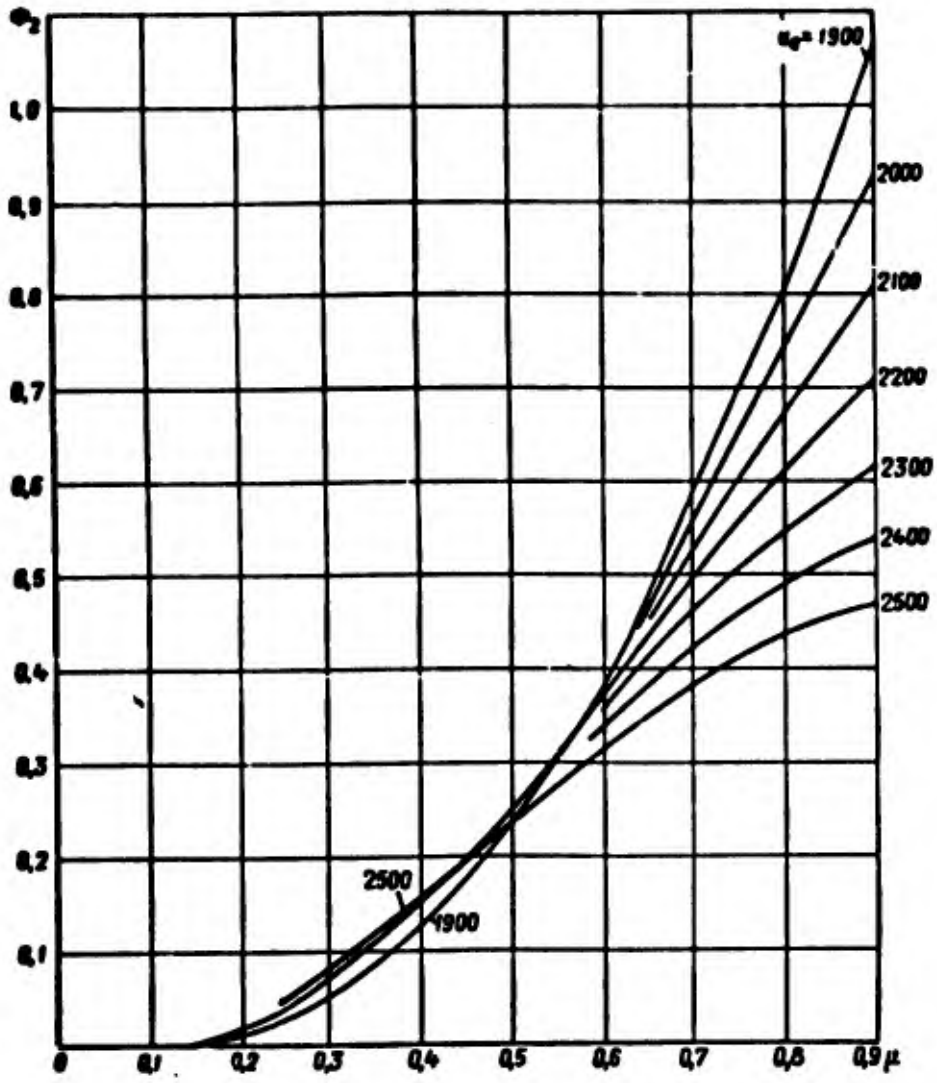
Annex 3 (continued)

$q = 0$



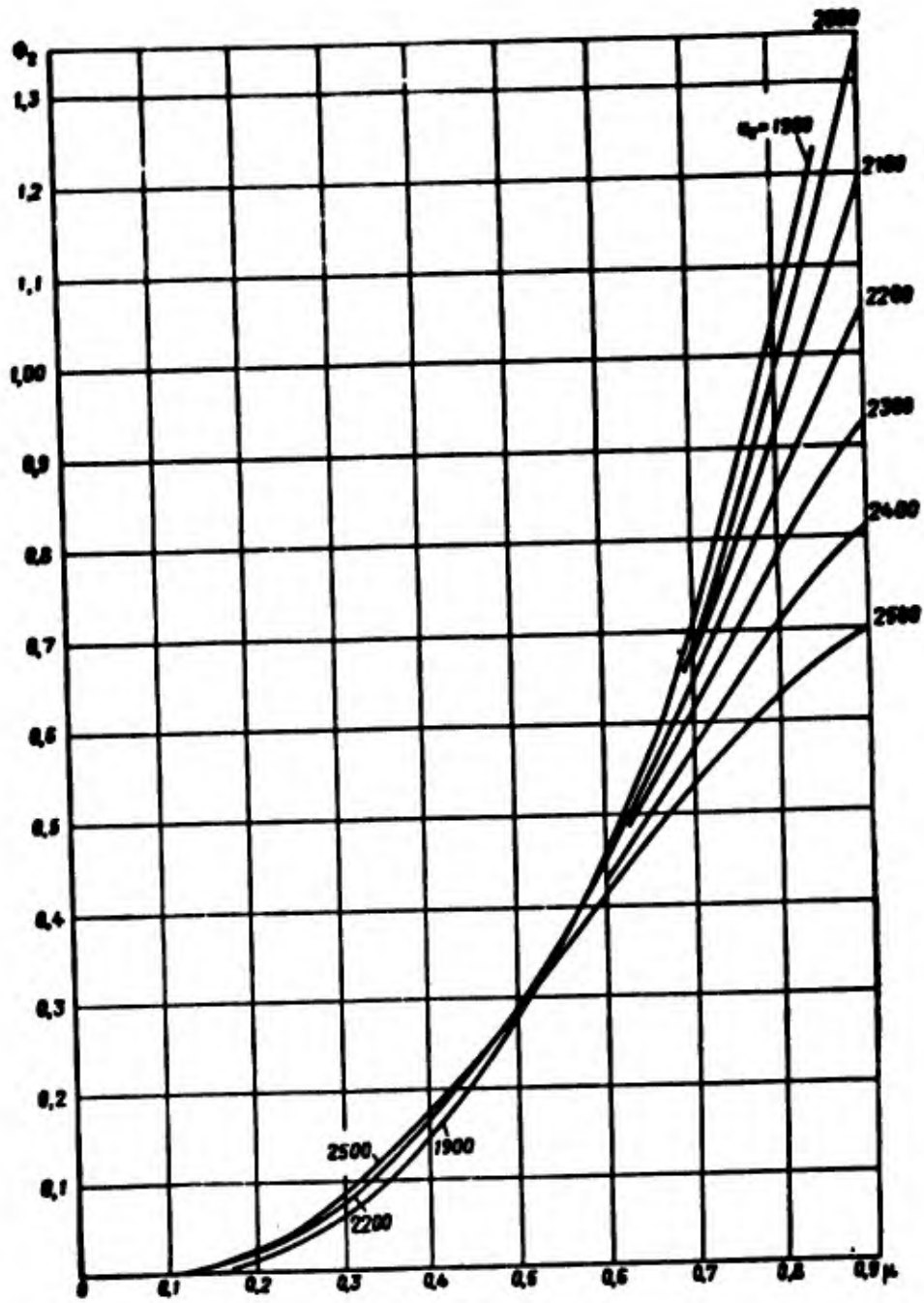
Annex 3 (continued)

$$\eta = 8$$



Annex 3 (continued)

$\eta = 0$



- END -

- 379 -

**DATA HANDLING PAGE**

01-ACCESSION NO.  TM9001853	98-DOCUMENT LOC	39-TOPIC TAGS  motion equation, solid rocket engine, aerodynamic moment, trajectory determination, thrust vector control, missile design, surface to surface missile, tensile strength, unguided missile
09-TITLE PRINCIPLES OF SOLID-FUEL ROCKET DESIGN -U-		
47-SUBJECT AREA  16, 20, 21		

42-AUTHOR CO-AUTHORS SHAPIRO, Ya. M. ; 16-MAZING, G. Yu. ; 16-PRUDNIKOV, N. Ye.	10-DATE OF INFO ----68
43-SOURCE OSNOVY PROYEKTIROVANIYA RAKET NA TVERDOM TOPLIVE (RUSSIAN)	68-DOCUMENT NO. FTD-HT-23-268-69
	69-PROJECT NO. 60401

63-SECURITY AND DOWNGRADING INFORMATION  UNCL. 0	64-CONTROL MARKINGS  NONE	97-HEADER CLASN  UNCL
--	---------------------------------	-----------------------------

76-REEL / FRAME NO. 1890 1531	77-SUPERSEDES	78-CHANGES	40-GEOGRAPHICAL AREA UR	NO. OF PAGES 389
CONTRACT NO.	X REF ACC. NO. 65-	PUBLISHING DATE 94-	TYPE PRODUCT TRANSLATION	REVISION FREQ NONE

STEP NO. 02-UR/0000/68/000/000/0001/0352

**ABSTRACT**

(U) On the basis of materials published in the domestic and foreign press this book offers a survey of the designs of guided and unguided rockets for various purposes and having solid-fuel engines. The design elements of individual assemblies and units, the composition layouts of rockets, and questions relating to the regulation of thrust as regards quantity and direction are examined. Engineering methods for calculating the elements of trajectories of guided and unguided rockets are given, as they apply to the problem of ballistic designing. The factors affecting the scatter of unguided rockets are examined. Optimum parameters for rockets and design units are evaluated via synthesis and analysis of weight equations for rockets, approximate external ballistic relations being utilized. The fundamentals of calculations of solid-fuel rocket engines and of charges for them as regards sturdiness are set forth. The book can be used as a manual for engineers working in the field of rocket technology, and also for students at institutes of higher education.